AGARD-AG-278 Volume I

AGARD-AG-278 Volume I

AGARD

ADVISORY GROUP FOR AEROSPACE RESEARCH & DEVELOPMENT

7 RUE ANCELLE 92200 NEUILLY SUR SEINE FRANCE

AGARDograph No.278

AGARD Corrosion Handbook Volume 1 Aircraft Corrosion: Causes and Case Histories

NORTH ATLANTIC TREATY ORGANIZATION

DISTRIBUTION AND AVAILABILITY ON BACK COVER

AGARD-AG-278
Volume 1

NORTH ATLANTIC TREATY ORGANIZATION

ADVISORY GROUP FOR AEROSPACE RESEARCH AND DEVELOPMENT

(ORGANISATION DU TRAITE DE L'ATLANTIQUE NORD)

AGARDograph No.278

AGARD CORROSION HANDBOOK

VOLUME 1

AIRCRAFT CORROSION: CAUSES AND CASE HISTORIES

by

W.Wallace
Head, Structures and Materials Laboratory
National Aeronautical Establishment
National Research Council Canada
Ottawa, Ontario, Canada

and

D.W.Hoeppner
Cockburn Professor of Engineering Design
Department of Mechanical Engineering
University of Toronto
Toronto, Ontario, Canada

with a chapter by

P.V.Kandachar
Fokker, B.V. Technical Centre
Schiphol, The Netherlands

This AGARDograph was prepared on behalf of the Corrosion Subcommittee of the Structures and Materials Panel of AGARD.

THE MISSION OF AGARD

The mission of AGARD is to bring together the leading personalities of the NATO nations in the fields of science and technology relating to aerospace for the following purposes:

— Exchanging of scientific and technical information;

— Continuously stimulating advances in the aerospace sciences relevant to strengthening the common defence posture;

— Improving the co-operation among member nations in aerospace research and development;

— Providing scientific and technical advice and assistance to the North Atlantic Military Committee in the field of aerospace research and development;

— Rendering scientific and technical assistance, as requested, to other NATO bodies and to member nations in connection with research and development problems in the aerospace field;

— Providing assistance to member nations for the purpose of increasing their scientific and technical potential;

— Recommending effective ways for the member nations to use their research and development capabilities for the common benefit of the NATO community.

The highest authority within AGARD is the National Delegates Board consisting of officially appointed senior representatives from each member nation. The mission of AGARD is carried out through the Panels which are composed of experts appointed by the National Delegates, the Consultant and Exchange Programme and the Aerospace Applications Studies Programme. The results of AGARD work are reported to the member nations and the NATO Authorities through the AGARD series of publications of which this is one.

Participation in AGARD activities is by invitation only and is normally limited to citizens of the NATO nations.

The content of this publication has been reproduced
directly from material supplied by AGARD or the authors.

Published July 1985

ISBN 92-835-1505-6

Printed by Specialised Printing Services Limited
40 Chigwell Lane, Loughton, Essex IG10 3TZ

PREFACE

Aircraft corrosion is a very expensive phenomenon in terms of inspection, of maintenance and repair, of manpower requirements, and of decreased aircraft availability. In the Spring of 1981 the Corrosion Sub-Committee of the Structures and Materials Panel called a Specialists' Meeting at which experts in the various corrosion-related disciplines discussed problems of mutual interest. There was strong support from this meeting for a proposal which had already been mooted by the Panel to publish a Handbook on Aircraft Corrosion.

The work was put in hand forthwith, and this volume, the first of a two-part Handbook, is a result of the Panel's initiative. This part covers the theory of, and some experiences with, metallic corrosion as related to the observed behaviour of real aircraft structures. The second part will concentrate on specifications for corrosion protection as practised by various NATO nations.

AGARD CORROSION HANDBOOK

VOLUME 1: AIRCRAFT CORROSION, CAUSES AND CASE HISTORIES

TABLE OF CONTENTS

SECTION II

CHAPTER 1

INTRODUCTION

1.1 General

Aircraft structures experience severe conditions in service. The loads developed in flight and during ground maneouvres are generally high, and in the interest of achieving low overall weight structural materials are selected that have high strength, high stiffness and low specific gravity. High strength materials allow excess weight to be kept to a minimum. However other properties, such as the ability of the materials to resist corrosive attack are also important. Unfortunately low weight and high strength in aircraft structures and materials may not always be compatible with high resistance to corrosion, and therefore trade-offs may need to be made. By proper attention to corrosion at the design stage and in assembly, and by careful inspection and early repair of corrosion damage and repair of damaged protective systems, it is generally agreed that corrosion consequences of these trade-offs can be minimized.

1.2 The Deterioration of Aircraft Structures

Aircraft structures will begin to deteriorate from the time they leave the manufacturers plant. Deterioration will occur in the form of mechanical damage such as abrasion, galling, wear or fatigue, which depend primarily on the design of the aircraft and the loads experienced in service. Deterioration will also occur by corrosion, which depends on the detailed design of the structure, the materials used for fabrication and protection, and also on the chemical nature of the operating environment of the aircraft. Other modes of deterioration will occur, such as corrosion fatigue, stress corrosion and fretting, which depend on both the chemical and mechanical aspects of the environment. This handbook is concerned with corrosion in aircraft structures, and with mechanical forms of deterioration to the extent that they are affected by corrosion.

Corrosion damage generally increases with time, and as an aircraft becomes older the effects of corrosion will become more severe. If corrosion damage is not detected early and repaired it may eventually become a serious hazard to the structural integrity of the aircraft. A particularly serious consequence of corrosion is that it can accelerate other forms of damage, such as fatigue, and it acts conjointly with fatigue to lower the overall structural integrity of the aircraft. It can therefore have a marked effect in reducing the life of the aircraft, particularly with aircraft intended to remain in service for long periods of time.

This is shown schematically in Figure 1-1 (Ref. 1-1) where corrosion damage is superimposed on fatigue damage of short-life and long-life aircraft. Since corrosion damage occurs slowly it may represent a small part of the total damage of a short-life aircraft at retirement. However, since corrosion damage is cumulative it may represent a substantial part of the total damage of a long-life aircraft at retirement, and hence be responsible for major reduction in life.

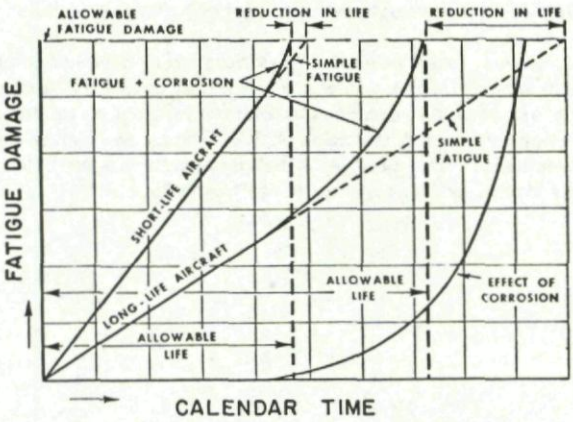

Fig. 1-1 The effect of corrosion on the fatigue lives of long and short-term aircraft (Ref. 1-1)

It is obvious that if an aircraft is to remain operationally effective for the whole of its long-life, corrosion-preventative measures must be of the highest possible standard at all times so that the designers' original fatigue and operational-life predictions remain valid.

1.3 The Costs of Corrosion

The costs of corrosion are known to be large, but accurate estimates are difficult to obtain. The direct costs of corrosion, including material lost and preventive measures taken, have increased steadily over the past four decades, as indicated in Table 1-1.

Table 1-1 Estimates of the total annual cost of corrosion in the U.K. and U.S.A. over the period 1950-1978

	Direct cost of corrosion ($ Millions)			
Year:	1950	1960	1970	1978
United Kingdom (Refs. 1-1, 1-3)		1500	3000	
United States (Refs. 1-2, 2-14)	5500		12000	7×10^4

Even though our knowledge of engineering design, materials science, and corrosion theory have increased considerably over the past thirty years, Table 1-1 indicates that corrosion costs have continued to escalate.

The estimates of Table 1-1 assume particular significance when it is appreciated that the costs of corrosion and protection in industrialized countries correspond to 2.5-3.5% of the gross national product (Ref. 1-3). Some of these costs are unavoidable such as those due to the higher price of more corrosion resistant materials, or the cost of painting or other protective measures. However, it has become clear that doing something about corrosion is in most cases cheaper than just letting it run its course, if only by avoiding unplanned down-time of equipment (Ref. 1-4). It has also been estimated (Ref. 1-3) that about 15% of the present corrosion costs could be saved by the application of existing knowledge of corrosion prevention and control, i.e., by using better protective systems, by improving design, and by improved materials selection.

The information in Table 1-1 is not specific to aircraft, but the information that is available indicates that corrosion costs in aircraft have followed a similar upward trend. An unconfirmed report has estimated the total cost of detecting and repairing corrosion in the U.S. Air Force at $1 billion/year, while the total direct cost of corrosion to members of the International Air Transport Association (IATA) (Ref. 1-2) in 1979 has been estimated to be $100 million, based on 1976 operations. The study also found that maintenance costs due to corrosion represented between 6% and 8% of direct air frame maintenance costs, and between $5 and $12 per flying hour depending on operations and aircraft type. These latter figures excluded maintenance overhead. Ryan (Ref. 1-5) has extimated that maintenance and operational costs exceed 50% of the total cost of ownership of military aircraft, and that 30% of each maintenance dollar is spent on corrosion and corrosion related problems. Furthermore, he estimates that corrosion related deterioration accounts for almost 25% of all causes of component failure and replacement.

It is obviously difficult to determine the costs of corrosion accurately, but it should be understood that corrosion in aircraft systems can lead to severe penalties in terms of;

(a) systems failures and loss of aircraft and human life.

(b) non-availability of aircraft due to corrosion damage.

(c) direct costs associated with inspection, and with both preventative and corrective maintenance.

1.4 Purpose and Scope of this Handbook

A need exists to keep aircraft operators and maintenance personnel aware of the science and technology of corrosion as it applies to aircraft structures. Manuals on aircraft corrosion have been prepared by some of the larger NATO countries (Refs. 1-1, 1-6), but similar documents do not exist in some of the smaller countries.

This handbook aims to address this problem and to provide state-of-the-art information which will be available to all NATO member countries. It has been prepared in two sections. Section I consists of Chapters 1 to 6, and includes information on the aircraft operating environment, a simple outline of corrosion theory, the common airframe materials andtheir response to corrosion, the detection of corrosion, and finally a description of methods employed to control or prevent corrosion in aircraft structures and materials.

Section II, Chapters 7 to 14, provides case histories of the deterioration or failure of components in aircraft typical of those in use in NATO member countries. Where possible information is also given of the means by which damage was detected and the remedial actions taken. The case histories are selected to describe the common forms of corrosion observed in aircraft systems. It is hoped this information will assist inspection and repair personnel in all NATO countries to make early diagnosis of developing corrosion problems, and to select appropriate corrective measures. Because of the special nature of microbiological corrosion a special chapter has been prepared on this by Dr. P.V. Kandachar, and this is included as Chapter 15.

SECTION I

CHAPTER 2

THE OPERATING ENVIRONMENT

2.1 General

The operating environments of aircraft in the collective NATO fleet vary widely, even within any one country. Consequently corrosion can also vary considerably. For stationary structures the corrosion severity of the atmosphere can provide an indication of the probable life of the part. For many reasons the problem is much more complicated with aircraft structures, not the least of which is the fact that in flight the aircraft experiences widely varying conditions, as a result of geographical location, range, altitude and weather changes. Nevertheless, an aircraft spends a considerable amount of time on the ground, and the environment of the base is an important consideration.

It should also be remembered that aircraft may experience particularly severe conditions for short periods of time. During take-off and landing an aircraft will be impacted by dust, gravel, stones and de-icing salts from the runway, which can damage bare metal or paint. Similarly, aircraft are exposed to a wide variety of cleaning and de-icing fluids which also create unusual environmental conditions, although these are obviously selected to minimize corrosive attack. Aircraft operating from ocean carriers will be exposed to severe salt spray, while the emission from the ships stack will contain a wide variety of corrosive gases and particulate matter which may also be damaging. A more complete list of hazards associated with normal operating and maintenance activities has been given by Mitchell, Table 2-1, Ref. 2-7.

Table 2-1 Operational/Maintenance materials and hazards affecting aircraft

(a) Oils and hydraulic fluids.
(b) Cleaning materials and paint strippers.
(c) Maintenance actions causing scratches and abrasions.
(d) Accidental damage during maintenance and in operation.
(e) Battery acid.
(f) Exhaust gases.
(g) De-icing and de-frosting fluids.
(h) Toilet and galley spillages.
(i) In flight turbulence causing spillage.
(j) Cargo breakage and/or spillage.
(k) Contaminated fuel (kerosene).

2.2 Classification of Atmospheres

For corrosion purposes atmospheres are usually classified as rural, industrial, marine or marine-industrial, although it should be realized that wide variations in corrosive attack may occur in any one atmosphere. This classification is based largely on the cleanliness of the atmosphere, since industrial pollutants such as suphur dioxide, ammonia, or smoke particles can accelerate corrosion markedly. Similarly, sodium chloride in marine or coastal atmospheres is also extremely damaging. A listing of impurities and their typical concentrations in various atmospheres is given in Table 2-2 (Ref. 2-8).

Table 2-2 Typical concentrations of atmospheric impurities, (Ref. 2-8)

Impurity	Typical concentrations ($\mu g/m^3$)
Sulphur dioxide	Industrial region: winter 350, summer 100 Rural region: winter 100, summer 40
Sulphur trioxide	Approximately 1% of the sulphur dioxide content
Hydrogen sulphide	Industrial region: 1·5-90 Urban region: 0·5-1·7 Rural region: 0·15-0·45 } values measured in the spring
Ammonia	Industrial region: 4·8 Rural region: 2·1
Chloride (air sampled)	Industrial inland: winter 8·2, summer 2·7 Rural coastal: annual average 5·4
Chloride (rainfall sampled)	Industrial inland: winter 7·9, summer 5·3 Rural coastal: winter 57, summer 18 (these values in mg/l)
Smoke particles	Industrial region: winter 250, summer 100 Rural region: winter 60, summer 15.

Climate is also a major factor affecting corrosion since it introduces the two important variables of temperature and humidity. A simple classification of atmospheres according to corrosion severity is given in Table 2-3 (Ref. 1-1).

Table 2-3 Types of corroding atmospheres

Rate of corrosion	Type of atmosphere		
Highly conducive to corrosion	Tropical	Industrial	Marine
Moderate corrosion	Temperate	Suburban	Inland
Low rate of corrosion	Arctic	Rural	

Table 2-3 shows that the atmosphere most conducive to corrosion is the tropical industrial marine atmosphere. Fortunately this is fairly uncommon due to lack of heavy industry in most tropical countries. However the temperate industrial marine atmosphere is also aggressive and is common to many of the NATO countries.

Table 2-4 gives a crude guide to the relative corrosivity of various atmospheres throughout the world on the light alloys used in aircraft construction. Corrosivity index (1) in the classification is the most corrosive atmosphere while index (8) indicates the least corrosive atmosphere.

TABLE 2-4 Relative corrosivity of the atmosphere at various sites on aircraft alloys (Ref. 1-1)

Location	Atmosphere	Corrosivity Index
Persian Gulf	Tropical marine	1
Singapore	Tropical marine	2
Guinea	Tropical marine	3
Halifax (Canada)	Industrial marine	4
London (UK)	Temperate industrial	5
Brixham (UK)	Temperate marine	6
Banbury (UK)	Semi-rural temperate	7
Cold Lake (Canada)	Arctic marine	8

The effects of long time exposure of a selection of aluminium alloys to rural, industrial and marine (sea-coast) atmospheres in the United States are shown in Figure 2-1. In this figure the extent of corrosive attack is indicated by loss of tensile strength on pre-machined tension specimens of the various materials. The loss of tensile strength could be appreciable since the tension specimens were thin.

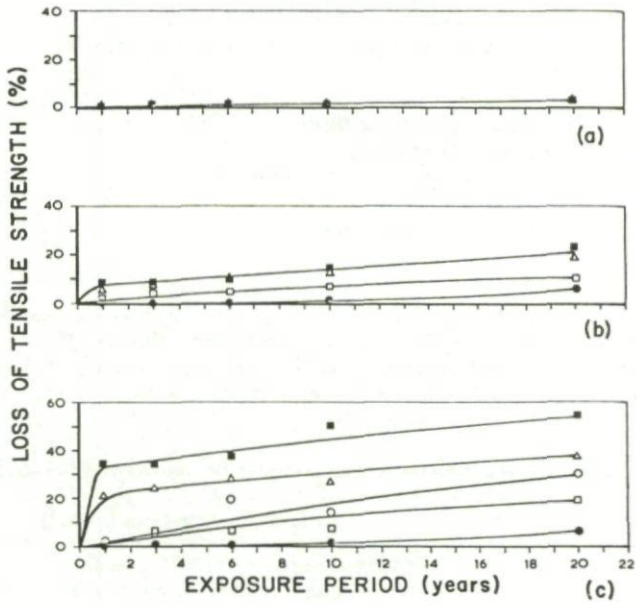

Fig. 2-1 A.S.T.M. 20-year corrosion tests: ■ 2017-T3, □ 3003-H14, △ 6051-T4, ○ 1100-H14, ● Alclad 2017-T3

(a) State College, Pa. (rural). Premachined tension specimens 0.89 mm thick. Curves for 1100-H14, 3003-H14 and Alclad 2017-T3 fall below curve shown;
(b) New York, N.J. (industrial);
(c) La Jolla. Calif. (seacoast) (Ref. 2-9)

The results show that the severity of attack increases in moving from the rural to the industrial to the marine atmosphere. The figure also shows that corrosive attack occurs rapidly at first and then tends to slow down, probably as protective corrosion products or films form on the surface. The effects of protective surface films is discussed later in Section 3.3.

2.3 Temperature

Temperature is an important variable and its effects are demonstrated in Tables 2-3 and 2-4. High temperature generally increases the rate of corrosive attack on metals since corrosion reactions are thermally activated. Corrosion in steel for example is strongly affected by temperature, while only a slight effect is observed with zinc (Refs. 2-10, 2-11). Temperature can change the mode of attack on aluminium alloys in moist or wet atmospheres from localized corrosion, or pitting, to uniform attack (Ref. 2-12). Temperature is also important since it affects the drying of corrosive solutions on the metal surface, and the consequent concentration of damaging impurities.

2.4 Humidity

Water vapour in the atmosphere is important since it can lead to the formation of a thin, often invisible film of water on the metal surface. The moisture will provide an electrically conducting medium to create an electrolytic cell on the metal which allows rapid corrosion to occur. This is described in Chapter 3.

Most metals will form a very thin surface oxide film at low humidities, which is usually protective, and serious corrosion will not occur until a critical level of humidity is reached. This is usually about 60% R.H. Further rapid increases in corrosion rate may occur at higher humidities due to the condensation of moisture in the oxide layers, or the vapourization of the corrosion products. In iron such accelerations of corrosion rate occur at about 75-80% R.H. and 90% R.H. respectively.

For some metals critical humidity may be influenced by impurities in the atmosphere which react with the water vapour. This is illustrated in Figure 2-2 for copper. This shows that corrosion on copper is slow in an atmosphere containing up to 63% relative humidity and 10% sulphur dioxide. At higher levels of humidity the adsorbed sulphur dioxide can collect sufficient water for catalytic oxidation to form sulphuric acid, which attacks copper readily in the presence of oxygen. Thus, at relative humidities of 75% and 99% the rates of corrosion are much higher.

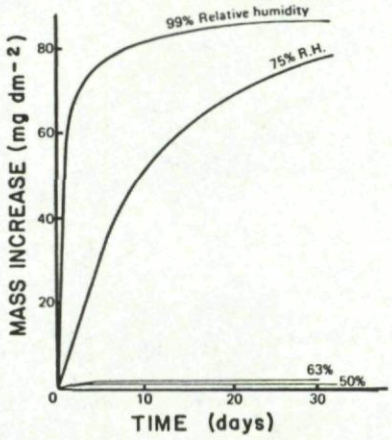

Fig. 2-2 Corrosion of copper by air containing 10% sulphur dioxide and different degrees of moisture (Ref. 2-13)

2.5 Atmospheric Impurities

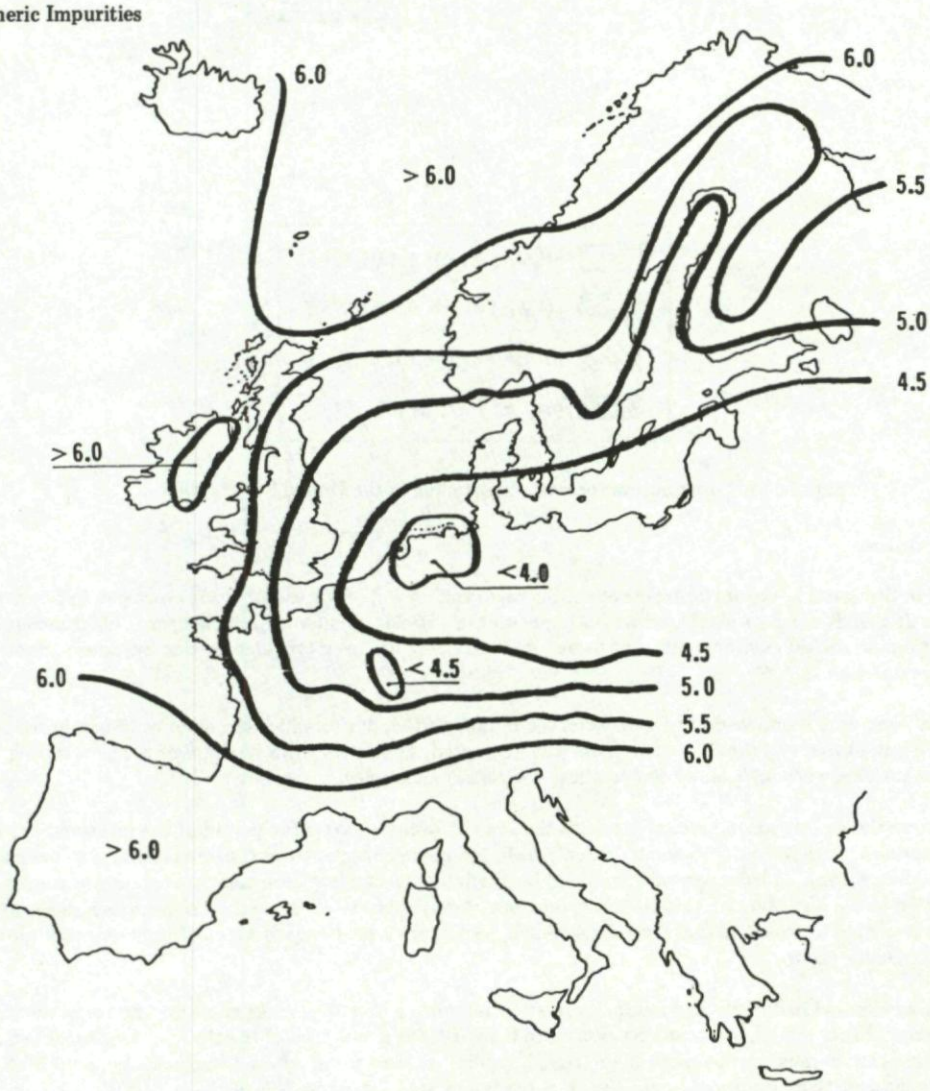

Fig. 2-3 Plots of iso-pH for rain water falling over Western Europe, 1980

The damaging effects of industrial and marine atmospheres noted in Tables 2-3 and 2-4 are due to the presence of impurities such as sulphur dioxide, hydrogen sulphide, ammonia, sodium chloride, and smoke particles. Typical concentrations of these constituent in various atmospheres are given in Table 2-2. Other damaging contaminants may be found in the local environments of chemical plants or behind the smoke stack on aircraft carriers where particularly severe corrosion can occur.

The general effect of these impurities is to acidify the atmosphere and the rainfall produced from it. A recent survey of rainfall analyses for Europe has shown that, with the exception of the U.K., the acidity and sulphate content of rainfall markedly increased during the period 1956 to 1966, pH values having fallen by 0.05 to 0.10 units per year (Ref. 2-8). Even in the U.K. a pH of 4 is not uncommon for rainfall in industrial areas. Figure 2-3 indicates the acidity of rainwater falling over Western Europe in 1980, while Figure 2-4 shows similar data for the United States. The data in Figure 2-3 is in the form of iso-pH lines and it indicates the high acidity (pH < 4.0) of the rain falling over parts of West Germany and Holland. Figure 2-4 shows that similarly high acidity is observed in the rain falling over many of the large industrial cities in the United States.

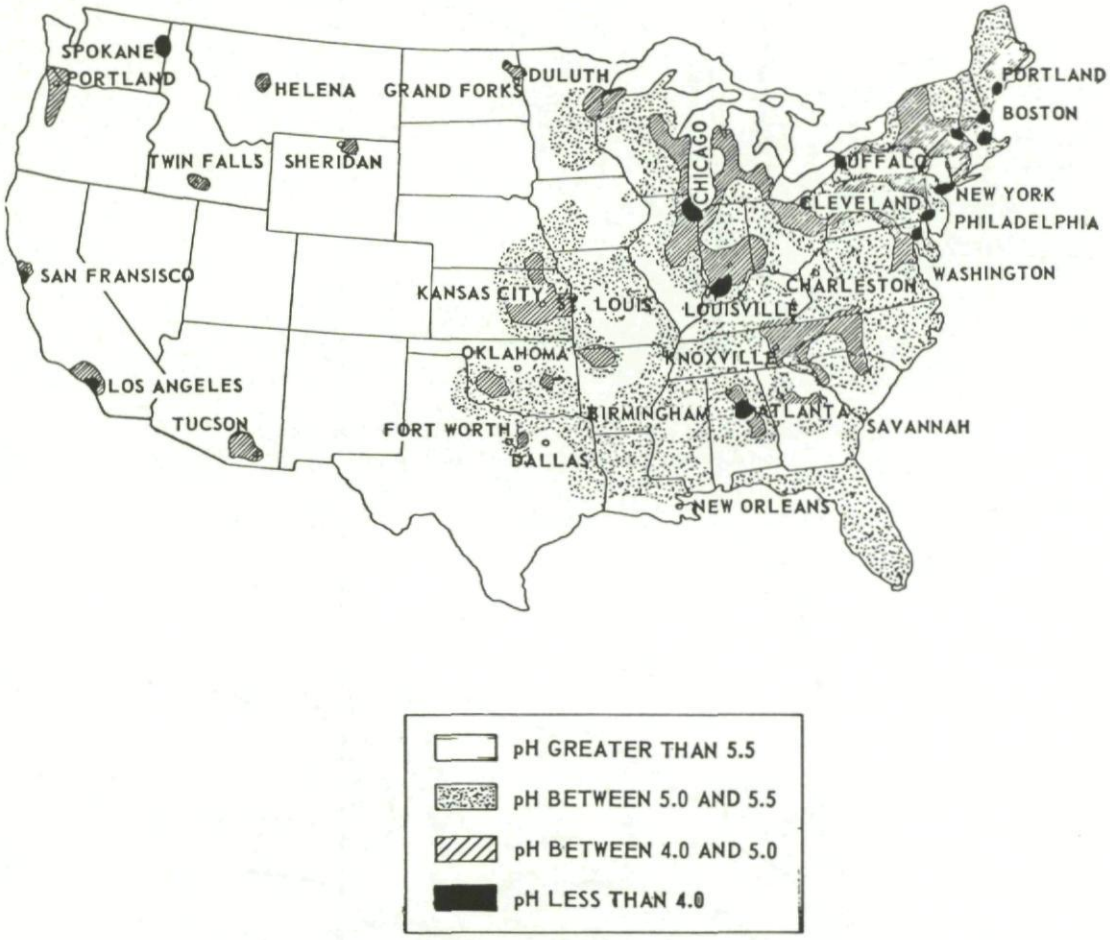

Fig. 2-4 pH distribution for rain water falling in the United States, 1980

2.6 The Environment at Base

As explained in Section 2.1, the environment of the air base is an important factor affecting corrosion in aircraft structures. This is because the aircraft spends much of its life, either outdoors on the airfield, or indoors in the hangar. Unfortunately there is no published data on different airfield environments, but some interesting data has been provided by one European country which is probably typical of several others.

Weather conditions were monitored outdoors over a ten month period, during which the amount of precipitation, the maximum and minimum humidities, and the time of wetness were measured. This latter was a measure of the time during which exposed non-conducting surfaces were sufficiently wet to allow the passage of an electric current.

Figure 2-5 shows the weekly mean precipitation and the time of wetness during the period of the investigation. It can be seen that the total precipitation varied from 0 to about 50 mm/week, but more important was the observation that the mean time of wetness was about 50 hours/week. A large part of this should be attributed to condensation and dew forming at sunrise. Although it may not be possible to relate a high time of wetness to the measure of corrosive attack, since the presence or absence of impurities is not considered, it is reasonable to conclude that for a considerable part of the time the outdoor environmental conditions were such that corrosion might easily occur.

From the daily measured maximum and minimum relative humidity a humidity range could be plotted as shown in Figure 2-6. This figure shows that the relative humidity was more than 70% for about 50% of the time. As explained in Section 2.4, fairly rapid corrosion will occur in most metals when the relative humidity exceeds some critical value, usually about 60%. The present results therefore indicate that conditions conducive to corrosion existed for about 70% of the time during the period of the investigation.

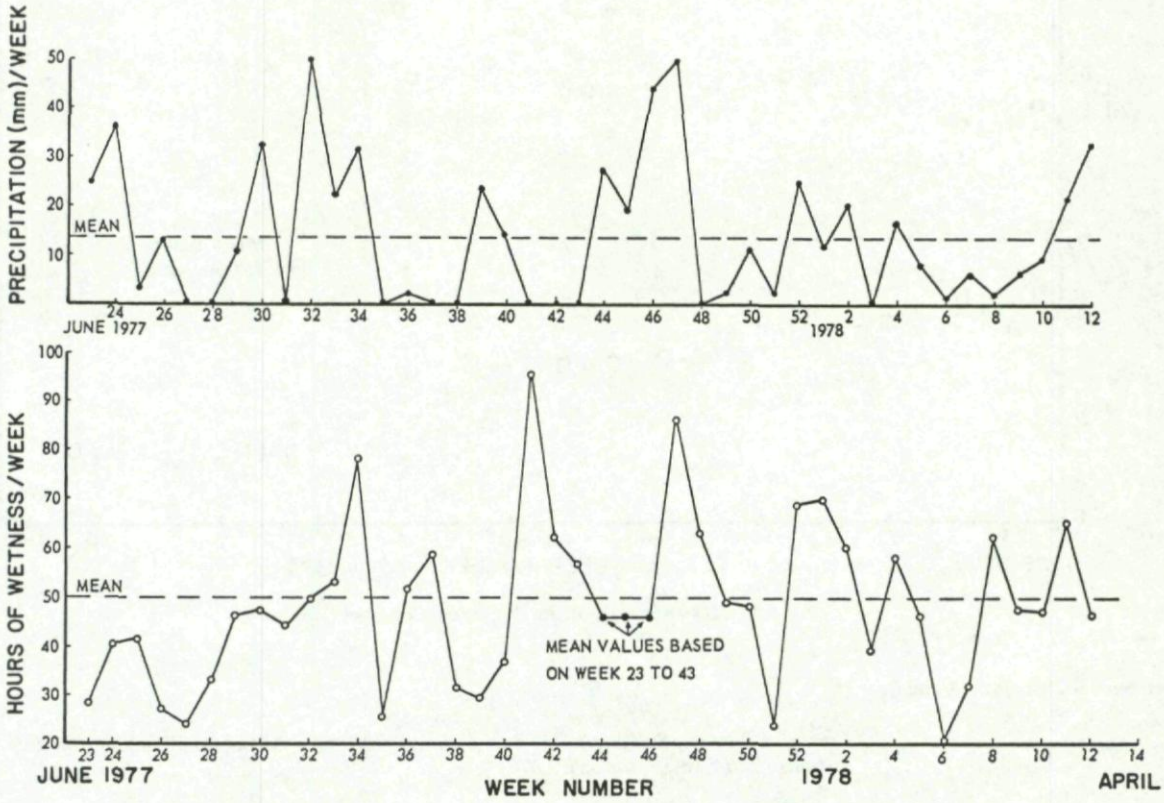

Fig. 2-5 Recorded time of wetness and precipitation during the total exposure period at a European airfield

During the course of this investigation measurements were also made of the temperature and the relative humidity in one of the aircraft shelters at the same base. From the records the mean values for each week were determined, and the results are shown in Figure 2-7. The results show that the relative humidity increases with decreasing temperature, and for a long period of time exceeds the 80% level. At these high relative humidity values an electrolyte can be easily formed by the water absorbent pollution products, and fairly rapid corrosion may occur.

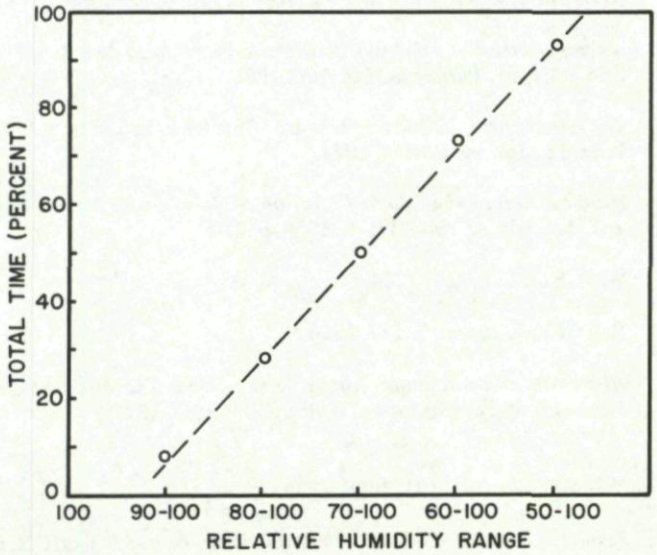

Fig. 2-6 Duration of humidity ranges from 1 June 1977 to 31 March 1978 at a European airfield

It was noted during this investigation that a large percentage of flights from this base involved either low altitude flights in a marine environment, or navigation flights performed in industrial environments at low level in the range 150-1500 m. Thus the contamination experienced in operational flights may result in severe corrosive attack when the aircraft return to the humid shelter climate.

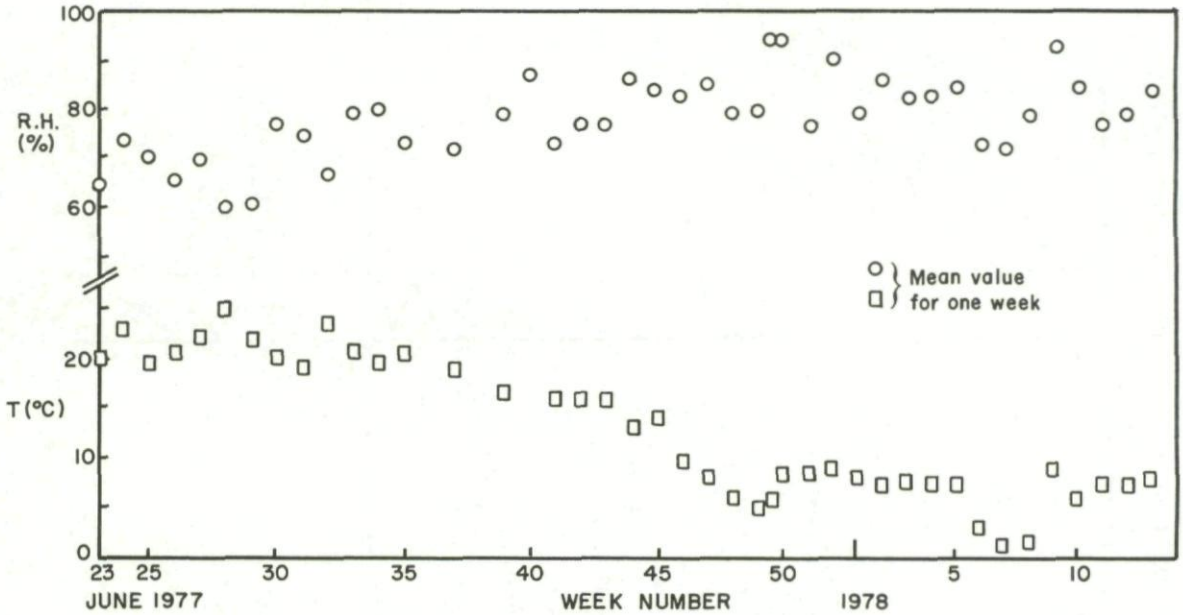

Fig. 2-7 Measurements of the shelter environment

2.7 References (Chapters 1 and 2)

1-1		*Corrosion Manual*, Section 1, Air Publication 119A-0200-1A, United Kingdom, Ministry of Defence, 2nd Edition, October 1978.
1-2		*Guidance Material on Design and Maintenance Against Corrosion of Aircraft Structures*, Doc. Gen/2637, International Air Transport Association, February 1979.
1-3		Report of the Committee on Corrosion and Protection, Chairman, T.P. Hoar, London, Her Majesty's Stationary Office, 1971.
1-4	Gellings, P.J.	*Introduction to Corrosion Prevention and Control for Engineers*, Delft University Press, Delft, The Netherlands, 1976.
1-5	Ryan, N.E.	Materials Division, Aeronautical Research Laboratories, Australia. Private Communication.
1-6		*Aircraft Weapons Systems Cleaning and Control*, Technical Manual, NAVAIR 01-1A-509, Naval Air Systems Command, Washington, September 1980.
2-7		*Aircraft Corrosion*, AGARD Conference Proceedings No. 315, Proceedings of a Conference held at Çeşme, Turkey, 5-10th April 1981.
2-8	Rowlands, J.C.	*The Atmosphere*, in Corrosion, Vol. 1, Chapter 2, Edited by L.L. Schrier, Newnes-Butterworths Press, London and Boston, 1977.
2-9		*Symposium on Atmospheric Corrosion of Non-Ferrous Metals*, American Society for Testing and Materials, ASTM-STP-175, 1956, p. 27.
2-10	Schikorr, A.	Werk. Korr., 15, 457, 1964.
2-11	Stanners, J.F.	B. Corrosion Journ., 5, 117, 1960.
2-12	Bailey, J.C. Porter, F.C. Pearson, A.W.	*Aluminum and Aluminum Alloys*, in Corrosion, Vol. 1, Chapter 4, Edited by L.L. Schrier, Newnes-Butterworths Press, London and Boston, 1977.
2-13	Vernon, W.H.J.	Trans. Faraday Soc., 31, 1668, 1935.
2-14	Berman, E.B., et al.	*Economic Effects of Metallic Corrosion in the United States*, U.S. Department of Commerce/ National Bureau of Standards NBS Special Publication 511-1, Washington, May 1978.

CHAPTER 3

AN OUTLINE OF CORROSION THEORY

3.1 General

Metals are seldom found in nature in their elemental state. They usually exist as compounds such as oxides, hydroxides, sulphides, silicates, carbonates and nitrates, which are fairly stable. Much energy is consumed in extracting the base metals from their compounds, in melting and mixing them to form alloys, and in forming these alloys into useful engineering structures. Most pure metals and alloys are not stable and will tend to revert back to their natural states by combining with elements in the atmosphere to form stable compounds. If this happens the engineering structure is weakened, or even destroyed, and the energy and money expended in producing the structure is lost.

The chemical reactions by which metals revert back to their natural state are known as corrosion reactions and the detailed path followed by these reactions depends on the metal or alloy and the conditions under which the reactions occur.

For simplicity it is convenient to consider two types of corrosion;

(i) *corrosion involving a liquid phase where an electrically conducting solution is present to assist in the transfer of metal ions* and electrons between the oxidizing or anodic site of the metal and the reducing or cathodic site. The corrosion reaction is therefore an electrochemical reaction, and the anodic and cathodic sites may be different areas of the same metal, or two completely different metals that are in electrical contact.

(ii) dry corrosion involves a metal/gas or metal/vapour reaction, where non-metals such as oxygen, halogens, hydrogen sulphide or sulphur vapour lead to the formation of a film or scale on the metal surface without the intervention of a liquid electrolyte. However, these reactions may also be considered in terms of electrochemical processes.

Corrosion reactions can be understood if the system is fully described in terms of the prevailing thermodynamics, electrochemistry, physical chemistry and metallurgical condition of the metals involved. Thermodynamics is based on knowledge of the equilibrium condition of a system and therefore can be used to indicate whether a chemical change is energetically feasible. Electrochemistry can be used to describe the transfer of electrons in the system and to predict the reaction products that will be produced. Metallurgy is able to describe the internal structure of the metals involved, in terms of their grain and grain boundary structures and the distribution of alloying elements and alloy phases that may affect local electrochemical conditions at an exposed surface. Finally, physical chemistry can provide information on the surface condition of the reactants and hence can describe the physical sites where electrochemical reactions may occur. In the following sections of this chapter the important aspects of metallic corrosion will be examined in terms of these four scientific disciplines.

3.2 Thermodynamics

Chemical reactions, such as those involved in corrosion, will only occur spontaneously if a driving force exists. The driving *force for a corrosion reaction is the change in free energy* ΔG *of the system, if this is negative it denotes a loss, or decrease in free* energy. The reactants, therefore, will tend to combine spontaneously since by doing so they change their total free energy from a relatively high value to a lower value. If the change in free energy were positive, the reaction would involve an increase in energy, and

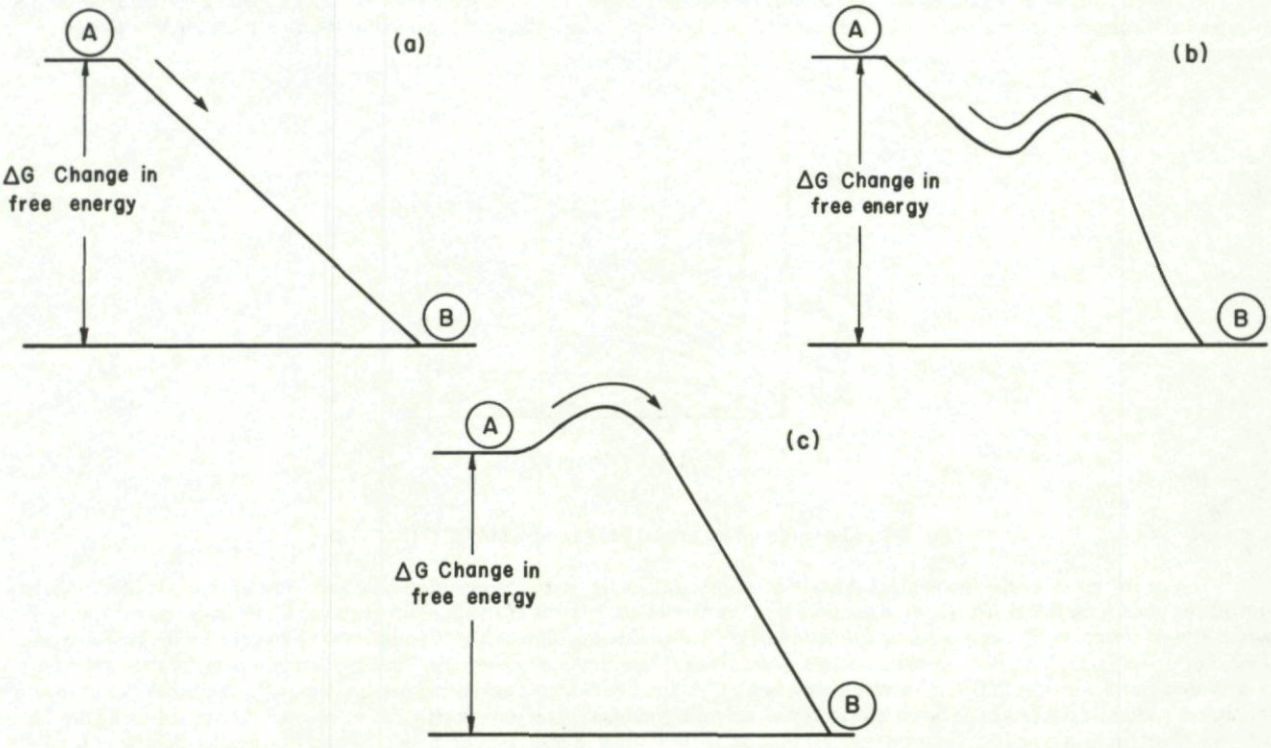

Fig. 3-1 The mechanical analogy of the free energy change of a corrosion reaction proceeding by different paths

additional energy would be required by the system from some external source to cause the reaction to occur. The change in free energy of a reaction therefore provides an indication of the direction that the reaction will tend to follow. However, it provides no information on the velocity of the reaction, since it is independent of the path by which the reaction occurs.

These points can be understood by considering the analogy of a ball rolling down a hill, Figure 3-1a. If the ball rolls from point A to point B it lowers its potential energy, and this represents a decrease in free energy ΔG. This is the spontaneous direction for this system, while the reverse reaction is not spontaneous since it would require the input of energy.

If the ball were required to negotiate any humps (Fig. 3-1b), such that it covered a longer path in rolling from A to B, it would obviously take a longer time to complete the journey. Thus while the free energy change ΔG is the same as before, the reaction rates are much slower. If a hill lay in the path of the ball, Figure 3-1c, between A and B, the ball would not roll to B unless it were first pushed to the top of the hill. The free energy change involved in rolling from A to B would be the same as before, but energy would have to be provided from an external source to allow the reaction to occur. Situations of this type can occur in corrosion, where the reaction will not occur unless external energy is provided to overcome some barrier. The external energy may be in the form of heat from the sun or from aircraft engine exhausts, or mechanical energy that may result in a rubbing action between components to break up protective oxide films.

The free energy change ΔG for an electrochemical reaction is given by the equation:

$$\Delta G = -nFE \tag{3.1}$$

where n is the number of electrons involved in the reaction, F is the Faraday constant, and E is the cell potential which is discussed later.

3.3 Dry Corrosion and Oxidation

When a metal combines with the atoms or molecules of a gas it loses electrons and an oxidation reaction is said to have occured. At the same time the electrons must be accepted by the non-metal involved, which is said to be reduced. Oxidation therefore involves a transfer of electrons, and may therefore be considered an electrochemical process. It need not involve oxygen itself. Any combination of metal and non-metal that can react to form a compound, and transfer electrons in the process are capable of producing oxidation reactions. The overall reaction can be described by two separate reactions occurring simultaneously:

$$\text{Metal } M \rightarrow M^{n+} + n \text{ electrons} \qquad \text{Oxidation} \tag{3.2}$$

$$\text{Oxygen } O_2 + n \text{ electrons} \rightarrow \frac{n}{2} O^{2-} \qquad \text{Reduction} \tag{3.3}$$

$$M + O_2 \rightarrow MO_{n/2} \qquad \text{Combination} \tag{3.4}$$

The oxidation of the metal, reduction of the non-metal, and their combination to form a compound occur at the same time and at the same place on the metal surface to form a film or scale.

3.4 Nature of Films and Scales

The films or scales produced by corrosion will affect the corrosion process, since they will tend to form a barrier between the metal and the corrosive environment. This is illustrated in Figure 3-2, which shows the oxidation reaction rates for several iron-aluminum alloys at 900°C.

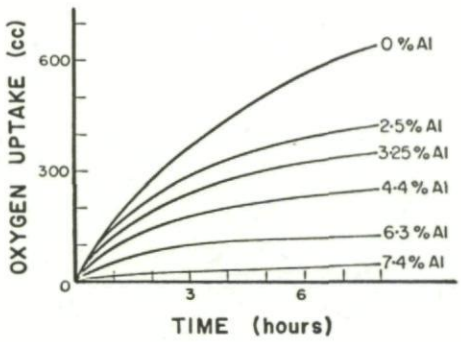

Fig. 3-2 The oxidation of several FE-Al alloys at 900°C (Ref. 3-1)

For any given aluminium content the rate of oxygen uptake, or corrosion rate, decreases with time as an oxide film forms to protect the underlying metal. The figure also shows that the aluminium content of the iron has a marked effect in decreasing the overall rate of corrosion. This is due to the formation of protective alumina films at high aluminium contents as opposed to iron oxide (FeO, Fe_2O_3 or Fe_3O_4), or mixed iron-aluminium oxide scales at low aluminium contents. Thus the reaction rates for the oxidation of iron-aluminium alloys at 900°C may vary depending on aluminium content, exhibiting parabolic growth rate behaviour at low aluminium contents to logarithmic behaviour at high aluminium contents. These growth rate laws are shown schematically in Figure 3-3a. Alloying clearly provides an important method for improving the corrosion resistance of metals, and may be applied in bulk or locally at the surface of the metal.

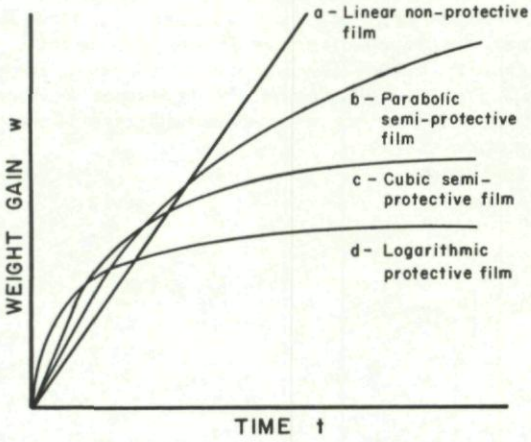

Fig. 3-3a Oxidation rate laws

(a) Linear oxidation $w = kt + k^1$
(b) Parabolic oxidation $w^2 = kt + k^1$
(c) Cubic oxidation $w^3 = kt + k^1$
(d) Logarithmic oxidation $w = k \log (1 + k^1 t)$

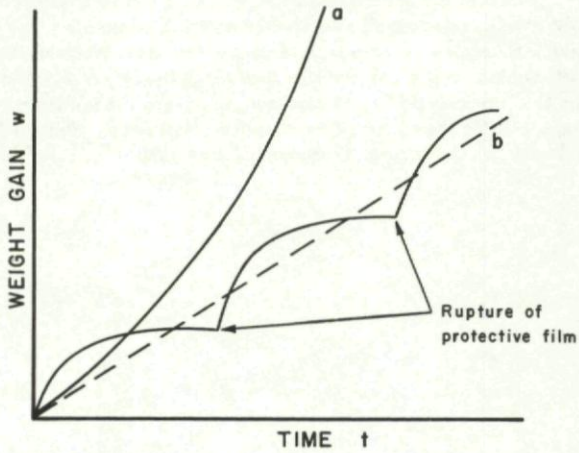

Fig. 3-3b Curve 'a' indicates an accelerating reaction rate, perhaps due to an exothermic reaction, curve b indicates a pseudolinear rate due to the periodic rupture of a protective film

Situations may arise where the oxides, or other corrosion products fail to protect the underlying metal and various results can occur.

(1) The oxides may react chemically or combine with water vapour to produce films that are not impervious to the passage of oxygen. The reaction will then continue at the initial rapid rate or at only a slightly reduced rate, as indicated by curves "a-b" in Figure 3-3a.

(2) If the volume of the oxide is less than the volume of metal from which it was produced the oxide may not give adequate protection from the very start (Ref. 3-2). An oxidation curve similar to 'b' in Figure 3-3a might be expected.

(3) If the volume of the oxide is much higher than the volume of the metal large stresses will be set up in the oxide, which will tend to crack and spall off. (Ref. 3-2). If the oxide film is inherently protective the rupture of the film may lead to an overall rate of reaction which appears to be linear, rather than logarithmic or parabolic. This is indicated by curve b, in Figure 3-3b. Cracking and spalling may also occur during temperature changes as a result of thermal expansion mismatch between the oxide and the metal.

(4) The oxide may volatize; for example molybdenum dioxide (MoO_2) volatilizes above 750°C. Or the reaction may be exothermic so that temperature increases and an accelerating growth-rate occurs (Ref. 3-3). This is indicated by curve 'a' in Figure 3-3b. Equivalent situations can occur during wet corrosion, for example when the corrosion products are soluable in the liquid environment.

(5) An otherwise protective film may be mechanically damaged due to impact from foreign objects (e.g. stones or sand) or due to rubbing of moving metal surfaces.

As a result of the above, oxidation rates or corrosion rates may not decrease in time in the expected logarithmic manner, but may show any one or any combination of the growth rate laws shown schematically in Figure 3-3. In all cases, if these reactions occur spontaneously the change in state of the system involves a decrease in free energy and the free energy change ΔG is negative.

3.5 Corrosion Involving a Liquid Phase

It was pointed out in Section 3.1 that corrosion is an electrochemical process involving the action of minute electrical cells on the surface of the metal. Corrosion involving liquids often provides conditions more typical of the conventional electrolytic cell than dry corrosion, because the reaction often occurs between discrete anodic sites where electrons are produced, cathodic sites where electrons are consumed, and an electrolyte such as water which allows the passage of charged particles. The reaction involves the corrosion and dissolution of the anodic area, while the cathodic area remains unharmed. These two areas may be minute local regions within the same piece of metal or may be areas of dissimilar metal or non-metal structure.

Before considering the conventional electrochemical cell it is worth considering the dissolution of a single piece of metal by an acid, which is probably the simplest form of electrochemical process. Most metals, such as aluminium, will dissolve in dilute acids. The process involving hydrochloric acid can be described by the reaction:

$$2Al + 6HCl \rightarrow 2AlCl_3 + 3H_2 \tag{3.5}$$

In this reaction aluminium metal is converted to aluminium ions, hydrogen ions are converted to molecular hydrogen gas, and the chloride ions remain unchanged. Therefore the reaction can be considered as two partial reactions, one involving the oxidation of aluminium and the other the reduction of hydrogen ions. Thus two reactions are involved, one of which is anodic and involves the oxidation or corrosion of aluminium, and the other which is cathodic and involves the reduction of hydrogen.

$$2Al \rightarrow 2Al^{3+} + 6e \qquad \text{Anodic Reaction} \tag{3.6}$$

$$6H^+ + 6e \rightarrow 3H_2 \qquad \text{Cathodic Reaction} \tag{3.7}$$

The electrochemical nature of corrosion can be illustrated further by referring to Figure 3-4, which shows a very simple electrolytic cell, consisting of two dissimilar metals, aluminium and copper, connected by a wire and partially immersed in water. The aluminium or anode will corrode, its atoms entering the electrolyte as positively charged particles or ions. This results in electrons being left behind on the anode which flow along the external conductor (wire) to the cathode. This flow of an electric current along the wire could be detected and the current measured if a milliameter were added to the circuit. Alternatively, the potential difference or voltage, causing the current flow could be measured by adding a millivoltmeter. However, the voltage measured in a case such as this would depend on the current, if any, being drawn from the cell. This point is explained later.

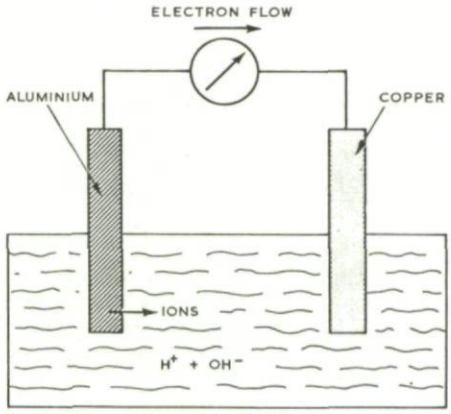

Fig. 3-4 Copper, aluminium and water electrolytic cell

This description of the corrosion process can be broken down into three distinct components or reactions.

(1) The electrolyte reaction involves, in this case, the partial dissociation of water;

$$H_2O \rightleftharpoons H^+ + OH^- \tag{3.8}$$

(2) At the anode electrons are generated according to the reaction;

$$Al \rightarrow Al^{3+} + 3e^- \tag{3.9}$$

(3) At the cathode electrons are consumed according to the reaction;

$$\tfrac{1}{2}O_2 + H_2O + 2e^- \rightarrow 2OH^- \tag{3.10}$$

The net result of these reactions is that the anode (aluminium) dissolves into the solution while the cathode reaction leaves the copper essentially unaffected.

It is apparent that four elements must be present at the same time for corrosion to occur. These include an anode, a cathode, a metallic path for the conduction of electrons, and an electrolyte — or continuous liquid or ionized gas path — capable of conducting an ion flow. If any one of these elements is removed the corrosion process stops, or at least is substantially reduced. This set of conditions required to cause corrosion has been described in one corrosion manual (Ref. 1-6) as the 'Vicious Circle', and is illustrated in Figure 3-5.

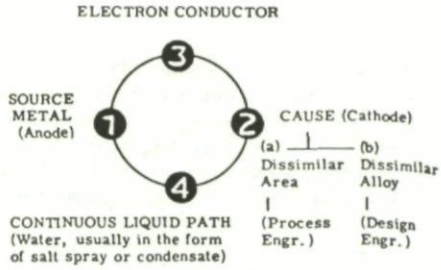

Fig. 3-5 The "Vicious Circle" of corrosion

The electrochemical cell shown in Figure 3-4 involved large, easily identifiable anode and cathode sites which were separate pieces of dissimilar metals. In other cases, the entire surface of a single piece of metal may consist of anodic and cathodic sites which may be continually changing (Ref. 3-3). This is shown schematically in Figure 3-6.

The anodic and/or cathodic sites may correspond to local regions within the microstructure of the material that differ from their surroundings in either a chemical manner or in the way their atoms are arranged. Examples include grain boundaries, which may be either enriched or depleted in alloying elements compared to the grain interiors and which have an irregular arrangement of atoms, and precipitates or inclusions of a second phase. Distorted and strained areas in metals resulting from processes such as shearing or abrading may act anodically with respect to adjacent unstrained areas, and therefore suffer electrochemical corrosion if the remaining conditions

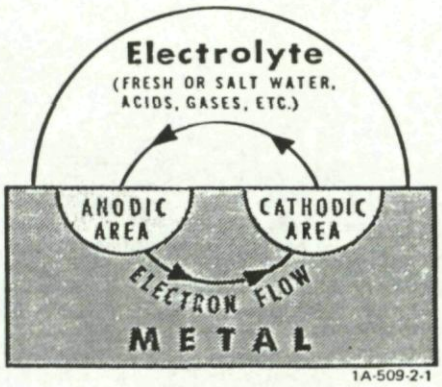

Fig. 3-6 Simplified corrosion cell (Ref. 1-6)

shown in Figure 3-5 are satisfied. Sheet metal forming processes such as stamping or deep drawing can also crack naturally protective oxide films on metals formed under harmless dry conditions. Such cracks may expose unprotected bare metal to the atmosphere, and again if the critical conditions of Figure 3-5 are satisfied, then accelerated local electrochemical attack of the exposed bare metal will occur.

Damage of any protective film or covering is potentially dangerous, whether it be a naturally formed oxide layer, an artificially formed oxide (anodized) layer, a layer of cadmium, tin or zinc plate, or a layer of paint or primer. This damage may lead to local corrosion, and possibly pitting of the exposed bare metal which is more severe than if no protective coating were there at all. Examples of this type can be found in Section II. However, to reinforce this discussion of corrosion as an electrochemical process we will consider the corrosion of iron at a break in an oxide scale, when the iron is immersed in sodium chloride solution.

The physical situation is shown schematically in Figure 3-7, and represents an electrochemical cell where an electric current will flow from the bare metal, which acts as the anode, to the oxide scale which acts as the cathode.

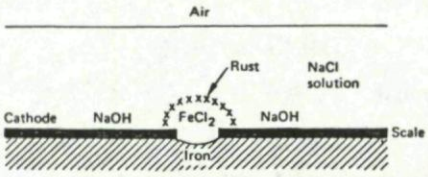

Fig. 3-7 Corrosion at breaks in oxide scale on iron immersed in sodium chloride solution (Ref. 3-4)

The current will continue to flow so long as the cathode has a ready supply of oxygen so that a cathodic reaction, such as that described earlier (3.10) can proceed unabated:

$$\tfrac{1}{2}O_2 + H_2O + 2e^- \rightarrow 2OH^- \tag{3.11}$$

At the anodic site the iron will pass into solution, usually as ferrous ions, according to the reaction:

$$Fe \rightarrow Fe^{2+} + 2e^- \tag{3.12}$$

Since sodium and chloride ions are present in solution, the product of the cathode reaction can be regarded as sodium hydroxide, while the anode product is ferrous chloride. Both products are soluable and therefore they will not precipitate to block the reaction. They may however revert to form ferrous hydroxide which will usually oxidize to ferric hydroxide ($Fe_2O_3 \cdot H_2O$) which is recognized as yellow rust.

3.6 Electrode Potentials

In the example of the two-metal (aluminium-copper) electrolytic cell used in Section 3.4, it is apparent that only one of the electrodes (aluminium) actually dissolved, while the other (copper) remained unaffected. Thus it is clear that the aluminium could more easily enter the electrolyte and build up a high electrical charge or potential then could the copper. Any metal immersed in a solution containing its ions will tend to dissolve, its ions going into solution, until an equilibrium is established between the metal and the solution.

The thermodynamic driving force for the aluminium-copper cell, or indeed any two metal cell, is the difference in galvanic potential of the two metals. The metal of lower potential in such a cell forms the anode and is oxidized or corroded, while the cathode receives electrons from the anode reaction which are consumed at the cathode surface by the cathode reaction.

As a further example we can consider the electrochemical cell containing copper and zinc plates partially immersed in dilute suphuric acid, which are electrically connected through an ammeter and voltmeter, Figure 3-8a. A potential difference exists between the plates, which causes a current to flow in the direction shown in Figure 3-8a. The zinc forms the anode to the cell and is oxidized to its positively charged ions which dissolve in the suphuric acid electrolyte. At the surface of the copper plate, which is the cathode of the cell, a balancing reaction occurs when the electrons formed in the anode reaction and conducted through the external circuit of the cell, meet with positively charged hydrogen ions to give hydrogen gas.

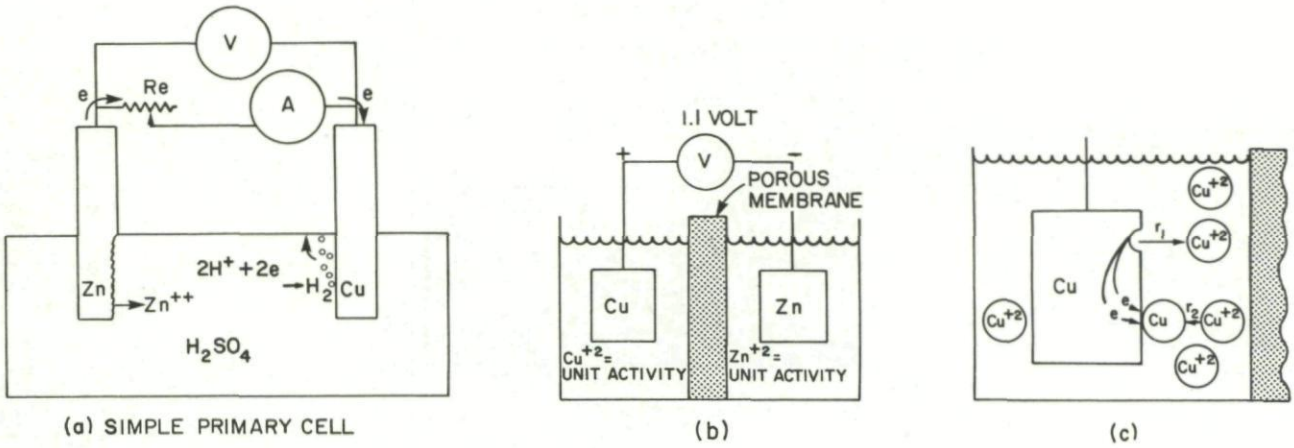

Fig. 3-8 Electrochemical reactions in the copper-zinc primary cell showing (a) the simple cell, (b) the electrochemical potential in the equilibrium cell, and (c) the reaction occurring in the copper half cell at equilibrium

Electrochemical corrosion processes with balanced anodic and cathodic reactions occur in acidic electrolytes or neutral electrolytes such as water, or water containing traces of dissolved inorganic matter. The anodic reaction will involve oxidation (corrosion) of the metal with the lower galvanic potential, but the cathodic reaction will usually be the reduction of oxygen dissolved in the electrolyte.

The electrode processes can be expressed chemically as:

(1) Anode reaction

$$M \rightarrow M^{2+} + 2e^- \tag{3.13}$$

where M is a divalent metal.

(2) Cathode reaction in an acidic electrolyte

$$2H^+ + 2e^- \rightarrow H_2 \tag{3.14}$$

(3) Cathode reaction in a neutral electrolyte

$$O_2 + 2H_2O + 4e^- \rightarrow 4OH^- \tag{3.15}$$

The net direction of reactions such as these depends on the electrode potentials generated by each electrode for the reactions that they sustain. To understand the source of the electrode potentials it is convenient to consider individual half cell reactions for electrodes that are at equilibrium with their ions in solution. The corresponding cell for the two metals used in the example of Figure 3-8a is shown in Figure 3-8b. In this example the two electrodes are separated by a porous membrane to retard mixing and a high impedance voltmeter is used to measure the voltage between them so that no current flows. The equilibrium reactions in each half-cell can be written

$$Cu \rightleftharpoons Cu^{2+} + 2e^- \tag{3.16}$$

$$Zn \rightleftharpoons Zn^{2+} + 2e^- \tag{3.17}$$

When the concentrations of metal ions are maintained at unit activity, that is each solution contains approximately 1 gram-atomic weight of metal ions per litre and both electrodes are at equilibrium each will generate a certain potential which is known as the reversible half-cell potential (E_r). The equilibrium reaction in the copper half-cell involves the simultaneous oxidation of copper atoms to cupric ions, and the reduction of cupric ions to metallic copper at other sites on the electrode as indicated in Figure 3-8c. An equivalent reaction occurs in the zinc half-cell.

The oxidation and reduction reactions required to maintain equilibrium at each electrode can be considered as separate anodic and cathodic reactions respectively, with a current I_a or I_c associated with each one. Thus for the copper electrode:

$$Cu \underset{I_c}{\overset{I_a}{\rightleftharpoons}} Cu^{2-} + 2e^- \tag{3.18}$$

Since this electrode is in equilibrium there is no net transfer of material between the electrode and solution and no net current flows. This implies that the anode and cathode currents are equal and opposite, and since normal sign convention establishes the anode current as positive and the cathode current negative $I_a = -I_c$. In contrast to this situation, if this single electrode were not in equilibrium a net transfer of material would occur, either to or from the electrode, a net transfer of charge would occur, and therefore a current would flow. For a net dissolution reaction the local anode current would exceed the cathode current $|I_a| > |I_c|$, while for a net deposition process the cathode current would exceed the anode current and $|I_c| > |I_a|$. According to Faraday's Law the mass (M) of material transferred in a time (t) is proportional to the net current (I) flowing, where $I = I_a + I_c$, and

$$M = e\,I\,t = \frac{A_m}{nF}\,I\,t \tag{3.19}$$

where e is the electrochemical equivalent Am is the atomic mass and n is the valency of the metal. The flow of current indicates a net chemical reaction, and the case where $|I_a| > |I_c|$ would represent a corrosion reaction. In practice the important consideration is

corrosion rate (M/t), which is proportional to the current flowing, and these quantities are often considered in terms of corrosion rate per unit area of specimen or anode, and current density (i) accordingly. Any changes made to a system to reduce current density would lead to a decrease in corrosion rate.

The reversible half-cell potentials of individual electrodes can be measured by means of a suitable reference electrode and high impedance voltmeters to prevent any current and hence maintain equilibrium. The most convenient reference electrode is based on the equilibrium hydrogen ionization reaction;

$$H_2 \rightleftharpoons 2H^+ + 2e^- \tag{3.20}$$

and the electrode potential for this reaction is arbitrarily set at zero. Since it is not possible to make an electrode out of gas, for experimental measurements an inert electrode such as platinum is used. The platinum is immersed in a solution containing hydrogen ions and hydrogen gas is bubbled through the solution at 1 atmosphere pressure to maintain unit activity. The platinum simply provides a stable surface and sites where hydrogen ions can be reduced to hydrogen gas, and other sites where hydrogen gas can be oxidized to hydrogen ions. Electrons flow between the different sites to maintain the balance. This hydrogen oxidation/reduction reaction is indicated by Equation (3.14).

When the reversible potentials of the equilibrium copper and zinc electrodes shown in Figure 3-8b are measured against the standard hydrogen electrode it is found that the potential of the copper is higher than that of the zinc. That is, the zinc is more electronegative and therefore it is anodic with respect to copper. Since the two cells are at equilibrium there is no net transfer of charge, $|I_c| = |I_a|$, and the potential between the electrodes or the reversible cell potential or electromotive force (e.m.f.) is a maximum and is equal to the difference between the reversible potentials of the two electrodes

$$E_{r,cell} = E_{r,c} - E_{r,a} \tag{3.21}$$

where $E_{r,cell}$ is the reversible e.m.f. of the cell and $E_{r,c}$ and $E_{r,a}$ are the reversible potentials of the cathode and anode respectively. However, once these electrodes are joined by an external conductor to allow a current to flow as shown in Figure 3-8a equilibrium conditions will not be maintained and the potentials of each electrode will deviate from their equilibrium values. This change in electrode potential is known as polarization and is explained later.

3.7 Electrochemical Series

Because of the large number of different half-cells which can exist, it would be a massive task to measure and catalogue the full cell potentials or e.m.f. for every combination of these. To simplify the problem the standard H_2/Pt half-cell, described in Section 3.6 has been established against which all others can be measured. The half-cell potentials for some common oxidation-reduction reactions at unit activity and 25°C are given in Table 3-1. The full listing of such potentials for all metals provides the electrochemical series. The cell potential for many electrochemical reactions can be determined by taking the algebraic difference between the half-cell reactions for the individual reactions. For the copper-zinc cell discussed earlier the difference in half-cell potentials for the two reactions (3.16) and (3.17) is 1.1v and zinc, which is more electronegative, would be the anode of the cell and current would flow as indicated in Figure 3-8a.

Table 3-1 Standard Oxidation-reduction (redox) Potentials (Ref. 3-5)

35°C, volts vs. normal hydrogen electrode*

$Au = Au^{+3} + 3e$	+1.498
$O_2 + 4H^+ + 4e = 2H_2O$	+1.229
$Pt = Pt^{+2} + 2e$	+1.2
$Pd = Pd^{++} + 2e$	+0.987
$Ag = Ag^+ + e$	+0.799
$2Hg = Hg_2^{++} + 2e$	+0.788
$Fe^{+3} + e = Fe^{+2}$	+0.771
$O_2 + 2H_2O + 4e = 4\ OH$	+0.401
$Cu = Cu^{+2} + 2e$	+0.337
$Sn^{+4} + 2e = Sn^{+2}$	+0.15
$2H^+ + 2e = H_2$	0.000
$Pb = Pb^{+2} + 2e$	-0.126
$Sn = Sn^{+2} + 2e$	-0.136
$Ni = Ni^{+2} + 2e$	-0.250
$Co = Co^{+2} + 2e$	-0.277
$Cd = Cd^{+2} + 2e$	-0.403
$Fe = Fe^{+2} + 2e$	-0.440
$Cr = Cr^{+3} + 3e$	-0.744
$Zn = Zn^{+2} + 2e$	-0.763
$Al = Al^{+3} + 3e$	-1.662
$Mg = Mg^{+2} + 2e$	-2.363
$Na = Na^+ + e$	-2.714
$K = K^+ + e$	-2.925

* Electrode potential values are given and are invariant (e.g., $Zn = Zn^{+2} + 2e$, and $Zn^{+2} + 2e = Zn$, are identical and represent zinc in equilibrium with its ions with a potential of -0.763 volts vs. normal hydrogen electrode).

SOURCE: A.J. de Bethune and N.A.S. Loud, "Standard Aqueous Electrode Potentials and Temperature Coefficients at 25°C," Clifford A. Hampel, Skokie, Ill., 1964.

Both temperature and concentration of the reactants (activity) affect the potential of any cell. Where the reactants are not at unit activity the cell potential (E) can be obtained from the equation:

$$E = E_o + 2.3 \frac{RT}{nF} \log \frac{a_{oxid}}{a_{red}} \tag{3.22}$$

where E_o is the standard half cell potential, R is the gas constant, T is the absolute temperature, a_{oxid} and a_{red} are the activities (concentrations) of oxidized and reduced species, and n and F are as defined previously.

For engineering purposes it may not be necessary to know half-cell reactions and cell potentials accurately, but a knowledge of the electrochemical potential of a metal or alloy, relative to another in a given solution may be sufficient to provide an indication of the corrosion susceptibility of the system. Tables such as that shown in Table 3-2 have been prepared for some of the common engineering alloys. A metal appearing high in the table would generate a high (negative) electrical potential with respect to a second metal standing lower in the table and would therefore behave anodically and would corrode when coupled to the second metal and immersed in sea water. It should be noted that the term 'High Potential End', in this table indicates a high negative potential.

Table 3-2 Grouping of Metals and Alloys (Ref. 3-7)

ANODIC	GALVANIC SERIES (SEA WATER)
	Magnesium
	Magnesium Alloys
	Beryllium
	Zinc
	Galvanized Steel
	Aluminum Alloys
	Chromium
	Gallium
	Cadmium
	Mild Steel
	Wrought Iron
	Indium
	Low-Alloy Steels
	Cast Iron
	Low-Alloy Cast Iron
	4.—6% Cr Steel
	Ni Cast Iron
	12—14% Chromium Steel and 25—30%
	Lead-Tin Solders
	16—18% Chromium Steel
	Austenitic Cr-Ni Stainless Steel
	Austenitic Cr-Ni-Mo Stainless
	Lead
	Tin
	Manganese Bronze
	Naval Brass
	Cobalt
	Nickel
	Inconel (13% Cr, 6.5% Fe, Bal. Ni)
	Yellow Brass
	Admiralty Brass
	Aluminum Bronze
	Red Brass
	Antimony
	Copper
	Silicon Bronze
	Nickel Silver
	70-30 Copper Nickel
	Titanium
	Monel
	Composition G Bronze (88% Cu, 2% Zn, 10% Sn)
	Composition M Bronze (88% Cu, 3% Zn, 6.5% Sn, 1.5% Pb)
	Silver Solder
	Nickel (Passive)
	70-30 Nickel Copper
	Stainless Steels (Passive)
	Silver
	Palladium
	Gold
	Rhodium
	Platinum
	Carbon
CATHODIC	

High Potential End ↑ ↓ Low Potential End

The greater the difference in electrochemical potentials between dissimilar metals in a couple the greater is the driving force for corrosion, and generally the more rapid will be the corrosive attack. However, in real situations the rate of corrosive attack is influenced by many other factors, some of which are discussed below, and therefore Tables 3-1 and 3-2 should only be used as guides to the probable direction of a corrosion reaction. Taking the opposite view, half-cell potentials or thermodynamics can indicate unambiguously when corrosion will not occur.

A further useful engineering guide of the corrosion susceptibility of bimetallic contacts has been given in Reference 3-8, and is reproduced in Table 3-3.

Table 3-3 Degree of Corrosion at Bimetallic Contacts (Ref. 3-8)

METAL CONSIDERED ↓ / CONTACT METAL →	1 Gold, platinum rhodium, silver	2 Monel Inconel, nickel/molybdenum alloys	3 Cupronickels, silver solder, aluminium bronzes, tin bronzes, gunmetals	4 Copper, brasses, nickel silvers	5 Nickel	6 Lead tin, and soft solders	7 Steel and cast iron	8 Cadium	9 Zinc	10 Magnesium and magnesium alloys (chromated)	11 Stainless steels: Austenitic 18/8 Cr/Ni	12 Stainless steels: 18/2 Cr/Ni	13 Stainless steels: 13% Cr	14 Chromium	15 Titanium	16 Aluminium and aluminium alloys
1 Gold, platinum, rhodium, silver	–	A	A	A	A	A	A	A	A	A	A	A	A	A	A	A
2 Monel, Inconel, nickel molybdenum	B	–	A	A	A	A	A	A	A	A	A	A	A	A	A	A
3 Cupronickels, silver solder, aluminium bronzes, tin bronzes, gunmetals	C[k]	BorC	–	A	A	A	A	A	A	A	BorC	B	A	BorC	BorC	A[e]
4 Copper, brasses, nickel silvers	C[k]	BorC	BorC[q]	–	BorC	BorC[p]	A	A	A	A	BorC	BorC	A	BorC	BorC	A[e]
5 Nickel	C	B	A	A	–	A	A	A	A	A	BorC	BorC	A	BorC	BorC	A
6 Lead, tin and soft solders	C	BorC[t]	BorC[q]	BorC[q]	B	–	AorC[r]	A	AorC[r]	A	BorC	BorC	BorC	BorC	BorC	A
7 Steel and cast iron [a, f, w]	C	C	C	C	C[k]	C[k]	–	A[m]	A[ml]	A	C	C	•C	C[k]	C	B[m]
8 Cadmium [u]	C	C	C	C	C	B	C	–	A	A	C	C	C	C	C	B
9 Zinc [u]	C	C	C	C	C	B	C	B	–	A	C	C	C	C	C	C[i]
10 Magnesium and magnesium alloys (chromated) [b, a]	D	D	D	D	D	C	D	BorC	BorC	–	C	C	C	C	C	BorC[e]
11 Stainless steels: Austenitic 18/8	A	D	A	A	A	A	A	A	A	A	–	A	A	A	A[v]	A
12 Stainless steels: 18/2 Cr/Ni	C	AorC[s]	AorC[s]	AorC[s]	A	A	A	A	A	A	A	–	A	A	•	A
13 Stainless steels: 13% Cr	C	C	C	C	BorC	A	A	A	A	A	C	C	–	C	C	A
14 Chromium	A	A	A	A	A	A	A	A	A	A	A	A	A	–	A	A
15 Titanium	A	A	A	A	A	A	A	A[x]	A	A	A	A	A	A	–	A
16 Aluminium and aluminium alloys [n, a, w]	D	C	D[e]	D[e]	C[k]	BorC	BorC	A	A	A[ch]	BorC	BorC	BorC	BorC[d]	C	–

Key A indicates the corrosion of the metal is not likely to be increased by the contact metal

B indicates the corrosion of the metal may be slightly increased by the contact metal

C indicates the corrosion of the metal may be markedly increased by the contact metal. (Accelerated corrosion, however, is likely to occur only when the metal is wetted with moisture containing an electrolyte such as salt, acid, combustion products, etc. Under less severe conditions the increase in corrosion may be slight.)

D indicates that when moisture is present this combination is inadvisable without adequate protective measures.

Superscript symbols refer to the Table notes printed below.

Notes to Table 3-3

(a) The exposure of iron, steel, magnesium alloys and unclad aluminium-copper alloys in an unprotected condition in corrosive environments should be avoided wherever possible even in the absence of bimetallic contact.

(b) The behaviour of magnesium alloys in bimetallic contacts is particularly influenced by the environment and depends especially on whether an electrolyte can collect and remain as a bridge across the contact. The behaviour indicated in Table 3-3 refers to fairly severe conditions. Under conditions of total immersion, magnesium alloys should be electrically insulated from other metals. In less severe conditions complete insulation is not necessary, but steel, brass and copper parts should be galvanized or cadmium plated and jointing compound used during assembly. Under conditions of good ventilation and drainage, even contacts classified as D have given satisfactory service.

(c) Where contact between magnesium alloys and aluminium alloys is necessary, adverse galvanic effects will be minimized by using aluminium alloys containing little or no copper (0-1% max).

(d) If aluminium and aluminium alloys are in contact with thin (decorative) chromium plate, the symbol is C, but with thick plating (as used for wear resistance) the symbol is B.

(e) When contacts between copper or copper-rich materials and aluminium alloys cannot be avoided, a much higher degree of protection against corrosion is obtained by first plating the copper-rich material with tin or nickel and then with cadmium, than by applying a coating of cadmium of similar thickness.

(f) The corrosion of mild steel may sometimes be increased by coupling with cast iron, especially when the exposed area of the mild steel is small compared with the cast iron.

(g) Instances may arise in which corrosion of copper or brasses may be accelerated by contact with bronzes or gunmetals. For example, the corrosion of copper, seawater-carrying pipelines may be accelerated by contact with gunmetal valves, etc.

(h) When magnesium corrodes in sea water or certain other electrolytes, alkali formed at the aluminium cathode may attack the aluminium.

(j) When it is not practicable to use other more suitable methods of protection (for example, spraying with aluminium), zinc may be useful for the protection of steel in contact with aluminium despite the accelerated attack upon the coating.

(k) Statement (j) should not necessarily discourage the use of the contact metal as a coating for the metal considered, provided that continuity is good. Under abrasive conditions, however, even a good coating may become discontinuous.

(l) In most waters at temperatures above 60° C, zinc may accelerate the corrosion of steel.

(m) In the circumstances indicated in the Table the contact metal may provide an excellent protective coating for the metal considered. The latter is usually electrochemically protected at gaps in the coating.

(n) When aluminium is alloyed with appreciable amounts of copper it becomes more noble and when alloyed with appreciable amounts of zinc it becomes less noble. These remarks apply to bimetallic contacts and not to inherent corrosion resistance. Such efforts are mainly of interest when the aluminium alloys are connected with each other.

(o) No data available.

(p) In some immersed conditions the corrosion of copper or brass may be seriously accelerated at pores or defects in tin coatings.

(q) In some immersed conditions there may be serious acceleration of the corrosion of soldered seams in copper or copper alloys.

(r) When exposed to the atmosphere in contact with steel or galvanized steel, lead can be rapidly corroded with formation of PbO at narrow crevices where the access of air is restricted.

(s) Serious acceleration of corrosion of 18/2 stainless steel in contact with copper or nickel alloys may occur at crevices where the oxygen is low.

(t) Normally the corrosion of lead/tin soldered seams is not significantly increased by their contact with the nickel-base alloys but under a few immersed conditions the seams may suffer enhanced corrosion.

(u) The corrosion product on zinc is, in certain circumstances, more voluminous and less adherent than that of cadmium. Where this is known to be so it should be considered in making a choice between these two metals.

(v) Joints of the metals shown are liable to enhanced corrosion in crevices where these are not filled with jointing compound.

(w) Corrosion products from iron or steel reaching aluminium, or corrosion products from aluminium reaching iron or steel, may sometimes cause serious local corrosion through oxygen screening or in other ways.

(x) Under some conditions cadmium can penetrate titanium alloy and embrittle it.

3.8 Polarization

When the electrodes in the copper-zinc cell of Figure 3-8a are connected through an external variable resistance (R_e) a driving force exists for an electrochemical reaction which is related to the reversible or equilibrium e.m.f. of the cell. This driving force is the free energy change ΔG, which is given by Equation (3.1) where E is the cell potential equal to $E_{r,cell}$ when the external resistance is high. In this case no current flows between the electrodes and no corrosion occurs. However, in practice if the external resistance is not high, a current will be drawn from the electrochemical cell, corrosion will occur and the cell potential will deviate from its initial value. This deviation in cell potential due to the current flow is known as polarization and is of practical importance since it influences the current flowing and therefore the corrosion rate. In the example of Figure 3-8a, a current would flow if the value of the external resistance R_e were lowered from its initial high value and corrosion would occur. The net reaction would be given by:

$$Zn \rightarrow Zn^{2+} + 2e^- \tag{3.23}$$

and the rate of this reaction would be determined by the current flowing. The electrodes would become mutually polarized and their potentials would be mutually displaced from their equilibrium values, as indicated by Figure 3-9. The polarized potential of the anode (Zn^{2+}/Zn) would become more positive, while that of the cathode (H^+/H) would become more negative. The displacement of the potential of an electrode from its equilibrium value is the overpotential z, and is given by

$$z = E_p - E_r \tag{3.24}$$

where E_p is the polarized potential and E_r is the equilibrium (reversible) potential.

The cathode overpotential z_c is always negative, while the anode overpotential z_a is always positive, and these overpotentials are given by (3.24) as

$$z_a = E_{p,a} - E_{r,a} \tag{3.24a}$$

$$z_c = E_{p,c} - E_{r,c} \tag{3.24b}$$

The polarization or overvoltage in a cell is simply the sum of the magnitudes of the overvoltages at each electrode $z_a + z_c$, where the negative sign of the cathode overvoltage is omitted.

As the current is increased by decreasing the value of the external resistance R_e, the magnitudes of z_a and z_c increase thus decreasing the magnitude of the polarized e.m.f. of the cell $E_{p,cell}$. For any given current I, the polarized potential of a cell $E_{p,cell}$ is given by

$$E_{p,cell} = E_{r,cell} - (z_a + z_c + I\,R_{soln}) \tag{3.25}$$

where z_a and z_c are the magnitudes of the overpotentials and R_{soln} is the resistance of the solution. Since the polarized cell potential $E_{p,cell} = I\,R_e$, then

$$I = \frac{E_{r,cell} - (z_a + z_c + I\,R_{soln})}{R_e} \tag{3.26}$$

which shows that for any given value of R_e the current flowing and therefore the rate of the corrosion reaction increases as:

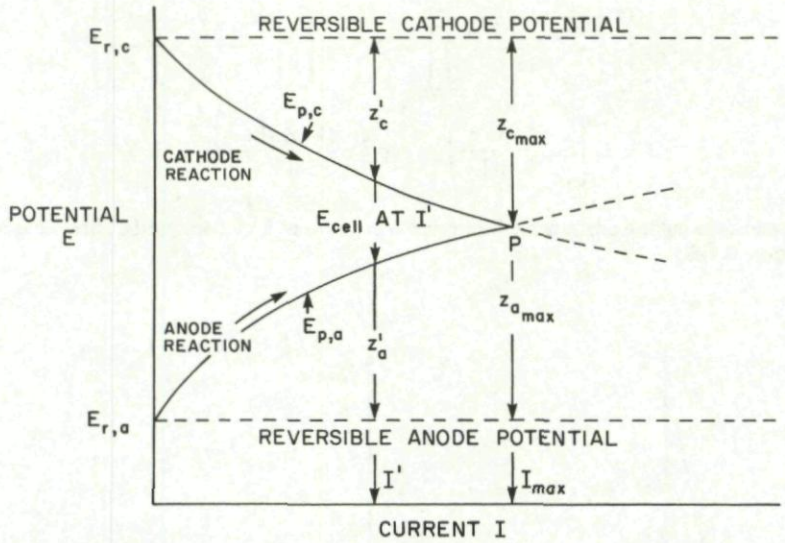

Fig. 3-9 Current-potential diagram for a typical corrosion reaction showing the relationship between reversible electrode potential (E_r), polarized potential (E_p) and overvoltage for the cathodic and anodic half reactions

(a) the magnitude of the reversible e.m.f. of the cell increases

(b) the magnitudes of the anode and cathode overpotentials decrease

(c) the electrolytic resistivity of the solution decreases.

However low the resistance of the total circuit the current flowing could never exceed the value represented by the value of the abscissa at the intersection point, P. In practice the maximum current I_{max} is always slightly less than indicated by P because of the finite resistance of the solution. However at currents close to I_{max} the acting e.m.f. would become vanishingly small. If the current flowing is I amperes, the corrosion rate will be I/F gram-equivalent per second.

3.9 Polarization at Single Electrodes

The reaction at any single electrode can be considered in terms of counteracting anodic and cathodic components, as indicated by the forward and reverse reactions and the currents I_a and I_c in Equation (3.18) for the copper dissolution reaction. Considering the cathodic reaction, copper ions which are the oxidized species must migrate through the electrolyte to the surface of the electrode where they must take up the required number of electrons, and then locate themselves as atoms in the metal lattice. If the cathode product was a gas, then in the final stage the gas molecules would have to move away from the surface to make room for other ions to make contact and participate in charge transfer. Each one of these stages in the overall process involves an activation energy and this energy must be supplied to allow each stage to proceed. Whichever reaction occurs slowest will determine the overall rate. Different types of polarization may be observed depending on which step in the overall reaction is rate controlling. If the process of charge transfer is rate controlling the polarization occurring is known as activation or charge transfer polarization. If the transfer of ions through an electrolyte is rate controlling then diffusion polarization is said to occur. This is also known as transport polarization or concentration polarization.

Activation polarization

In Equation (3.18) the currents I_a and I_c and therefore the current densities i_a and i_c are equal and opposite if the electrode is in an equilibrium condition. The current density in this case is known as the exchange current density and is identified as i_o. These electrode reactions are governed by Arrehenius equations of the type $K = A\,e^{\frac{-\Delta G}{RT}}$ where K is the rate constant, A is a pre-exponential factor and ΔG is the activation energy representing the energy barrier between the transition states. The forward (anode) and reverse (cathode) reactions are influenced by their respective activation energies ΔG_a and ΔG_c and since the electrode is at equilibrium the exchange current density $i_o = i_a = i_c$, or

$$i_o = A_a \exp\left\{\frac{-\Delta G_a}{RT}\right\} = A_c \exp\left\{\frac{-\Delta G_c}{RT}\right\} \tag{3.27}$$

where i_o is in amps/cm^2, and A_a and A_c are dimensionless constants. ΔG_a and ΔG_c are in joules/mole and these are approximately equal.

If a potential is applied to cause an imbalance in the forward and reverse reactions so that metal dissolution occurs, this potential is the anodic overpotential z_a. This imbalance arises from the effect of the applied potential on the free energy changes associated with the forward and reverse reactions. For the forward reaction the free energy change ΔG is decreased by an amount $\alpha n z_a F$, while ΔG for the reverse reaction is increased by an amount $(1-\alpha) n z_a F$. These free energy changes are derived from Equation (3.1), and α is the charge transfer coefficient with values in the range 0 to 1.

The current flowing as a result of the imbalance is the difference between the rates of the forward and reverse reactions. The reaction can be made to flow in either the forward or reverse directions depending on polarity of the overpotential, and the current flowing (i) is given by,

$$i = A_a \exp\left[-\left\{\frac{\Delta G_a - \alpha nFz}{RT}\right\}\right] - A_c \exp\left[-\left\{\frac{\Delta G_c + (1-\alpha)nFz}{RT}\right\}\right]$$

and

$$i = i_o\left[\exp\left\{\frac{\alpha nFz}{RT}\right\} - \exp\left\{-\frac{(1-\alpha)nFz}{RT}\right\}\right] \tag{3.28}$$

The polarization curves showing the relationship between the net current i, the two partial currents i_a and i_c, and applied overpotential are shown in Figure 3.10a.

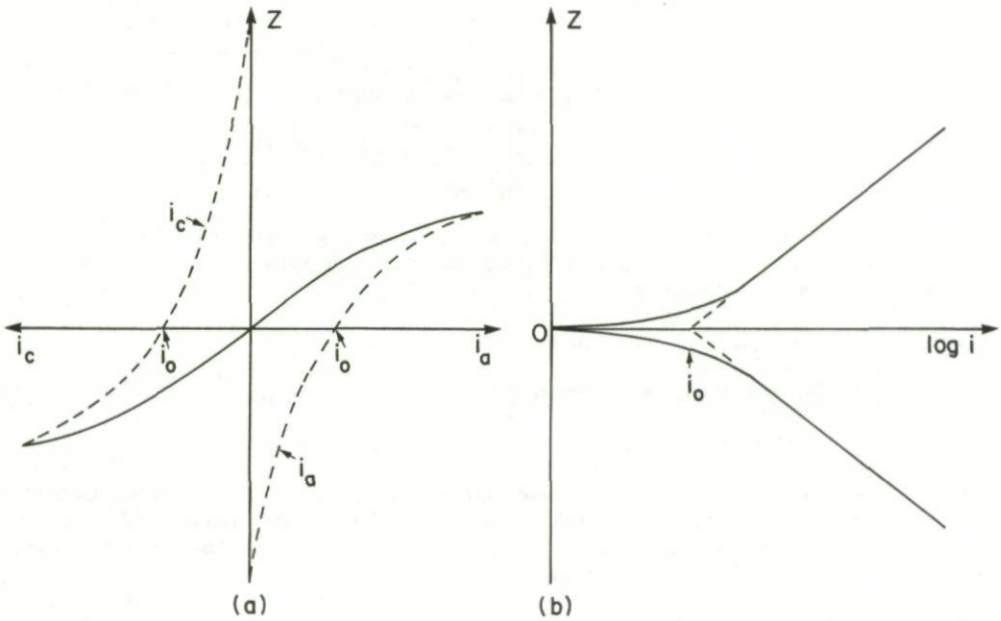

Fig. 3-10 Polarization diagrams for a single electrode showing activation polarization
(a) Overpotential versus current
(b) Overpotential versus log. current

For large values of overpotential ($|z| > 0.1$v) one of the two terms in Equation (3.28) may be neglected and the equation may be written

$$z_a = \frac{2.3\,RT}{\alpha nF}\left(\log i_a - \log i_o\right) \quad \text{for anodic overpotential}$$

or

$$z_c = \frac{-2.3\,RT}{(1-\alpha)nF}\left(\log i_c - \log i_o\right) \quad \text{for cathodic overpotential}$$

or in the general case

$$z = a + b \log i \tag{3.29}$$

where a and b are the Tafel constants.

Equation (3.29) indicates that a plot of overpotential versus log i would yield a straight line at high values of overpotential and the extrapolation of this straight line to zero overpotential would indicate the exchange current density i_o, as indicated in Figure 3.10b. This diagram is known as a Tafel diagram. The exchange current density is an important characteristic of an electrode reaction and provides an indication of the response of the reaction to any overpotential. For reactions with a large exchange current density the overpotential required to reach a certain external current is smaller than for reactions with a small exchange current density, and therefore resistance to polarization is small. See Reference 3-6 for a further discussion of these points.

Diffusion polarization

The above discussion dealt with electrode processes controlled by the rate of charge transfer occurring at the electrode, but if the rate of charge transfer is high or a high overpotential is applied the electrode process may be controlled by the rate of arrival of ions at the electrode surface or the removal of molecules. These reactions are effected by mass transfer through the solution, which is controlled primarily by diffusion behaviour with moderating effects due to migration and convection.

For a diffusion controlled electrode reaction the current density i is given by Reference 3-6 as,

$$i = -nFD\frac{C_o - C}{\delta} \tag{3.30}$$

where D is the diffusion coefficient, C_o is the concentration of the bulk solution, C is the concentration at the electrode surface and δ is the width of the boundary layer. A limiting current may exist corresponding to the greatest concentration gradient, where the concentration at the electrode surface is negligible compared to the bulk concentration. In this case Equation (3.30) becomes

$$i_L = -nFD\frac{C_o}{\delta} \tag{3.31}$$

The limiting current therefore increases as the concentration of the solution increases, and the relationship between diffusion overpotential and current is given by the equation

$$z = \frac{RT}{nF}\log\left(1 - \frac{i}{i_L}\right) \tag{3.32}$$

This shows that the smaller i_L and the lower the concentration of the solution the greater is the overpotential due to diffusion. Any factor which causes i_L to increase will result in an increase in the corrosion rate.

The polarization curve for a cathodic reaction showing diffusion polarization is indicated by Figure 3-11a, where the variation of overpotential with current is given by Equation (3.32). When both diffusion and activated charge transfer are rate controlling the curve is modified to that shown in Figure 3-11b, where a linear region of slope 'b' appears corresponding to the Tafel region.

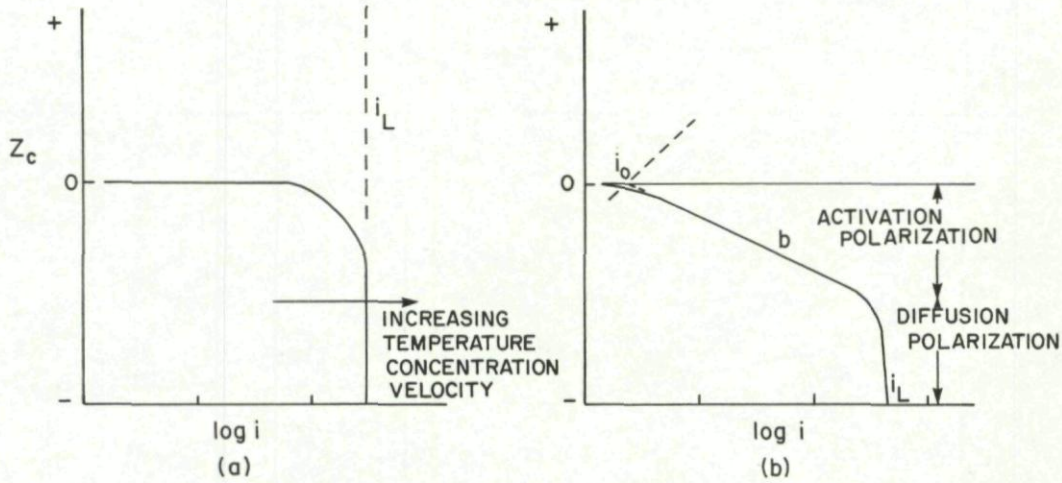

Fig. 3-11 Plots of overpotential versus current when the reaction rates are controlled (a) by diffusion (b) a combination of diffusion and charge transfer or activation

3.10 Graphical Representation of Corrosion Rates

Diagrams of the type shown in Figure 3-9 provide a simple means of visualizing corrosion reactions and of estimating the effects of changes in polarization behaviour of the electrode(s) on corrosion rates. These diagrams are known as Evans diagrams after their originator (Refs. 3-9, 3-10), and can be applied to single metals dissolving in corrosive solutions or to dissimilar metal couples undergoing galvanic corrosion. In either case the diagrams indicate the change in electrode potentials with current for each anodic and cathodic reaction. These changes were originally presented by straight lines, and the points of intersection of the lines indicate the corrosion potential E_{corr} and corrosion current I_{corr}. A typical diagram where the corrosion rate is equally affected by changes in anodic and cathodic polarization is shown in Figure 3-12a. However, this diagram assumes that the resistance of the electrolyte (or corrodent) is small so that the anodic and cathodic lines intersect. For neutral salt solutions of low concentration the resistance may be high so that a significant IR drop occurs in the solution and the lines may not intersect. This is shown in Figure 3-12b, where the corrosion rate indicated by I_{corr} is said to be under resistance control. A similar result may occur if a non-conducting oxide film forms on the metal surface.

For reactions where the rate of the cathodic polarization reaction is much greater than the rate of the anodic polarization reaction, indicated by the slope of the appropriate E_p – I line, the reaction is said to be under cathodic control and any change in the rate of this polarization reaction will exert a greater influence on the rate of corrosion than a similar change in the anodic process. If the slope of the anodic curve is much greater than the slope of the cathodic curve, the opposite occurs and the reaction is said to be under anodic control. These cases are illustrated in Figures 3-12c and 3-12d respectively. In the case of cathodic control, the anodic reaction is important since a change in anode metal which would lead to a significantly higher or lower reversible cell potential, indicated by E_a' in Figure 3-12c, would cause a corresponding change in corrosion rate indicated by I_{corr}'.

It was stated earlier, Section 3.7, that the greater the difference in electrode potentials between dissimilar metals the greater the driving force for corrosion, and generally the more rapid will be the rate of corrosive attack. In practice however the corrosion current, and therefore the rate of corrosion, is influenced by many variables including potential difference and polarization behaviour. Figure 3-12e illustrates a situation where the corrosion current I_{corr}' between electrodes with potentials E_a' and E_c', is greater than that

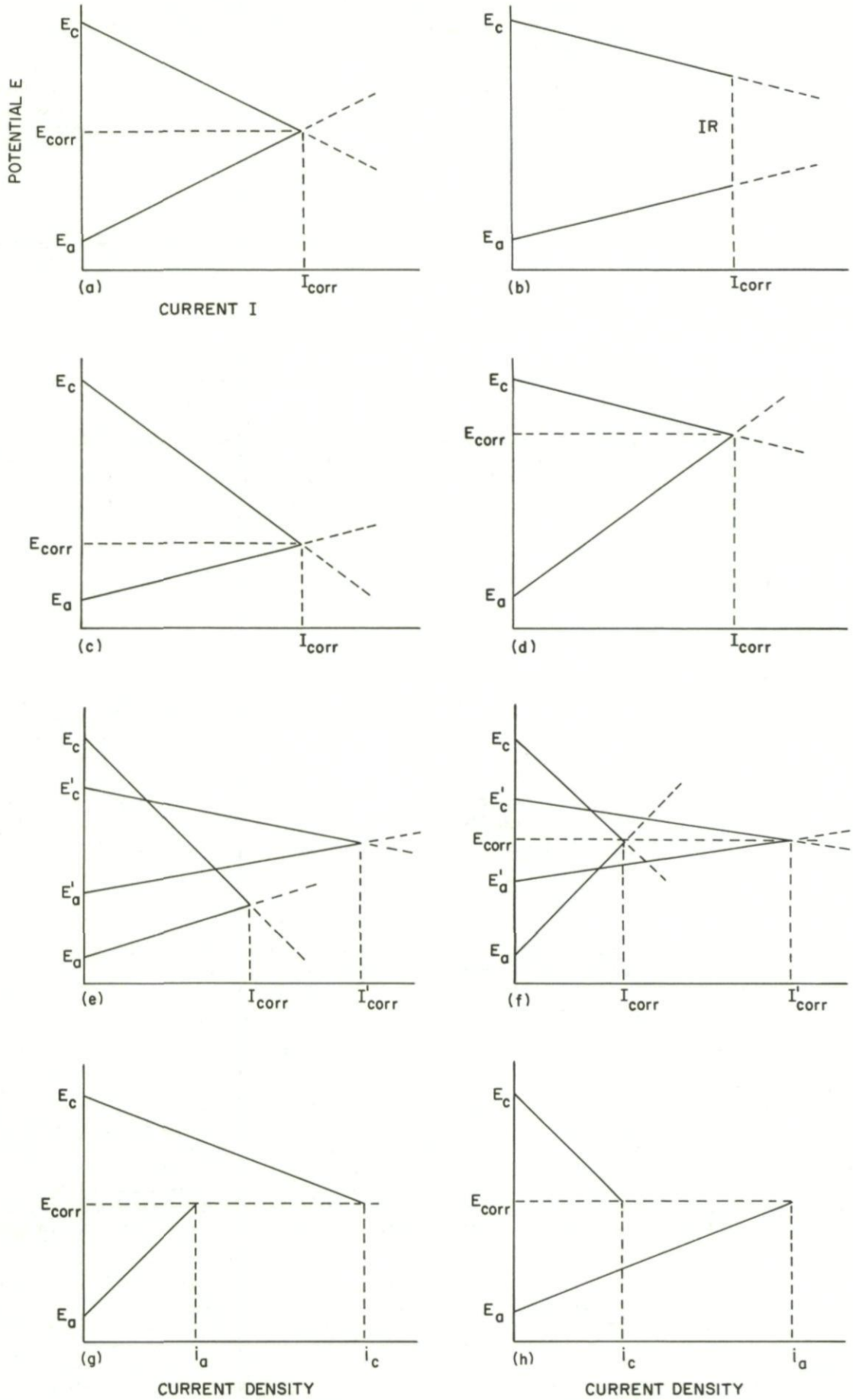

Fig. 3-12 Plots of E_p - I (or i) for typical corrosion reactions or Evans diagrams showing;

(a) Mixed control (b) Resistance control (c) Cathodic control (d) Anodic control (e) Situation where corrosion current is greater at low thermodynamic driving force than for high driving force, determined by rates of polarization (f) Situations involving different corrosion currents for the same corrosion potential E_{corr} (g) Dissimilar metal corrosion when the anode is larger than the cathode (h) Dissimilar metal corrosion when the cathode is larger than the anode (Ref. 3-11)

occurring between two electrodes E_a and E_c, even though the potential difference is greater in the latter case. This arises since the rates of polarization of the electrodes in the former case are much less than in the latter. Examination of Figures 3-12a to d will indicate that E_{corr} provides no indication of corrosion rate, and this is further illustrated in Figure 3-12f. In this illustration the corrosion potential E_{corr} is the same for two cases where the corrosion currents, I_{corr} and I'_{corr}, and potential differences $E_c - E_a$ and $E'_c - E'_a$ are widely different.

It is evident from Section 3.9 that the polarization of electrode reactions depends on current density i, rather than current I. In the case of single electrodes $I_c = I_a$, and since the same surface area is available for the anode and cathode reactions $i_c = i_a$. To understand corrosion reactions in dissimilar metal couples where the surface areas available to support the anode and cathode reactions are different it is preferable to plot E_p versus i for such reaction. Typical cases are illustrated in Figure 3-12g and 3-12h. Figure 3-12g illustrates the case where the surface area of the anode is much greater than the surface area of the cathode, and therefore for the overpotentials indicated the anode current density is much less than the cathode current density. Figure 3-12h illustrates the reverse situation where the cathode surface area is much greater than the anode surface area, and therefore for the overpotentials indicated, the anode current density is much greater than the cathode current density, this case of large cathode and small anode is the most serious case and should be avoided.

3.11 Pourbaix Diagrams

Corrosion reactions are not only affected by cell potentials but also by the acidity or hydrogen ion concentration (pH) of the electrolyte. In practice both can be varied independently, cell potentials can be varied by coupling dissimilar metals with different half-cell potentials or by applying an external potential, and hydrogen ion concentration can be adjusted by the addition of acids or bases.

The influence of these variables on chemical and electrochemical equilibrium can be represented graphically using a series of diagrams due to M. Pourbaix, which indicate the equilibrium between a metal and a liquid under various conditions of potential and pH. Each diagram indicates conditions under which a metal would either corrode, be immune or develop a protective solid film to become passive. The diagrams are constructed from calculations based on thermodynamics and the Nerst Equation (3.22), and on solubility data for the chemical compounds tending to form.

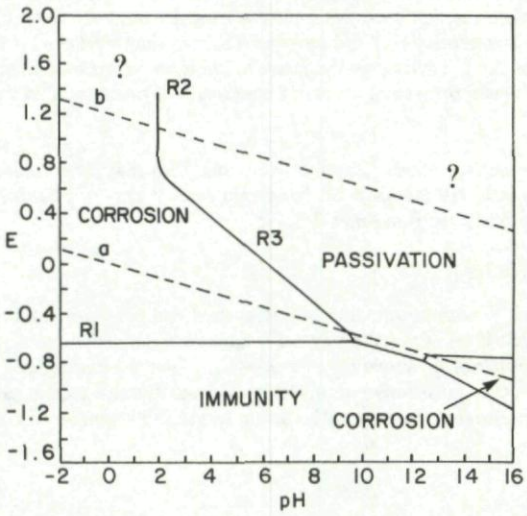

Fig. 3-13a Simplified Pourbaix diagram for Iron

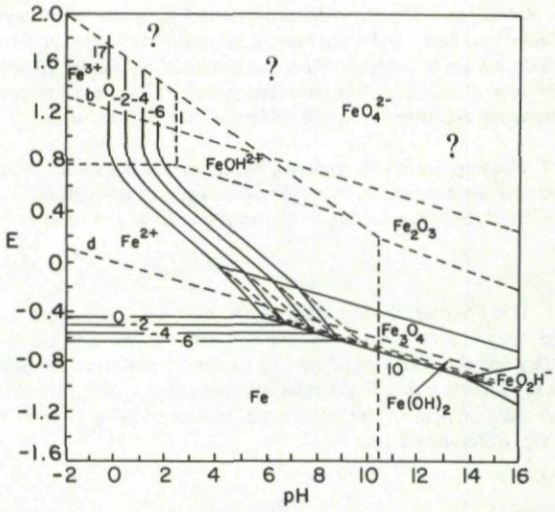

Fig. 3-13b Pourbaix diagram for iron at 25°C (Ref. 3-4)

A typical diagram is shown in Figure 3-13a, and is composed of lines representing different types of equilibria. Horizontal lines represent equilibrium reactions that involve electrons, but which are independent of pH. For example the horizontal R1 represents the equilibrium:

$$Fe \rightleftharpoons Fe^{2+} + 2e^- \tag{3.33}$$

The potential for this, and any other dissolution reaction is dependent on the activity of the ferrous ions in solution in accordance with Equation (3.22). According to this equation the potential of a univalent metal will change by 59.9 mV for every tenfold change in activity of the metal ions in solution at 25°C. Thus a complete Pourbaix diagram would show sets of parallel reaction lines indicating conditions for solutions of different activity, instead of the single lines shown in Figure 3-13a. A more complete version of this diagram is shown in Figure 3-13b which contains sets of parallel lines 0, −2, −4 and −6, corresponding to ferrous ion activities of 10^0, 10^{-2}, 10^{-4} and 10^{-6} times normal, and spaced at intervals of 2 × 59.9 mV as determined by Equation (3.22). The important point to note is that iron will not dissolve below the horizontal line R1 once the liquid in which it is immersed contains Fe^{2+} ions at the concentration appropriate to the line selected, and therefore it will be immune. Conversely if the potential were to be raised above the line R1, the metal would corrode.

The vertical lines in Figure 3-13a and 3-13b represent reactions involving hydrogen ions (H^+) or hydroxyl ions (OH^-), but not electrons. Thus they are affected by pH but not cell potential. The line marked R2 represents the hydrolysis:

$$Fe^{3+} + H_2O \rightleftharpoons Fe(OH)^{2+} + H^+ \tag{3.34}$$

The sloping lines in Figure 3-13a indicate reactions involving both hydrogen ions (H^+) and electrons, and therefore they are affected by both pH and potential. The line marked R3, for example, indicates the reduction and dissolution of solid ferric oxide to ferrous ions in the liquid;

$$2Fe^{2+} + 3H_2O \rightleftharpoons Fe_2O_3 + 6H^+ + 2e^- \tag{3.35}$$

Considering, for example, the corrosion of iron in a mildly acid solution (e.g. pH = 6) at an applied potential of -0.4 volt, the corrosion could be arrested by raising the potential above line R3, so that a solid oxide film would form to obstruct the passage of further iron into the solution. Under these conditions the iron would become passive. If, on the other hand, a strong acid were to be added to the solution to increase pH and move the equilibrium to the left of the sloping line R3, the corrosion reaction would continue with the dissolution of the ferric oxide film.

The region between the lines marked 'a' and 'b' on Figure 3-13a indicate conditions under which water is stable. Above the oxygen line 'b' oxygen is evolved, while below the hydrogen line 'a' hydrogen is evolved. The oxygen and hydrogen evolution reactions involve the release or capture of electrons respectively, and therefore potential must move in opposite direction to support each reaction:

$$2H^+ + 2e \rightarrow H_2 \ (\uparrow \text{gas}) \tag{3.36}$$

$$4OH^- \rightarrow O_2 \ (\uparrow \text{gas}) + 2H_2O + 2e \tag{3.37}$$

3.12 Passivity

Figure 3-13a indicates that the anodic reaction occurring at a metal surface may involve the dissolution of the metal by forming ions which are soluable in the corrosive solution, or the formation of a insoluable solid compound. When the solid compound forms as tightly adherent and impermeable film on the metal surface it tends to impede the corrosion reaction and the metal is said to be passive. The conditions of potential and pH which allow passivation to occur are indicated by the appropriate Pourbaix diagram. Under conditions where passivation may occur, the anodic polarization curve of a metal will be markedly different to that observed in a freely corroding situation.

If a metal is cleaned by pickling in a strong acid, and then immersed in an electrolyte it will establish a potential in the active region E_A, as indicated in Figure 3-14. If the electrolyte contains metal ions at unit activity the potential developed will be the reversible potential E_r. If an external potential is applied to raise the electrode potential the corrosion current will increase. However, in metals capable of passive behaviour a maximum current will be reached at some potential E_s, depending on the metal and the electrolyte. The potential E_s is known as the passivation potential, and above E_s the corrosion current suddenly begins to decrease. According to Hoar, Reference 3-12, this is caused by the formation of an oxide monolayer which becomes a compact barrier between the metal and the solution. As a result, the corrosion current fails abruptly to a very low density (i_o) and remains stable at that level even if the potential continues to increase. At some potential E_T at the positive end of the passive range the passive film loses its protective properties and even with no further potential increase the corrosion current increases by several orders of magnitude. The material is now in the transpassive condition where it undergoes rapid dissolution.

The appearance of transpassive behaviour is an indication of a secondary anodic reaction occurring. This may occur when the passivating oxide is anodized to a soluable substance by high positive potentials, Reference 3-12. In certain cases it may not be due to the metal itself, but may be due to the appearance of the oxygen evolution reaction, Reference 3-6, e.g.

$$H_2O \rightarrow O_2 + 4H^+ + 4e \ (\text{at } 1.23\text{v}) \tag{3.38}$$

It is because of their tendency to become passive that metals such as aluminium, zinc, stainless steel and titanium exhibit low corrosion rates in many corrosive environments. However it is important that if an external potential is applied to any such metal, for example by coupling with a conducting dissimilar material, the potential must not lie above E_T or below E_s. When the dissimilar material is a highly cathodic material, such as carbon, high potentials above the transpassive potential may arise. For this reason careful attention must be paid to the selection of metals to be used in airframe structures in contact with carbon or graphite reinforced composites, e.g. Reference 3-13.

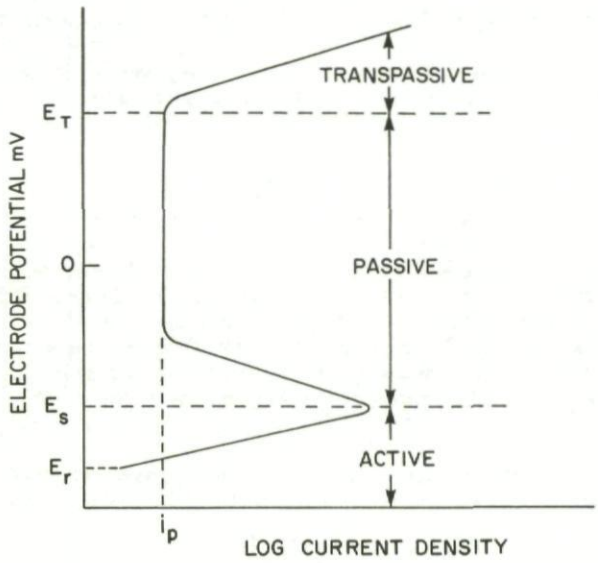

Fig. 3-14 Schematic anodic polarization curve for a metal which can be passivated

To establish the corrosion current flowing, and therefore the corrosion rate for a metal which exhibits active-passive behaviour it is necessary to consider the anodic polarization curve together with the cathodic polarization. Several types of behaviour may be observed, and three of the more important have been described by Reference 3-6, and these are illustrated in Figure 3-15.

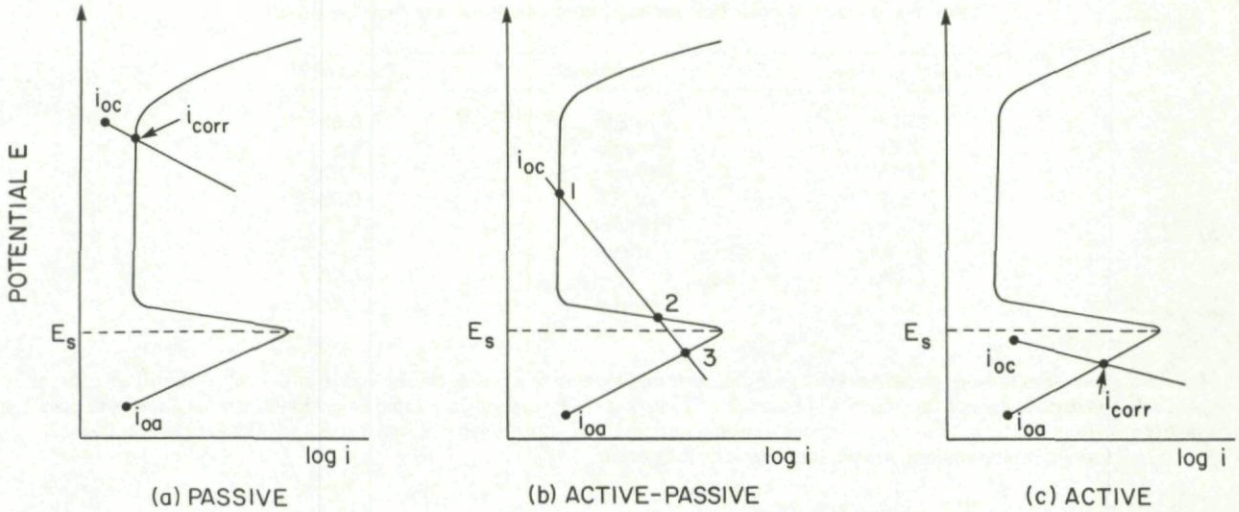

Fig. 3-15 Polarization diagrams for metals which can be passivated, Ref. 3-6

In Figure 3-15a, where the cathode reaction has a high equilibrium potential, the anodic and cathodic polarization curves cross only in the passive region and the corrosion current (i_{corr}) is equal to the anode passivation current (i_p), and spontaneous and stable passivity is obtained. If the cathode equilibrium potential is much lower several situations can arise as illustrated in Figure 3-15b and 3-15c. In Figure 3-15b, the curves cross at three points and the processes occurring depend on the physical condition of the anode at any time. If the anode is initially passive the reaction will be represented by point 1, where the corrosion current is low. However, if the passive film becomes damaged to expose an active spot, the active spot cannot be repassivated and the reaction occurs at a corrosion rate indicated by point 3. This condition is known as an active-passive state, and it involves the combination of a small anode and a large anode. Since the cathode reaction is unable to lift the active metal over its critical passivation current density this situation usually leads to serious localized corrosion of the type observed, for example in pitting. Point 2 in Figure 3-15b is of no practical interest since it is electrically unstable and the system would move spontaneously to points 1 or 3.

The final diagram, Figure 3-15c, shows the case where the cathode equilibrium potential is below the passivation potential (E_s) for the anode, and passivation is no longer possible. The corrosion rate is given by the point of intersection of the two curves, and this represents the case of corrosion of an active metal.

3.13 Special Cases of Practical Interest

Area effects

As indicated in Section 3-11 above, particularly serious localized corrosion can occur where the active site or anode is small with respect to the cathode area. In this situation the anodic current density (i_a) will be high and the corrosion rate correspondingly high. The lower is the ratio of the cathode area to the anode area, the lower is the rate of corrosion. Conversely, where there is a large cathode and a small anode the rate of corrosion tends to be severe.

An important practical application of these rules occurs in fastener selection where invariably the fastener surface area will be small with respect to the surrounding area of structure. Generally therefore, it is a sensible precaution to select a fastener material which will respond as a cathode to the adjacent structure, rather than the reverse situation. In this case any corrosion occurring as a result of electrical contact between the fastener and structure would be minimized. However, in the ideal case the galvanic potential between the fastener and the structure would be eliminated completely, or if dissimilar metals were unavoidable, the two would be electrically isolated.

Oxygen concentration corrosion

Corrosion cells can be set up by local differences in composition of an electrolyte. This frequently occurs where one part of the electrolyte is exposed to the atmosphere and therefore contains the maximum of dissolved oxygen while another part may be isolated from the atmosphere and may become deficient in oxygen as a result of the initial stages of oxidation. This is sometimes referred to as differential aeration, and may occur in a tight crevice or underneath loosely adhering surface deposits or coatings.

Regions of metal in contact with liquid having a high concentration of oxygen will become cathodic and be protected from corrosion, while regions where the oxygen concentration is low will become anodic and will corrode. The electrochemical conditions in crevices also change due to decreases in pH arising from hydrolyses of metal ions, and the decreased oxygen content will tend to make repassivation more difficult and corrosion more severe.

Electrochemical corrosion between alloy phases

Galvanic corrosion of a highly localized nature can occur in single metals due to the presence of inclusions or second phase particles with chemical compositions and therefore electrochemical potentials that are different to the major phase. Since the different phases are in electrical contact with each other, electrochemical corrosion will occur in the presence of an electrolyte with the dissolution of the anodic phase. Values for the electrode potentials of some of the common intermetallic compounds found in aerospace aluminium alloys are given in Table 3-4, where they are compared with values for the bulk alloys. These values are all measured against a standard calomel electrode.

Table 3-4 Electrode potentials for some common alloys and their inclusions

Alloy or Phase	Condition	Potential V
2024	Wrought, T3-	-0.69
6061	Wrought, T6	-0.83
7075	Wrought, T6	-0.83
356	Cast, T6	-0.82
Silicon	Particles	-0.26
Fe $A\ell_3$	Particles	-0.56
Cu $A\ell_2$	Particles	-0.73
Al_8 M_5	Particles	-1.24

If the inclusion is more electronegative than the surrounding matrix it will form the anode of the cell, and will corrode, and since generally the surface area of the anode will be small with respect to the cathode the rapid corrosion described above will occur. If the inclusions are in the form of long continuous or semi-continuous stringers deep pits may form, or if they are concentrated at grain boundaries severe intergranular corrosion and cracking may occur.

Electrochemical corrosion due to temperature variations

Corrosion may occur in a single metal exposed to an electrolyte if it is exposed to local heating which produces temperature gradients within the metal. It follows from Equation (3.22), that the warm spots will develop higher electrode potentials than the cooler areas and the potential differences between the different areas may be sufficient to create corrosion cells. This may be important in the corrosion of heat exchangers and boilers, but it may also be a factor in areas of aircraft structure close to engines or areas heated locally by the sun.

3.14 References

3-1 Portevin, A.M., Pretel, E., Joliver, H. — J. Iron and Steel Inst., 103, 219, 1934.

3-2 Pilling, N.B., Bedworth, R.E. — J. Inst. Metals, 29, 529, 1923.

3-3 Scully, J.C. — *The Fundamentals of Corrosion*, Pergamon International Library, Pergamon Press, London, 1975.

3-4 Evans, U.R. — *An Introduction to Metallic Corrosion*, 3rd Edition, Edward Arnold, London, 1981.

3-5 Fontana, M.G., Greene, N.D. — *Corrosion Engineering*, McGraw-Hill Book Company, New York, 1967.

3-6 Gelling, P.J. — *Introduction to Corrosion Prevention and Control for Engineers*, Delft University Press, Delft, The Netherlands, 1976.

3-7 *Aircraft Weapons Systems Cleaning and Control*, Technical Manual, NAVAIR, 01-1A-509, Naval Air Systems Command, Washington, September 1980.

3-8 *Corrosion Manual*, Section 2, AP-119A-0200-1B, 2nd Edition, United Kingdom, Ministry of Defence, 1977.

3-9 Evans, U.R. — *The Corrosion and Oxidation of Metals*, Arnold, London, 1961.

3-10 Evans, U.R. — J. Franklin Inst., 208, 1929, p. 52.

3-11 *Corrosion*, Volume 1: Metal — Environment Reactions, Ed. L.L. Schrier, Newnes-Butterworths, London, 1977.

3-12 Hoar, T.P. — *The Production and Breakdown of the Passivity of Metals*, Corrosion Science, Vol. 2, Pergamon Press, London, 1967, p. 341.

3-13 Morris, A.W. — *Materials Performance*, October 1980, pp. 38-42.

CHAPTER 4

COMMON AIRCRAFT ALLOYS AND THEIR RESPONSE TO CORROSIVE ATTACK

4.1 Introduction

By far the most widely used materials in airframe structures are aluminium alloys, but titanium alloys, and a wide range of specialty steels and occasionally magnesium alloys and nickel alloys are also used. The nickel, cobalt, titanium and ferrous alloys used in engines will not be dealt with specifically in this review, except where their use is related to airframe or undercarriage applications. Copper and various copper alloys are used in electrical equipment, and cadmium, zinc, aluminium, chromium, nickel and silver are used either alone or in combination for protective coatings. The main airframe and undercarriage structural alloys can be sub-divided into different alloy types, such as casting alloys and wrought alloys, and further sub-divisions can be made depending on whether the alloys are strengthened by mechanical working or heat treatment. Examples of the main alloy types are given in Table 4-1, along with notes describing some of their typical applications. Their general metallurgical and corrosion characteristics are described below. More detailed accounts of the mechanisms of the different modes of corrosive attack are given in Section II.

4.2 Steels — General

Many different steels are used in airframe structures and the susceptibility to corrosion and the modes of corrosive attack vary enormously depending on alloy composition and heat treatment condition. Plain carbon steels or low alloy steels can suffer from uniform corrosive attack, pitting or intergranular attack. Many high alloy and stainless steels are virtually immune to uniform attack, being protected from all but the most aggressive environments by thin passive films. However, these alloys are nevertheless prone to pitting attack, hydrogen embrittlement, stress corrosion cracking and other forms of mechanically aided corrosive attack. Generally, when moisture is present the corrosion products are reddish-brown scales or films, which are easily recognized.

4.2.1 Carbon and low alloy steels

Quenched and tempered low alloy steels such as T1 (Table 4-1) may be used where yield strengths of 620-700 MPa are required together with good toughness. Corrosion resistance depends on alloy composition, but small additions of Ni, Cr and Cu lead to improved corrosion resistance compared to plain carbon steels. In the specific case of T1, atmospheric corrosion resistance is about four times greater than for equivalent plain carbon steels (Ref. 4-1). It is also fairly resistant to stress corrosion cracking in water and sodium chloride containing atmospheres, but water saturated with H_2S and agricultural ammonia contaminated with air are both known to cause stress corrosion cracking (Ref. 4-2).

Higher yield strengths can be obtained in quenched and tempered low alloy steels such as 4130, but these alloys are also prone to general rusting, pitting, and stress corrosion cracking, particularly in industrial and marine atmospheres. These alloys should therefore be protected by electroplating or painting, or a combination of the two. However these alloys are also susceptible to hydrogen embrittlement in chromium, nickel and cadmium plating solutions and in hydrochloric acid pickling. Alkaline cleaners and anodic acid cleaners usually cause fewer problems. Baking at 190°C for times up to 24 hours, depending on the severity of the embrittlement is effective in relieving the embrittlement (Refs. 4-3, 4-4).

4.2.2 Ultra high strength steels

Ultra high strength steels such as 4340 and 8630 are also low alloy steels but have superior hardenability than those discussed previously. They may be used therefore where yield strengths are required in excess of 1400 MPa. The higher strength alloys such as 4340 can provide yield strengths up to 2000 MPa.

The general corrosion resistance of these steels is poor, and similar to other low alloy steels where corrosion protection is required. Ferritic and martensitic steels such as 8630 exhibit uniform corrosion in the presence of moisture or moist air. The rate of corrosive attack increases with temperature, acidity of the corrosive solution, and the velocity of the fluid flow. Under normal conditions these steels do not develop protective oxide films and they suffer from galvanic attack when in contact with more noble (cathodic) metals.

Heat treatment of alloys such as 4340 to strength levels in excess of 1400 MPa produces material with severe sensitivity to hydrogen embrittlement and processes involving exposure to hydrogen, such as acid pickling, cathodic cleaning or electroplating must be carried out with care. Hydrogen embrittlement may lead to brittle failures at very low stress levels, and particularly at stress concentration in notches. Delayed failure under sustained static loads may also occur as a result of hydrogen embrittlement (see Chapter 12). Relief from hydrogen embrittlement may be achieved by baking at temperatures in the range 150-350°C, and times of 1-24 hours depending on the alloy and the type of surface treatment causing the embrittlement.

The 18% nickel maraging steels can also be included in this group, and three types of alloy exist in this class providing strength levels up to 1400, 1725 and 1950 MPa respectively. The alloys contain 18% nickel, together with varying amounts of cobalt, molybdenum, titanium and aluminium, while carbon is held at very low levels up to 0.03%. Quenching from the austenitic region causes the transformation to martensite at relatively low temperatures (95-200°C), and a very fine structure. Alloys of very high strength and toughness are then developed by aging.

The alloys were designed to provide better resistance to crack propagation then the low alloy steels. The alloys also provide superior resistance to oxidation, corrosion, stress corrosion cracking (Refs. 4-5, 4-6), corrosion fatigue (Refs. 4-7, 4-8) and hydrogen embrittlement (Refs. 4-7, 4-9) then low alloy steels such as 4340.

4.2.3 Austenitic stainless steels

The austenitic stainless steels include a wide range of iron based alloys containing a minimum of 16% chromium and 6% nickel, and which possess outstanding corrosion resistance and good formability when in the annealed condition. Both cast and wrought forms are available. The high corrosion resistance of these alloys is due to the formation of very thin, highly adherent and uniform oxide films of chromium and nickel, and corrosion resistance increases as the concentration of these elements increases. Accordingly, alloys similar to type 310 stainless steel, which contains about 25% Cr and 20% Ni, provide the greatest corrosion resistance.

Table 4-1 Common metals used in airframe construction

Alloy Type	Examples	UNS* Code	Typical Uses
Carbon and low alloy steels	T1: Fe, 0.15C, 0.92Mn, 0.88Ni, 0.5Cr, 0.46Mo, 0.32Cu, 0.26Si	K11576	Quenched and tempered low alloy steels, used where strengths are required to 700 MPa.
	4130: Fe, 0.3C, 0.95Cr, 0.2Mo	G41300	
Ultra high strength steels	4340: Fe, 0.4C, 1.8Ni, 0.8Cr, 0.25Mo	G43400	Gears, landing gear components, pinions, connecting rods, bolts.
	8630: Fe, 0.3C, 0.55Ni, 0.5Cr, 0.25Mo	G86300	
Austenitic stainless steels	316: Fe, 18Cr, 13Ni, + Mo	S31600	Used predominantly in engine applications such as exhaust manifolds and after-burners. Minor use for specialty fittings in airframe.
	347: Fe, 18Cr, 12Ni, + Nb	S34700	
	310: Fe, 25Cr, 20Ni	S31000	
Martensitic stainless steels	403: Fe, 12Cr, low carbon	S40300	Used predominantly in engines in the form of forgings and castings. Used for specialty low volume parts in airframe where corrosion resistance without protection is required.
	440: Fe, 17Cr, 0.5Mo, high carbon	S44004	
Age hardening steels	17-4PH: Fe, 17Cr, 4Ni, 4Cu	S17400	High strength fasteners and forgings, cold drawn thin section parts, aircraft pressure vessels.
	Custom 455: Fe, 12Cr, 8Ni, 2Cu, 1Ti, + Nb, low carbon	S45500	
	AM362: Fe, 15Cr, 7Ni, Ti	S36200	
Nickel chromium steels	A286: Fe, 25Ni, 15Cr, 2Ti, 1.5Mn, 1.3Mo, 0.3V	K66286	Turbine discs, exhaust components. Little use in airframe.
	RA330: Fe, 35Ni, 19Cr, 1.25Si	N08330	
	Incoloy 800: Fe, 32Ni, 20Cr, 0.75Mn		
Cast aluminium alloys	355: Al, 5Si, 1.3Cu, 0.5Mg	A03550	Impellors and compressor parts, sand and permanent mold castings.
	A356: Al, 7Si, 0.3Mg	A13560	Aircraft wheels, pump parts, valve bodies, control brackets, pulleys.
	518: Al, 8Mg	A05180	Die castings with good corrosion resistance, instrument casings.
Wrought heat treatable aluminium alloys	2024: Al, 4.5Cu, 1.5Mg, 0.6Mn	A92024	Wing and fuselage skins, cowls, fasteners.
	6061: Al, 1Mg, 0.6Si, 0.25Cu, 0.2Cr	A96061	Applications requiring intermediate strength, with corrosion resistance and weldability, water tanks, tubing.
	7049: Al, 7.6Zn, 2.5Mg, 1.5Cu, 0.15Cr	A97049	Forgings requiring high strength and SCC resistance.
	7050: Al, 6.2Zn, 2.25Mg, 2.3Cu, 0.127Zr	A97050	Landing gear forgings, sheet, plate and extrusions. Replaces 7075 where resistance to exfoliation, stress corrosion, and high toughness are required.
	7075: Al, 5.6Zn, 2.5Mg, 1.6Cu, 0.3Cr	A97075	Wing spars, forgings, sheet, plate and extruded products. One of the first high strength alloys.
	7178: Al, 6.8Zn, 2.7Mg, 2.0Cu, 0.26Cr	A97178	Machined integrally stiffened skins, space vehicles.
	7475: Al, 5.7Zn, 2.3Mg, 1.5Cu, 0.21Cr, low Si, Fe, Mn, Ti	A97475	Wing spars, integrally stiffened panels, components requiring good strength and toughness.
Wrought, non-heat treatable aluminium alloys	5052: Al, 2.5Mg, 0.25Cr	A95052	Electrical housings, hydraulic tubing; spun, drawn or cast pressure receptacles.
	5456: Al, 5.1Mg, 0.8Mn, 0.1Cr	A95456	
Cast magnesium alloys	AZ92A: Mg, 9Al, 2Zn	M11920	Sand, permanent mold, and die castings for low cost, lightweight parts. The alloys provide a range of strengths, weldability and castability. Alloys such as QE22A maintain tensile strengths to temperatures in the region of 200°C.
	QE22A: Mg, 2.5Ag, 2.0Di, 0.4Zr	M18220	
	EZ33A: Mg, 3Re, 2.5Zn, 0.6Zr	M12330	
	ZH62A: Mg, 1.5Th, 5.7Zn, 0.7Zr	M16620	
	ZK61A: Mg, 6Zn, 0.8Zr	M16610	
Wrought, heat treatable magnesium alloys	AZ80A: Mg, 8.5Al, 0.5Zn	M11800	Forgings, aircraft wheels, extrusions.
	LA141A: Mg, 14Li, 1Al	M14141	Instrument housings, armour plate, aerospace structures.
Wrought, non-heat treatable magnesium alloys	AZ31B: Mg, 3Al, 1Zn	M11311	Sheet and plate with good formability and corrosion resistance. Extrusions and forgings.
	AZ61A: Mg, 6Al, 1Zn	M11610	Extrusions and forgings.
Cast titanium alloys	Ti-6Al-4V	R56400	Impellors, compressor wheels, window frames, hubs, bearing housings.
	Ti-5Al-2.5Sn	R54520	
Wrought titanium alloys	Ti-5Al-2.5Sn, ELI**	R54521	An intermediate strength alloy used where good toughness is required. Sheet, plate, bar, wire and forged products.
	Ti-8Al-1Mo-1V	R54810	Used in high temperature applications.
	Ti-6Al-2Sn-4Zr-2Mo	R54620	Jet engine compressor parts and airframe skin components.
	Ti-6l-4V, ELI	R56401	A wide range of sheet, plate, bar, wire and forged airframe and engine products.
	Ti-6Al-6V-2Sn	R56620	Replaces Ti-64 where higher strength is required, but at the expense of toughness.
	Ti-6Al-2Sn-4Zr-6Mo	R56260	Disc and fan blade compressor forgings.
	Ti-8Mo-8V-2Fe-3Al	R58820	High strength sheet.
	Ti-13V-11Cr-3Al	R58010	Sheet, bar and forged products. High strength fasteners.

*UNS = Unified numbering system
**ELI = Extra low interstitial grade

Carbon is another key element affecting corrosion resistance since it will tend to combine with chromium to form $Cr_{23}C_6$ carbides, which will precipitate at intergranular and intragranular sites when the alloys are cooled through the temperature range 880°-425°C. Similar precipitation can occur during long time service exposure in this temperature range. Since these carbides are rich in chromium they will deplete the surrounding matrix or grain boundary regions of chromium and may render them sensitive to corrosive attack. Intergranular corrosion will often occur because of this problem, although it can usually be prevented by annealing the alloy to dissolve the carbides and to relieve residual stresses. This problem may be severe in high carbon alloys, and in the fusion zones and heat affected zones of welds which are allowed to cool slowly through their critical carbide precipitation ranges. To avoid this problem low carbon alloys are available, as well as alloys such as types 321 and 347 which contain additions of niobium, titanium, tantalum or molybdenum that act as carbide stabilizing elements.

Since the alloys are austenitic at room temperature they cannot be strengthened by allotropic transformations and they do not exhibit significant precipitation hardening. They are strengthened therefore by cold, or warm working, although certain alloys such as type 304 contain small amounts of nitrogen (0.1%-0.16%) to increase strength and creep resistance through the formation of nitrides. In the cold worked condition many of the alloys are susceptible to stress corrosion cracking.

Some of these alloys, such as type 310 are embrittled by hydrogen, although only in very thin sections and therefore it is not considered a serious problem. Pitting and crevice attack may also occur in several of these alloys when exposed to severe atmospheric conditions. The addition of molybdenum (2-4%) in types 316 and 317 stainless steel provides increased resistance to pitting corrosion and stress corrosion cracking compared to the other 300 series alloys, although these forms of attack may still occur in sea-water. By comparison, type 321 is resistant to stress corrosion cracking in sea-water but is still susceptible to stress corrosion cracking and pitting in coastal regions or on aircraft carriers where alternate wetting and drying of chloride containing rain or spray can occur. It is usually recommended that most austenitic stainless steels be protected by coatings, and anodic protection is often applied when the steels are used in marine atmospheres for significant lengths of time (Ref. 4-10).

4.2.4 Martensitic stainless steels

The 400 type stainless steels are air hardening alloys, generally providing high strengths but lower corrosion resistance than the 300 series austenitic stainless steels. They contain chromium in amounts from 12-17% to provide corrosion resistance, and a wide range of minor alloying additions including nickel, molybdenum, tungsten, niobium and vanadium in amounts up to 3%. Both wrought and cast forms of these alloys are used.

These alloys are generally resistant to atmospheric corrosion and attack by fresh water, however they are prone to stress corrosion cracking and to hydrogen embrittlement. Their sensitivity to these forms of attack depends on the particular alloy chemistry and its heat treatment. For example type 420, which is a simple iron-chromium alloy, is particularly sensitive to salt water stress corrosion cracking when quenched or air cooled and then tempered in the range 370-480°C. Resistance to general corrosion also decreases as a result of this type of treatment. Generally, the higher strength conditions are more prone to stress corrosion cracking and hydrogen embrittlement. The addition of minor elements nickel, molybdenum, tungsten and vanadium, found in type 422 steel, provides increased resistance to stress corrosion cracking and also improved creep strength. However sensitization to salt water stress corrosion cracking also occurs if tempering is performed in the intermediate range of 370-570°C, and temperatures outside this range are therefore recommended.

Many of these alloys possess outstanding oxidation resistance and alloys such as Greek Ascoloy, niobium modified 410 and type 440 can be used continuously at temperatures up to 600°C, 670°C and 760°C respectively. For this reason they are often used in the hot sections of gas turbine engines.

4.2.5 Age hardening steels

This series of alloys includes the martensitic and semi-austenitic stainless steels such as 17-4PH and PH15-7Mo, which are also amenable to strengthening by precipitation hardening. They contain chromium and nickel as the major alloying elements, and their combined content is generally in excess of 20%. These elements are used in combination with smaller additions of Mo, Al, Ti, Co, and occasionally Cu and Nb. The alloys have atmospheric corrosion resistance similar to 304 stainless steels and oxidation resistance generally better than the martensitic 400 type stainless steels. Various heat treatments and thermomechanical processing treatments are available to produce ultimate tensile strengths at room temperature up to 2000 MPa, and yield strengths up to 1800 MPa in alloy 17-7PH. Several of the alloys retain high strengths at temperatures in the range 425-540°C.

The corrosion resistance of these alloys also depends on their heat treatment condition. Most alloys in this series are resistant to general corrosion in rural or moderate industrial atmospheres, but they are prone to crevice corrosion and pitting. Several of the alloys, such as AM-350 are susceptible to stress corrosion cracking in severe atmospheres such as coastal marine atmospheres and salt spray. Stress corrosion cracks tend to form at corrosion pits and to propagate intergranularly along prior austenite boundaries, or grain boundaries containing delta ferrite. These alloys are also prone to corrosive attack in weld heat affected zones unless post weld heat treatments involving full solutioning and aging are carried out.

4.2.6 Nickel chromium steels

These alloys are similar to the age hardening steels in providing outstanding combinations of strength, corrosion resistance and oxidation resistance. The alloys however have more stable austenitic matrix structures which are achieved by large additions of nickel, usually in excess of 20%, supplemented by smaller additions of chromium. Included in this class are the single phase austenitic alloys, such as RA-330 and Incoloy, which may contain additional elements such as Si and Mn. These alloying additions provide no age-hardening response, and therefore the alloys can only be strengthened by cold or warm working.

Several alloys contain smaller amounts of alloying additions such as Ti, Mo and V which allow strengthening by age hardening through the precipitation of various carbide phases. Several high carbon alloys are available, including Incoloy 802, which provide strengthening through a carbide dispersion-hardening mechanism which remains effective to quite high temperatures.

Also included in this class are alloys such as A-286 which exhibit age hardening characteristics through the precipitation of a γ'-$Ni_3(Al, Ti)$ phase, similar to that which forms in nickel-base superalloys. These alloys are therefore sometimes called iron-base superalloys or stainless superalloys. The age hardenable alloys provide high strength levels, with ultimate tensile strengths up to

1050 MPa and yield strengths of 760 MPa at ambient room temperature. However these alloys are prone to over-aging at very high temperatures and therefore service operating temperatures are generally limited to 650-850°C. The non-age hardenable alloys provide lower strengths, usually in the range 400-700 MPa at 25°C, but service temperatures up to 1200°C are feasible. Carbide dispersion strengthened alloys provide higher strengths in the intermediate temperature range, 760-1000°C.

The age hardenable alloys were originally developed for use in gas turbine engines and they provide good oxidation resistance in engine atmospheres in the temperature range given above. Consequently they can be used for continuous operation at these temperatures, and for intermittent service at higher temperatures. However, as noted in Chapter 12, alloy A-286 is susceptible to hydrogen embrittlement which leads to brittle intergranular fracture.

The non-age hardenable alloys also exhibit high resistance to oxidation and alloys such as Incoloy are resistant to corrosion in strongly oxidizing solutions such as nitric and sulphuric acids. Like other austenitic alloys, these alloys can be sensitized to intergranular attack by prolonged heating or slow cooling in the range 540-760°C. This problem is particularly severe in the high carbon alloys. Full solution treating and controlled aging should be used to stabilize these alloys and produce the correct grain boundary carbide phases. Stabilization annealing in the range 940-960°C is also used with age hardenable alloys like Incoloy 801 to provide maximum resistance to stress corrosion cracking.

4.3 Aluminium and Aluminium Alloys — General

As indicated by its position in the electrochemical series, aluminium is thermodynamically one of the most reactive metals, behaving anodically with respect to all metals except magnesium, beryllium and zinc. In practice however it is often resistant to corrosion since it is protected by oxide films which form rapidly in most environments.

The conditions for thermodynamic stability of the oxide film are given by the Pourbaix diagram of Figure 4-1. Aluminium is passive in the pH range of about 4 to 8.5, depending on temperature and the rate at which the oxide film dissolves in the electrolyte. Outside of this range aluminium may corrode, by the formation of Al^{+++} ions in acid solutions or the formation of AlO_2^- ions in alkaline environments. Some special cases exist where aluminium does not corrode outside the passive region, and these may occur for example when the oxide film is not soluble or where it is maintained by the oxidizing nature of the solution.

Very localized corrosion of aluminium may occur in the passive range, leading for example to pitting. The propensity for pitting can be established from the pitting potential, which is simply the potential in a particular solution above which pits will initiate and below which they will not. The pitting potential can be found by applying a variable external potential between the metal (as anode) and a cathode which are immersed in an electrolyte free of cathodic reactants. The relationship between anode potential and current is determined, and conditions are established where the metal polarizes, potential levels off to a steady value and rapid increase in current occurs. This potential is the pitting potential, and this is indicated in Figure 4-2 for 1100 aluminium immersed in neutral sodium chloride solution. Only when cathodic potential is sufficient to polarize the metal to its pitting potential will significant current flow and pitting occur. Pitting is common in aluminium alloys in aerated solutions containing halide ions since it develops electrode potentials that equal or exceed the pitting potential. In deaerated solutions of equal halide (e.g. chloride) concentrations, in the absence of the cathodic reactant O_2, aluminium may not corrode by pitting since it is not polarized to its pitting potential. Generally, aluminium does not develop pitting in aerated solutions of most non-halide salts because its pitting potentials in these solutions are considerably more cathodic than those in halide solutions, and it is not polarized to these potentials (Ref. 4-12).

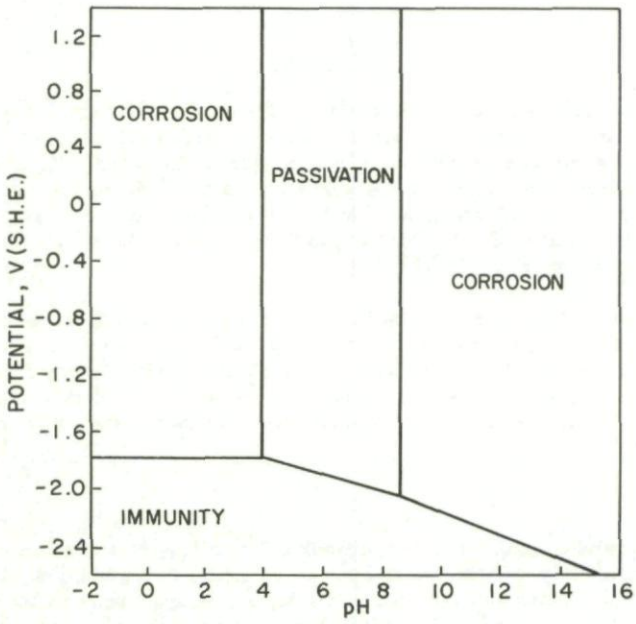

Fig. 4-1 Pourbaix diagram for aluminium (Ref. 4-11)

Diagram is for aluminum with an oxide film of hydragillite ($Al_2O_3, 3H_2O$) at 25°C. Potential values are for the standard hydrogen electrode scale.

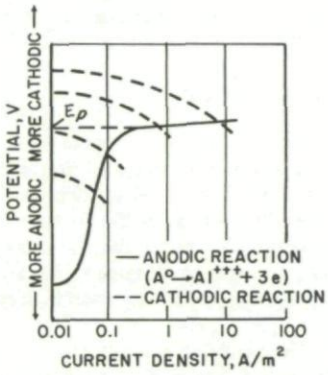

Fig. 4-2 Anodic polarization curve for aluminium 1100

Specimens were immersed in neutral deaerated NaCl solution free of cathodic reactant. Pitting develops only at potentials more cathodic than the pitting potential, E_p. The intersection of the anodic curve for aluminium (solid line) with a curve for the applicable cathodic reaction (one of the representative dashed lines) determines the potential to which the aluminium is polarized, either by cathodic reaction on the aluminium itself, or on another metal connected to it electrically. The potential to which the aluminium itself, or on another metal connected to it electrically. The potential to which the aluminium is polarized by a specific cathodic reaction determines corrosion current density and corrosion rate (Ref. 4-12).

The corrosion behaviour of aluminium alloys is strongly influenced by the chemical composition of the alloys as determined by impurity elements and alloying additions, since these affect the electrolytic solution potentials of the alloys. The solution potential is primarily determined by the composition of the aluminium-rich solid solution which is the predominant phase in the alloys. But second phase particles such as inclusions, dispersoids and precipitates are also important to corrosion since they will have electrochemical potentials different from the aluminium solid solution and may therefore create local galvanic couples. These may be responsible for special cases of corrosion such as intergranular corrosion or exfoliation.

The principal alloying elements in aluminium alloys include Zn, Mg, Si, Cu, and Mn, and the effects of these elements on the solution potential of aluminium are shown in Figure 4-3. The reactive elements zinc and magnesium decrease the solution potential of aluminium, producing very reactive binary alloys. Silicon, copper and manganese have the opposite effect on solution potential, and since the effects of these alloying elements in ternary or higher order alloys are approximately additive the solution potentials of commercial alloys span a wide range.

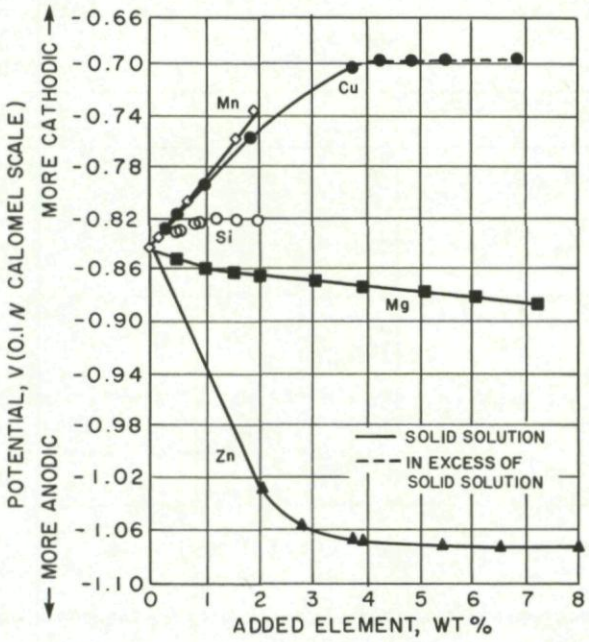

Fig. 4-3 Effects of principal alloying elements on electrolytic solution potential of aluminium (Ref. 4-12)

Potentials are for high-purity binary alloys solution heat treated and quenched. Measured in a solution of 53 g/L NaCl plus 3 g/L H_2O_2 maintained at 25°C.

4.3.1 Cast aluminium alloys

The cast aluminium alloys used in the aerospace industry are heat treatable alloys based on the Al-Si-Mg, Al-Si-Cu-Mg and the Al-Cu-Mg alloy systems. They are used because of their high fluidity, low solidification shrinkage tendencies, high resistance to hot cracking and good pressure tightness. These are the main properties required to ensure good castability. However the major alloys also have high corrosion resistance and weldability.

Silicon is a major alloying element in many alloys and free silicon or silicide particles exist in large amounts. These particles are highly cathodic to the aluminium matrix by several hundred millivolts and therefore they would be expected to promote corrosion. However the effects on corrosion resistance are minimal because of the low corrosion current densities resulting from the fact that the silicon particles are highly polarized (Ref. 4-11).

The ternary Al-Si-Mg alloy 356 has outstanding corrosion resistance and it can be used in industrial and sea coast environments without cracking. It is also highly resistant to stress corrosion cracking and no service failures due to SCC have been reported. Alloy 355 which contains 1.3% Cu also has high resistance to corrosion and stress corrosion cracking, although it is inferior to alloy 356. Other higher strength casting alloys are available. However, as the strengths of these alloys increase their propensity for corrosion, and particularly for stress corrosion cracking increases. Copper is added up to about 5% and this has a significant and generally deleterious effect on corrosion resistance.

4.3.2 Wrought heat treatable aluminium alloys

These are by far the most important and most widely used alloys in airframe construction and many different types are in service. The most important alloys are of the Al-Cu-Mg type (2xxx series) or Al-Zn-Mg type (7xxx series). Alloys of the 6xxx series, Al-Mg-Si system, such as 6061 are also used to a lesser extent. Table 4-2 gives the solution potentials for a number of such alloys used in aerospace, while Table 4-3 gives their typical room temperature mechanical properties.

Table 4-2 Solution potentials of some commercial heat treatable aluminium alloys used in aerospace

Alloy	Temper	Potential V versus standard calomel electrode
2014	T4 T6	-0.69 -0.78
2219	T3 T6	-0.64 -0.8
2024	T3 T6	-0.69 -0.81
6061	T4 T6	-0.80 -0.83
7005	T6	-0.94
7049	T73 T76	-0.84 -0.84
7050	T73 T76	-0.84 -0.84
7075	T6 T73	-0.83 -0.84
7475	T6 T73	-0.83 -0.84
7178	T6	-0.83

Table 4-3 Typical room temperature mechanical properties of some common aerospace aluminium alloys

Alloy	Form and condition		Tensile Yield MPa	Tensile Ultimate MPa	% Elong. in 50 mm	Modulus of elasticity MPa × 10^3 (d)	Brinell Hardness 500 Kg load 10 mm ball	Fatigue strength MPa	Fracture toughness MPa $\sqrt{m}$ (g)
2014	T4	sheet (a)	290	428		73	105	140 (e)	
	T6	sheet (a)	414	483		73	135	125 (e)	23-26
2219	T351	sheet (a)	248	359	17	73		103 (e)	
	T62	sheet (a)	290	415	10	73			
	T8	sheet (a)	390	475	10	73			28-32
2024	T3	sheet (a)	345	480	18	73	120	140 (e)	33-50
	T4	sheet (a)	325	470	20	73	120	140 (e)	
	T8	sheet (a)	450	480	6	73			22-27
6061	T4	sheet (a)	145	241	22	69	65	97 (e)	
	T6	sheet (a)	276	310	12	69	95	97 (e)	
7005	T6351	extrusions (b)	320	375	12	71.5		130-150 (f)	50-53
7049	T73	forgings (c)	475	535	11.5	70	135	275-315 (f)	32-36
7050	T7351	plate (b)	462	525	13.8	72		170-300 (f)	34-36
	T7651	extrusions (b)	530	575	13	72			30-32
7075	T7351	plate (b)	435	500	10	72			31-35
	T651	sheet (a)	500	580	9	72	150	159 (e)	27-31
7475	T7351	plate (b)	430	500				205-235 (f)	51-53
	T651	sheet (a)	462	524	12	72			41-43
7178	T6	plate (b)	538	607	10	72			21-25
	T76	plate (b)	504	573	11	71		200-290 (f)	29-33

(a) 1.6 mm thick sheet.
(b) 50 mm thick plate or extrusions.
(c) Properties of forgings across grain flow.
(d) Average of tension and compression values.
(e) 5×10^8 cycles of completely reversed stress, R.R. Moore type, tests.
(f) Axial tests on smooth specimens (R = 0.0), 50 mm thick plate.
(g) Longitudinal-transverse orientation.

The alloys are strengthened by precipitation hardening treatments which involve solution heat treatment, rapid quenching and either natural aging at room temperature or artificial aging at elevated temperatures. The hardening response of these alloys, as well as many other properties such as corrosion resistance are sensitively dependent on heat treatment parameters, the details of which are beyond the scope of this handbook, however some general effects should be noted. Solution temperatures, quenching rates, and the degree of aging as influenced by aging time and aging temperature are the most important parameters to be considered and information will be given on these with respect to specific alloy systems.

Figure 4-4 illustrates the effect of quenching rate on the corrosion resistance of alloys 2024-T4 and 7075-T6, in terms of the percentage loss in tensile strength caused by exposure to corrosive solutions. It can be seen that slow quenching rates, of about 1°C/s lead to intergranular corrosion in 2024 and mixed intergranular corrosion plus pitting corrosion in 7075. As the quenching rate increases the rate of corrosion also increases until a maximum is reached at between 10 and 50°C/sec. At even higher quenching rates the corrosion resistance increases and the mode of corrosion changes from intergranular to pitting. These variations in cooling rate during quenching lead to slightly different effects on the age hardening response of the alloys. In the case of 7075, a decrease in quenching rate below 10^3°C/sec will lead to a significant loss of age hardening response and strength before any significant change in corrosion resistance occurs. However, with alloy 2024 age hardening response remains fairly constant over a wide range of quenching rates from about 50°C/s to about 10^4°C/s, while corrosion resistance decreases rapidly as quenching rate drops below about 10^3°C/s. For this reason many heat treatment specifications will require demonstration of both strength or hardness and resistance to intergranular corrosion.

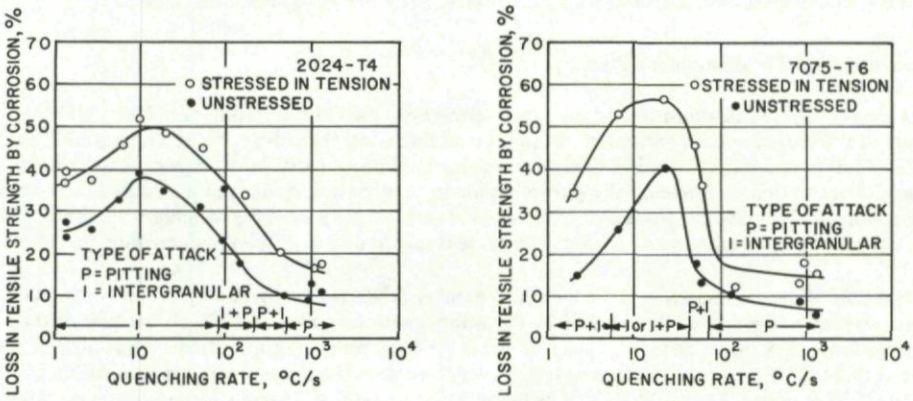

Fig. 4-4 Effect of quenching rate on corrosion resistance of nonclad wrought aluminium alloy specimens (Ref. 4-25)

Corrosion resistance is indicated by percentage loss in tensile strength due to corrosion and by changes in predominant type of corrosive attack. Specimens of alloy 2024-T4 (left), 1.63 mm (0.064 in.) thick, were exposed to 48 h of alternate immersion in standard sodium chloride — hydrogen peroxide solution. Specimens of alloy 7075-T6 (right), also 1.63 mm thick, were exposed to three months of alternate immersion in a 3.5% aqueous solution of sodium chloride.

These types of alloy are used in a number of temper conditions, the most common of which are as follows:

F or O	:	As fabricated or annealed respectively.
H	:	Strain hardened wrought products.
W	:	Solution heat treated (treatment prior to natural aging).
T3	:	Solution treated, cold worked and naturally aged.
T4	:	Solution treated, naturally aged.
T6	:	Solution treated, artificially aged.
T7	:	Solution treated, stabilized (overaged).
T8	:	Solution treated, cold worked, artificially aged.

One or more digits following these basic temper designations are indicative of variations in the amount of cold work, aging time or both.

Alloys of the 2xxx series are used in all of the above temper conditions and their corrosion behaviour varies accordingly. Electrochemical effects on corrosion can be stronger in these alloys than in many others because of the presence of copper. As indicated in Figure 4-3, variations in the concentration of copper in solid solution lead to appreciable changes in electrode potential and local variations in composition can therefore give rise to local galvanic cells. There is also a tendency for copper which has first dissolved in a solution to replate on the free surface to form small copper cathodes which again cause local microscopic galvanic cells. These alloys are particularly susceptible to stress corrosion, particularly when stressed in the short transverse direction. However both stress corrosion resistance and exfoliation resistance can be improved by heat treatments such as T6 or T8 involving artificial aging.

The 6xxx series alloys are intermediate strength materials which provide corrosion resistance superior to most of the 2xxx and 7xxx series alloys. They are strengthened by the precipitation of an ionic compound Mg_2Si, which is both anodic to aluminium and reactive in acidic solutions. However the precipitation of Mg_2Si has a negligible effect on the electrode potential of aluminium and therefore corrosion resistance is not markedly affected. Small amounts of chromium, manganese and zirconium may be added for control of grain structure, but at levels which do not affect corrosion resistance significantly. Copper is used in alloys such as 6061 to enhance strength, and this may be responsible for the slightly inferior corrosion resistance of this alloy compared to copper free alloys such as 6063. Corrosion resistance generally decreases as copper content increases, but most commercial alloys have copper contents less than 1%.

The 7xxx series alloys contain large amounts of zinc and magnesium and include copper free alloys such as 7005, and a greater number of alloys such as 7010, 7050, 7075, 7178 and 7475 which contain copper. The alloys are strengthened by the sequential precipitation of solute rich zones (G-P zones) and precipitates such as η' and η ($MgZn_2$). These alloys provide strengths over a wide

range, and are among the highest strength materials available when considered on the basis of strength to density ratios. The alloys are also more resistant to general corrosion than the 2xxx series alloys, however they are particularly susceptible to stress corrosion cracking and exfoliation corrosion unless appropriately heat treated to develop immunity to these forms of attack.

Copper is a key alloying element in terms of both strength and corrosion resistance. Copper is needed to develop the highest strength levels possible, and it is present in amounts in excess of 1.8% in alloys such as 7050 (2.3%) and 7178 (2%). Although lower in strength the copper free alloys are quite resistant to general corrosion, and they compare quite well with some of the corrosion resistant alloys of the 3xxx, 5xxx and 6xxx series. The addition of copper leads to a general decrease in the resistance to general corrosion, but at the same time has a beneficial effect on stress corrosion resistance. Of particular importance is the fact that high copper content allows the alloys to be aged at higher temperatures without excessive loss of strength, and therefore the T76 and T73 treatments have been developed to provide resistance to exfoliation corrosion and stress corrosion cracking with only moderate loss of strength from the T6 peak strength condition. These strength losses typically amount to 6-8% and 10-15% for the T76 and T73 conditions respectively.

Many of these alloys are used with surface claddings to provide corrosion protection. The cladding alloy is selected to be anodic to the core alloy by 80 to 100 mV so that it provides cathodic protection to the core. The cladding, which is normally used with sheet and tube products, is applied in such a way as to achieve a metallurgical bond with the core and may be applied to one or both faces of the product. Because of the cathodic protection provided by the cladding, any corrosion will progress only to the core-cladding interface, and then spread laterally. This is an effective method to avoid perforation of thin sheet products such as wing and fuselage skins. 7072 is a widely used cladding, used with 2219, 6061, 7075 and 7178 aluminium alloys.

4.3.3 Wrought, non-heat treatable aluminium alloys

The 5xxx series alloys are the most important alloys of this type used in the aerospace industry and they contain magnesium with smaller amounts of manganese and, or chromium. In alloys containing less than about 3% of alloying additions, the elements either remain in solid solution or are distributed as finely dispersed second phase particles of Al_8Mg_5. These alloys have high corrosion resistance, almost equivalent to that of commercially pure aluminium. In more heavily alloyed materials an almost continuous network of Al_8Mg_5 may form along grain boundaries unless precautions are taken during processing to achieve a uniform distribution within the grains. Continuous intergranular precipitation of Al_8Mg_5 can cause susceptibility to exfoliation corrosion and stress corrosion cracking.

The most heavily alloyed materials in this series, such as alloy 5090, may contain magnesium contents up to 7% and are capable of developing strengths in excess of those for 2024-T3. Although not as strong as 7075-T6, because of their lower density and excellent corrosion resistance they might be used in place of alclad 7075-T6 for some applications. While 5090 is anodic to other high strength alloys such as 2024, 7075 and other 5xxx series alloys which contain less magnesium, it is compatible with 7072 which is one of the most common cladding alloys. Alloy 5090 is also highly resistant to exfoliation and stress corrosion cracking (Ref. 4-14).

4.4 Magnesium Alloys — General

Unalloyed magnesium is not extensively used for structural purposes and therefore interest is principally with the higher strength alloys of magnesium which contain additions of aluminium, lithium, zinc, rhenium, thorium and silver. Minor additions of elements such as cerium, manganese and zirconium may also be used. These alloying elements are selected to enhance response to strengthening treatments and also to provide compatibility with magnesium in terms of corrosion resistance. Other elements such as iron, nickel, cobalt and copper have severely deleterious effects on corrosion resistance of magnesium and are therefore regarded as impurity elements with definite tolerance limits imposed to ensure acceptable corrosion resistance.

Table 4-4 Standard four-part ASTM system of alloy and temper designations for magnesium alloys (Ref. 4-25)

First part	Second part	Third part	Fourth part
Indicates the two principal alloying elements	Indicates the amounts of the two principal alloying elements	Distinguishes between different alloys with the same percentages of the two principal alloying elements	Indicates condition (temper)
Consists of two code letters representing the two main alloying elements arranged in order of decreasing percentage (or alphabetically if percentages are equal)	Consists of two numbers corresponding to rounded-off percentages of the two main alloying elements and arranged in same order as alloy designations in first part	Consists of a letter of the alphabet assigned in order as compositions become standard	Consists of a letter followed by a number (separated from the third part of the designation by a hyphen)
A-Aluminium E-Rare Earth H-Thorium K-Zirconium M-Manganese Q-Silver S-Silicon T-Tin Z-Zinc	Whole numbers	Letters of alphabet except I and O	F-As fabricated O-Annealed H10 and H11-Slightly strain hardened H23, H24 and H26-Strain hardened and partially annealed T4-Solution heat treated T5-Artificially aged only T6-Solution heat treated and artificially aged T8-Solution heat treated, cold worked and artificially aged

The alloy designation system used in this document is the four part system of alloy and temper designations developed by ASTM. This is explained in Table 4-4. As applied to alloy AZ92A listed in Table 4-1, the first two letters indicate that aluminium (A) and zinc (Z) are the two principal alloying elements. The second part of the designation, 92, indicates that the alloy has an aluminium content nominally of 9% and a zinc content of 2%. The third part of the designation, A, indicates this alloy was the first alloy standardized with 9% Al and 2% Zn as the principal elements. The fourth part of the designation, which is not shown in Table 4-1, is the temper designation which is similar to that used for aluminium alloy. For example T6 indicates that an alloy is solution treated and artificially aged.

Aluminium and zinc are among the most widely used alloying elements in magnesium alloys because they have high solubility and give rise to some of the highest strength alloys available with tensile strengths of about 275 MPa at room temperature. Manganese is often used as a ternary addition with aluminium and zinc to improve corrosion stability, and is present in AZ92A at about 0.1%.

Because of the position of magnesium and magnesium alloys at the anodic end of the galvanic series they will corrode rapidly when coupled with most other metals in a high conductivity environment. The rate of galvanic attack is approximately in proportion to the potential difference between the metal and the cathode. In the case of aluminium alloys the galvanic effect with magnesium is strongly influenced by the presence of elements such as iron, copper, nickel and zinc in the aluminium. Small amounts of iron up to 1% in 6061-T6 aluminium can increase galvanic corrosion rates of magnesium alloy AZ31B by almost two orders of magnitude in 3% NaCl solution. It follows that low iron content in 6061 aluminium would render this alloy more compatible with AZ31B in terms of corrosion resistance. However, effects of this type depend on the particular magnesium alloy and the potential that the alloy is able to generate. For example the improvement observed with Mg-Th alloys, such as HK31A, is small because they develop appreciably higher potentials.

To determine galvanic corrosion hazzards requires that exposure tests be carried out on typical joint assemblies using the same bolt or rivet materials intended to be used in the structure. Generally it is found that magnesium alloys are reasonably compatible with certain aluminium alloys such as 5052, 6053, 6061 and 6063, and these are the alloys that would normally be considered for use in washers, shims, fasteners and mating structural members. Stainless steel, titanium, copper, Monel, and aluminium alloys such as 2024, Alclad 2024, 7075 and Alclad 7075 will corrode magnesium when coupled with it under corrosive conditions, and therefore protection is required. The corrosion protection systems may take many different forms. A moisture impervious film should be applied at least to the dissimilar metal so that any defect in the film allowing electrochemical contact between the metals will result in the least damaging combination of small cathode area and large anode area. The magnesium metal surface should also be protected. Faying surfaces between metal to metal joints should also be protected. Magnesium to magnesium assemblies may be protected by an inhibited (e.g. chromate pigmented) primer or the use of wet assembly techniques. In wet assembly a sealing compound is placed between the surfaces during assembly to ensure that there is no crevice at the joint into which water can gain access by capillary action.

4.4.1 Cast magnesium alloys

Both sand and permanent mold castings are made from magnesium alloys and all of the alloys used in aerospace applications are made from heat-treatable alloys. At least five different alloy systems are used, including the Mg-Al-Zn system (AZ series), Mg-Ag-Rare Earth system (QE series), Mg-Rare Earth-Zn system (EZ series), Mg-Zn-Th system (ZH and HZ series) and the Mg-Zn-Zr system (ZK series). Selection of a particular alloy system is made on the basis of foundry qualities and the ability to produce the required shape, and the physical, mechanical and chemical properties of the resulting casting.

All of these alloys are subject to general and pitting corrosion when exposed to most natural environments, and must be properly surface treated and protected. It is doubtful whether these alloys are suitable for use where continuous or long time immersion in water or salt solution is involved because of the rapid corrosion that would occur in the event of a breakdown in the corrosion protection system.

The highest strength levels are achieved in alloys such as AZ63A, where tensile strengths of about 275 MPa can be obtained at ambient room temperature (21°C). However the higher strength alloys are inferior with respect to porosity, pressure tightness and weldability, compared to lower strength alloys such as AZ91. The thorium containing alloys, HZ31A and HZ32A, provide outstanding high temperature properties among the magnesium casting alloys, and the presence of 2.1% Zn in HZ32A provides optimum creep resistance at temperatures of 260°C and above.

4.4.2 Wrought, heat treatable magnesium alloys

Several of the alloy systems discussed above are also used to produce wrought products in the form of forgings, extrusions, sheet and plate, and the corrosion properties of the wrought alloys are similar to those of their cast equivalents. Several alloys are prone to stress corrosion cracking, including AZ80A, HK31A, HM31A and ZK60A. Consequently efforts have been made to develop stress corrosion resistant alloys, and several such alloys are now available. These include alloy EK31A, which is relatively free from stress corrosion cracking and which exhibits a low corrosion rate in 3% NaCl immersion tests. The Mg-Th-Mn alloy HM21A is also resistant to SCC, and sheet specimens in the T8 condition have been found to be immune to SCC when exposed to rural environments for over 7 years when stressed to 75% of their yield strength.

Several lithium containing alloys have been developed, and these are among the newer wrought magnesium alloys available. Alloy AL91A is a two phase material, consisting of hexagonal α-phase in a body-centered-cubic β-phase matrix, while AL141A containing a larger amount of lithium (14%) is an all beta alloy. These alloys are among the lightest weight structural alloys available, and they have high stiffness-to-weight ratios, ductilities and impact properties.

Alloy LA141A is strengthened by an age hardening reaction involving precipitation of a transition phase, however there is some doubt whether LA91A is also a heat-treatable alloy. Full strength appears to be developed by working treatments which break-up and disperse the α-phase.

The corrosion resistance of these alloys varies inversely with lithium content, and therefore LA91A is the more corrosion resistant of the two. However chrome pickle or dichromate or anodic surface treatments are required, together with painting to provide corrosion protection. Resin based coatings have also been used. The corrosion products on LA91A are less adherent than those on most other commercial magnesium alloys and the corrosion rates, particularly in salt water or salt spray, are more rapid. While corrosion rates will decrease with time for most alloys as oxide films form, the films formed on magnesium-lithium alloys will provide little or no protection and corrosion rates will tend to remain constant. For alloy LA141A evidence has been found of intergranular corrosion occurring in unprotected weldments.

4.4.3 Wrought, non-heat treatable magnesium alloys

Magnesium-aluminium-zinc alloys containing less than about 8% aluminium plus zinc do not respond to heat treatment and must be strengthened by mechanical working. The two important alloys of this type are AZ31B and AZ61A, which contain 3% and 6% aluminium respectively together with 1% zinc. AZ31B is a widely used alloy providing good mechanical properties and excellent formability. However, surface treatments and painting are required to provide corrosion protection. AZ61A provides improved corrosion resistance, due to the higher aluminium content, and it is resistant to attack by most alkalies and some acids and salt solutions. The alloy does not corrode in dry air, but corrosion occurs in moist air particularly in the presence of chloride ions, and the alloy is also prone to stress corrosion cracking.

4.5 Titanium Alloys — General

Titanium is an attractive metal for aeronautical applications because it has a low density of about 4.5 Mg/cm^3, and its alloys also have low densities in the range 4.5-4.84 Mg/cm^2, high strength-to-weight ratios, and high corrosion resistance. Titanium itself is resistant to corrosion in industrial environments, sea water, other chloride salt solutions, and salts such as $Fe\ Cl_3$ and $Cu\ Cl_2$ which tend to pit most other metals actually inhibit corrosion of titanium. The outstanding corrosion resistance of titanium is due to the formation of an extremely protective film of $Ti\ O_2$. The most protective films form when the atmosphere contains water, even in trace amounts. Exposure to strongly oxidizing atmospheres in the absence of moisture produces a non-protective film. Similarly, titanium and its alloys corrode rapidly in environments that destroy the protective oxide film. Hydrochloric, hydroflouric, sulphuric, phosphoric and formic acids will attack titanium. Dry chlorine and dry fuming nitric acid will oxidize titanium rapidly and the reactions can be pyrophoric. However titanium is resistant to wet chlorine (1% moisture) and to other oxidizing gases such as SO_2 and CO_2.

Titanium and its alloys passivate rapidly in acqueous (wet) environments and it has surprisingly good compatibility with many other alloys. Since it behaves cathodically with respect to all aluminium and magnesium alloys, and most ferrous alloys except some passive stainless steels, when coupled with these metals in airframe structures it is the coupled metal rather than titanium that would tend to corrode in a galvanic cell. Titanium is anodic to carbon, and therefore galvanic corrosion of titanium might be expected to occur if it were brought in contact with carbon or graphite fibres of the type now being used in fibre-reinforced composites. However this does not occur with titanium alloys because of the stability of the passive film, and it has been shown that very high potentials are required to cause the transition from passive to transpassive behaviour, when the passive film would be anodized to a soluble substance (Ref. 4-15). This study (Ref. 4-15) showed that of six common fastener materials investigated Ti-6Al-4V exhibited the highest transpassive potential, Table 4-5, and was likely therefore to be the most resistant to galvanic corrosion when in contact with carbon. It was concluded that Ti-6Al-4V, Inconel 718 and MP35N could be used with confidence for fastener in composite structures, PH13-8Mo and A286 were considered marginal while Monel was considered unsatisfactory because it could be raised to the transpassive state by contact with carbon.

Table 4-5 Comparison of galvanic cell potentials with transpassive potentials and comparison of galvanic corrosion currents with sweep corrosion currents (Ref. 4-15)

Material	Short circuit cell potential (mV) SCE		Transpassive potential (mV) SCE	Cell corrosion current ($\mu A/cm^2$)		Sweep corrosion current at cell potential ($\mu A/cm^2$)	
	7 Days	24 Days		7 Days	24 Days	7 Days	24 Days
Ti-6Al-4V	-12	370	2500	0.005	0.001	0.96	0.214
Inconel 718	203	165	900	0.028	0.006	0.201	0.20
MP35N	33	270	815	0.055	0.025	1.54	1.43
A286	75	100	130	0.010	(1)	7.5	5.3
PH13-8Mo	54	-28	200	0.086	3.31	0.93	5.17
Monel	-55	106	-275	14.7	0.004	27.63	

(1) Broken lead wire prevented measurement.

Titanium is resistant to oxidation up to about 590°C, but nevertheless it is a reactive metal that absorps interstitial elements such as oxygen, nitrogen and hydrogen. Pick up of these elements causes hardening and embrittlement and therefore strict limits are imposed on these elements in commercial alloys. Also, the use of titanium at high temperatures is limited, even though the pure metal has a very high melting point of about 1668°C.

Titanium has a hexagonal-close-packed (HCP) structure at room temperature, known as the α-phase, but this transforms to the body-centred-cubic β-phase at about 882°C. This temperature is strongly affected by the presence of interstitial elements, oxygen, nitrogen and hydrogen, and also by alloying elements. The alloying elements are classified either as α-stabilizers which raise the α-β transformation temperature, or β-stabilizers which lower this temperature. Aluminium and tin are the principal α-stabilizers, while vanadium, molybdenum and chromium are the main β-stabilizers. These elements also affect the strength and corrosion resistance of the principal phases. Other elements such as zirconium and silicon may be used to enhance strength and creep resistance.

The presence of an allotropic transformation allows titanium alloys to be strengthened by heat treatment, with martensitic structures being produced by quenching from the β-phase field. A wide range of two phase α-β structures can be produced, where the amount and morphology of each phase can be adjusted by control of alloy chemistry, thermo-mechanical working and heat-treatment. The control of microstructure in these alloys is discussed in detail elsewhere (Ref. 4-16) and therefore this information will not be repeated. However it is convenient to point out that the commercial titanium alloys fall into one of three classes; alpha or near alpha alloys, alpha-beta, and beta alloys. The alloys listed in Table 4-1 are among the most widely used titanium alloys in aerospace. Of the wrought alloys listed the first two are alpha or near-alpha alloys, Ti-64, Ti-6242, Ti-6246 and Ti-662 are alpha-beta alloys, while the last two are beta alloys. The typical room temperature properties of these alloys are listed in Table 4-6.

Table 4-6 Typical room temperature mechanical properties of some common aerospace titanium alloys

Alloy	Form and Condition	Tensile Yield MPa	Tensile Ultimate MPa	% Elong.	Modulus of elasticity MPa × 10^6	Charpy impact J	Fatigue strength at 10^7 cycles MPa	Hardness
Ti-6Al-4V	As-cast Low oxygen	895	1014	10	11.7	23	483(a)	311 BHN
Ti-5Al-2.55n	Ann sheet	793	827	10	11	25.8		36 R_c
Ti-8Al-1Mo-1V	Ann forgings	827	896	10	12.7	20-33	565	36 R_c
Ti-6Al-2Zn-4Zr-2Mo	Ann	827	896	10	11.3			36 R_c
Ti-6Al-4V	Ann sheet	827	896	10	11.3	24.4		36 R_c
Ti-6Al-6V-2Sn	Ann sheet	999	1069		11.7	13.6-20.3	159_n-276_{un}	
Ti-6Al-2Sn-4Zr-6Mo	Ann sheet	1172	1269	10	11.3			42 R_c
Ti-8Mo-8V-2Fe-3Al	STA sheet	1283	1366	7	11-11.25		427	40 R_c
Ti-13V-11Cr-3Al	STA sheet	1173	1311	10	10.34	8.13	552	32-36 R_c

n = notched, un = un-notched, a = annealed, STA = solution treated and annealed

4.5.1 Cast titanium alloys

The α-β alloy Ti-6Al-4V is the most common titanium alloy used for castings, although other alloys such as Ti-5Al-2.5Sn and Ti-6Al-2Sn-4Zr-2Mo have also been used. The alloys are melted by induction heating or by consumable electrode skull melting, and cast by precision or investment casting techniques. In general, for comparable heat treatments these cast alloys exhibit the same or slightly lower strengths, ductilities, creep and fatigue strengths, and elevated temperature stabilities than their wrought counterparts. Corrosion properties are also similar to those of the wrought alloys.

Molten titanium alloys have inferior fluidity, compared to steels, and severe porosity and hot tears are common problems. Techniques such as hot isostatic processing are now being examined to close and heal shrinkage porosity, but hot tears must be repaired by welding and therefore alloys used for casting must be weldable.

4.5.2 Wrought titanium alloys

The wrought titanium alloys are remarkably resistant to pitting, stress corrosion, galvanic corrosion, crevice corrosion, erosion-corrosion, and corrosion fatigue in marine environments (Ref. 4-17). However many alloys are susceptible to stress corrosion cracking in aqueous environments containing halide ions when a pre-crack is present, and liquids such as methanol, ethanol, and ethylene glycol have been found to cause cracking in titanium alloys even in the absence of a pre-crack and occasionally when no externally applied stress has been present.

Stress corrosion cracking. A detailed review of the stress corrosion cracking of titanium alloys has been given in Reference 4-18. It has been shown that SCC occurs in aqueous solutions, organic liquids, hot salts, nitrogen tetroxide (N_2O_4), red fumic nitric acid, molten salts, liquid metals and gases. It has also been shown that the α-phase, the β-phase, or both may be susceptible to SCC.

Alloys such as Ti-8Al-1Mo-1V and Ti-5Al-2.5Sn are susceptible to SCC in distilled water. The addition of halide ions Cl^-, Br^- and I^- can increase the rate of cracking in alloys that are susceptible to SCC in distilled water, and also induce SCC in alloys that are immune in distilled water. Alloys such as Ti-6Al-4V are included in this latter group which includes the majority of alloys. In α and $\alpha+\beta$ alloys the characteristic mode of SCC in aqueous solutions is cleavage of the α-phase and a compilation of the environment-material combinations for which α-cleavage during SCC occurs has been given by Reference 4-19.

Table 4-7 Relative resistance of titanium alloys to hot-salt stress corrosion (Ref. 4-23)

Least Resistant	Moderately Resistant	Most Resistant
Ti-5Al-2.5Sn (M.A.)	Ti-8Mo-8V-2Fe-3Al	Ti-4Al-3Mo-1V
Ti-12Zr-7Al	Ti-5Al-5Sn-5Sr-1Mo-1V	Ti-10Sn-5Zr-2A-1Mo-0.2Si
Ti-8Al-1Mo-1V (M.A.)	Ti-6Al-2Sn-4Zr-2Mo	
Ti-5Al-5Sn-5Zr	Ti-5Al-2.75Cr-1.25Fe	Ti-11.5Mo-6Zr-4.5Sn
Ti-6Al-6V-2Sn	Ti-13V-11Cr-3Al	
Ti-5Al-1Fe-1Cr-1Mo	Ti-8Al-1Mo-1V (T.A.)	Ti-8Mn
	Ti-2Fe-2Cr-2Mo	
	Ti-4Al-4Mo	
	Ti-6Al-4V	

M.A. = Mill annealed
T.A. = Triple annealed

In β alloys the β-phase may be susceptible to stress corrosion cracking in aqueous salt solutions, and this may occur by intergranular and transgranular fracture. In the case of the more highly susceptible alloys the presence of a pre-crack is not necessary, and mill and duplex annealed Ti-8Al-1Mo-1V is susceptible to SCC when a notch is present, while the same alloy and Ti-13V-11Cr-3Al are susceptible without a notch when they are step-cooled (Refs. 4-20, 4-21).

However not all alloys are susceptible to aqueous stress corrosion cracking and at least one alloy, Beta-C with a nominal composition Ti-3Al-8V-6Cr-4Mo-4Zr, has been reported to be immune to salt water stress corrosion cracking at ambient temperature (Ref. 4-22). Specimens which had been aged at 565, 621 and 676°C were fatigue pre-cracked and submerged in 3.5% NaCl solution with crack tip stress intensities equal to the fracture toughness of the alloy, and no crack growth was observed in more than 2000 hours of exposure.

Stress corrosion cracking can also occur in organic solutions such as methanol, ethanol or ethylene glycol. This is of practical concern since these solutions are constituents of many industrial substances such as marking fluids, de-icers, and paint removers. In methanol at least two types of SCC behaviour have been identified (Ref. 4-18). Type-A cracking occurs intergranularly in titanium and all alloys when halogens are present in the solution. Type-B cracking occurs transgranularly in alloys which are also susceptible to aqueous SCC.

Hot salt stress corrosion cracking. The presence of solid salts containing Cl^-, Br^- or I^- ions can cause embrittlement and, or stress corrosion cracking in titanium alloys at high temperature. The measured salt deposits and operating temperatures and stresses of compressor components in current turbine engines are sufficient to cause failure by this mode in laboratory specimens, but no such service failures have been reported to date. In laboratory tests the phenomenon has been observed at temperatures of about 290°C and above, and stresses as low as one third of the yield strength of the material. A wide variety of halogen salts have been found to produce stress corrosion cracking, and pure sodium chloride has been found to be among the most damaging and is more severe than artificial sea salt (Refs. 4-23, 4-24). The mechanisms of hot salt cracking are not well understood but many ideas have been proposed which involve complex chemical reactions leading eventually to the formation of either chlorine, oxygen, hydrogen, or hydrogen chloride gas which cause embrittlement. The general consensus is that oxygen is involved in some form, such as TiO_2, and that corrosion is more rapid in moist rather than dry environments. The mechanisms of hot salt cracking have been reviewed in References 4-18, 4-23, and 4-24. This latter reference has provided a rating of the resistance of some of the commercial titanium alloys to hot-salt stress-corrosion, as shown in Table 4-7.

Most titanium alloys are susceptible to some degree, and the response of an individual alloy may be affected by heat treatment condition. For example, as shown in Table 4-7, the alloy Ti-8Al-1Mo-1V is less susceptible in the triple annealed condition than in the mill annealed condition. The alpha alloys appear to be more susceptible than the alpha-beta alloys, but the degree of susceptibility increases with increasing aluminium content.

4.6 References

4-1	Brown, W.F., Jr.	Aerospace Structural Metals Handbook, Vol. 2, U.S. Department of Defence, Belfour Stulen Inc, 1972, Code 1103.
4-2	Doty, W.D.	Metals Engineering Quarterly, February, 1969.
4-3	Cataldo, C.E.	*Compatibility of Metals with Hydrogen.* NASA TM X-53807, George C. Marshall Space Flight Centre, December 1968.
4-4	Groeneveld, T.P. Fletcher, E.E. Elsea, A.R.	*A Review of the Literature on the Cleaning, Pickling and Electroplating Processes and Relief Treatments to Minimize Hydrogen Embrittlement of Ultra-High Strength Steels.* Battelle Memorial Institute, Columbus, Ohio, October 1966.
4-5	Dean, S.W. Copson, H.R.	Corrosion, 21, March 1965, pp. 95-103.
4-6	Kirk, W.W. Covert, R.A. May, T.P.	Metals Engineering Quarterly, 8, Nov. 1968, pp. 31-38.
4-7	Spitzig, W.A. Talda, P.M. Wei, R.P.	Journ. Eng. Fracture Mechanics, 1, 1968, p. 158.
4-8	Wei, R.P. Talda, P.M. Che-Yu, Li	*Fatigue Crack Propagation of Some Ultra-High Strength Steels.* ASTM-STP-415, 1967, pp. 460-485.
4-9	Wei, R.P. Landes, J.D.	Materials Research and Standards, ASTM, Vol. 9, 1969, p. 25.
4-10	Morrison, J.D.	*Corrosion Study of Base and Coated Stainless Steels.* NASA TN D-6519, John F. Kennedy Space Center, July 1972.
4-11	Pourbaix, M. et al.	Atlas of Chemical Equilibria in Aqueous Solutions, Pergamon Press, Oxford, New York, 1966.
4-12	Hollingsworth, E.H. Hunsicker, H.Y.	*Corrosion Resistance of Aluminium and Aluminium Alloys.* IN Metals Handbook, Volume 2, 9th Edition, Properties and Selection of Non-ferrious Alloys and Pure Metals, American Society for Metals, Ohio, 1979.

4-13		Heat Treatment of Aluminium Alloys, Ibid, page 34.
4-14	Kattus, J.R.	Aerospace Structural Metals Handbook, Volume 3, Code 3304, U.S. Department of Defence, Materials Information Centre Publication, Belfour Stulen Inc, June 1979.
4-15	Morris, A.W.	Materials Performance, Oct. 1980, pp. 38-42.
4-16		Titanium and Titanium Alloys Source Book, American Society for Metals, Metals Park, Ohio, 1982.
4-17		Military Handbook — Titanium and Titanium Alloys, MIL-HDBK-697A, United States Department of Defence, June 1, 1974.
4-18	Blackburn, M.J. Feeney, J.A. Beck, T.R.	*Stress Corrosion Cracking of Titanium Alloys.* IN Advances in Corrosion Science and Technology, Vol. 3, ed. M.G. Fontana and R.W. Staehle, Plenum Press, New York, 1973.
4-19	Wanhill, R.J.H.	British Corrosion Journal, Vol. 10, No. 2, 1975, pp. 69-78.
4-20	Fager, D.N. Spurr, W.F.	Trans. A.S.M., 61, 1968, p. 283.
4-21	Feeney, J.A. Blackburn, M.J.	IN The Theory of Stress Corrosion Cracking in Alloys, ed. J.C. Scully, 1971, p. 355, NATO Scientific Affairs Division, Brussels.
4-22	Hagemeyer, J.W. Gordon, D.E.	*Properties of Two Beta Titanium Alloys After Aging at Several Different Temperatures.* IN Titanium Science and Technology, Plenum Press, New York, 1973.
4-23	Heimerl, G.J. Braski, D.N. Royster, D.M. Dexter, H.B.	*Salt Stress Corrosion of Ti-8Al-1Mo-1V Alloy Sheet at Elevated Temperature.* ASTM-STP-397, 1965.
4-24	Rideout, S.P. Louthou, M.K., Jr. Selby, C.L.	*Basic Mechanisms of Stress Corrosion Cracking of Titanium.* ASTM-STP-397, 1965.
4-25	Petersen, V.C.	Journal of Metals, 23, April 1971, pp. 40-47.
4-26		ASM Metals Handbook, Vol. 2, Ninth Edition, p. 34, Metals Park, Ohio, 1979.

CHAPTER 5

AIRCRAFT INSPECTION FOR CORROSION

5.1 Introduction

All aircraft must be inspected for signs of corrosion and condition of protective coatings during scheduled inspections. These must be carried out more frequently when the aircraft is known to contain materials or structural details that are highly susceptible to corrosion, and when the aircraft is operated under extreme conditions of humidity and temperature. Usually inspections for corrosion are carried out along with more general inspections for other forms of damage such as fatigue, and would be carried out at different times at different levels of scrutiny.

Prior-to-flight inspections involve simple walk-around visual inspections of airframe and control surfaces, as well as operational checks on engines and flight controls. Line inspections are carried out at pre-determined intervals, typically of 50-150 hours, depending on aircraft type and operational role. These would involve detailed examinations of prescribed areas of structure and components and typically may involve three levels of effort (Ref. 5-1).

- Visual inspections would be carried out on all visible external structural surfaces, plus all internal structure visible through quick access doors either by direct line of sight or by using mirrors.
- Aided visual inspection would be carried out less frequently, but would represent the standard thorough inspection carried out on all internal and external surfaces accessible without major disassembly. Simple inspection aids such as mirrors, magnifying glasses, fibre-optics probes, mechanical probes and gauges would be employed.
- Special inspections are carried out on known problem areas using the same devices as above together with simple non-destructive inspection methods such as liquid penetrants, or eddy currents.
- Detailed inspections are performed on parts requiring special inspection methods such as x-ray, magnetic particle, flourescent penetrant, ultrasonic inspection, or on components or areas of structure requiring unusual levels of disassembly (Ref. 5-2).

These inspections should be designed and timed to detect all forms of structural deterioration at an early stage. A serious consequence of even minor corrosion is that it may obscure the presence of other forms of damage such as fatigue cracks and therefore an aim of current research is to develop NDI techniques that can differentiate between different types of damage, see Reference 5-3.

5.2 Inspection for Corrosion

The first appearance of corrosion on unpainted surfaces may be in the form of deposits or spots. This occurs around skin seams; lap and butt joints; areas where sand and dirt collect; or in crevices or joints where traces of chemicals such as cleaning compounds or corrosion removal compounds have collected. Particular attention must be paid towards areas where moisture does not rapidly evaporate. Areas exposed to battery electrolytes, engine exhaust products, smoke and gunfire gases must be inspected carefully and frequently. Several metals produce corrosion products with characteristic colours and the appearance of discolouration and streaking on clean metal surfaces may also provide an early indication of corrosion. The appearance of the corrosion products on some common aircraft alloys is indicated in Table 5-1.

Table 5-1 Corrosion of Metals — Nature and Appearance of Corrosion Products (Ref. 5-4)

Alloys	Type of attack to which alloy is susceptible	Appearance of corrosion product
Aluminium Alloys	Surface pitting, intergranular and exfoliation.	White or gray powder.
Titanium Alloys	Highly corrosion resistant. Extended or repeated contact with chlorinated solvents may result in degradation of the metals structural properties.	No visible corrosion products.
Magnesium Alloys	Highly susceptible to pitting.	White powdery snow-like mounds, and white spots on surface.
Low Alloy Steels (4000-8000 series)	Surface oxidation and pitting, surface and intergranular.	Reddish-brown oxide (rust).
Corrosion Resistant Steel (CRES) (300-400 series)	Intergranular corrosion (due to improper heat treatment). Some tendency to pitting in marine environment (300 series more corrosion resistant than 400 series). Stress corrosion cracking.	Corrosion evidenced by rough surface; sometimes by red, brown or black stain.
Nickel-base Alloys (Inconel)	Generally has good corrosion-resistant qualities. Sometimes susceptible to pitting.	Green powdery deposit.
Copper-base Alloy, Brass, Bronze	Surface and intergranular corrosion.	Blue or blue-green powder deposit.
Cadmium (used as a protective plating for steel)	Good corrosion resistance. If attack occurs, will protect steel from attack.	White, powdery corrosion products.
Chromium (used as a wear-resistant plating for steels)	Subject to pitting in chloride environments.	Chromium, being cathodic to steel, does not corrode itself, but promotes rusting of steel where pits occur in the coating.

Corrosion should be less severe on painted, clad or plated surfaces than on unprotected surfaces. However corrosion will occur if the protection system is damaged and the bare metal is exposed to the corrosive medium. The corrosion protection system may then tend to hide the corrosion damage, and the first indications may be discolouration of the coating system or blistering or flaking of paint. Damaged areas of coatings must be removed to allow closer inspection of the underlying metal, and repairs effected in both the metal and the coating system.

5.3 Corrosion Prone Areas

Recurring corrosion problems may appear in different areas of aircraft depending on the aircraft type and the local operating environment. Figure 5-1 shows some of the corrosion prone areas in a typical small transport aircraft (Ref. 5-5). Other corrosion prone areas that are not shown specifically in Figure 5-1 include:

Transport aircraft
- Main undercarriage.
- Nose undercarriage.
- Rudder and elevator shroud areas.
- Aileron and flap track area, flap tracks and trailing edges.
- Freight doors and ramps.
- Access doors.
- Control cables.
- Leading edges, hinge lines and air ducts.
- Radome area.

Jet fighter aircraft
- Missile and gun blast areas.
- Engine intake areas.
- Cockpit frames.
- Wing fold areas.

Helicopters
- Main rotor head assembly.
- Tail rotor assembly.
- Transmission housing.
- Main rotor blades and leading edges.

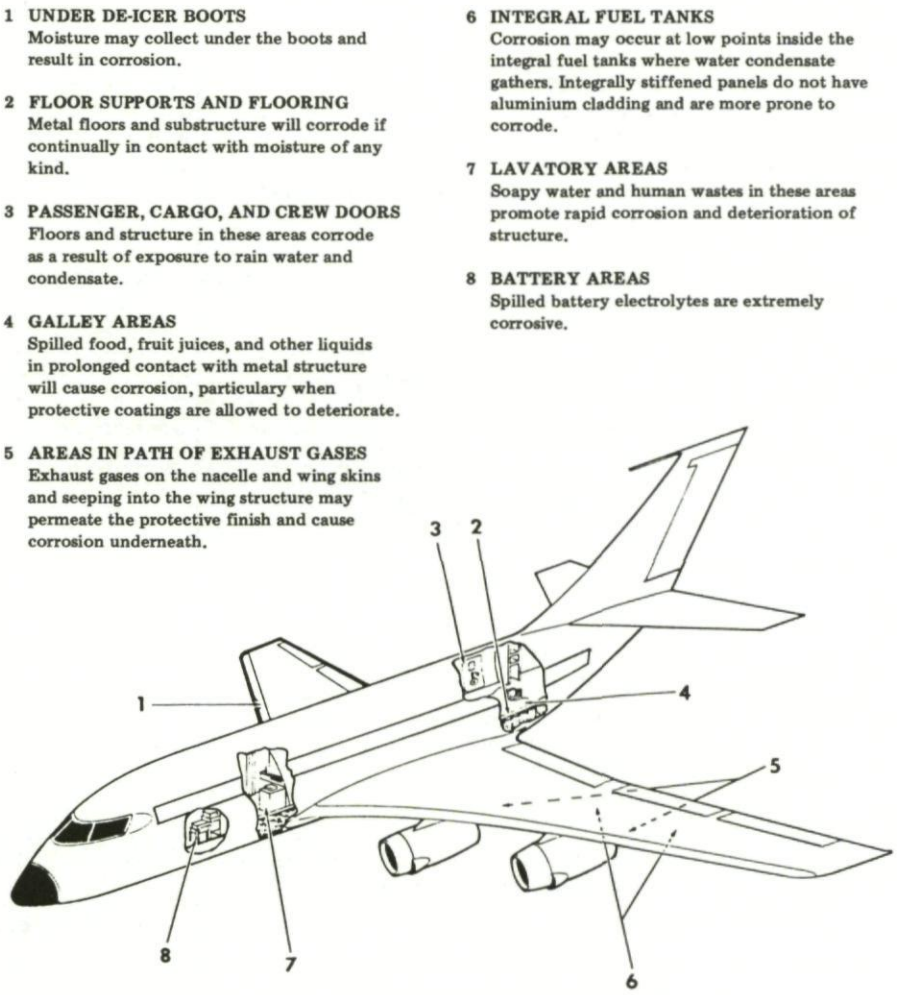

Fig. 5-1 Most susceptible areas (Ref. 5-5)

External skins

The external surfaces of magnesium alloy or aluminium alloy skins are particularly susceptible to corrosion along rivet lines, lap joints, fasteners, faying surfaces, or where protective coatings have been damaged or neglected. These areas must be carefully examined by visual inspection, employing visual aids such as magnifying glasses, mirrors, fibre-optic probes, mechanical probes, and various other devices. These inspections would normally pay particular attention to the following areas.

- Corrosion may be evident in spot-welded skins by corrosion products appearing at the crevices through which the corrosive agents entered and is usually more prevalent on external areas (Fig. 5-2).
- Piano-type hinges are also prime sites for corrosion, Figure 5-2, as are edges of honeycomb panels and drilled holes.
- Lower fuselage, wing and flap areas aft of wheels suffer damage in protective coatings due to impact from particles thrown up from the runway on take-off and landing.
- Canopy and passenger/crew/cargo door structures and associated hinges, fittings, and mechanisms may be damaged due to the combined effects of mechanical and corrosive action.
- Windows and door frames may be similarly affected.

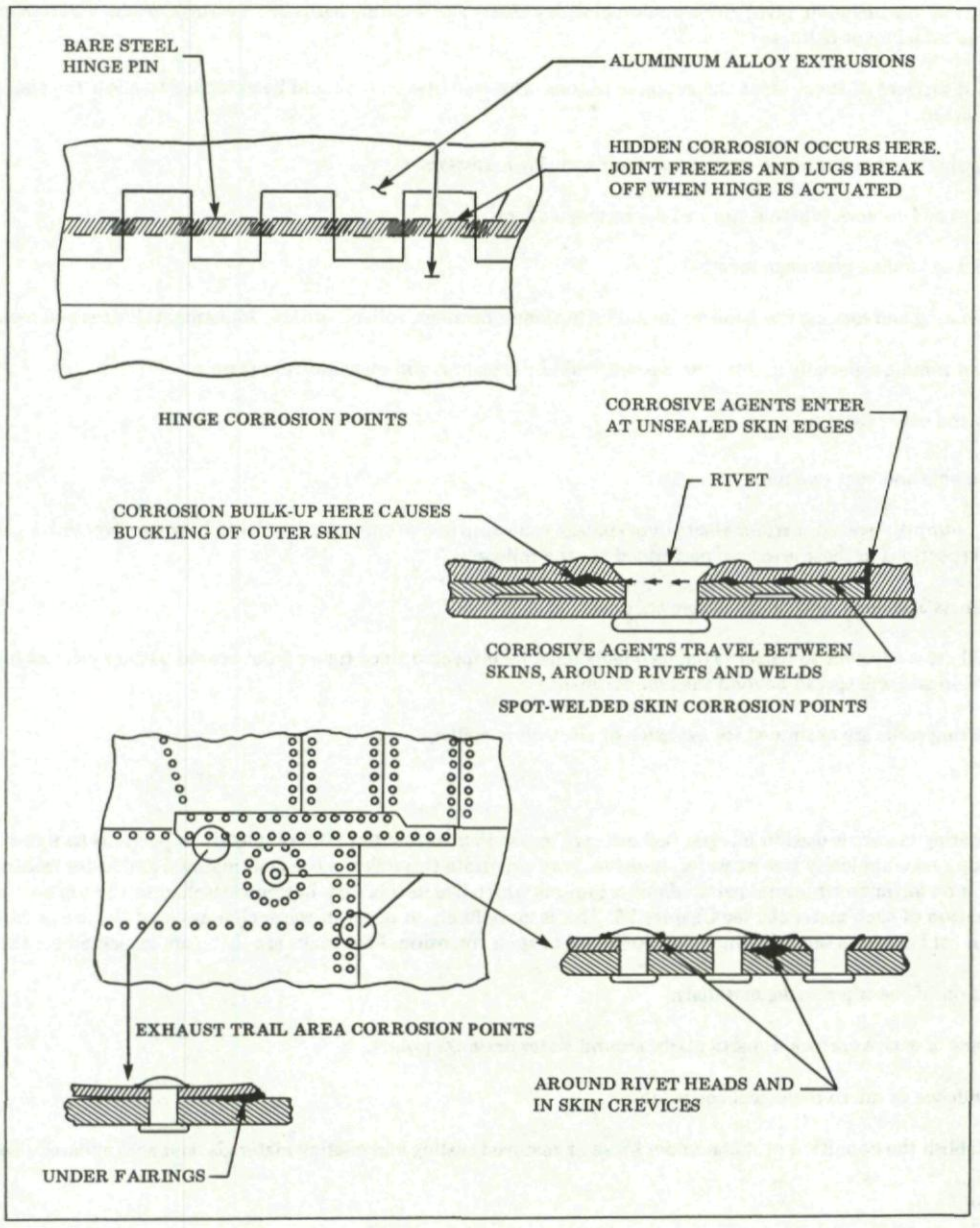

Fig. 5-2 Vulnerable areas (Ref. 5-5)

Exposed hardware

Exposed hardware such as control surface actuating rods, fittings, attaching and hinge bolts, nuts, washers and cotter pins, are generally made from alloys different to those of the structure on which they are mounted, and several dissimilar metals may be used in the hardware itself. These items and the adjacent areas of airframe structure are therefore prime sites for galvanic corrosion. Corrosion may occur in these parts particularly when organic or chemical coatings have been damaged or have deteriorated, or when protective films or lubricants have been removed by cleaning solvents or detergents during cleaning. Protective films and lubricants can also be removed by de-icing fluids. Other areas requiring close inspection include:

- Bonding jumpers, grounding studs and receptacles, attaching hardware and adjacent areas.
- Access panels, antenna and radome attaching screws, countersinks and adjacent areas.
- Navigation lights, landing lights and other external light installations and their attaching hardware and adjacent areas.
- Jacking pads, tie-down fittings, attaching hardware and adjacent areas.
- Boarding and access ladder mounting devices and attachments for engine run-up screens and blanking devices.

Undercarriage bays

Wheel wells are exposed to flying debris from landing strips which damages paintwork and lodges in inaccessible areas, between stiffeners, ribs and lower surfaces. Undercarriage assemblies must be examined with particular attention to magnesium wheels, paintwork, exposed switches and electrical equipment. Frequent cleaning is required followed by treatment by water displacing fluids and re-lubrication to ensure continued safe operation. Other areas of the undercarriage requiring regular inspection and maintenance are:

- All pivot points including pivot and trunnion pins, lay shafts and securing hardware; bearings, bushings, attachment and pivot lugs, and attachment fittings.
- Exposed surfaces of shock strut and actuator pistons. These components should be extended to allow the piston surfaces to be inspected.
- Axles, wheels, wheel bearings, brakes and their securing hardware.
- Openings and recesses where water and debris may collect.
- Surfaces of landing gear main members.
- All operating and locking mechanisms including bushings, bearings, rollers, springs, adjustment devices and securing hardware.
- Exposed tubing, especially at nuts and sleeves, and under clamps and identification tags.
- Valves and other fittings.

Battery compartments and vent openings

If not promptly treated, battery electrolyte spillage can cause severe corrosion particularly where protective paintwork has been damaged. Inspections in these areas are performed for the following:

- Cleanliness and condition of protective coatings.
- Internal areas adjacent to battery compartments must be inspected since fumes from heated battery electrolytes are difficult to contain and will spread beyond the compartment.
- Supporting racks are examined for evidence of electrolyte spillage.

Fuel tanks

Top coating materials used in integral fuel cells are impervious to fuel but not completely impervious to water. Since it is impossible to keep fuel completely free of water, moisture may penetrate through the top coat material and cause fretting or inter-granular corrosion on airframe structural parts. Micro-organisms which live in fuel may become attached to the top coating and may result in deterioration of such materials, see Chapter 15. This is more likely to occur in warm climates, and the use of fuel system icing inhibitors in cold climates should reduce the likelihood of such corrosion. Fuel tanks are therefore inspected for the following:

- Condition of the top coating materials.
- For signs of active corrosion, particularly around water drainage points.
- For evidence of micro-biological corrosion.
- To establish the condition of metal under loose or removed sealing and coating materials, and accumulated residues.

Exhaust trail areas

Fairings and skins located in engine-exhaust areas are subject to highly corrosive exhaust gas. They should be examined and cleaned regularly to ensure that exhaust deposits do not accumulate in joints, crevices, seams or hinges. The following inspections are usually carried out:

- Fairings and access panels in the exhaust gas path are removed and all surfaces are inspected.
- Special attention is paid to skin joints, hinges, fasteners and fairings since deposits may become trapped and not be removed during routine cleaning.
- Internal areas of structure in the path of exhaust gases, such as wings, flaps and nacelles are inspected.

Engines and nacelles

The protective finish on leading edges and engine intake areas may be subject to rain erosion and abrasion by dust. These areas should be cleaned, examined and reprotected as regularly as possible, particularly when operating in marine or desert environments. Problems occur both in jet engines and reciprocating engines and inspections usually include the following specific tasks:

- Frontal areas of engines are inspected, particularly cylinders and push rod housings on reciprocating engines.
- Accessory mounting brackets and particularly cadmium plated parts are examined for signs of corrosion or mechanical damage.
- Cooling air paths that can become obstructed are inspected, as are any crevices where salt deposits may build up.
- Carburettors and other air intake structures are examined, particularly at faying surfaces and fasteners.
- Propellor surfaces and particularly leading edges are examined for nicks, pits or other damage that might lead to corrosion or fatigue.
- Engine mounts and struts are examined, and particularly under clamps or tape, and at welded joints.

Toilet and galley areas

Fluid spillage in toilet and galley areas often gains access to inaccessible places beneath floor structure. Waste products from these areas are highly corrosive and should be removed as soon as possible. The inspections in these areas should ensure that:

- All areas, particularly deck areas behind toilets, sinks and ranges where spilled food and waste products may collect are clean, dry and free of corrosion.
- Bilge areas under galleys and toilets should likewise be inspected for cleanliness and to ensure integrity of protective treatments and coatings.

Helicopter rotating assemblies

Helicopter rotor heads, main rotor blades, tail rotor blades, gearboxes, transmission shafts and bearings are susceptible to corrosion as a result of exposure to the elements. Several of these components may be made of high strength steels which may be susceptible to stress corrosion cracking and therefore very regular cleaning and careful inspection using available non-destructive testing methods are required to detect pits or cracks before they become serious.

Titanium alloys, aluminium alloys and fibre reinforced composites are now being used in rotor heads and blades, and regular inspections are required to ensure the good condition of these materials, particularly in joints and seals. Rotor blades may contain foam fillers, and these must be kept in good condition to avoid the absorption of moisture. Careful inspection is required wherever moisture absorbing materials such as leather, paper, foam rubber, sound proofing and insulation materials are used either in helicopters or other forms of aircraft.

Miscellaneous areas

Any areas where foreign matter and moisture may accumulate are potential sites for corrosion. Containers or enclosures of all types, including housings for electrical and avionics equipment are prime areas for concern. Access panel seals may deteriorate to allow ingress of water, and the housings may be vented which may allow moist air or spray to enter and corrosion to occur. Electrical equipment may not be adequately designed to resist corrosion and therefore this should be inspected for signs of corrosion and performance at regular intervals. Examples of corrosion problems in electronic systems have been given in Reference 5-6.

Potential corrosion areas exist in wing fold joints, flaps, ailerons, elevators, spoilers and speed brake recesses where dirt and moisture may collect when such control surfaces are in the closed condition. Control cables are also prone to corrosion, particularly where they are exposed or where they pass through seals. Aircraft exposed directly to salt spray such as fighter aircraft or helicopters operating from aircraft carriers, or amphibious aircraft must be inspected more frequently than land based aircraft.

5.4 Specialized Non-Destructive Inspection Techniques

When it is not possible to monitor the corrosion deterioration of a structure by direct visual examination or when the corrosive attack is highly localized and not visibly apparent, special techniques of non-destructive inspection are required to provide reliable indications. The general techniques employed include:

- liquid penetrant inspection
- magnetic particle flaw detection
- x-ray and neutron radiography
- ultrasonic inspection
- eddy current inspection
- acoustic emission

With the exception of acoustic emission, these techniques are able to detect cracks in metal structures, including those due to fatigue, corrosion fatigue and stress corrosion cracking. However they are generally less effective in detecting uniform hidden corrosion, and the accumulation of corrosion products in and around fatigue cracks can render these techniques significantly less sensitive and less reliable than they would be on clean cracks. Reference 5-3 describes a study performed to determine probability of dection, sensitivity and accuracy in the detection of fatigue cracks in aluminium alloy sheet specimens, using eddy currents, ultrasonics, x-rays and penetrants. In this study ultrasonics and radiography were the least reliable and accurate, while penetrant inspection gave a probability of detection greater than 90% for corrosion free cracks of 1 mm depth or greater. After corrosion sensitivity and probability of detection for all NDI methods fell although eddy current and ultrasonic inspections retained the original accuracy. After corrosion, penetrant inspection remained the most sensitive but eddy current inspection appeared to be more reliable (Figs. 5-3, 5-4, 5-5).

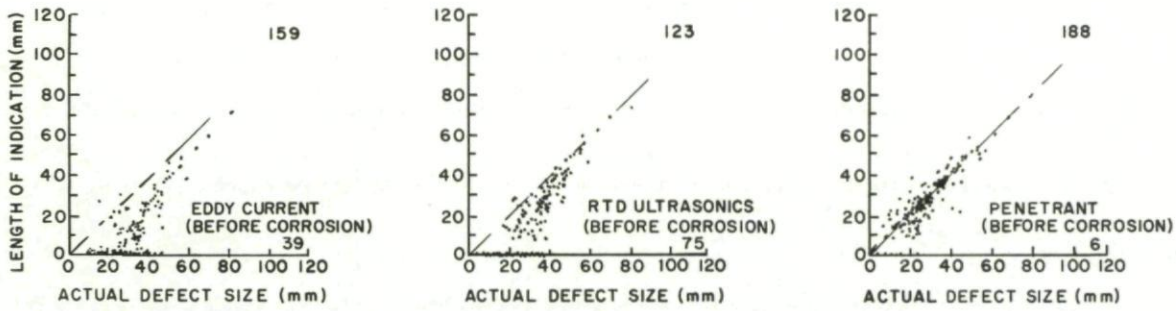

Fig. 5-3 Inspection accuracy, the degree of correspondence between the size of the defect indication and the actual crack size (Ref. 5-3)

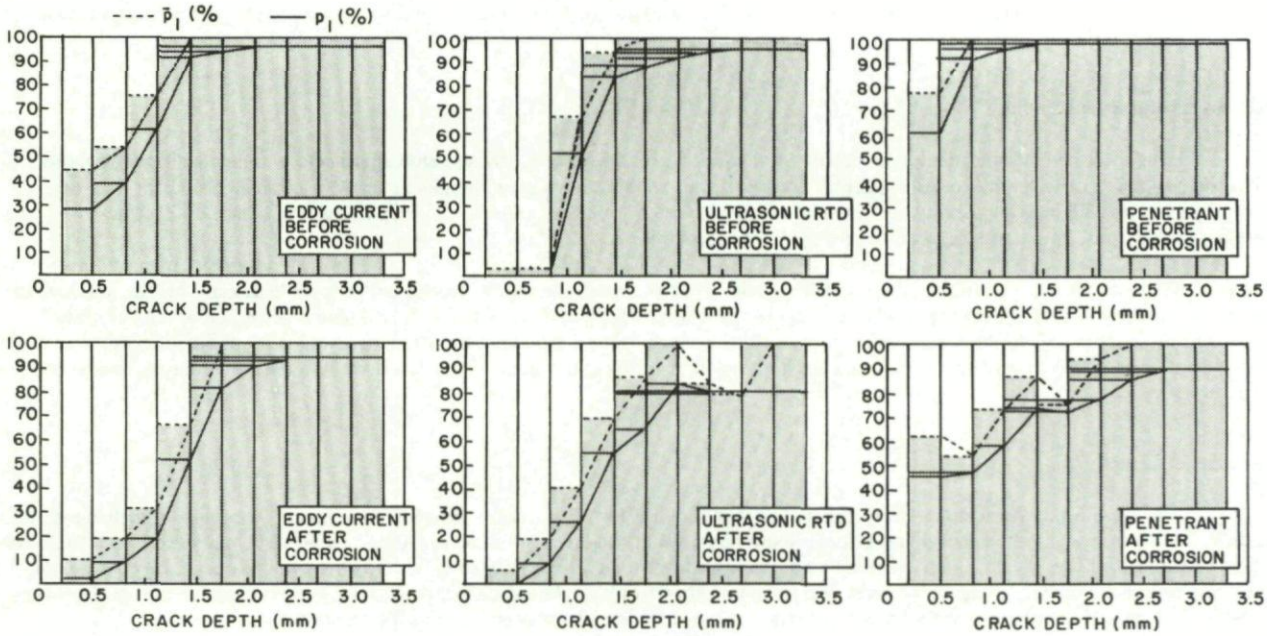

Fig. 5-4 Plots of POD vs. crack depth

The dashed horizontal lines represent the point estimates ($\bar{p}$) in every interval, the area underneath has been shaded. The continuously drawn horizontal lines give the lower limit (p_ℓ) of the 95% confidence interval with the available data grouped according to the optimized probability method. To produce conservative graphs both types of calculated data were considered to be applicable to the largest flaw in each interval; therefore the right hand sides of the horizontal lines were connected (Ref. 5-3).

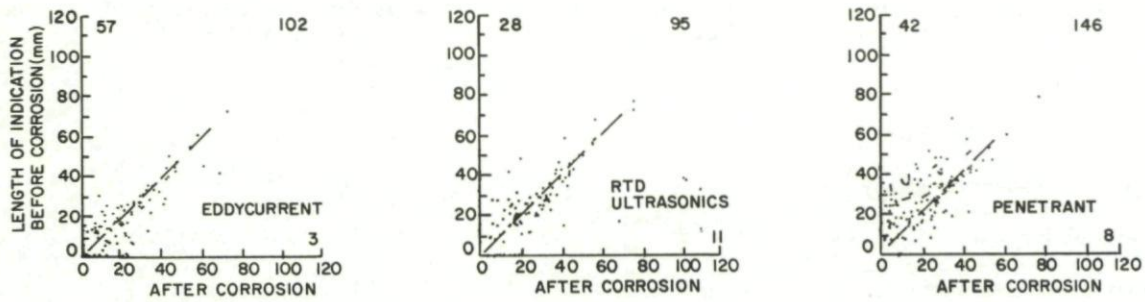

Fig. 5-5 Comparison between inspection indication lengths before and after exposure to corrosion (Ref. 5-3)

5.5 Liquid Penetrant Inspection (LPI)

Liquid penetrant inspection is a physical-chemical NDI method used to detect and expose surface discontinuities, such as cracks, porosity, laps, seams and other surface defects. The method can be applied rapidly, economically and with a high degree of reliability. The surface length of a defect can be determined but not its depth. The method can be used to detect cracks whether they be due to fatigue, corrosion fatigue, stress corrosion cracking, or intergranular corrosion cracking. However, as stated in Section 5.3, it becomes less reliable when the component is uniformly and heavily corroded. Surfaces for examination must be accessible for visual or optical inspection, and must be clean, dry and preferably free from oxide scales and coatings. Clearly therefore, the method is not useful for determining the depth of uniform corrosion on a surface.

The technique employs oil or water based solutions with good wetting characteristics which are wiped or sprayed onto a surface. The penetrants contain coloured dyes which are clearly visible under white light, or fluorescent dyes which respond to ultra-violet light. The penetrant will seep into a surface connected crack and the surface excess is removed. The presence of the crack is then indicated under the appropriate illumination by the penetrant seeping out of the crevice. A developer may be used to enhance the indications by the penetrant.

LPI is outstanding for its simplicity and remarkable sensitivity in revealing very small surface cracks and surface-connected discontinuities. Equipment varies from a simple kit of cleaning agents and aerosol spray penetrant to major automated installations (Ref. 5-7). In its simplest form the technique can be applied to aircraft in the field and power supplies are not required. Many penetrants and developers provide magnification of the width of fine cracks allowing otherwise invisible cracks to be detected. Also the colour or brightness contrast of penetrants provides a further aid, both for visual inspection and automated inspection systems. These latter typically involve television cameras or flying-spot laser scanners with photo-electric detectors which are used to produce remote displays for computer analysis (Ref. 5-1).

As stated in Section 5.3, LPI becomes less reliable when the component is uniformly corroded. Painted or coated surfaces must be stripped and cleaned prior to inspection, and these coatings must usually be replaced to protect sound parts during subsequent service. In virtually all cases, surfaces must be thoroughly cleaned after liquid penetrant inspection to remove any residues which might cause corrosion.

An excellent review of the methods and materials used in LPI, and its application to engineering problems is given in Reference 5-1.

5.6 Magnetic-Particle Inspection (MPI)

In MPI a magnetic field is induced in the component to be inspected using a magnet or electromagnetic coil. Crack-like discontinuities or cavities at the exposed surface interfer with the induced magnetic field, and the discontinuity is revealed by the pattern produced by magnetic particles attracted to the surface. The advantage of MPI over LPI is its ability to reveal discontinuities filled or coated with contaminants that could prevent entry and formation of indications by liquid penetrant.

In practice magnetic-particle inspection is severely limited in all aircraft applications because it is limited to magnetic materials, the components must be made part of an electrical or magnetic circuit, and magnetized components must be demagnetized after inspection and all magnetic particles must be removed. The majority of aircraft materials are non-magnetic, and for the few magnetic components, the requirements for magnetization and demagnetization are difficult to satisfy without removing the component from the aircraft. Also, false indications can be obtained in parts containing screw threads or sharp changes in section. As with LPI, the method can only be used on visibly or optically accessible surfaces and only for detecting sharp and relatively clean cracks.

5.7 Radiography

Radiography is based on the differential absorption of penetrating radiation by the component being inspected. The radiation may be electromagnetic radiation of very short wavelength such as x-rays or γ-rays, or particulate radiation such as a neutron beam. When the component is bathed in radiation differential absorption may occur in the component due to local variations in thickness or composition. The unabsorbed radiation passing through the part may be recorded on a film to produce a permanent image or viewed on a fluorescent screen or image-intensifier as a real time image. These latter methods are sometimes referred to as fluoroscopy.

Radiographic examinations are carried out by NDT operators to detect corrosion in areas of aircraft such as the internal surfaces of skins, stringers, engine-bearer tubes and the mating surfaces of rivetted structures. The suitability of radiography to detect service induced degradation of engineering alloys has been summarized in Reference 5-8, as shown in Table 5-2. This table deals with engineering alloys in a general sense and problems may arise when these methods are applied to actual engineering components or structures which are characteristic of the particular application. For example in aircraft structures the presence of chromate paints, Redux bonding and various jointing compounds reduces the sensitivity of the technique. Also, loss of material or change in density must occur for radiographic methods to be successfully employed. This does not always take place, especially when the corrosion is between mating surfaces. Corrosion of metals usually has only a small net effect on the absorption of x-rays and, except where corrosion is advanced, only low-contrast detail is obtained on a radiograph. As a consequence of these problems the early stages of corrosion are difficult to detect. Also, the complex structure of an aircraft limits the coverage which can be obtained and consequently radiographic corrosion-detection techniques are restricted to areas of relatively simple construction.

One factor limiting the detection of defects by radiography is poor contrast in the x-ray film. A recent development has been the use of image enhancement techniques to increase contrast in those parts of the image corresponding to regions where corrosion might be expected to occur. Packer (Ref. 5-9) digitized radiographs of corroded 7075-T6 specimens using a spatial resolution of 100 μm and 256 uniformly spaced grey levels to quantitize the data. Contrast in regions of interest around fastener holes was enhanced by expanding the grey scale in appropriate ranges and compressing bands of lower interest. The detection of corrosion was made much easier, and it was suggested that further analysis of the digitally processed image might lead to a method for determining the sequence of events in regions where corrosion had occurred.

Table 5-2 Suitability of three radiographic methods for inspection of light and heavy metals

	Light Metals			Heavy Metals		
	X-ray	Fluoroscopy	γ-ray	X-ray	Fluoroscopy	γ-ray
Fatigue cracks	F(a)	U	P(a)	P	U	P
Stress corrosion	F	U	P	F	U	P
Blistering	P	U	P	P	U	P
Thinning	F	P	F	F	P	F
Corrosion pits	F	P	P	G	P	P

G = Good, F = Fair, P = Poor, U = Unsatisfactory.
(a) = Radiation must be parallel to the cracks.

5.8 Ultrasonic Inspection

In ultrasonic inspection high frequency sound waves are introduced into the material being inspected to detect surface and subsurface flaws. The sound waves travel through the material with some attendant loss of energy (attenuation) and are reflected at interfaces. The reflected beam is detected and analyzed to define the presence and location of flaws. Most ultrasonic inspections are performed at frequencies between 1 and 25 MHz, and the instrumentation will attempt to measure one or more of the following:

- reflection of energy at an interface in the specimen
- time of transit of a wave through the specimen
- attenuation of the beam of sound waves by absorption and scattering in the specimen.

These measurements are made either by the pulse-echo method, or the through transmission method. In the pulse-echo method short bursts of ultrasonic energy are introduced into the test article at regular intervals of time. If the pulses encounter a reflecting surface some or all of the energy is reflected. The proportion of energy reflected is dependent on the size of the reflecting surface in relation to the size of the incident beam. The direction of the reflected beam depends on the orientation of the reflecting surface with respect to the incident beam. Both the amount of energy reflected in a specific direction and the time delay between transmission of the initial pulse and receipt of the echo are measured. In transmission testing flaws are detected by comparing the intensity of ultrasound transmitted through the test piece with the intensity transmitted through a reference specimen. Transmission testing can be performed either with direct beams or reflected beams, and it requires two ultrasonic heads, one to transmit the beam and a transducer to receive it.

The reflection of a wave at a surface depends on the physical state of the interface and the process is more efficient for gas/solid interfaces than for liquid/solid or solid/solid interfaces. Thus when applied to corrosion problems, the method can be useful for detecting crack-like discontinuities such as stress corrosion cracks, intergranular corrosion cracks, corrosion fatigue cracks or deep pits. The sensitivity of the method decreases when the cracks are filled with dense, chemically bonded oxide scales since these effectively change the nature of the interface.

In order to detect corrosion with ultrasonic methods on one surface of a component, access to the other side of the component or exceptionally to the same side must be available. This access is not always possible. Also the conventional methods of ultrasonic inspection are less reliable on thin-gauge materials than on thick sections, and therefore only severe corrosion can be detected.

Some recent research efforts have concentrated on the application of computer based pattern recognition procedures for differentiating between stress corrosion cracks and other defects in metal structures (Ref. 5-10), and the use of deconvolution procedures to increase the time resolution of signals from corroded thin plates (Ref. 5-11). Further work in these areas may resolve some of the problems now affecting aircraft corrosion inspection.

5.9 Eddy Current Inspection

In eddy current inspection a coil carrying an electrical current is brought into close proximity with the part to be tested to cause an eddy current to be set up in the part by induction. The method involves electromagnetic induction and does not rely on direct electrical contact with the part. The part to be inspected must be electrically conductive and may be made of a ferromagnetic or non-ferromagnetic material. The induced currents in the part flow within closed loops and their magnitude and phase depend on the primary field established by the excitation current, the electrical properties of the part and the electromagnetic fields established by the currents flowing within the part. The excitation current is kept low to minimize heating in the part and frequencies are usually in the range 200 Hz to 6 MHz, depending on thickness of the part to be inspected, the desired depth of penetration, the degree of sensitivity or resolution required, and the purpose of the inspection. The lower the frequency in the inspection coil the greater is the penetration of the induced current in the part.

The induced electromagnetic field is affected by the presence of cracks in the part or the presence of non-conductive or non-magnetic coatings on a conductive or magnetic base metal. The condition of a part can be monitored by observing the effect of the resulting field on the electrical characteristics of the exciting coil, such as its electrical impedance, induced voltage or induced currents. Alternatively, the effect of the electromagnetic field can be monitored by observing the induced voltage in one or more other coils placed within the field near the part being inspected. The techniques and equipment used for eddy current inspection are described in detail in Reference 5-8.

Eddy current inspection is used extensively for detecting fatigue, corrosion fatigue, stress corrosion and intergranular corrosion cracks in airframe structures and engine components. Several commercial instruments are available with specially designed probes for inspection of fastener holes and some are capable of dealing with holes with fasteners installed.

An application of eddy current inspection for the measurement of corrosion depth in thin sheet aluminium specimens has been described in Reference 5-12. The specimens were riveted and adhesively bonded lap joints in 1.25 mm thick sheet, with a reinforcing stringer as shown in Figure 5-6. This specimen is typical of modern aircraft construction and corrosion is known to occur both in the lap joint and on the rear surface of the skin. Ultrasonic thickness gauges were found to be unsuitable for this inspection because of the number of interfaces in the joint and the thin gauge of the skin. An amplitude sensitive eddy-current gauge also gave spurious readings due to thickness changes, dents and other irregularities. However, by using a phase and amplitude sensitive eddy current inspection system and tuning the coil frequencies to suit the thickness of the sheet a clear phase separation was obtained to distinguish between the effects of corrosion and the bond line spacing. The phase relationships for three frequencies are shown in Figure 5-7. From Figure 5-7(b) at 28 KHz, which provided the optimum tuning for the 1.25 mm thick skin, the approximate depth of corrosion on the back face could be determined. The method was used for sheet specimens ranging in thickness from 0.8 mm to 3 mm using frequencies from 5 KHz to 30 KHz, and the minimum depth of corrosion was found to be about 5% of skin thickness.

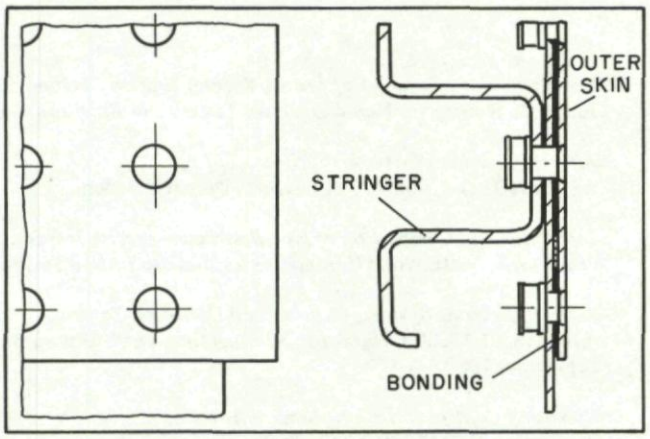

Fig. 5-6 Outer skin lap-joint produced with adhesively bonded sheet of various thicknesses and a riveted stringer (Ref. 5-12)

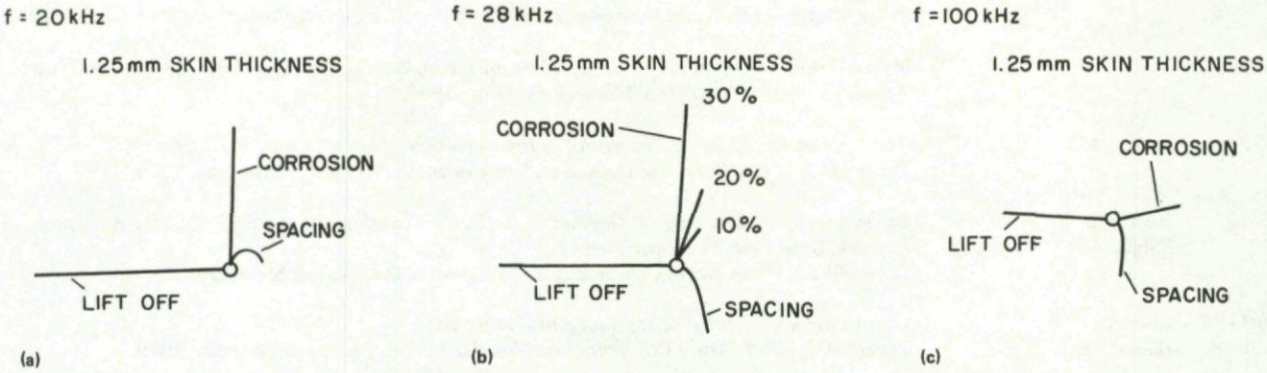

Fig. 5-7 Eddy current indications obtained using phase and amplitude sensitive equipment with the assembly shown in Figure 5-6. Plots (a) to (c) show the effects of frequency, plot (b) shows the optimum phase separation between back face corrosion and aluminium sheet spacing for 1.25 mm thick sheet

5.10 Acoustic Emission

Acoustic emission is defined as the high-frequency stress-waves generated by the rapid release of strain energy that occurs within a material during crack growth, plastic deformation or phase transformation. This energy may originate from stored elastic energy as in crack propagation, or from stored chemical free energy as in phase transformation (Ref. 5-8). Acoustic emissions can be detected and recorded to provide information on the intensity and rate of occurrence of acoustic events. The typical equipment is described in Reference 5-8.

Acoustic emission can be used in the detection of subcritical growth of flaws, such as fatigue crack growth, stress corrosion cracking and hydrogen embrittlement. The technique is capable of detecting growing flaws at least an order of magnitude smaller than those detectable by any other known non-destructive testing method and is capable of locating one or more discontinuities while they are growing (Ref. 5-14). When the discontinuity approaches critical size, the acoustic-emission count rate increases markedly, warning of impending instability and failure.

As indicated above, acoustic emission has been used to detect crack propagation due to stress corrosion cracking, but it also has the potential to detect general corrosion in its early stages and at hidden interfaces. The early applications of acoustic emission

monitoring to corrosion have been reviewed in Reference 5-15. The majority of subsequent applications have involved the detection of corrosion induced crack growth. Thus a number of studies have been carried out of stress corrosion crack growth, including intergranular crack growth in welded stainless steels (Ref. 5-16) and aluminium alloys (Refs. 5-17 and 5-18). In a study of exfoliation corrosion the authors, Reference 5-19, suggested that acoustic emission was not expected because of the purely electrochemical nature of the corrosion process, however they found that AE signals varied over a wide range depending on transducer location. Reference 5-20 studied galvanic corrosion of aluminium alloys and suggested that acoustic emissions in these alloys occur as a result of hydrogen formation in pits. Reference 5-15 has reviewed the information available on the nature of the acoustic emission events associated with corrosion and has concluded that such events can be readily detected and are not always due only to hydrogen bubble formation. This paper also reviews some applications of AE to aircraft corrosion inspection. In one application an AE system was used to detect hidden corrosion in honeycomb material in the F-111 aircraft. The ingress of moisture to metal honeycomb material causes corrosion which is concentrated in the bond region and therefore leads to local bond failure. A single transducer was used to scan the surface of the structure until the source of acoustic activity was located. Since the honeycomb material was highly attenuative to sound waves it was necessary to inspect within 150 mm of the source to detect the corrosive reaction. Local heating was also used to increase the corrosion reaction rate and to generate detectable noise from differential expansion at regions of disbond.

5.11 References

5-1		Non-destructive Testing Handbook, Second Edition, Volume 2, Liquid Penetrant Inspection, American Society for Non-destructive Testing and American Society for Metals.
5-2		*Aircraft Corrosion Control.* AP-119A-0201-1, Ministry of Defence, United Kingdom.
5-3	De Graaf, E.A.B. De Rijk, P.	*Evaluation and Comparison of Non-destructive Service Inspection.* Paper 4A-1, Ninth World Conference on Non-destructive Testing, Melbourne, Australia, 1979.
5-4		*Aircraft Weapons Systems Cleaning and Corrosion Control.* NAVAIR 01-1A-509, Naval Air Systems Command, United States Department of Defence, September 1980.
5-5		*Corrosion Control and Precautions — Aircraft.* Publication No. C-12-010-040/TR-021, Canadian Department of National Defence, September 1978.
5-6	Shaffer, I.S.	*Corrosion In Naval Aircraft Electronic Systems.* Paper No. 13, AGARD Conference Proceedings No. 315 on Aircraft Corrosion, 1981.
5-7	Borucki, J.S.	*Utilization of the Zyglo Hydrophilic Penetrant System for Improved Process Control, Inspection Reliability, Water Conservation and Pollution Control.* Paper 4A-12, Ninth World Conference on Non-destructive Testing, Melbourne, Australia, 1979.
5-8		Metals Handbook, Volume 11 (Eighth Edition): Non-destructive Inspection and Quality Control, American Society for Metals, Metals Park, Ohio, 1976.
5-9	Packer, M.E.	*The Application of Image Processing to the Detection of Corrosion by Radiography.* Paper 4D-7, Ninth World Conference on Non-destructive Testing, Melbourne, 1979.
5-10	Rose, J.L. Singh, G.P.	*Stress Corrosion Cracking vs. Geometric Reflector Classification Analysis for 304 Austenitic Stainless Steel Pipe Weld Specimens.* Paper 3B-12, Ninth World Conference on Non-destructive Testing, Melbourne, 1979.
5-11	Forli, O. Haugen, R.	*Corrosion Detection by Ultrasonics and Radiography.* Paper 2A-4, Ninth World Conference on Non-destructive Testing, Melbourne, 1979.
5-12	Nagel, G. Schur, F.	*Application of Low Frequency Eddy-Current For Inspection of Civil Aircraft.* Paper 2A-2, Ninth World Conference on Non-destructive Testing, Melbourne, 1979.
5-13	Funke, G. Pawlowski, Z.	*Acoustic Emission and Fractographic Analysis Applied to the Estimation of Crack Growth During Low Cycle Fatigue.* Paper 3K-10, Eight World Conference on Non-destructive Testing, Cannes, 1978.
5-14	Hartbower, C.E. Morais, C.F. Reuter, W.G. Crimmins, P.P.	*Development of a Non-destructive Testing Technique to Determine Flaw Criticality.* AFML-TR-71-218, Air Force Materials Laboratory, Wright Patterson Air Force Base, Ohio, 1972.
5-15	Scott, I.G. Wilson, L.	Materials Note 122, Aeronautical Research Laboratories, Melbourne, 1978.
5-16	Stahlkopf, K.E. Hutton, P.H. Zebroski, E.L.	Publication 1976-10 75-83, Institution of Mechanical Engineers, 1976.
5-17	McIntyre, P. Green, G.	British Journal of Non-destructive Testing, 20, 1978, pp. 135-140.

5-18	Dickson, J.I. Martin, P. Bailon, J-P.	Materials Science and Engineering, 58, 1983, pp. L5-L8.
5-19	Bakulin, A.V. Malyshev, V.N.	Protection of Metals, 14, 1978, pp. 157-160.
5-20	Mansfeld, F. Stocker, P.J.	J. Electrochemical Society, 1301-2, 1977.

CHAPTER 6

PREVENTION AND CONTROL OF CORROSION IN AIRCRAFT

6.1 Introduction

It has been stated (Ref. 6-1) that the present state-of-the-art in aircraft structural technology should allow a design objective of at least 20 years of operational life free from significant corrosion to be achieved. However to meet this objective requires a full awareness of the consequences of corrosion and careful attention to detail at all stages in the design, manufacture, assembly, and eventually the use and maintenance of aircraft. It is also generally recognized that careful attention to detail at the design stage in terms of materials selection, surface preparation, and design detail will lead to significant cost benefits over the life of the aircraft, although the initial procurement costs may be increased. The corrosion requirements of most aircraft structural assemblies and components will be satisfied if the following are taken into consideration;

(a) proper choice of environmentally stable materials,

(b) parts should be designed to minimize exposure of corrosion prone 'end' grain boundaries to moisture,

(c) parts should be designed to prevent the ingress and accumulation of moisture,

(d) protective treatments or surface coating should be carefully selected to enhance corrosion resistance of components operating in particularly aggressive environments,

(e) assembly techniques should be used to avoid damage to protective coatings and to seal structure against moisture penetration,

(f) parts should be designed to allow access to all areas of structure for inspection and maintenance,

(g) inhibitors and water displacing fluids may be used for supplementary protection but should not be relied upon as the primary form of corrosion protection,

(h) since corrosion is inevitable in the long term, some allowance should be made for the effects of corrosion in the initial design.

6.2 Materials

Materials for structural applications must meet a wide range of design requirements, not the least of which are high static yield and ultimate strengths, high stiffness, fatigue and fracture mechanics properties, good formability and low cost. However since the economic life of an aircraft may be limited by corrosion, rather than fatigue, it is important that corrosion resistance be given due consideration during the design stage.

Operating experience with aircraft has led to the identification of several structural materials which should not be used in aircraft structures. These include the following.

Aluminium alloys such as 7079-T6 in all forms, and 7075-T6 plate, forgings or extrusions should be avoided because of their inferior stress corrosion resistance. It should be noted that 7079 does not respond to the T76 and T73 averaging treatments for improved corrosion resistance, as 7075 does, and therefore the effectiveness of treatments of this type must be established for any new 7000 series alloys that are introduced. Alloys such as 7178 and 2020 are generally not recommended, and the International Air Transport Association has recommended they not be used (Ref. 6-1). References 6-2 and 6-3 have provided tables showing the relative susceptibilities of various aluminium alloys to general corrosion, exfoliation corrosion and stress corrosion cracking. Both references provide information on the effects of product form, and include data on thin sheet, plate, tube, extruded bar and sections, and forgings. Reference 6-3 provides information on the effects of grain orientation, while Reference 6-2 provides additional information on the relative susceptibilities of various steels to stress corrosion cracking and includes data on bars and forgings, bolt stock, sheet and plate, tube, and castings. These two references provide a broad data base that may be useful in the selection of material during preliminary design.

Although having reasonably good corrosion resistance in mild environments, magnesium alloys suffer severe pitting in aggressive environments, and particularly when natural protective coatings or artificial coatings are damaged. Because of their position in the galvanic series they suffer severe corrosion when coupled with conductive dissimilar materials. Corrosion of magnesium alloys is also difficult to inhibit and while chromates can be effective, much higher concentrations are required than can be achieved by leaching chromate pigments from a paint film. The United Kingdom Ministry of Defence has developed specifications for the corrosion protection of magnesium alloy structure, and these involve a complex process involving mechanical and chemical cleaning, chromate filming or anodizing, sealing by the application of a stoving epoxy resin in several layers, and finally one or more coats of epoxy paint primer and one or more coats of paint finish or a plastic (e.g. nylon) coating (Ref. 6-2). The aim is to completely encapsulate the magnesium and to isolate it from the environment and where possible from any surrounding structure. This latter however may not be possible with studs or interference fit bushings, and in these cases maximum use should be made of sealants and caulking compounds to provide a barrier through which moisture diffusion is minimized. Notwithstanding these measures, there is concern over the use of magnesium in aircraft structures, and Reference 6-1 has recommended against its use.

Titanium alloys are generally resistant to corrosion in aircraft structures and they provide strong resistance to corrosion in chloride containing solutions, as discussed in Chapter 4. However they are rapidly attacked by phosphate ester fluids at high temperatures, and this type of exposure can lead to severe corrosion. Also, as noted in Table 3-3, cadmium may penetrate titanium under certain circumstances and cause embrittlement, and contact between these two metals should therefore be avoided.

Non-corrosion resistant steels should not be used in high temperature areas, and high strength maraging steels which have been used in the past for bolts have a poor record of failures due to hydrogen induced delayed static failures or stress corrosion cracking, and their use in bolts is therefore not recommended by some authorities. For example, Reference 6-1 includes maraging steel bolts in a list of materials that should be "prohibited in structural applications except in controlled situations", where "controlled" refers to complete part development, from design through manufacture to aircraft application, and must account for all environmental aspects.

Materials which absorb moisture should be avoided. A basic aim in aircraft design is to exclude moisture and prevent the build up of pools of water, and this is dealt with later under design principles. However, this objective will be aided if internal pockets are filled with adherent, inert, non-porous and lightweight materials (Ref. 6-2). The use of moisture absorbent porous materials should be avoided. Similarly the use of structural adhesives, such as the cold curing adhesives which are sometimes used to improve the dynamic strength of riveted joints, should be used with caution since they absorb moisture and may cause corrosion in the joint. These adhesives should only be used on anodized surfaces which are pre-treated with corrosion inhibiting adhesive primer. The use of phosphoric acid anodizing has been recommended (Ref. 6-4). Structures manufactured in this manner require appropriate mechanical and environmental testing.

One of the most important requirements in aircraft structural design is that of galvanic compatibility between dissimilar structural materials in contact. Materials selection must therefore be carried out early in the design process, using information such as that given in Table 3-3. This allows compatible materials to be selected and their strength and damage tolerance limitations to be recognized early in the design process. Where significant galvanic potentials cannot be avoided, even greater attention must be paid to detailed design and assembly to ensure a corrosion free structure over the targeted design life. Further information on these points is given later. Further information on the corrosion resistance of specific airframe alloys is given in Chapter 4.

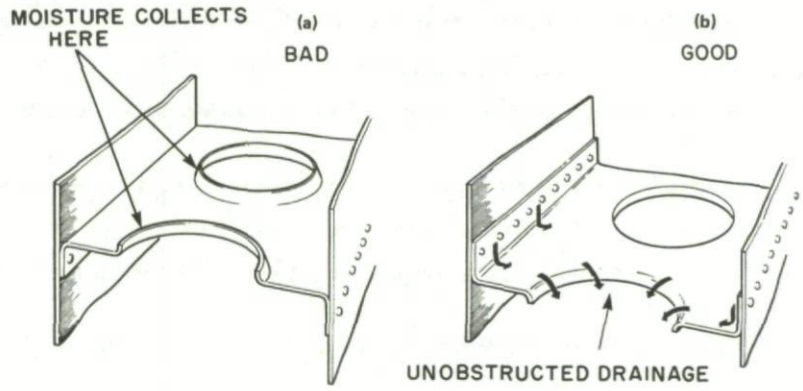

Fig. 6-1 Lightening holes in horizontal diaphragms

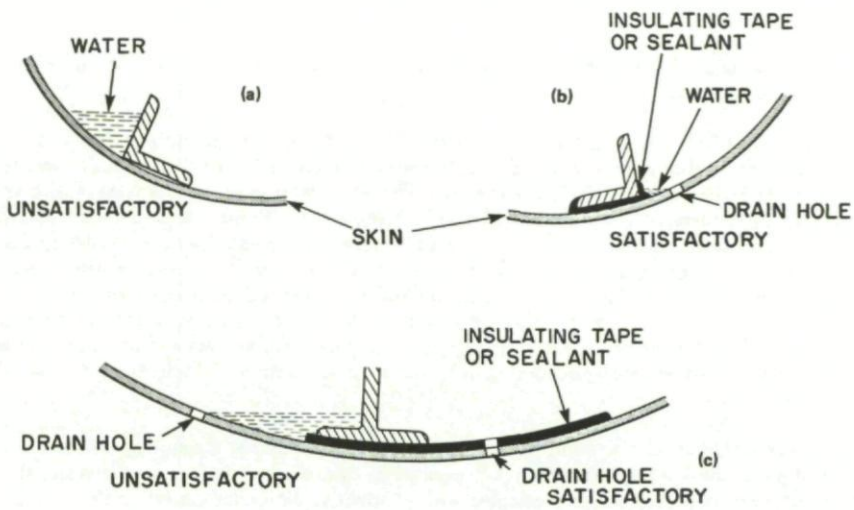

Fig. 6-2 Water traps and faying surfaces

6.3 Design Principles

The requirements for corrosion prevention and control should be considered at all stages of the design process. The aim should be to ensure that the final structure is of an optimum configuration, not only for immediate flight performance, but also to allow manufacture, assembly, and in-service inspection and maintenance to be performed easily and in a manner that will maintain the quality of the structure and its ability to resist corrosion.

During preliminary design, basic structural shapes should be considered to avoid those which introduce natural traps for water or other corrosive fluids. Channel-type structures or U-section structures should be arranged where possible with the open side facing downward so that moisture will not collect in the bottom of the channel, and all areas of structures where moisture may collect should be provided with drainage holes. This applies particularly in the case of closed, or box structures which may be difficult or impossible to gain access to for inspection. In these cases multiple holes in the lower surface will not only aid drainage, but will allow free circulation of air to help drying and avoid condensation. Drainage holes should always be located in gravity fed areas, and the internal structural details so arranged to allow moisture to run freely to the drain for escape. Similarly, flanges or lips on sheet metal structures should be directed downwards to allow moisture to run freely over their edges to escape. This point is illustrated in Figure 6-1, with reference to the design of a lightening hole in a horizontal diaphragm (Ref. 6-5).

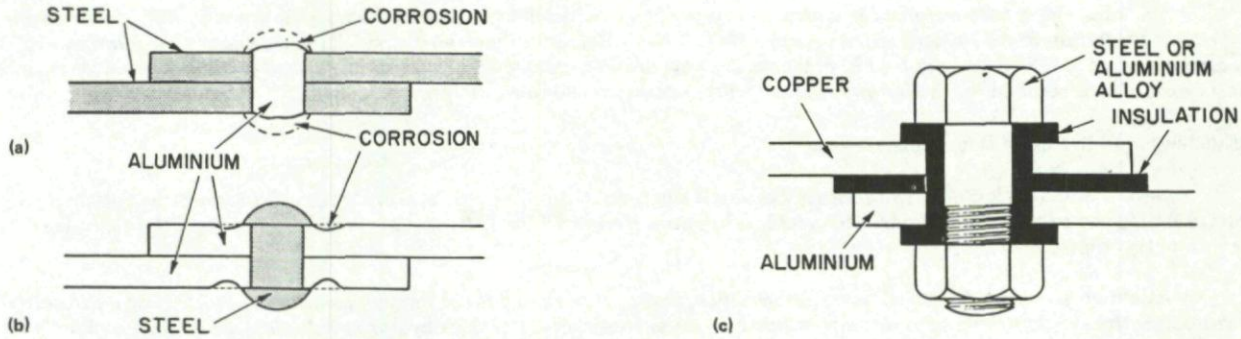

Fig. 6-3 Dissimilar-metal corrosion (bolted and riveted joints). (Ref. 6-5)

The first requirement in design is to avoid the initial entry of moisture into the structure, and where possible this is achieved by sealing. However since this is impossible to achieve in practice, all parts should be designed to allow access for inspection, and have geometries which are easily cleaned and repaired. Sharp corners and cavities where dirt and moisture can collect should be avoided, and curved surfaces should have a large radius to facilitate cleaning, inspection and repair.

Faying surfaces provide natural crevices where moisture may collect and corrosion occur, assisted in a detrimental sense by mechanical interactions at the interface and any galvanic differences between the contacting metals. Faying edges should be sealed in all cases, and where dissimilar metals are involved interface compounds or films should be inserted to isolate the metals. Many of the sealants presently in use are heavily enriched with chromates which provide additional protection as inhibitors. Figure 6-2 illustrates the use of an insulating tape or sealant at a faying surface formed between a fuselage skin and an angle section of an internal stiffener. This figure also illustrates the correct location of drainage holes, and demonstrates that the isolation of dissimilar metals must take into account the natural water level of any small pools that may collect.

Mechanically fastened joints invariably involve dissimilar metals, either in the structural members being joined or the fastener which holds them together. The detailed design of joints is therefore a matter requiring careful attention. Figure 6-3(c) shows one method of dealing with a bolted or riveted joint where the fastener and the sheet materials are all dissimilar. The aim of this design is to avoid metal-metal contact in all areas. It also ensures that the fastener which provides the smallest surface area is made of the most cathodic material so that in the event of a breakdown in the protection system the requirement of large anode and small cathode, as indicated in Figure 6-3(b), is maintained. In recent years there has been a move towards "wet installation" of fasteners where the fastener hole is filled with an inhibiting sealing compound prior to insertion of the fastener. This leaves a film of sealant between the bore of the hole and countersink and the shank and head of the fastener to provide insulation and to prevent moisture from penetrating. This practice is now generally recognized as an effective measure for preventing corrosion. In butt-joints the same precautions must be taken to exclude moisture from crevices. Usually a gap of between 2 and 5 mm is left between the ends of the plates or sheet and the joint is made through a backing plate or strap. The butt-joint gap is then filled with sealant so that the sealant forms a head overlapping the butting ends. Typical arrangements are shown in Figure 6-4. The exposed edges of butt and lap joints should be sealed in a similar way, as indicated in Figures 6-5 and 6-6.

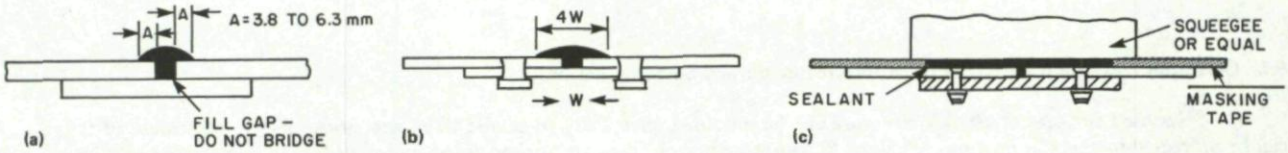

Fig. 6-4 Sealing butt-joint gaps

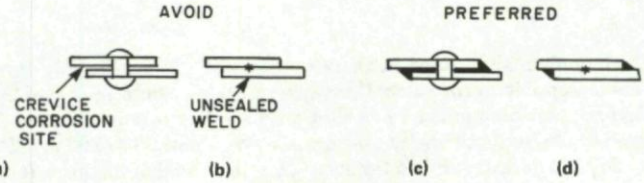

Fig. 6-5 Sealing of a butt joint

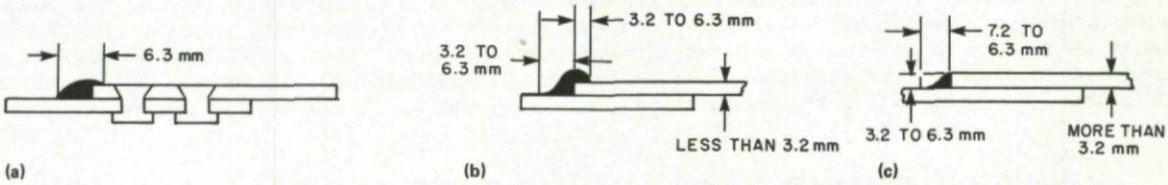

Fig. 6-6 Sealing lap joints

The most widely used material for sealants are polysulphides, cross-linked to remain elastomeric down to -60°C, and capable of operating for the life of the airframe at temperatures up to 120°C (Ref. 6-2). Fluorcarbons which remain elastomeric down to -15°C and can be used up to 200°C are used for higher temperature applications. Non-setting materials are used as jointing compounds in areas where disassembly is required for routine servicing and where sealants would cause problems (Ref. 6-2).

6.4 Attention to Corrosion During Manufacture

Review of the corrosion case histories of Section II will reveal that many problems occur because of insufficient attention to detail during component manufacture. This problem has been recognized by Scolaris (Ref. 6-4), who has listed the following precautions that should be taken.

Attention should be paid to all forms of machining, heat treatment, and metal forming processes to avoid residual stresses. Since residual stresses may contribute to problems such as stress corrosion cracking or hydrogen induced delayed static failure in otherwise lightly loaded structures, they should be eliminated before proceeding with the next stage of manufacture.

Corrosion may occur during the manufacturing process itself, and while this may not be serious on its own, it may provide initiation sites for further corrosion damage or mechanical damage in service. The temporary protection and cleanliness of parts during manufacture and storage should therefore be recognized as priority requirements.

Several cases can be found in Section II where corrosion occurred because of the removal of previously applied corrosion protection systems during hole drilling or boring operations. If this is unavoidable, a corrosion protection system at least as effective as the original one should be applied later. Such drilling operations may be particularly damaging if they expose grain boundaries lying perpendicular to the short transverse direction in plate or extruded products. This is because of the susceptibility of transverse grain boundaries to stress corrosion cracking. The same concern arises during machining of thick section components, and the designer can partly alleviate these concerns by selecting preforms, such as forgings, in which the grain flow follows as closely as possible the final contour of the finished part. This principle is illustrated in Figure 6-7, where the length of the horizontal leg in Figure 6-7(b) is increased over that shown in Figure 6-7(a). This leads to improved grain flow in the forging where fewer transverse grain boundaries are exposed to the environment by machining.

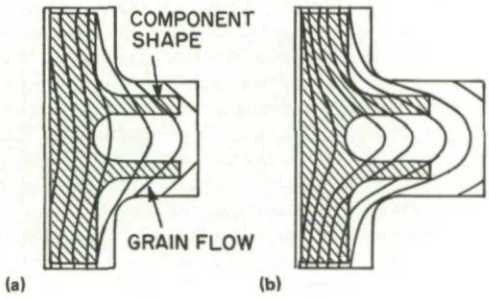

Fig. 6-7 Improving grain flow (Ref. 6-5)

6.5 Corrosion Prevention Through Protective Treatments and Surface Coatings

Exposed surfaces of aircraft structure can be modified chemically to render them less susceptible to corrosion, or they can be protected by metallic coatings or paints. Processes such as cladding are applied at the mill stage by the manufacturers of sheet, plate or tubing. Processes such as anodizing, chromate filming or plating are usually applied by the aircraft manufacturers or their subcontractors. Surface pre-treatment by chemical or mechanical means is also important in painting, and the methods used are designed to ensure good adhesion of the paint to the alloy surface. The methods used for surface preparation prior to painting depend on the type of alloy to be protected, as indicated in Table 6-1.

6.5.1 Cladding

Many of the high strength aluminium alloys used in aircraft structures, and particularly those containing copper as the principal age hardening constituent are susceptible to corrosion. Corrosion resistance can be improved by metallurgically bonding to the susceptible core alloy a surface layer of pure aluminium, or an alloy with good corrosion resistance. The cladding is selected not only to have good corrosion resistance but also to be anodic to the core alloy by about 80 to 100 mv. Thus if the cladding becomes damaged by scratches, or if the core alloy is exposed at drilled fastener holes, the cladding will provide cathodic protection by corroding sacrificially. Because of the cathodic protection provided by the cladding, corrosion progresses only to the core/cladding interface and then spreads laterally, thus helping to prevent perforations in thin sheet. The cut edges of the clad product should be protected by the normal aircraft finish, or by jointing-compound squeezed out during wet assembly.

For aluminium-copper alloys (2000 series) dilute aluminium alloys such as 1230, 6003 or 6053, containing small amounts of manganese, chromium or magnesium may be used as cladding material. These contain low copper contents, less than 0.02%, and low iron content less than 0.2%. However these alloys are not sufficiently anodic with respect to the Aℓ-Zn-Mg-Cu alloys of the 7000 series, and they do not provide cathodic protection in these cases. The 7000 series alloys are therefore usually clad with aluminium alloys containing about 1% zinc, such as 7072, or aluminium-zinc-magnesium alloys such as 7008 and 7011, which contain higher zinc contents.

The thickness of the cladding is usually between 2% and 5% of the total sheet or plate thickness, and since the cladding is usually a softer and lower strength alloy, the presence of the cladding can lower the fatigue strength and abrasion resistance of the

Table 6-1 Typical protection schemes for aluminium, magnesium and non-corrosion resistant steels. Derived from Reference 6-2

Treatment	Aluminium alloys	Magnesium alloy castings	Non-corrosion resistant steels
1. Cleaning	One or more of the following: (a) degrease (b) alkaline clean (c) abrasive clean (d) pickle or etch	(a) Preliminary cleaning by an approved method, or — rough machining — pickling — chemical milling. (b) Fluoride anodizing.	Various methods are allowed depending on the strength of steel. See Reference 6-2 for typical specifications.
2. Pre-treatment	One or more of the following: (a) anodize (b) chromate film (c) etch primer.	(a) Hard anodize, or (b) Fluoride film removal followed by chromate filming.	Cadmium plate or (a) aluminium, (b) zinc or (c) phosphating.
3. Surface sealing	May be required by anodizing specification, see Reference 6-15.	Sealing by stoving epoxy resins to a minimum thickness of 25 μm. Resins may be chromate pigmented.	
4. Paint primer	Epoxy primer, typically 20 μm or 40 μm minimum thickness depending on corrosion severity.	Chromate pigmented epoxy.	Epoxy.
5. Paint finish (a) interior (b) exterior	Primer only or primer plus. Acrylic or polyurethane, typically 30 μm minimum thickness.	Epoxy or polyurethane.	Depends on position in aircraft as for aluminium alloys.
6. Further protection	Polyurethane finish may be specified where high resistance to polar liquids is required.	Organic coatings such as nylon with a thickness of 100 μm may be used for finishing.	Stoving enamel to replace 5 and 6 where ultra high performance is required.

product. In the case of thick plate where substantial amounts of material may be removed from one side by machining so that the cladding becomes a larger fraction of the total thickness, the decrease in strength of the product may be substantial. In these cases the use of the higher strength claddings such as 7008 and 7011 is preferred.

6.5.2 Surface-conversion coatings

Surface-conversion coatings are produced by chemical action, with or without electrical assistance. The treatments change the immediate surface layer of metal into a film of metallic oxide or compound which has better corrosion resistance than the natural oxide film and provides an effective base or key for supplementary protection such as paints.

Anodizing: This involves the electrolytic oxidation of a surface to produce a tightly adherent oxide scale which is thicker than the naturally occurring film. The oxidized surface is hard and abrasion resistant, and it provides some degree of corrosion resistance. However anodizing cannot be relied upon to provide corrosion resistance to corrosion prone alloys, and further protection by painting is usually required. Fortunately the anodic coating provides an excellent surface both for painting and for adhesive bonding. Anodic coatings break down chemically in highly alkaline solutions (pH > 8.5) and highly acid solutions (pH < 4.0). They are also relatively brittle and may crack under stress, and therefore supplementary protection, such as painting, is particularly important with stress corrosion prone alloys.

Anodic coatings can be formed in chromic acid, sulphuric acid, phosphoric acid or oxalic acid solutions. Chromic acid anodizing is widely used with 7000 series alloys to improve corrosion resistance and paint adhesion, and unsealed coatings provide a good base for structural adhesives. However these coatings are often discoloured and where cosmetic appearance is important sulphuric acid anodizing may be preferred. International standards for chromic acid anodizing include processes performed at 20 v DC and 40 v DC. However processes may be modified so that voltage is increased in a stepwise fashion to 50 v to give an anodic film of about 2 μm thick (Ref. 6-2).

The $A\ell_2O_3$ coating produced by anodizing is typically 2 μm to 25 μm thick, and consists of a thin non-porous barrier layer next to the metal with a porous outer layer that can be sealed by hydrothermal treatment in steam or hot water for several minutes. This produces a hydrated oxide layer with improved protective properties. Improved corrosion resistance is obtained if the sealing is done in a hot metal salt solution such as a chromate or dichromate solution. The oxide coatings may also be dyed to provide surface colouration for decorative purposes, and this can be performed either in the anodizing bath or afterwards. International standards for anodic treatment of aluminium alloys have been published by the International Standards Organization and cover dyed and undyed coatings (Refs. 6-6 to 6-9).

Anodizing treatments are also available for magnesium and titanium alloys. Two treatments are commonly used with magnesium alloys, the Dow 17 treatment and the HAE treatment. These both involve several processing options to produce either thin coatings of about 5 μm thickness for flexibility and surfaces suitable for paint adhesion, or thick coatings, up to about 30 μm for maximum corrosion and abrasion resistance. Details of the solutions used, temperatures, current densities and coating times are given in Reference 6-3, page 603. In the Dow treatment a magnesium flouride coating is formed by anodizing at low voltage and low current density (55-540 A/m^2) in an ammonium hydrofluoride solution.

Anodic coatings are also used on titanium and titanium alloys. When used on fasteners they provide limited protection of less noble metals against galvanic corrosion, and when used together with solid film lubricants they help to prevent galling. One draft international standard has been prepared covering a sulphuric acid process (Ref. 6-10). This process employs a variable current DC power supply to provide an initial current of 0.2 A/dm^2 at 15 to 20 volts which decreases to 0.05 A/dm^2 over the anodizing cycle. The process produces a smooth coating with a uniform texture and appearance, and a uniform blue to violet colour.

Chromate filming: A number of proprietary chromate filming treatments are available for aluminium, magnesium, cadmium and zinc alloys. The treatments usually involve short time immersion in strongly acid chromate solutions, but spraying or application by brushing or swabbing can also be used for touch-up of parts. The resulting films are usually about 5 μm thick, and are coloured depending on the base alloy, being golden yellow on aluminium, dull gold on cadmium and zinc, and brown or black on magnesium. The films contain soluble chromates which act as corrosion inhibitors, and they provide a modest improvement in corrosion resistance of the base metal. However their main purpose is to provide a suitable surface for sealing resins or paints. Epoxy primer, for example, which does not adhere well to bare aluminium, adheres very well to chemical conversion coatings. Among the best known coatings used with aluminium alloys are those produced by the Alodine 1200 or Alocrom 1200 processes. A draft international standard covering chemical conversion coatings for aluminium alloys has been prepared (Ref. 6-11).

A process for zinc alloys has been described in Reference 6-12, to consist of immersion for a few seconds in a sodium dichromate solution at a concentration of 200 g/litre and acidified with sulphuric acid at 8 ml/litre. The treatment is performed at room temperature and is followed by rinsing and drying to produce a dull yellow zinc chromate coating.

Phosphate coatings: A number of proprietary treatments such as 'Parkerizing' or 'Bonderizing' are available for use on steel. They are applied by brushing, spraying or prolonged immersion in an acid orthophosphate solution containing iron, zinc or manganese. For example a solution might contain $Zn\ H_2\ PO_4$ plus $H_3\ PO_4$. The coatings consist of a thick porous layer of fine phosphate crystals, tightly bonded to the steel. The coatings do not provide significant corrosion resistance when used alone, but they provide an excellent base for oils, waxes or paints, and they help to prevent the spreading of rust under layers of paint. Phosphating is not widely used for aircraft structures since electroplated cadmium, although more expensive, is generally considered more effective.

Phosphating should not be applied to nitrided or finish-machined steel, and steel parts containing aluminium, magnesium or zinc are subject to pitting in the bath. Some restrictions apply also to heat treated stainless and high-strength steels (Ref. 6-5).

Nitriding: Steels containing nitride forming elements such as chromium, molybdenum, aluminium and vanadium can be treated to produce hard surface layers providing improved wear resistance. Many of the processes employed are proprietary, but typically they involve exposure of cleaned surfaces to anhydrous ammonia at elevated temperatures. The nitrides formed are not only hard, but also more voluminous than the original steel and therefore they create compressive residual surface stresses. Because of this nitrided steels usually exhibit improved fatigue and corrosion fatigue resistance. Similar beneficial effects can be achieved by shot peening.

Passive films: Austenitic stainless steels and hardenable stainless steels such as martensitic, precipitation hardening and maraging stainless steels are seldom coated but their corrosion resistance depends on the formation of naturally occurring transparent oxide films. These films may be impaired by surface contaminants such as organic compounds, metallic or inorganic materials. Treatments are available for these materials to clean and degrease surfaces and produce uniform protective oxide films under controlled conditions. These usually involve immersion in an aqueous solution of nitric acid and a dichromate solution, and details are given in draft international standards (Refs. 6-13 and 6-14).

6.5.3 Metallic coatings

Metallic coatings are deposited by electroplating, electroless plating, spraying, hot dipping, chemical vapour deposition and ion vapour deposition. The most important coatings in airframes and landing gear structures are cadmium, chromium, nickel, aluminium and zinc. Copper, gold and silver are also used in electrical equipment and occasionally for specialty fastener applications. Copper is used as a base layer in multiple-plate electroplatings, silver is used for anti-fretting purposes, and both silver and gold are sometimes used to provide electrical conductivity in waveguides and at contacts (Ref. 6-5).

Cadmium: Cadmium is widely used as an electroplating on steel fasteners and bearing assemblies because it provides a galvanically acceptable couple with aluminium. Cadmium is also anodic to steel and will cathodically protect the substrate at scratches or gaps in the coating and at cut edges. It also exhibits surface lubricity, conductivity, resists fretting and fatigue, and its corrosion products do not cause binding. Platings are usually deposited from cyanide baths, but baths containing fluoborates or sulphamates are also used. The baths may contain special additives to reduce hydrogen penetration, and the coatings are usually 5 to 25 μm thick.

The use of cadmium introduces four problems. The first problem is that it is highly toxic and environmental protection agencies have been concerned about its release into the environment. Disposal of wastes from cyanide baths is therefore a problem, as is the eventual disposal of the finished coated part. These problems are discussed in Reference 6-2. The second problem is that the electroplating process also exposes parts to cathodically produced hydrogen and since many of the high strength steels involved are highly susceptible to hydrogen embrittlement, stringent requirements exist to bake parts immediately after plating to remove this hydrogen. Most process specifications for cadmium plating include requirements for baking and subsequent testing of coupons to demonstrate absence of embrittlement. The problem of hydrogen embrittlement can be avoided by applying cadmium coatings by an ion-vapour deposition process which does not produce hydrogen. This process is sometimes used on very high strength steels where hydrogen would be difficult to remove by baking. Once deposited these coatings are essentially similar to electro-deposited coatings, and should receive the same type of additional paint protection. The third problem is that cadmium has been reported to cause solid metal embrittlement both of steel and titanium alloys (Refs. 6-15 and 6-16). Finally, cadmium has also been reported to cause exfoliation corrosion of susceptible aluminium alloys when used on fasteners in contact with these alloys in a riveted or bolted structure (Ref. 6-17).

Chromium: Chromium is used as a protective coating providing resistance to wear, abrasion and corrosion. It has a hardness in the range 900 to 1100 HV, low friction characteristics and high reflectivity. It is used as a thin coating, usually in the range 0.2 to 1 μm thick, as the final layer in a multiple-plate copper-nickel-chromium electroplating, or as a thick coating up to 300 μm to provide wear resistance. When used as a constituent of a multiple-plate coating, chromium provides hardness, reflectivity and tarnish resistance. The corrosion resistance is derived primarily from the barrier effect of the thick nickel plate under the chromium. However, copper,

nickel and chromium are all cathodic with respect to steel, and corrosion can be accelerated once the coating is breached and the underlying steel is exposed. For this reason these coatings are not chosen where corrosion protection is the primary concern.

Hard chromium plating is usually applied directly to steel parts in thicknesses up to about 300 μm, to provide resistance to wear, abrasion and corrosion. It is also used to build up worn or undersized parts. In the thicker applications it may be impervious but is subject to microcracks.

Chromium is a metal with low cathode efficiency, and substantial amounts of hydrogen are deposited on the part along with the metal being plated. Because of this parts must be baked as soon as possible after plating to drive-off the hydrogen and prevent embrittlement. Baking temperatures can be used up to the tempering temperature of the steel, and therefore they tend to be less effective for very high strength steels where tempering temperatures are low.

Nickel: By far the greatest use of nickel plating is on steel in conjunction with copper and chromium as described above. However nickel can also be deposited, both on metals and non-metals by an electroless or non-electrolytic process. The metal is deposited spontaneously on the surface of a catalytic substrate immersed in an aqueous solution containing the metal ion and a reducing agent together with a compound (frequently the salt of an organic acid) which acts as a buffer and a complexing agent for the metallic ion (Ref. 6-5).

The baths often contain phosphorous or boron, and they provide coatings of uniform thickness even over sharp corners and into deep recesses. The coatings have low internal stress and are less magnetic than electro-deposited nickel platings, and they have hardness values of about 500 HV. The coatings can be heat treated to higher hardness of about 1000 HV, which provides wear and abrasion resistance. This increase in hardness is achieved by a precipitation hardening process involving the phosphorous which is usually present in amounts of 5 to 10%. The heat treatment is carried out at temperatures of about 400°C.

Electroless nickel coatings about 25 μm thick are often used, after baking to remove hydrogen, to provide protection against stress corrosion cracking of precipitation hardenable stainless steels.

Aluminium: Aluminium coatings can be applied to steel by hot-dipping, cementation, ion vapour deposition or spraying. Ion vapour deposition is a relatively new process and spraying is the only process that has been used extensively over a long period of time with airframe parts. Pack cementation is widely used for gas turbine components.

In soft waters aluminium is cathodic with respect to steel, however in sea water or some fresh waters containing chloride ions or sulphate ions aluminium may become anodic to steel and aluminium coatings should therefore corrode sacrificially and provide cathodic protection to steel. However, as noted below this may not always be the case.

Sprayed aluminium coatings provide an adherent, somewhat absorbent film about 100 to 150 μm thick. They provide very good protection to steel, and they may be sealed with organic lacquers or paints to provide further protection and delay the formation of visible surface rust. The surface of the steel must first be grit-blasted to provide a rough surface to aid adhesion. Unfortunately the thickness and relative roughness of the coatings make them unsuitable for close tolerance parts.

Ion vapour deposited aluminium coatings have been used on a variety of parts including steel and titanium fasteners, electrical connectors, engine mounts and stator vanes, landing gear components, integrally machined wing skins and a large number of miscellaneous components (Ref. 6-17). These coatings are soft and ductile and are prepared using commercially available aluminium (1100 alloy) feed wire which is melted, vapourized and ionized in a glow discharge created by an inert gas. The process is applied in a batch mode, where parts to be coated are held at a high negative potential relative to the evaporation source. The positively charged gas ions bombard the surface of the part and perform a final cleaning action. When this is done the aluminium is vapourized and ionized and the ionized aluminium is accelerated towards the part surface where it plates as a dense, tightly adherent coating.

Minimum coating thicknesses are in the range 8 to 25 μm, and coatings may be used as-prepared or with a supplementary chromate treatment. The thinner coatings are used when close tolerances are required, such as on threads, intermediate thickness coatings (> 13 μm) are used on interior parts or where only mildly corrosive environments are expected, and the thicker coatings (> 25 μm) are used for exterior parts operating in highly corrosive environments and for engine parts. Ion vapour deposited aluminium has been considered as a replacement for diffused nickel cadmium and aluminium pigmented paints for use in the cooler sections of gas turbines, where temperatures are less than 454°C. The process has also been considered as an alternative to pack cementation for the preparation of aluminide coatings on hot section components. In this case the ion vapour deposited aluminium is diffused into the nickel base superalloy substrates to form the nickel aluminide coating (Ref. 6-17).

Ion vapour deposition of aluminium is attractive since it avoids the environmental and toxicological problems associated with cadmium. It does not cause hydrogen embrittlement of steel, nor solid metal embrittlement of steel or titanium, and it should be more galvanically compatible with aluminium alloy structure and avoid the exfoliation corrosion of sensitive aluminium alloy structure reported in Reference 6-17. However, views on the ability of aluminium to protect steel fasteners appear to vary. Reference 6-17 reports that cadmium plated steel fasteners in a 7075-T6 alloy plate were more severely rusted, and the aluminium countersinks more severely corroded when exposed to SO_2—salt spray tests for 168 hours, than when the steel fasteners were coated with IVD aluminium. However, in another study of the corrosion protection afforded by several coatings on steel and titanium fasteners, aluminium coated steel fasteners showed red rusting within weeks of exposure in a coastal environment (Ref. 6-18). In contrast cadmium and zinc plated fasteners showed no rust after 52 weeks. However, it is not clear how the aluminium was deposited in this latter study (Ref. 6-18) and whether the coatings are comparable to the IVD coatings of Reference 6-17. A view expressed in Reference 6-2 is that the presently available pure aluminium coatings are not able to provide adequate sacrificial protection to steel in a chloride ion environment, and for this reason a recommendation is made for the development of aluminium coatings containing small amounts of zinc, or other elements for improved protection.

Zinc: Zinc coatings may be applied either by electroplating or spraying. Electroplatings are normally less than 25 μm thick, and may be as thin as 5 μm on threaded parts. However while they provide good protection to steel in rural atmospheres, they do not perform as well in marine or industrial environments. Reference 6-12 reports that 30 μm thick zinc coatings lasted about 11 years or longer in rural or suburban locations, about 8 years in marine locations and only 4 years in industrial atmospheres. The short life in industrial atmospheres was attributed to attack by sulphuric acid in polluted atmospheres. Reference 6-5 reports that zinc plating does not perform as well as cadmium in tropical and marine atmospheres, and therefore cadmium is preferred for aircraft use.

Where thicker coatings are permissible zinc may be deposited by spraying, but must compete with aluminium which is usually the preferred material.

6.6 Supplementary Protection Systems

Supplementary protection is provided to surfaces which already have some form of permanent or semi-permanent form of protection such as cladding or conversion coating. The supplementary protection may be in the form of a material that can be easily applied and removed, and which will be replaced periodically during the life of the aircraft. Jointing compounds and sealants are examples of this type. Supplementary protection is also provided in the form of paints and primers, which although intended to last for the life of the aircraft will generally require renewal and repair periodically.

6.6.1 Jointing compounds and sealants

Jointing compounds are used for protection at joints where they act by excluding dirt and moisture, and by providing a reservoir of slightly soluble chromates which act as inhibitors. Sealants are applied to joints to prevent the escape of fluids, such as fuel, but they also exclude moisture.

As explained in Section 6-3, jointing compounds are required to remain flexible so as to allow easy disassembly of parts. Various synthetic resins are used for this purpose, see for example Reference 6-5. The compounds harden sufficiently at edges to take paint, but they remain tacky within the joint so that flexure does not cause cracking. Sealants of the type now being specified are also elastomeric, and the most popular are polysulphide sealants containing corrosion inhibitors. The inhibitive sealants are very effective when used in faying surfaces and butt joints, for wet installation of fasteners and over fastener patterns. They are also effective in insulating dissimilar metals (Refs. 6-19 and 6-20).

6.6.2 Paint systems

Primers: Primers perform two functions, they provide a good surface for topcoat adhesion and they provide a supply of inhibitors to impede corrosion. To perform satisfactorily they must themselves adhere well to the base metal or any surface conversion coating that might be present. They should also contain an adequate concentration of a leachable inhibitor, where this is considered an important feature of the protection system, and this is usually a chromate pigment. Primers for magnesium alloys must contain a chromate pigment, and are generally required to be free from compounds of mercury and lead. Pigmented-synthetic-resin primers give superior corrosion protection to etch primers, but inferior adhesion (Ref. 6-5). However, epoxy primers are widely used both in Europe and North America (Refs. 6-2, 6-4 and 6-19).

A single application of primer might be sufficient to protect internal areas of aircraft where condensation or contamination does not occur. In other areas a second layer of primer might be used, followed soon after a single layer of a suitable topcoat. Since paint adds significant weight to an aircraft the use of multiple coatings is avoided where possible.

Topcoats: These provide further protection and provide a decorative function in the case of civil aircraft or, perhaps, camouflage in the case of military aircraft. They are required to be durable, abrasion resistant, resistant to chalking and crazing, to retain gloss and to be easy to clean (Ref. 6-19).

The topcoats commonly used include air drying paints and oil-based varnishes which harden by oxidation, acrylics and other lacquers which dry by solvent evaporation, and polyurethane and epoxy paints which dry by cold-curing chemical reactions. High temperature curing or stoving can also be used with certain types of epoxy to produce a harder finish, but this also makes them more difficult to remove.

Polyurethane paints have been widely used on both sides of the Atlantic (Refs. 6-2, 6-4 and 6-19). However these paints are quite brittle and tend to chip and crack, and Reference 6-2 has indicated a preference for solvent drying acrylic paints for the exterior finish. These paints can be removed locally by chemical solvents down to the primer and are reported to be easier to touch-up (Ref. 6-2). Which ever paint system is selected for exterior use it is usual to qualify the system on the basis of its ability to prevent filiform corrosion. Reference 6-1 describes one such test, although most manufacturers have equivalent test methods.

Flexible paints: References 6-2 and 6-19 have both reported interest in flexible paint systems. Coatings of polysulphide polymers have been used as intermediate layers below polyurethane topcoats, but these are reported to be dense, thick and difficult to apply because of short pot life. Other types of elastomeric coatings are being evaluated (Ref. 6-19).

6.6.3 Inhibitors

Inhibitors lead to a decrease in corrosion rate when introduced to the environment at a corroding metal surface. Several types of inhibitors exist including passivators, organic inhibitors, and vapour phase inhibitors. Further information on these types of inhibitors are given in Reference 6-12.

Passivators are the most important types in aircraft protection since they are capable of reducing corrosion rates to very low values. They act by moving the corrosion potential of the metal in the noble direction and this shift may be several hundred milivolts. The common passivating inhibitors include chromates, nitrates and molybdates (Ref. 6-12), but by far the most important are chromates which are able to suppress the corrosion of aluminium under a wide range of conditions. Chromates also reduce corrosion rates in steels, cadmium, zinc and even magnesium under certain conditions (Ref. 6-2).

Passivators in contact with a metal surface are believed to act as depolarizers, initiating high current densities at residual anodic areas which exceed $i_{critical}$ for passivation, as indicated in Figure 6-8. Only those ions which have both an oxidizing capacity and which are readily reduced can serve as passivators. However, the passivator concentration must exceed a certain critical value to be effective, as indicated in Figure 6-8. Below this concentration they act as active depolarizers and maintain an increased corrosion rate at local areas. The critical concentrations for the inhibitors given above are in the range 10^{-3} to 10^{-4} M, and for a typical inhibitor such as sodium chromate 10^{-3} M would be equivalent to about 160 ppm. Chloride ions and elevated temperatures increase $i_{critical}$ and $i_{passive}$, which in effect increases the critical concentration required for the passivator to be effective.

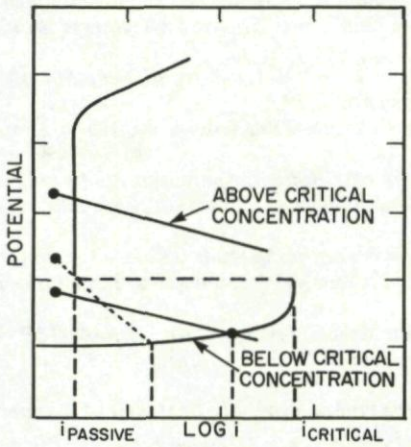

Fig. 6-8 Polarization curves that show effect of passivator concentration on corrosion of iron. An oxidizing substance that reduces sluggishly does not induce passivity (dotted cathodic polarization curve). (Ref. 6-12)

Adequate concentrations of inhibitor can be maintained at metal surfaces by incorporating them in surface coatings such as chromate conversion coatings, chromic acid anodized coatings, pigmented primers or paints, or by introducing them to sealants or jointing compounds. They can also be released from strategically placed inhibitor sacks to protect local structure, or they can be added to wash water so that a thin film of inhibitor is left behind as the structure dries.

Reference 6-21 has listed some of the important requirements for inhibitors used with aircraft structures, and these include low toxicity and biodegradibility. Unfortunately chromate salts are toxic and carcinogenic and they create a number of environmental pollution problems, as discussed in Reference 6-2. A great deal of effort is therefore being focussed on the development of alternative inhibitors which avoid these problems. Reference 6-2 has discussed the development of zinc thioglycollate which appears to be as effective as chromate salts in inhibiting the corrosion of aluminium alloys, while Reference 6-21 has described various borax-nitrite based inhibitors which have also been found to provide protection for high strength aluminium alloys and steels used in aerospace applications. These latter compounds were also reported to protect the copper-bearing alloys used in electronic components.

6.6.4 Water displacing compounds

Water displacing compounds may be useful in providing supplementary protection for paint systems that have deteriorated or become damaged in service. They are applied as fluids by wiping, brushing, spraying or dipping, and they are usually immiscible with water and displace water from surfaces and crevices.

A number of fluids used in the United Kingdom are based on lanolin (PX-1, PX-3 and PX-9) and contain various solvents and inhibitors. The evaporation of the solvents leave either thin soft films (PX-1), semi-hard films (PX-9) or hard resin films (PX-3) providing varying degrees of protection. PX-3 contains a zinc chromate pigment which acts as an inhibitor and it can be used in place of paint on bare metal where only light protection is needed (Ref. 6-5). It may therefore be used on areas of internal structure, but it is not normally used on external surfaces or on naval aircraft.

Other fluids such as PX-10 and PX-24 may be used to provide short term protection. They exhibit better water displacing characteristics than PX-1, PX-3 and PX-9, and they leave a thin oily film providing short term corrosion protection. PX-28 is a wax thickened protective with water displacing properties but without the penetrating power of PX-24. It does not harden with time, but remains tacky and has an ability to self-heal when damaged. It is not used on exterior surfaces, or areas where regular access is needed, but it can be used in closed sections or inaccessible areas of structure. PX-7 is a petroleum based product, used to protect battery terminals and other parts, while PX-13 is a petroleum wax containing inhibitors and other additives and is used to protect engine cylinder bores, valves and springs (Ref. 6-5).

Water displacing compounds similar to these are used in North America, and two of these have been described in Reference 6-19. AML-350 is a petroleum sulfonate in a mineral spirit solvent. When applied to a metal surface it spreads over the surface and under water droplets, and as the solvent evaporates it leaves a soft oil-like film of sulfonate which isolates the metal from the environment and acts as a corrosion inhibitor. The film is built up to a thickness of 2 to 5 μm.

AMLGUARD is another North American product (Ref. 6-19), which is a water displacing compound containing solvents, silicone and silicone alkyd resins, barium petroleum sulfonate and several other additives. It dries to the touch in about 18 hours, but continues to cure for 1 to 3 months to form a hard, dry, but flexible finish between 25 and 51 μm thick. It not only displaces water but it also leaves a protective barrier coating containing barium petroleum sulfonate and alkyl ammonium organic phosphate as inhibitors (Ref. 6-19).

AML-350 is intended for use on internal metallic parts and electrical connectors. AMLGUARD is intended for temporary use on external aircraft parts, such as wheels, wheel wells, cables, landing gear parts, wing leading edges and helicopter blades (Ref. 6-19).

6.7 References

6-1 *Guidance Material on Design and Maintenance Against Corrosion of Aircraft Structures.*
Doc. Gen. 2637, International Air Transport Association, Montreal, February 1979.

6-2 McLoughlin, V.C.R. *Corrosion Control Measures for Military Aircraft — Present UK Requirements and Future Developments.*
AGARD Conference Proceedings No. 315 on Aircraft Corrosion, August 1981.

6-3 *Properties and Selection: Nonferrous Alloys and Pure Metals.*
ASM Metals Handbook, Volume 2, Ninth Edition, American Society for Metals, Ohio, 1979.

6-4 Scolaris, M. *Corrosion Prevention Methods Developed From Direct Experience With Aerospace Structures.*
AGARD Conference Proceedings No. 315 on Aircraft Corrosion, August 1981.

6-5 Corrosion Manual, Section 2, AP 119A-0200-1B, United Kingdom Ministry of Defence, 2nd Edition, June 1977.

6-6 *Aerospace Process — Anodic Treatment of Aluminium Alloys — Chromic Acid Process 20 VDC, Undyed Coating.*
International Organization for Standardization, ISO 8077, 1984(E), Geneva, Switzerland.

6-7 *Aerospace Process — Anodic Treatment of Aluminium Alloys — Chromic Acid Process 40 VDC, Undyed Coating.*
International Organization for Standardization, ISO 8076, 1984(E), Geneva, Switzerland.

6-8 *Aerospace Process — Anodic Treatment of Aluminium Alloys — Sulphuric Acid Process, Undyed Coating.*
International Organization for Standardization, ISO 8078, 1984(E), Geneva, Switzerland.

6-9 *Aerospace Process — Anodic Treatment of Aluminium Alloys — Sulphuric Acid Process, Dyed Coating.*
International Organization for Standardization, ISO 8079, 1984(E), Geneva, Switzerland.

6-10 *Aerospace Process — Anodic Treatment of Titanium and Titanium Alloys — Sulphuric Acid Process.*
Draft International Standard, International Organization for Standardization, ISO/DIS 8080, 1984, Geneva, Switzerland.

6-11 *Aerospace Process — Chemical Conversion Coating for Aluminium Alloys — General Purpose.*
Draft International Standard, International Organization for Standardization, ISO/DIS 8081, 1984, Geneva, Switzerland.

6-12 Uhlig, H.H. *Corrosion and Corrosion Control.*
Wiley Interscience, 2nd Edition, John Wiley and Sons Inc., New York, 1971.

6-13 *Aerospace Process — Surface Treatment of Austenitic Stainless Steel Parts.*
Draft International Standard, International Organization for Standardization, ISO/DIS 8074, 1983, Geneva, Switzerland.

6-14 *Aerospace Process — Surface Treatment of Hardenable Stainless Steel Parts.*
Draft International Standard, International Organization for Standardization, ISO/DIS 8075, 1983, Geneva, Switzerland.

6-15 Frager, D.N.
Spurr, W.F. *Solid Cadmium Embrittlement: Steel Alloys, Corrosion.*
NACE, 27, 1971, pp. 72-76.

6-16 Frager, D.N.
Spurr, W.F. *Solid Cadmium Embrittlement: Titanium Alloys, Corrosion.*
NACE, 26, 1970, pp. 409-419.

6-17 Fannin, E.R. *Ion Vapor Deposited Aluminium Coatings for Improved Corrosion Protection.*
AGARD Conference Proceedings No. 256 on Advanced Fabrication Processes, March 1979.

6-18 McLoughlin, V.C.R. *An Evaluation of Coatings for Steel and Titanium Alloy Fasteners for Aircraft Applications.*
AGARD Conference Proceedings No. 256 on Advanced Fabrication Processes, March 1979.

6-19 Ketchum, S.J.
DeLuccia, J.J. *Recent Developments in Materials and Processes for Aircraft Corrosion Control.*
AGARD Conference Proceedings No. 315 on Aircraft Corrosion, August 1981.

6-20 Miller, R. *Sealants.*
Chapter 6, in A Handbook of Protective Coatings for Military and Aerospace Equipment, Ed. S.J. Ketchum, First Edition, to be published by National Association of Corrosion Engineers, Houston, Texas.

6-21 Khobaib, M.
Vahldiek, F.W.
Lynch, C.T. *New Concepts in Multifunctional Corrosion Inhibition for Aircraft and Other Systems.*
AGARD Conference Proceedings No. 315 on Aircraft Corrosion, August 1981.

CHAPTER 7

UNIFORM CORROSION AND EROSION

7.1 Introduction: Uniform Corrosion

Corrosion of metals by uniform chemical attack is the simplest and most common form of corrosion. It may occur in moist air or other gases, and in a wide variety of liquids including water. It is probably the most common form of corrosion in aircraft structures, occurring under normal service conditions and particularly in areas where water or condensation is apt to collect. High temperature oxidation is a special form of uniform attack. In uniform corrosion the anodes and cathodes of the electrolytic cells are numerous and closely spaced on the surface of a single piece of metal, and therefore uniform corrosion can be considered as localized electrolytic attack occurring consistently and evenly over the surface.

Uniform corrosion generally produces large areas of damage, and provided the corrosion prone area is accessible for visual inspection, it can usually be detected fairly early and remedial action taken. Uniform corrosion occurring in sealed interior areas, or other visually non-inspectable areas can lead to serious damage unless special non-destructive inspection methods, such as x-radiography or ultrasonic inspection are used for early detection followed by corrective maintenance.

Most of the common engineering metals and alloys produce characteristic corrosion products which allow corrosion to be recognized fairly easily. Probably the best-known form of corrosion occurs on non-stainless iron and steel and is easily recognized by the familiar red iron rust (Figs. 7-1 and 7-2). Figure 7-1 shows rusting on a steel track rod adjuster and eye end, originally cadmium plated but operating in an exposed environment. The cadmium had presumably been totally sacrificed after loss on threads during assembly or maintenance. Use of a supplementary protective material should have prevented this. Figure 7-2 shows a steel jet pipe end cap liner which had been subjected to high temperature oxidation over a long period of time. In this figure the blistering and flaking of a surface protective coating is apparent, and the formation of red rust products in the underlying steel can be seen. The materials chosen for this application had simply proven unsuitable for the environment, though quite possibly they were the best available when the design was established. The fact that the aircraft life had been extended, and these components had been required to operate for much longer times than originally intended is also an important factor.

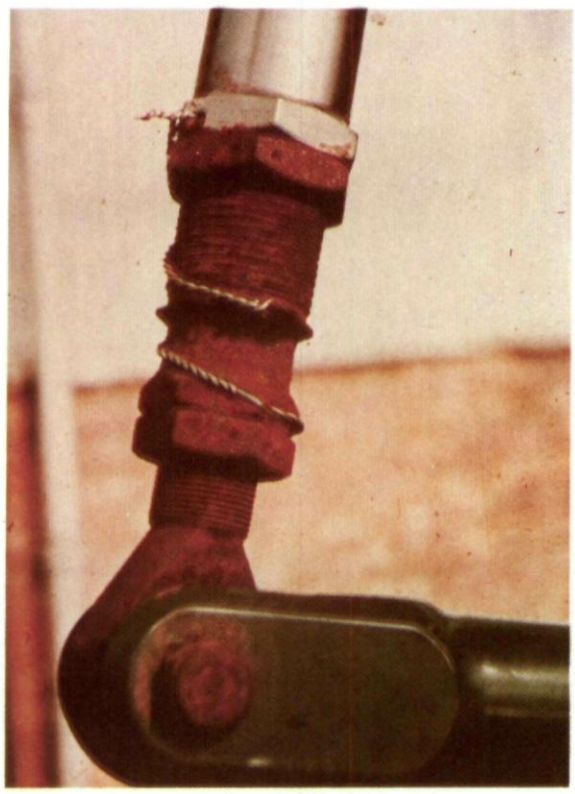

Fig. 7-1 Rusting on a steel track rod adjuster and eye after damage occurred to the protective cadmium plating

Fig. 7-2 Rusting in a jet pipe end cap liner following damage to its protective coating

The corrosion products of aluminium and magnesium alloys are evident as white to grey powdery deposits, the latter are often of a fluffy or granular nature. Figure 7-3 shows the surface corrosion damage to an aluminium alloy stringer, where the chromate pre-treatment and primer coat had failed, probably through aging and exposure to moisture. Early identification of aluminium or magnesium corrosion is essential, and frequently the first indications are flaking or blistering of the surface finish. Figure 7-4 shows an area of general surface corrosion on a magnesium alloy skin of a helicopter on which the chromate pre-treatment had locally failed.

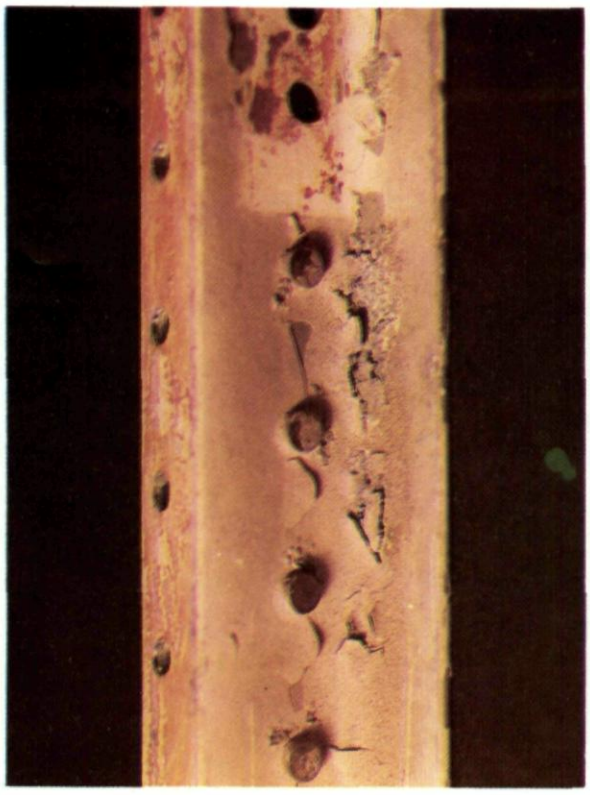

Fig. 7-3 Flaking of the chromate pre-treatment and primer on an aluminium alloy stringer and corrosion of the exposed metal

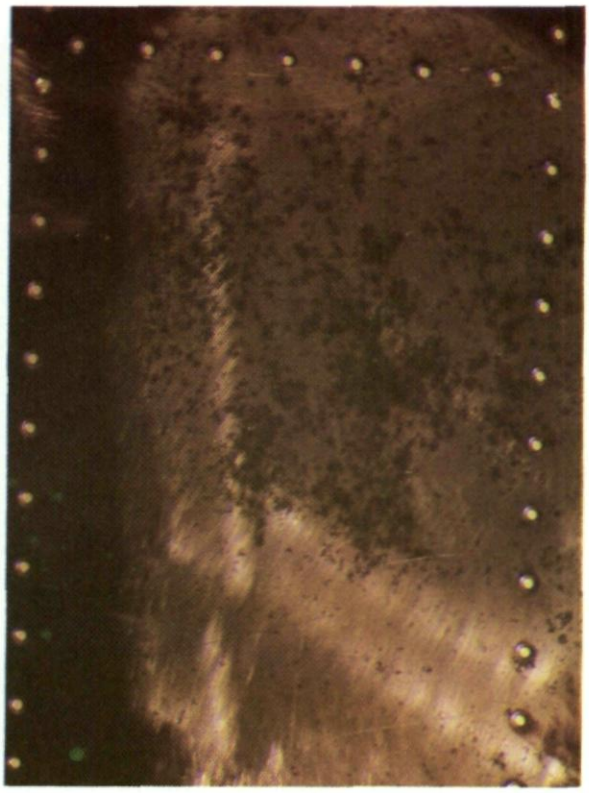

Fig. 7-4 Uniform corrosion in a magnesium alloy helicopter skin after damage to the chromate pre-treatment

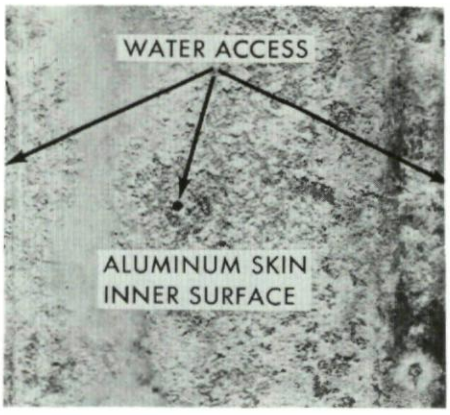

(a)

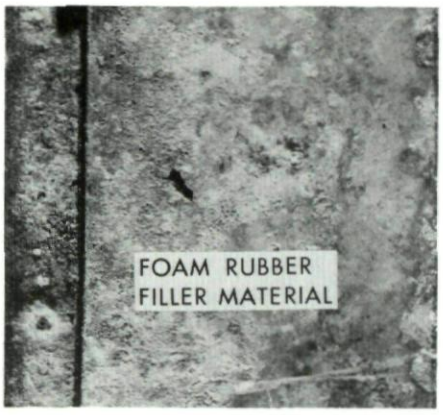

(b)

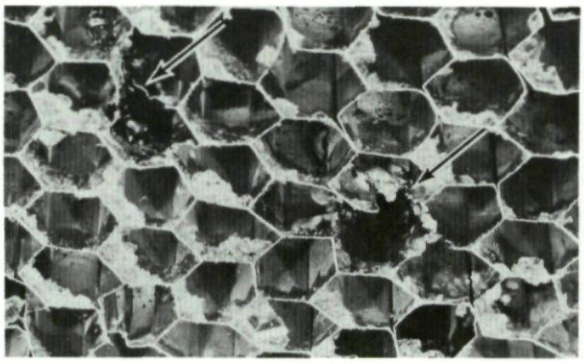

(c)

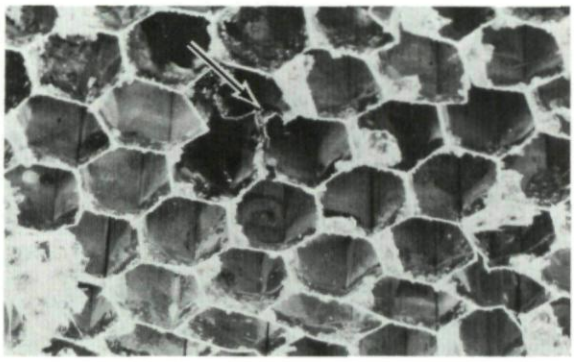

(d)

Fig. 7-5 Corrosion damage in an aluminium alloy honeycomb structure from a fighter aircraft

(a) Inner surface of the aluminium skin showing perforations.
(b) Foam rubber filler material.
(c) and (d) Arrows point out areas of severe corrosion damage in the honeycomb.

Early attention to uniform corrosion damage is particularly important where the metal skin is used as an outer layer of a honeycomb sandwich structure, or closed box structure. Failure to do so may lead to penetration of the skin by corrosion, and the entry of water or other corrodents into the internal structure. Figure 7-5 shows the corrosion damage to an aluminium honeycomb structure from a fighter aircraft. Figure 7-5(a) shows heavy corrosion on the inner surface of the aluminium skin, with holes which allowed the ingress of water. Figures 7-5(c) and 7-5(d) show areas of corrosion damage to the aluminium honeycomb, which are indicated by arrows. Figure 7-5(b) shows a sample of foam rubber filler material which formed a layer between the skin and the honeycomb. It is uncertain whether the rubber in this case contributed to the corrosion reactions, but the operators of this particular aircraft did note that the rubber was usually not present. This simply serves to point out that all material combinations should be evaluated with respect to corrosion before a design is finalized, since one material may contribute to the corrosive environment of another.

The need to prevent the ingress of water and other corrodents to internal structure and equipment is nowhere more important than with electrical and avionics equipment. In the interests of obtaining specific electrical characteristics, the materials used are often inferior in terms of corrosion resistance, and serious corrosion problems and often malfunction of equipment can occur if the equipment is not properly sealed. Figure 7-6(a-c) shows examples of corrosion of electrical equipment in a military aircraft due to water intrusion around the access door. The general reddish-orange discolouration of the compartment walls and floor, in Figure 7-6(a), indicates that uniform corrosion has occurred in these areas. The close-up photographs of Figure 7-6(b) and -6(c) show local eruptions of corrosion products around a screw and binding post, which are probably examples of galvanic corrosion and crevice corrosion.

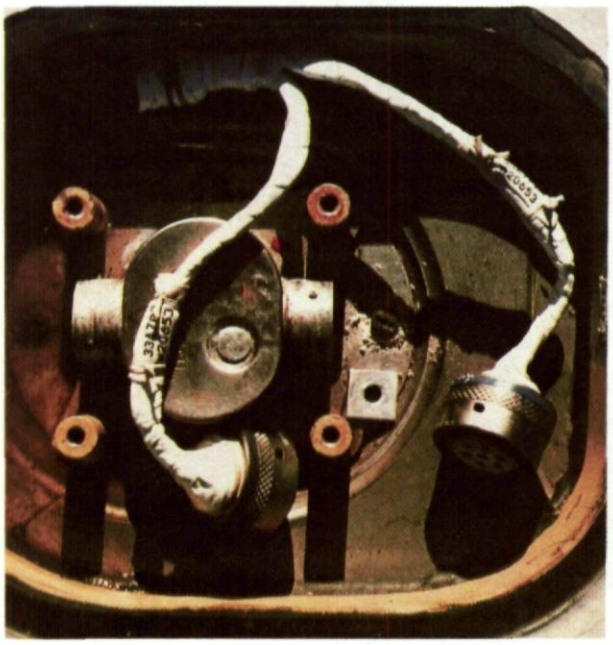

(a)

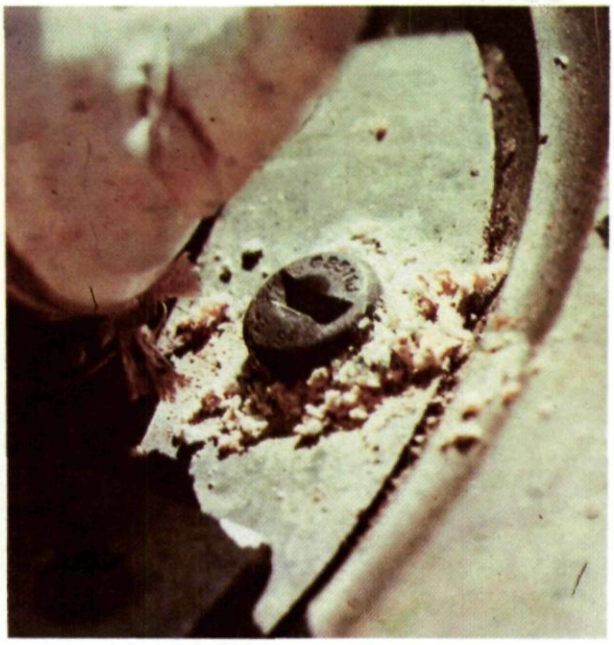

(b)

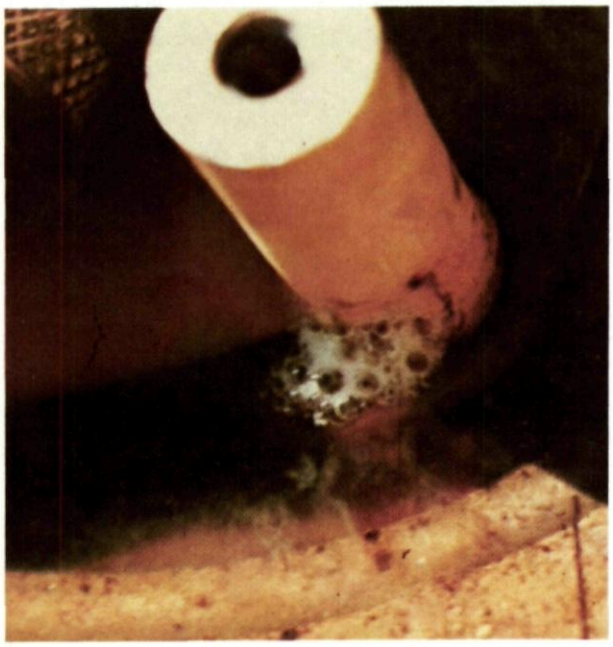

(c)

Fig. 7-6 Corrosion in a container used to house electrical equipment

(a) Discolouration indicates general corrosion of the walls and floor of the compartment.
(b) Localized corrosion around a screw.
(c) Localized corrosion at the base of a binding post.

7.2 Introduction: Erosion-Corrosion

When corrosion occurs in the presence of a fast moving fluid the rate of attack may be much higher than would occur in a still, or slow moving environment. This form of attack is known as erosion-corrosion, and the fluid may be either a liquid or a gas. Metal may be removed from the surface either as dissolved ions in a solution, or as solid particles. In this latter case the process will usually involve the formation of a corrosion product such as an oxide, hydroxide, sulphate or nitrate, which is then removed from the surface by mechanical wear and abrasion. Erosion-corrosion will therefore tend to be more severe where the corrosive fluid contains solid particles which can impact on the metal surface to cause mechanical damage to the corrosion products and any surface protective coatings.

Erosion-corrosion problems can be quite severe in transport aircraft operating in hot desert climates. Though dry in the sense of having low rainfall, desert areas are nevertheless often very humid, especially at night. High temperatures accelerate corrosion, distort skin surfaces and crack protective finishes, while dust and sand often containing a high proportion of salt erode surface finish and also mix with oils, grease and hydraulic fluid to form extremely abrasive compounds. Loose stones and rocks thrown up from temporary landing strips damage protective finish leaving areas of bare metal open to corrosive attack. Figure 7-7 shows erosion-corrosion damage to the undercarriage components of a transport aircraft as a result of operation from a desert landing strip. Damage to the protective coating system by stone impact and sand erosion has led to exposure of the bare metal which then continues to deteriorate by a combination of corrosion and erosion.

Erosion-corrosion is a common form of damage to aircraft propellors and turbine engine components operating either in the intake air stream, or in the hot gas path. Components such as impellors, compressor blades, turbine blades, nozzles and guide vanes are particularly prone to damage. Figure 7-8(a) shows erosion-corrosion damage on the concave surface of a compressor blade from a fighter aircraft engine after 16.5 hours in an erosion test cell. This particular blade was protected by a proprietary protective coating, applied by a vapour deposition process. Figure 7-8(b) shows a similar blade protected with a bias sputtered Ti Cr C coating after a similar 16.5 hour exposure in the test cell. A great number of hard, erosion resistant coatings are available for protection of engine coatings, and a great deal of research and development on new coatings continues.

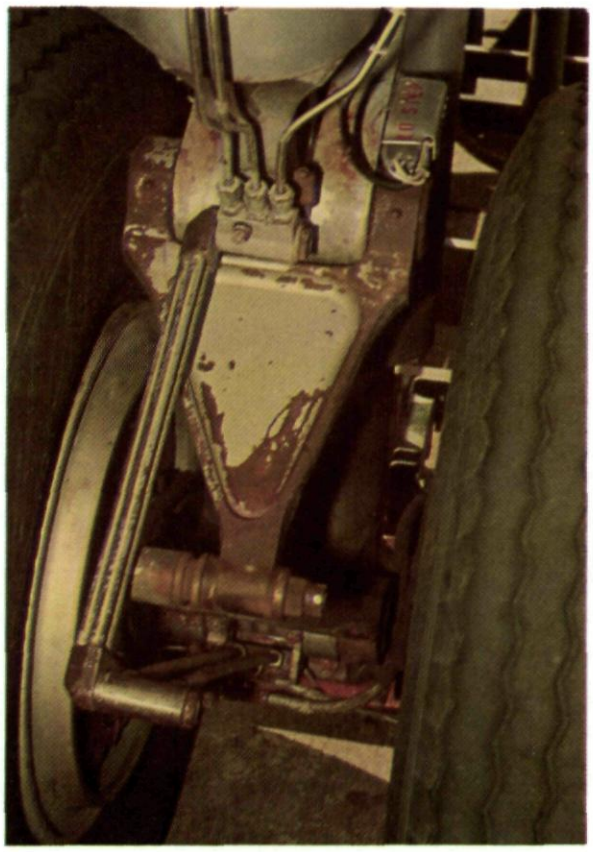

Fig. 7-7 Erosion-corrosion damage on the undercarriage of a transport aircraft

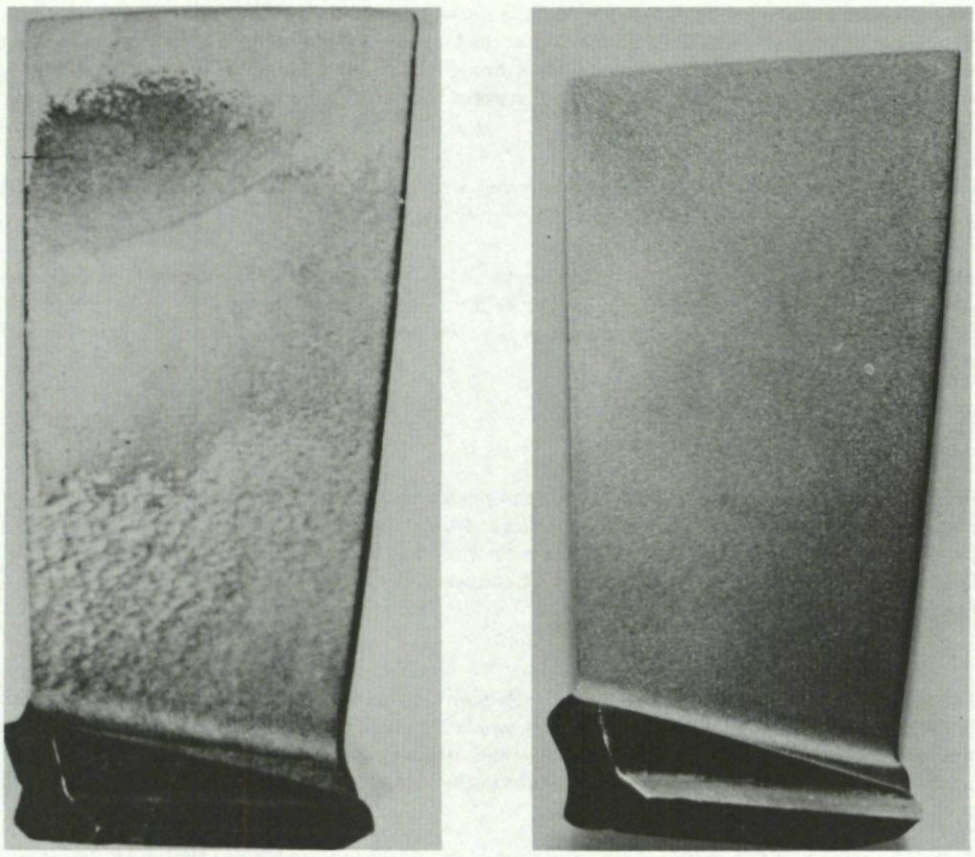

(a) VAPOUR DEPOSITED (b) BIAS SPUTTERED

T-58 COMPRESSOR BLADES AFTER 16-1/2 HOURS EROSION TEST (CONCAVE SURFACE)

Fig. 7-8 Erosion-corrosion damage on the airfoil of a fighter aircraft compressor blade

(a) Damage to a vapour deposited coating after 16.5 hours exposure in an erosion-corrosion test cell.
(b) Blade coated with a bias sputtered Ti Cr C coating after a similar exposure.

7.3 Case Histories

Case history 7-1. Brake disc failure.

The brake disc assemblies were removed from both main wheels of a light single engine aircraft (Fig. 7-9(a)). Both brake disc assemblies were severely corroded in the fillet radius area between the disc and the sidewall, and there was a 12-15 mm band of corrosion around the outside surface of the wall as shown in Figure 7-9(a).

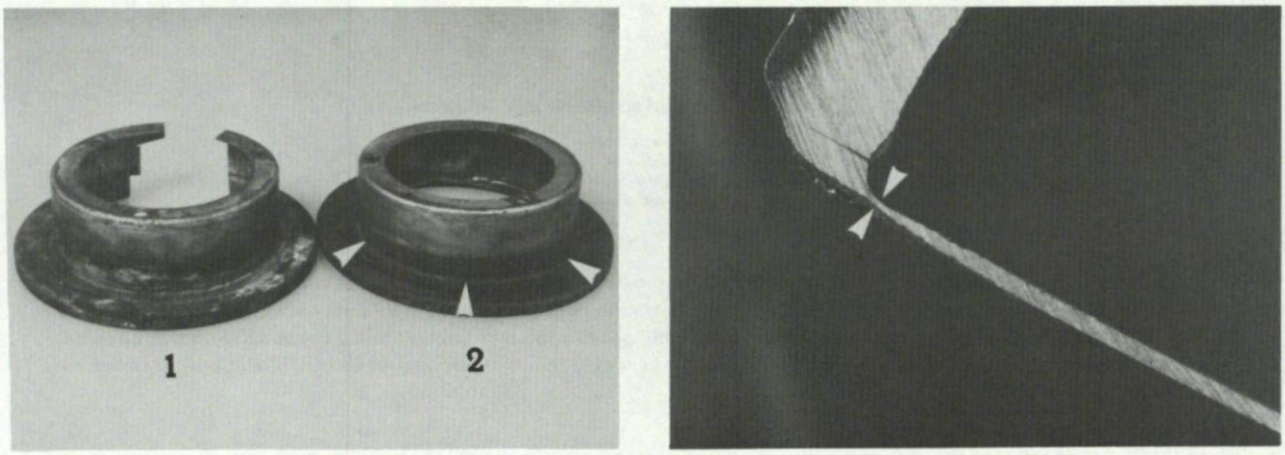

(a) (b)

Fig. 7-9 Corrosion failure of a brake disc assembly

(a) Disc assemblies showing 15 mm wide band of corrosion around the sidewall adjacent to the disc. The right hand brake disc had a completely fractured wall next to disc where arrowed.
(b) Typical area between disc and sidewall showing severe loss of wall thickness near to disc (arrows).

The brake disc assembly number 2 had failed around the sidewall circumference adjacent to the disc; this area was severely weakened due to corrosion to the extent that the wall thickness at the failed section was reduced to approximately one-quarter of the original thickness. Figure 7-9(b) shows the corresponding section through the disc and sidewall of the unfailed assembly, number 1. Even though this particular unit had not failed, a serious loss of material had occurred leading to a reduction of sidewall section thickness, as indicated by the arrows in Figure 7-9(b).

The final mode of failure was shear overload of the severely weakened area, resulting from brake application during towing of the aircraft. Moisture plus salt residues were suspected to be the corrosive agents in this case.

Close visual examination of the disc surfaces alone would have indicated that both brake assemblies were in an unserviceable condition prior to failure. Proper maintenance and inspection procedures are necessary to prevent the occurrence of such failures. The materials used for the brake assemblies were not reported in this investigation, but a substitution with materials with improved corrosion resistance would appear to be warranted.

Case history 7-2. Corrosion of structural steel fasteners.

A substantial amount of corrosion, and high repair and replacement costs are associated with structures and equipment at airports and ground support stations. Structural steel assemblies and their fasteners located in hot and humid coastal environments are particularly prone to damage. A sample set of ten nuts and bolts which had been used for about eight years on a mobile service tower at a base in a temporate coastal climate were inspected for corrosion. The samples examined were representative of 3000 similar parts still in service, and were originally specified to conform to ASTM-A325. The parts submitted for examination are shown in Figure 7-10(a).

Visual and optical examination verified that considerable corrosion existed on all part surfaces. However, the most severely affected areas were found to be on the surfaces of the nuts, as shown in Figure 7-10(b). Cross-sections through the nuts and bolts revealed the severity of corrosion, and showed that nearly one-third of the cross-sectional area on all ten nuts had been lost to corrosion. The depth of corrosion, in some areas, extended almost to the bolt surface, as shown in Figure 7-10(c).

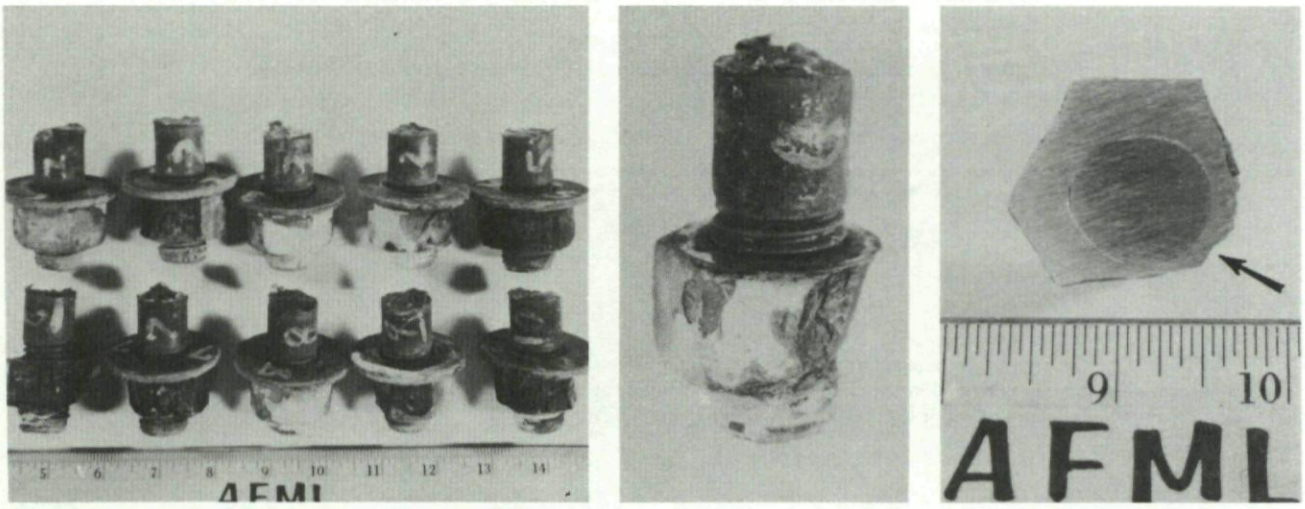

(a) (b) (c)

Fig. 7-10 Corrosion of structural steel fasteners

(a) Parts submitted for examination.
(b) Showing severe corrosion on the nut face surfaces.
(c) Cross-section through a typical bolt and attached nut showing areas most affected by corrosion.

Metallographic examinations of nut-bolt interfaces showed little evidence of intergranular cracking, while the microstructures were typical of quenched and tempered low carbon steels. Hardness values obtained from the nuts were in the range R_B 80 to 83, and for the bolts R_c 28 to 30. These values were in accordance with the specification requirements called for in ASTM-A325. Chemical analyses performed on the nuts and bolts showed the materials to be within the compositional limits for 1025 and 1035 carbon steel, as shown in Table 7-1.

It was concluded that the nuts and bolts conformed to the requirements of ASTM-A325, with respect to hardness and chemical composition. In view of the substantial corrosion on all component surfaces, and the considerable deterioration of the nut face surfaces, it was concluded that the future integrity and reliability of the equipment would be seriously jeopardized if these nuts and bolts were left in service.

It was recommended that all corroded nuts and bolts be removed from service and replaced with corrosion resistant steel nuts and bolts, or with fasteners that had been coated with a protection system designed for marine use.

Table 7-1 Chemical analyses for nuts and bolts

Component	Chemical Composition, Weight %				
	C	Mn	Si	S	P
Steel nuts (AISI-1025)	0.24	0.57	0.10	0.10	0.04
ASTM-A315 Spec.	—	—	—	0.23 max.	0.12 max.
Steel bolts (AISI-1035)	0.35	0.75	0.26	0.008	0.010
ASTM-A325 Spec.	0.30 min.	0.50 min.	—	0.05 max.	0.04 max.

Case history 7-3. Hydrofluoric gas corrosion of a stainless steel pipe.

A particularly serious consequence of uniform corrosion is that it may lead to some other more serious and less obvious form of corrosion if remedial action is not taken quickly. The full extent of the corrosion damage, which may be in the form of fine cracking, may be hidden by the initial corrosion products.

Hydrofluoric gas was found leaking from a section of flexible stainless steel pipe on a laser test aircraft. The stainless steel pipe was subsequently replaced with a section of polyvinyl chloride (PVC) pipe which also leaked gas.

Visual examination of the flexible stainless steel pipe, Figure 7-11(a), revealed the outside surface to be covered with a light tan powdery residue or corrosion product. A dark brown residue was found on the inside surface when the pipe was sectioned (Fig. 7-11(b)). The wire mesh was stripped from the convoluted flexible pipe and large cracks were found running circumferentially around the inside or small radius bends of the convolutes (Fig. 7-11(c)).

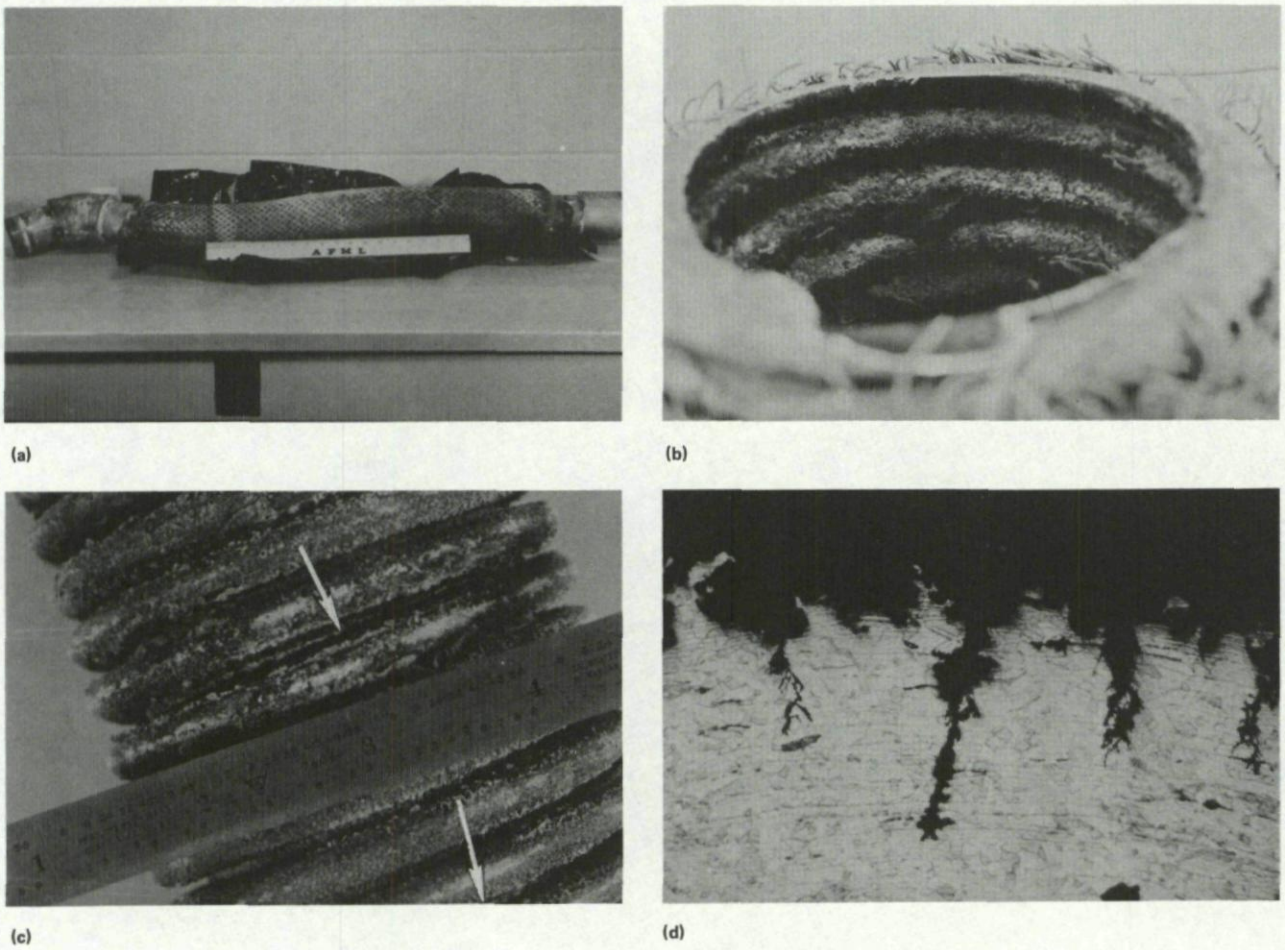

Fig. 7-11 Hydrofluoric acid corrosion of an austenitic (316) stainless steel pipe

(a) Section of stainless steel pipe used to vent hydrofluoric gas from laser on a flight test aircraft.
(b) Interior of the flexible pipe showing iron rich corrosion products.
(c) The arrows indicate circumferential cracks running around the outside of the pipe, while general corrosion is indicated. The corrosion products had a light tan appearance.
(d) Optical micrograph through the wall of the flexible pipe showing general surface corrosion, pitting and stress corrosion cracks running from the bottom of the pits.

Chemical analysis of the convoluted stainless steel showed it to be of the 316 type, while the end fittings were 304 stainless steel. Both residues on the pipe were determined to be corrosion products consisting predominantly of iron, with nickel, chromium, and small amounts of other elements. The dark residue on the inside of the pipe was found to have higher concentrations of nickel and chromium than the light tan residues from the outside of the pipe.

Microscopic examination of the convoluted pipe, Figure 7-11(d), showed that pitting had occurred beneath the corrosion products and that stress corrosion cracks had initiated at the base of the pits. The stress corrosion was observed only on the inside or small radius bends of the convolutes, while pitting was observed over the entire internal surface of the flexible pipe.

The polyvinyl chloride pipe was also examined and no damage that would cause a gas leak was observed. However it was though that PVC might be attacked by hydrofluoric gas and it was therefore recommended to replace all remaining sections of the stainless steel pipe by polyethylene pipe.

The consequences of the leakage of a highly corrosive gas, such as hydrofluoric gas, in an aircraft structure are particularly serious and precautions against this should involve frequent careful inspections. In the case of the stainless steel pipe direct visual inspection was hampered by the outer sheathing of wire mesh. Carefully controlled compatibility studies should be performed before hardware of this type is placed in service.

CHAPTER 8

GALVANIC CORROSION

8.1 Introduction

Galvanic corrosion occurs when metals of different electrochemical potential are in contact in a corrosive medium. Common examples of metal couples susceptible to galvanic corrosion include combinations such as a copper pipe connected to an iron pipe, a bronze propellor in contact with a steel hull, cold worked metal in contact with the same metal annealed, and grain boundaries in a metal in contact with the grains of the same metal. The less noble metal will form the anode of the electrolytic cell and will be corroded while the more noble metal will act as the cathode and will remain largely unaffected. The resulting damage to the anodic metal will be more severe than if the same metal were exposed to the corrosive environment without the presence of, and contact with the cathode.

Galvanic corrosion can often be identified from other forms of corrosion because the corrosive attack is usually more severe at the interface between the two dissimilar metals. Perhaps the most common example of this in aircraft structure is the corrosion which occurs at fastener holes in aluminium or magnesium alloy skin when steel bolts or rivets are used. Examples of this are shown in Figures 8-1 and 8-2. In Figure 8-1, the skin was 7075-T6 aluminium alloy and the fasteners cadmium plated steel. Figures 8-1(b) and 8-1(c) show individual fasteners with substantial corrosion damage occurring in the adjacent aluminium.

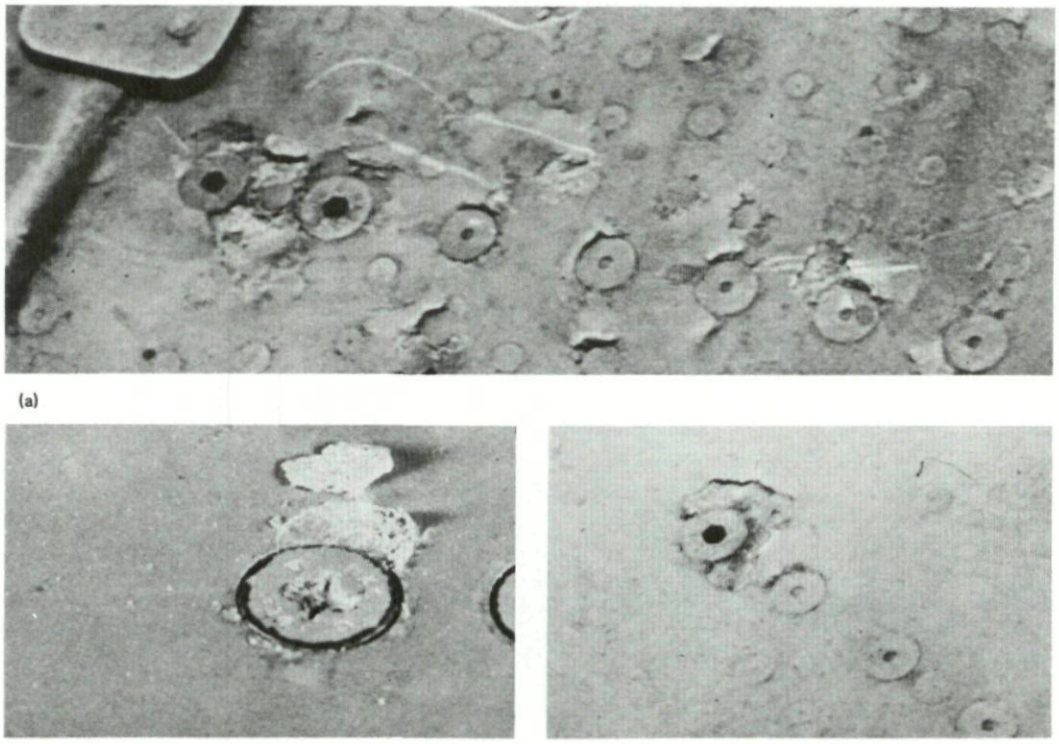

(a)

(b) (c)

Fig. 8-1 Galvanic corrosion occurring around cadmium plated steel fasteners in a 7075-T6 aluminium skin

(a) General view.
(b) and (c) Close-up of individual fasteners.

Cadmium is used as a protective coating and to provide a compatible surface between dissimilar metals in contact. It can be seen from the galvanic series given in Table 3-2 that cadmium lies between aluminium alloys and the common alloy steels and therefore the electrochemical potentials formed by the aluminium/cadmium cell, and the cadmium/steel cell are less than the unprotected aluminium/steel cell and therefore galvanic corrosion will be less severe. In general the greater the difference in electrochemical potential between two metals in a dissimilar metal cell the greater the rate of chemical attack. The use of cadmium as a protective coating on steel fasteners therefore serves to moderate any corrosive reactions, but will not stop them completely. In practice therefore attempts are made to prevent metal contact by placing an insulating material, usually a sealant or jointing compound between the two parts before assembly. In the example of Figure 8-1, an elastomeric sealant applied over the fastener heads after insertion would also have assisted by preventing the ingress of moisture between the fasteners and skin. The use of a more corrosion resistant aluminium alloy tempers such as T76 or T73, would also have assisted.

The example of Figure 8-2 shows dissimilar metal, or galvanic corrosion damage at fastener holes where steel bolts fastened through a magnesium alloy skin. The positions of these two materials in the electrochemical series, or galvanic series indicates that a high electrochemical potential would exist between them when in contact, and severe galvanic corrosion could be expected to occur.

Some care must be taken when using the galvanic series to assess the galvanic corrosion potential of dissimilar metals, since some metals may occupy different positions in the series. This is most commonly observed with metals such as stainless steels which can exist in either a passive or active state. In the passive state most stainless steels will occupy positions towards the noble end of the galvanic series, while in the active state they will behave more anodically. This behaviour is believed to be due to the state of the protective oxide films which tend to form on stainless steels, and which resist further corrosive attack. When the oxide film is intact and effective as a protective covering the metal behaves cathodically, whereas a damaged film leaves the metal unprotected and it therefore tends to behave anodically.

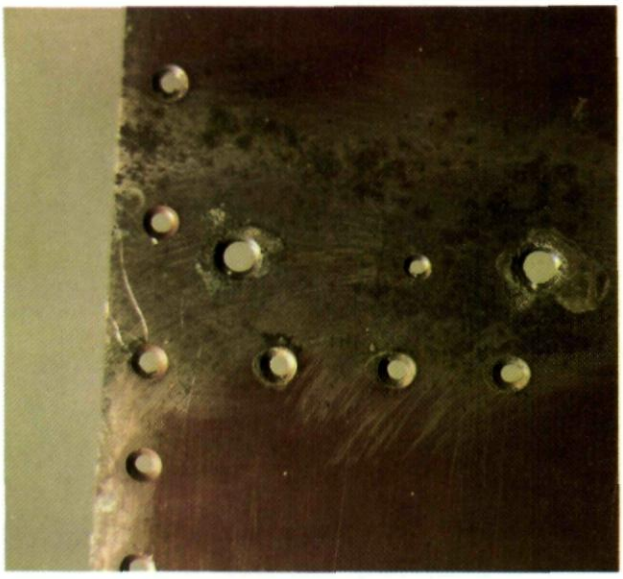

Fig. 8-2 Galvanic corrosion around fastener holes used to locate steel fasteners in a magnesium alloy skin

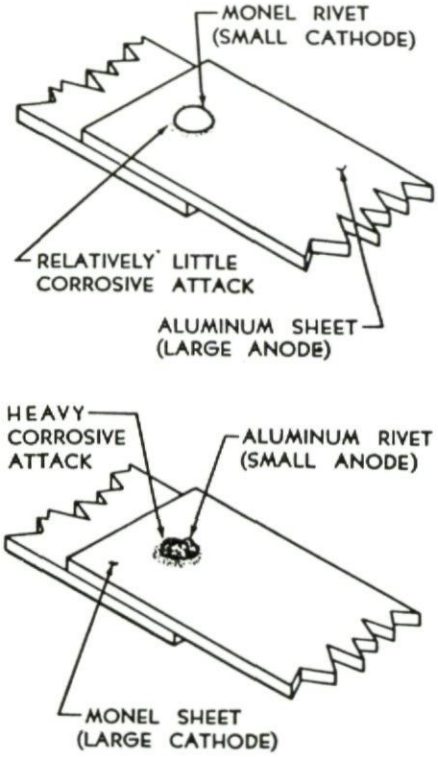

Fig. 8-3 Diagrams showing the effects of anode/cathode surface area ratio in dissimilar metal couples (Ref. 3-8)

An important practical consideration which can usually be addressed at the design stage is that galvanic corrosion will be severe if the surface area of the anode is small with respect to that of the cathode. Conversely, the corrosion will tend to be superficial if the surface area of the anode is large compared to the cathode. Thus in the case of the fastener/skin dissimilar metal combination, more severe corrosive attack would occur if the fastener were the anode and the skin were the cathode. This is illustrated schematically in Figure 8-3, using an aluminium/monel metal combination.

8.2 Case Histories

Case history 8-1. Galvanic corrosion in an aluminium alloy skin due to contact with a conductive cement.

Severe corrosion was found during a visual inspection of the outer wings and tail of a light aircraft operating in the Mediterranean region. The corrosion was found along the edges of an anti-icing boot on the leading edges (Fig. 8-4(a)) and was associated with an exposed band of the cement used to bond the de-icing boot to the wing. The damage is shown at higher magnification in Figure 8-4(b), where flaking of the cement and corrosion in the underlying metal can be seen. More detailed visual inspection of the tail revealed the presence of a 25 cm long area of complete metal penetration in the corroded region, which formed a crack like discontinuity in the structure. The area affected by this penetration is shown in Figures 8-5(a) and 8-5(b). Figure 8-5(a) shows the damage visible on the exterior surface, while Figure 8-5(b) shows the same area viewed from the inside after the affected material was cut from the structure.

The wings and tail units were fabricated from Alclad 2024 sheet, but metallographic examinations revealed that the aluminium cladding had been removed during previous servicing operations. The de-icer cement was a proprietary product, but of particular importance is that it was found to be electrically conducting. Thus, when in direct contact with the bare 2024 aluminium in a moist corrosive environment the cement would form the cathode of the electrolytic cell while the aluminium would form the anode and would be prone to severe corrosive attack.

Metallographic specimens of the damaged aluminium skin showed areas of uniform corrosion on the outer exposed surface (Fig. 8-6(a)) and regions of deep intergranular corrosion (Fig. 8-6(b)), which had led to perforation of the skin panel. Areas of the tail and wings away from the de-icing cement were protected by Corogard 22 paint, and these areas were not damaged by corrosion.

The personnel involved in the repair and overhaul of this aircraft recommended the use of a rain erosion resistant anti-static coating system (MIL-C-7439) to replace the conductive de-icer cement. The important requirement is to avoid the use of a conductive cement in exposed contact with the aluminium. In the example cited, corrosion damage to the 2024 aluminium would have been much reduced had the bare cement been covered by a protective coating to prevent mechanical damage to the cement and to prevent the intrusion of water.

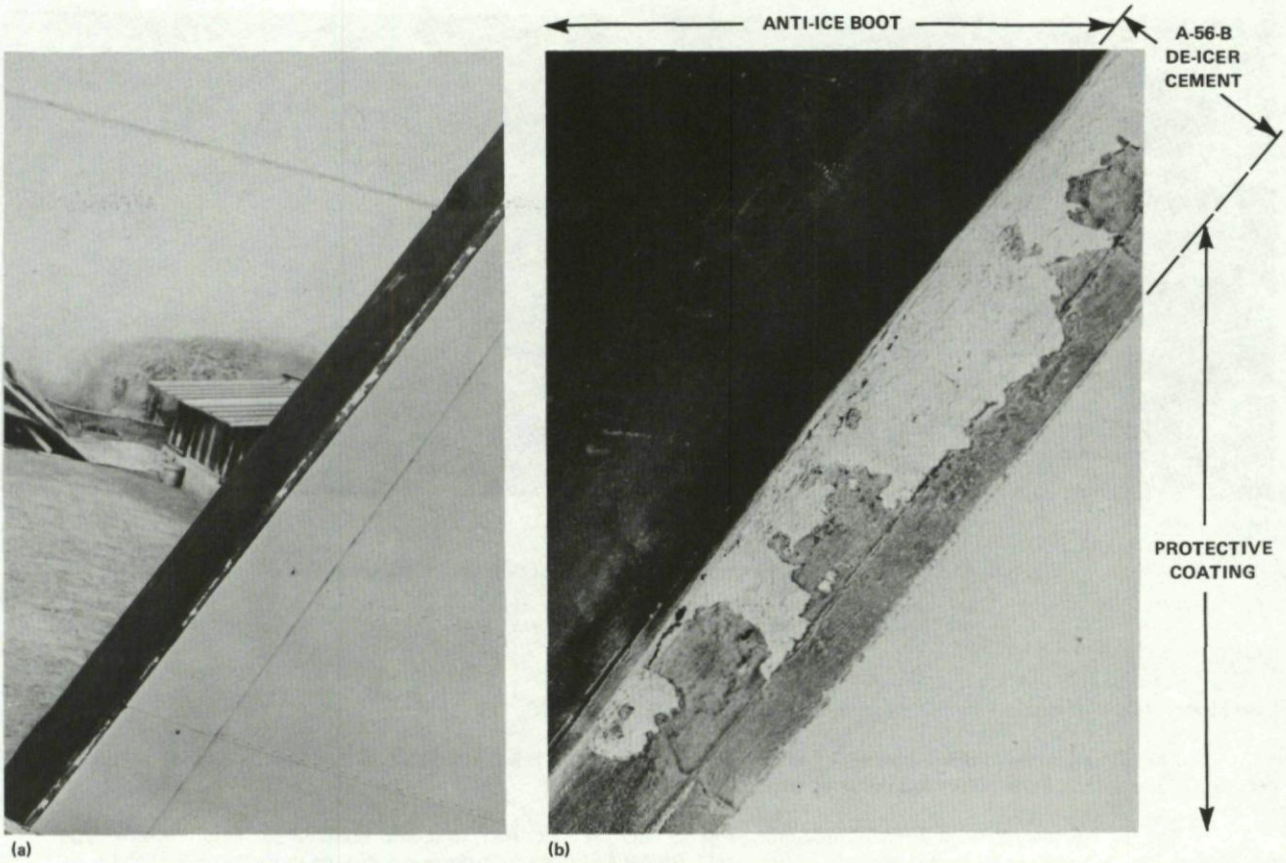

Fig. 8-4 Galvanic corrosion in an aluminium alloy skin due to contact with a conductive cement

(a) General view of a tail section leading edge showing de-icing boot and aluminium panels.
(b) Close-up showing the exposed cement between the de-icing boot and aluminium skin.

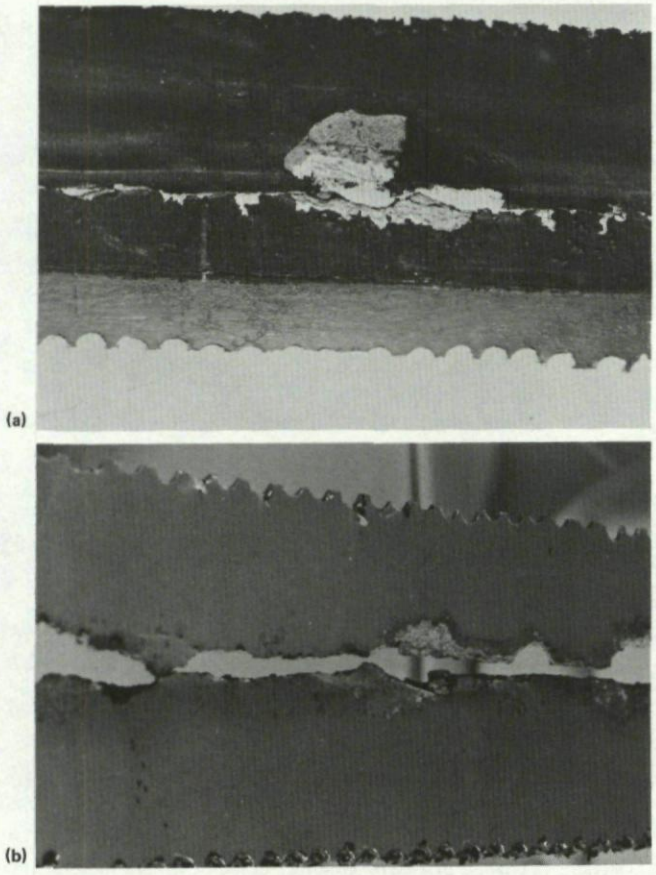

Fig. 8-5 Selected areas of corrosion from Figure 8-4

(a) Penetration of the aluminium skin viewed from the outside.
(b) Corrosion and penetration of the aluminium skin viewed from the inside.

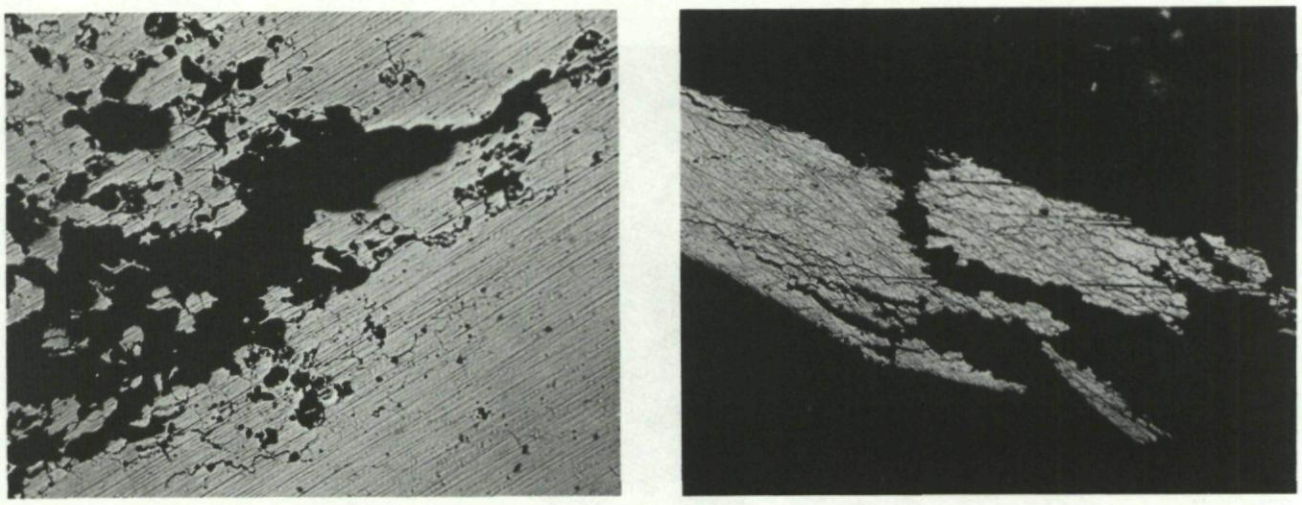

(a) (b)

Fig. 8-6 Metallographic sections through the aluminium skin shown in Figures 8-4 and 8-5

(a) General surface corrosion leading to intergranular attack on the outer surface.
(b) Deep intergranular attack and perforation of the skin.

Case history 8-2. Failure of a king pin lug from the main legs of a fighter aircraft.

The circumstances of this failure were not reported to AGARD, but it is fairly certain that substantial damage would have occurred to the aircraft if the failure had occurred either on take-off or landing.

The lug was made from a 7075-T6 aluminium forging, and the holes used to mount the king pin were protected from mechanical damage and wear by steel bushings. The lug, steel bushings and fracture surfaces can be seen in Figures 8-7(a) and 8-7(b). Visual inspection of the lug revealed corrosion damage. This was restricted to the region between the two steel bushings, as indicated in Figure 8-7(c). This suggested that galvanic corrosion of the aluminium lug which was in contact with the steel bushings was the cause of the corrosion damage. The severity of the corrosion damage is indicated by the cross-section of the lug, shown in Figure 8-7(d).

Figures 8-7(e) and 8-7(f) show one of the fracture surfaces produced by the failure. Figure 8-7(e) shows that the fracture originated at the site of the corrosion damage. Electron fractography of the same fracture surface (Fig. 8-7(f)) revealed mainly ductile dimples indicative of ductile failure.

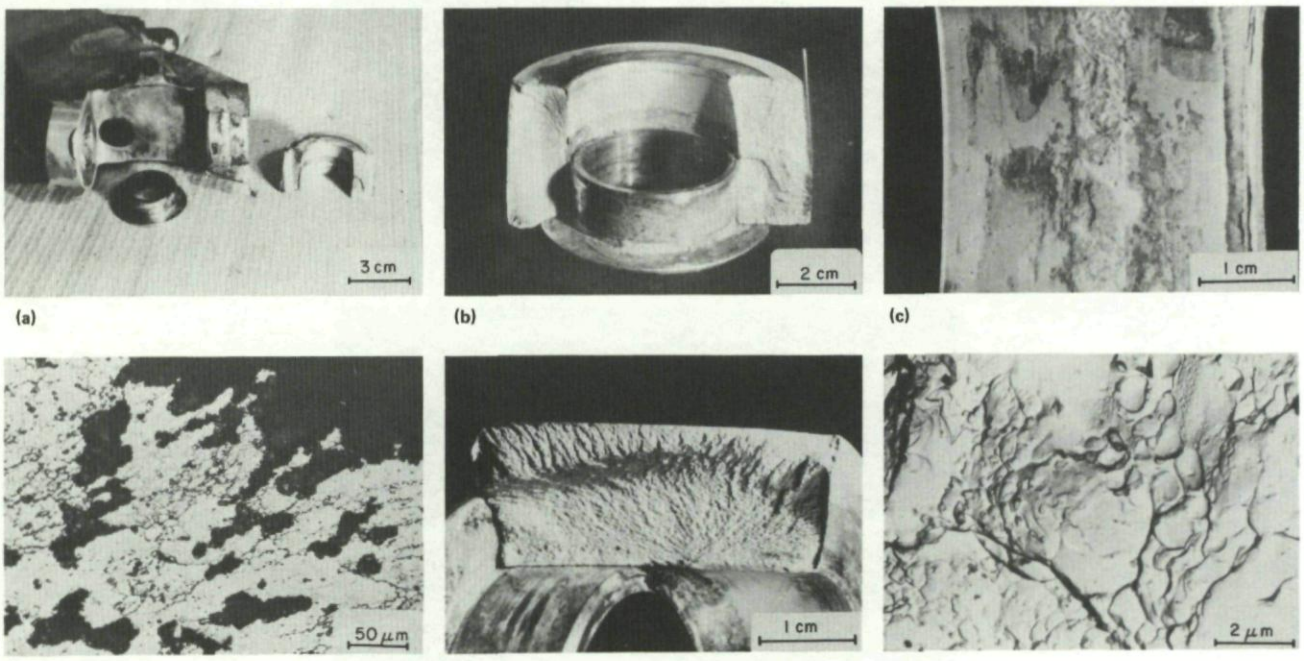

(a) (b) (c)

(d) (e) (f)

Fig. 8-7 Galvanic corrosion in a 7075-T6 king pin lug of a fighter aircraft main leg

(a) General view of the failed lug. (Mag. × 0.3)
(b) Fracture faces and steel bushing. (Mag. × 0.7)
(c) Band of corrosion in the lug between the bushings. (Mag. × 1.7)
(d) Deep corrosion pits revealed in a cross-section. (Mag. × 200)
(e) Crack initiation site in the corrosion band. (Mag. × 1.7)
(f) Dimpled fracture surface indicating ductile fracture. (Mag. × 7000)

It was concluded that the king pin lug failed in a ductile manner by overload, but that the fracture was initiated by severe corrosion damage in a ring of exposed material between the two bushings. This corrosion damage could have been prevented by proper application and maintenance of a protective coating on the aluminium alloy. It was not reported whether the steel bushings were cadmium plated, but if so this should have provided a degree of compatibility between the steel and the aluminium. A significant factor in this failure is that the corrosion damage occurred in a closed area which was not readily visible without dissassembly of the parts.

Case history 8-3. Corrosion of a nose gear strut assembly.

A nose gear strut assembly from an executive twin-engined aircraft was found, during a visual inspection, to be severely corroded around the drag brace attachment lugs. The strut and the areas of corrosion attack are shown in Figure 8-8(a). The strut assembly was a magnesium alloy casting and the lugs contained cadmium plated low alloy steel bushings. The steel type was not revealed to AGARD, but was reported to contain a high chromium content.

Visual inspection of the corroded lugs (Fig. 8-8(b)) showed that the steel bushings were undamaged while severe corrosion of the magnesium alloy which was in contact with the steel had occurred. The preferential corrosive attack of the magnesium at the magnesium/steel interface suggests that the damage was caused by galvanic corrosion, where the magnesium formed the anode of the electrolytic cell and the steel the cathode. The aircraft in question had been operated in a marine environment, and the moist salt laden atmosphere would have contributed to the problem. However even a milder environment would likely give rise to a similar problem given sufficient time.

Both cadmium and zinc type coatings protect steel by anodic protection, which involves the sacrificial corrosion of the anodic coating to prevent or minimize corrosion in the cathodic steel. However in sea water magnesium alloys are strongly anodic with respect to both steel and cadmium, and therefore cadmium serves no useful purpose in this case other than to protect the bore of the steel bushing. It is doubtful whether magnesium alloy castings would be selected at the present time for a component such as this nose gear strut, which experiences severe conditions and aggressive environments in service. However, in other cases it is important to provide an insulating interface material between magnesium and any steel parts.

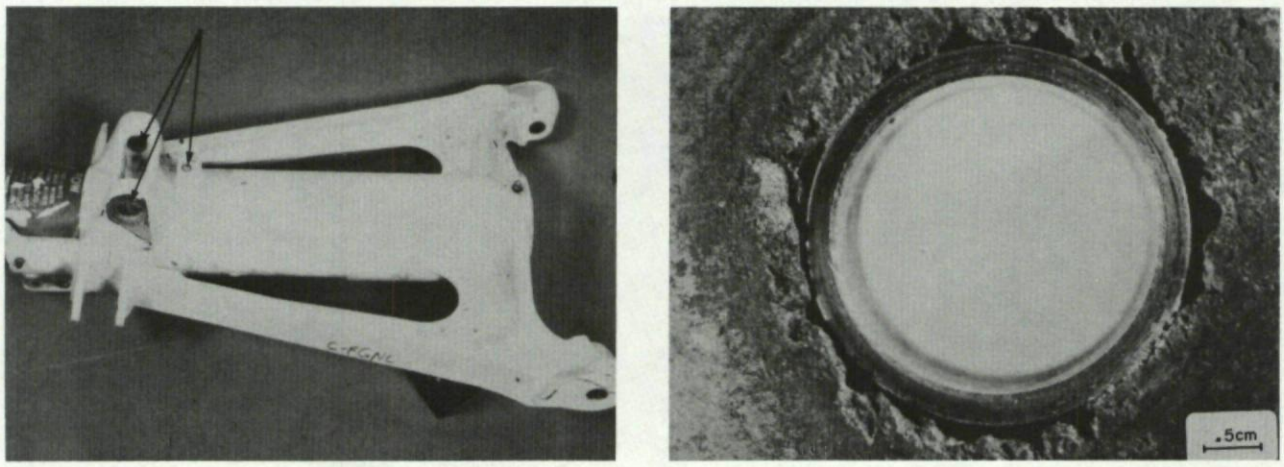

(a) (b)

Fig. 8-8 Galvanic corrosion between a steel bushing and a cast magnesium alloy nose gear strut

(a) General view showing areas of attack (arrows).
(b) Close-up of corrosion adjacent to the cathodically protected steel bushing. (Mag. × 2)

Case history 8-4. Galvanic corrosion of an aluminium alloy wing skin caused by the use of a graphite marker.

A maintenance technician reportedly noticed a small nick in the lower wing skin of a fighter aircraft. He circled the defect using a conventional graphite pencil; however the nick and the pencil marking were not removed immediately. Some months later a disc of the lower skin, matching the pencilled circle reportedly "fell out of the wing".

In order to verify that the lost disc might be associated with the pencil marking, laboratory specimens of the high strength aluminium alloy skin material were marked with a conventional graphite pencil and with a grease pencil, and were then exposed to salt mist accelerated corrosion testing. One week of exposure showed no effect on the grease pencilled panel (Fig. 8-9(a)) while the graphite pencilled panel showed severe corrosion damage (Fig. 8-9(b)).

Whether the reported "lost disc" actually fell out of the wing cannot be ascertained, but nevertheless the laboratory trials demonstrate unequivocally that severe galvanic corrosion can occur, even when a thin film of graphite comes in contact with a high strength aluminium alloy. Table 3-2 shows that graphite (carbon) is one of the most noble materials, and will give rise to a strong electrochemical potential when coupled with aluminium alloys. Marking of any aerospace hardware should only be performed with safety-checked markers, such as grease pencils.

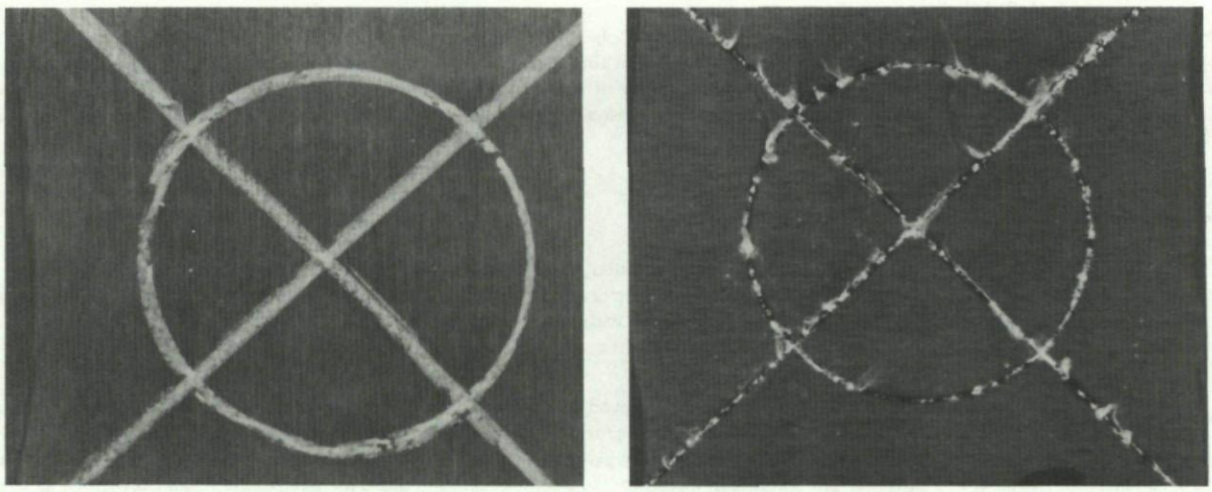

Fig. 8-9 Galvanic corrosion in aluminium alloy wing skin due to conductive markers

(a) Panel after 7 days exposure to salt mist when a grease pencil was used.
(b) Panel after the same exposure when a graphite marker was used, showing galvanic corrosion.

Case history 8-5. Galvanic corrosion in a magnesium alloy flap deflection control lever.

The control levers of a flap deflection mechanism of an aircraft were made from a magnesium casting alloy with a nominal composition Mg - 6%, Zn - 2%, Th - 0.75 Zr, similar to ZH62A. The levers were protected with a zinc-chromate primer and an epoxy top-coat. Galvanic corrosion was found in the levers in a socket where steel balls had been located. The ends of the lever arms are shown in Figures 8-10(a) and 8-10(b), which also show the corrosion damage. Figure 8-10(c) shows a cross-section through the lever arm in the corroded area and shows deep cavities due to this galvanic corrosion.

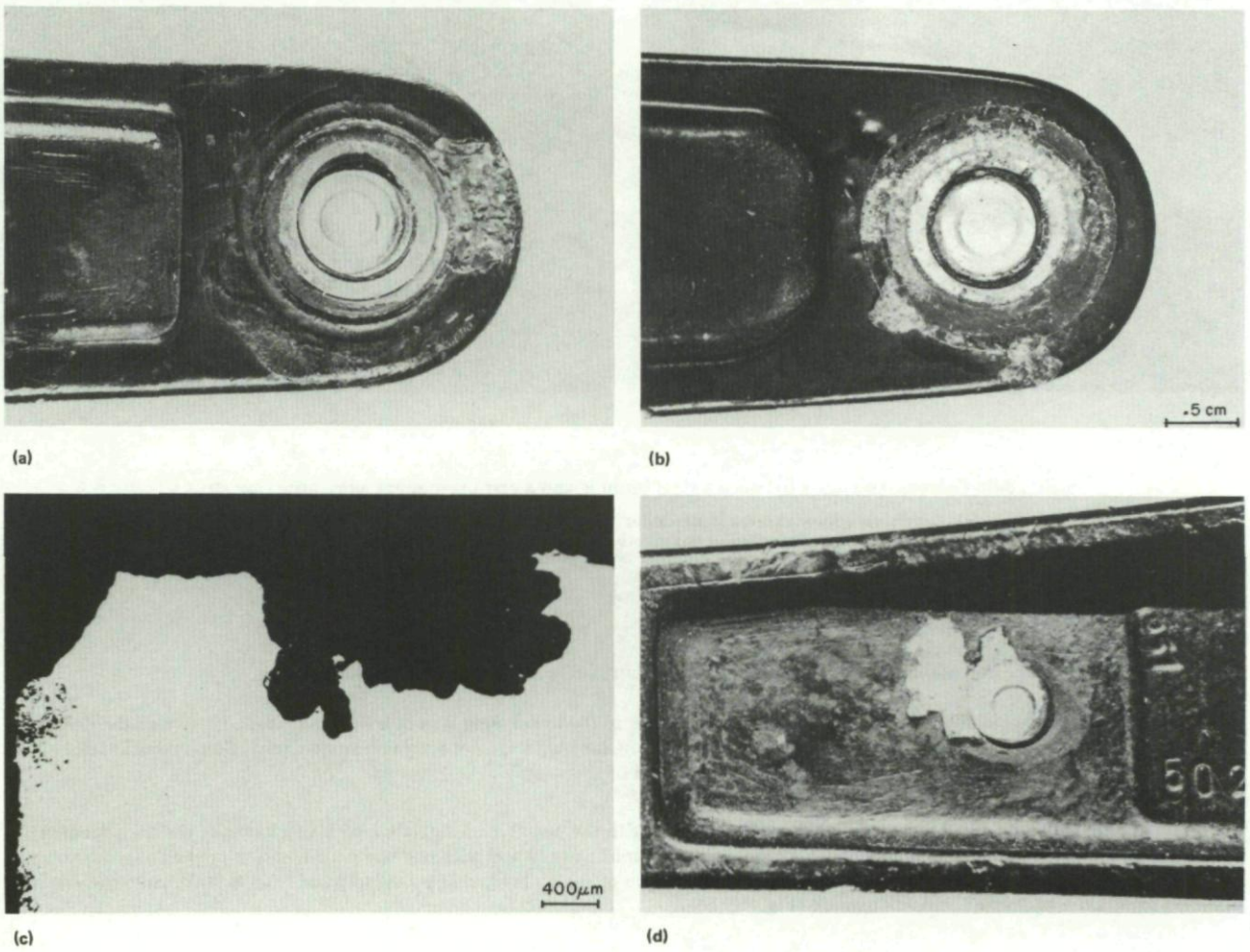

Fig. 8-10 Galvanic corrosion in a cast magnesium alloy flap control lever arm

(a) and (b) End of the magnesium lever showing ball socket and corrosion. (Mag. × 2)
(c) Cross-section through the corroded region of Figure 8-10(a), showing deep pitting. (Mag. × 25)
(d) Galvanic corrosion in the magnesium lever around a press-fit aluminium bushing.

Other examples of galvanic corrosion were found in the same fittings. Figure 8-10(d) shows an area of galvanic corrosion around an aluminium bushing which was press fitted into the lever.

In both these cases the galvanic corrosion occurred because of the highly anodic behaviour of the magnesium with respect to the metals in contact, and the inability of the protection system to isolate the metals and to exclude moisture. In the case of the aluminium bushing, a sealant might have prevented ingress of moisture, while an elastic paint was considered as a means of delaying the galvanic corrosion in the steel ball bearing sockets. However, current aircraft designs tend to avoid use of magnesium alloys, and particularly when the components are in contact with moving parts of a dissimilar metal where damage will inevitably occur to protective coatings and allow galvanic corrosion to occur.

CHAPTER 9

PITTING, CREVICE AND FILIFORM CORROSION

9.1 Introduction: Pitting

Pitting corrosion is a strongly localized type of attack which leads to the formation of deep and narrow cavities. All engineering metals and alloys are susceptible, and the conditions leading to pitting vary from metal to metal, depending in part on whether the metal is normally active or passive.

For active metals uniform exposure of a large surface area to a corrosive medium would tend to cause uniform corrosion. Pitting of an active metal will therefore occur as a result of local wetting, or defects in a protective coating which allow very localized exposure. A severe case of pitting corrosion damage to an active metal component is shown in Figure 9-1(a). The component was a magnesium alloy casting used as a helicopter structural cleat, and this was originally chromated and sealed. The protective treatment was damaged locally, possibly by the tools used in applying the fasteners, and not repaired. A similar example is illustrated in Figure 9-1(b) which shows a corroded magnesium alloy casting of a stringer end cap. This was also chromated and primed, but severe pitting corrosion occurred, probably due to failure of protection by aging and exposure to moisture.

In passive metals such as certain stainless steels and aluminium alloys, which form naturally protective oxide films, pitting occurs as a result of localized damage to this protective film. However, whether the metal is active or passive, pitting involves the formation of small areas which are anodic with respect to the rest of the surface, and which therefore suffer severe corrosive attack in the presence of an electrolyte.

In aircraft structures pitting corrosion may occur in many areas, but areas subject to local contamination by highly corrosive media, such as battery compartments, toilet and galley areas, are prime sites. Pitting corrosion is particularly common in aircraft structures operating in marine environments since the chloride ions promote the local dissolution of protective oxide films. Pitting in passive metals is uncommon in solutions which do not contain halide ions, since the oxide films would tend to be stable and remain protective.

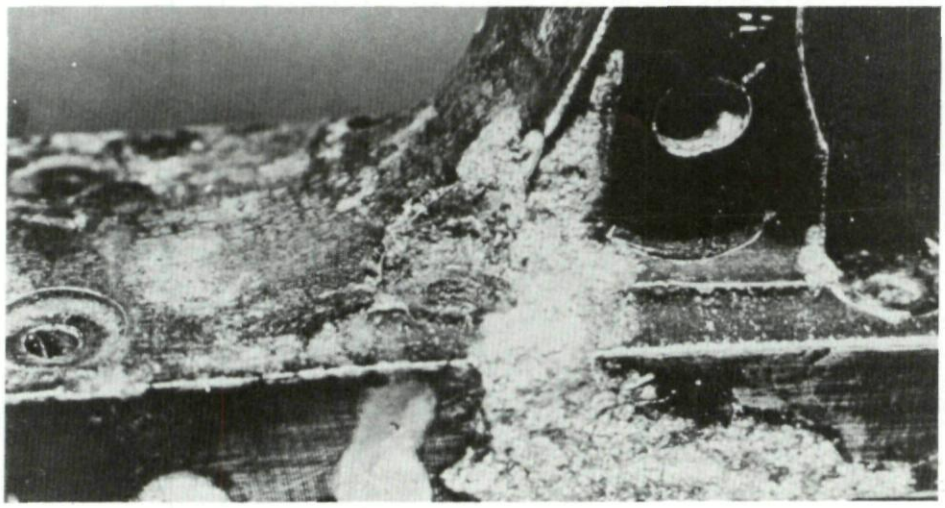

Fig. 9-1(a) Severe pitting in a magnesium alloy casting

Fig. 9-1(b) Severe pitting in a cast magnesium alloy stringer end cap

Pitting occurs in two stages, initiation and growth. The initiation stage involves the period before visible pits have formed and may extend over periods of several months or several years, even for nominally constant environmental conditions. Under actual service conditions, it is likely that a transient exposure to a severe environment involving high concentrations of chloride ions or high acidity (ph) will be responsible for initiation. Once a pit has formed it can penetrate the metal at an ever increasing rate. This is because the corrosion process occurring within the pit produces conditions which favour the continued and accelerating dissolution of metal. In the pitting of a metal by an aerated sodium chloride solution, rapid dissolution of metal within the pit tends to produce an excess of positive charge in this area. This causes the migration of chloride ions into the pit to balance the positive charge, and the formation of $MC\ell$. The high concentration of chloride ions, together with the high concentration of hydrogen ions arising from hydrolysis, provides conditions which favour the continued dissolution of the metal. This build-up of high concentrations of metal, chloride and hydrogen ions in the pit is favoured by a stagnant, or only slowly moving solution, and also by the growth of the pit in the direction of gravity forces. By increasing the velocity or turbulence in a corrosive solution, or by creating conditions which oppose the formation of highly acidic conditions in the pit, the pitting action can often be stopped.

Pitting corrosion is one of the most insidious forms of corrosion because the pits are often very small and difficult to see with the naked eye, and particularly if they are hidden by general corrosion products or coatings. The electrochemical conditions at the base of a pit can be such that other forms of corrosion, such as intergranular attack will occur, leading to widespread subsurface damage. In highly loaded structures the stress concentration at the base of a pit can be sufficient to cause fatigue or stress corrosion cracking to occur. Examples of these forms of combined corrosion action are given in the case histories described below.

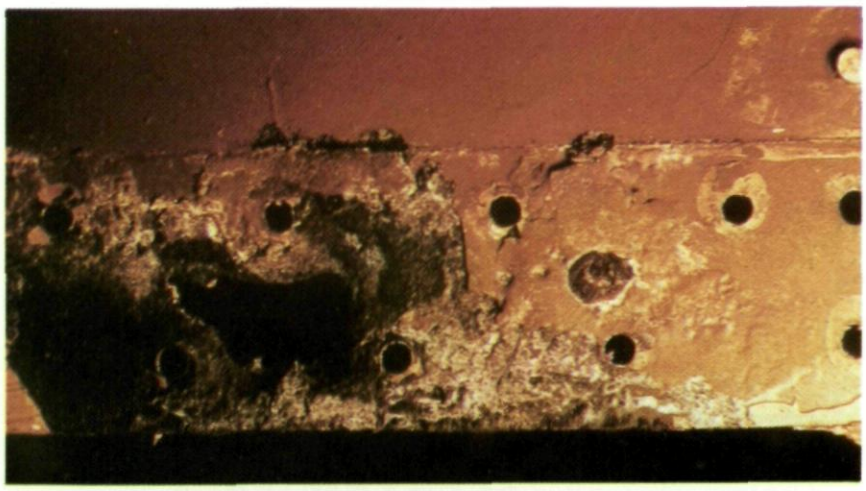

(a) Dismantled joint in a magnesium alloy panel.

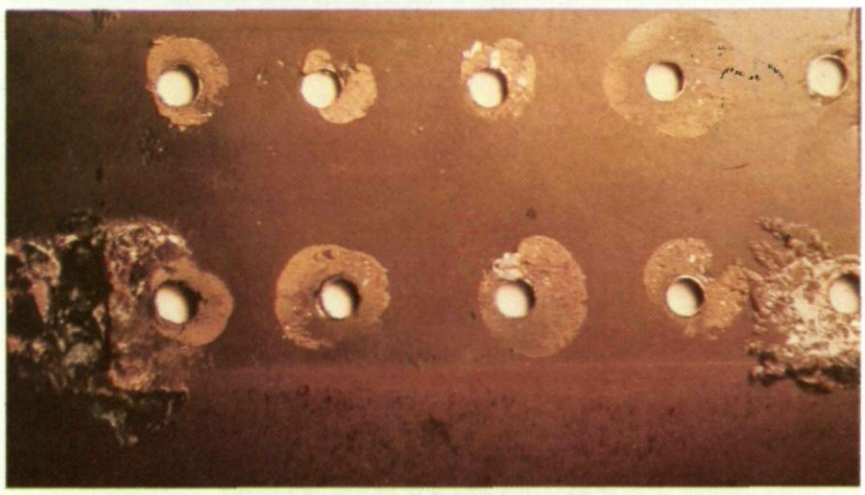

(b) Crevice corrosion in a magnesium alloy skin joint due to inadequate sealing.

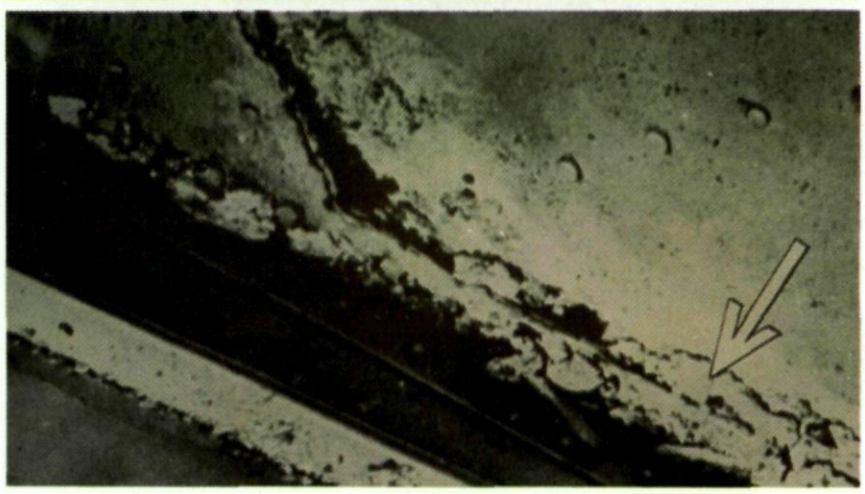

(c) Crevice and galvanic corrosion between a magnesium alloy floor panel and aluminium alloy frame member.

Fig. 9-2 Examples of crevice corrosion in aircraft structural parts

9.2 Introduction: Crevice Corrosion

This is a form of attack which occurs when a corrosive liquid, such as salt spray, gains access to crevices in, or between components. It is usually associated with small volumes of stagnant solution which become trapped in holes, between gasket surfaces or lap joints, under surface deposits, or in crevices under bolt or rivet heads. If there are differences in the concentration of dissolved salts or dissolved oxygen in the entrapped liquid, anodic and cathodic regions may result, and the anodic areas will be attacked. This anodic region is usually at the bottom of a crevice and a pit develops. The corrosive action at the bottom of the pit accentuates the difference in concentration of the electrolyte at that point and corrosive attack progresses more rapidly as the depth of the pit increases. Crevice corrosion has many characteristics in common with pitting. For example it is common in passive metals such as stainless steels and aluminium alloys which form protective oxide films, and it is often observed in solutions containing high concentrations of chloride ions and hydrogen ions, which promote the breakdown of these films.

Some examples of crevice corrosion are shown in Figures 9-2(a), 9-2(b) and 9-2(c). Figure 9-2(a) shows a corroded and perforated magnesium panel in a dismantled joint area from a transport aircraft structure. The corrosion damage was due to inadequate sealing. Figure 9-2(b) presents a similar case of crevice corrosion at the interface of a magnesium alloy skin joint, which was also due to inadequate sealing. In both examples the most severe damage is away from the edges of the fastener holes which suggests that galvanic corrosion was not the major factor. Figure 9-2(c) shows a situation where both galvanic corrosion and crevice corrosion contributed to the damage. The corrosion damage has occurred at the junction between a magnesium alloy floor panel and aluminium alloy frames and angle plates. This problem was probably aggravated by poor drainage conditions, and inadequate sealing and surface protection.

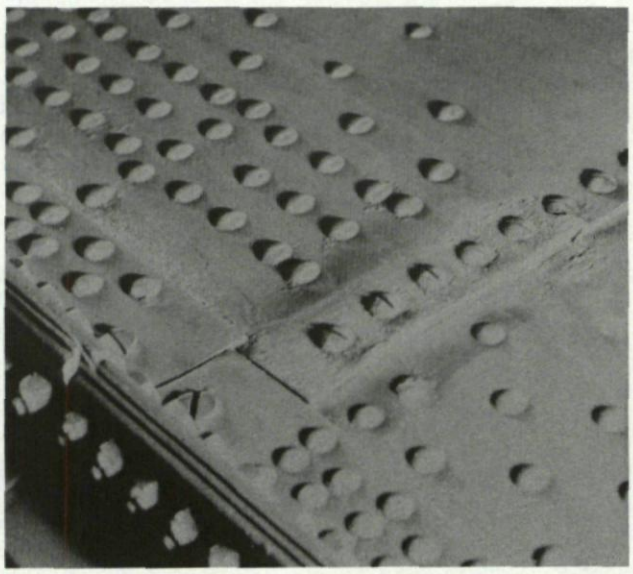

(a)

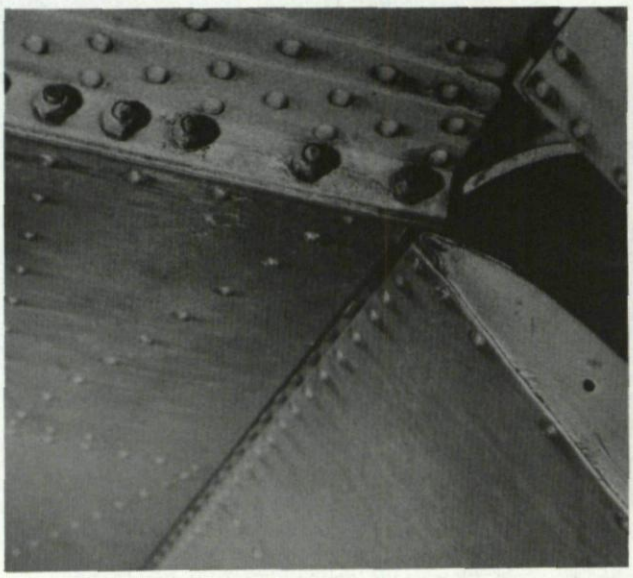

(b)

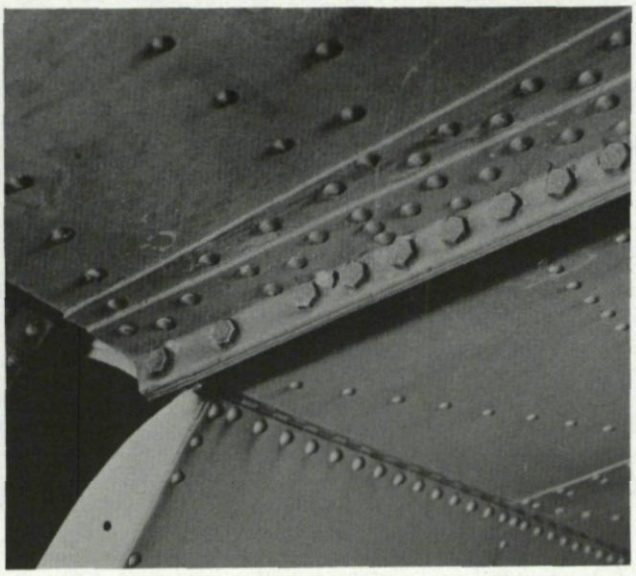

(c)

Fig. 9-3 *Crevice corrosion in the outer wing coupling flange of a transport aircraft*

(a) Crevice corrosion in aluminium lap joint.
(b) and (c) Corrosion around bolts and under nuts in the under wing structure.

Crevice corrosion may be particularly severe with magnesium alloys since they are the most anodic of the common airframe structural alloys, however similar problems also exist with aluminium alloys. Figures 9-3(a), 9-3(b) and 9-3(c) show examples of crevice corrosion in the outer wing coupling flange of an older type small transport aircraft which had been operating in the Mediterranean region. The damage was observed during routine visual inspection, and subsequently x-ray inspection was used to measure the depth of corrosion in the different areas of structure. The structure was predominantly aluminium alloy sheet and flanges, with steel fasteners, and the structure was protected by a titanium dioxide (TiO_2) pigmented paint finish. Crevice corrosion is evident between the aluminium alloy flanges and sheet, and at the aluminium lap joints (Fig. 9-3(a)). Corrosion cavities were also observed under the bolts and nuts (Figs. 9-3(b) and 9-3(c)), and the corrosion can be seen to extend beyond the area of contact of the fasteners. Measurements of the depth of corrosion showed that this was greatest under the heads of the bolts and nuts, rather than at the immediate edges of the fastener holes. This suggests that the crevice effect was probably at least as significant as the galvanic effect in this case. The corrosion repair work led to this aircraft being out of commission for a reported "long period", although the precise details were not available. The repair work involved the use of a pigmented zinc chromate primer and top coat, in place of the TiO_2 finish used originally.

9.3 Introduction: Filiform Corrosion

Filiform corrosion is one of the less common forms of corrosion in aircraft structures and consequently is not as well understood, or as well documented as some others. It has some of the characteristics of pitting corrosion and also of intergranular corrosion. It often starts from a corrosion pit, but instead of penetrating deep into the thickness of the metal it spreads out sideways to form threadlike lines of corrosion near the surface. It is often found in clad aluminium alloys, where the initial pit will penetrate the cladding, and then will be diverted by the underlying grains to run parallel with the surface in numerous meandering filaments. It is also found under organic coatings such as paints, and it has been suggested that this may be due to the permeation of moisture through the painted surfaces under conditions of high humidity and high ambient temperatures. However it is also often found that the corrosion starts at fastener holes, where the metal is unprotected, and then extends along the surface of the sheet and beneath the paint.

This form of corrosion may become quite severe before it is detected, since it will often be hidden by either cladding or paint, and in the latter case may be indicated by blistering. A typical example is shown in Figure 9-4(a), where the paint blistering is concentrated around the rivet holes in an aluminium alloy sheet. Figure 9-4(b) shows the same area after the paint has been removed, and the threadlike meanderings of the corrosion filaments can be seen. Filiform corrosion has been observed in magnesium, aluminium, steel and chromium-plated nickel.

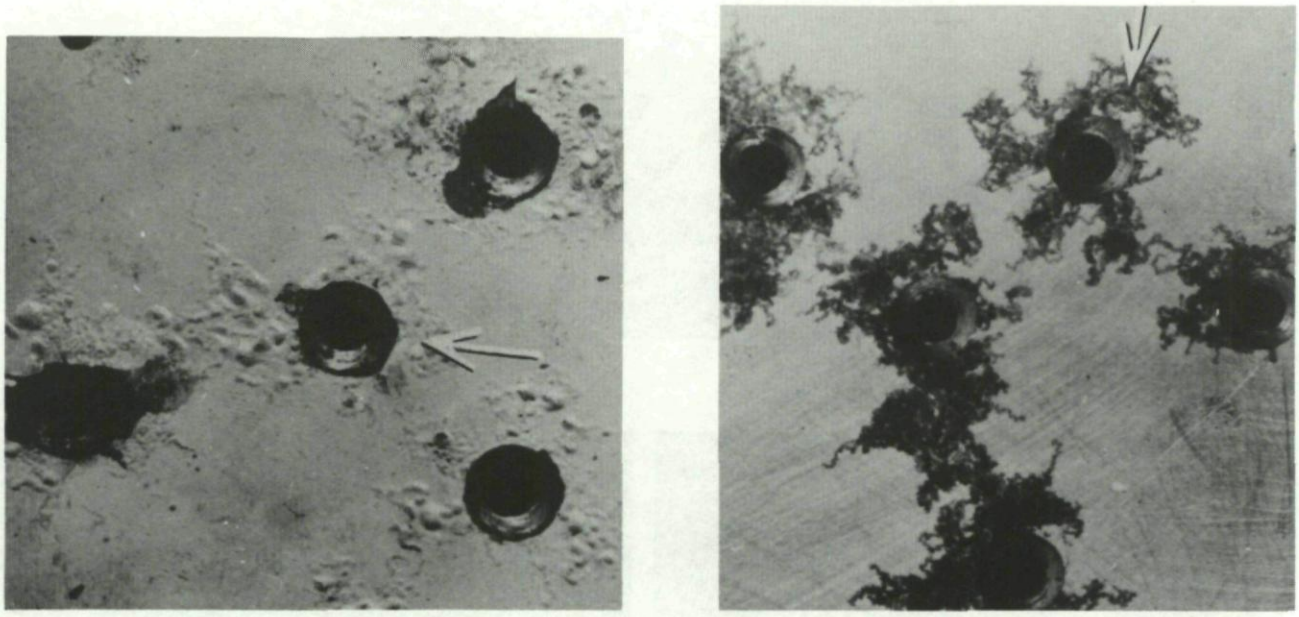

(a) (b)

Fig. 9-4 Filiform corrosion in an aluminium alloy sheet structure

(a) Blistering of paint due to underlying corrosion.
(b) Filiform corrosion revealed by removing paint.

9.4 Case Histories

Case history 9-1. Loss of an engine's thrust reverser doors due to pitting corrosion.

A large commercial jet lost the thrust reverser doors from one of its engines in cruise flight, but nevertheless landed safely. Subsequent investigation showed one thrust reverser door driver link had fractured, allowing the leading edge of the door to spring up into the 550 knot airstream. Figure 9-5(a) shows the general arrangement of the thrust reverser system with the failure location indicated by an arrow. The resulting air loads on the thrust reverser had torn the doors away from the aircraft. Closer inspection showed that the link failed in fatigue, but the fatigue crack initiated at pitting corrosion sites in the link surface. The latter was coated by a protective molybdenum disulphide type dry film lubricant. Figure 9-5(b) shows the broken driver links, with the primary fatigue fracture indicated by arrows.

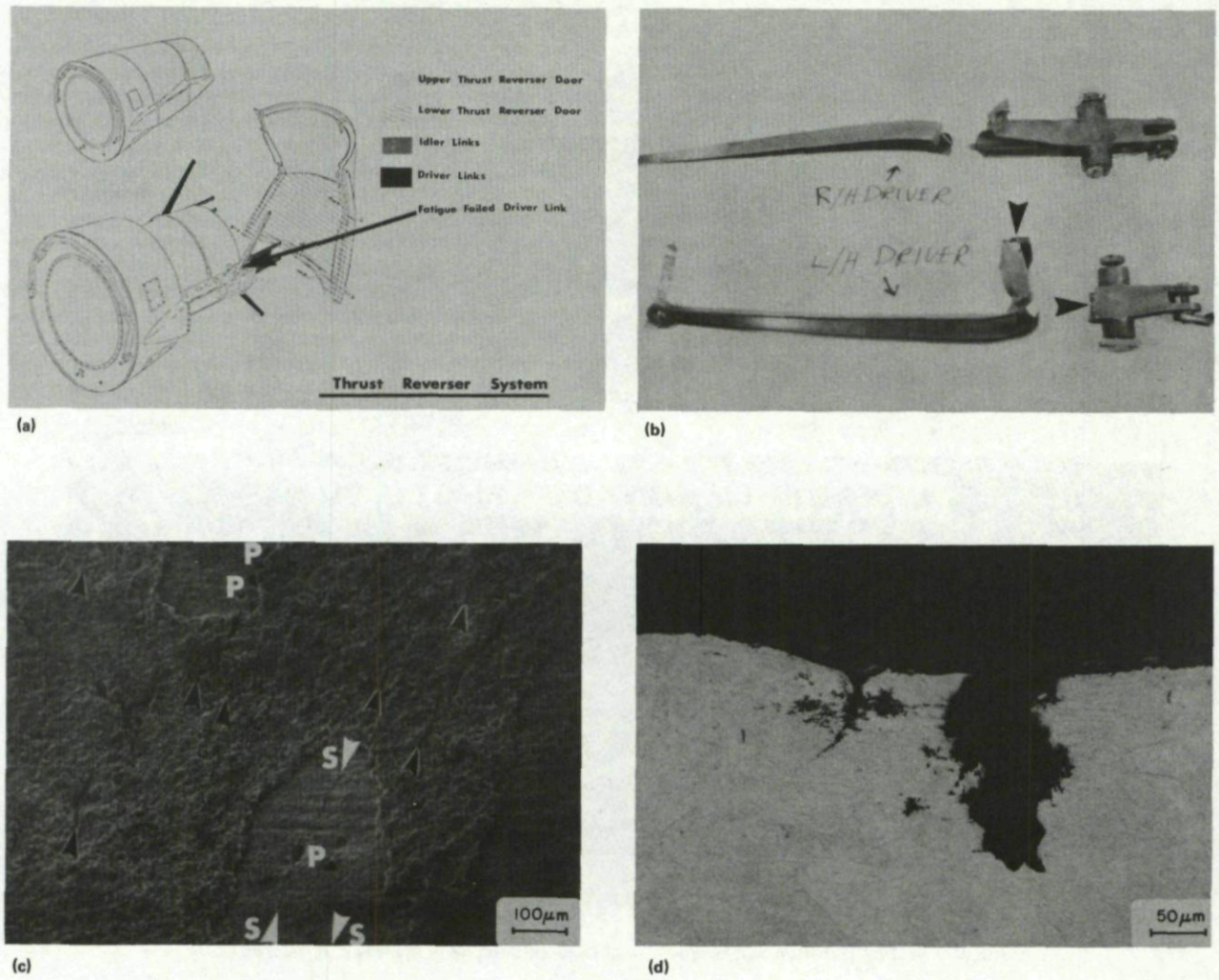

Fig. 9-5 Pitting corrosion and fatigue failure of a thrust reverser driver link

(a) General arrangement of thrust reverser system showing location of failure.
(b) Broken driver links showing primary fatigue fractures (arrows).
(c) Scanning electron microscope photograph of link surface near fracture, showing fissures in coating (black arrows). White arrows 'S' show cracks growing from pits 'P' in areas where coating has spalled off. Black arrows show fissures in coating. (Mag. × 100)
(d) Cross-section through a typical pit (P in Fig. 9-5(c)) showing depth of attack. Villela's etch. (Mag. × 200)

Scanning electron microscopic (SEM) examination of the surface near the fracture showed that the coating was fissured, and that pits were being formed at the roots of these fissures. Small fatigue cracks were growing from almost every such pit, and all were parallel to the major fracture surface. These features are shown in Figure 9-5(c).

Since the operating cyclic stress was close to the yield stress for this 422 type stainless steel link, any pit represented a sufficient stress concentration site to rapidly initiate high stress, low cycle fatigue. Pitting was the result of entrapment of fuel combustion by-products and moisture, collecting in fissures in the coating and attacking the stainless steel. A cross-section through a typical pit is shown in Figure 9-5(d).

Prevention could be accomplished by lowering the very high stress level in the link, or by preventing the corrosion pitting of the link. However, the corrosive medium in this case could not be eliminated since combustion products will inevitably condense on the part. The most practical immediate approach to preventing further failures was to strip the coating from all existing links, inspect for corrosion or cracks, and recoat the sound links with an improved coating while maintaining an ongoing inspection programme to identify early signs of corrosion. In the longer term, a redesign of the link system to reduce the service stresses would also be beneficial.

Case history 9-2. Main landing gear strut failures in a fighter aircraft.

Within a one month period, three naval aircraft were damaged due to failure of their main landing gear struts. The failed struts were submitted for laboratory examination, which showed the strut outer barrel was fabricated from 2014-type aluminium alloy, and all were within the specified dimensional tolerances with respect to wall thicknesses.

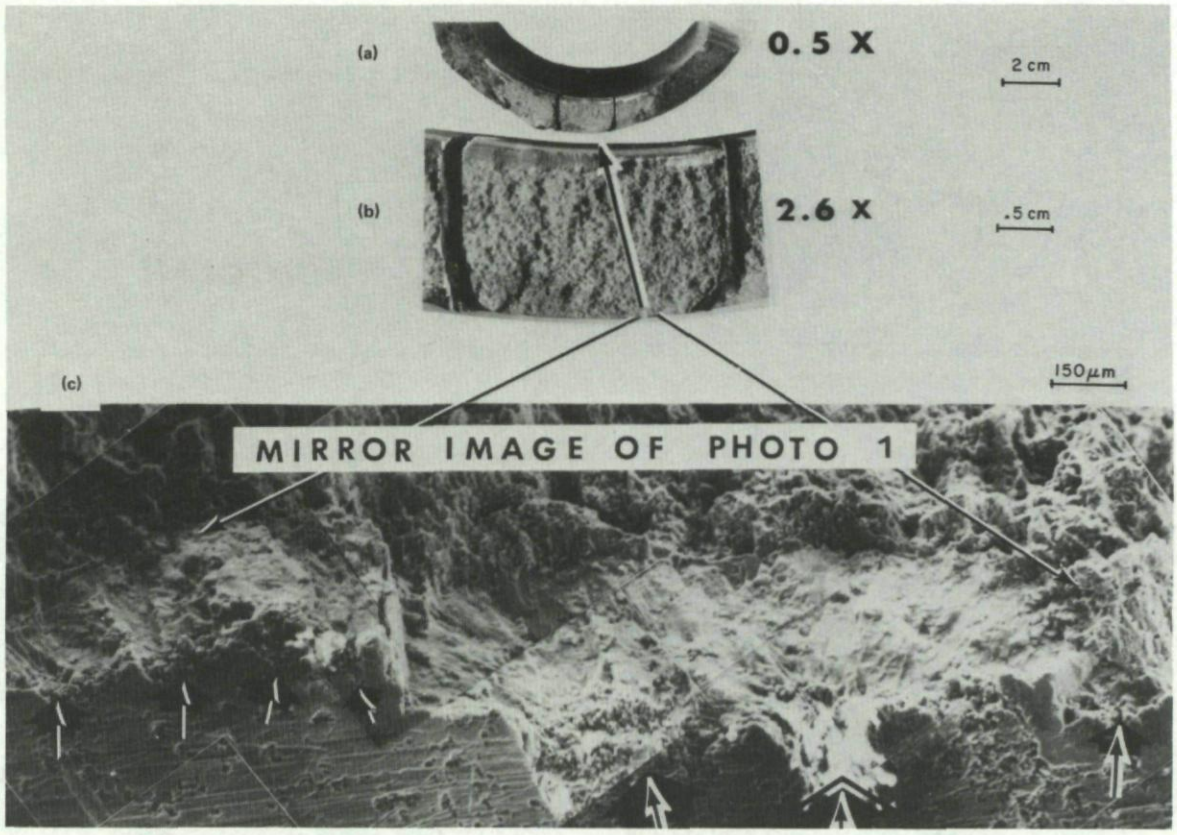

Fig. 9-6 Pitting corrosion and fatigue of a 2014 aluminium alloy main landing gear strut

(a) and (b) Low magnification photographs of the fracture surface.
(c) Montage showing the crack initiation region and portions of the landing gear outer surface showing pitting.

The three failed struts were cleaned ultrasonically in an acetone solvent and then examined macroscopically, and by transmission electron microscopy. Two of the three parts exhibited corrosion pits followed by fatigue, while the third showed characteristics of fatigue failure but no pits. Figure 9-6 shows a section of the fracture surface of one of the parts at three different magnifications. Extensive corrosion pitting can be seen along the machined surface in Figure 9-6(c), in the vicinity of the fatigue crack initiation.

The surface details of the fracture shown in Figure 9-6, were partially obliterated by corrosion products, but not sufficiently to obscure the presence of fatigue striations. In the other two components the fracture surfaces were relatively clean and fatigue striation counts and spacing measurements could be made fairly reliably. The striation spacings were found to vary from area to area on each fracture surface, and in specific areas both coarse and fine striations were found together. However, based on average striation count measurements it was found that the total striations to failure were 15100, 18000, and 16400 respectively for the three different struts. These values were reported to be between 1.5 and 2.5 times the actual number of landings, therefore indicating that each landing produced more than one striation. Notwithstanding the uncertainties in this analysis, the data was found to be useful as a guide in establishing inspection intervals.

No information was given in this investigation on any surface protective coatings used on these landing gear struts, and they may not have been used. Alloy 2014 has excellent resistance to corrosion in most common environments because it passivates spontaneously under normal oxidizing conditions (Ref. 9-1). In outdoor environments the alloy weathers to a grey colour with some initial pitting which gradually ceases (Ref. 9-2). Industrial soot, sulphur dioxide, sulphur trioxide and marine spray tend to increase atmospheric corrosion, but the alloy is resistant to hydrogen sulphide and carbon dioxide (Ref 9-3). In aqueous environments, the corrosion resistance is greatest under neutral or slightly acidic conditions. Strong alkalies and strong non-oxidizing acids destroy the oxide and accelerate corrosion. Pitting can occur if the alloy is in water containing chlorides or other halogen ions. Since aluminium is anodic to most other common metals, galvanic coupling with them generally results in severe attack on the aluminium alloy, especially in sea water (Ref. 9-4).

It is evident that the marine role of these aircraft was a significant factor in the pitting and failure of at least two of the landing gear struts. A surface protective coating, if not used, would have aided in combating corrosion. Further information on the gear design would be needed to assess the possible role of galvanic corrosion in the overall degradation process.

Case history 9-3. Pitting corrosion and fatigue of a tip tank latch knob.

The analysis of this component failure is illustrated in Figures 9-7(a) to 9-7(f). A tip tank latch knob is shown in Figure 9-7(a), and is typical of three similar parts which failed with almost identical fracture features. The material in all cases was AISI 4340 steel, which is a low alloy steel with poor corrosion resistance. No information was given in this investigation on the presence of a protective coating, and one would certainly be needed to avoid corrosion damage.

Two of the three failures occurred just underneath the head of the latch knob, at location I in Figure 9-7(b), while the third failure occurred in the second radius, at location II in Figure 9-7(b). An example of the fracture surface of the first type is given in Figure 9-7(c), while the second type of fracture surface is illustrated in Figure 9-7(d). Figure 9-7(e) shows one of the fracture surfaces in greater detail.

All of the failures initiated at the side of the latch knobs facing towards the wing lower side, and in every failure almost half the cross-section showed a fatigue fracture surface. An investigation with the scanning electron microscope revealed that the failures were initiated by corrosion pits. This is illustrated in Figure 9-7(f), showing a corrosion pit at the origin of one of the fatigue fractures.

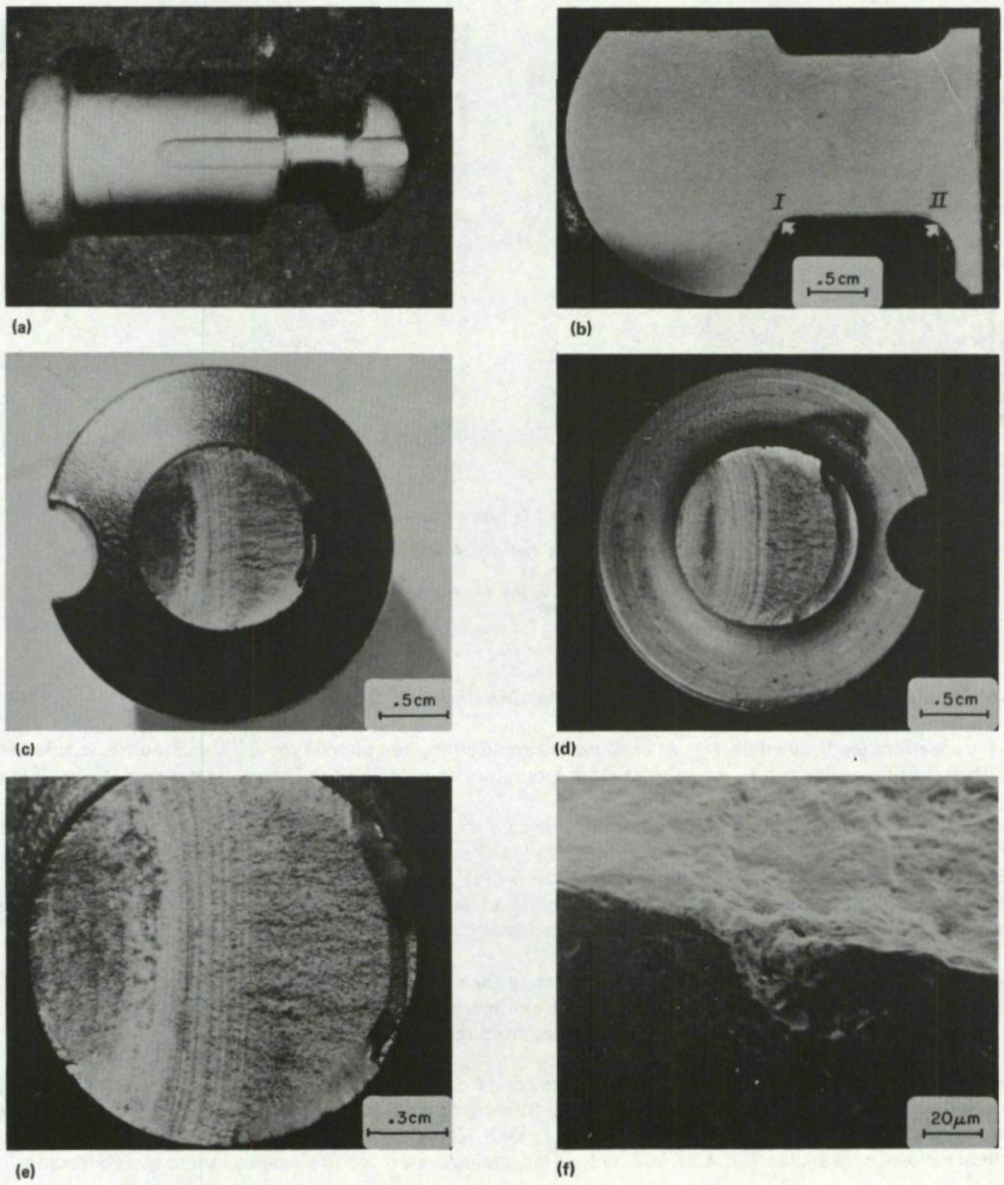

Fig. 9-7 Pitting corrosion and fatigue failure of a 4340 steel tip tank latch knob

(a) General view of the latch knob.
(b) Cross-section through the knob show crack initiation sites. (Mag. × 2)
(c) Fracture surface of crack initiating at site I. (Mag. × 2.5)
(d) Fracture surface of crack initiating at site II. (Mag. × 2.5)
(e) Fracture surface of (9-7c) at higher magnification. (Mag. × 5)
(f) Corrosion pitting at a fatigue crack initiation site. (Mag. × 500)

It was concluded that the main cause of the failures was the corrosion pits in critical areas of the latch. Since other similar parts were in service on aircraft, it was recommended that all latch knobs be inspected visually with the aid of a binocular microscope for evidence of corrosion. Any components showing signs of pitting corrosion were rejected. For a long term solution it was recommended that a change of material be made, involving the use of an alloy such as 17-4 PH stainless steel which has much improved corrosion resistance compared to 4340, and can be heat treated to similar strength levels and hardness. However this alloy is also susceptible to crevice, pitting and edge corrosion in sea water (Ref. 9-5) and therefore periodic inspection would be required.

Case history 9-4. In-flight failure of an engine exhaust valve.

A light single engine aircraft suffered in-flight engine failure and was destroyed in the subsequent forced landing. Engine teardown revealed engine seizure was the result of an exhaust valve failure. The valve stem fractured in fatigue, the crack initiating at pitting corrosion sites on the valve stem. The push rod also showed extensive pitting corrosion. Both parts are shown in Figure 9-8(a).

Figure 9-8(b) shows a typical pit in the valve stem, filled with a complex series of corrosion products containing iron, chromium and silicon oxides, and aluminium, copper, lead, sulphur and bromine compounds. Pitting near the fracture was so severe as to overlap the pits and reduce the section diameter by approximately 0.25 mm. Since this engine continued to run for some time after the valve head had separated and had fallen into the cylinder head, extensive secondary damage resulted from the valve head ingestion and eventually seized the engine.

Teardown revealed extensive pitting of several other valves and push rods. The engine was found to have been inactive for long periods, during which the engine oil was not drained and replaced by inhibiting oil. This improper maintenance resulted in pitting corrosion of the valves and push rods from acid compounds formed in the old engine oil.

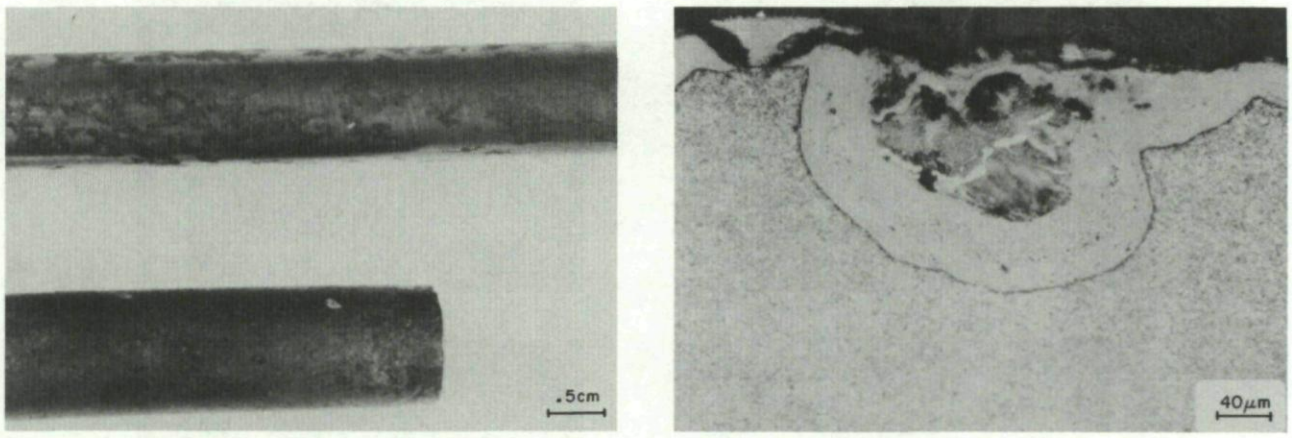

(a) (b)

Fig. 9-8 Pitting induced failure of an engine exhaust valve

(a) Pitted push rod (top) and pitted and fatigue fractured valve stem (bottom). (Mag. × 2)
(b) Typical corrosion pit in the valve stem near the fracture face. Nital etch. (Mag. × 250)

Case history 9-5. Pitting induced failure of 440C martensitic stainless steel wing flap hinge bearings.

Visual inspections led to the discovery of cracking in several chromium plated type 440C martensitic stainless steel wing flap hinge bearings. Three of the suspect parts were submitted for laboratory examination, and these are shown in Figure 9-9(a).

Bearings 1 and 2 were found to be cracked, while bearing 3 was found to be uncracked. In bearing No. 1, two separate cracks were found; one crack took the path shown in Figure 9-9(b), while the second crack, which is not shown, ran straight across the bearing cross-section. Bearing No. 2 showed the crack path seen in Figure 9-9(c). Further visual examination of the bearing crack fractures showed the cracks were flat and slightly fibrous, as indicated in Figure 9-9(d). The fracture face of bearing No. 2 differed slightly from the two fractures seen on bearing No. 1 in that there was a chip missing on the outer edge of the bearing.

Optical examination revealed numerous corrosion pits on the inner diameter of the failed bearings, and also on bearing No. 3 which had not failed. A typical example is shown in Figure 9-9(e). Figure 9-9(f) shows a cross-section through one of the corrosion pits, and a network of fine intergranular cracks can be seen emanating from the base of the pit.

Type 440C stainless steel is a 17% chromium, air hardening martensitic stainless steel. It is resistant to atmospheric and fresh water corrosion, and its corrosion resistance is maximum in the fully hardened condition. However the alloy is susceptible to both stress corrosion and hydrogen embrittlement if heat treated to high strength. Chemical analysis of the failed bearings, Table 9-1, showed that they met the compositional requirements of AMS 5630D for 440C stainless steel for all elements except molybdenum which was low.

Table 9-1 Chemical analysis of failed bearings, No. 1 and 2, and composition ranges for AMS 5630D

	Chemical Analysis Weight %					
	Cr	Mn	Mo	Si	C	Fe
AMS 5630D Max.	18.00	1.00	0.65	1.00	1.20	Balance
For 440C Min.	16.00		0.40		0.95	
Bearing No. 1	17.10	0.41	0.23	0.45	1.17	Balance
Bearing No. 2	17.50	0.41	0.27	0.43	0.98	Balance

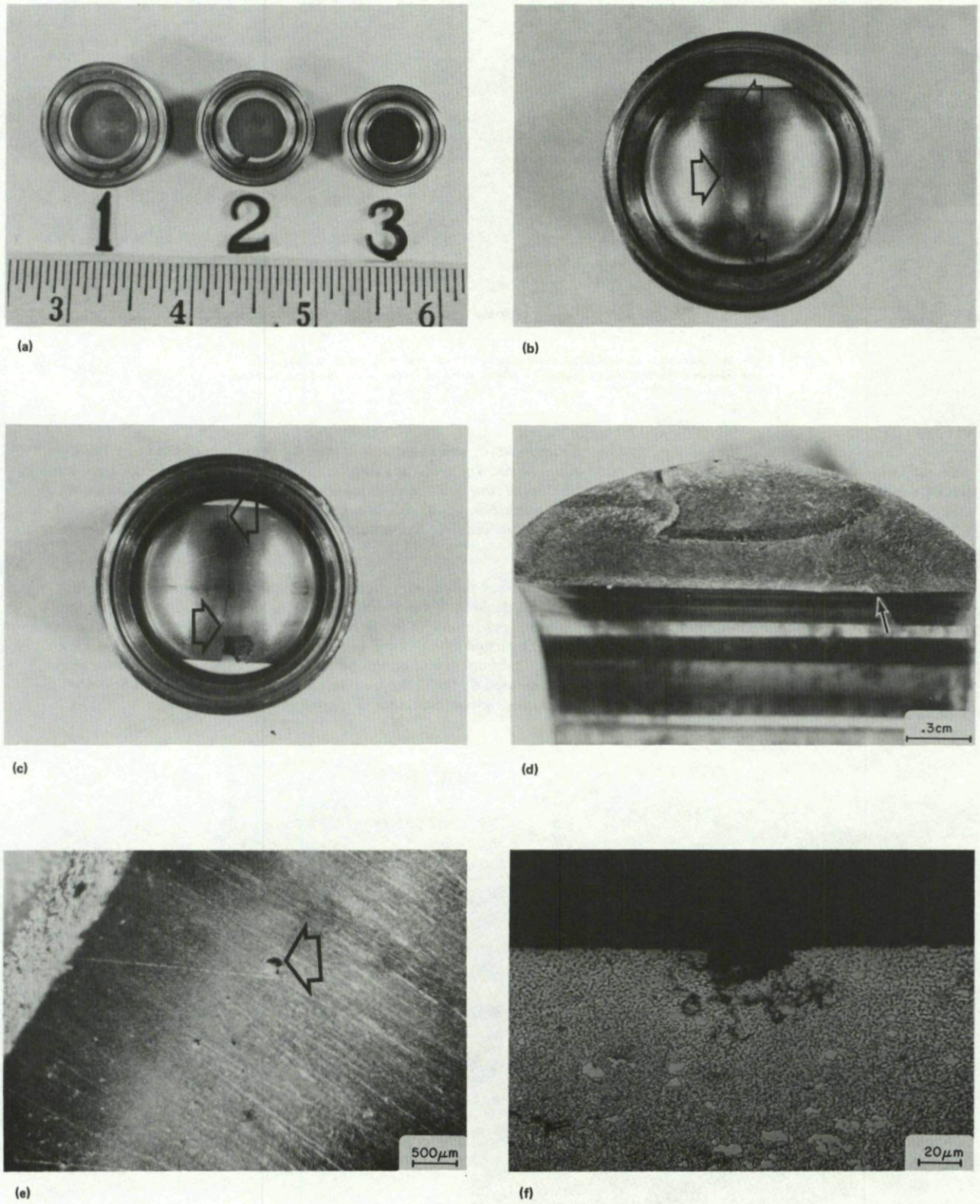

Fig. 9-9 Pitting induced failure of some 440C stainless steel hinge bearings

(a) Three hinge bearings from a fighter aircraft.
(b) Bearing number 1, showing crack configuration.
(c) Bearing number 2, showing crack pattern and fragment missing at end of crack.
(d) Fracture face of second crack in bearing number 1. Arrow shows probable crack initiation area. (Mag. × 5)
(e) Corrosion pits on the inner diameter of a bearing which are typical of all three bearings submitted. (Mag. × 20)
(f) Cross-section of corrosion pit found on bearing showing intergranular cracking at the base of the pit. Picric acid etch. (Mag. × 500)

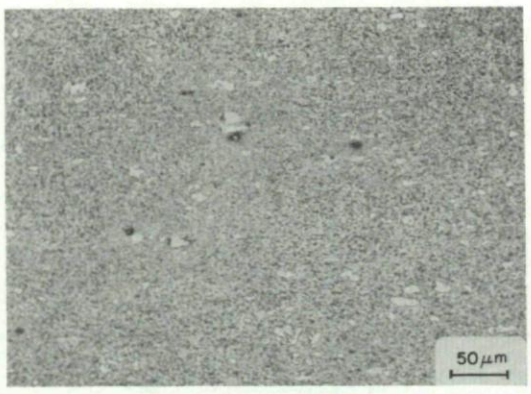

(g)

(h)

Fig. 9-9 Pitting induced failure of some 440C stainless steel hinge bearings (Cont'd)

(g) Microstructure typical of all three bearings. Picric acid etch. (Mag. × 200)
(h) Electron fractograph of bearing number 1 showing intergranular mode of fracture. (Mag. × 3960)

The microstructure of the bearings is shown in Figure 9-9(g), and shows fine spheroidal chromium carbide together with larger carbide globules dispersed in the tempered martensitic matrix. The material had a hardness of R_c 54-55, and both the microstructure and hardness were considered acceptable for this class of steel and the intended application. Figure 9-9(h) shows a replica transmission electron micrograph of the fracture surface of bearing No. 1, and indicates an intergranular mode of fracture. Similar observations were made for bearing No. 2, and both fracture surfaces showed indications of corrosion products on the intergranular facets.

It was concluded that the failures were caused by corrosion pitting which led to crack initiation and propagation either by stress corrosion cracking or hydrogen embrittlement. It was decided to carry out a fleet wide non-destructive examination to determine the extent of the flap hinge bearing cracking problem, and to inspect for pitting on the inner diameter. Since it is known that hydrogen cracking can occur during chromium plating of hardened 440C, it was decided to review the chromium plating and baking sequence to ensure that a source of hydrogen was not introduced during the plating operation. To counteract the pitting problem it was suggested that electroless nickel plating could be used on the entire bearing, since electroless nickel can be heated to 340°C for 1 hour subsequent to plating to provide wear resistance equivalent to that of chromium.

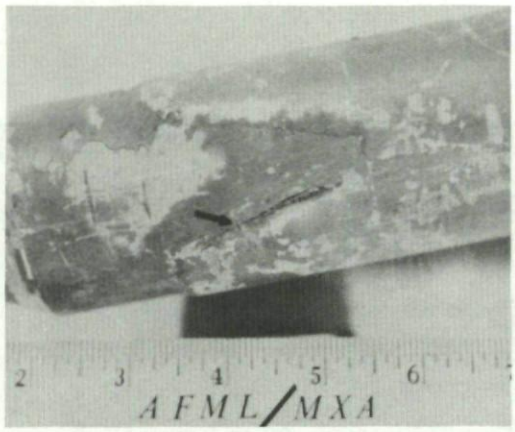

(a)

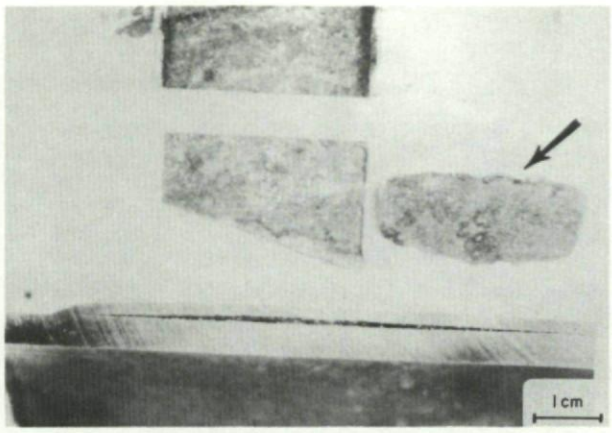

(b)

(c)

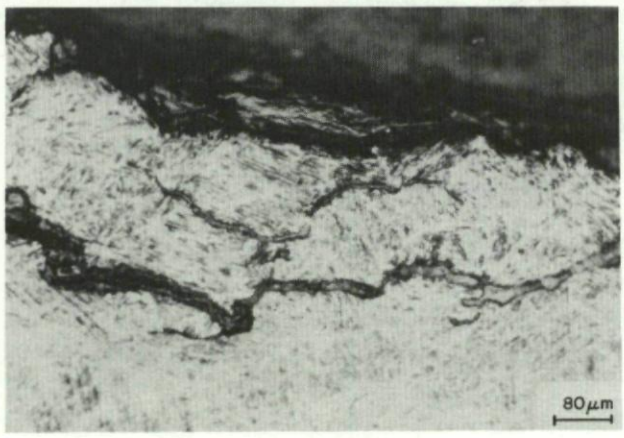

Fig. 9-10 Crevice corrosion in a welded steel joint

(a) Appearance of the as-received torque tube showing the cracked weld.
(b) Composite photograph showing corrosion deposit after the first cut (bottom) and second cut (top) of the tube section. Arrow indicates corrosion deposits found. (Mag. × 1.2)
(c) Evidence of intergranular cracking in the weld bead. (Mag. × 125)

Case history 9-6. Crevice corrosion in a welded steel joint.

A crack was found in a weld bead in an elevator torque tube on a coast guard patrol aircraft. The torque tube serves as part of the elevator control linkage, and the crack which was found during a routine visual inspection is shown in Figure 9-10(a).

The torque tube was fabricated from two hollow telescoping steel tubes which were joined by welding. The geometry of the weld bead was not circumferential but rather followed the double trapezoidal cut out of the outer tube as shown in Figure 9-10(a). The weld bead appeared excellent in all respects except for one section which was cracked along the centre of the weld bead for a distance of about 46 mm. The outer tube appeared to be bulging outwards just at the crack defect.

The cracked area was sectioned whereupon a large amount of ferrous corrosion product was discovered (Fig. 9-10(b)). The volume of deposit was much greater than the displaced metal from which it had formed, with the result that the outer tube was bulged outward to develop stresses in the weldment. Evidence of intergranular fracture was found in the adjacent weldment, suggesting that stress corrosion cracking had occurred to relieve the internal pressure (Fig. 9-10(c)).

It was concluded that cracking was due to crevice corrosion occurring between the telescoping steel tubes. The corrosion product had built-up to a sufficient quantity and thickness to expand against and fracture the weld bead. Stress corrosion cracking was also suspected as playing a secondary role in the failure. The obvious recommendation was to employ proper corrosion control measures. It was observed that the torque tube was primed and painted on the outside, but was devoid of corrosion control coatings on the inside. It was also noticed that the tube was not sealed to prevent water access to the interior of the tube. In problems of this type, where welded joints are involved, proper design of the weld geometry is important to avoid crevices where corrosive fluids can collect. The joint should also be stress relieved after welding, and inspected by magnetic particle or dye penetrant to ensure a crack free weld.

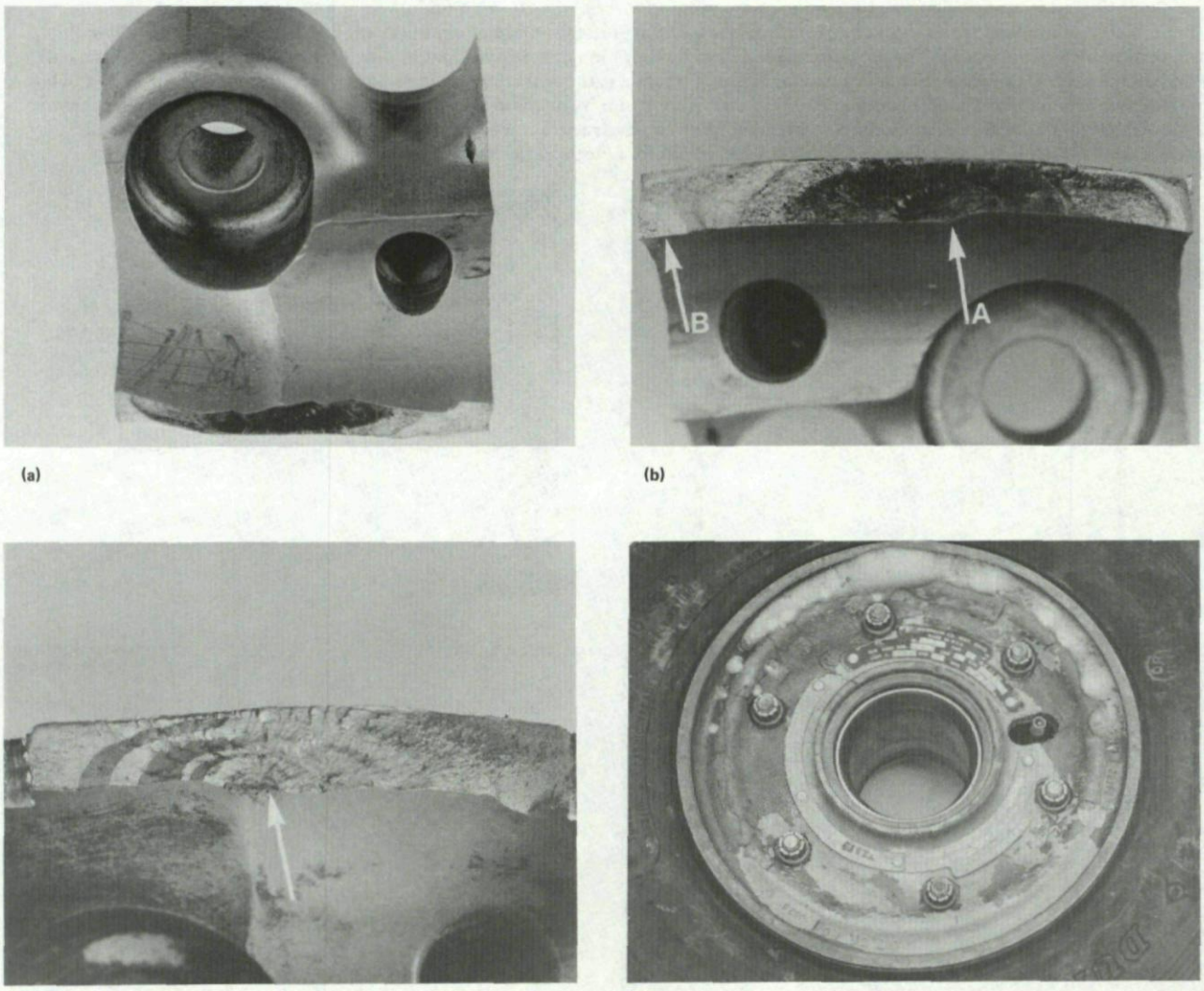

(a) (b) (c) (d)

Fig. 9-11 Pitting corrosion and fatigue of a 2014-T6 aluminium alloy main landing gear wheel

(a) Piece of the failed wheel received for examination.
(b) Fracture surface showing the fatigue crack initiation site (arrow 'A'). Arrow 'B' indicates where an adjacent fatigue crack was cut during sectioning.
(c) Fatigue crack initiating at a corrosion pit.
(d) Inflated nose wheel tyre indicating air leakage through the wheel wall, when liquid detergent was applied.

Case history 9-7. Pitting corrosion and fatigue failure of a fighter aircraft main landing gear wheel.

The armed forces of several NATO countries have experienced corrosion and fatigue cracking problems in the main landing gear wheels of a common fighter aircraft type. The wheels are made from 2014 aluminium alloy in a T6 temper. Problems have also been reported with the nose wheels on the same aircraft, although these were made from the magnesium alloy ZK 60A-T5.

Figure 9-11(a) shows a piece of an aluminium alloy main wheel, while Figure 9-11(b) is the same piece at higher magnification and shows a portion of the fracture surface involved. The fracture surface in this area showed beach marks, characteristic of fatigue, and the fatigue crack could be traced back to an initiation site at a corrosion pit, which is indicated by the arrow 'A'. The adjacent arrow 'B' points to a neighbouring fatigue crack which had also initiated at a corrosion pit. The total length of these two cracks was about 80 mm, and both had propagated through the wall of the wheel until air had escaped and the tyre deflated.

Striation spacing analysis on the fracture surfaces showed that the cracks had propagated initially at a slow rate, however the propagation rate increased significantly when the cracks reached about 10 mm in length. This particular wheel had undergone only four landings since the last overhaul, and therefore the crack propagation analysis indicated quite clearly that the cracks had been missed during inspection.

Figure 9-11(c) shows another example of a fatigue crack originating at a corrosion pit in a main wheel. In all these cases it was observed that the cracks initiated at corrosion pits, and in all cases the corrosion pits occurred in the same area where the wheel was in contact with a stainless steel heat shield. As explained in case history 9-2 above, aluminium alloy 2014 is normally a passive corrosion resistant metal, forming a protective anodic film on exposure to corrosive environments. However, in this case the repeated contact between the stainless steel heat shield and the wheel had resulted in the removal of both the paint finish on the wheel and the anodic film. The bare metal would then be in direct contact with the stainless steel, and in the presence of an electrolyte a corrosion cell would be set up in which the aluminium would be the anode and the stainless steel the cathode. The pitting situation was aggravated by the large cathodic surface area of the stainless steel and very small area of rubbed and unpassivated aluminium anode.

These problems led to more regular maintenance of the protective finishes, especially around the key boss areas where the heat shields contact the wheels. The problem also led to an investigation of adhesive tapes to provide insulation between the stainless steel and the aluminium wheel, and an aluminium foil tape which was thought would provide better heat dissipation properties and less likely to damage the wheel anodic coating. The heat shields could not be removed since high temperatures would occur in the wheels and lead to fuse plug release. A more rigorous programme of non-destructive inspection was also implemented, involving eddy current inspection about the bead seat radius and ultrasonic inspection for defects in the key boss radius-heat shield contact area.

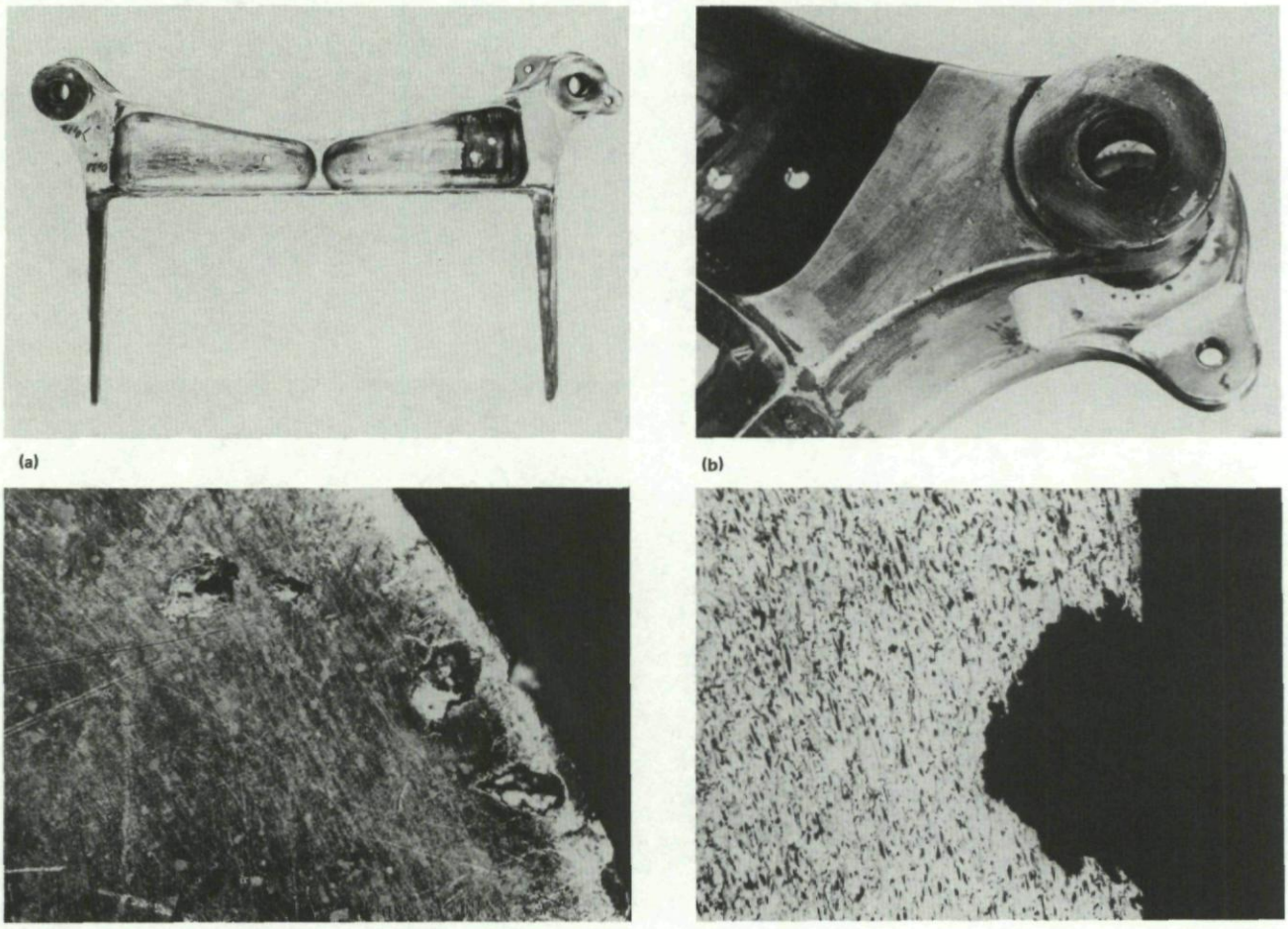

Fig. 9-12 Pitting corrosion of a 7075 aluminium tail cone fitting

(a) General view of the tail cone fitting.
(b) Close-up of the right lug.
(c) Corrosion pits on the outer perimeter of the lug.
(d) Cross-section through the lug showing corrosion penetration.

The problems in the magnesium nose wheels are illustrated in Figure 9-11(d), which shows bubbling in a soap solution which was applied to the wheel in the bead seat radius. In these cases the problems were attributed to excessive porosity due micro-shrinkage and intergranular corrosion in these magnesium alloy castings.

Case history 9-8. Pitting corrosion of a 7075 aluminium tail cone fitting.

Deep corrosion pits were found in the lug area of an aluminium alloy tail cone fitting during routine inspection. The fitting, shown in Figure 9-12(a), was determined to be made of 7075 aluminium alloy and the pitting was found around the outer perimeter of the lug, shown at higher magnification in Figure 9-12(b). Typical corrosion pits are shown in Figure 9-12(c), and a cross-section is shown in Figure 9-12(d). The corrosion pits were measured to be up to 1.5 mm in diameter and up to 0.65 mm in depth. These corrosion pits were found to contain corrosion deposits which were determined to consist of aluminium hydroxide $Al(OH)_3$ containing sodium and chloride ions, suggesting that the pitting was due to salt water corrosion.

The lugs of the tail-cone fittings contained beryllium-bronze bushings, and therefore the possibility of galvanic corrosion arises. However, the pitting did not occur in the aluminium in immediate contact with the bronze bushings, but rather some distance away, which suggests that galvanic corrosion was not a factor.

The use of corrosion protection systems of the type now in common use with aluminium alloys should be capable of preventing the recurrence of this problem, provided coatings are properly maintained.

Case history 9-9. Filiform corrosion in a 6061-T6 pylon tank.

The aircraft in question had been operating in the Mediterranean region and the corrosion damage was detected during a routine visual inspection. The damage to the pylon tank was largely superficial affecting isolated areas over the full length of the tank, as indicated by open arrows in Figure 9-13(a). However at one point, penetration had occurred, as indicated by the solid arrow in Figure 9-13(a).

Closer surface examination showed that the corrosion followed the characteristic wandering path of filiform corrosion, as shown in Figure 9-13(b), while metallographic sections through the corrosion damage showed areas resembling broad pits and intergranular tunnelling (Fig. 9-13(c)). The alloy was found to be 6061 aluminium with a hardness of H_B 52, suggesting the alloy was in a T6 temper condition. The protective coating on this part had been removed by the operator prior to laboratory inspection, and therefore is unknown, however modern epoxy primers and polyurethane paint finishes, if properly maintained, should be sufficient to prevent this type of problem from recurring.

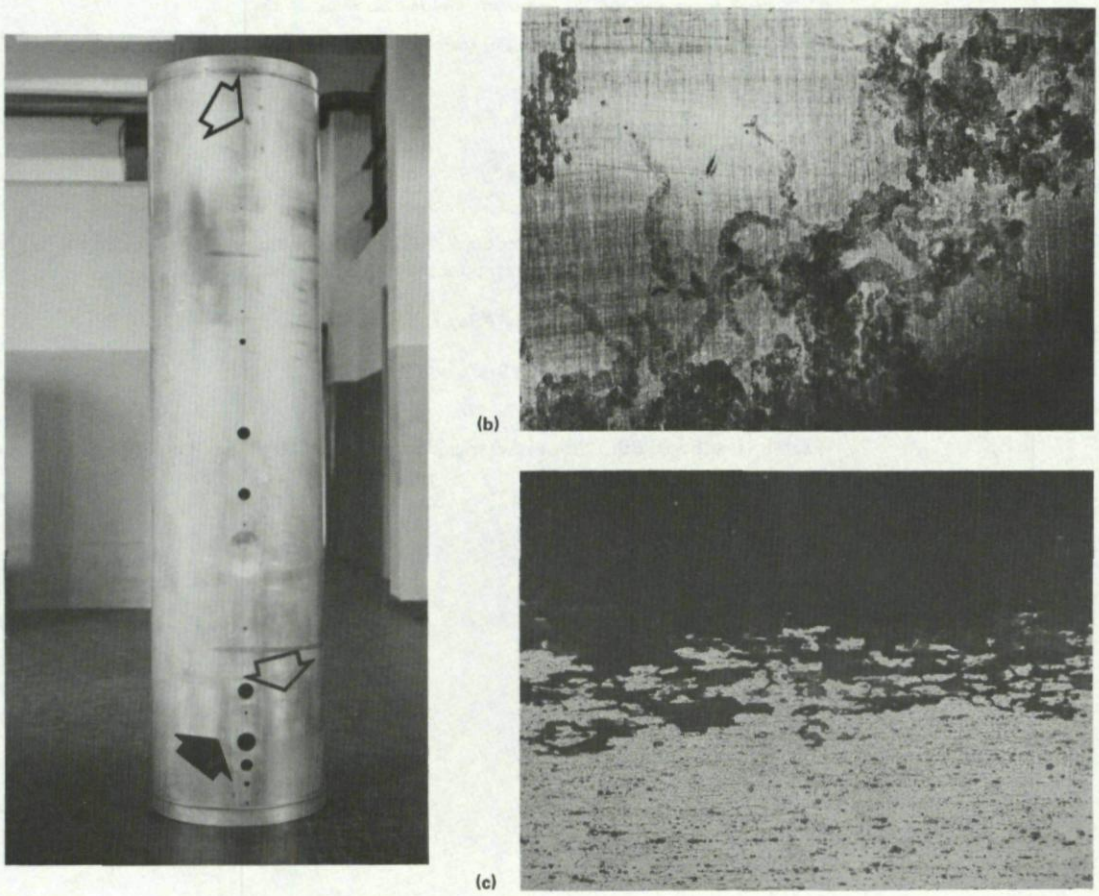

(a) (b) (c)

Fig. 9-13 Filiform corrosion in a fighter aircraft pylon tank

(a) General view of the tank showing areas of general corrosion (open arrows) and penetration (solid arrows).
(b) Indications of filiform corrosion.
(c) Pitting and intergranular corrosion.

Case history 9-10. Filiform corrosion in some 2024 aluminium ailerons and flaps.

This aircraft had also been operating in the Mediterranean region, and the corrosion damage was again detected during visual inspection. The structure in this case was made from 2024 aluminium and had been protected by a nitro-alkyd resin paint system. Areas of corrosion damage are shown in Figure 9-14(a), and in Figure 9-14(b) after removal of the paint system. The corrosion was largely superficial, although penetration had occurred in one area. The surface corrosion showed the thread-like meanderings of filiform corrosion, and appeared to have originated in the fastener holes, as indicated in Figure 9-14(b).

A strontium chromate epoxy primer and polyurethane finish were recommended to replace the nitro-alkyd protection system used previously.

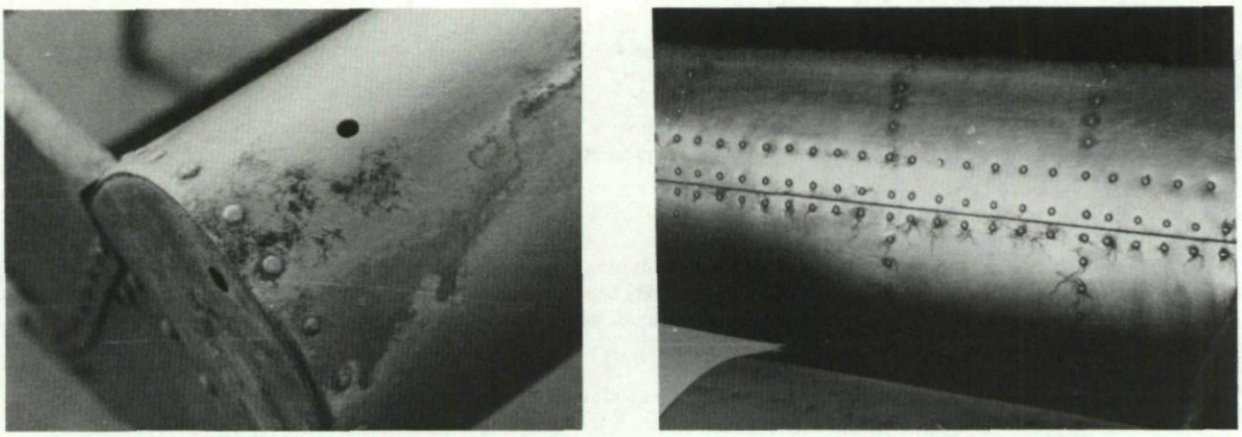

(a) (b)

Fig. 9-14 Filiform corrosion in some 2024 ailerons and flaps

(a) General appearance of the corrosion showing blistering of the paint.
(c) Filiform appearance of the corrosion tracks radiating away from fastener holes.

9.5 References

9-1 Aerospace Structural Metals Handbook, Vol. 3, 1982 Edition, U.S. Department of Defence, Mechanical Properties Data Center, published by Belfour Stulen Inc.

9-2 Shrier, L.L. Corrosion, Vol. 1, Sect. 4.1, John Wiley and Sons, 1963.

9-3 Aziz, P.M. Goddard, H.P. Corrosion, 1959. (See Reference 9-1, Code 3201).

9-4 Metals Handbook, 8th Edition, American Society for Metals, Cleveland, Ohio, 1961.

9-5 See Reference 9-1, Volume 2.

CHAPTER 10

INTERGRANULAR CORROSION AND EXFOLIATION CORROSION

10.1 Introduction

Intergranular corrosion is a highly localized form of dissolution which affects the grain boundary regions in a polycrystalline metal. The corrosive attack can produce a network of corrosion or cracking on the metal surface, occasionally dislodging whole grains, or it may penetrate deeply into the metal leaving behind very little visible evidence of the damage. An example of a network of fine surface cracking is shown in Figure 10-1(a), where the part is a forged aluminium alloy hydraulic valve.

In heavily rolled or extruded products where the grains are flattened and elongated in the direction of working, the presence of intergranular corrosion can lead to layering and flaking, producing a delamination effect with surface grains being pushed out by the underlying corrosion products. This is known as exfoliation corrosion, and is essentially a severe form of intergranular corrosion occurring in the direction of grain flow. Examples of exfoliation are shown in Figures 10-1(b) and 10-1(c). Figure 10-1(b) shows a specimen cut from the edge of an access hole in a aluminium alloy skin panel, and reveals the severely destructive effect of exfoliation. This damage occurred due to the use of a susceptible rolled alloy with inadequate protection to the flat land of the access holes, combined with operations in a maritime environment. Figure 10-1(c) shows the voluminous dark corrosion products forming in the intergranular fissures and the substantial delamination occurring in the skin.

In intergranular corrosion or exfoliation the material in the grain boundary areas behaves anodically with respect to the bulk of the metal in the grain interiors. In corrosive environments dissolution of the anodic grain boundaries usually occurs at a very rapid rate while the bulk alloy is little affected. The small area of the anode with respect to the cathode area is an important factor influencing the corrosion rate. The anodic nature of the grain boundary may be due to the local segregation of impurities, or either the enrichment or depletion of the grain boundary in alloying elements. These effects may be associated with the precipitation of grain boundary phases, which may themselves behave anodically with respect to the adjacent alloy.

A common example of intergranular corrosion occurs in some austenitic stainless steels when these are slowly cooled after exposure to solution heat treatment temperatures. Slow cooling through the temperature range 800 to 500°C allows the precipitation of large particles of chromium carbide ($Cr_{23}C_6$) along grain boundaries, and the formation of a chromium depleted zone in the matrix adjacent to the grain boundary. Similar results can also occur by aging these alloys in this same temperature range. When these sensitized alloys are exposed to even mildly corrosive solutions, intergranular corrosion may occur by the preferential dissolution of the depleted zones. Either the chromium carbide particles or the chromium rich grain interior may act as the cathode sites in the local electrochemical cells. Susceptible steels include most of the high chromium (18-8) stainless steels, containing more than about 0.03% carbon. Since steels with chromium levels less than about 10% exhibit corrosion characteristics similar to carbon or low alloy steels, the presence of intergranular corrosion in sensitized steels is an indication that the chromium levels in the depleted zones are less than about 10%. However laboratory attempts to measure the chromium depletion have indicated much lower levels. Various low carbon versions of these alloys are available to avoid these problems, or alternatively the higher carbon alloys must be rapidly quenched after solution heat treatment and exposure to temperatures in the critical range avoided.

Similar problems can occur in some of the high strength aluminium alloys used in airframe construction. Alloys of the 2000 (Al Cu) series may be sensitive to intergranular corrosion if they are not quenched rapidly enough after solution heat treatment. These alloys are strengthened by the precipitation of copper-aluminium, or copper-magnesium-aluminium phases such as $CuAl_2$ or $CuMgAl_2$ during aging at room temperature (natural aging) or moderately elevated temperatures (artificial aging). However slow cooling through the range 400-260°C may lead to the formation of coarse grain boundary precipitates with substantial potential differences arising between the copper-depleted zones and adjacent material. Figure 4-4, Chapter 4 shows the effect of cooling rate on the corrosion resistance of 2024-T4 and 7075-T6 aluminium alloys respectively. Corrosion resistance is indicated by the percentage loss in tensile strength of 1.64 mm thick non-clad specimens, as well as the predominant type of corrosive attack (pitting or intergranular) occurring. The data indicates that maximum corrosion resistance requires a rapid quenching rate, preferably not less than about 200°C per second. The data also shows that the effects of a slow quench on corrosion are magnified when a sustained tensile stress is imposed during corrosion (Ref. 10-1).

Parts must therefore be solutioned at temperatures high enough to dissolve all precipitated phases, usually in the region of 490°C, and then quickly immersed in the quenching bath to ensure rapid cooling to room temperature. When quenching is by total immersion in water, the water must be at room temperature and cooled to maintain a temperature below 38°C during the quench.

The degree of aging after quenching, which is affected by the aging temperature and the aging time, also have marked effects on intergranular corrosion. Over aging treatments such as T8 (or T851) for 2000 series alloys, or T76 (T7651) or T73 (T7351) for 7000 series alloys generally produce increased resistance to intergranular corrosion.

10.2 Case Histories

Case history 10-1. Exfoliation corrosion of an aluminium alloy stabilizer bracket.

The left hand rear stabilizer bracket from a light single engine aircraft was found, during a routine inspection, to be severely corroded, as indicated in Figure 10-2(a). The steel bearing bushing was isolated from the bracket by a nylon sleeve, but atmospheric moisture and contaminants had collected on the bracket's horizontal surface and seeped into the bracket-to-nylon interface.

The bracket had been machined from an aluminium alloy extrusion, and consequently the end grains were exposed around the nylon sleeve. Intergranular corrosion occurred, which because of the extremely elongated grain structure, propagated as exfoliation corrosion, as indicated in Figure 10-2(b). As the corrosion attack continued, the exfoliated grains separated and general surface corrosion of the exposed and unprotected core grains also occurred, as seen in Figure 10-2(a). The other surfaces of the bracket were protected by a chemical conversion coating and were uncorroded.

In this example, inadequate design and maintenance were both a problem. It is necessary to ensure that corrosive agents do not have the opportunity to attack exposed end grains. While the nylon sleeve around the steel bushing prevented galvanic corrosion,

the interface between the nylon bushing and the aluminium was not sealed to prevent corrosive medium seepage. Since the horizontal orientation of the corroded surface seen in Figure 10-2(a) retained moisture-born corrodents, regular inspection was required to allow early detection of corrosive attack.

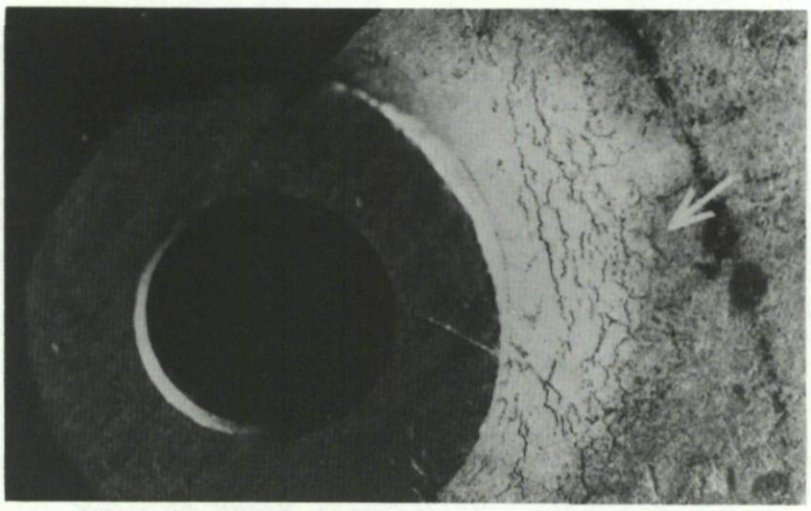

(a)

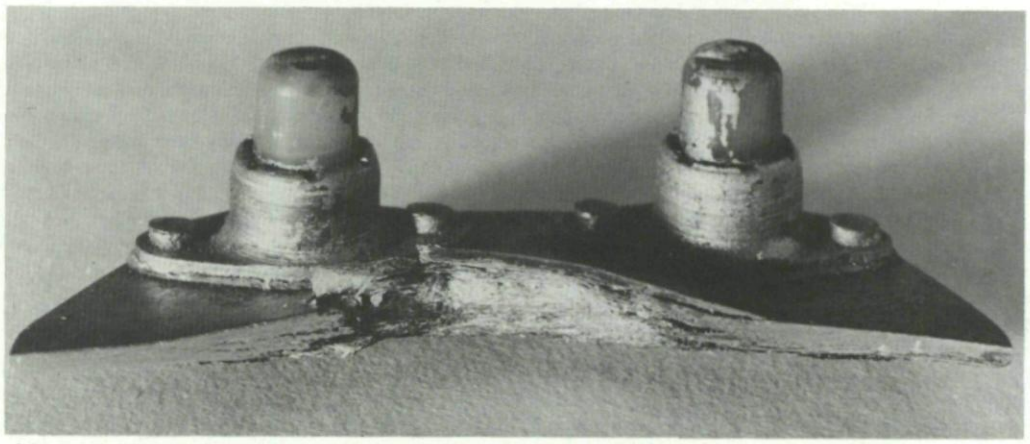

(b)

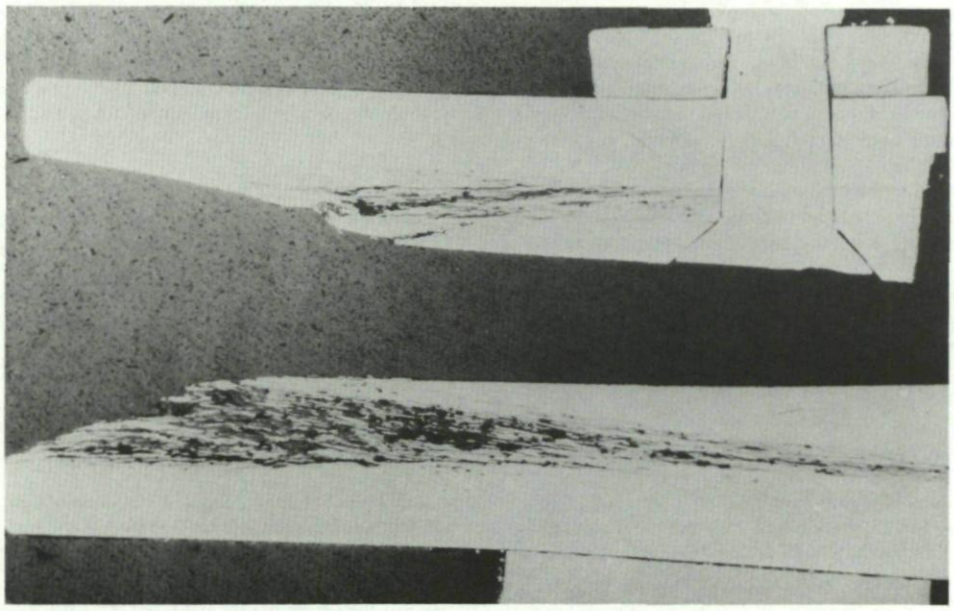

(c)

Fig. 10-1 Examples of intergranular and exfoliation corrosion in aircraft structure and components

(a) Intergranular surface cracking in a forged aluminium alloy valve.
(b) Exfoliation corrosion in an aluminium alloy skin.
(c) Cross-section through an aluminium alloy skin showing dark corrosion products and delamination due to exfoliation.

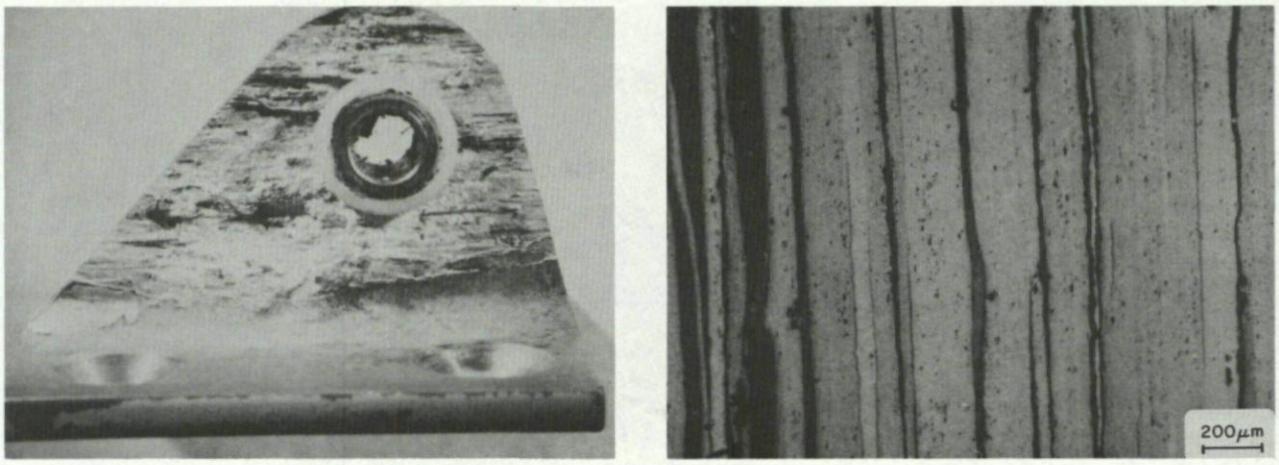

(a) (b)

Fig. 10-2 Exfoliation corrosion in an aluminium alloy stabilizer bracket

(a) Heavy surface corrosion of the stabilizer hinge bracket.
(b) Cross-section through the bracket showing the corroded surface grains at the right, and corrosion of elongated grain boundaries only. Keller's etch. (Mag. × 50)

Case history 10-2. Intergranular corrosion and fatigue of a light aircraft engine exhaust.

A custom silencing muffler was added to a light aircraft engine exhaust, as shown in Figure 10-3(a). This muffler and most of the exhaust separated in flight, and the unrestrained hot exhaust gases caused an in-flight fire. The exhaust pipe broke near its flange support, the pipe and silencing muffler were otherwise unsupported. Examination revealed the austenitic stainless steel exhaust had suffered intergranular corrosion (Fig. 10-3(b)), and the corrosion cracks had served as stress concentration sites to initiate fatigue. The loading causing fatigue was due to vibration of the cantilevered pipe and muffler, which was excited by fluctuating air loads as well as engine induced vibration.

Intergranular corrosion of austenitic stainless steel exhaust pipes is common, since the cycles of hot and cold exposure to combustion by-products and condensates represents a severe corrosive environment. However, since the pipes are usually well supported and hence subject only to low loads, normally they will not fracture until virtually perforated. In this case, the heavy, cantilevered, unsupported muffler extension created high cyclic stresses. The problem was alleviated by adding an extra support for the muffler. The grade of austenitic stainless steel used in the exhaust was not disclosed in this investigation, and therefore the possibility of sensitizing occurring due to the high temperature of the exhaust gases cannot be ruled out. The oxidation resistance and corrosion resistance of these alloys generally increase with increasing chromium and nickel contents, while microstructural stability improves with lower carbon levels.

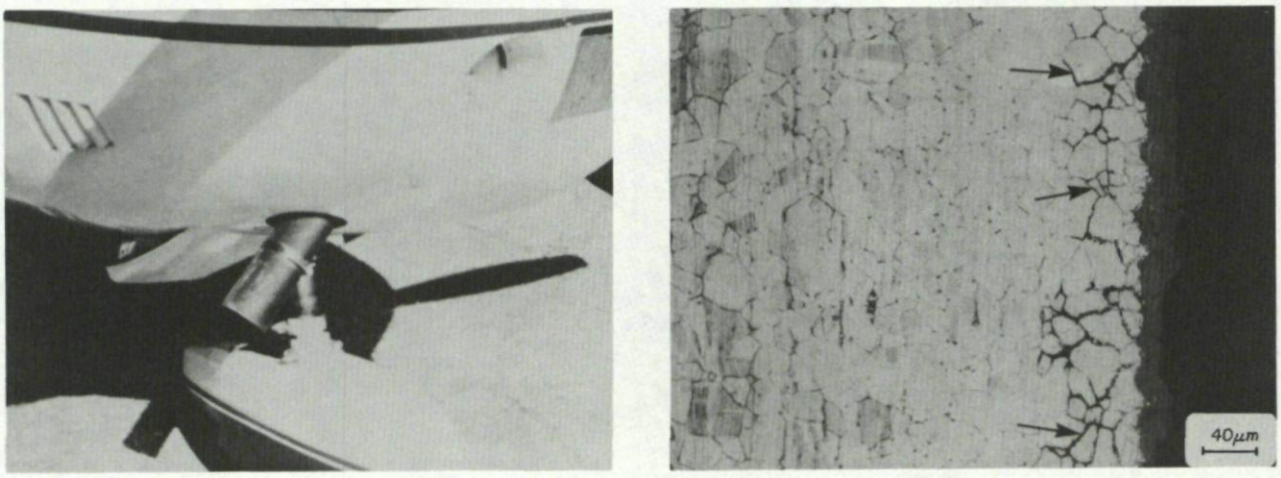

(a) (b)

Fig. 10-3 Intergranular corrosion and fatigue of a light aircraft engine exhaust

(a) Silencer extension fitted onto the exhaust pipe.
(b) Intergranular attack of the austenitic stainless steel pipe. Kalling's etch. (Mag. × 250)

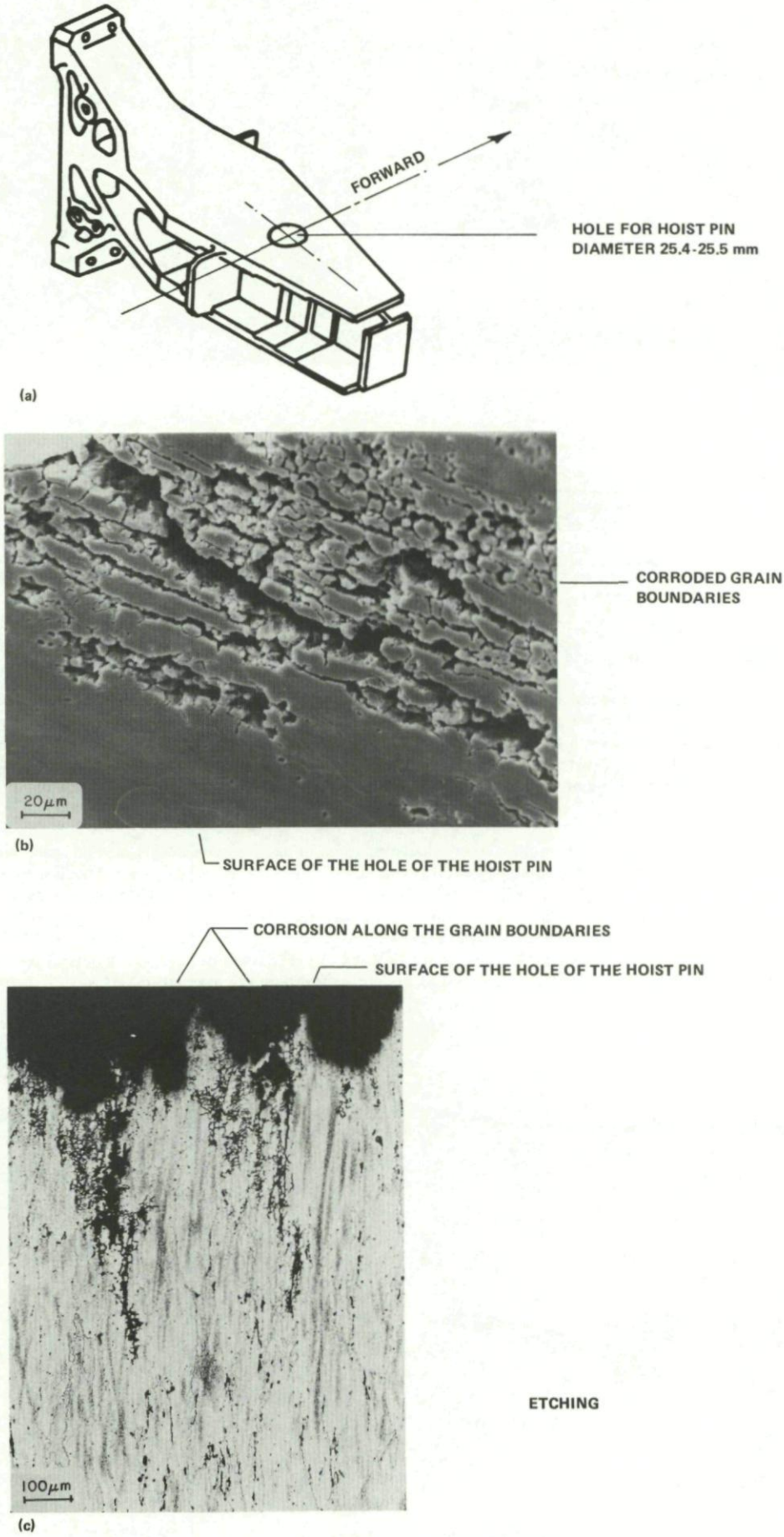

Fig. 10-4 Intergranular corrosion of an Al-Zn-Mg-Cu alloy wing attachment forging

(a) Wing attachment fitting indicating the corroded hoist pin hole.
(b) Macroscopic view of the corroded area. (Mag. × 500)
(c) Representative microstructure showing intergranular corrosion. (Mag. × 100)

Case history 10-3. Intergranular corrosion in an aluminium alloy wing attachment fitting.

Eddy current methods were used during the periodic inspection of a fighter aircraft to detect corrosion damage in the hole of the hoist point in a wing attachment fitting. A sketch of the attachment fitting showing the affected hole is given in Figure 10-4(a). The attachment fitting was made from an aluminium alloy forging and the alloy was determined to be an Al-Zn-Mg-Cu alloy, similar to 7075, but containing small amounts of silver. A chemical analysis of the material showed that it conformed to the specification of a German aerospace structural alloy 3.4354, as indicated in Table 10-1. Also, the mechanical properties indicated that the material was in a solution treated and mechanically aged condition (0.7), which is similar to the T6 condition. The mechanical properties are listed in Table 10-2.

The surface preparation of the fitting included shot peening on all surfaces, including the hole of the hoist pin, together with chemical conversion coating using Alodine 1200 and a zinc chromate primer. Notwithstanding this treatment, corrosion occurred in service and this is shown in Figure 10-4(b) to have occurred preferentially along grain boundaries in the forging. This was confirmed by preparing metallographic cross-sections through material adjacent to the hoist hole, and a typical example is shown in Figure 10-4(c). This shows that the forging has an elongated grain structure with grains boundaries running normal to the axis of the hole. There was also evidence of fine recrystallized grains forming a necklace structure around the boundaries of the coarser grains. The intergranular nature of the corrosive attack is very clear in Figure 10-4(c).

Intergranular corrosion occurred in this component due to a combination of circumstances. Material of this type is susceptible to intergranular corrosion when aged to a peak strength 'T6' condition. Greater resistance to corrosion can generally be achieved by overaging to a T76 or T73 condition, although the response of this sepecific alloy to this type of treatment would need to be verified. Intergranular attack is clearly promoted when grain boundaries intersect a free surface. By drilling the hoist hole perpendicular to the direction of grain flow leads to many grain boundaries being exposed. And finally, the surface protection system was probably damaged during insertion of the hoist pin, and appears not to have been adequately repaired. Similar parts remaining in service were also inspected, and where corrosion damage was detected the holes were re-drilled and ground to remove the corrosion and the full protection system was re-applied.

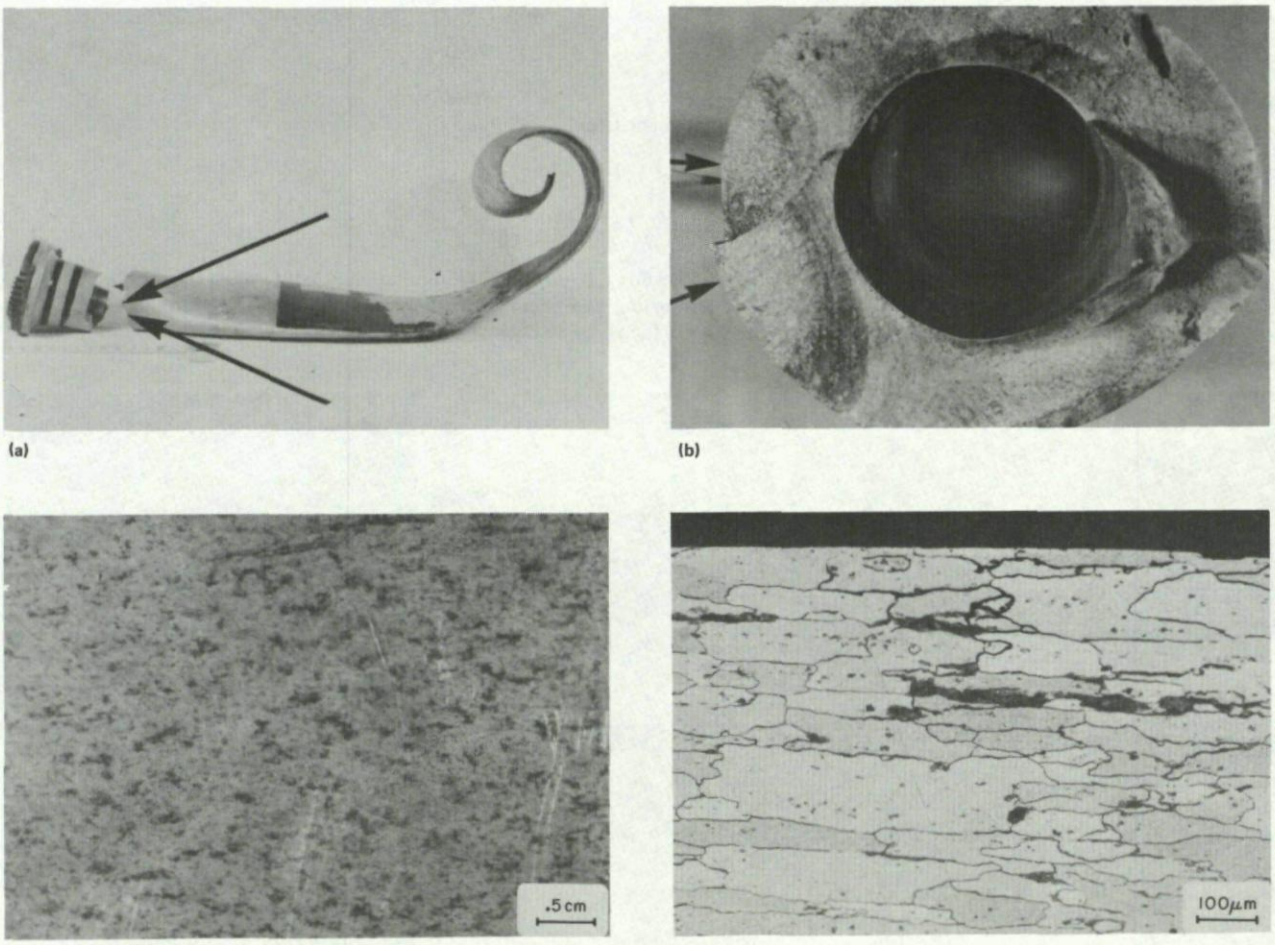

Fig. 10-5 Intergranular corrosion and fatigue of an aluminium alloy propeller

(a) Failed propeller showing the fatigue crack initiation sites near the leading edge root (arrows).
(b) Fracture face showing two major fatigue cracks whose origins correspond to the arrows in Figure 10-5(a).
(c) Surface of the propeller blade near the fatigue initiation sites showing a mottled appearance but no indications of widespread corrosion. (Mag. × 2)
(d) Section through the area seen in Figure 10-5(c) showing severe intergranular corrosion. Keller's etch. (Mag. × 100)

Case history 10-4. Intergranular corrosion of an aluminium alloy propeller.

An aircraft used for crop dusting lost a propeller blade just after taking off. The resulting severe imbalance ripped the engine out of its mounts and the aircraft crashed and was destroyed by fire. Figure 10-5(a) shows the damaged propeller and the arrows indicate the crack initiation sites. Figure 10-5(b) shows the fracture surface, and scanning electron microscopy showed that crack growth occurred by fatigue through about 40% of the root section before catastrophic rupture occurred under centrifugal loading.

Two major fatigue crack initiation sites were apparent, as indicated by the arrows in Figure 10-5(b), but no obvious stress concentration sites were visually apparent at the origins. Figure 10-5(c) shows the surface of the blade around the fracture zone exhibited a slightly mottled effect, apparently due to mild surface corrosion. However, sections cut from this area showed that severe intergranular attack had occurred, as shown in Figure 10-5(d). This attack provided the stress concentration sites which had initiated fatigue cracking. The corrosive medium responsible was found to be the agricultural spray chemicals used in crop dusting.

No information was provided in this investigation of the alloy type or the inspection procedures used with this aircraft propeller. Most of the high strength aluminium alloys used for safety critical aircraft parts are susceptible to intergranular corrosion unless properly heat treated and protected. Satisfactory heat treatment generally involves rapid quenching, of the order of several hundred °C per second, to avoid grain boundary precipitation during the quench. Subsequent precipitation heat treatment must also be extensive enough to avoid introducing susceptibility to intergranular corrosion. It is possible that intergranular corrosion may occur even in correctly heat treated parts, if particularly aggressive corrodents are present in the atmosphere. Hence to avoid corrosion in a case such as this it would be recommended to carefully wash off all chemicals after each flight, and wax the surfaces to protect them.

Case history 10-5. Intergranular corrosion leading to fatigue cracking of a helicopter main rotor blade.

A long crack was found in a helicopter rotor blade. The crack had initiated at the trailing edge and had propagated across the blade in a chordwise direction to a length of 225 mm. The blade chord was 350 mm, and the crack was located 650 mm from the blade root. The rotor blade and crack are shown in Figures 10-6(a) and 10-6(b).

The main elements of the rotor blade included

(a) an extruded aluminium alloy nose spar.

(b) a 4 mm thick aluminium alloy skin.

(c) a 0.8 mm thick aluminium alloy trailing edge reinforcement strip.

(d) a 0.25 mm thick stainless steel leading edge capping strip.

(e) a moltoprene foam filler.

The aluminium alloy skin was found to be an Al-Cu-Mg alloy (all 4G1-T546) similar to alloy 2024, while the aluminium alloy trailing edge reinforcement strip was an alloy AG 5-TX516. The leading edge capping strip and the skin were bonded to the spar, the foam filler and the trailing edge. Rivets were installed along the trailing edge to prevent the skin from peeling off the trailing edge strip.

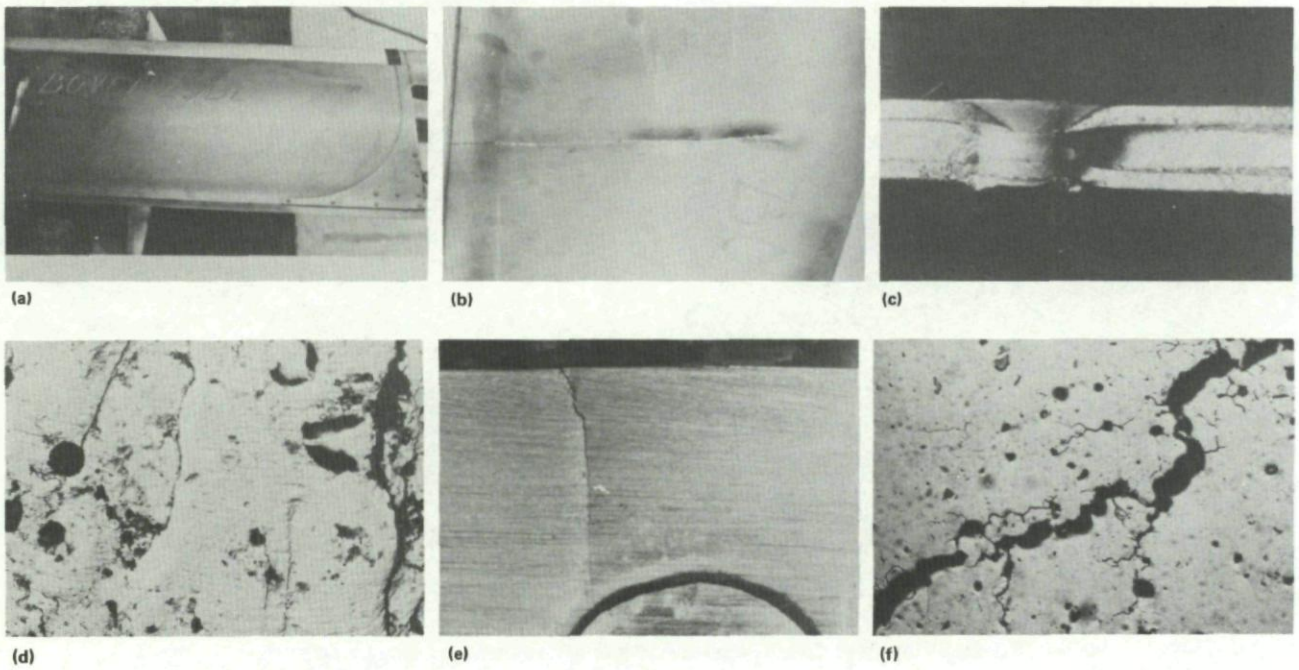

Fig. 10-6 Intergranular corrosion and fatigue in a helicopter main rotor blade

(a) Trailing edge of the blade.
(b) 225 mm long crack growing from the trailing edge.
(c) Fracture surface on either side of a rivet.
(d) Fatigue striations on the crack face in the lower skin.
(e) A secondary crack adjacent to the main crack.
(f) Intergranular cracking in the trailing edge skin.

Figure 10-6(c) shows the fracture surface after opening of the crack, and Figure 10-6(d) is an electron fractograph showing fatigue striations on the fracture surface of the bottom skin behind a rivet. Since the main crack ran through a rivet hole, further inspections were carried out involving removal of paint from the locations of all other rivets. Many other cracks were found, similar to that shown in Figure 10-6(e), and in all cases it was found that the cracks had grown into the rivet holes but had initiated elsewhere. Thus it was found that the stress concentration sites responsible for fatigue crack initiation were not associated with the rivet holes, but were due to intergranular corrosion in the skin in the trailing edge region.

Figure 10-6(f) shows the typical metallographic evidence of the intergranular corrosion in the trailing edge skin. Further examination showed that the bond line along the trailing edge was not completely sealed, so that moisture could penetrate and be absorbed by the foam filler. It was also found that the bottom skin had undergone a hot-dimpling operation. Reheating wrought aluminium alloys during such operations must be carried out with caution because of the danger of lowering the corrosion resistance of the metal. For example, 2024 aluminium in the T3 and T4 conditions should not be reheated to temperatures in the range 150-230°C, because of its harmful effect on corrosion resistance, while material in the more stable T81 or T86 conditions must be limited to exposure times varying from 20-40 hours at 150°C to 5 minutes at 230°C (Ref. 10-1).

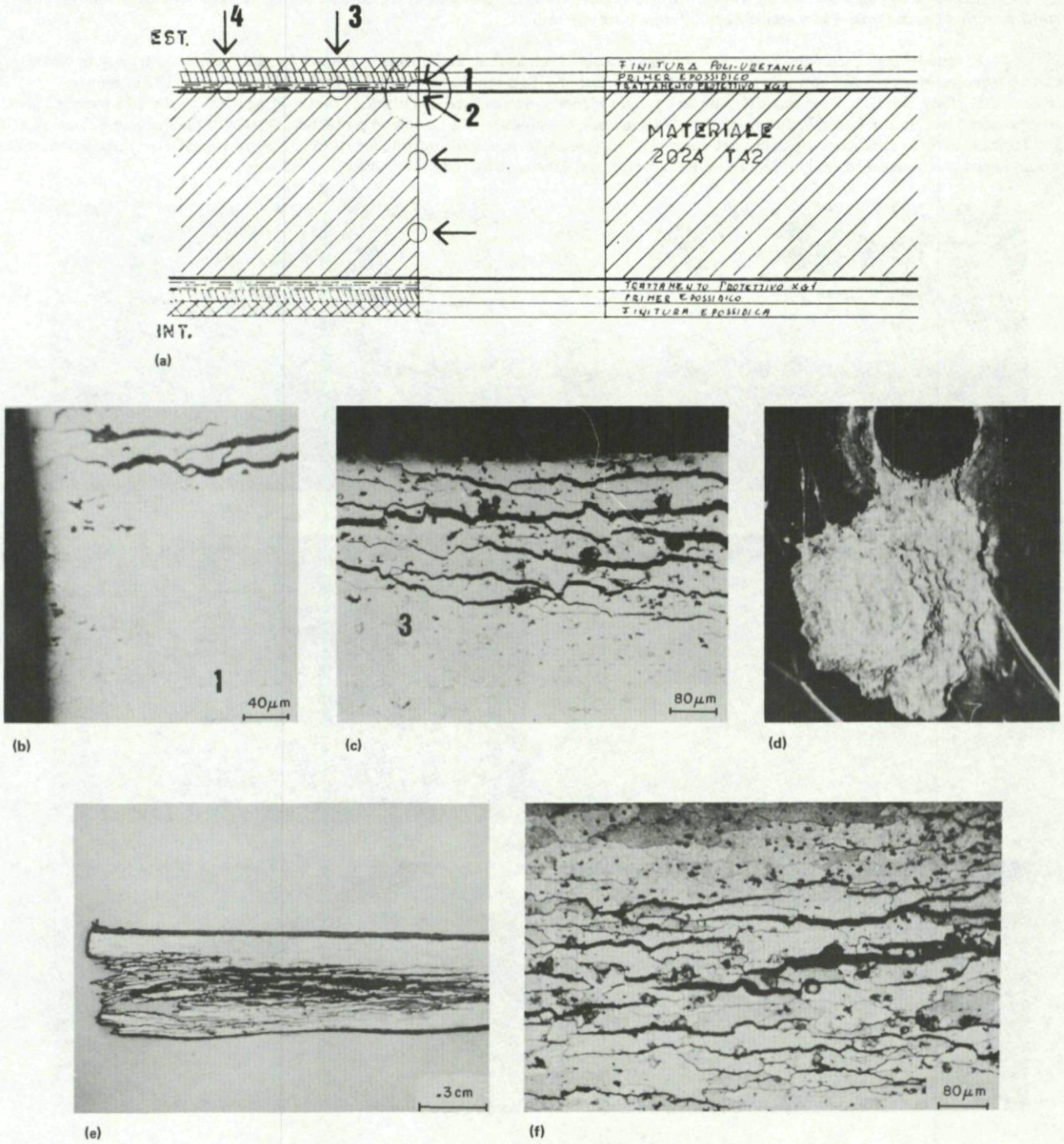

Fig. 10-7 Intergranular corrosion and exfoliation in a 2024-T42 vertical fin and horizontal stabilizer

(a) Diagram showing the aluminium skin and corrosion protection system.
(b) Intergranular corrosion observed at location 1 in a fastener hole. (Mag. × 250)
(c) Intergranular corrosion observed under the corrosion protection system at location 3 in the skin outer surface. (Mag. × 130)
(d) Corrosion products at a fastener hole.
(e) Severe exfoliation and delamination. (Mag. × 5)
(f) Intergranular corrosion associated with delamination of Figure 10-7(e). (Mag. × 130)

Case history 10-6. Intergranular corrosion and exfoliation in a transport aircraft vertical fin and horizontal stabilizer.

Corrosion damage was detected during visual inspection of the vertical fin and horizontal stabilizer of a transport aircraft. The structure involved the extensive use of rivetted and bolted joints in 2024-T42 aluminium alloy. The surface skin was coated with the corrosion protection system shown schematically in Figure 10-7(a). All non-machined surfaces were protected by a layer of chromic acid anodizing and an epoxy primer. On the inside surface of the skin the top-coat was a layer of epoxy paint, while on the outside (exterior) surface a coating of polyurethane enamel was employed. The machined surfaces of the fastener holes were bare.

Corrosion damage was found to have initiated in the bores of the fastener holes. Since the fasteners were installed without the use of sealants, moisture could easily penetrate between the fastener and skin to cause corrosion damage in the bare metal. Figure 10-7(b) shows evidence of the corrosion damage in the bore of a fastener hole, and Figure 10-7(c) shows evidence of the intergranular attack in the skin immediately below the exterior coating away from the fastener hole. In areas of severe corrosion, for example at fastener holes, substantial build-up of corrosion products had occurred (Fig. 10-7(d)), while internal propagation exhibited the characteristic delamination effects of exfoliation corrosion (Figs. 10-7(e) and 10-7(f)).

Accelerated corrosion testing was carried out on specimens cut from unprotected bare metal, according to MIL-H-6088. This confirmed that the material was susceptible to intergranular corrosion.

Several forms of remedial action are possible in a case such as this. The optimum temper for 2024 aluminium alloy in terms of resistance to intergranular corrosion and exfoliation is not the T42 temper as used, but is the T81 (T851 or T861) temper (Refs. 10-2, 10-3). For thin sheet the T81 temper provides higher yield strength and ultimate tensile strength than the T42 temper for an equivalent section thickness. In the case of the T42 temper, the absence of a corrosion protection system in the fastener holes was a key factor leading to corrosion. By using wet assembly, with sealing compounds introduced to the holes during fastener installation, it would have been possible to exclude the corrosive solution and substantially reduce corrosion.

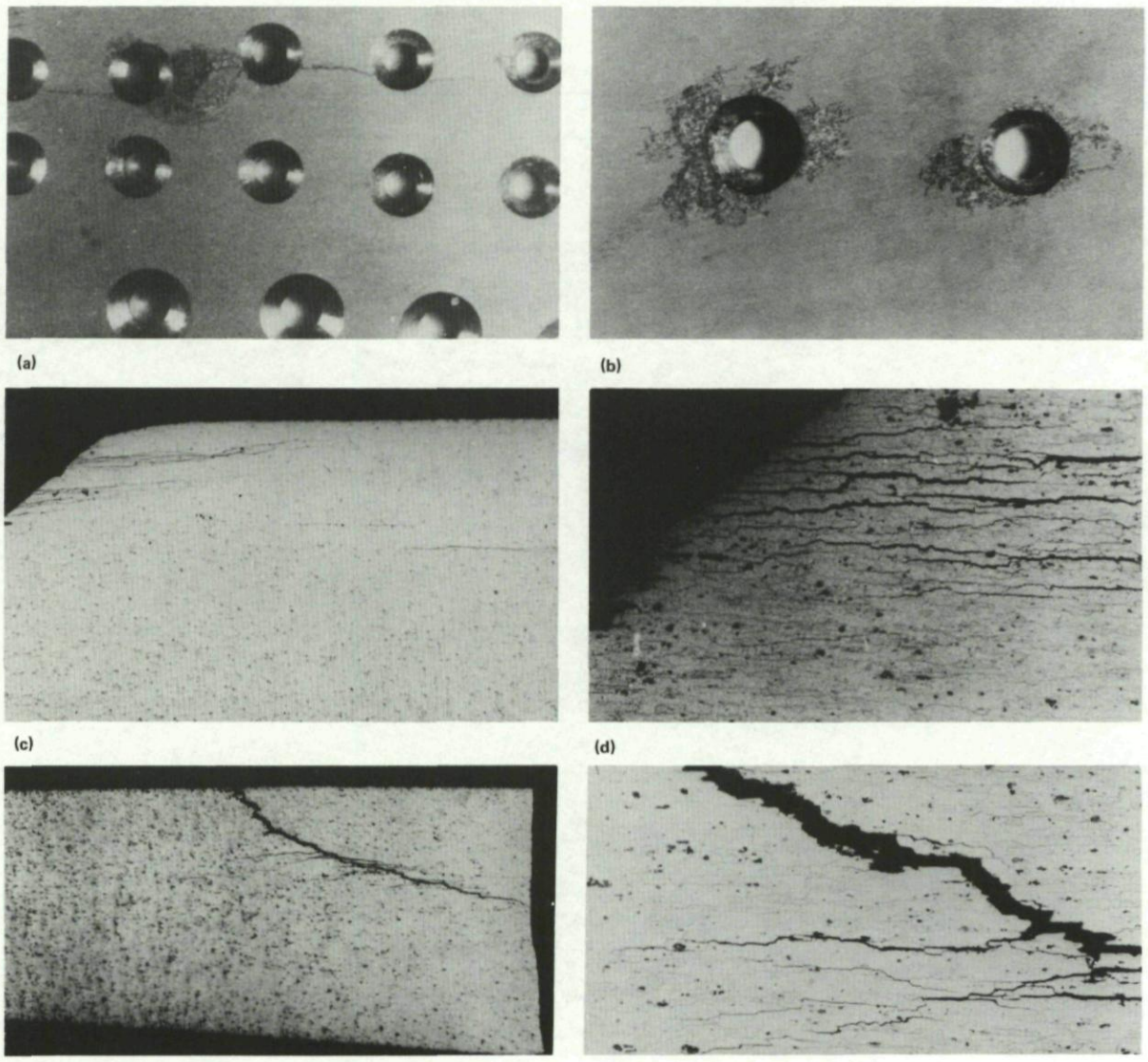

Fig. 10-8 Intergranular corrosion and exfoliation of a 7075-T6 wing box lower panel

(a) Deep corrosion between the fastener holes of the wing panel bolted joints.
(b) Localized corrosion around fastener holes.
(c) Traces of pitting and intergranular corrosion at the fastener countersink holes.
(d) Similar area to Figure 10-8(c) at higher magnification.
(e) Intergranular corrosion extending from a fastener hole and running out to the free surface of the plate.
(f) Cracking shown in Figure 10-8(e) at higher magnification.

Case history 10-7. Intergranular corrosion and exfoliation of a fighter aircraft wing box lower panel.

Corrosion damage to the wing box lower panel of a fighter aircraft was detected during visual inspection. The wing panel was fabricated from 7075-T6 aluminium, and the areas suffering from corrosion damage had undergone a manufacturing process involving shot peening, chromic acid anodizing, and final painting of the external surfaces with a vinyl wash primer and an acrylic enamel top-coat.

Corrosion damage was located primarily around fastener holes, as shown in Figures 10-8(a) and 10-8(b), but damage was also found in areas away from fastener holes. The damage included pitting, areas of filiform type corrosion and extensive intergranular cracking. The predominant type of damage was pitting in the bores and countersink areas of the fastener holes, from which extensive intergranular cracking emanated (Figs. 10-8(c) and 10-8(d)). Several surface connected cracks can be seen running between fastener holes in Figure 10-8(a). Metallographic examinations showed that substantial intergranular cracking was associated with the surface connected cracking, as shown in Figs. 10-8(e) and 10-8(f).

Samples for mechanical property testing were machined from the wing box panel, and the results are shown in Table 10-3, where they are compared with minimum allowable properties for 7075-T6 aluminium (Ref. 10-4).

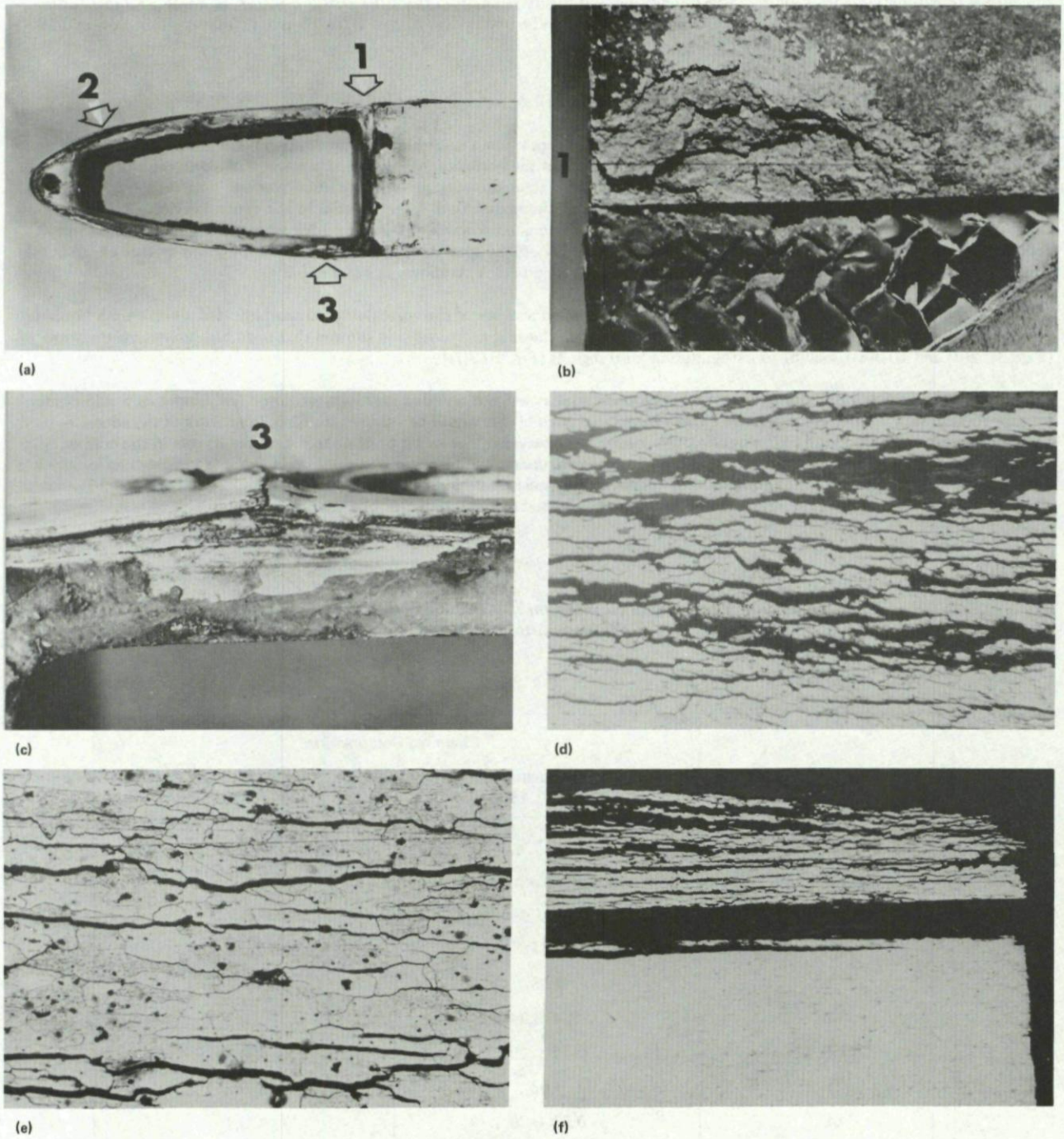

Fig. 10-9 Corrosion of a 2024 aluminium alloy helicopter rotor blade

(a) Leading edge at the blade tip showing three areas of severe corrosion.
(b) Corrosion in the aluminium alloy skin at location '1'.
(c) Rupture of the surface skin at location '3', due to the build-up of corrosion products in the underlying spar.
(d) and (e) Evidence of intergranular corrosion in spar.
(f) Exfoliation corrosion in the surface skin.

This data shows that the material properties were above the minimum design allowables for this alloy. Accelerated corrosion testing was also performed according to MIL-H-6088, and this confirmed that the material was susceptible to intergranular corrosion.

Several courses of action are possible to resolve problems of this type, involving either enhanced corrosion protection of the existing structure, or change of either the alloy type or the heat treatment condition of the metal structure. For aircraft already in-service, major up-grading of the corrosion protection system was carried out involving touch-up of fastener hole bores and countersinks using a chemical conversion coating (Alodine 1200). This was followed by wet assembly of fasteners and the use of a strontium chromate primer and an acrylic finish. It was reported that similar treatments had also been applied to new aircraft in manufacture, resulting in marked improvements in their corrosion resistance.

The use of 7075-T6 aluminium in corrosion prone airfract structure is now being seriously questioned by aircraft designers. The newer T76 or T73 tempers provide marked improvements in resistance to exfoliation resistance and stress corrosion resistance with only moderate losses in tensile strength. Several newer aluminium alloys are available to designers and these provide increased resistance to intergranular corrosion and exfoliation. Of these newer alloys, 7475 is the closest in chemical composition to 7075, differing mainly with respect to lower limits on the impurity elements silicon, iron, manganese and titanium. These chemistry controls lead to an alloy with strength levels very similar to 7075 but much improved fracture toughness and exfoliation resistance. Alloy 7475 is slightly susceptible to exfoliation corrosion in the T61 condition, but highly resistant in the T761 condition (Ref. 10-5). In a temper-for-temper comparison, the exfoliation resistance of 7475 sheet was found to be better than that of 7075-T6 and T76 sheet (Refs. 10-6 and 10-7).

Case history 10-8. Intergranular corrosion and exfoliation of a helicopter main rotor blade.

Severe corrosion was found in the tip region of a helicopter main rotor blade during routine inspection. Corrosion was found to be most severe in the leading edge and disassembly showed that the corrosion had occurred preferentially between the leading edge spar and the surface skin, as indicated in Figure 10-9(a). Three areas showing signs of particularly severe corrosion can be seen in Figure 10-9(a). Area '1' lay between the leading edge spar and the honeycomb filler material in the centre section of the blade. Corrosion in this area is shown in Figure 10-9(b). Area '2' was located towards the leading edge where the build-up of corrosion products between the skin and the spar had caused the skin to lift off the spar. Area '3' was located on the lower surface of the blade where severe corrosion of the spar had caused the skin to lift off and crack, as shown in Figure 10-9(c).

The leading edge spar was made of 2024 aluminium and analysis of the corrosion products indicated aluminium hydroxide containing approximately 1.3% chlorine. Cross-sections through the spar and outer skin showed that both had intergranular corrosion (Figs. 10-9(d) and 10-9(c)), leading to exfoliation in local regions (Fig. 10-9(f)).

The corrosion protection system used in this component was not revealed in this investigation, although this would clearly be important in view of the very aggressive environments that such blades would be exposed to. Also, the nature of the adhesives used to bond the skin to the spar and to the honeycomb core was not revealed, nor was it possible to determine its role in the corrosion process discussed. However, an investigation of the alloy microstructure and mechanical properties in the spar indicated an incorrect heat treatment which had led to the formation of coarse $Cu\,Al_2$ precipitates in grain boundaries. As indicated in Section 10-1, and Chapter 4, the correct heat treatment of 2024 aluminium is essential to avoid sensitivity to intergranular corrosive attack.

Table 10-1 The chemical composition of the Aluminium Alloy 3.4354 (Wt %) (Case history 10-3)

Source	Chemical Composition	
	Wing attachment fittings 3.4354	Specification [1] 3.4354
Zn	5,6-5,7	5,5-6,5
Mg	2,4-2,45	2,1-2,9
Cu	1,2-1,4	0,6-1,3
Ag	0,31	0,25-0,40
Cr	0,18	0,10-0,25
Mn	0,024-0,044	≤ 0,1
Fe	0,17-0,19	≤ 0,4
Ti	0,03	≤ 0,2
Si	0,03-0,06	≤ 0,4
Others		≤ 0,15
Al	Remainder	Remainder

[1] Specification according to Material Handbook of the German Aviation

Table 10-2 Mechanical and physical properties of the Aluminium Alloy 3.4354 (Case history 10-3)

Specification Form Condition Thickness Basis	3.4354 forging artificially aged (0.7) $\leqslant$ 75 mm s
Mechanical properties:	
F_{tu} [N/mm^2]	
L	510
LT	490
F_{ty}	
L	451
LT	431
F_{cy}	
L	451
LT	402
F_{SU}	314
e [%]	
L	7
LT	4
E_T [N/mm^2]	70730
E_C	72103
G	26781
Brinell Hardness HB	140
Electrical conductivity $\left[\frac{m}{\Omega mm^2}\right]$	15-18

Table 10-3 Tensile properties of the 7075-T6 wing box lower panel (Case history 10-7)

Orientation	Yield Strength MPa	Ultimate Strength MPa	% Elong
Longitudinal (L)	467	534	10
Transverse (T)	404	474	11
Minimum allowable (L)	455	531	7

10.3 References

10-1 Source Book on Selection and Fabrication of Aluminium Alloys, ASM Engineering Bookshelf, American Society for Metals, Metals Park, Ohio, 1978.

10-2 *Aluminum Standards and Data.*
The Aluminum Association, Sixth Edition, Washington, March 1979.

10-3 Van Horn, K.R. *Aluminium, Volume 1, Properties, Physical Metallurgy and Phase Diagrams.* American Society for Metals, Metals Park, Ohio, 1967.

10-4 Standards for Wrought Aluminum Mill Products, Aluminum Association, Washington, September 1965.

10-5 Aerospace Structural Metals Handbook, Volume 3, U.S. Department of Defence, Mechanical Properties Data Center, Balfour Stulen Inc., 1982 Edition.

10-6 Dickson, J.A. *Alcoa 467 Process X7475 Alloy.* Alcoa Green Letter GL 216 5-70, Aluminum Company of America, Pittsburgh, May 1970.

10-7 Newcomer, R.E. *Improved Aluminum Alloys.* McDonnell Aircraft Company, Report MDC A1666, May 12, 1972.

CHAPTER 11

FRETTING CORROSION

11.1 Introduction

Fretting is a form of wear which occurs between contacting surfaces which are undergoing vibratory motion involving relative displacements, or slip of small amplitude. The degradation of the rubbing surfaces usually involves a combination of wear and a corrosion reaction, and therefore the terms fretting corrosion or wear oxidation are frequently used. It usually gives rise to the formation of pits or grooves in the metal surrounded by corrosion products.

In the classic case fretting occurs between parts which are intended to be fixed by some form of mechanical fastener, but where vibratory stresses cause loosening of the fastener system to allow small cyclic displacements to occur between the two contacting faces. However exceptions occur, for example between ball bearings and their races, or between mating surfaces in oscillating bearings and flexible couplings. The basic requirements for fretting corrosion are that there is repeated relative motion between the surfaces, that the surfaces are under load and that the load is sufficient to cause slip or plastic deformation on the surfaces. The fretting action will be more severe the more aggressive is the corrosive environment. Studies have shown that fretting damage is less severe when oxygen and moisture are both excluded, and the debris produced is different. For example fretting damage to steel in nitrogen was found to be only one-sixth that in oxygen; and the debris produced was metallic whereas in the presence of air oxide was formed (Ref. 11-1). Therefore it does not appear that fretting can be stopped entirely by excluding a corrosive atmosphere; but that stick-slip action, localized at a single point, can produce a quantity of metallic debris which will oxidize when the surface is exposed to air for examination (Ref. 11-2).

Slip amplitudes as small as 10^{-7} mm have been known to cause fretting, but the displacements must be sufficient to cause plastic deformation in the surface layers. If the deformation remains elastic fretting will not occur. Because of the limited motion which occurs between the surfaces the corrosion products remain in the general area of the damage, and this differentiates fretting corrosion from common wear. In this latter case the wear debris, whether it be metallic debris or oxide scale, will be removed from the local area from which it originated because of the large relative movements between the contacting surfaces.

Figure 11-1 shows fretting damage in two flying control hinge pins, in the form of broad bands of deep pitting with associated accumulations of corrosion products. In service these pins would experience a combination of large amplitude displacements associated with deliberate movements of the control surfaces, and small amplitude displacements associated with normal aircraft vibrations in steady-state flight. Thus the damage observed may be due to a combination of wear and fretting corrosion. These problems are probably due to lack of adequate lubrication to alleviate the rubbing action.

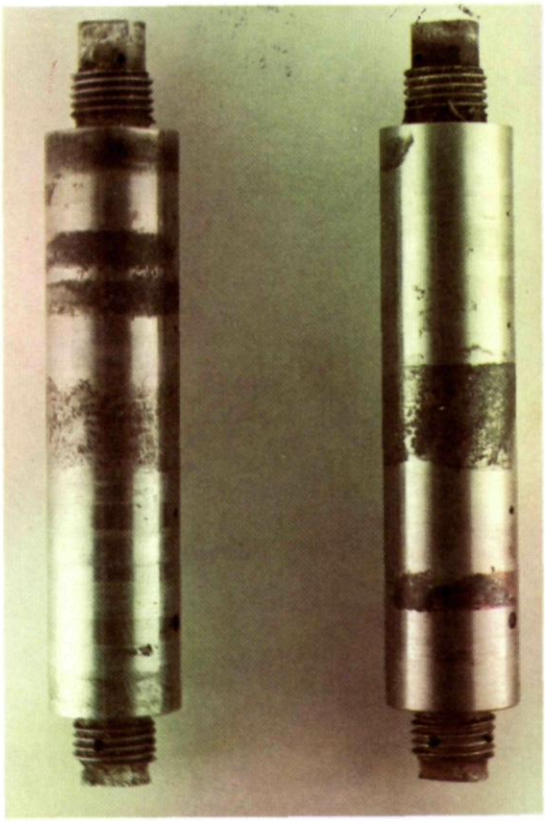

Fig. 11-1 Fretting damage in two flying control hinge pins

The mechanisms of fretting corrosion are not completely understood, however they are generally thought to include either mechanical wear followed by oxidation of metallic wear debris, or mechanical rupture and decohesion of naturally occurring oxide films followed by re-oxidation of the exposed bare metal. In either case the damage occurs locally at high points on the contacting surfaces. These mechanisms have been reviewed in more detail elsewhere (Refs. 11-3 and 11-4).

If the fretting couple consists of dissimilar metals the softer metal will deform the greatest amount, so that the oxide film on the softer metal will be disrupted but that on the harder metal will remain intact. The softer metal will therefore tend to suffer the greatest damage due to fretting corrosion. This concentration of damage will also tend to increase if the softer metal is the more electrochemically active metal in the couple so that it corrodes anodically. An example of fretting corrosion damage in a dissimilar metal couple is shown in Figure 11-2. This shows fretting in a magnesium alloy (EZ-33) low pressure compressor casing. Fretting has occurred in an annular ring due to the vibrating rubbing action of a row of steel stator vanes. This problem might be alleviated either by changing to a harder and more wear resistant casing alloy, or by using a wear resistant coating.

Fretting damage is particularly serious since it can lead to unexpected fatigue failures. Under fretting conditions fatigue cracks are initiated at very low stresses, well below the fatigue limit of non-fretted specimens. The initiation of fatigue cracks in fretted regions depends mainly on the state of stress in the surface and particularly on the stresses superimposed on the cyclic stresses. The direction of growth of the fatigue cracks is associated with the direction of contact stresses and takes place in a direction perpendicular to the maximum principal stress in the fretting area.

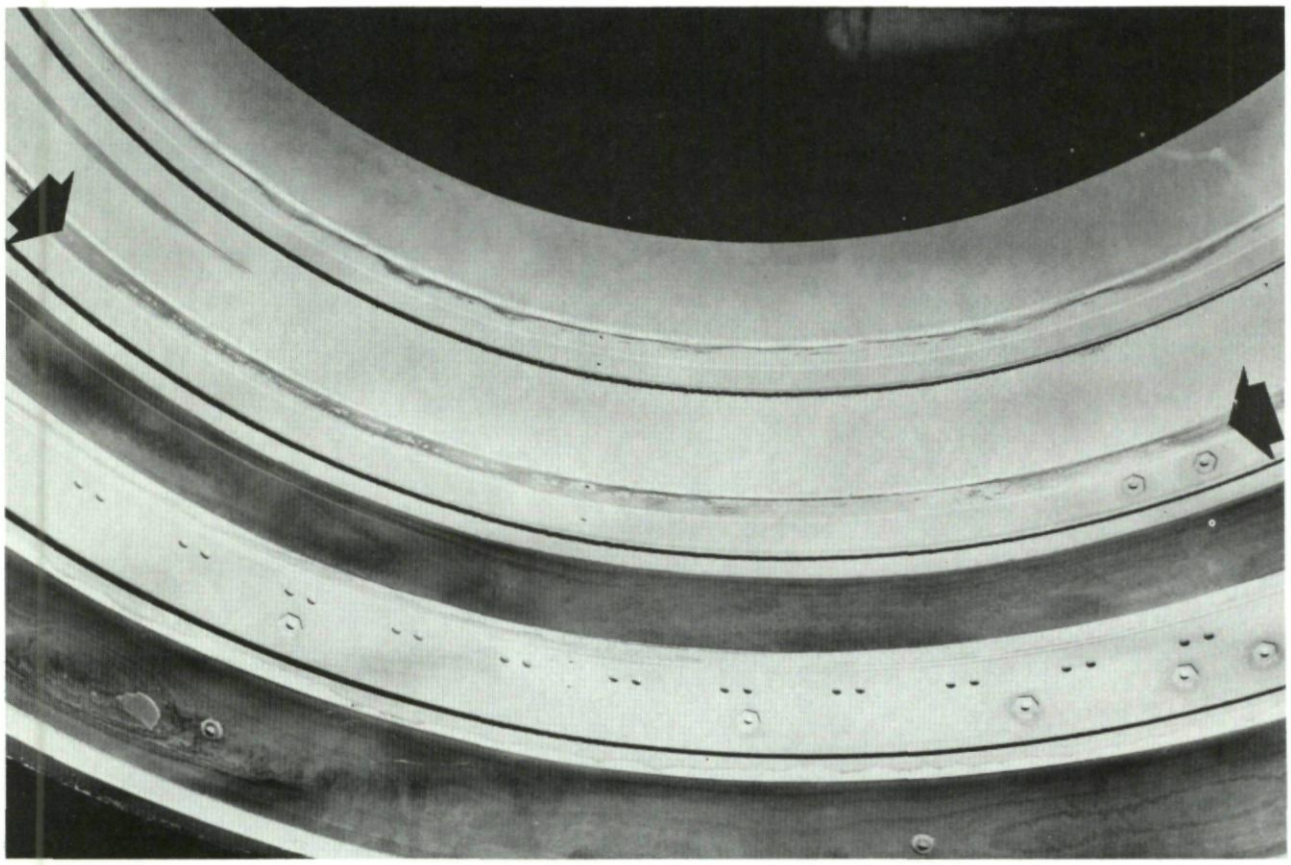

Fig. 11-2 Fretting corrosion in a magnesium alloy (EZ-33) compressor casing, indicated by arrows

11.2 Fretting Corrosion Case Histories

Case history 11-1. Fretting induced fatigue failure of a helicopter engine connecting rod.

A piston engined helicopter crashed due to in-flight engine failure after a connecting rod broke. The shattered connecting rod is shown in Figure 11-3(a). The primary fracture is shown by an arrow in Figure 11-3(a), and is shown in plan view in Figure 11-3(b). The origin of this fatigue failure is on the bore wall, and this coincides with a small region of fretting damage which can be seen in Figure 11-3(c).

Scanning electron microscopic examination of the fretting zone clearly shows the surface damage and the initiation of a multitude of small fatigue cracks parallel to the major fracture (Fig. 11-3(d)). Fretting occurred because of the rotational oscillatory motion of the shell bearing within the connecting rod big end bore.

This and other similar failures were the result of inadequate restraint of the bearing shells. By increasing the "crush" of the shell, that is by increasing the circumference of the shells relative to the bore of the connecting rods, and by increasing the bolt loadings, the high crush shells were effectively restrained and prevented from initiating such fretting damage.

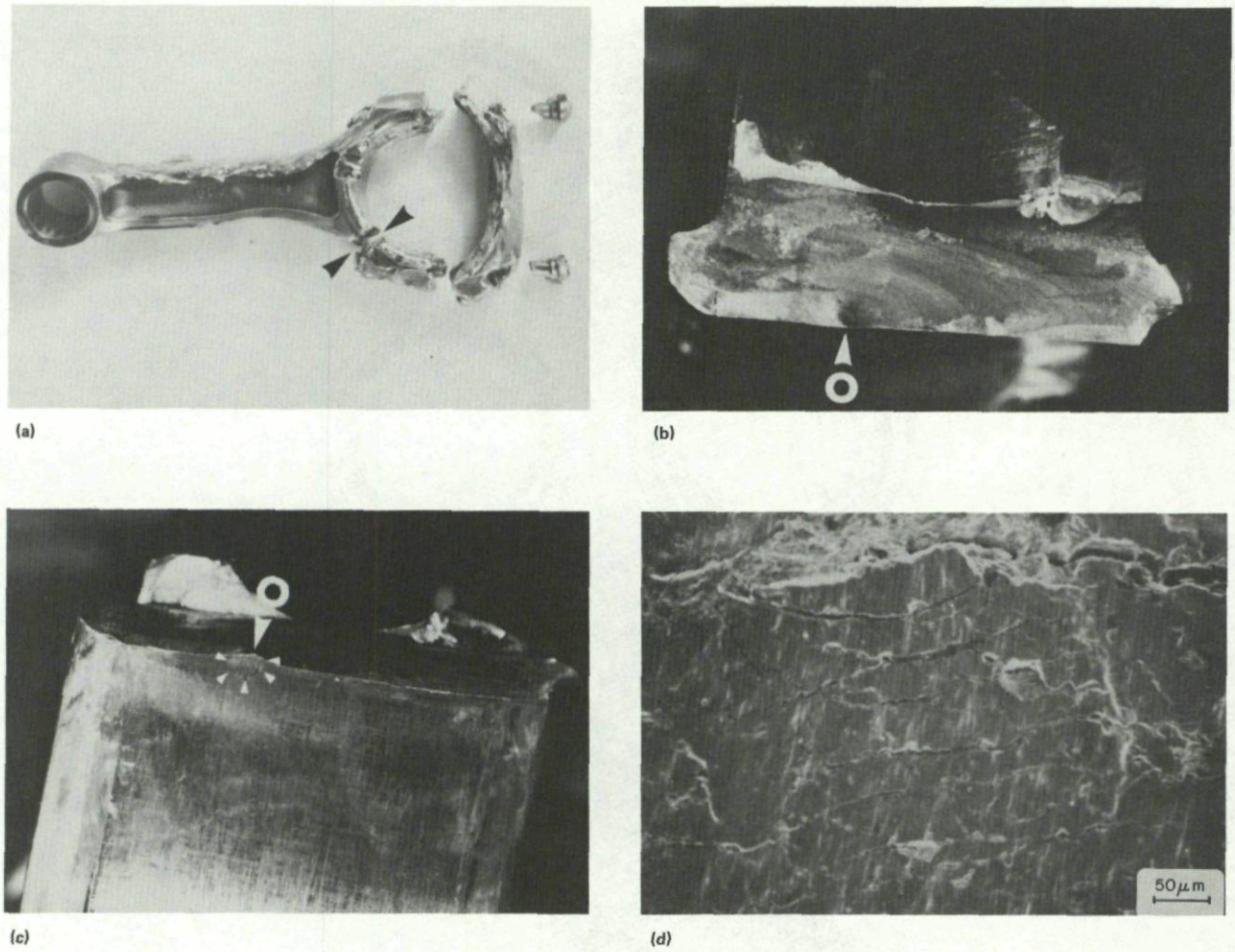

Fig. 11-3 Fretting corrosion and fatigue of a helicopter engine connecting rod

(a) Broken connecting rod indicating the location (arrows) of the fracture surface shown in Figure 11-3(b).
(b) Close-up of arrowed fracture from Figure 11-3(a), showing the fatigue crack initiation site 'O'.
(c) Small fretted zone on the bearing surface at the fatigue origin, marked 'O' in Figure 11-3(b).
(d) SEM image of the fretted area showing multiple cracks running parallel to the main fracture face seen at the top. (Mag. × 200)

Case history 11-2. Fretting corrosion in propeller shaft ball bearings.

It was explained earlier that fretting corrosion is not expected to occur between components subject to large relative displacements. However exceptions do occur, for example between ball bearings and bearing races when abnormal operating conditions arise. Figures 11-4(a) and 11-4(b) show an example of this type where fretting has occurred in the inner and outer bearing races of a propeller shaft.

These bearing races were from a light aircraft which had been operating in the Mediterranean region. The bearings were made from AISI-E-51100 steel and were heat treated to produce a fine tempered martensite with a hardness $H_{RC} = 63$. The fretted regions can be seen as the slightly lighter appearing pitted areas on the outer bearing race shown in Figure 11-4(b).

Fretting of shafts and bearing surfaces usually occurs as a result of one or more of the following (Ref. 11-1):

(a) Minute oscillatory motion between the two components, (b) bearing loads on a limited-contact area, (c) adhesion of asperities and transfer of metal between components, and (d) surface deterioration by abrasion.

According to Reference 11-1, oscillatory motion may occasionally lead to the appearance of a series of elliptical-shaped blemishes that develop centrally located cavities as the fretting progresses. Some indications of this exist in Figure 11-4(b). Strictly static loads applied perpendicular to the bearing surface should not cause wear; however in conjunction with a minute oscillating motion they are conducive to fretting corrosion. The vibratory stresses associated with the propellers appear to have been sufficient in this case to cause the fretting action. The problem of abrasion is one which may affect either non-lubricated bearings where contacting surfaces have equal hardness and are therefore mutually abraded, or in bearings where lubrication fails. The extent of abrasion in the bearings of Figure 11-4 is not known.

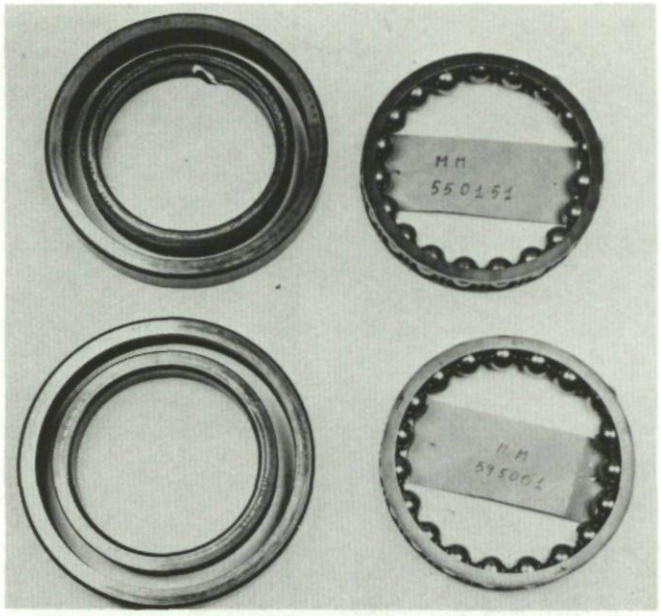

(a)

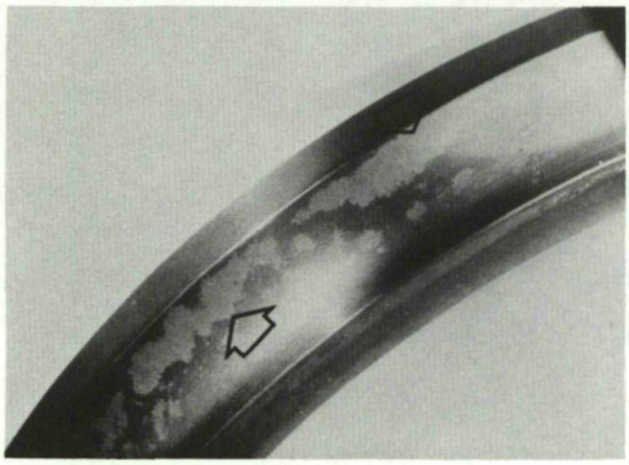

(b)

Fig. 11-4 Fretting corrosion in propeller shaft ball bearings

(a) Bearings and bearing races exhibiting fretting.
(b) Areas of fretting in an outer bearing race.

Case history 11-3. Electrical connector malfunction in an engine starting circuit due to fretting corrosion.

An in-flight mishap occurred when an assisted air start of a military aircraft engine could not be accomplished. It was found that the problem was due to an open circuit malfunction of electrical connectors which were employed in the engine starting circuit.

The receptacle halves of two connectors were submitted for laboratory examination. The mating plug connector halves were not available for study. The connectors were standard five wire threaded collar and flange secured type, and are shown in Figure 11-5(a). Connectors from two different manufacturers were reported to be prone to similar malfunction.

The receptacles were dismantled to retrieve the hollow and split pin contactors, one side of which was bent over to expose the internal contact surface as shown in Figure 11-5(a). The split configuration is normally compressed by a stainless steel tube swaged over the reduced shoulder of the contactor. The sockets were formed from what appeared to be unalloyed copper and were gold plated. Of the two contacts shown in Figure 11-5(a), one was vacant, and one active with a nickel wire remnant still crimped in place. The dark deposit visible within the contact areas was observed in varying amounts on all ten of the available sockets which were examined. Figure 11-5(b) is a higher magnification scanning electron photograph of the unusual deposit showing its crumbly nature. The flattened appearance was thought to have been caused by the mating pin.

A massive deposit which extended the length of the cavity was found in one of the connectors (Fig. 11-5(c)). The wavy appearance of the residue suggests a dried-up liquid (Fig. 11-5(d)). The residue was analyzed and found to be primarily copper oxides, CuO and Cu_2O. Other elements such as Fe, Ni, Au, Rb, Ta, S and P were also detected but were not of sufficient quantity or uniformity to be of significance. An attempt to resolve metallic copper particles within the residue which would be an indication of fretting corrosion was not successful. Nevertheless, the source of the deposit could not be determined other than to assume that it occurred due to fretting action between the recepticle and the pin.

Metallographic cross sections of the female socket connector were prepared in an attempt to gain some insight into the problem. It was found that the connectors were not made of electronic grade, high conductivity oxygen free (OFHC) copper, but rather a cold worked copper containing large oxide inclusions. The electrodeposited coating was found to consist of a very thin gold

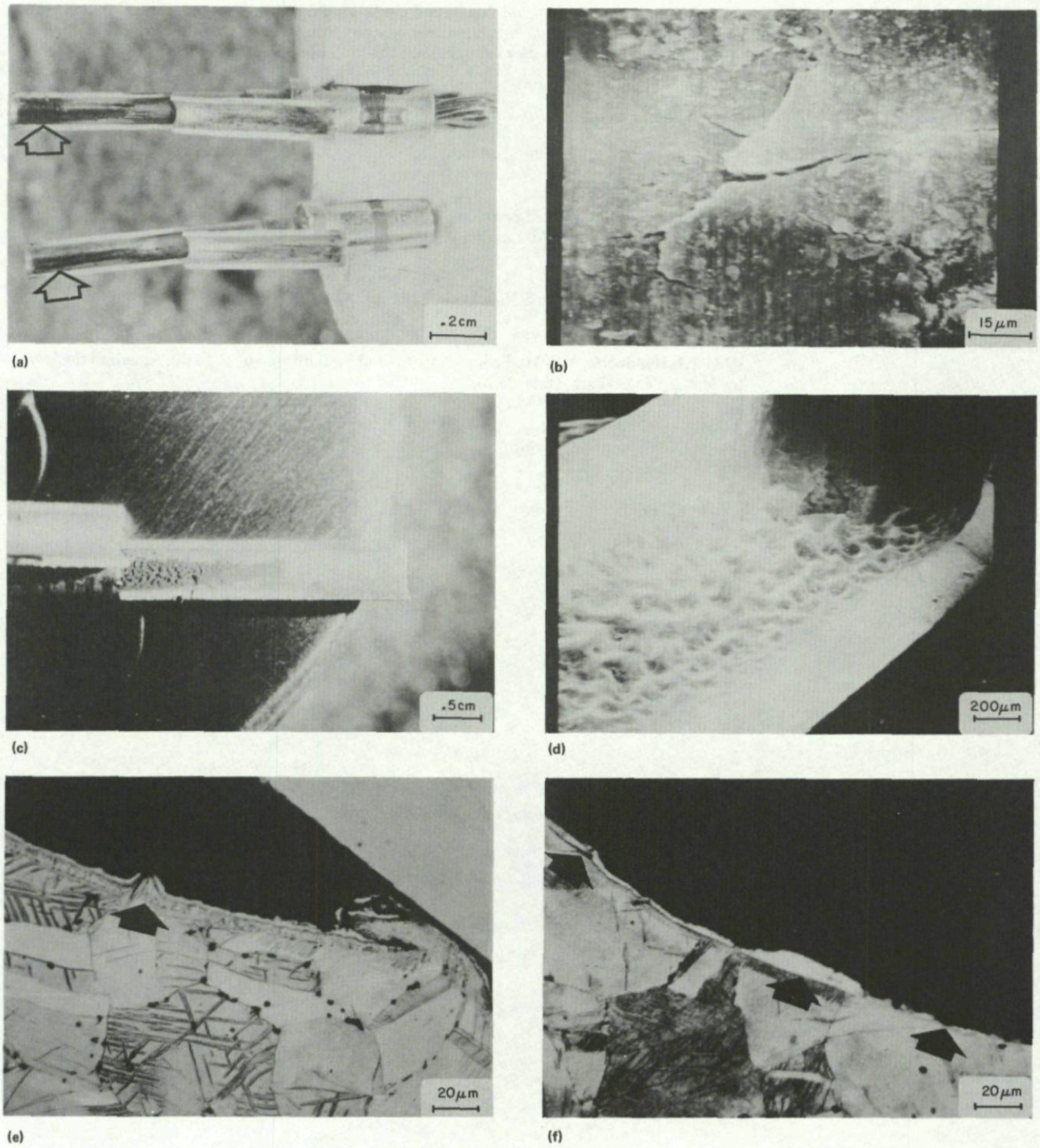

Fig. 11-5 Fretting corrosion in electrical connectors

(a) Dark corrosion products observed inside the connector sockets (arrows). (Mag. × 6)
(b) Higher magnification view of the deposits shown in Figure 11-5(a). (Mag. × 900)
(c) Residue found in No. 2 socket of one connector. (Mag. × 2)
(d) As in Figure 11-5(c). The wavy appearance suggests a dried up liquid contaminant. (Mag. × 50)
(e) Evidence of gas expulsion through plating layers. (Mag. × 500)
(f) Evidence of non-uniform and lack of adhesion of plating. (Mag. × 500)

layer plated on a thicker copper plate, as indicated in Figure 11-5(e). Local areas were found where the coating appeared to be separating from the socket wall, and other areas were found showing what appeared to be gas expulsion through the plating. These defects are indicated by arrows in Figures 11-5(e) and 11-5(f). Figure 11-5(f) also shows that the plating was non-uniform, and that bare copper was exposed in certain areas. It was thought that hydrogen picked up during plating may have combined with the abundant oxygen in the copper to produce water vapour and, possibly aided by electrical heating, this built up sufficient pressure to cause the observed plating decohesion. Thinning of the gold plating, as indicated by Figure 11-5(f), might be due to a wear or fretting action between the pin connector and its receptacle.

It was concluded that the connector was of poor quality and design, and a poor choice of hardware for this application where only two of the five wire connectors were actually used. The fretting action was believed to be due to vibration induced motion between the male pin connector and the female receptacle. It was decided to replace this vibration sensitive electrical connector with a threaded stud and eye type connector.

11.3 References

11-1	Feng, I-M. Uhlig, H.H.	J. App. Mech. 21, 1954, p. 395.
11-2	Evans, U.R.	*An Introduction to Metallic Corrosion.* 3rd Edition, Edward Arnold, London, 1981, pp. 172-173.
11-3	Fontana, M.G. Greene, N.D.	*Corrosion Engineering.* McGraw-Hill Book Company, New York, 1967, pp. 88-91.
11-4	Krueger, F.E.	*Fretting Failures.* IN Metals Handbook, Vol. 10, Failure Analysis and Prevention, pp. 154-160, American Society for Metals, Metals Park, Ohio, 1975.

CHAPTER 12

HYDROGEN INDUCED FAILURES – HYDROGEN EMBRITTLEMENT

12.1 Introduction

A great deal of information has been collected in recent years to demonstrate that environmentally induced failure processes may often be the result of hydrogen damage rather than oxidation. Atomic hydrogen is a cathodic product of many electrochemical reactions, forming during many naturally occurring corrosion reactions as well as during many plating or pickling processes. For example hydrogen is formed, and liberated as a gas when iron is immersed in HCl or dilute H_2SO_4. Whether hydrogen is liberated as a gas, or atomic hydrogen is absorbed by the metal depends on the surface chemistry of the metal. Many substances which are readily adsorbed on metal surfaces can affect both the evolution of hydrogen gas and the absorption of atomic hydrogen. Substances such as phosphorous, arsenic, antimony, sulphur, selenium, tellurium, iodine, cyanide ions, thiourea and naphthalene can act as cathode poisons, impeding the combination of pairs of hydrogen atoms to form gas molecules and favouring the entry of atomic hydrogen into the metal. Benzonitrile and other nitriles act in the opposite way to diminish the entry of hydrogen into the metal (Ref. 12-1).

Due to its small size and mass, atomic hydrogen has very high diffusivity in most metals. It will therefore penetrate most clean metal surfaces quite easily and will migrate rapidly to favourable sites where it may remain in solution, precipitate as molecular hydrogen to form small pressurized cavities, cracks or large blisters, or it may react with the base metal or with alloying elements to form hydrides.

12.2 Hydrogen Blisters

Very large blisters or bubbles can form, particularly in commercial steels exposed to cathodic electrochemical processes in steam plants or petrochemical plants. The bubbles form as a result of the generation of atomic hydrogen at the cathode surface, some of which enters the steel only to condense as molecular hydrogen at internal microvoids or at lines of oxide or sulphide inclusions. The blistering which occurs is evidence of the very high pressures that can occur in the voids, and these have been estimated to be up to several hundred thousand atmospheres (Ref. 12-2).

12.3 Hydrogen Induced Cracking

The accumulation of hydrogen in high strength alloys often leads to cracking, and this often occurs in statically loaded components several hours or even days after the initial application of the load or exposure to the source of hydrogen. Cracking of this type is often referred to as hydrogen-stress cracking, hydrogen delayed cracking, or hydrogen induced cracking. Similar fracture processes can occur in new and unused parts when heat treatments or machining treatments have left residual stresses in the parts, and have then been exposed to a source of hydrogen. For this reason all processes such as pickling or electroplating must be carried out under well controlled conditions to minimize the amount of hydrogen generated.

In pickling, suitable inhibitors such as certain polyamines can be added to the pickling solutions to eliminate or minimize attack on the metal and the generation of hydrogen. In plating processes, both the plating solutions and the applied voltages are controlled to provide high cathode efficiencies which minimize the amount of hydrogen generated. Cadmium plating is widely used in the aerospace industry and hydrogen embrittlement following cadmium plating from cyanide baths is a well known problem. Several alternative plating baths have been developed which diminish this problem, see for example Reference 12-3. With both pickling and plating processes it is usually recommended to bake the component at high temperature to drive off any absorbed hydrogen. The times and temperatures used depend on the particular alloy and on the nature of any surface platings which may impede the effusion of hydrogen. Temperatures are normally in the range 150-300°C for most engineering alloys. Figure 12-1 shows that the times to failure and the stresses required to cause failure by hydrogen delayed cracking increase as hydrogen content in 4340 steel is decreased by baking at 150°C. It also shows that long times in excess of 24 hours are required to restore the normal, hydrogen free, notch strength of this alloy by baking at 150°C.

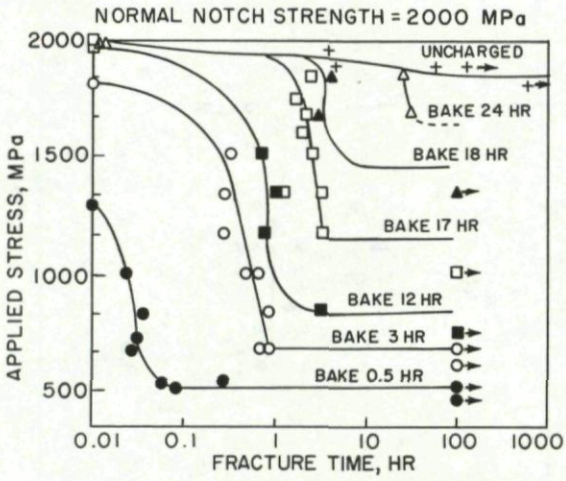

Fig. 12-1 Static fatigue curves for various hydrogen concentrations obtained by baking 4340 steel for different times at 150°C. (Ref. 12-2, data from Ref. 12-4)

12.4 The Nature of Hydrogen Embrittlement

Laboratory investigations have shown that the effect of hydrogen is to lower the ductility or strain to fracture in metals (Ref. 12-5). However the phenomenon is only observed under certain conditions of temperature and strain rate as indicated in Figure 12-2. The most pronounced effects are observed at temperatures around ambient room temperature and at very slow strain rates, since these conditions allow atomic hydrogen to migrate to sites of high triaxial stress in the metal to promote brittle fracture.

Metals which are held under static load at ambient temperature would normally sustain the load indefinately. However statically loaded metal specimens which are pre-charged with hydrogen electrolytically, or which are exposed to environmental conditions where hydrogen is formed, may suffer sudden brittle failures. This type of delayed fracture process is similar to fatigue or stress corrosion cracking in the sense that it involves a period of time required to initiate a crack, and a time required to grow the crack to a size where it will cause complete rupture. Plots of the type shown in Figure 12-3, giving the times for crack initiation and for crack

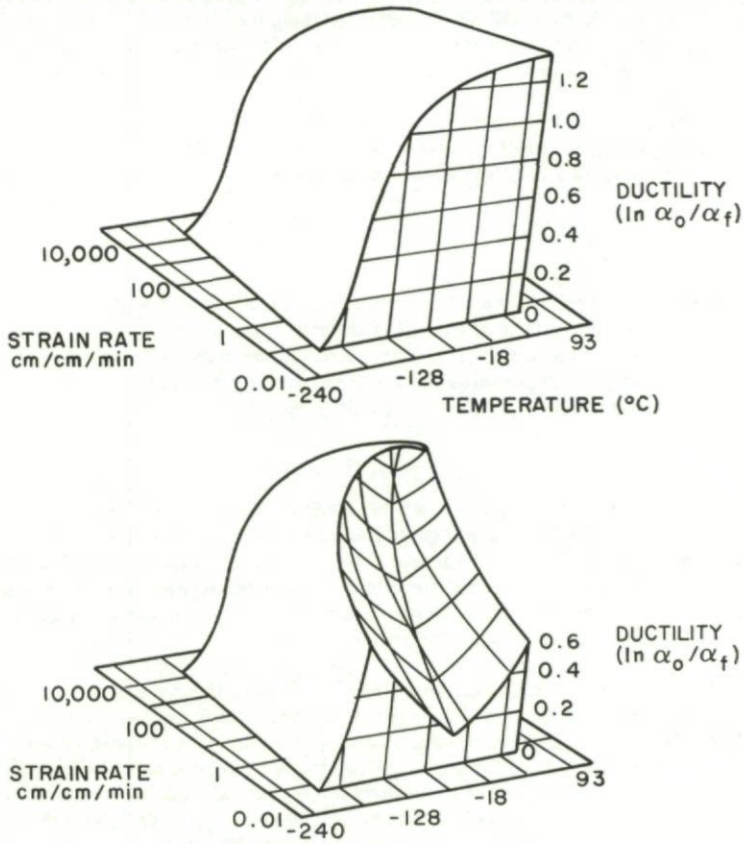

Fig. 12-2 Ductility, expressed as strain to fracture (e_f), of spheroidized 1020 steel as a function of strain rate and temperature. Hydrogen free specimens, top; hydrogen-charged specimens, bottom. (Ref. 12-8, data from Ref. 12-5)

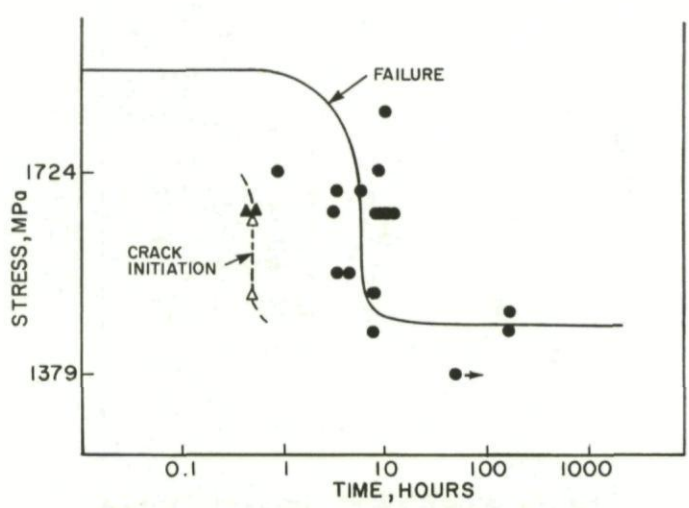

Fig. 12-3 Static fatigue behaviour of 4340 steels at 77°K. The times for crack initiation and for crack propagation are shown as a function of stress. (Ref. 12-6, data from Ref. 12-7)

propagation as a function of applied stress are therefore often referred to as static fatigue curves. The curves are affected by hydrogen content, or pressure, and temperature as discussed by Birnbaum (Ref. 12-6).

This type of delayed fracture process can occur both in smooth or notched specimens and the time to failure will increase as the applied notch stress decreases. The lowest stress intensity which causes failure is called K_{th}, the threshold K for failure (Ref. 12-8).

12.5 Effects of Metallurgical Variables on Hydrogen Embrittlement

Many of the alloys used in airframe and engine construction are affected by hydrogen embrittlement, including steels, aluminium and titanium alloys, and nickel-base alloys. Only brief notes will be given on the metallurgical variables of these alloys that affect hydrogen embrittlement and further details are available elsewhere, see References 12-9 to 12-13. The most important variables are composition, microstructure and strength level. These variables are interrelated, and the variable of microstructure can be subdivided in terms of grain size, crystal structure, precipitate type and morphology, and texture.

Steels

Strength level is an important variable affecting several types of steel, and possibly other alloys as well. The general rule is that susceptibility to hydrogen embrittlement increases as the alloy strength level increases. This is shown in Figure 12-4 which also indicates that the time to failure in 4340 steel decreases as the tempering temperature decreases and the strength increases. However this relationship is observed primarily for high strength steels, since steels with yield strengths below about 700 MPa are usually not markedly affected by hydrogen embrittlement.

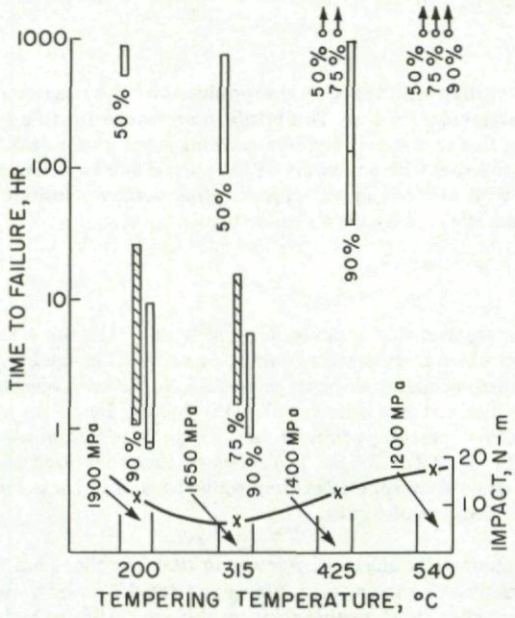

Fig. 12-4 Time to failure versus tempering temperature for 4340 steel at stress levels of 50, 75 and 90% of the yield stress. Specimens exposed to wetting and drying 3.5% NaCl solution at room temperature. (Ref. 12-2, data from Ref. 12-14)

Ferritic and martensitic steels are probably the most commonly affected aerospace materials, and their susceptibility to hydrogen embrittlement is affected by their microstructures. Untempered martensites are the most susceptible, followed by normalized pearlitic/ferritic steels, spheroidized steels, and quenched and tempered martensitic or bainitic steels which are the most resistant to hydrogen (Ref. 12-10). However the composition of any alloy within a grade is also important since alloying elements may either increase (e.g. Mn) or decrease (e.g. Si) susceptibility to hydrogen embrittlement (Ref. 12-8).

Austenitic stainless steels and age hardening austenitic stainless steels are also affected by hydrogen embrittlement. In austenitic stainless steels compositions which increase austenite stability generally provide increased resistance to hydrogen embrittlement. This implies high nickel contents and chromium levels either below 15% or above 20% (Ref. 12-9).

The precipitation hardenable stainless steels such as A-286 are adversely affected by hydrogen, and this alloy has been shown to be susceptible to sustained-load cracking in hydrogen containing atmospheres (Ref. 12-15). The extent of hydrogen embrittlement and the appearance of hydrogen induced intergranular cracking are related to the precipitation of the γ' phase (Ni_3Al, Ti) and η phase (Ni_3Ti) in this alloy. The precipitation of the γ' phase lowers ductility in hydrogen, while the η phase at grain boundaries promotes intergranular fracture (Ref. 12-16).

Aluminium alloys

Most of the early reports on environmentally enhanced fracture in aluminium alloys dealt with stress corrosion cracking (SCC) and the mechanism of cracking was often considered to be stress assisted anodic dissolution of active paths. However new interest has developed as information has been published to show that at least in some cases of SCC hydrogen embrittlement is the operative fracture mode.

The aluminium alloys most widely used in aircraft structures belong to the 2000 series and 7000 series alloys, and evidence now exists, at least in the case of the 7000 series alloys, that hydrogen embrittlement contributes to stress corrosion cracking (Ref. 12-18 to Ref. 12-24). Most studies have been carried out on Al-Zn-Mg alloys made from high purity ingredients, but some work has also been performed on commercial 7075 and 7475 alloys (Refs. 12-25 and 12-26). These studies have shown that hydrogen bubbles may form on grain boundaries in alloys exposed to moist atmospheres. Interestingly the bubbles have been found to form only in overaged alloys, and not in the underaged or peak-aged T6 temper conditions. This has been taken as an indication that if hydrogen is able to precipitate as a gas at suitable grain boundary sites then the amount of hydrogen remaining in solid solution at the grain boundaries will be reduced, and the embrittling effects of this hydrogen will also be reduced. These investigations have been useful in showing that microstructural changes caused by heat treatment in 7075-type alloys lead to similar changes in susceptibility to both hydrogen embrittlement and stress corrosion cracking. Underaged materials appear to be the most susceptible and overaged (T73 type tempers) materials the most resistant.

The source of hydrogen in these embrittlement studies is believed to be the reaction between aluminium and water, which at 70°C produces a duplex film consisting of aluminium oxyhydride (Al OOH) and bayerite ($Al(OH)_3$). The reaction has been written (Ref. 12-27):

$$\text{Anodic} \quad Al + \begin{Bmatrix} 3H_2O \\ 2H_2O \end{Bmatrix} \longrightarrow \begin{matrix} Al(OH)_3 \\ Al\,OOH \end{matrix} + 3H^+ + 3e$$

$$\text{Cathodic} \quad 3H_2O + 3e \longrightarrow \frac{3}{2} H_2 + 3OH^-$$

In the case of the Al-Zn-Mg alloys discussed, the hydrogen produced by this reaction can penetrate the metal, and in the presence of a stress can lead to brittle intergranular fracture. This brittle intergranular fracture can occur with no evidence of concurrent anodic dissolution of the metal, suggesting that true stress corrosion cracking is not responsible. The embrittlement effect is reversible and hydrogen evolution may be detected together with a recovery of the normal ductile failure mode. Interestingly, these phenomena are not observed with pure aluminium or with Al-Mg-Si alloys, suggesting that both composition and heat treatment are important in determining the susceptibility of aluminium alloys to hydrogen embrittlement.

Titanium alloys

Three types of titanium alloys are available commercially, including, (1) the α-phase alloys consisting of hexagonal close-packed α-phase, (2) the α-β alloys in which body centered cubic β-phase exists in equilibrium with α, and (3) metastable β alloys. These different alloy types are formed by adding elements such as Al, Sn, Zr or oxygen which stabilize and strength the α-phase, or elements such as Mo, V, Cr, Nb or Ta which stabilize and strengthen the β-phase. By far the most common types of titanium alloys used in aircraft structures are two phase alloys consisting of dispersions of β-phase in an α-phase matrix, such as Ti-6Al-4V, or dispersions of α-phase in a β-matrix, such as Ti-11.5Mo-6Zr-4.5% Sn. The alloys are therefore often said to have $\alpha+\beta$, or $\beta+\alpha$ microstructures and the two phases can exist with a wide range of morphologies from equiaxed grains to acicular or martensitic laths. Various minor phase precipitates and intermetallic compounds can also exist.

The majority of data on environmentally enhanced fracture in titanium alloys has related to stress corrosion cracking in α-β alloys, and a wide range of environments are known to be damaging (Ref. 12-9). However some work has been performed on commercially pure titanium and several α-β alloys to show that they are also susceptible to hydrogen embrittlement (Refs. 12-28 to 12-32). This work has shown that microstructural parameters such as grain size, grain shape, and precipitate morphology, that affect stress corrosion cracking also affect hydrogen embrittlement in a similar way. The general trend is for acicular α-β microstructures to be more resistant to SCC than equiaxed structures. Figure 12-5 shows that the fracture behaviour of Ti-6Al-4V in hydrogen gas also depends on microstructure. The stress intensity (K_{scg}) required to cause subcritical crack growth in the equiaxed α-β alloy in hydrogen is less than 80% of the stress intensity required to cause unstable fast fracture (K_Q). This hydrogen embrittlement is independent of hydrogen gas pressure. The alloy microstructure in this case had a continuous α-matrix containing dispersed equiaxed grains of β. When

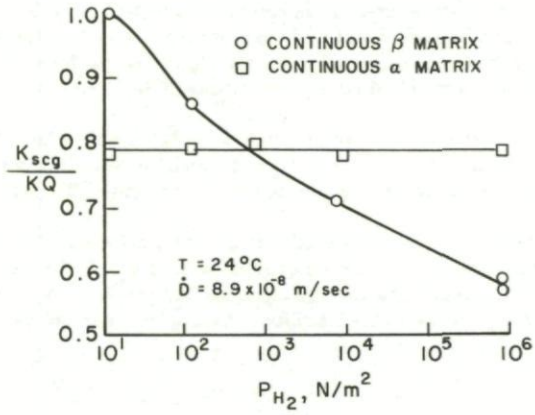

Fig. 12-5 Environmental hydrogen embrittlement of the titanium alloy Ti-6A1-4V as a function of hydrogen pressure. (Ref. 12-31)

the alloy is processed to have an acicular structure, consisting of Widmanstatten laths of α-phase in a continuous matrix of β-phase its susceptibility to hydrogen embrittlement is dependent on hydrogen gas pressure. At very low pressures the alloy is relatively unaffected and it retains its high toughness and resistance to crack growth. With increasing gas pressure the resistance to subcritical crack growth decreases and the alloy is severely embrittled.

Hydrogen embrittlement may also contribute to stress corrosion cracking in titanium alloys, as it has been suggested for aluminium alloys. Important results supporting this view have been obtained by electrochemical experiments (Refs. 12-33 and 12-34), and by experiments involving comparisons of the effects of torsional loading (mode III) versus tension loading (mode I) on the cracking of titanium alloys in sodium chloride solution (Ref. 12-35). In torsion loading there is no hydrostatic component of stress which would cause hydrogen to accumulate at the crack tip, whereas in tension there is. The results of Figure 12-6 show that stress corrosion cracking did not occur in Ti-8Al-1Mo-1V when torsion loading was employed, whereas stress intensities less than 80% of the fracture toughness caused SCC with failures occurring in times less than 1 hour when tensile loading was applied. Additions of arsenic to the solution, which as explained earlier should promote the entry of hydrogen atoms into the metal increased the stress corrosion cracking susceptibility of this alloy. This data provides strong evidence of a relationship between SCC and hydrogen embrittlement. Similar results have been obtained for 7075-T6 aluminium tested in sodium chloride and potassium dichromate solutions (Ref. 12-35). Some special cases of stress corrosion cracking, such as hot salt SCC in titanium alloys, have been established to be due to hydrogen embrittlement (Refs. 12-36 and 12-37).

The mechanism whereby hydrogen embrittles titanium alloys is not completely understood, although the formation of hydrides has been widely discussed (Ref. 12-9).

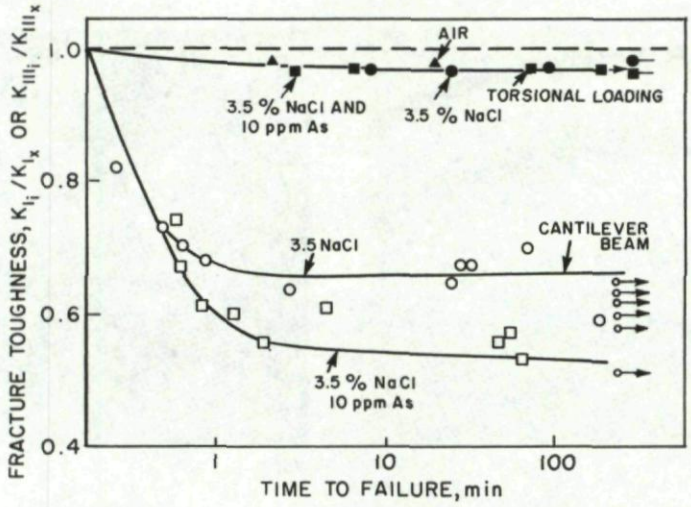

Fig. 12-6 Resistance to SCC of Ti-8Al-1Mo-1V as a function of loading mode in 3.5% NaCl solution with and without arsenic additions to facilitate hydrogen entry, at -500 mV versus a standard calomel electrode. (Ref. 12-35)

12.6 Case Histories

Case history 12-1. Hydrogen embrittlement of a flap control return spring.

During a pre-flight inspection of a light aircraft the pilot lowered the flaps, heard a loud noise and found the flaps jammed down. The flap control return spring was found to be shattered into many pieces (Fig. 12-7(a)). All the fracture faces revealed similar small, dark, crescent shaped areas radial to the wire axis on the inside surface of the coil. These areas followed a 45° helical path with respect to the wire centre line (Figs. 12-7(b) and 12-7(c)). The remaining portion of each fracture face was characteristic of sudden overload rupture, confirmed as mixed ductile dimpling and cleavage mode by scanning electron microscopy. The pre-cracked helical zones were all damaged by corrosion.

Magnetic particle inspection (MPI) revealed many other helical cracks on the spring coil's inner surface (Fig. 12-7(c)). The spring was found to be cold wound carbon steel of about 1900 MPa strength. Axial sections cut through the cracks revealed by MPI showed them to be corroded, however some subsurface cracks were also found (Fig. 12-7(d)). The large number of simultaneous fractures at failure, and the multitude of surface and subsurface cracking indicated that this was an unusual failure.

Figure 12-7(d), showing an entirely internal crack, is indicative of hydrogen embrittlement. The conditions for hydrogen assisted cracking were all present; (1) the material and its strength level were appropriate, (2) the material was subjected to high sustained stresses in service (207 MPa initial tension set, plus residual coiling stresses, plus elongation stresses in service) all of which were concentrated at the coil inner surface where all the cracking was located, (3) the spring was exposed to a source of hydrogen during cadmium electroplating.

As discussed in Section 12-3, hydrogen absorbed during pickling and electroplating can be removed by baking after each stage of processing. In this case there was no record of any baking after cadmium plating. The spring was replaced and precautions taken to ensure that the springs were baked for 24 hours at 190°C, and that this baking was performed immediately after the plating.

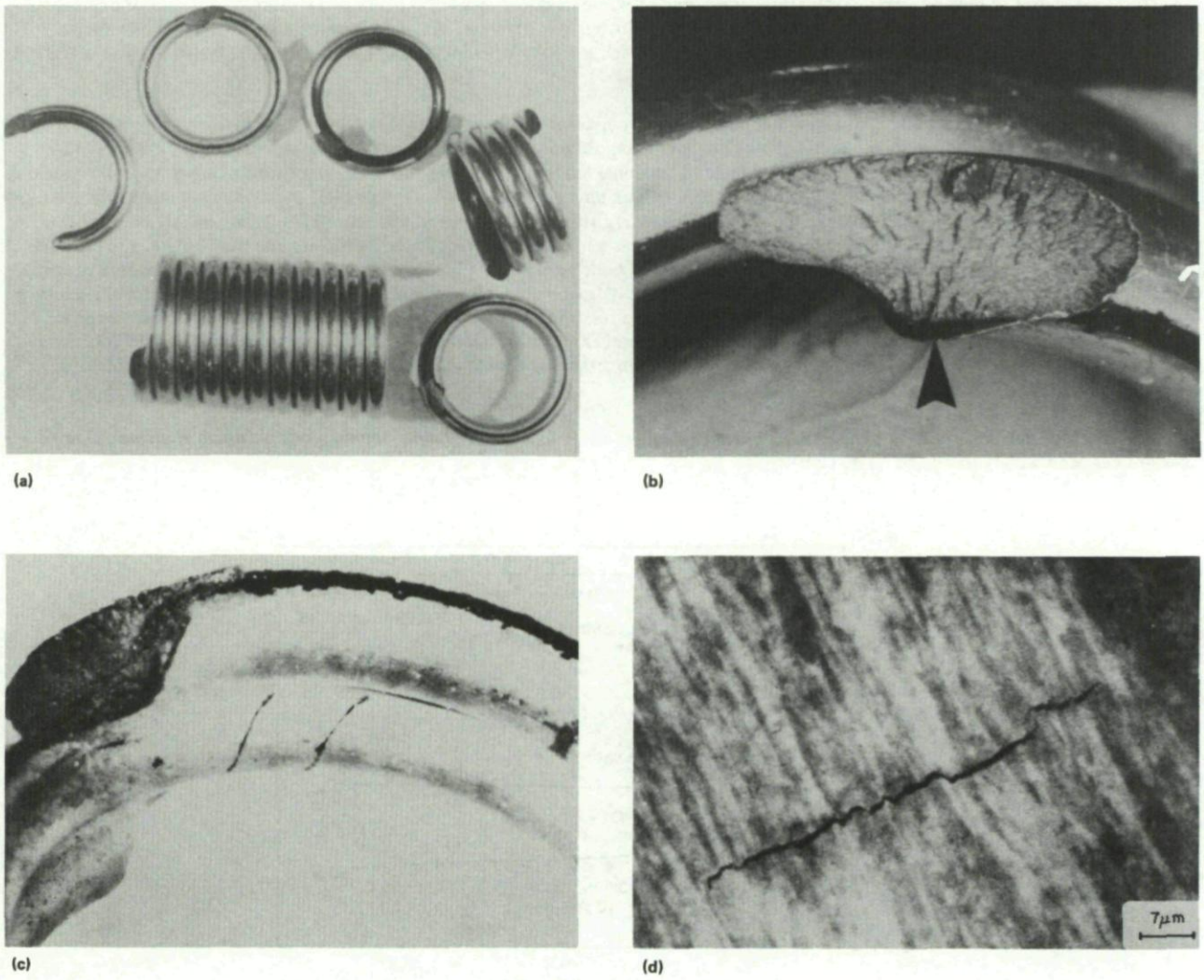

Fig. 12-7 Hydrogen embrittlement of a carbon steel flap control return spring

(a) General view of the broken flap control spring.
(b) Close-up of a typical spring fracture surface. Note the dark radial/helical oriented precrack on the spring's inner surface (arrowed).
(c) Magnetic particle indications of other helically oriented cracks on the spring inner surface.
(d) SEM image of a subsurface crack in spring section (inner surface of coil at upper right). Note the absence of corrosive attack. Nital etch. (Mag. × 1500)

Case history 12-2. Hydrogen delayed cracking in a 4340 steel main landing gear pivot pin.

Over a period of time a number of pivot pins from the main landing gear retraction system of a fleet of fighter aircraft were found to be fractured. The pins were made from a chromium plated 4340 low alloy steel in a high strength condition. One of the pins was found to be broken into three pieces and the central piece, having fracture surfaces at both ends, is shown in Figure 12-8(a). One of the two fracture surfaces is shown in Figure 12-8(b). The fracture surface was found to be very clean and free of any significant indications of corrosion. It was also found to be very rough, and it was not possible to identify the initiation point with any certainty. However there were some indications that the fracture started near the lower edge of the surface shown in Figure 12-8(b).

Palladium shadowed two-stage replicas were made of various areas of the fracture surface and these were examined in a transmission electron microscope. The fractures were predominantly intergranular, and evidence of ductility was minimal (Fig. 12-8(c)).

Intergranular fracture in a high strength low alloy steel, in the absence of temper discolouration or discolouration due to corrosion and pitting, is strongly indicative of hydrogen embrittlement. In order to test the hypothesis that the failures were due to hydrogen embrittlement, some sustained load tests were performed. All specimens failed within a fairly short time, and the replicas of the fracture surfaces showed the same clean intergranular features as the service failures. An example of the sustained load fracture surfaces is given in Figure 12-8(d).

It was concluded that the failures were due to hydrogen embrittlement, and the source of hydrogen was most probably the galvanic chromium plating process. The baking treatment used for the relief of hydrogen embrittlement was evaluated and modifications made to the process.

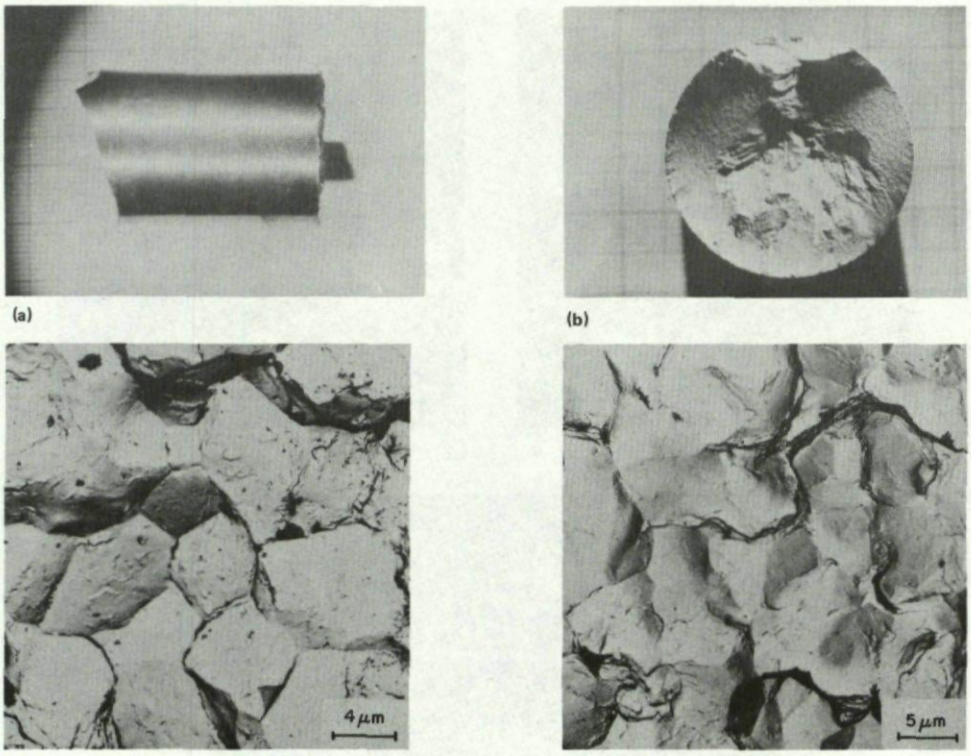

Fig. 12-8 Hydrogen delayed cracking in a 4340 main landing gear pivot pin

(a) Central portion of the broken pivot pin.
(b) One of two fracture surfaces on the piece shown in Figure 12-8(a).
(c) Replica transmission electron microscope picture of an area from Figure 12-8(b). (Mag. × 2800)
(d) Fracture surface of a specimen which failed during a sustained load test. (Mag. × 2200)

Case history 12-3. Hydrogen embrittlement of a 4340 steel bolt from a main landing gear drag link.

A cadmium plated 4340 steel bolt from a fighter aircraft main landing gear drag link was found to be fractured during a visual inspection of the aircraft. The part is shown in Figure 12-9(a), and it can be seen that the fracture occurred in the root of the first engaged thread, under a nut. The fracture appeared to have initiated in the region of the arrow, in Figure 12-9(b), and the fracture surface was quite clean and flat except for two ledges at the top and bottom edges as viewed in Figure 12-9(b).

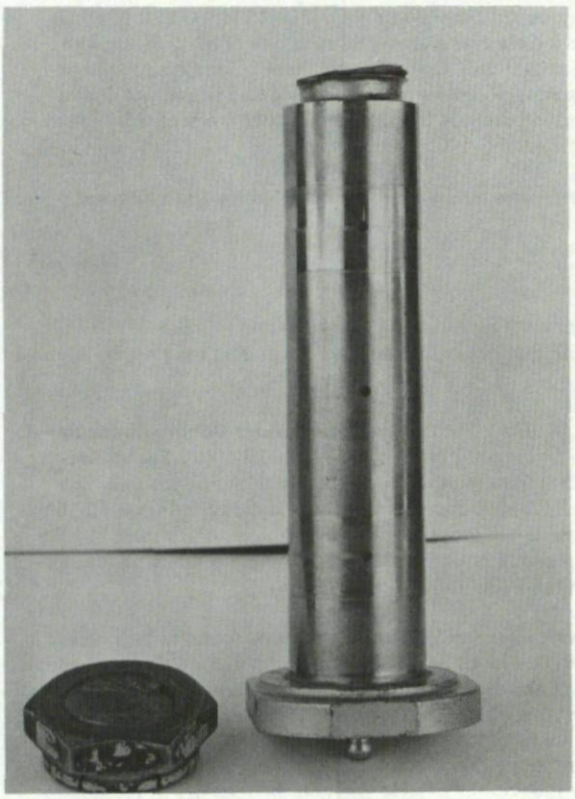

(a)

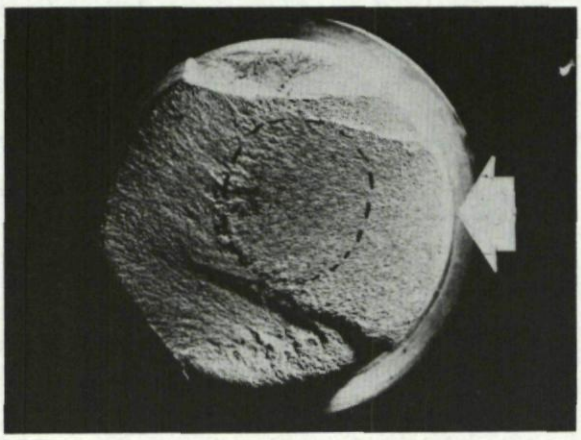

(b)

Fig. 12-9 Hydrogen embrittlement of a 4340 steel bolt from a main landing gear drag link

(a) General view of the failed bolt.
(b) Fracture surface of the failed bolt.

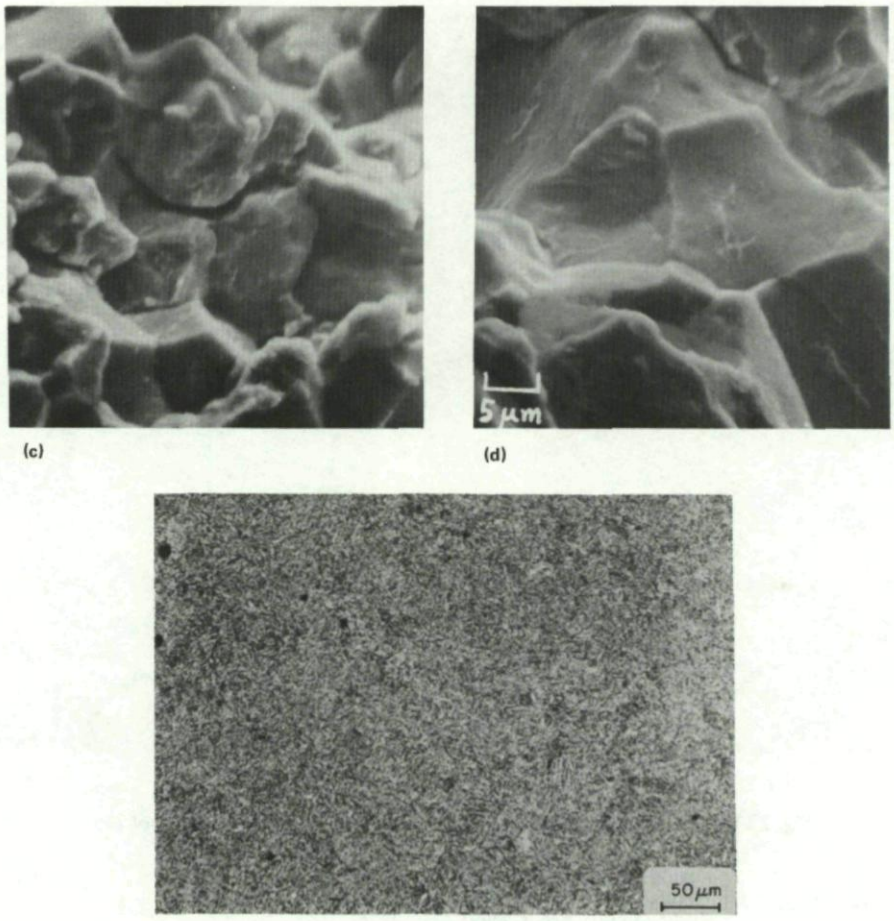

(c) (d) (e)

Fig. 12-9 Hydrogen embrittlement of a 4340 steel bolt from a main landing gear drag link

(c) and (d) SEM pictures of the fracture surface shown in Figure 12-9(b) showing intergranular fracture.
(e) Microstructure of the 4340 steel. (Mag. × 200)

Scanning electron microscopy revealed a predominantly intergranular fracture topography (Fig. 12-9(c)), with fine hair lines on the equiaxed grain faces (Fig. 12-9(d)). The material was found to have a fine martensitic structure (Fig. 12-9(e)), with a hardness R_c = 52. This suggests the material was tempered in the range 200-260°C, and would have a tensile strength of 1800-1950 MPa. The bright and clean intergranular fracture in a steel of this strength level strongly suggests that failure was due to hydrogen embrittlement. As indicated in Figure 12-4, sustained load cracking will occur in hydrogen embrittled steels of this type in times as short as 1 hour when stresses of about 75% of the yield stress are applied.

The source of hydrogen was believed to be the cadmium plating process, and a more rigorous baking treatment was recommended.

Case history 12-4. Hydrogen assisted cracking in a 4340 steel tie rod end.

Over a period of time at least seventeen defective parts were found in the main landing gear actuating cylinder tie rod ends of two fighter aircraft. Although two aircraft were involved the parts were identical in design, materials and manufacturing methods, and a typical part is shown in Figure 12-10(a).

On inspection two cracks were found in the part shown in Figure 12-10(a). The first crack was clearly visible with the naked eye, and was found on the outside of the rod end emanating from the grease fitting hole, as shown in Figure 12-10(b). The second crack was not readily apparent until the two bushings shown in Figure 12-10(a) were removed from the eye of the tie rod end. The crack was located on the inside of the eye opposite the threaded rod section. The appearance of this crack is shown in Figure 12-10(c) as a separated fracture face. It can be seen that the crack was quite extensive and had propagated from several initiation sites. In both cases the cracks appeared to be driven by stresses arising from pressed inserts, and in both cases the inserts were cadmium plated steel. The rod end was analyzed and found to meet specifications for 4340 steel in the 1250-1400 MPa condition.

The cracks were examined metallographically and by scanning electron microscopy. The cracks were found to be multiple in nature, with numerous initiation sites and extensive branching, as shown in Figure 12-10(d). The fracture path was mainly transgranular, and no oxide scale or corrosion deposits were evident. No decarburization was observed and there was no evidence of cadmium within the crack formations. Figures 12-10(e) and 12-10(f) are scanning electron photographs of the fracture surface exposed by breaking open the crack in the tie rod eye. The direction of crack propagation is from bottom to top in both photographs, and the fracture characteristics are primarily of brittle transgranular fracture, with little or no evidence of intergranular fracture or ductile dimples. The appearance of the fracture surface most closely resembled mechanical fatigue except for the absence of striations and the presence of multiple

secondary cracks running both transverse to the direction of primary crack propagation (axial cracks), Figure 12-10(e), and parallel to this direction (radial cracks), Figure 12-10(f). The absence of corrosion products and intergranular cracking would seem to rule out stress corrosion cracking, while the absence of ductile dimples would rule out overload cracking.

It was thought that hydrogen assisted delayed failure was the most likely explanation for this unusual fracture behaviour, although this was not unequivocally established. The driving stresses were thought to arise from the interference fit bushings and grease fittings, rather than from service loading. The source of the hydrogen was conjectured to be from the cadmium plated bushings and fittings, and/or from the cadmium plated tie rod threads. It was recommended to remove the cadmium from the bushings and grease fittings, and the surfaces that they are in contact with, and to reinstall using wet assembly techniques with an epoxy primer for corrosion control. It was also recommended that the cadmium plated threaded ends of the tie rod be examined to insure that no hydrogen assisted delayed cracking was occurring in those regions.

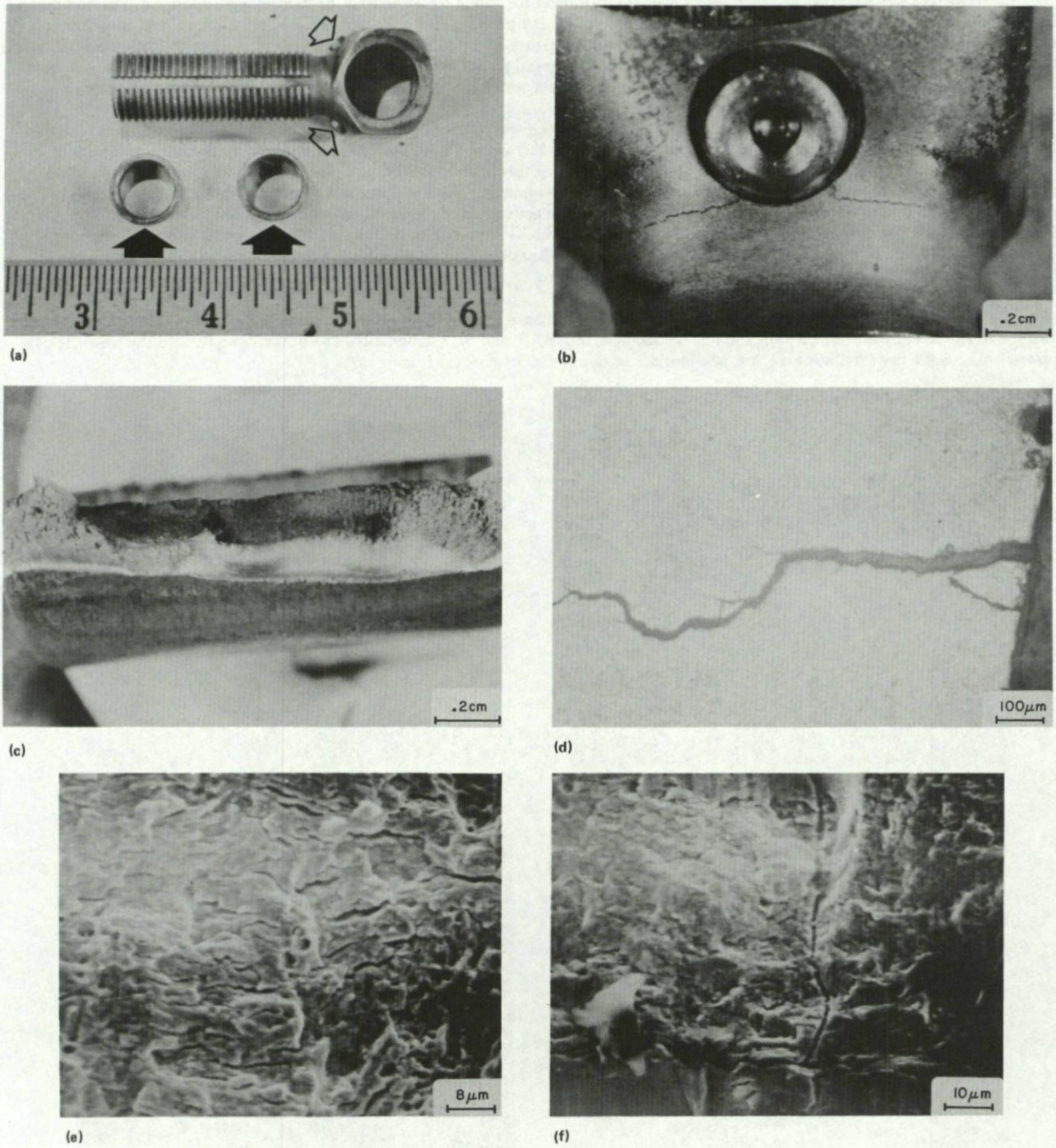

Fig. 12-10 Failure of a 4340 steel tie rod end

(a) As received tie rod end showing (open arrows) cadmium plated grease fittings and (solid arrows) cadmium plated steel bearing inserts. Both are press fitted.
(b) Cracks propagating from the grease fitting hole. (Mag. × 7)
(c) Fracture surface of the crack in the eye section. The surface was prepared by bending the section to open and expose the crack. The dark area is the crack formation, the lighter area is overloaded sound metal. (Mag. × 7)
(d) Metallographic section through a typical crack. (Mag. × 100)
(e) SEM picture of the fracture face showing secondary transverse tearing. (Mag. × 1250)
(f) SEM picture of the crack initiation surface showing cracking in the direction of crack propagation. Same orientation as Figure 12-10(e). (Mag. × 1000)

In cases of diagnostic uncertainty such as this, the problem can sometimes be resolved by performing tensile strength tests on notched specimens covering a range of strain rates which would in one case suppress hydrogen embrittlement, and in another case allow it to occur. Some results from tests of this type are shown in Reference 12-17. An alternative method, used in Case history 12-2, involves the determination of times to failure of specimens loaded statically to stresses below the yield strength.

Case history 12-5. Failure of a low alloy steel bolt from a fighter aircraft rudder post bearing retainer cap.

The failed bolt shown in Figure 12-11(a) was found during a training exercise of a fighter aircraft rudder assembly. The inspection was not scheduled maintenance. Of eight bolts securing the rudder post, two were discovered to have separated. One of the two bolts was examined in the laboratory.

The bolt was specified as a cadmium plated shear fastener for which either 4340 or 8740 steel were approved. The bolt was found to have a hardness of R_c 41-42. The threads were rolled and incorporated a locking feature, for a crimp nut, consisting of notches in the thread crown. These can be seen by the arrows in Figure 12-11(b). The crimp nut was not used on the failed bolt. It was observed that the fracture path coincided with these notches in several places. It was also evident that a sealer or primer had been used on the bolt. Distress observed on the bolt threads and on the nut suggested that an over-torqued condition could have occurred.

The fracture surface of the bolt, shown in Figure 12-11(c), was studied by optical and scanning electron microscopy. It was observed that the fracture originated at multiple sites in the upper thread root and also at the notches shown in Figure 12-11(b). The cracks propagated radially towards the centre of the bolt. The fracture surface of the bolt was free of corrosion deposit, and no prominent beach marks or arrest pattern were apparent. The intergranular crack propagation shown in Figure 12-11(d) suggests that stress corrosion or hydrogen embrittlement failure mechanism was active during the initial crack propagation. However low alloy steels of this type have poor corrosion resistance and signs of rust might be expected in the case of aqueous stress corrosion cracking. Hydrogen embrittlement might therefore be the more likely explanation. Ductile dimples indicating overload failure were apparent toward the centre of the bolt.

An effort was made to identify a corrodent which could have contributed to the stress cracking observed. Dispersive electron analysis of the fracture area of the bolt and nut revealed Cd, Mo, S, Cr, and Si in abundance. These findings indicated the presence of a primer/sealer and a dry film lubricant, but no chlorides or other corrodents were found.

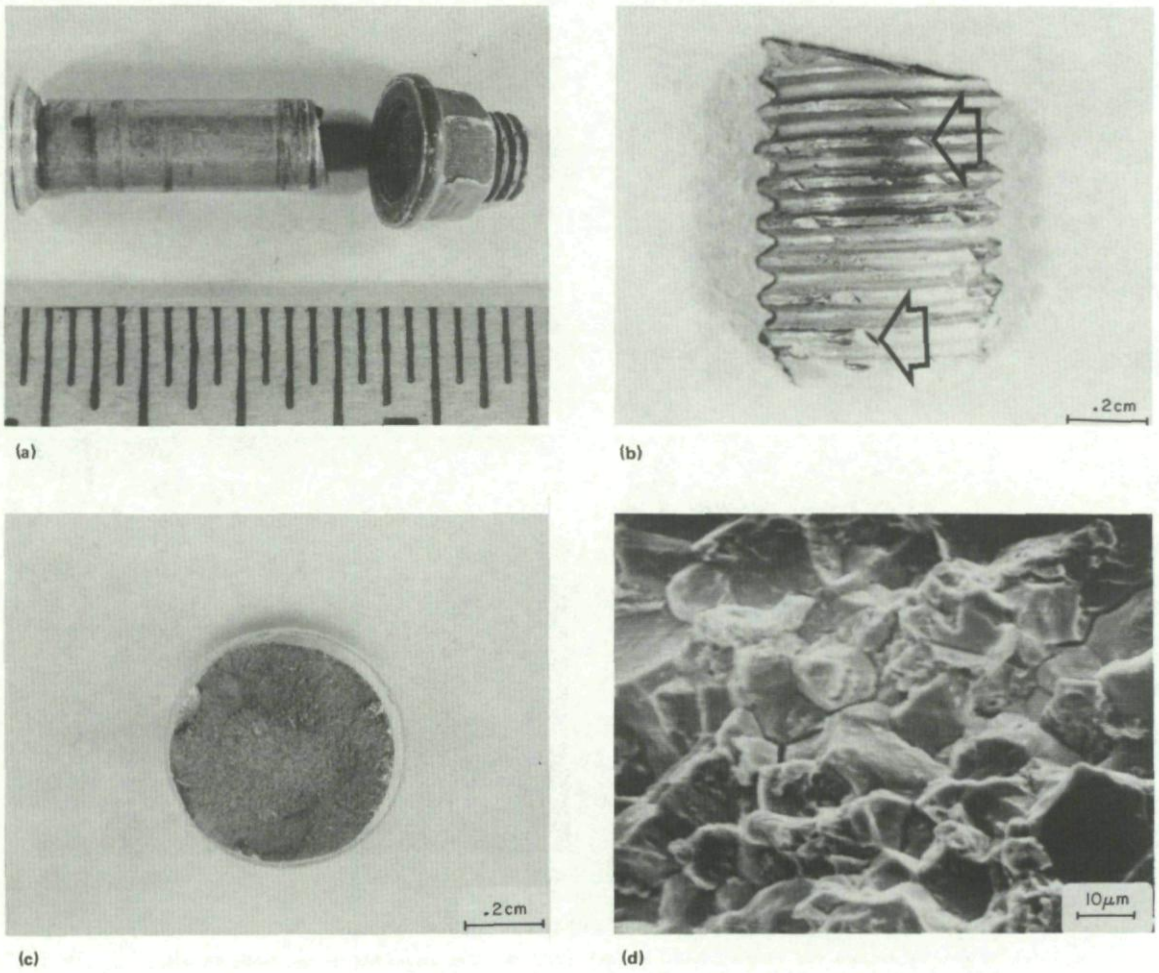

Fig. 12-11 Failure of a low alloy steel bolt

(a) General view of the failed bolt and nut.
(b) Threaded end of the failed bolt removed from the nut. (Mag. × 7)
(c) Fracture face of the head end of the bolt. Multiple initiation sites are present. (Mag. × 7)
(d) SEM picture of the fracture surface showing intergranular topography. (Mag. × 1000)

It was concluded that the rudder assembly bolt failed by hydrogen embrittlement. Several factors may have contributed to the failure, including excessive torque on the bolt and the presence of notches on the thread crowns. The source of hydrogen was not established, although this may have been from the cadmium plating. The dry film lubricant was also considered to be a potential corrodent, but this was not established.

Case history 12-6. Hydrogen induced failure of 4037 steel setscrews from a helicopter clutch.

Several setscrews from a single batch failed in service in the clutch assembly of a military helicopter. Samples of the failed setscrews were submitted for laboratory examination along with a number of unused and intact setscrews from the same batch. The setscrews, shown in Figure 12-12(a), were 25 mm × 6.35 mm × 28 cadmium plated steel and were used for clutch adjustments. The procurement specifications allowed the use of 4032, 4037, 4137, 4140, 8630 or 8740 low alloy steels, having a hardness in the range R_c 45-53, and required cadmium plating to be used.

One setscrew was analyzed and found to meet the requirements for 4037, having a composition 0.37% C, 0.79% Mn, 0.28% Si and 0.20% Mo. Its hardness was R_c 49-50. The microstructure was examined with respect to grain size, inclusion content and extent of surface decarburization and all were within acceptable limits. The cadmium plating was found to have a thickness of 5μm-8μm.

The fracture surface of a failed setscrew exhibited predominantly intergranular fracture (Fig. 12-12(b)), but some areas of ductile dimples and secondary cracking were evident (Fig. 12-12(c)). These features suggested that hydrogen embrittlement may be involved. An unused setscrew was loaded in tension until failure occurred at 23.14 KN. Another setscrew was loaded to 19.58 KN, or 85% of the ultimate load, and held under sustained static load. The setscrew failed in 51 hours, the fracture face again exhibiting a mixed mode brittle intergranular and ductile dimpled appearance. This behaviour confirmed hydrogen embrittlement.

The subject batch of setscrews was recalled from service to preclude future embrittlement failures. It was thought that the hardness of the setscrews was excessively high for the specific application even though allowed by the specifications. It was recommended to lower the hardness of the setscrews in order to improve their toughness and resistance to service induced embrittlement.

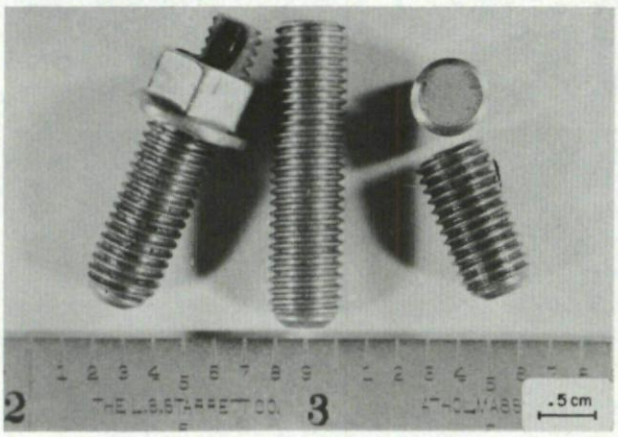

(a)

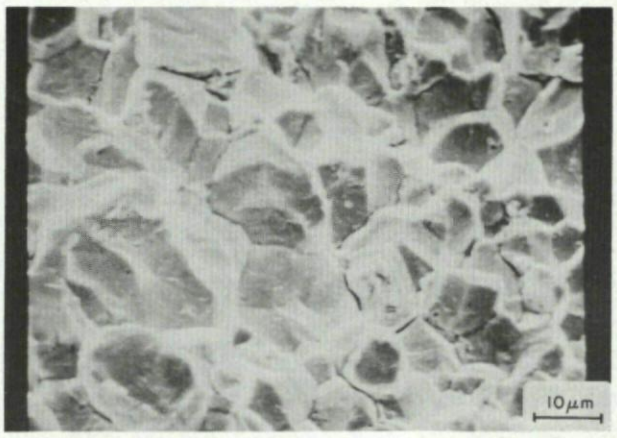

(b)

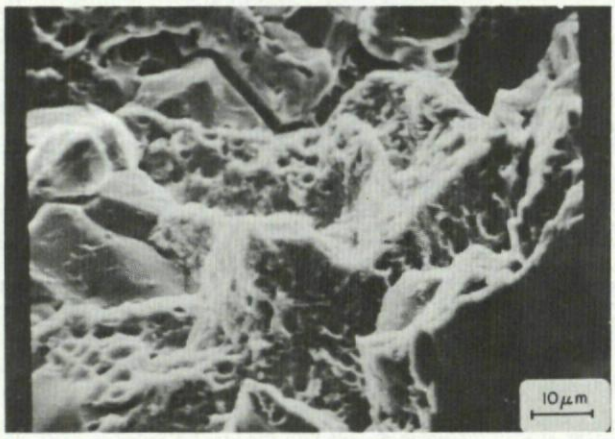

(c)

Fig. 12-12 Hydrogen induced failure of some 4037 steel setscrews

(a) General view of some new and unused, and used and failed setscrews. (Mag. × 2)
(b) SEM picture showing intergranular fracture and secondary cracking of setscrew fracture face. (Mag. × 1200)
(c) SEM picture showing mixed mode brittle intergranular and ductile dimpled fracture. (Mag. × 1200)

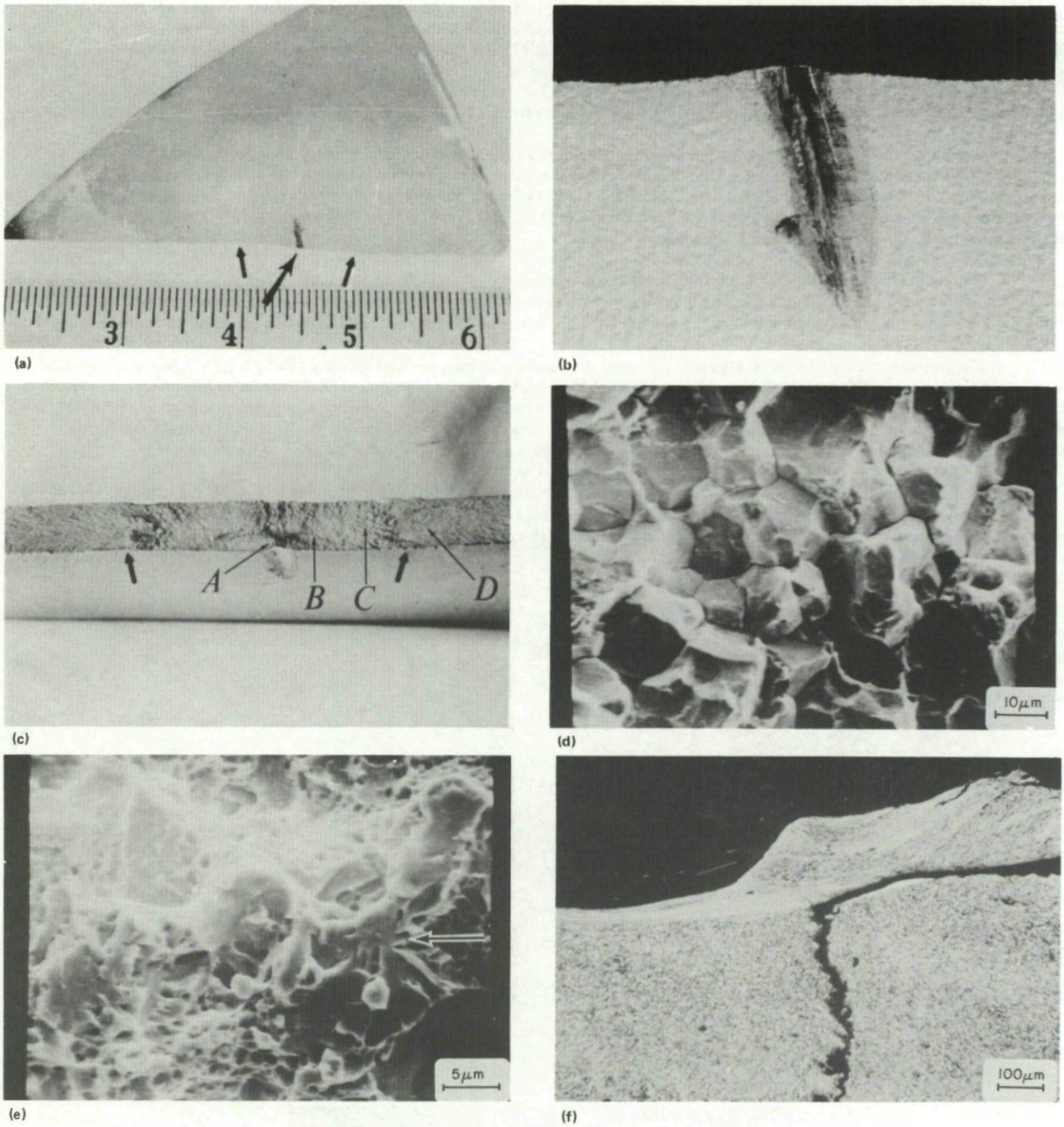

Fig. 12-13 Failure of a 4340 steel landing gear cylinder

(a) Piece of cylinder with paint removed. Large arrow indicates gouge which initiated fracture. The fracture surface between the small arrows is free of a shear lip.
(b) Close-up of the gouge with a build-up of material to the left. The gouge was free of corrosion products and bare steel was exposed in some areas with residual cadmium plating in others.
(c) Fracture surface at the gouge. Small arrows indicate the start of shear lip formation. Long arrows A and D indicate the locations of SEM pictures shown in Figure 12-13(d) and Figure 12-13(e).
(d) SEM picture of Area A showing clean and unpitted intergranular fracture facets. (Mag. × 1100)
(e) SEM picture of Area D showing mixed ductile dimples and quasi-cleavage (arrow) typical of overload fracture in high strength steels of good toughness. (Mag. × 2400)
(f) Metallographic cross-section through the gouge showing a secondary crack which follows a light band of untempered martensite under the burr (upper right), and then turns into the wall section and proceeds by an intergranular mode. (Mag. × 100)

Case history 12-7. Failure of a 4340 steel outer cylinder from an aircraft landing gear.

The outer cylinder of a military aircraft landing gear failed during taxi for take-off. The failure occurred only five weeks and four flights after the landing gear had been installed, and prior to installation it had been held in storage since its last overhaul almost two years earlier.

A piece of the outer cylinder, shown in Figure 12-13(a), was submitted for laboratory examination and was found to contain a gouge which extended from the fracture surface. Closer examination revealed no evidence of paint or primer in the gouge (Fig. 12-13(b)), although there were signs of solvent contact with the outer surface in the vicinity of the gouge. The walls of the gouge were bright in some areas and dark in others, but exhibited no obvious signs of general corrosion.

Inspection of the fracture surface showed that the outer surface gouge was centred in a roughly clamshell-shaped area whose boundaries were not well defined but could be generally discerned by the texture of the chevron marks, as indicated in Figure 12-13(c). There was no shear lip on the outer surface for a length of about 12 mm on either side of the gouge, but the rest of the fracture edges, including the entire inner wall surface, had well formed shear lips. There was no rust or other evidence of corrosion to be seen anywhere on the fracture surface. Rather, it appeared clean and bright, even near the gouge.

Scanning electron microscopy of the fracture surface revealed a predominantly intergranular cracking mode near the initiation site at the gouge, with small patches of transgranular dimpling. The grain facets were very clean and not pitted (Fig. 12-13(d)). Moving progressively farther from the initiation zone, the fracture surface revealed an increasing proportion of transgranular tearing, still mixed with clean intergranular cracking and little or no quasi-cleavage. Estimates of the proportion of intergranular cracking occurring at sites A, B, C and D (in Fig. 12-13(c)) indicated values of 90%, 60%, 50% and less than 10% respectively. The fracture surface at location D is shown in Figure 12-13(e), and consists of a mixture of ductile dimples and quasi-cleavage, producing a predominantly transgranular fracture. No definite transition from intergranular cracking to ductile transgranular tearing was seen. Such a transition is commonly found in slow, stable-growth cracks, such as stress corrosion cracks, which may progress to instantaneous failure.

Energy-dispersive x-ray analysis of the fracture surface revealed no evidence of corrosion products. Similarly, inspection of the gouge walls gave no indication of elements whose anions are often implicated in corrosion reactions, e.g. Cl^- or $SO_4^=$. The gouge walls were free of cadmium in many areas, while the remaining cylinder outer surface was cadmium plated.

A metallographic cross-section was taken parallel to and approximately 5 mm below the fracture surface. This section traversed the lower portion of the gouge and is shown, polished and etched, in Figure 12-13(f). The microstructure of the steel away from the gouge was that of a normal tempered martensite, but in the immediate vicinity of the gouge light bands of untempered martensite were observed. A secondary crack, running perpendicular to the main fracture surface, had followed one of the light bands under the gouge burr, and then turned toward the cyclinder inner surface and progressed intergranularly. Micro-hardness tests, performed to compare the hardness of the light bands to that of the tempered matrix confirmed that the bands were untempered martensite with a hardness of R_c 61.5.

Hardness measurements on the tempered martensite gave an average value of R_c 48.5, and chemical analysis showed that the material was 4340 alloy steel with a composition 1.8% Ni, 0.88% Cr, 0.76% Mn, 0.22% Mo, 0.22% Si, 0.38% C, 0.025% P (max), 0.025% S (max), balance Fe. The hardness indicates a tensile strength of about 1670 MPa.

It was concluded that failure of the landing gear cyclinder had initiated at a surface gouge which contained brittle untempered martensite. The age of the gouge could not be established, but the fact that the exposed steel walls of the gouge appeared clean and uncorroded suggested that the gouge had been formed recently, and certainly either during or after the gear installation five weeks earlier.

It was thought that the propagation of the crack, after it formed in the martensite was due to hydrogen embrittlement. Hydrogen was implicated particularly since the cylinder had been exposed to sustained-load conditions for only five weeks. It was considered improbable that a stress-corrosion crack could grow to a 25 mm length in that time under the conditions experienced by this component.

Case history 12-8. Failure investigation of two filter bowl securing studs.

A problem involving the failure of securing studs from a helicopter filter bowl persisted for several years. Two failed studs, as shown in Figure 12-14(a), were submitted for laboratory examination. Stud No. 1 was determined to be a 41XX steel with a hardness of R_c 26, while stud No. 2 was found to be a 43XX type steel with a hardness of R_c 38. The carbon contents were found to be 0.36% and 0.46% respectively and the alloys were assumed to be 4130 and 4340 with 0.03% carbon in excess. No significance was attached to the high carbon values since many other similar failures had been examined where the compositions were within specification.

The fracture surface of the lower strength stud, No. 1, closely resembled a fatigue fracture surface. It was relatively flat and had an unusually small final overload area. The fracture surface of the higher strength stud was not typical of mechanical fatigue. The numerous crack propagation planes, multiple initiation sites and different inclinations of the various fracture facets were thought to be indicative of an environmentally enhanced fracture mode. However, cross-sectional examination of stud No. 1 also revealed multiple sub-surface cracking on planes parallel to the main fracture plane. A similar examination of stud No. 2, and its mating nut showed that the nut also contained cracks, one of which is shown in Figure 12-14(b). Again the condition is not typical of mechanical fatigue. Further evidence of environmentally enhanced fracture was found in the form of a multiple jagged crack in stud No. 2, which had propagated almost all the way across the section without causing complete failure. This crack is shown in Figure 12-14(c).

Examination of the fracture surfaces in a scanning electron microscope failed to provide conclusive information. The fracture surface on stud No. 1, resembled fatigue but fatigue striations could not be discerned (Fig. 12-14(d)). The fracture surface of stud No. 2 was found to have a rough topography, having a slight rock candy appearance but indisputable intergranular fracture could not be found. No corrosion deposit or evidence of cadmium was detected on the fracture surfaces by dispersive x-ray analysis. The absence of a corrosion deposit indicated that the active corrodent or embrittling agent was hydrogen.

The two studs differed not only in chemistry and strength level but also in the type of threading. The higher strength stud (No. 2) exhibited machine cut threads, while the lower strength stud (No. 1) had rolled threads. Thread rolling is usually to improve fatigue resistance of the stud. Figure 12-14(e) shows a cross-section of a rolled thread stud where cracking has occurred in both the root and the crown of the thread. It would appear that folds and laps generated in the rolling operation act as stress raisers from which cracks initiate. It could not be determined whether the rolled threads, designed to prevent mechanical fatigue were better or worse than the machined threads when delayed static failure was involved. The cracking in the thread crown was puzzling, but the observations suggest that thread rolling does not necessarily prevent delayed static failure.

It was concluded that the failure mechanism in both studs was hydrogen assisted delayed failure. Mechanical fatigue was thought to have contributed, particularly in the case of the lower strength stud. The differences in appearance of the two fracture surfaces was attributed to the different properties of the two steels. The excessive carbon content of the alloys and the inferior threading were not desirable but were not considered to be the primary cause of failure. The source of hydrogen could not be determined but was thought to be related to the cadmium plated nuts, one of which was also cracked.

It was recommended to replace the fastener hardware with a moderate strength corrosion resistant alloy that is also insensitive to hydrogen. It was recommended to replace the stud and nut with similar parts made from A-286 alloy. However, as noted earlier in Section 12-5, this alloy is also adversely affected by hydrogen, and so while this substitution may reduce the tendency to cracking it may not eliminate it completely.

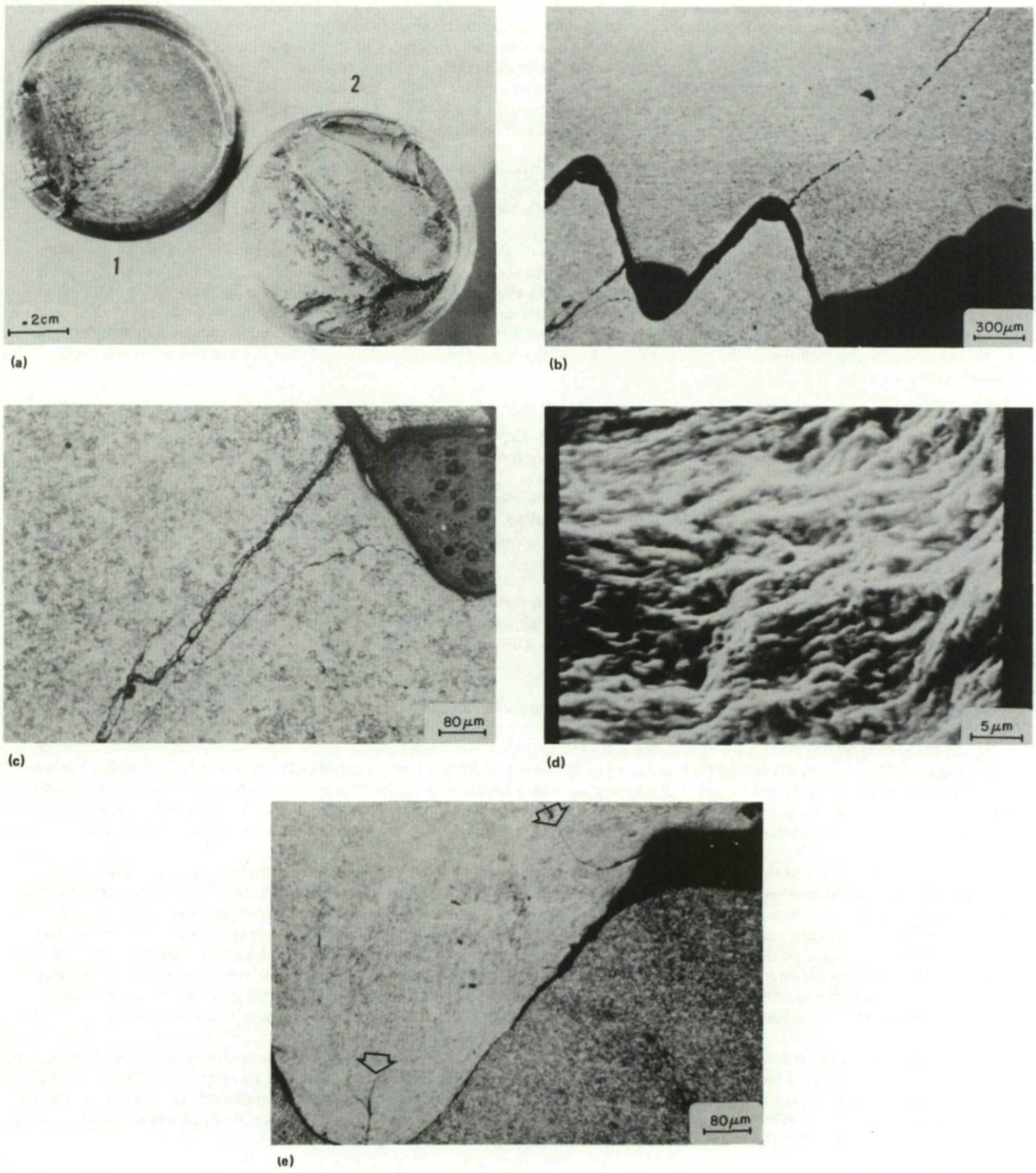

Fig. 12-14 Failure of two low alloy steel bolts

(a) Fracture surfaces of the failed bolts. (Mag. × 6.5)
(b) Secondary cracking in the nut (top) and the high strength R_c 38 bolt (bottom). (Mag. × 37.5)
(c) Longitudinal section through bolt No. 2, showing additional secondary cracking. (Mag. × 125)
(d) SEM picture of the fracture surface on bolt No. 1. (Mag. × 2200)
(e) Cracking in the root and crown of the rolled thread in bolt No. 1. (Mag. × 125)

12.7 References

12-1 Evans, U.R. *An Introduction to Metallic Corrosion.* 3rd Edition, Edwin Arnold, London, 1981.

12-2 Fontana, M.G., Greene, N.D. *Corrosion Engineering.* McGraw-Hill Book Company, New York, 1967.

12-3 Beck, W., Glass, A.L., Taylor, E. *Plating.* July 1968, p. 232.

12-4 Johnson, H.H., Schneider, E.J., Troiano, A.R. Trans A.I.M.E., 212, 1958, pp. 526-536.

12-5 Toh, T., Baldwin, W.M. *Stress Corrosion Cracking and Embrittlement.* Wiley, New York, 1956, p. 176.

12-6 Birnbaum, H.K. *Hydrogen Related Failure Mechanisms in Metals.* Proc. Symposium on Environment-Sensitive Fracture of Engineering Metals, Chicago, October 1977, Metallurgical Society of AIME, Ed. Z.A. Foroulis, pp. 326-360.

12-7 Barth, C.F., Steigerwald, E.A. Met. Trans, 1, 1970, p. 3451.

12-8 Thompson, A.W. *Effect of Metallurgical Variables on Environmental Fracture of Engineering Materials.* IN Ref. 12-6, pp. 379-410.

12-9 Thompson, A.W., Bernstein, I.M. *Advances in Corrosion Science and Technology.* Ed. R.W. Staehle and M.G. Fontana, Vol. 7, 1980, Plenum Press, New York, pp. 53-175.

12-10 Bernstein, I.M., Thompson, A.W. Int. Metals Reviews, Review No. 212, Vol. 21, 1976, pp. 269-287.

12-11 Thompson, A.W., Bernstein, I.M. Reviews on Coatings and Corrosion, Vol. 2, 1975, pp. 3-44.

12-12 Scamans, G.M., Tuck, C.D.S. *Embrittlement of Aluminium Alloys Exposed to Water Vapour.* IN Ref. 12-6, pp. 464-483.

12-13 Proc. International Conference on Hydrogen in Metals, ed. I.M. Bernstein and A.W. Thompson, Seven Springs, American Society for Metals, Metals Park, Ohio, 1973.

12-14 Davis, R.A., Dreyer, G.H., Gallaugher, W.C. *Corrosion.* 20: 93t, 1964.

12-15 Walter, R.J., Chandler, W.T. *Influence of Gaseous Hydrogen on Metals.* NASA Report No. CR-124410, Rocketdyne Division, Rockwell International, Canoga Park, California, Oct. 1973.

12-16 Thompson, A.W., Brooks, J.A. Met. Trans, Vol. 6A, 1975, pp. 1431-1442.

12-17 Aerospace Structural Metals Handbook, Vol. 1, Code 1206, U.S. Department of Defence, Mechanical Properties Data Center, Belfour Stulen Inc., 1982.

12-18 Scamans, G.M., Alani, R., Swann, P.R. Corros. Sci, 16, 1976, pp. 443-459.

12-19 Scamans, G.M. J. Mater. Sci., 13, 1978, pp. 27-36.

12-20 Jacko, R.J., Duquette, D.J. Met. Trans., 8A, 1977, pp. 1821-1827.

12-21 Latanision, R.M., Gastine, O.H., Compeau, C.R. IN Environment-Sensitive Fracture of Engineering Materials, TMS-AIME, New York, 1979, pp. 48-70.

12-22 Scamans, G.M., Tuck, C.D.S. IN Mechanisms of Environment-Sensitive Cracking of Materials, Metals Society London, 1977, pp. 482-491.

12-23 Bursle, A.J., Pugh, E.N. IN Mechanisms of Environment-Sensitive Cracking of Materials, Metals Society, London, 1977, pp. 471-480.

12-24	Klimowicz, T. Latanision, R.M.	Met. Trans., 9A, 1978, pp. 597-599.
12-25	Rajan, K. Wallace, W. Beddoes, J.C.	Journ. Mat. Sci, 17, 1982, pp. 2817-2824.
12-26	Islam, M.U. Wallace, W.	Metals Technology, 10, Oct. 1983, pp. 386-392.
12-27	Scamans, G.M. Tuck, C.D.S.	IN Environment-Sensitive Fracture of Engineering Materials, TMS-AIME, New York, 1979, pp. 464-483.
12-28	Livanov, V.A. Bukhanova, A.P. Kolachev, B.A.	*Influence of Grain Size on Hydrogen Embrittlement of Ti Alloys and Commercially Pure Ti.* Moscow Aviation Technology Institute, Moscow, 1966.
12-29	Nelson, H.G. Williams, D.P. Stein, J.E.	Met. Trans., 3, 1972, pp. 469-475.
12-30	Williams, D.P. Nelson, H.G.	Met. Trans., 3, 1972, pp. 2107-2113.
12-31	Nelson, H.G.	Met. Trans., 4, 1973, pp. 364-367.
12-32	Nelson, H.G.	IN Hydrogen in Metals, Ed. I.M. Bernstein and A.W. Thompson, ASM, Metals Park, Ohio, 1974, pp. 445-464.
12-33	Green, J.A.S. Sedriks, A.J.	*Corrosion.* 28, 1972, pp. 226-230.
12-34	Scully, J.C.	IN Effect of Hydrogen on Behaviour of Materials, Ed. J.M. Bernstein and A.W. Thompson, TMS-AIME, New York, 1976, pp. 129-147.
12-35	Green, J.A.S. Hayden, H.W. Montague, W.G.	IN Effect of Hydrogen on Behaviour of Materials, Ed. I.M. Bernstein and A.W. Thompson, TMS-AIME, New York, 1976, pp. 200-215.
12-36	Gray, H.R.	*Corrosion.* 25, 1969, pp. 337-341.
12-37	Ondrejcin, R.S.	Met. Trans., 1, 1970, pp. 3031-3036.

CHAPTER 13

STRESS CORROSION CRACKING

13.1 Introduction

Alloys are often selected because they are known to be resistant to corrosion in a particular operating environment. However experience has shown that components may still fail by a process involving the corrosion induced initiation and growth of cracks when a tensile stress exists above some critical level in the surface of the part. The mechanisms of crack growth involve the synergistic action of the corrosive environment and the sustained stress acting at an exposed surface, and the failure mode is known as stress corrosion cracking (SCC). This mode of failure has been called sustained load environmental cracking and is dependent on the simultaneous occurrence of three distinct elements.

1. The existence of a sustained surface tensile stress of a sufficient magnitude in the part concerned.
2. The presence of an aggressive environment with access to the surface of the part.
3. A material which is susceptible to localized corrosion along specific paths which may or may not link up.

If any one of these factors is absent, the stress corrosion phenomenon will not develop.

13.2 General Features of Stress Corrosion Cracking

Stress corrosion is a particularly insidious form of corrosion since it will often occur with little or no visual evidence of surface corrosion such as discolouration or the build up of noticeable corrosion products. This is illustrated in Figure 13-1(a), which shows stress corrosion cracking in the bosses of a forged aluminium alloy component. The cracks can travel over long distances with time, as indicated in Figure 13-1(b), and as they propagate they lower the residual strength of the affected part. Figure 13-1(b) shows stress corrosion cracking which initiated at corrosion pits in the flat lower surface of an undercarriage leg, the corrosion pits having served as local stress raisers. Stress corrosion cracks may propagate deeply into thick section parts, as indicated in Figure 13-1(c), while the visible surface crack length may often be quite small. The banded appearance of the fracture surface in Figure 13-1(c) is an indication that crack growth occurred in a slow, time dependent manner, and macroscopically the fracture surface may resemble

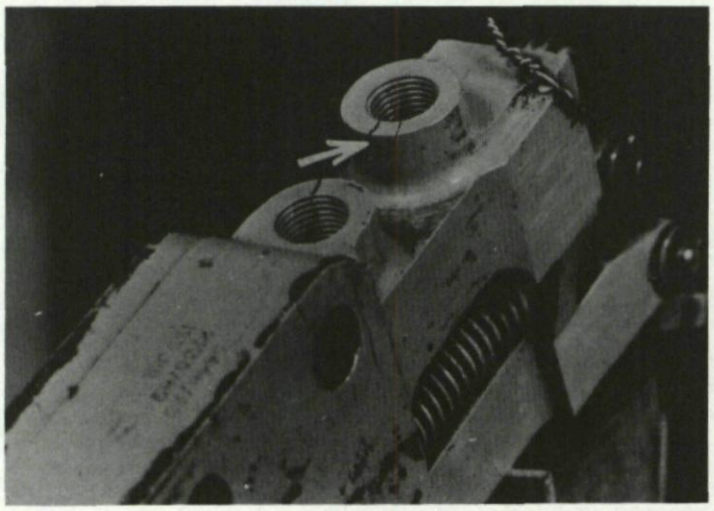

(a)

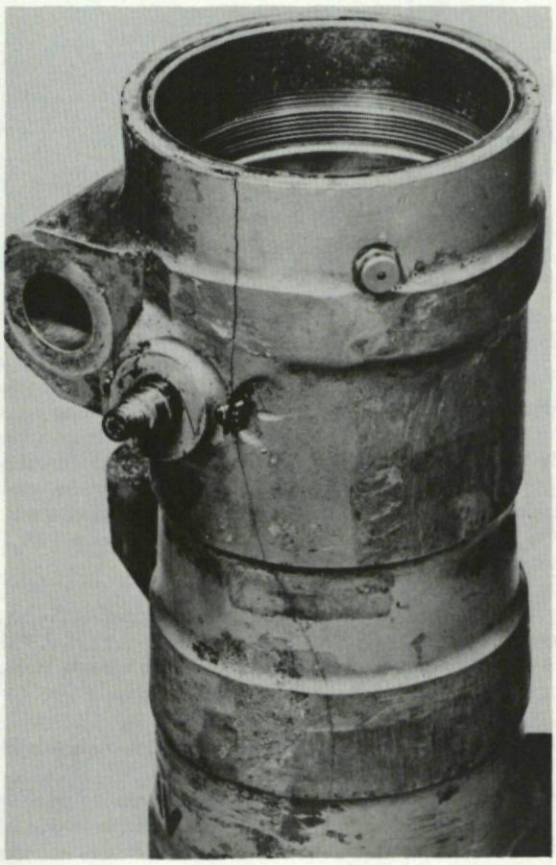

(b)

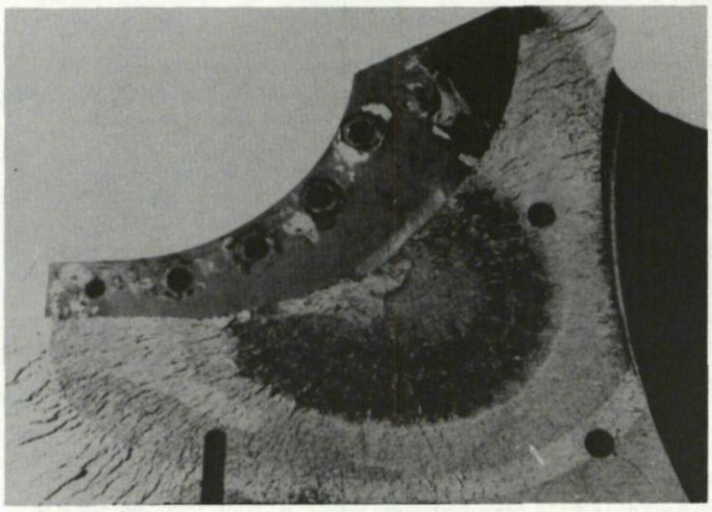

(c)

(a) Cracks in the bosses of a forging.
(b) SCC in an undercarriage leg.
(c) Stress corrosion fracture surface in an aluminium forging.

Fig. 13-1 Examples of stress corrosion cracking in aluminium alloy components

fatigue. The part shown in Figure 13-1(c) was a high strength aluminium-zinc alloy forging and the stress corrosion cracking was attributed to poor forging and heat treatment practice which produced a microstructure susceptible to SCC. The part was also thought to have contained high residual stresses as a result of poor machining practices, and the corrosive environment experienced in service was the final parameter leading to SCC.

Stress corrosion cracking is essentially a localized form of corrosion affecting either grain boundaries or specific crystallographic planes, and leading either to intergranular decohesion, transgranular cracking, or a combination of the two. In the case of transgranular cracking the fracture surface may exhibit brittle, cleavage-like markings as well as areas of ductile fracture. Irrespective of the microstructural path followed by the crack, the fracture occurs approximately perpendicular to the direction of the tensile stress, and extensive crack branching may be observed. The stresses involved may be residual stresses resulting from manufacture, fabrication or heat treatment, assembly stresses associated for example with interference fit bushings or fasteners, or they may be due to loads developed in flight or ground operations. Once a stress corrosion crack has initiated, the build up of corrosion products between the crack faces can create additional stresses at the crack tip to sustain crack growth beyond the region of influence of the stresses responsible for SCC initiation.

Reference 13-1 provides an estimate of the number of stress corrosion service failures affecting the aerospace communities of Western Europe and North America between 1960 and 1970. The data, shown in Figure 13-2, was extracted from over three thousand individual failure reports from six aerospace companies and a number of government agencies and research laboratories in the United States and five countries in Western Europe. The majority of the failures affected small aircraft, but failures were also reported for helicopters, jet aircraft and rockets. Since it was not possible to identify all SCC failures, and since classified information was deliberately excluded, the data shown in Figure 13-2 underestimates the real problem but nevertheless indicates its magnitude and shows certain trends. Of the four alloy classes considered in Figure 13-2, high strength aluminium alloys accounted for by far the greatest number of SCC failures and this is due at least in part to the fact that they are the most widely used airframe alloys. High strength steels were the next most severely affected materials, while magnesium alloys represented about 10% of the reported cases and the number of service failures of titanium components was considered completely insignificant. It is interesting to note that the case histories collected during the preparation of this Handbook show similar trends, with high strength aluminium alloys accounting for 61% of the reported SCC service failures, high strength steels 32%, magnesium alloys 7%, and no cases involving titanium were reported.

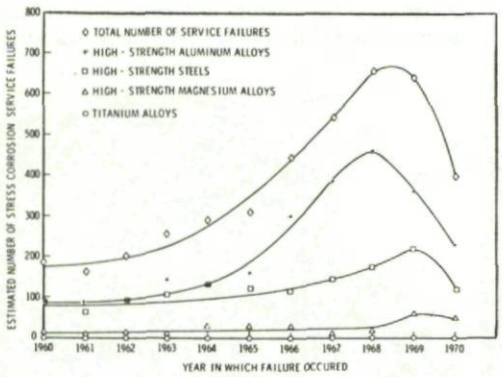

Fig. 13-2 Estimated number of stress corrosion service failures of aerospace products in Western Europe and North America from 1960 to 1970. (Ref. 13-1)

It is interesting to note that the number of SCC service failures rose from 1960 to 1968, and then began to decline between 1969 and 1970. The author (Ref. 13-1) speculated that this might be due to the introduction of less susceptible alloys, better service protection, inhibited environments, and reduced sustained stresses. It was reported that 7079-T6, 7075-T6 and 2024-T3 contributed to more than 90% of the service failures of aluminium alloys. Of the cases collected during this study, 71% of the aluminium failures involved these three alloys, while another 17% involved alloys that were not identified and may therefore have involved these alloys. In the earlier study more than 80% of the steel failures involved 4340, 4330 and 17-7 PH. In this study approximately 50% of the reported cases involved these materials, but maraging steels, plain carbon steels, and high strength springs steels were also reported. Of the magnesium alloy failures reported in Reference 13-1, more than 70% involved AZ91C-T6 and AZ80A-F. In this study all the magnesium alloy SCC failures involved AZ91C.

Stress corrosion cracking is influenced by the corrosive nature of the environment, the stresses acting on the part and the composition and microstructure of the alloy employed. These factors are discussed below with respect to high strength (7000 series and 2000 series) aluminium alloys and some high strength steels. However a short outline will be given first of the phenomenological and mechanistic aspects of stress corrosion cracking.

13.3 Initiation and Propagation of Stress Corrosion Cracks

The site of initiation of a stress corrosion crack may be submicroscopic and may be determined by local differences in alloy composition, thickness of protective films, concentration of corrodent and stress concentrations. A pre-existing mechanical flaw such as a scratch, indentation or crack can act as an initiation site, or stress corrosion can start at a site of pre-existing corrosion damage. Other forms of corrosion such as pitting, fretting, intergranular corrosion or exfoliation often precede stress corrosion cracking and SCC often initiates at sites created by these forms of attack. For example in the study by Speidel (Ref. 13-1) approximately 12% of SCC failures were found to initiate at corrosion pits, 5% initiated at damage caused by galling, fretting or wear, and approximately 4% initiated at sites created by intergranular corrosion or exfoliation. Examples of these types can be found among the case histories presented later.

In laboratory tests on smooth specimens under constant load, stress corrosion involves an incubation period where no detectable crack is present, and a period of time dependent crack growth leading to final overload failure. A certain minimum stress is required to cause a stress corrosion crack to initiate and grow, and as explained earlier, pitting or intergranular corrosion may contribute to the initiation process by creating stress concentration sites.

Once the stress corrosion crack has formed it will continue to grow, stopping only when the tensile stress has fallen below the critical value, or when the corrosive environment is excluded. The crack may permanently arrest if tensile residual stresses are relaxed by the initial crack advance. If the stresses are due to assembly forces, such as from interference fit bushings or fasteners, or are a result of service operations the cracks may continue to grow until the component can no longer sustain them. The speed of crack growth for a given material-environment combination is dependent on the crack tip stress state, and the crack tip stress intensity can sometimes provide an indication of the crack velocity. Numerous laboratory studies have shown that for a given system the velocity of stress corrosion crack growth will remain constant over a range of stress intensities, but as the stress intensity is decreased a point will be reached where the crack velocity will begin to decrease and eventually the velocity, if plotted on a logarithmic scale, will decrease linearly with decreasing stress intensity. These two regions of stress corrosion cracking are indicated as Region II, sometimes referred to as the plateau region, and Region I, the stress dependent region in Figure 13-3. This figure also shows a second stress dependent region, Region III, at higher stress intensities but this is usually difficult to establish experimentally. In the region of slow crack growth a value of stress intensity K_{ISCC} can often be established below which crack growth occurs so slowly that the crack can be considered to be at rest. This is referred to as the threshold stress intensity for stress corrosion cracking and for aluminium alloys the values of K_{ISCC} correspond to growth rates of about 10^{-10} m/sec.

13.4 Mechanisms of Stress Corrosion Cracking

The mechanisms of stress corrosion cracking are still under review, but it is now generally considered that different mechanisms may apply in different situations. The early views of stress corrosion involved stress assisted dissolution of the material at the crack tip, e.g. References 13-2 and 13-3. In the case of intergranular cracking the grain boundaries are likely to be more active with respect to corrosion than the adjacent grains, due perhaps to the segregation of alloying elements or the depletion of alloying elements through the precipitation of second phases. The anodic paths are often associated with heterogeneous phases such as $CuAl_2$ which will precipitate along grain boundaries in 2000 series aluminium alloys during heat treatment and produce copper depleted paths adjacent to the grain boundaries. Differences in potential can sometimes be measured between grain boundaries and their adjacent grains, and grain boundaries are found to be anodic with respect to grain interiors in environments causing intergranular SCC. In such cases cathodic polarization can be used to retard or arrest the attack.

Once the crack has initiated the crack tip should remain anodic while the rest of the metal including the walls of the crack should act as a cathode. Stress is thought to contribute to the process by rupturing protective films, which would otherwise tend to isolate the metal from the corrosive environment. Susceptibility to stress corrosion cracking, according to this model, depends on the rate at which the metal exposed by film rupture is repassivated vis-a-vis the rate of metal dissolution. This is known as the Film Rupture-Metal Dissolution Mechanism and is described schematically in Figure 13-4.

An alternative mechanism for SCC is one proposed by Uhlig (Refs. 13-5 and 13-6), which involves the stress assisted adsorption of damaging ions at the crack tip. According to this Stress-Sorption Mechanism, specific ionic species interact with the strained bonds at the crack tip to lower the surface energy, γ, and a decrease in the stress required to produce brittle fracture. The relationship between the theoretical stress to produce brittle fracture, σ_f, and γ is given by the expression

$$\sigma_f = \left(\frac{E\gamma}{d}\right)^{1/2}$$

where E is the elastic modulus and d is the atomic spacing. The adsorption of a damaging species at a crack tip lowers σ_f and therefore the threshold stress for SCC is the minimum value to which γ is lowered by adsorption. Supporting evidence for this mechanism is

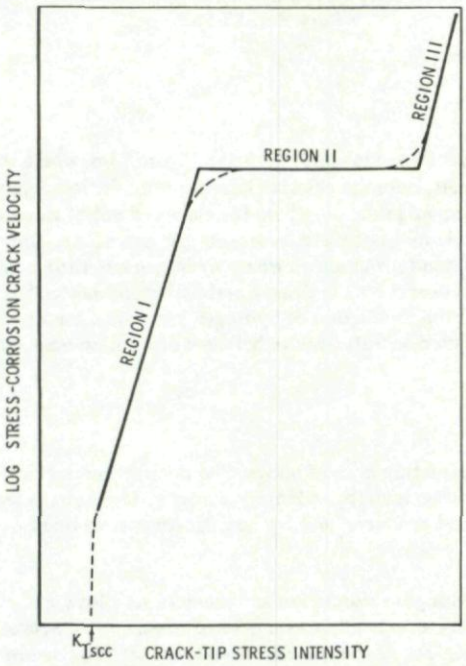

Fig. 13-3 Schematic representation of the effect of stress intensity on the growth rate of stress corrosion cracks.

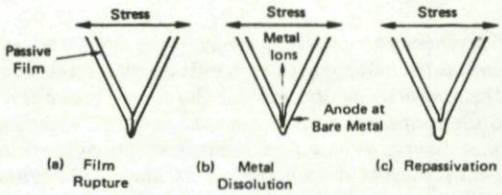

Fig. 13-4 Film rupture-metal dissolution mechanism for SCC. (Ref. 13-4)

(a) Rupture of the protective film at tip of a crack by the application of a tensile stress.
(b) Dissolution of the metal exposed when film is ruptured. Tip of crack is an anode and film covered walls of the crack is a cathode.
(c) Repassivation of the exposed metal at the tip of the crack.

obtained from observations that SCC often occurs by a discontinuous process, often exhibits brittle fracture characteristics, and that both SCC and adsorption of damaging anions often do not occur below some minimum critical potential. Inhibiting anions can be introduced to the system to compete with the damaging species for adsorption sites, and thus retard the process. More positive potentials would then be required in the metal to reach a concentration of damaging species needed for adsorption and sustained cracking. However, a number of problems with this mechanism have been discussed by References 13-7 and 13-8. The mechanism is described schematically in Figure 13-5.

More recent theories of stress corrosion cracking have considered the possibility that crack advance is due to hydrogen embrittlement. According to these theories, cathodic reduction of hydrogen ions at the crack tip produces atomic hydrogen which enters the metal in the vicinity of the crack tip and gradually embrittles the metal immediately ahead of the advancing crack. The hydrogen is though to accumulate at preferred sites such as grain boundaries or selected crystallographic planes, and to gradually lower the local cohesive strength or fracture toughness of the material until the applied stress is sufficient to cause the crack to advance into a non-embrittled region. The process then repeats, giving rise to a mode of crack growth where the crack advances in a series of jumps. Laboratory experiments on stress corrosion cracking have often confirmed this discontinuous mode of crack growth, and the crack jumps can often be heard with the aid of appropriate acoustic transducers and amplifiers.

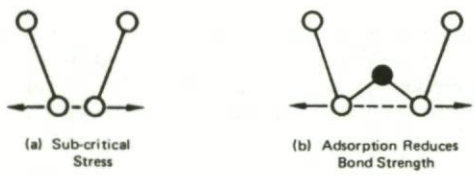

Fig. 13-5 Stress sorption mechanism for SCC. (Ref. 13-4)

(a) Chemisorption of ion at tip of crack.
(b) Weakening of interatomic bond at the tip of the crack so that applied tensile stress leads to the breaking of this bond.

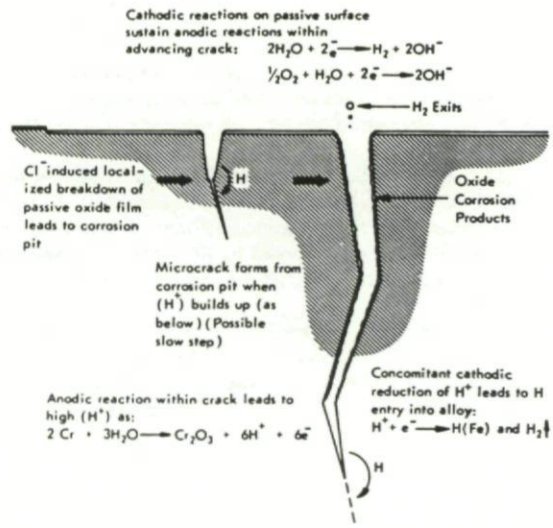

Fig. 13-6 Generalized model for crack initiation and propagation in SCC (chemical details here are for austenitic stainless steel in a chloride environment). From Ref. 13-9, based on an original model by Ref. 13-10.

A generalized model for the hydrogen embrittlement mode of stress corrosion cracking is shown in Figure 13-6, where the specific chemical details apply to austenitic stainless steels in a chloride environment. Here the chloride ions promote the initial breakdown of the passive oxide film and this allows a corrosion reaction to occur to form an initial pit where the electrochemical reactions leading to the formation of hydrogen ions and their cathodic reduction to atomic hydrogen and hydrogen gas, can occur. This illustration is thought to be typical of many situations involving both ferrous and non-ferrous alloys where hydrogen embrittlement is the dominant process of stress corrosion cracking. Stress corrosion cracking which occurs by a hydrogen embrittlement mechanism is unlikely to be arrested or retarded by cathodic polarization since this would assist the production of hydrogen and would tend to promote cracking. The response of the process to applied potentials is sometimes used to differentiate between dissolution controlled SCC processes and processes controlled by hydrogen embrittlement.

13.5 Effects of Metallurgical Variables

Stress corrosion cracking is influenced by alloy composition and microstructure in most alloys. The microstructural variables of interest include grain size, grain shape, and the nature of precipitates formed intragranularly and intergranularly. These characteristics are influenced by the primary working treatments used to produce the initial mill products, and by heat treatments or thermo-mechanical treatments employed during mill processing or at some later stage.

Aluminium alloys: Stress corrosion cracking in liquid metals has been observed with pure aluminium and many of its alloys, and all such alloys may be susceptible. In moist air or aqueous solutions fewer materials are affected, but examples of stress corrosion cracking have been reported for alloys belonging to the important Al-Mg, Al-Cu-Mg, Al-Mg-Zn, Al-Zn, Al-Zn-Mg-Cu, and Al-Mg-Si series. Generally, the high strength alloys of the Al-Cu-Mg type (2000 series) and Al-Zn-Mg type (7000 series) are more susceptible to SCC than the others. There are no general rules that allow susceptibility to SCC to be determined from basic alloy composition data, but it is known that susceptibility usually increases as the concentration of soluble alloying elements increases. The effects of individual elements depend not only on the absolute concentrations of the elements but also on the ratios of certain key elements.

Table 13-1 Estimate of the highest sustained tension stress at which test specimens of different orientations to the grain structure would not fail by SCC in the 3,5 pct NaCl alternate immersion test (84 days) or in inland industrial atmosphere (1 year), whichever is lower (Ref. 13-1)

Alloy and Temper	Direction of Applied Stress	Plates		Extrusions		Forgings	
		MPa	(ksi)	MPa	(ksi)	MPa	(ksi)
2014-T6	L	310	(45)	310	(45)	210	(30)
	LT	210	(30)	150	(22)	170	(25)
	ST	<55	(<8)	<55	(<8)	<55	(<8)
2219-T87	L	>270	(>40)	>240	(>35)	>260	(>38)
	LT	>260	(>38)	>240	(>35)	>260	(>38)
	ST	>260	(>38)	>240	(>35)	>260	(>38)
2024-T3, T4	L	170	(25)	>340	(>50)		
	LT	140	(20)	120	(18)		
	ST	<55	(<8)	<55	(<8)		
2024-T8	L	>340	(>50)	>410	(>60)	290	(43)
	LT	>340	(>50)	>340	(>50)	290	(43)
	ST	200	(30)	>310	(>45)	100	(15)
7039-T64	L	>290	(>42)				
	LT	240	(35)				
	ST	<35	(<5)				
7075-T6	L	340	(50)	410	(60)	240	(35)
	LT	310	(445)	220	(32)	170	(25)
	ST	<55	(<8)	<55	(<8)	<55	(<8)
7075-T76	L	>340	(>49)	>360	(>52)		
	LT	>340	(>49)	>340	(>49)		
	ST	170	(25)	170	(25)		
7075-T73	L	>340	(>50)	>360	(>53)	>340	(>50)
	LT	>330	(>48)	>330	(>48)	>330	(>48)
	ST	>300	(>43)	>300	(>43)	>300	(>43)
7178-T6	L	380	(55)	450	(65)		
	LT	260	(38)	170	(25)		
	ST	<55	(<8)	<55	(<8)		
7178-T76	L	>360	(>52)	>380	(>55)		
	LT	>360	(>52)	>360	(>52)		
	ST	170	(25)	170	(25)		
7079-T6	L	>380	(>55)	>410	(>60)	>340	(>50)
	LT	270	(40)	240	(35)	210	(30)
	ST	<55	(<8)	<55	(<8)	<55	(<8)
7049-T73	ST					≈170	(≈25)
7050-T736	ST					>170?	(>25?)
7175-T736	ST					≈170	(≈25)
RX 720	ST	>170	(>25)				
RR 58	L	>300	(>44)				
	ST	>270	(>40)				
DTD 3067	ST	140	(20)				
DTD 3066	ST	140	(20)				
AZ 74	ST					310	(45)

Table 13-1 provides estimates of the highest sustained tension stress at which test specimens of different orientation would not fail by stress corrosion cracking either in an 84 day alternate immersion test in 3.5% NaCl or in a 1-year exposure test to an inland industrial atmosphere. It can be seen that for most alloys the susceptibility to SCC is strongly dependent on the direction of the applied stress, most alloys being most susceptible when stressed in the short transverse direction, in contrast to the longitudinal or long transverse directions. Alloys such as 2014-T6, 2024-T3 and T4, 7039-T6, 7075-T6, and 7079-T6 exhibit marked susceptibility to stress corrosion cracking when loaded in the ST direction, while others such as 2219-T87 and 7075-T73 are somewhat resistant to SCC irrespective of the loading direction. This directionality of SCC susceptibility is related to the shape and orientation of the grains in heavily deformed wrought products. Components machined from rolled plate, extrusions or forgings have flat pancake shaped grains elongated in the longitudinal and long transverse directions and having small dimensions in the short transverse direction. When the ST direction is aligned with the stress axis and the susceptible "end grain boundaries" are exposed at a free surface stress corrosion cracks will form relatively easily and favourably oriented grain boundary paths will exist to assist crack propagation. It might be thought therefore that materials having more equiaxed grain structures would provide better resistance to SCC, but tests have shown that such materials are either as susceptible or more susceptible than the ST direction (Refs. 13-11 to 13-13). Thus the commercial grain structure not only restricts concern to one direction in the product, but it improves SCC resistance over an equiaxed structure (Ref. 13-14).

A particular sensitivity to stress corrosion cracking occurs at the parting plane of forgings. Cracking of this type is shown in Figure 13-7(a) where the component is a 7079-T6 H-link of a main landing gear assembly. This problem has been explained in Reference 13-11 to be due to the directionality of grain flow in forgings and the tendency for end grain boundaries to be exposed at the surface at the parting plane, as indicated in Figure 13-8. In the case of the H-link of Figure 13-7(a), examination showed that SCC was preceded by pitting and intergranular corrosion (Fig. 13-7(b)), and areas of intergranular separation evident on the fracture surface showed a distinctly equiaxed grain structure (Fig. 13-7(c)).

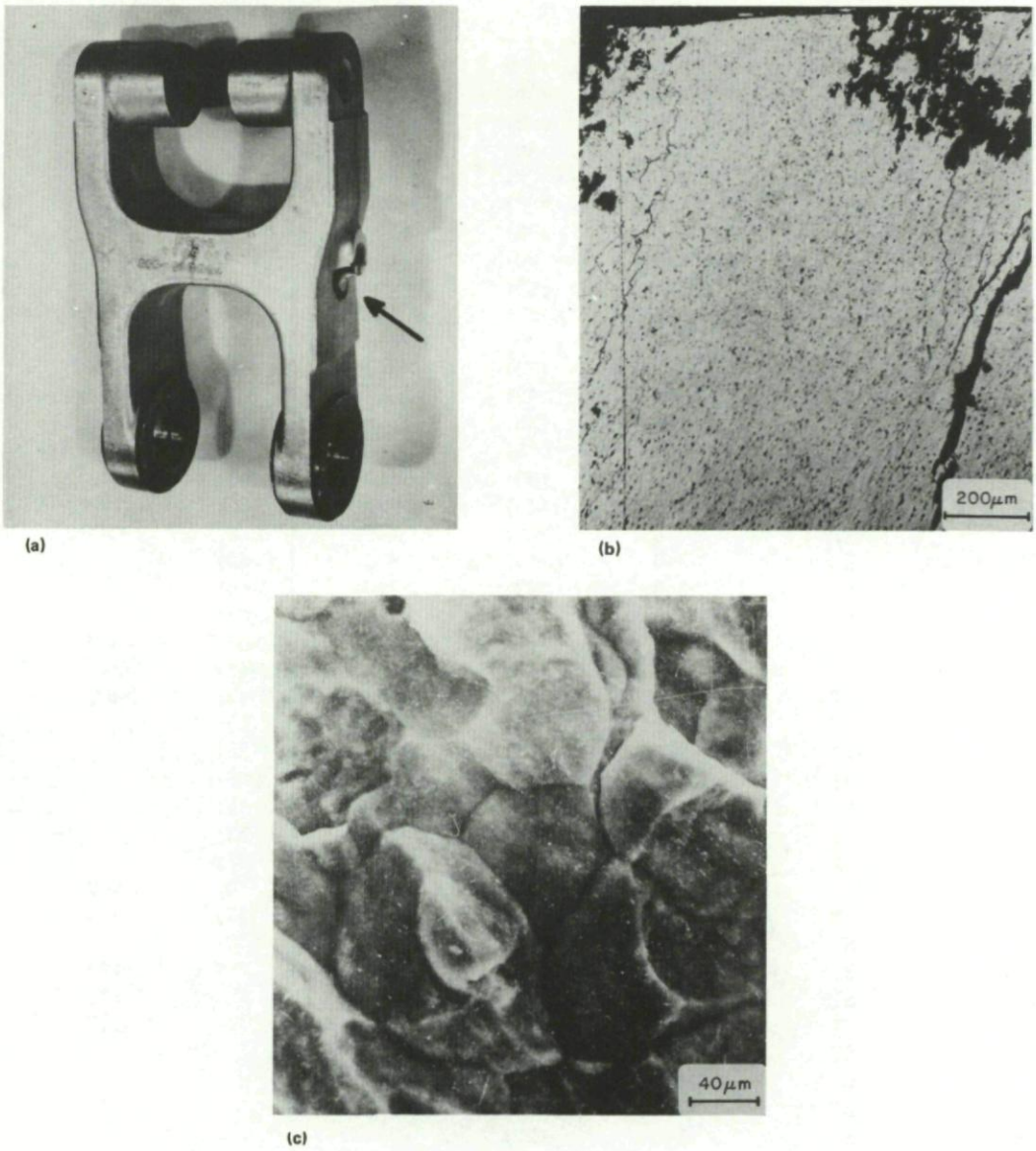

Fig. 13-7 Stress corrosion cracking occurring from corrosion pits and intergranular corrosion cracking in the parting plane of a 7079-T6 H-link.

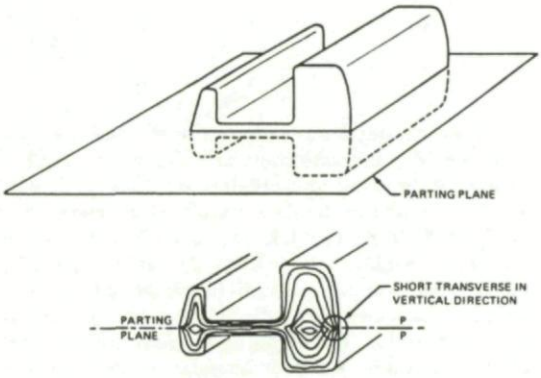

Fig. 13-8 Schematic representation of the grain flow in a section of a typical die forging. (Ref. 13-11)

The reason for the susceptibility of grain boundaries to stress corrosion cracking in aluminium alloys is not completely understood. In the case of Al-Mg alloys (5000 series) the grain boundaries are rendered anodic to the grain interior by the intergranular precipitation of Mg_2Al_3. This precipitation is continuous and forms an uninterrupted path for anodic dissolution (Ref. 13-15). The result is a susceptibility to intergranular attack in certain environments, and in the presence of a sustained tensile stress, to SCC. Grain boundary precipitation of $CuAl_2$ in the 2000 series alloys is usually not continuous (Ref. 13-15), but a difference in electrochemical potential between the grain boundary regions and the grain interiors arises from the depletion of Cu from the grain boundary regions. The $CuAl_2$ precipitates are cathodic and they promote the anodic dissolution of the copper depleted region adjacent to the grain boundary. This solute depletion is a consequence of grain boundary precipitation, and the grain boundaries have been shown to pit at potentials lower than the matrix (Ref. 13-16). Thus the selective pitting attack is thought to be an important factor leading to the intergranular SCC in these alloys. In this study (Ref. 13-16), susceptibility to intergranular SCC in a NaCl environment was found to depend on the difference between the pitting potential of the grain boundaries and grain interiors. Susceptibility increased with increasing difference in pitting potential.

References 13-15 and 13-16 report that a maximum in SCC susceptibility is reached in Al-Cu alloys as the alloys are aged, and that aging for longer times leads to a decrease in susceptibility. It is thought that the difference between the grain boundary and the interior pitting potential also goes through a maximum as a function of aging time, and this might be expected if the solute depleted zone produced during the early stages of precipitation tends to disappear due to diffusion or the generalized precipitation of Cu-rich phases in the grain interior. Reference 13-15 also reports that a small amount of intergranular corrosion susceptibility greatly increases SCC susceptibility in the naturally aged T3 and T4 tempers but the same is not true for artificially aged 2024 (T6 or T8) alloy in NaCl. In this case it is found that some intergranular corrosion can take place without influencing SCC. This is thought to be due to the fact that the grain boundary precipitate Al_2CuMg produced by these treatments will corrode at potentials more anodic than the grain boundary pitting potential. However if SCC does not occur until the grain boundary pitting potential is reached, some intergranular attack may be sustained but the grain boundaries are assumed to retain some degree of mechanical integrity sufficient to avoid long range cracking.

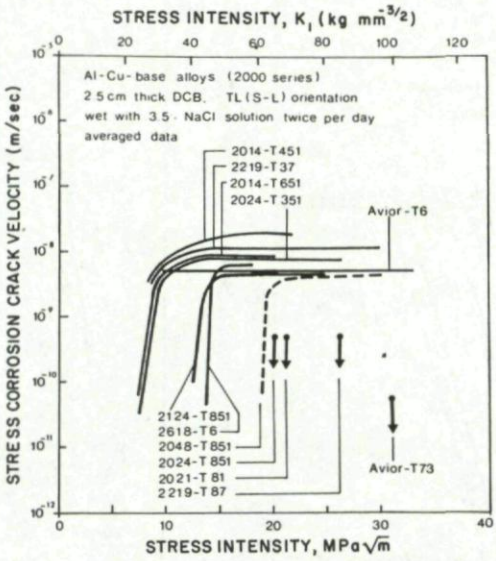

Fig. 13-9 Summary of stress corrosion crack growth rates in various alloys based on the aluminium-copper system. (Ref. 13-1)

Reference 13-1 has classified the commercial 2000 series alloys according to four groups. The most susceptible alloys include 2014-T451, 2219-T37, 2014-T651 and 2024-T351. As shown in Figure 13-9, these alloys exhibit high growth rates of about 10^{-8} m/sec in the plateau region (Region II) of the V-K plot, and their stress dependent crack growth rates are observed at very low stress intensities, i.e. below 9 MPa $m^{1/2}$. The second group includes alloys such as 2124-T851 and 2618-T6 which exhibit stress dependent crack growth at slightly higher values of stress intensity, typically between 13 and 15 MPa $m^{1/2}$. However, their plateau crack growth rates are similar to those of the first group. The third group of alloys is represented in Figure 13-9 by 2048-T851, which exhibits a very high threshold stress intensity for stress corrosion cracking, equivalent to or higher than the fracture toughness values of many other alloys in the 2000 series. However, in the stress intensity range where SCC occurs the growth rate for this alloy is similar to those of the most susceptible alloys. The fourth group included alloys such as 2219-T87 and 2021-T81 which were essentially immune to stress corrosion cracking. These alloys exhibited very high values of K_{ISCC} which correspond well with the smooth specimen threshold stresses of $\geq$ 240 MPa given in Table 13-1. This author (Ref. 13-1) points out the close relationship between values of K_{ISCC} and smooth specimen threshold stresses for most of these alloys, and suggests that 2000 series alloys should be ranked on the basis of K_{ISCC} rather than crack growth rates.

Stress corrosion cracking in 7000 series alloys is also strongly influenced by alloy composition, grain structure and heat treatments. The amounts and ratios of the principal alloying elements, Zn, Mg and Cu are important through their influence on the precipitation hardening reactions and the electrochemistry of the precipitate phases and matrix. Copper appears to be particularly important since it increases strength and stress corrosion resistance up to about 1% (Ref. 13-14), and higher concentrations may be needed for maximum stress corrosion resistance in some alloys (Ref. 13-17). However, since copper creates problems in welding, some attempts have been made to develop copper free alloys (Ref. 13-14). It might be noted that alloy 7079 with only about 0.6% copper is an alloy notoriously prone to SCC. Minor alloying additions of Cr, Mn and Zr are used for grain control and they act by

forming dispersoids such as $Al_{12}Mg_2Cr$, $Al_{20}Cu_2Mn_3$ and $ZrAl_3$ which are present during solution heat treatments and impede recrystallization and grain growth. These elements also improve stress corrosion resistance, and the most effective element is Zr followed by Cr. Both Cr and Mn accelerate the precipitation reactions and Cr increases quench sensitivity (Ref. 13-14).

Other alloying additions such as Ag have been used to improve SCC resistance (Ref. 13-18), but some doubts exist whether it is effective in commercially processed materials (Ref. 13-19), and it may be deleterious to other mechanical properties (Ref. 13-20). Elements such as Fe and Si are reduced to low levels in alloys such as 7475 and 7010, but this practice is to improve fracture toughness and it has little or no effect on stress corrosion resistance.

Precipitation heat treatments carried out after quenching cause an increase in strength and decrease in stress corrosion resistance. The stress corrosion resistance reaches a minimum in slightly underaged alloys, it then begins to increase as the alloys are aged to the peak strength condition, and it continues to increase as the alloys are overaged. The established T76 and T73 heat treatments have been developed to exploit this phenomenon, providing resistance to exfoliation in the case of T76 and resistance to both exfoliation and stress corrosion cracking in the case of T73. However not all alloys will respond favourably to these treatments, and both treatments involve strength penalties compared to the T6 temper which provides near peak strength. The strength penalty with T73 is about 15% in the case of 7075, while the T76 temper which was developed later provides a compromise in terms of strength and stress corrosion resistance between T6 and T73. Investigations of overaging using fracture mechanics specimens have shown that different alloys may respond in different ways. In 7079 aluminium overaging moves the stress dependent region (Region I) of the velocity-stress intensity plot to the right, but the plateau growth rates (Region II) are largely unaffected, as indicated in Figure 13-10. However, in alloys such as 7075 or 7178, overaging from the peak strength T6 or T651 conditions lowers the growth rates in the plateau region (Fig. 13-11). For these alloys overaging for about 15 to 20 hours at 160°C can lower the plateau velocities by about three orders of magnitude.

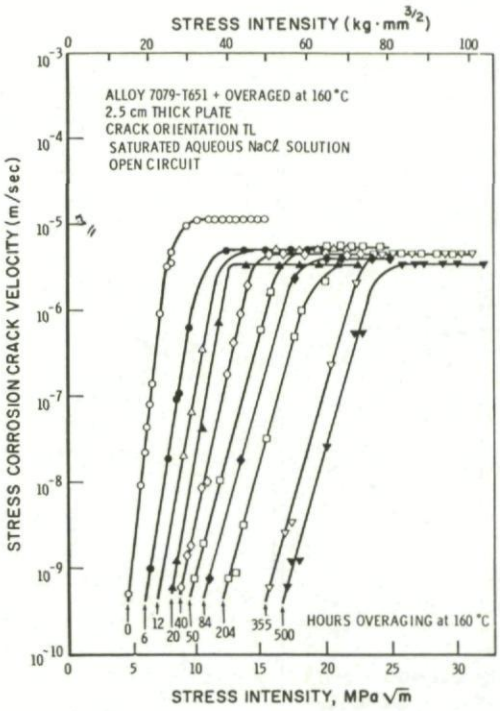

Fig. 13-10 Effect of overaging on stress corrosion crack velocity of high strength aluminium alloy 7079. (Ref. 13-1)

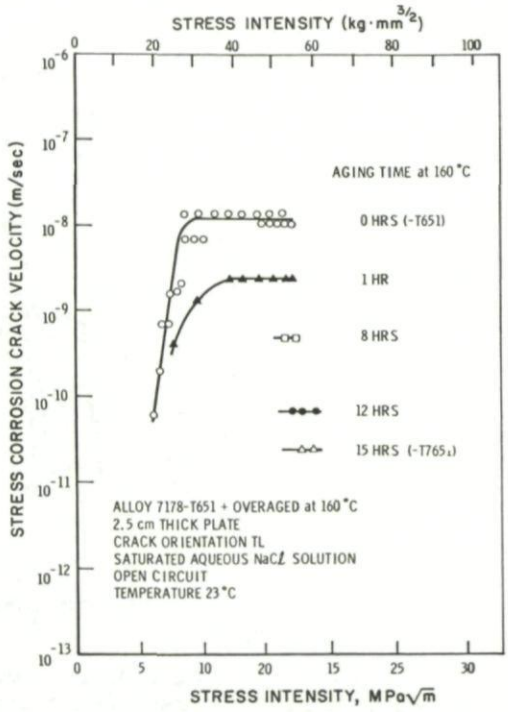

Fig. 13-11 Effect of overaging on stress corrosion crack velocity in aluminium alloy 7178. (Ref. 13-1)

Although 7075-T73 provides high resistance to exfoliation and stress corrosion cracking, designers have sometimes been reluctant to accept the strength penalty. 7075-T76 has been used in place of 7075-T6, sometimes without redesign or increase in weight, and it has been found to provide high resistance to SCC with ST-direction stresses up to about 170 MPa (Ref. 13-17). However for higher stress levels this condition may be inadequate, and alternative alloys such as 7175, 7049 and 7050 have been developed. They respond favourably to overaging treatments to provide high resistance to stress corrosion cracking at strength levels very close to those of 7075-T6 or 7079-T6. The development of these alloys has been reviewed in Reference 13-17.

Alloy 7175-T736 was developed for premium quality forgings and by using non-conventional heat treatments and fabricating processes it can provide strength levels very close to 7075-T6 and stress corrosion resistance almost as good as 7075-T73. Alloy 7049-T73 differs from 7075 principally in its higher Zn and lower Cr contents, but it also has more restrictive controls both on the major elements and impurities. The higher Zn/Mg ratio was found to provide superior combinations of strength and stress corrosion resistance, the lower chromium reduced quench sensitivity and Cu, Fe and Si were controlled to improve ductility and fracture toughness at the higher strength levels. In the T73 condition this alloy provides strength levels equivalent to 7079-T6 together with higher resistance to SCC, and it has been used to replace 7079-T6 in parts such as landing gear forgings. Alloy 7050 was introduced in the early 1970's (Ref. 13-17), and was intended for use in thick section parts where lower quenching rates are unavoidable. The alloy has a very high copper content of about 2.4%, together with a higher zinc content than 7075 (6.3% compared to 5.6%), and a slightly lower magnesium content. Zirconium replaces Cr and Mn as the grain refining agent, and it acts by forming small spherical particles of $ZrAl_3$ rather than copper or magnesium containing phases, which would decrease the role of these elements in the precipitation

hardening reaction. The alloy responds to overaging in a manner similar to 7075, and achieves high resistance to SCC at the expense of strength. In the T73 condition in thin sections it provides yield strengths about 10% higher than 7075-T73, but this advantage increases with section thickness reaching about 20% in sections over 100 mm thick.

One significant effect of overaging in 7075 is an increase in the size of precipitates on grain boundaries. Thus in the T6 condition the precipitates have an average size of about 14 nm, while in the T73 condition they are about 30 nm. It has been observed (Refs. 13-21 to 13-23), that exposure of overaged Al-Zn-Mg alloys to moist environments leads to the formation of what appear to be hydrogen bubbles on grain boundaries. This has provided evidence supporting the hydrogen embrittlement mechanism of stress corrosion cracking in these alloys, but since overaged alloys such as 7075-T73 are virtually immune to stress corrosion cracking the view is that by allowing hydrogen to condense as gas bubbles and removing it from solution in the grain boundaries, the embrittlement of the grain boundaries is prevented. Stress corrosion cracking by a hydrogen embrittlement mechanism occurs in underaged alloys or alloys aged to near peak strength, where the grain boundary precipitates are too small to act as effective trapping sites for hydrogen, and the hydrogen therefore remains in solution at the grain boundary.

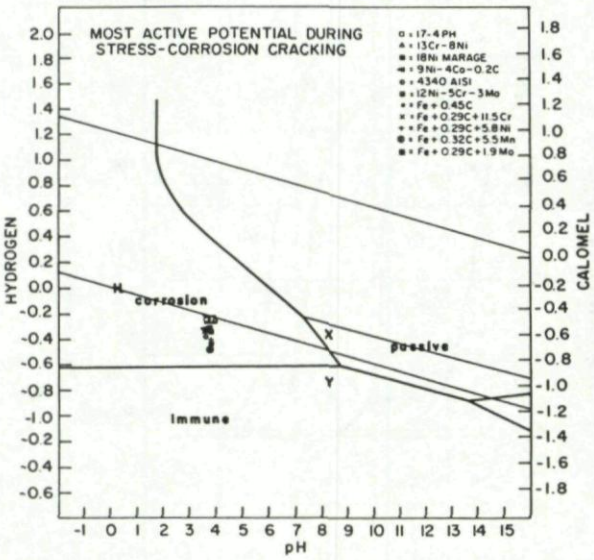

Fig. 13-12 Potential and pH of corrodent at crack tip for several alloy steels under freely corroding conditions. (Ref. 13-30)

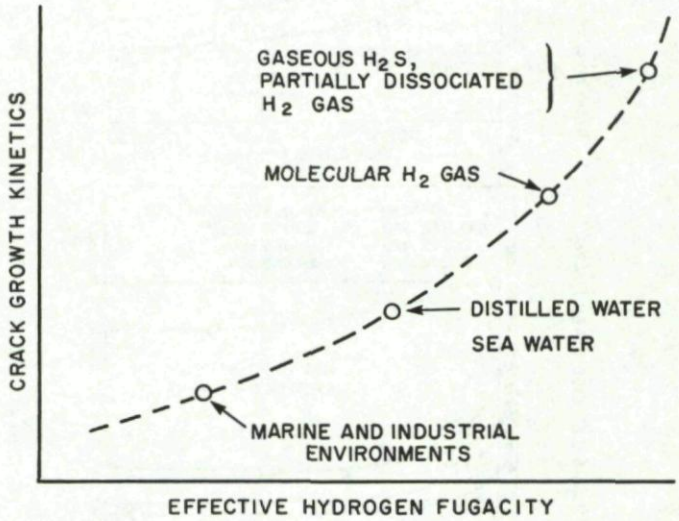

Fig. 13-13 Schematic illustration of severity of stress corrosion cracking environments. (Ref. 13-29)

An unconventional heat treatment, known as Retrogression and Reaging, was introduced in 1974 and was claimed to provide stress corrosion resistance in 7075-T6 equivalent to the T73 temper, while retaining the strength level of the T6 condition (Ref. 13-24). Starting with material in the fully processed T6 condition, the process involves very short time "Retrogression" in the temperature range 200-280°C, followed by "Reaging" which is a repeat of the initial T6 aging treatment. The benefits of this treatment have been confirmed by several workers, and it has been shown that it leads to an increase in size of grain boundary precipitates, similar to that of T73 overaged material, but it allows the important strengthening features of the T6 condition to be retained with only minor changes (Refs. 13-25 to 13-27). Since the process can be applied to finished T6 components without recourse to severe quenching treatments, which would introduce residual stress, it might be considered as a means of "re-conditioning" parts which are prone to SCC. However since the times required for retrogression are very short the process is difficult to apply, particularly in thick section parts, and if it is applied it is likely to be regarded as a surface conditioning treatment. At the present time it appears to have been used very little.

High strength steels: High strength steels are important materials in airframe and landing gear structures and interest in stress corrosion cracking has remained high since the higher strength versions of these alloys are both susceptible to SCC and sensitive to the presence of flaws. Thus stress corrosion cracks can initiate catastrophic brittle fracture or unexpected fatigue. The alloys of particular interest are the martensitic, precipitation-hardening and maraging steels, and like aluminium alloys their SCC behaviour is influenced by composition, grain structure, microstructure and strength. Reference 13-28 describes some of the early work on stress corrosion cracking of high strength steels used in aircraft and missiles, and indicates that both anodic dissolution and cathodic hydrogen embrittlement processes can result in cracking. However the more recent trend has been to view both stress corrosion cracking and hydrogen embrittlement as the same process in these materials (Ref. 13-29), and therefore the information given in Chapter 12 on these materials is relevant to this discussion. The clarification of this point is due largely to Reference 13-30, which shows that the pH and potential values at the tips of growing stress corrosion cracks are often quite different from the bulk system, and they provide conditions suitable for the production of hydrogen. This is shown in Figure 13-12, where pH values of about four exist at crack tips in a wide range of high strength steels under freely corroding conditions in neutral 3.5% NaCl. These conditions were found to prevail even if the bulk solution was made highly alkaline (pH = 10) or highly acid (pH = 2) by the addition of NaOH or HCl respectively. The logical extension of these ideas is that several forms of environmentally induced fracture, such as stress corrosion cracking, delayed static failure, hydrogen embrittlement and hydrogen sulphide cracking are the result of the same phenomenon, and the environment per se simply alters the effective hydrogen fugacity as indicated in Figure 13-13.

Steels that are susceptible to stress corrosion cracking will respond to stress in a similar manner to aluminium alloys. Both notched and un-notched specimens will fail under sustained static loads at stresses lower then those required to cause yielding. However for any given steel in a given environment a threshold stress will exist below which smooth specimens will not fail, and similarly for

pre-cracked specimens or components a crack tip stress intensity K_{ISCC} exists below which cracks will not propagate by SCC. These threshold values are dependent on the material-environment combination. The time-to-failure decreases as the stress or stress intensity increases above the threshold values, and for a given steel in a given environment time-to-failure decreases as strength level increases. Typical results for unnotched specimens of 4340 steel quenched and tempered to different strength levels are shown in Figure 13-14, where the corrosive environments were 3% NaCl and 0.1 N HCl aqueous solutions. Typical results for notched specimens are shown in Figure 13-15, where the data are for four alloy steels, quenched and tempered to the same strength level and statically loaded to failure in distilled water. For these four steels in this environment the values of K_{ISCC} were similar, but above the threshold the times-to-failure varied markedly with alloy type, alloy 4340 being the most susceptible to stress corrosion cracking. The effect of strength level in 4340 steel has also been investigated by Reference 13-32, where increased strength level was found to be detrimental in both gaseous and aqueous environments, and K_{ISCC} in 3% NaCl solution was found to fall from about 66 MPa $m^{1/2}$ at a yield strength of about 860 MPa, to about 15 MPa $m^{1/2}$ at a yield strength of about 1310 MPa.

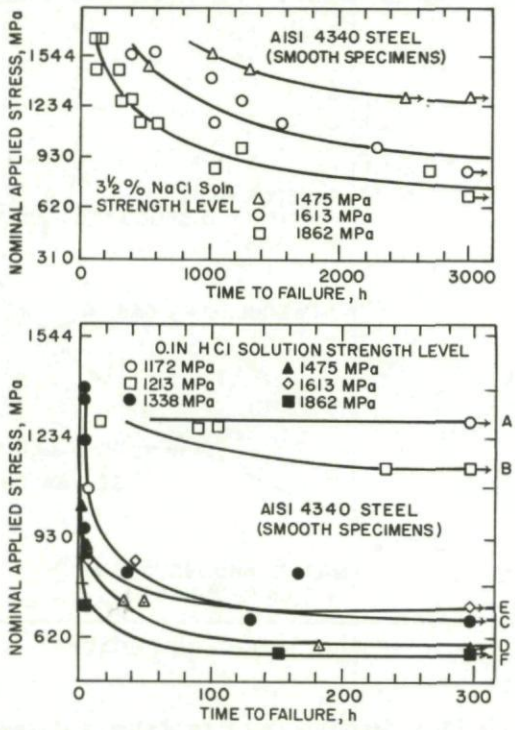

Fig. 13-14 Effect of strength level on delayed failure of AISI 4340 steel in aqueous solutions. (Ref. 13-34)

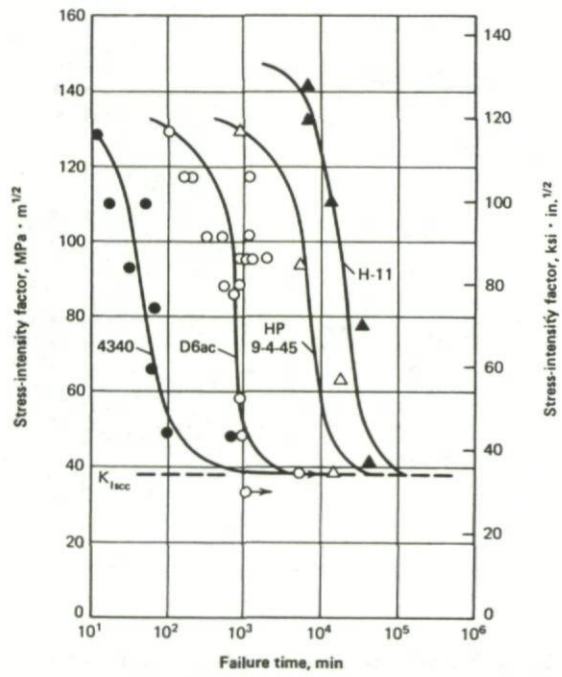

Fig. 13-15 Stress corrosion cracking in four high-strength steels. (Ref. 13-31)

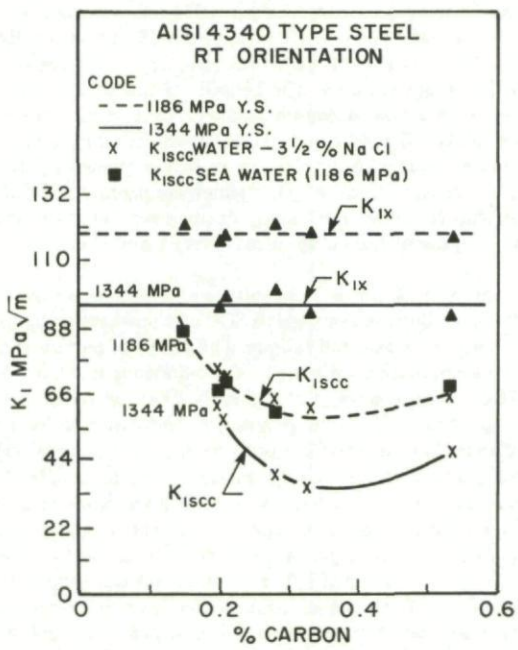

Fig. 13-16 The effects of carbon on the resistance to stress-corrosion cracking of AISI 4340-type steels quenched and tempered to either 1186 MPa or 1344 MPa yield strength. (Ref. 13-33)

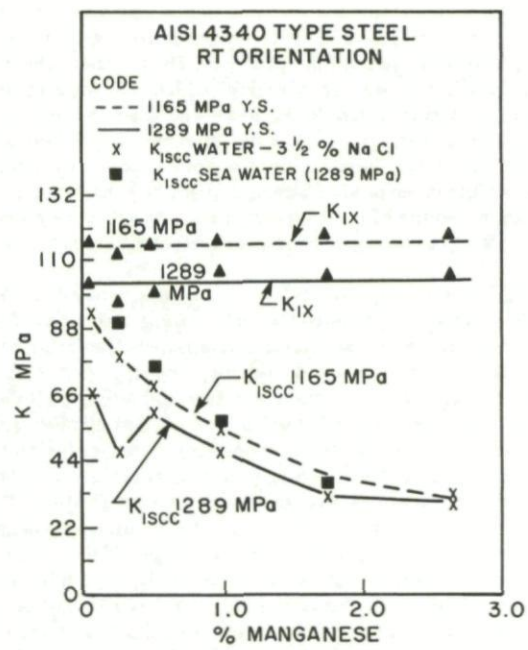

Fig. 13-17 The effects of manganese on the stress-corrosion cracking resistance of AISI 4340-type steels quenched and tempered to 1165 MPa and 1289 MPa yield strength. (Ref. 13-33)

Both composition and microstructure are important, but because of the number of variables involved only general trends have been indicated, and for any given steel microstructure appears to be more important than composition. Detailed studies of the effect of composition on SCC in martensitic steels have been reported in Reference 13-33. A detailed review of stress corrosion cracking in low alloy steels with yield strengths up to 1034 MPa has been given in Reference 13-42, and information on stainless steels and maraging steels is given in References 13-14 and 13-38 respectively. For 4340 type steels elements such as Cr, Mo, Ni, Co, P and S appear to have very little effect when the steels are of equivalent strength (Ref. 13-33). However, SCC was very sensitive to carbon and manganese levels. Figure 13-16 shows that as carbon is increased to about 0.35% resistance to SCC as indicated by K_{ISCC} decreases. However if carbon is increased beyond this level to about 0.45%, stress corrosion resistance again increases. Resistance to SCC decreased progressively as manganese was increased from about 0.1% to about 2.6%, as shown in Figure 13-17. The effect on microstructure was to produce either untempered martensite or twinned martensite, and the lowering of K_{ISCC} means that the load-carrying capacity of quenched and tempered steels containing flaws will be decreased when exposed to salt water. Therefore for maximum resistance to SCC, the manganese content should be as low as possible consistent with requirements on hardness and hardenability. Figure 13-15 shows that delayed failure times for precracked specimens of medium and high alloy martensitic steels (9 Ni-4 Co, H-11) in distilled water are substantially greater than failure times for low alloy steels (4340, D6AC). Silicon additions (1.6% or more) to 4340 steel have been found to substantially lower the stress corrosion crack velocities in 3.5% NaCl solution (Ref. 13-29).

For the steels studied in Reference 13-33 the values of K_{ISCC} decreased as yield strength increased, and similar behaviour is observed for many other steels as shown in Figure 13-18, and although a great deal of scatter is apparent in this data the trends are particularly clear for alloys such as 4340 and 18-Ni maraging steel. Other data from Reference 13-30 is presented in Figure 13-19 and this shows that as the strength of 4340 steel is increased by varying the tempering temperature, both toughness and stress corrosion resistance decrease, toughness decreasing from about 92 MPa $m^{1/2}$ to 64 MPa $m^{1/2}$ while K_{ISCC} decreases from about 71 MPa $m^{1/2}$ to about 11 MPa $m^{1/2}$ in flowing sea water.

The particular susceptibility of high strength martensitic steels to stress corrosion cracking has been attributed to the presence of ϵ-carbides, high dislocation densities, and coherency strains between twinned martensite plates, and the supporting evidence has been reviewed by Reference 13-29. Reference 13-35 has shown that for the same strength level, crack velocities are more than an order of magnitude greater for 4340 steel with a tempered martensite structure than for the lower bainite structure. Figure 13-20 shows crack velocity as a function of applied stress intensity for martensitic and bainitic steels. The difference was attributed to more effective trapping of hydrogen at coherently twinned interfaces in the plate martensite structure, as opposed to the incoherent bainite laths. Figure 13-20 also shows that the range of stress intensities required for cracking is notably lower for the martensite structure.

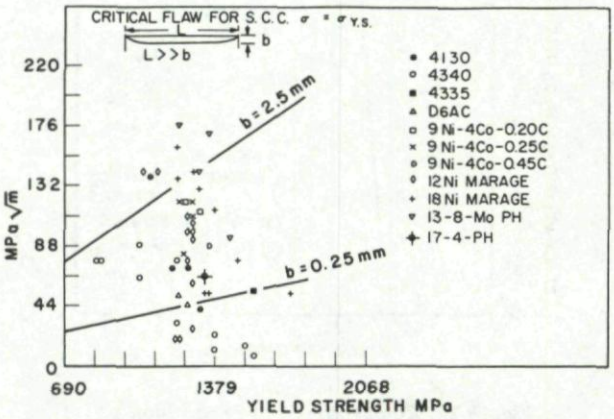

Fig. 13-18 K_{ISCC} data for a number of commercial steels of various yield strengths tested in salt water. Lines show K_{ISCC} at which a stress corrosion crack will initiate assuming yield strength stresses and assuming the crack depth indicated (2.5 mm or 0.25 mm).
(Data due to G. Sandoz, reported in Ref. 13-30)

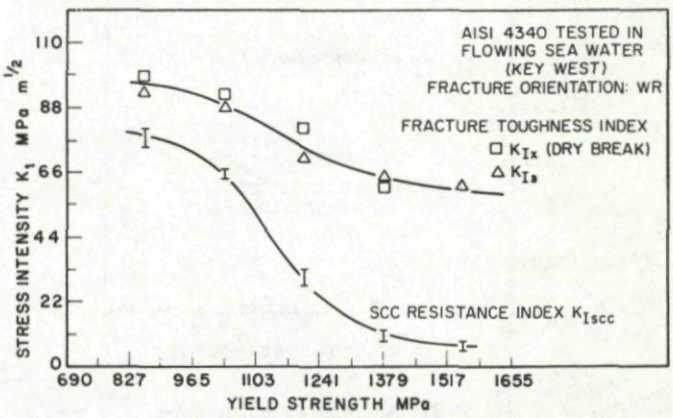

Fig. 13-19 The effect of yield strength (varied by varying tempering temperature) on stress corrosion resistance. K_{Ix} and $K_{I\delta}$ are approximations of fracture toughness. (Ref. 13-30)

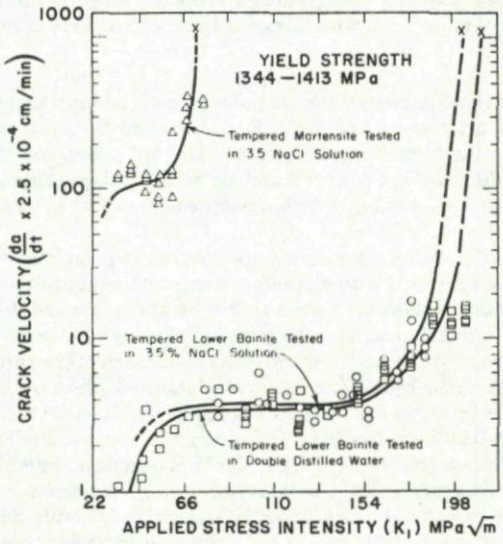

Fig. 13-20 Crack velocity vs stress intensity for AISI 4340 steel (martensitic and bainitic structures) in 3½% NaCl solution (pH = 6.0) and double distilled water. (Ref. 13-35)

The susceptibility of martensitic 400-series stainless steels to both stress corrosion and to temper embrittlement occurs within a range of tempering temperatures which promotes the resolution of one carbide species and the simultaneous reprecipitation of another (Ref. 13-29). Reference 13-36 shows SCC data for un-notched bent-beam specimens of several martensitic stainless steels including Types 410, 420, 422 and 436 in a 5% salt spray environment. Minimum failure times occurred after a 480°C temper, and other studies have shown that this coincides with the precipitation of M_3C carbides (Ref. 13-37). References 13-36 and 13-37 have shown that temper embrittlement and stress corrosion cracking occur over the same range of tempering temperatures.

The stress corrosion cracking and hydrogen embrittlement of 18-Ni maraging steels has been reviewed in Reference 13-38. Data from smooth bend specimens (Fig. 13-21) indicates that 18-Ni (250 grade) maraging steel is able to sustain stresses of approximately 80% of yield strength in 3.5% NaCl solution for approximately 1000 hours, and it survives as well as many lower strength steels carrying much lower stresses. Figure 13-22 shows that this resistance to stress corrosion cracking is due to lower Region II crack growth rates, compared to some other steels, and for maraging steels these growth rates increase with increasing strength level. Reference 13-44 reports that stress corrosion threshold stress intensities can be correlated with a parameter based on the concentrations of the major alloying elements Co, Mo, Al and Ti. Thus values of K_{ISCC} were reported to fall by a factor of about six (130 MPa $m^{1/2}$ to about 20 MPa $m^{1/2}$) as the parameter $(Co)^{1/2}$. Mo (Ti + Al) increased from about 4 to about 10. Reference 13-38 reports that C and P may be beneficial to SCC in maraging steels at high stress levels, while Cr may be deleterious.

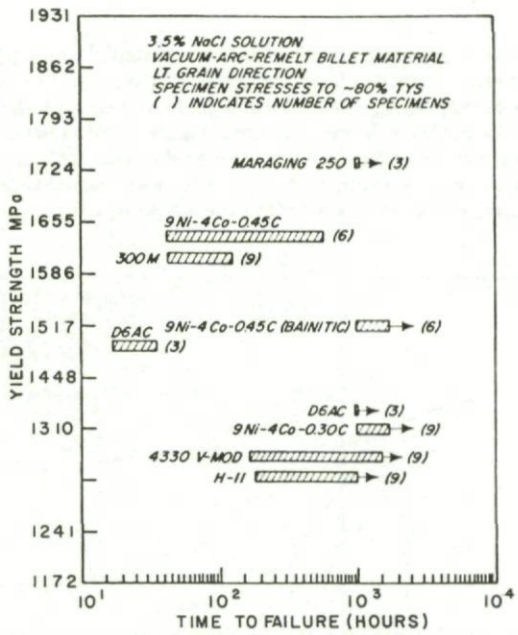

Fig. 13-21 Alternate immersion stress corrosion data from smooth bend specimens. (From Ref. 13-38)

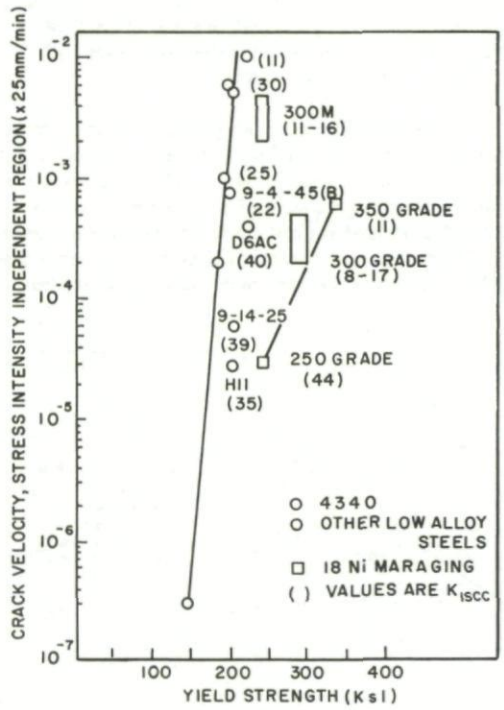

Fig. 13-22 Comparison of stress corrosion crack velocities in maraging and low alloy steels. (Ref. 13-43)

Notwithstanding these seemingly attractive properties of maraging steels problems of stress corrosion cracking and hydrogen embrittlement have occurred with maraging steel bolts in service, and as noted in Chapter 6, if they are used they should be used with caution.

Austenitic stainless steels are prone to both intergranular stress corrosion cracking and intergranular corrosion when slow cooled through the range of about 850°C to about 550°C. This sensitization is due to the precipitation of chromium carbides at grain boundaries and the formation of chromium depleted zones, and therefore the effects on SCC may be either electrochemical or structural. As discussed in Chapters 4 and 10, austenitic steels should be quenched rapidly from temperatures above about 850°C, and problems arising from welding or high service temperatures can be moderated by the addition of carbide stabilizing elements.

Stress corrosion cracking will also occur transgranularly in austenitic stainless steels exposed to aqueous solutions containing chlorides, but it appears this only occurs at temperatures above about 70°C. The role of alloying additions and microstructure on SCC in austenitic stainless steels has been reviewed by Thompson and Bernstein (Ref. 13-14), and this report and its references should be consulted for further details. The two principal alloying additions Ni and Cr both improve SCC resistance in certain composition ranges. Nickel additions above about 8% improve SCC resistance, while chromium additions are also beneficial except in the range of about 15% to 18% where the benefits are minimal. Manganese which is generally present in stainless steels in the 1% to 2% range may produce either beneficial or detrimental effects. Carbon above about 0.1% confers considerable resistance to SCC, while lower amounts in the range 0.01% to 0.06% are damaging, and a minimum resistance to SCC has been noted at about 0.06% (Ref. 13-39). Nitrogen and phosphorous both accelerate SCC, while silicon is beneficial. Interestingly, molybdenum which is added to improve pitting resistance is found to be deleterious to SCC resistance, producing a maximum effect at about 0.5%, and it promotes intergranular stress corrosion rather than the more usual transgranular behaviour (Ref. 13-40). Similarly the carbide stabilizing elements Nb and Ti which are added to improve resistance to sensitization and intergranular cracking are found to decrease resistance to SCC (Refs. 13-39 and 13-41).

Because of the number of variables that can affect stress corrosion cracking in commercial alloys laboratory tests usually lead to results with an appreciable amount of scatter, but nevertheless results for commercial austenitic stainless steels in boiling 42% $MgCl_2$ solution show that at least three groups of alloys exist (Fig. 13-23). This particular environment is one of the most aggressive and it is widely used for SCC testing of stainless steels. The data of Figure 13-23 shows that alloy 304 and its low carbon counterpart are more susceptible to SCC then types 305, 309, 316, and 347, while types 310 and 314 are more resistant. For each of these three groups times to failure fall in a fairly narrow scatter band, with times increasing as the applied stress decreases.

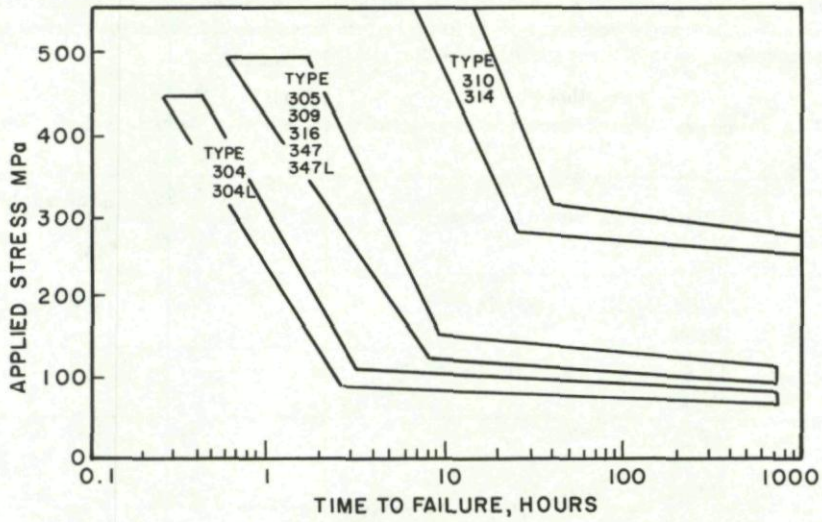

Fig. 13-23 Variation of time-to-failure with applied stress of several commercial austenitic stainless steels in a boiling 42% magnesium chloride solution. (From Ref. 13-41, data due to Denhard)

13.6 Environmental Aspects of Stress Corrosion Cracking

Table 13-2 provides a list of environments that may cause stress corrosion cracking in a number of metals and alloys. This table simply indicates the wide range of metals that may be affected by SCC and the wide variety of environments capable of producing damage. It is worth noting that very few of the materials listed are unlikely to be found in aircraft structures, and chloride containing environments such as seawater are damaging to many of the structural alloy classes listed. However, Table 13-2 is not complete, and it would in fact be difficult to prepare a complete list since new situations involving stress corrosion cracking in different metal-environment systems are still recorded periodically. Not included in Table 13-2 are liquid metal environments, aircraft fuels, hydraulic fluids and organic solvents many of which are damaging to a wide range of alloys including aluminium. Also halide ions such as Br^- and I^-, in addition to chloride ions, usually accelerate stress corrosion cracking in aluminium alloys and steels in aqueous solutions, and they can cause SCC in certain titanium alloys that would otherwise be immune to SCC (Ref. 13-46). A further listing of environments known

Table 13-2 Environments that may cause stress corrosion of metals and alloys (Ref. 13-45)

Material	Environment	Material	Environment
Aluminium alloys	$NaCl$-H_2O_2 solutions	Ordinary steels	NaOH solutions
	NaCl solutions		$NaOH$-Na_2SiO_2 solutions
	Seawater		Calcium, ammonium, and sodium nitrate solutions
	Air, water vapor		Mixed acids (H_2SO_4-HNO_3)
Copper alloys	Ammonia vapors and solutions		HCN solutions
	Amines		Acidic H_2S solutions
	Water, water vapor		Seawater
Gold alloys	$FeCl_3$ solutions		Molten Na-Pb alloys
	Acetic acid-salt solutions	Stainless steels	Acid chloride solutions such as $MgCl_2$ and $BaCl_2$
Inconel	Caustic soda solutions		$NaCl$-H_2O_2 solutions
Lead	Lead acetate solutions		Seawater
Magnesium alloys	$NaCl$-K_2CrO_4 solutions		H_2S
	Rural and coastal atmospheres		$NaOH$-H_2S solutions
	Distilled water		Condensing steam from chloride waters
Monel	Fused caustic soda	Titanium alloys	Red fuming nitric acid, seawater, N_2O_4, methanol-HCl
	Hydrofluoric acid		
	Hydrofluosilicic acid		
Nickel	Fused caustic soda		

to induce or accelerate SCC in aluminium alloys has been given by Speidel (Ref. 13-13), as shown in Table 13-3. Many of these environments also cause SCC in steels and titanium alloys. The environments in which SCC of low alloy steels has been observed include water and chloride solutions, hydrogen sulphide, sulphuric acid, gaseous hydrogen, nitrates, hydroxides, ammonia, carbon dioxide and carbonate solutions, water-carbon monoxide-carbon dioxide, ammonia-hydrogen sulphide-hydrogen cyanide-carbon dioxide, hydrogen cyanide, and various organic liquids (Ref. 13-42).

The environmental variables known to influence SCC are humidity in gaseous environments, pH, electrical potential, temperature, viscosity, concentration of certain halide ions in aqueous solutions, and the presence of cathode poisons such as As, Se, Te and S in aqueous solutions which may accelerate the entry of hydrogen into materials such as steels. These variables may influence times-to-failure in notched and un-notched specimens, raise or lower plateau crack growth rates in pre-cracked specimens, or influence the position of the stress dependent region of crack growth and hence influence K_{ISSC}.

Table 13-3 Some environments known to cause or not to cause SCC in aluminium alloys (Ref. 13-13)

	Environments known to cause		Additions known to	
	No SCC	SCC	induce SCC	accelerate SCC
Gases	A, He, O_2, N_2 dry air	H_2O, Hg	H_2O	H_2O
Liquid Metals	Li, Se, Bi, Te, Cd, Pb	Hg, Ga, Na, Te, Sn, Zn		
Molten Salts	$AlCl_3$-LiCl LiCl-KCl eutectic			
Inorganic Liquids	H_2SO_4	H_2O	H_2O	Br^-, Cl^-, I^-
Organic Liquids		CCl_4 alcohols hydrocarbons ketones esters } induced by traces of H_2O?		H_2O, Cl^-, Br^-, I^-

SCC in gaseous environments: Stress corrosion cracking does not occur in commercial aluminium alloys in dry argon, dry helium, dry oxygen, dry hydrogen, dry nitrogen or dry air, but it will occur when these environments contain moisture. Figure 13-24(a) shows the SC crack growth behaviour of several commercial aluminium alloys loaded to produce crack tip stress intensities just below the fracture toughness values for the different materials, and held under sustained load. No crack growth occurs for times up to 47 days when the environment is dry hydrogen with less than 0.01% humidity. However, crack growth begins immediately when water vapour is added, the actual crack velocity depending on the alloy composition. Speidel, Reference 13-13 has shown that Stage II (plateau) crack growth rate for 7075-T651 is a linear function of the relative humidity in air, with a slope of one in a double-logarithmic plot, as indicated in Figure 13-24(b). Increasing humidity also increases crack growth rates in the stress dependent region of crack growth (Stage I), that is V-K curves are displaced to higher stress intensities. Humidity also has an adverse effect on high strength steels and SC crack growth rates in H11 steel (yield strength 1586 MPa) in air have been found to increase as relative humidity is increased up to 60%, above which growth rates were similar to that observed in water (Ref. 13-47). However water vapour does not appear to be essential to SCC or hydrogen embrittlement in steels since delayed static failures have been observed in low pressure hydrogen and hydrogen sulphide environments (Ref. 13-29).

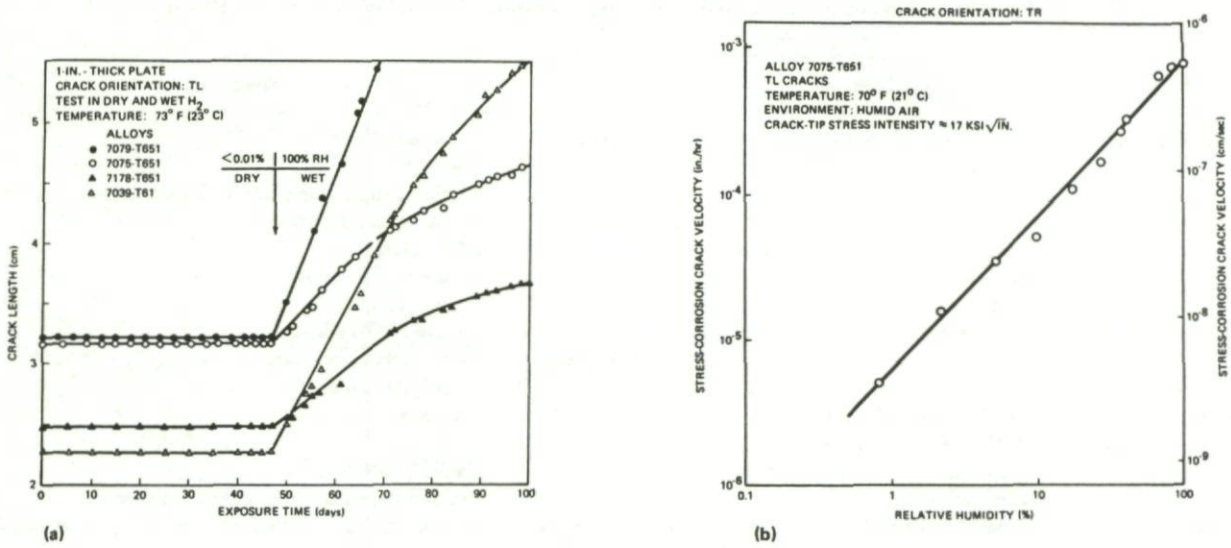

Fig. 13-24 Effects of humidity on stress-corrosion crack growth in high strength aluminium alloys. (Ref. 13-13)

(a) SC crack growth in various commercial alloys in dry and wet hydrogen.
(b) Effect of relative humidity on stress-independent stress-corrosion crack growth in 7075-T651 in air.

SCC in organic liquids: Aluminium alloys are prone to SCC in organic fluids including flight fuel, hydraulic fluids, engine oil and a wide variety of organic solvents including commercial methanol, ethanol, benzene and acetone. However these fluids all contain traces of moisture of about 0.05%, and Speidel has shown that SC crack growth rates in these fluids are similar to those observed in water. Thus it is thought that the water is the damaging constituent rather than the organic fluids themselves. If water contents are reduced below about 0.01% then SC crack growth rates are substantially decreased (Ref. 13-13).

SCC in aqueous solutions: Stress corrosion crack growth rates for aluminium alloys and steels in distilled water are similar to those observed in air at high relative humidities (> 60%), and this might be expected if condensation occurs at the crack tip in air at high humidities to create a liquid environment (Refs. 13-13 and 13-41). Anions such as chloride, bromide and iodide ions accelerate SC crack growth rates in aluminium and titanium alloys above and beyond the velocities observed in distilled water (Refs. 13-13 and 13-46). However fluoride ions decrease SCC growth rates in aluminium alloys, acting as an inhibitor rather than an accelerator (Ref. 13-13). Thus, the detrimental effects of Cl^-, Br^- and I^- are specific to these anions, and are not characteristic of all halides. These particular ions are also unique pitting agents for aluminium and its alloys, and many steels, and they also accelerate crevice corrosion and intergranular corrosion in these alloys. They can therefore influence both the initiation and growth stages of SCC. The acceleration of SC crack growth by Cl^-, Br^- and I^- depends on metallurgical factors such as alloy composition and strength level. For example SC crack velocity in 7075-T651 in water can be increased by a factor of four by the addition of chloride ions, while for 7079-T651, SC crack velocity can be increased by more than one thousand times (Ref. 13-13). In neutral aqueous solutions few cations appear to affect SCC in aluminium alloys, two exceptions being mercury and hydrogen ions, which are generally damaging, see Reference 13-13.

The addition of cathodic poisons, containing elements from Groups V and VI of the periodic table have been shown to promote hydrogen entry into iron or steel from aqueous solutions (Ref. 13-29). Cathodic poisons have been rated, in order of effectiveness in promoting hydrogen entry as:

$$As > Se > Te > S$$

These poisons have been shown to both increase hydrogen entry into high strength steels, and to lower the stress required for delayed failure in aqueous media. For example hydrogen sulphide additions to neutral or acidic aqueous solutions will reduce the stress required for delayed static failure of high strength steels by a factor of about five. The effect of H_2S additions appears most significant in the pH range of about 3 to 7 (Ref. 13-29).

The pre-exposure of steels to sulphur-containing environments, which lead to the formation of sulphided areas on the surface of the steel, will also lead to a decrease in times-to-failure in delayed static failure tests. This has been attributed to the effect of the sulphided areas in retarding the recombination of atomic hydrogen, and thereby promoting the entry of hydrogen into the steel. Chloride ions, per Se, appear to have no significant effect on the cracking susceptibility or kinetics of 4340 steel, as indicated in Figure 13-20, however this may not be the case in all types of steel. For example Reference 13-38 reports that cracking times in thin foil specimens of 18 Ni maraging steel decreased as Cl^- content was increased in aqueous solutions as indicated in Figure 13-25(a).

Figure 13-25(a) also shows that pH can affect stress corrosion cracking in maraging steel, and similar effects are observed for many other types of steel. Reference 13-29 reports that delayed failure times of smooth and notched specimens of high strength steels in aqueous media are rapidly decreased by a decrease in bulk solution pH.

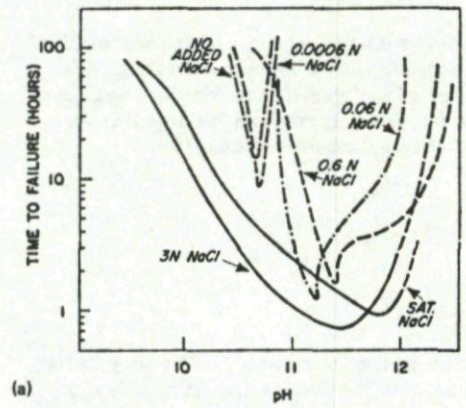

(a)

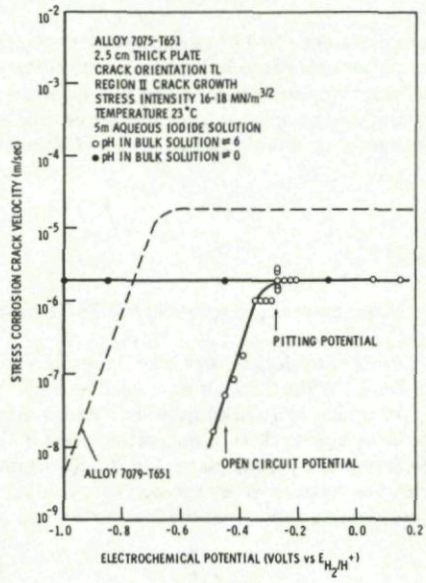

(b)

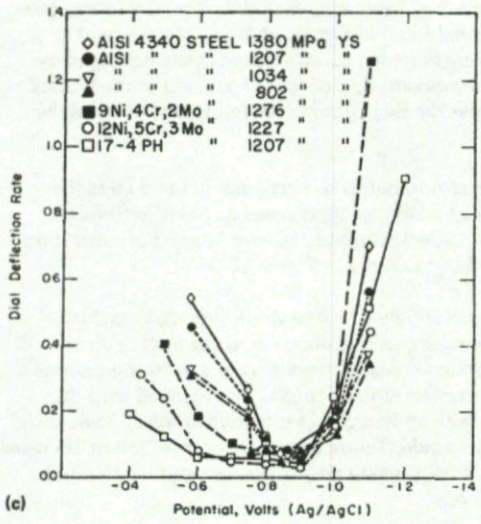

(c)

Fig. 13-25 Effects of solution pH and electrochemical potential on stress-corrosion cracking in several high strength steels and aluminium alloys in aqueous solutions.

(a) Relation between time-to-failure in 18 Ni maraging steel in deionized water with and without NaCl at various values of pH. (Ref. 13-48)
(b) Influence of potential and pH on stage II stress corrosion crack growth in 7075-T651 and 7079-T651. (Ref. 13-13)
(c) Influence of applied potential on crack growth rates in aqueous chloride solutions for various high strength steels. (Ref. 13-30)

In aluminium alloys the effect of lowering the pH of the bulk solution from 6 to 0 is to displace the stress dependent region of the V-K curve to lower stress intensities (Ref. 13-13). However the plateau crack growth rate (Stage II) remains remarkably constant over a wide range of pH up to about 11, while above pH = 11 crack velocity appears to decrease towards the general corrosion rate in the material (Ref. 13-13).

Effects of applied potentials: The effects of potential on SCC in steels and aluminium alloys are influenced by solution pH and various metallurgical parameters. In the case of aluminium alloys in neutral or mildly acidic solutions a shift in applied electrochemical potential to more negative values typically causes a shift in the stress dependent region of the velocity-stress intensity (V-K) curve towards higher values of K. At higher negative values of potential plateau growth rates are also decreased, as indicated in Figure 13-25(b), reaching very low values when the applied potential is about minus one volt versus the standard hydrogen electrode. Thus SCC in high strength aluminium alloys can often be suppressed by cathodic protection. However these effects are strongly influenced by bulk solution pH. In strongly acid solutions there may be no effect of potential on Stage II crack growth rates, as indicated in Figure 13-25(b), and cathodic protection may be impossible. Similar effects are observed for titanium alloys, where cathodic protection against SC crack growth is impossible at very low pH values (Ref. 13-46).

In the case of steels, Reference 13-30 has shown that impressed potentials, whether anodic or cathodic, strongly increase SC crack velocity in a variety of high strength steels, as indicated in Figure 13-25(c). Thus cathodic protection is impossible in these cases. Impressed potentials also increase the rate of hydrogen permeation through steels and in the case of anodic polarization, stress corrosion cracks are found to initiate at the base of corrosion pits (Ref. 13-29).

Effects of temperature: Since many aircraft spend considerable periods of time operating in tropical or semi-tropical climates, it is important to know how temperature will affect SCC in structural materials. But high temperatures can also be created in aircraft structures operating in colder regions, as a consequence of aerodynamic heating, and structure close to engines can also become heated as a result of normal engine operation. It is well known that higher temperatures will generally accelerate corrosion reactions, and times-to-failure for aluminium alloys susceptible to SCC decrease with increasing temperature (Ref. 13-49). Investigations of the effects of temperature using fracture mechanics specimens have shown that temperature may affect different alloys differently. For example, Reference 13-13 shows that increasing temperature from -11°C to 105°C in 3M KI solution causes an increase in stress independent crack growth velocity in 7079-T651 by approximately one order of magnitude from about 8×10^{-4} cm/sec to about 9×10^{-3} cm/sec. At the same time the stress dependent region of crack growth was displaced to lower values of stress intensity, so that high temperatures both increased SC crack growth rates and caused cracking to occur at lower applied stresses. However, studies on other alloys such as 7039-T61 (Ref. 13-49), have shown that the stress dependent crack growth rates may be unaffected by increasing temperature in the range 23°C to 110°C, while stress independent crack growth rates were increased by more than three orders of magnitude from about 6×10^{-7} cm/sec to about 10^{-3} cm/sec. Thus the specific effects of temperature are strongly influenced by metallurgical parameters.

In the case of steels the effects of temperature depend not only on the type of steel, its composition and microstructure, but also on the nature of the environment. In aqueous solutions stress corrosion crack growth rates increase with temperature, and the activation energies measured correspond quite well with that for hydrogen diffusion in steel (Ref. 13-29). However in gaseous environments different behaviour is observed. Tests on 4130 steel and H11 steel in hydrogen (Refs. 13-50 and 13-51), have shown that subcritical crack growth rates increase with temperature in the range from about -80°C to about 20°C, and then decrease as temperature is further increased to about 80°C. The activation energies reported in the literature for slow crack growth in various steels in distilled water, salt water and both hydrogen and hydrogen sulphide gas are given in Reference 13-29.

Effects of viscosity: Reference 13-11 has discussed the effects of solution viscosity on SCC in aluminium alloys. Relatively few alloy-environment combinations appear to have been investigated, but for 7079-T651 in 2M aqueous KI solution only the plateau crack growth rate was affected by viscosity, the stress dependent region of crack growth remaining largely unaffected. Viscosity was varied by more than two orders of magnitude from about 1 centipoise to about 600 centipoise by adding glycerol and the stage II crack growth rate was decreased by more than two orders of magnitude to produce a slope of -1 on a double-logarithmic plot.

13.7 Case Histories

Case history 13-1. Stress corrosion cracking in a 7079-T6 locking cylinder of a main landing gear.

An Al-Zn-Mg alloy forging was used to produce a locking cylinder for a main landing gear assembly. The alloy had a composition 4.3% Zn, 3.3% Mg, 0.5% Cu with small amounts of Mn and Cr and it conformed to the German material specification 3.4344, which is very similar to 7079 and the alloy was in the peak strength T6 condition. Cracks were detected after service exposure, and were found to lie in a plane close to the parting plane in the closed die forging, as indicated in Figure 13-26(a). Metallographic sections prepared through the parting plane (Fig. 13-26(b)), showed that the grains were flattened and elongated in the parting plane such that "end grain" boundaries were exposed at the free surface. Figure 13-26(b), shows surface pitting in the region of the parting plane and cracks propagating away from the free surface and following grain boundaries running approximately perpendicular to the surface.

Other areas of the surface of the forgings away from the parting plane were also found to be corroded. In these areas the corrosion led to pitting, as shown in Figure 13-26(c), and closer examination revealed a fibrous appearance in pitted regions as indicated in Figure 13-26(d). Metallographic sections through these areas showed that the grain boundaries were aligned in a direction approximately parallel to the surface, and exfoliation of the surface grains was occurring, as shown in Figure 13-26(e).

As explained in Section 13-5, alloys of the 7079 type are among the most susceptible alloys to stress corrosion cracking, and particularly when end grain boundaries are exposed at a free surface. The intergranular cracking observed in the parting plane (Fig. 13-26(b)), was attributed to stress corrosion cracking in this case, and the sustained tensile stresses were due to the internal pressurization of the locking cyclinder in service. No information was given on the corrosion protection system employed with this part, but the widespread corrosion indicates that this was inadequate. However, even with an improved protection system it is doubtful whether such parts would perform adequately. The long term solution to this problem would require a material change, and as discussed in Section 13-5, alloy 7049-T73 has been used to replace 7079-T6 in landing gear forgings, providing equivalent strength with much improved SCC resistance. Alloys 7175-T736 and 7050-T73 would be alternative choices.

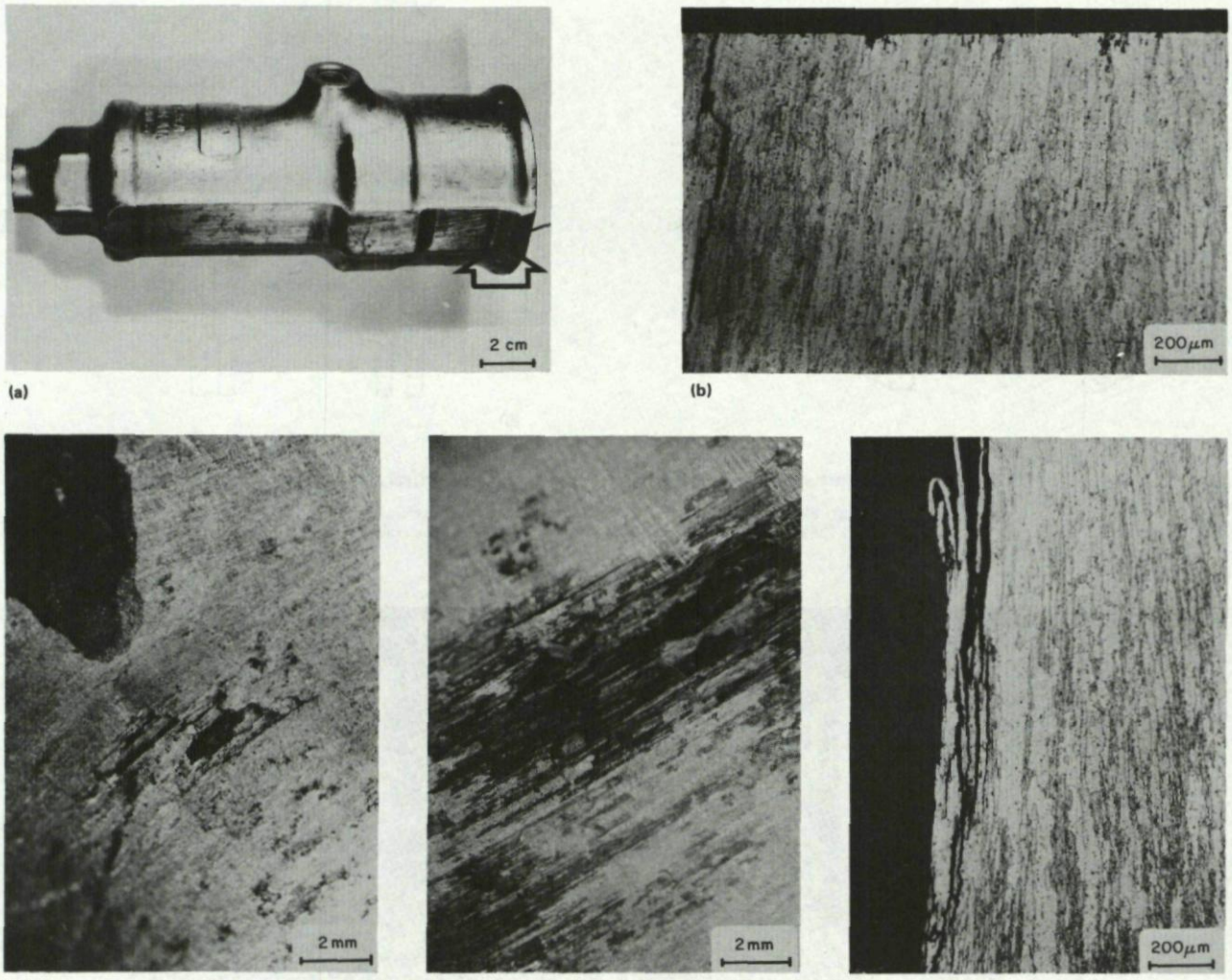

Fig. 13-26 Stress corrosion cracking in a 7079-T6 main landing gear locking cylinder, case history 13-1.

(a) Cracked cylinder showing location of cracking (arrow).
(b) Metallographic section in the region of the parting plane showing pitting and intergranular cracking.
(c) Surface pitting away from the parting plane.
(d) Close up of surface pitting showing fibrous appearance.
(e) Exfoliation in areas away from the parting plane.

Case history 13-2. Stress corrosion cracking in the 7079-T6 front and rear spars of a fighter aircraft vertical fin.

Several cracks were found in the front and rear spars of a fighter aircraft during a routine inspection using eddy current methods. The locations of the cracks in the parts are shown schematically in Figures 13-27(a) and 13-27(b), which show the front and rear spars respectively. The spars were made from 7079 die forgings, and were artificially aged to the peak strength condition according to the specification QQ-A-367. All surfaces of the spars had been shot peened after machining, and had been treated with a chromate conversion coating and a single layer of zinc chromate primer.

The spars were removed from the aircraft to allow closer visual inspection and the cracks could be seen clearly to be up to several centimetres long as indicated in Figure 13-28(a). Many of the cracks were found to propagate from fastener holes as indicated in Figures 13-27 and 13-28. The front and rear spars were mounted in a jig, and loaded statically to cause failure so that the crack surfaces were revealed. A typical fracture surface observed in the front spar is shown in Figure 13-28(b), and this shows a dull fan-shaped region which appears to have initiated in the radius at the base of a bolt access hole as indicated by the arrow, and a lighter area which was produced by the static overload fracture. The dull area was typical of stress corrosion cracking showing evidence of corrosion and arrest lines indicating that cracking had occurred progressively over a period of time. Metallographic examinations showed that the material had a fine-grained recrystallized microstructure, and the cracks were found to run along grain boundaries, as is expected with stress corrosion cracking in this class of alloy.

It was concluded that the cracking was due to stress corrosion which had occurred because of the use of a stress corrosion prone alloy. While the spars had received corrosion protection treatments, damage to the surface coatings during the installation of bolts had exposed bare metal and stress corrosion had occurred as a result of the high humidity and high sustained tensile stresses arising from fastener installation. To overcome this problem the spars were machined from 7075-T73 forgings, which as discussed in Section 13-5 provide high resistance to stress corrosion cracking. The surface protection system used previously, including shot peening to develop compressive residual stresses, followed by chemical conversion coating and zinc chromate priming, was retained. An alternative solution involving the use of 7175-T736 was also considered in order to maintain high strength, equivalent to or higher than the original 7079-T6 values, together with improved stress corrosion resistance.

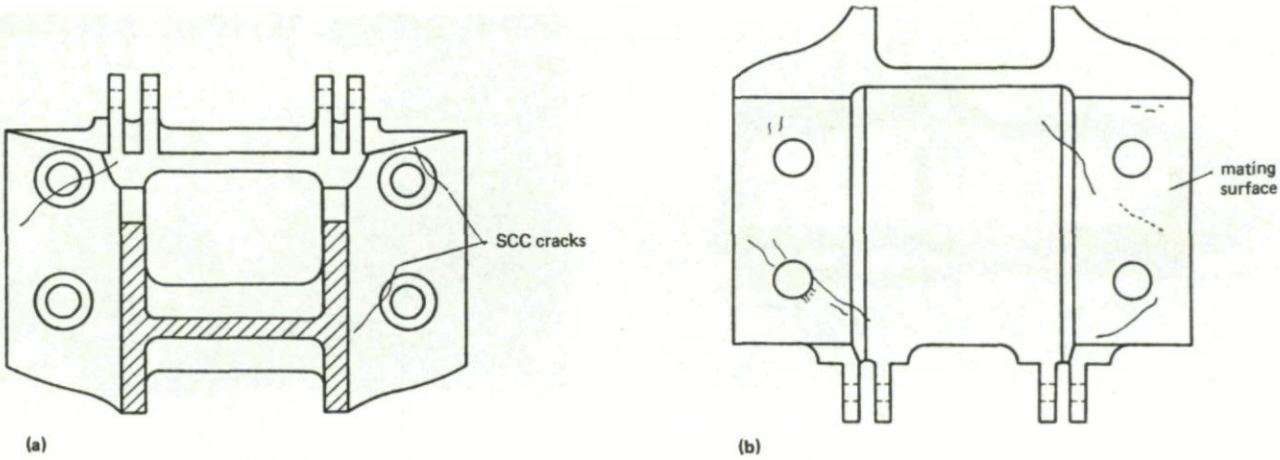

Fig. 13-27 Stress corrosion cracking in the 7079-T6 spars of a vertical fin, case history 13-2.

(a) Sketch of the front spar showing the location of the cracks.
(b) Sketch of the rear spar showing the location of the cracks.

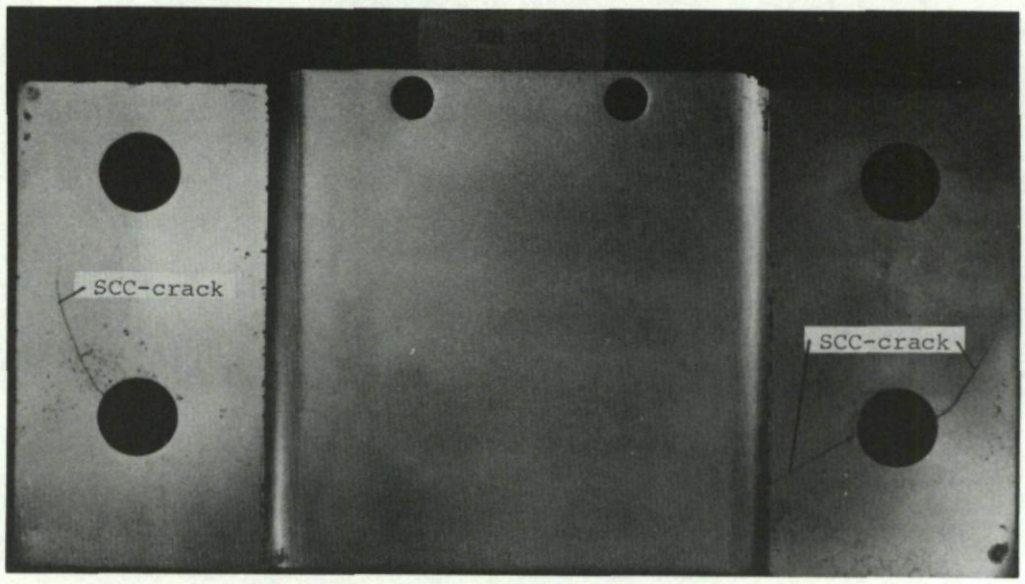

(a)

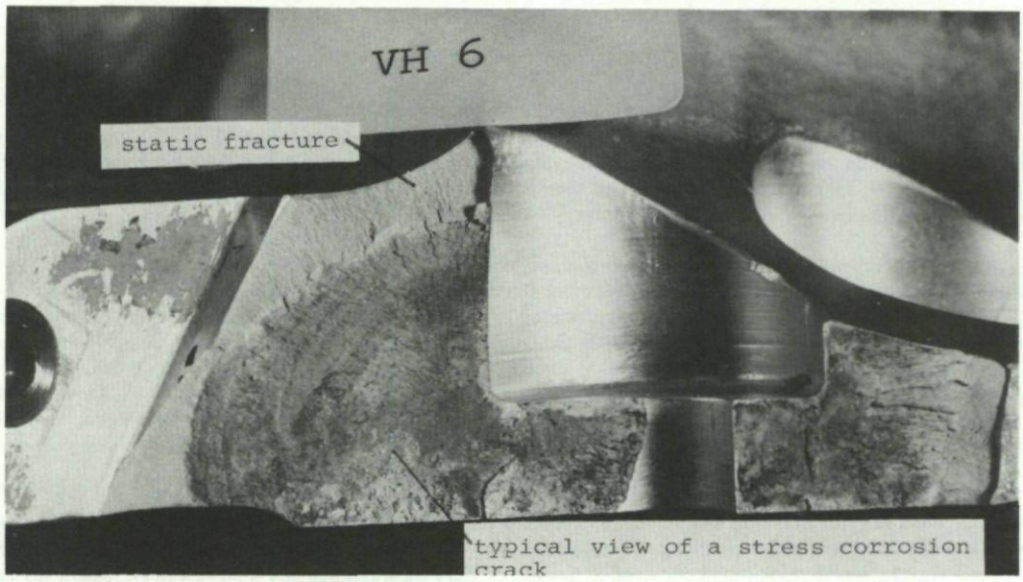

(b)

Fig. 13-28 Stress corrosion cracking in the 7079-T6 spars of a vertical fin, case history 13-2.

(a) Macroscopic view of the mating surface of the rear spar.
(b) Fracture surface of a statically broken front spar.

Case history 13-3. Stress corrosion cracking of a 7079-T6 bearing housing of a vertical stabilizer beam.

During a major repair of a fighter aircraft a crack was found in the pivot bearing housing at the top end of the vertical stabilizer beam. Figure 13-29(a) shows the crack as it was found by dye penetrant inspection. Figure 13-29(b) shows a metallographic cross section through the tip of the crack, and this shows that the crack follows grain boundaries aligned along the length of the bearing. Figure 13-29(c) shows a replica transmission electron micrograph of the fracture surface, which again reveals the intergranular nature of the fracture surface.

The alloy was reported to be a 7079-T6 forging and the presence of intergranular cracking suggests that stress corrosion was the operative fracture mode. The bearing was mounted in the housing by interference fit, and a calculation of the maximum interference-fit stress for this design revealed that it was close to the threshold value for stress corrosion cracking in this alloy. Thus stress corrosion cracks could be expected to form if the part was exposed to normal humid operating conditions. The operator was advised to maintain a high standard of cleanliness and to inspect these parts carefully and frequently. However the long term solution would require a change of material to either 7049-T73 or 7175-T736, as discussed earlier.

Case history 13-4. Stress corrosion cracking of a 7075-T6 main landing gear bogie.

The main landing gear bogie of a large turboprop transport aircraft failed on touchdown, fortunately without causing a serious accident. The part was found to be made from a 7075-T6 forging of the type shown in Figure 13-30(a), and was found to have split along the forging parting plane as indicated in Figure 13-30(b). The tip of the white arrow in Figure 13-30(b) indicates the position of the crack tip in the parting plane, and therefore indicates the maximum extent of cracking in the parting plane. The longest crack was nearly 30 cm long at failure, but since the forging surface had been fully shot peened, the surface residual compressive stresses had prevented the growing cracks from breaking through to the surface and hence revealing themselves to surface inspection. Cracking initiated at the main axle bore, where the most susceptible end grain boundaries on the forging parting plane were exposed by the machining process. Cadmium plated steel bushings were mounted in the main axle bore by interference fit, and corrosion pits were found in the aluminium forging underneath the bushings. Thus even though cadmium plating was used, there appears to have been a sufficiently high galvanic potential in the presence of moisture to initiate pitting attack which led in turn to stress corrosion cracking. The stresses driving SCC in this part were due to the interference fit bushings and residual stress resulting from the post-forge heat treatment operations.

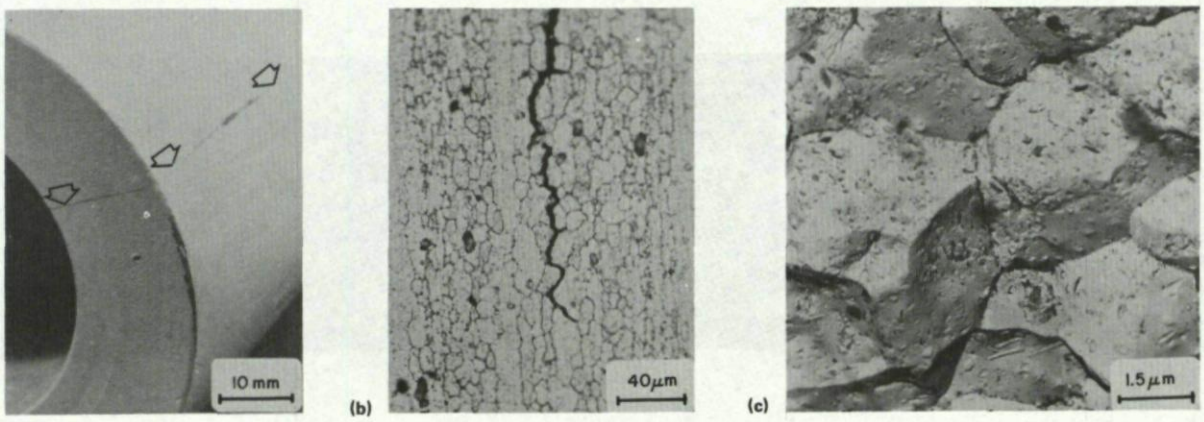

(a) (b) (c)

Fig. 13-29 Stress corrosion cracking in a 7079-T6 bearing housing, case history 13-3.

(a) End of the bearing housing showing the location of the crack.
(b) Metallographic section through the tip of the crack showing the intergranular nature of cracking.
(c) Electron micrograph showing the intergranular fracture topography.

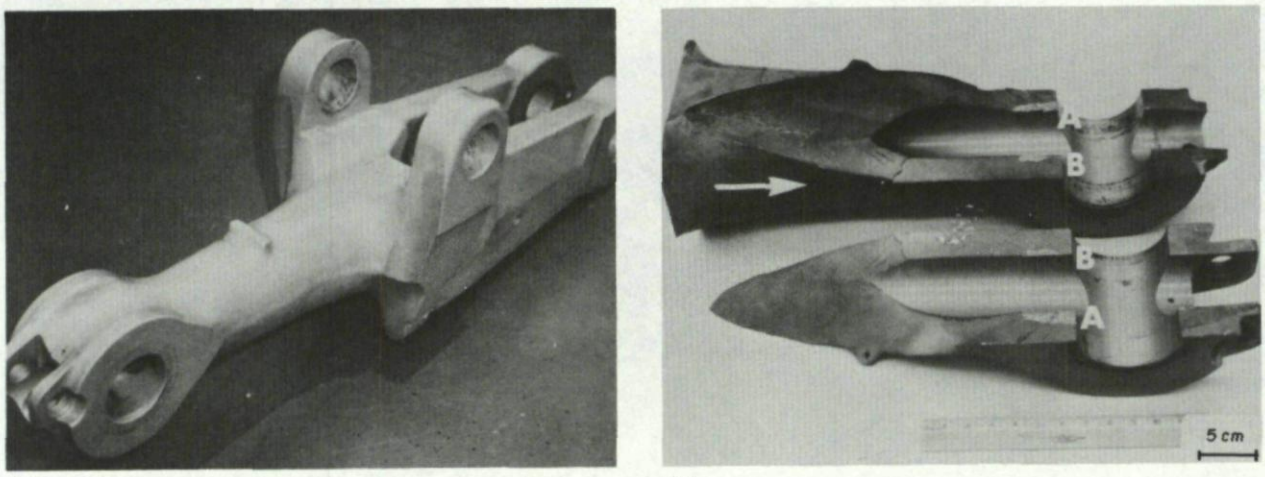

(a) (b)

Fig. 13-30 Stress corrosion cracking in a 7075-T6 main landing gear bogie, case history 13-4.

(a) New and unused bogie.
(b) Failed bogie beam showing the crack initiation sites (A and B) underneath the shrunk-in steel bushings for the main axle bearings. The arrow tip indicates the maximum extent of the crack in the parting plane.

Several options are available to prevent problems of this type. Since the parts had apparently operated for long periods of time with quite large cracks present, it appears that static and fatigue strengths are not of major concern. Therefore some loss of strength could probably be tolerated and the T73 temper could be employed to provide forgings with high resistance to stress corrosion cracking. In more heavily loaded parts where this strength penalty cannot be tolerated, the use of a higher strength alloys, such as 7050, in a stress corrosion resistant T73 temper would be preferred.

Case history 13-5. Stress corrosion cracking and fatigue of a 7075-T6 hydraulic cylinder.

Three main landing gear door actuating cylinders were found to contain cracks at, or near the parting planes of the as-forged 7075-T6 cylinders. Two of the cylinders were examined metallographically and fractographically, while the third was sectioned and its interior surface was inspected using fluorescent penetrants to reveal the cracks indicated in Figure 13-31(a).

Fractography on one cylinder revealed the presence of three distinct regions of fracture as indicated in Figure 13-31(b). Region I consisted of layered intergranular fracture, as shown in Figure 13-31(c); region II was found to contain fatigue striations as shown in Figure 13-31(d), while region III was the overload fracture region produced when the cylinder was broken open for examination.

Metallography revealed corrosion pits on the inside surfaces of the cylinders, as shown in Figure 13-31(e) where the pits can be seen to be aligned at about 45° to the surface in the direction of the grain boundaries. Since the cylinders in service were filled with hydraulic fluid which was not expected to cause pitting corrosion, it was thought that the pitting had occurred during storage prior to service use. However, Reference 13-11 has shown that stress corrosion cracking can occur in 7075-T651 when exposed to hydraulic fluids such as Aerosafe 2300W and Skydrol 500A. It was thought therefore that region I of the fracture surfaces of these cylinders was due to stress corrosion, and that this was the primary failure mode leading eventually to crack propagation by fatigue.

This problem may have been avoided if the inside surfaces of the cylinders had been protected during storage to prevent the initial pitting attack. However, to be safe a stress corrosion resistant material such as 7075-T73 should be used, subject to satisfactory static and fatigue design margins.

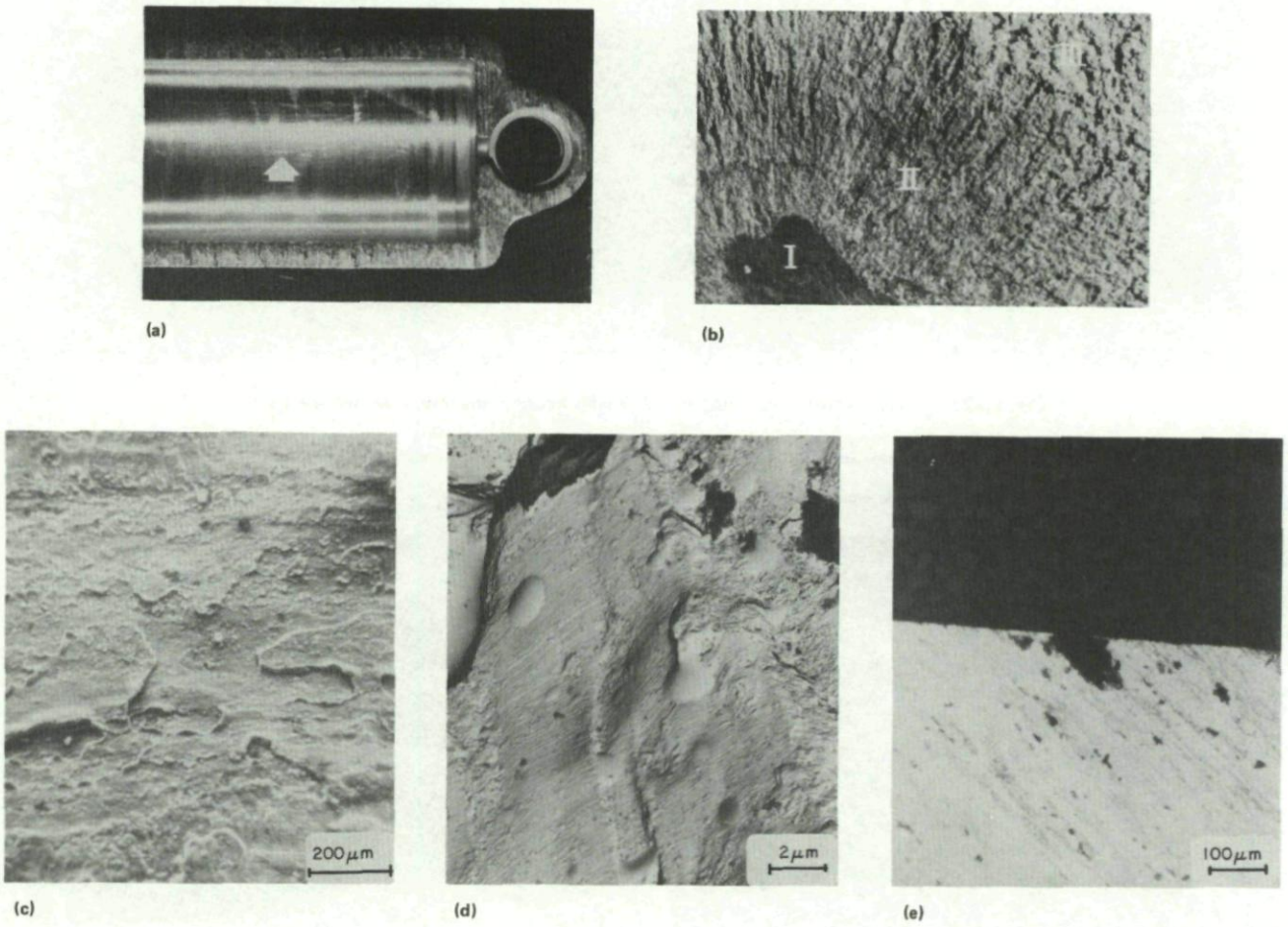

Fig. 13-31 Stress corrosion cracking of a 7075-T6 hydraulic cylinder, case history 13-5.

(a) Section through cylinder showing the location of cracks on the inside surface.
(b) View of the fracture surface showing three regions of cracking.
(c) Appearance of intergranular fracture in region I.
(d) Fatigue striations observed in region II.
(e) Cross-section through the inside surface showing corrosion pit.

Case history 13-6. Stress corrosion cracking in a 7075-T6 nose landing gear fork.

During a post-flight visual inspection of a fighter aircraft a long crack was found in the nose landing gear fork. The part is shown in Figure 13-32, and the crack which can be seen in this figure was found to lie in the parting plane of the aluminium alloy forging. The forging was made from 7075-T6 and its surfaces were treated with a single coat of wash primer plus two coats of acrylic paint.

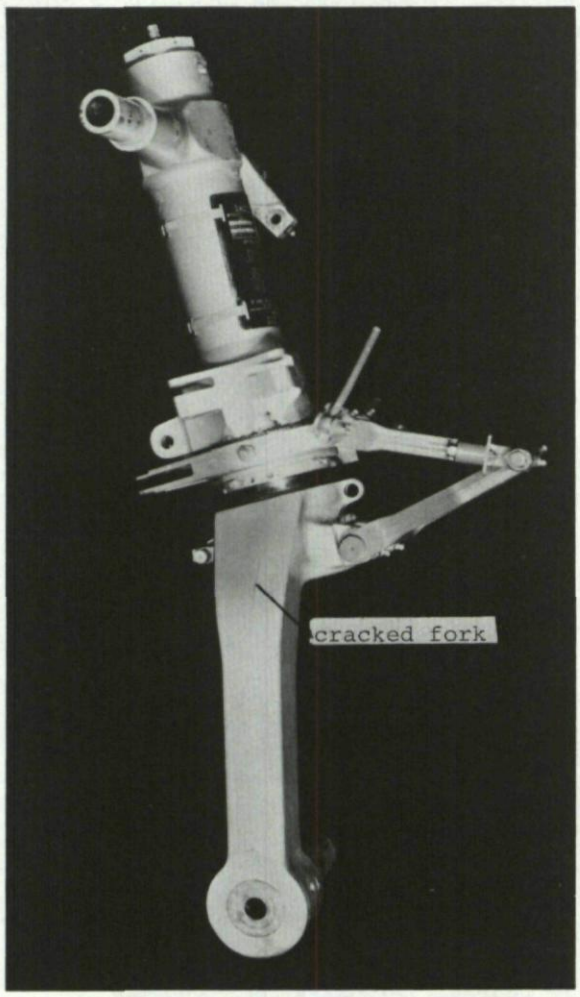

(a)

Fig. 13-32 Stress corrosion cracking in a 7075-T6 nose landing gear fork, case history 13-6.

(a) Complete landing gear assembly.
(b) Close-up of the fork outer surface showing the crack.
(c) Close-up of the fork inner surface showing the crack.

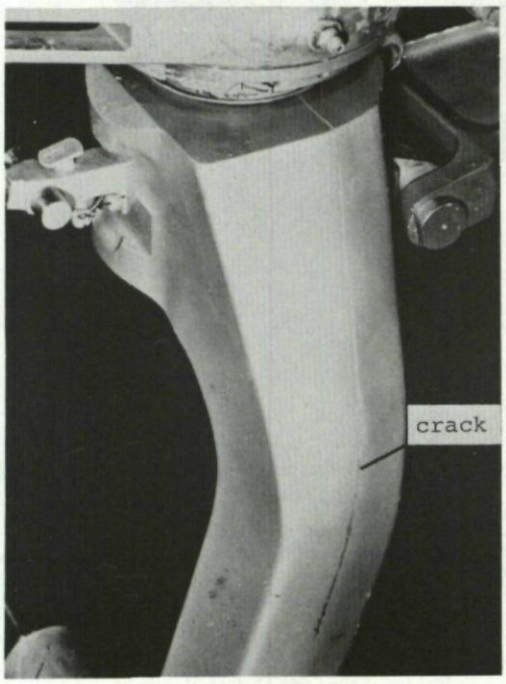

(b)

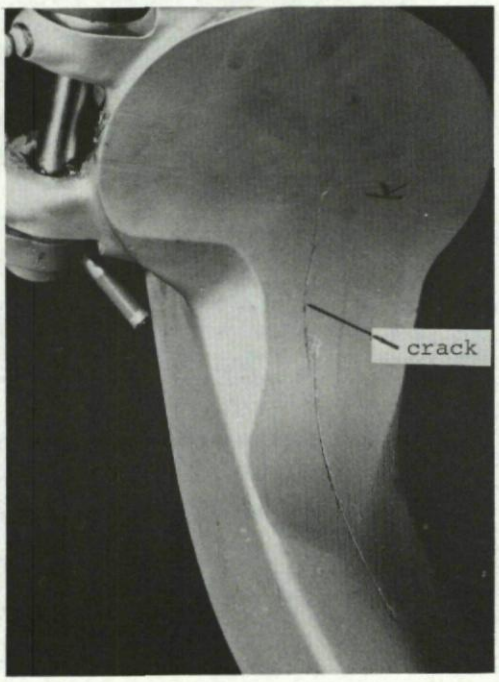

(c)

The crack was found to extend through the thickness of the fork, as indicated in Figures 13-32(b) and 13-32(c), and when the crack was opened up it was found to extend over about three quarters of the longitudinal cross section of the fork, as indicated in Figure 13-33. Figure 13-34(a) shows the fracture surface and reveals a dull fibrous fracture typical of stress corrosion cracking, where the crack appears to have started in the upper bore for the nose-landing gear leg attachment and the adjacent bore hole, which was introduced as a weight saving measure. However while the bores may have been effective in respect to weight savings, they provided natural traps for moisture. Figure 13-34(a) also reveals a narrow ribbon of material along both external surfaces which appear to have a lighter appearance than the area affected by SCC, and this suggests that the stress corrosion crack may have propagated over a substantial distance through the NLG-fork before breaking through to the external surfaces. Thus the crack may have been hidden for a substantial period of time prior to visual detection. Figure 13-34(b) shows a metallographic section through the crack tip and demonstrates quite clearly that the crack had propagated along grain boundaries, as expected for SCC in this type of alloy. The intergranular fracture mode was confirmed by scanning electron microscopy.

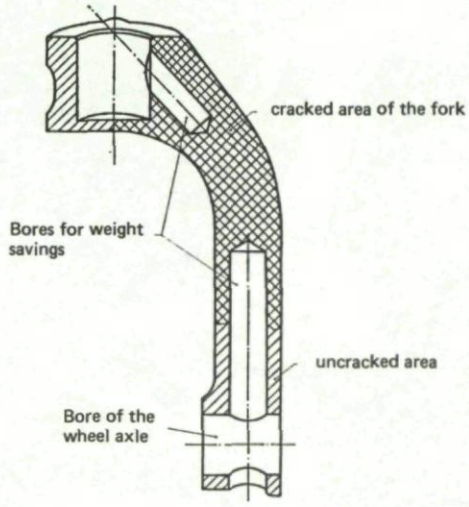

Fig. 13-33 Sketch of the cracked fork showing the area affected by stress corrosion cracking (double hatched area), case history 13-6.

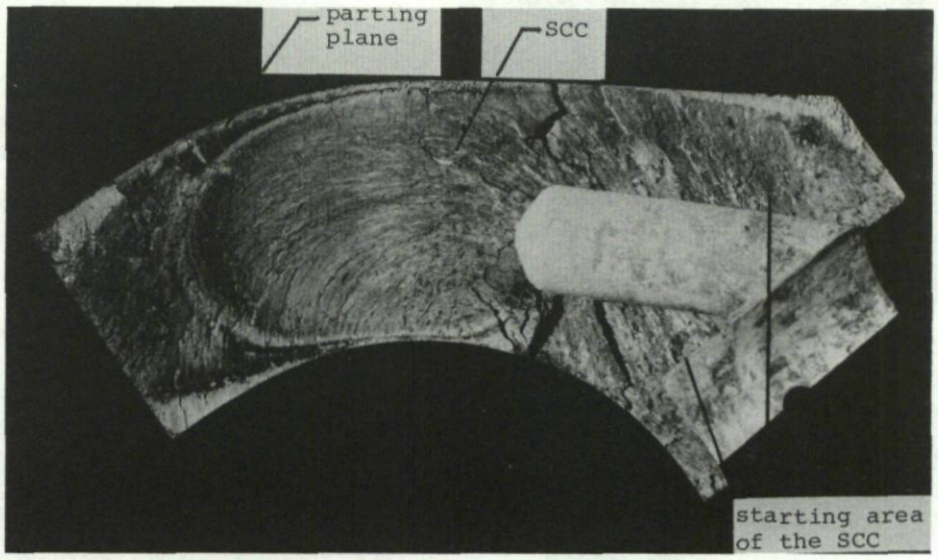

(a)

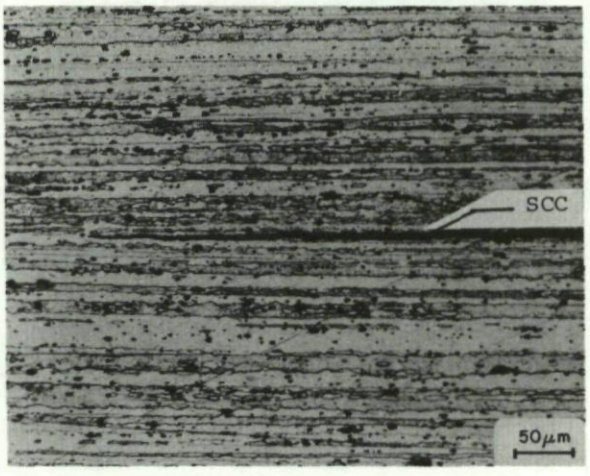

(b)

Fig. 13-34 Stress corrosion cracking in a 7075-T6 NLG fork, case history 13-6.

(a) Macroscopic view of the SC crack in the fork.
(b) Section through the tip of the crack showing the intergranular crack path.

It was concluded that cracking was due to stress corrosion and this was a consequence of the use of a stress corrosion susceptible alloy, exposure of end grain boundaries at the surfaces of internal bore holes, the entrapment of moisture in the bore holes, and the presence of internal stresses created by heat treatment.

The fact that the crack had propagated over a substantial distance by SCC without causing static or fatigue failure of the fork suggested that service induced stresses were not unduly high, and therefore the problem could be solved by resorting to the T73 temper. At the same time the corrosion protection system was improved by shot peening all surfaces, and by applying a chemical conversion coating (Alodine 1200) followed by a single coat of wash primer and two coats of epoxy paint.

Case history 13-7. Stress corrosion cracking of a 7075-T6 nose landing gear strut.

The nose landing gear strut of a fighter aircraft failed during a normal landing procedure after only 30 hours of flight had been accumulated. The failed part is shown in Figure 13-35, and closer examination of the fracture surfaces evident in the failed part revealed that pre-existing cracks had been present prior to the final failure. The fracture surfaces due to these pre-existing cracks are shown in Figure 13-36, and it can be seen that these had initiated at the corners of the bore holes used to locate the clamping attachment bolts for the retraction cylinder.

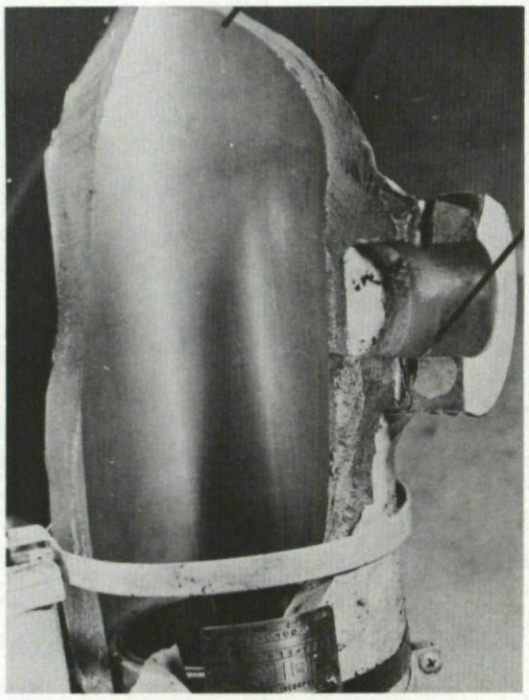

Fig. 13-35 Stress corrosion cracking in a 7075-T6 nose landing gear strut, case history 13-7.

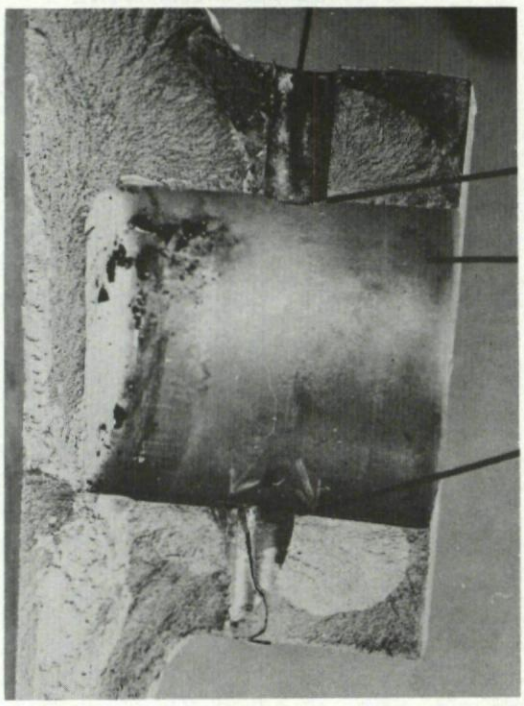

Fig. 13-36 Close-up of the stress corrosion crack initiation sites and the internal surface of the bore used to locate the retraction cylinder. Pitting can be seen at the base of this hole, case history 13-7.

The landing gear strut was made from a 7075-T6 die forging, and examination revealed that the initiating cracks had formed in the parting plane. The bore of the clamping attachment bolt was roll burnished on its cylindrical surface, and brush treated with sodium dichromate solution. An interference fit bushing had been installed, and the chamfer sealed with PR 1422 A2 sealant. In addition, an oversize bolt was wet installed with a zinc chromate primer and sealed again with PR 1422 A2.

Metallographic examinations showed that a series of cracks was present in the landing gear strut, lying in planes between the axis of the cylinder bore and the axis of the securing bolt hole (Fig. 13-37(a)). Figure 13-37(b) shows the tip of the longest crack of Figure 13-37(a), and this etched micrograph shows that the cracks follow the grain boundaries of the large pancake shaped grains. Some fine recrystallized grains lie around the perimeters of these larger grains.

The failure was a classical stress corrosion cracking problem and was influenced by the use of a susceptible material, the bored holes exposing end grain boundaries, assembly stresses due to interference fit bushings, and superimposed stress concentrations due to the intersecting bores. It was likely that high residual stresses were also present as a result of the T6 heat treatment.

A number of alternative designs were considered to resolve this problem including the use of one of the newer high strength, stress corrosion resistant forging alloys such as 7050-T73. However, it was decided to change to a high strength low alloy steel, AMS-6427 (0.3% C, 0.9% Cr, 0.2% Cu, 0.9% Mn, 0.42% Mo, 1.9% Ni) which provides higher strength together with good stress corrosion resistance. The design was also changed, replacing the clamping attachment bore with a forged steel pin, as indicated in Figure 13-38. The steel forging was protected by a vacuum deposited layer of cadmium plating followed by a layer of epoxy primer and a single coat of polyurethane paint.

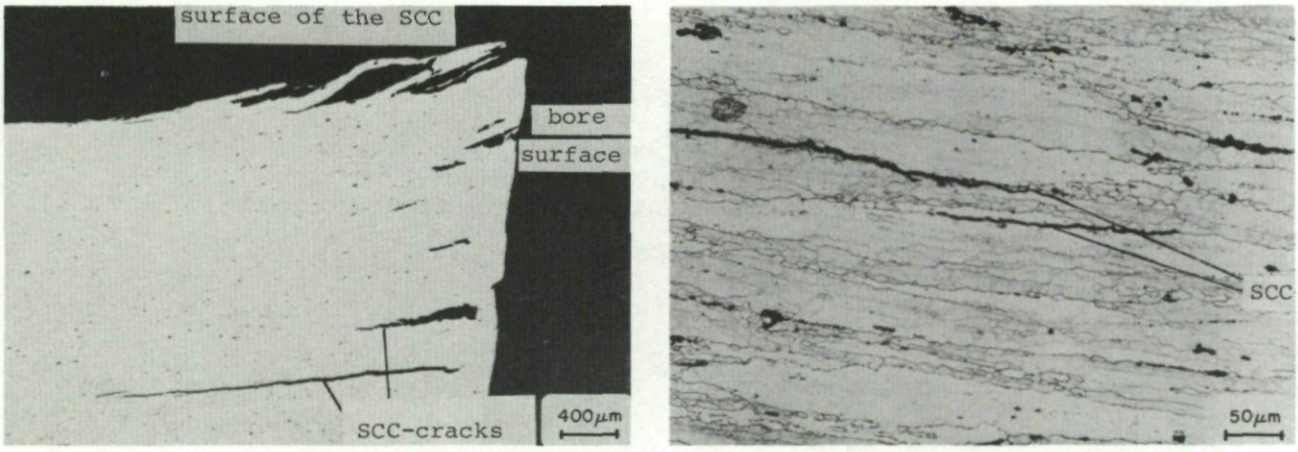

(a) (b)

Fig. 13-37 Cross sections through the nose landing gear strut adjacent to the retraction cylinder bore and bolt hole, case history 13-7.

(a) Showing multiple stress corrosion cracks.
(b) Shows the tip of the lower crack in (a) above and indicates that the crack path is intergranular.

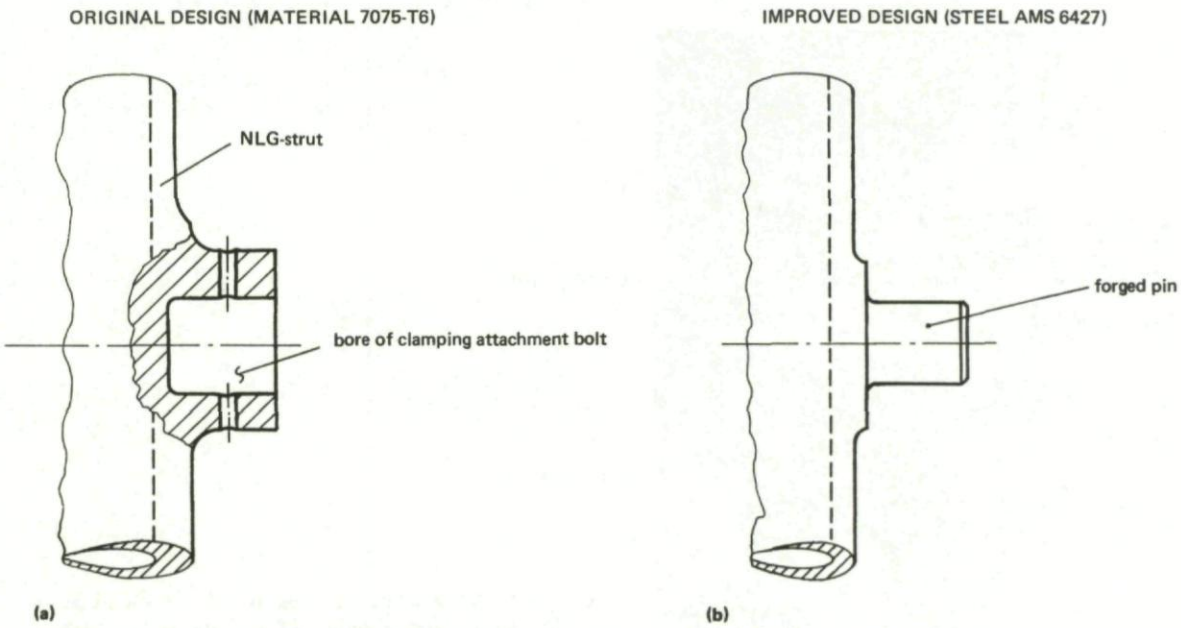

Fig. 13-38 Design details of the nose landing gear strut, case history 13-7.

(a) Original design.
(b) Modified design.

Case history 13-8. Stress corrosion cracking of a 7075-T6 fuselage frame flange.

A number of cracks was noticed in the fuselage frame of a fighter aircraft during a routine inspection. The cracks were observed to lie in line with a row of rivets in the upper flange as indicated in Figure 13-39. The rivets were removed and the presence of the cracks was confirmed using a magnifying lens and an eddy current fastener hole inspection device. Three cracks were found to run between adjacent fastener holes, linking adjacent holes, while three further cracks were found running away from fastener holes, but they had not yet reached the neighbouring holes. The locations of the cracks are indicated in Figure 13-39, and in all cases they were found to extend through the thickness of the flange.

A spectrographic analysis showed the alloy contained 3% Mg, 5.1% Zn, 1.8% Cu, 0.18% Cr and lesser amounts of Fe, Si and Mn. The alloy concentrations were consistent with specifications for 7075 and the alloy hardness indicated the material was in a T6 strength condition. A microstructural evaluation of the grain structure showed a heavily wrought structure of pancake shaped grains, where the crack plane was coincident with the plane containing the longitudinal-long transverse directions, and the short transverse direction was normal to the crack plane as indicated in Figure 13-40.

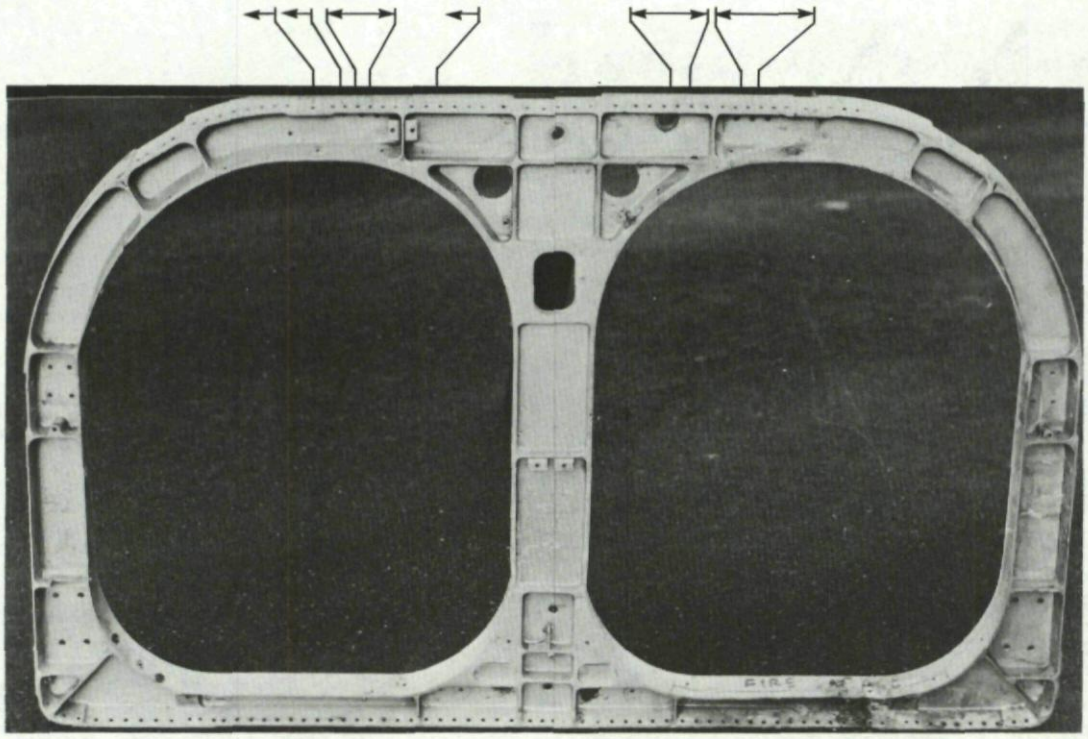

Fig. 13-39 Stress corrosion cracking in a 7075-T6 fuselage frame, case history 13-8. Arrows indicate the directions of cracking away from fastener holes.

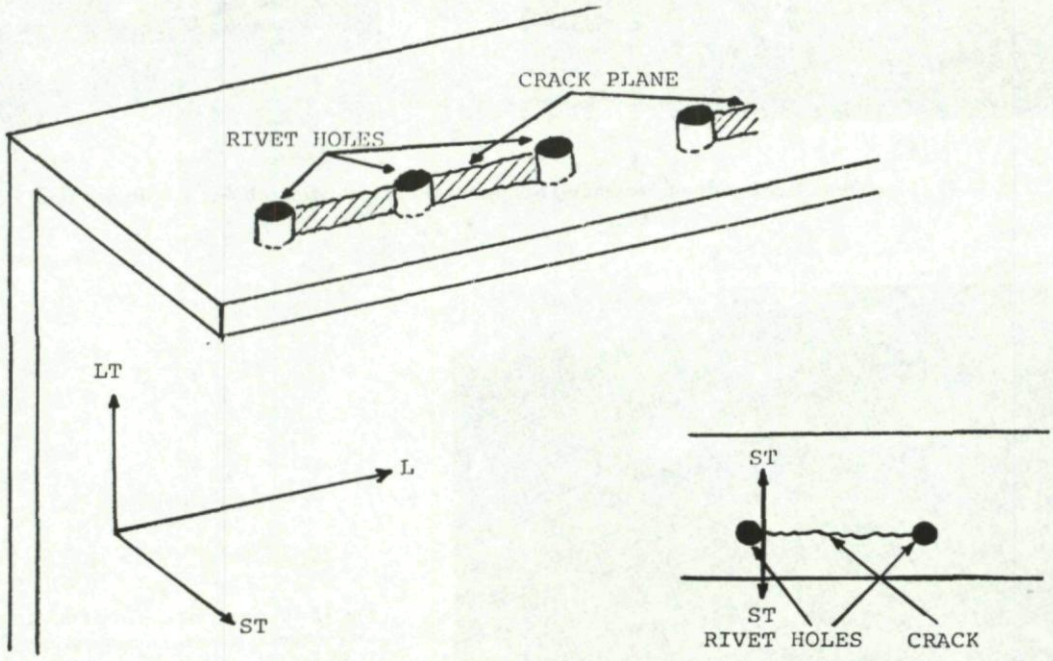

Fig. 13-40 Orientation of the crack plane with respect to the principal directions in the fuselage frame, case history 13-8.

Figure 13-41 shows a metallographic section normal to the LT direction and cracks can be seen running in the longitudinal direction along grain boundaries. The fracture surfaces were corroded, and in most cases they showed no recognizable feature other than flat grain boundary surface facets, as shown in Figures 13-42(a) and 13-42(b), and secondary cracking (Fig. 13-43). In a few cases striation like markings were present immediately adjacent to the fastener holes and in most cases the surfaces of the fastener holes contained corrosion pits. The failure analysis report made no mention of sealants or other forms of corrosion protection in the fastener holes and no information was given on the fastener materials used. However it was concluded that cracking was due to stress corrosion, initiating at corrosion pits in the bore of the fastener holes. The stresses were believed to be due to assembly and operating loads and a stress analysis showed that stresses in the ST direction in the region of the fastener holes were in excess of the threshold values for stress corrosion cracking given in Reference 13-1, Table 13-1.

It was recommended to replace these fuselage frames with 7075-T73 to prevent SCC. However, since there was evidence of fatigue in some areas and since threshold stress intensities for fatigue in 7075-T73 are slightly lower than for 7075-T6 it might be preferable to replace this alloy completely with a higher strength stress corrosion resistant alloy such as 7050-T73. Wet assembly of fasteners should also assist by excluding moisture from the fastener holes.

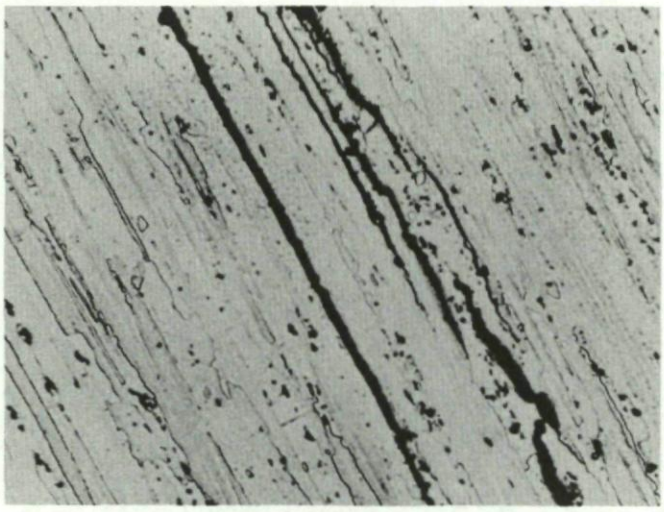

Fig. 13-41 Metallographic section indicating the intergranular crack path in the fuselage frame, case history 13-8.

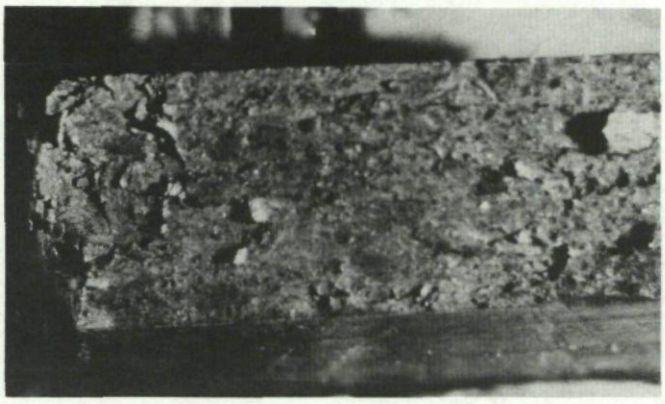

(a)

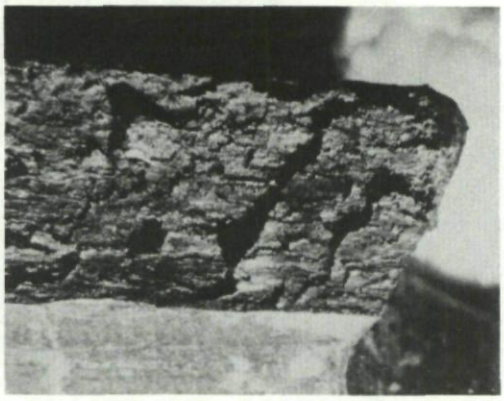

(b)

Fig. 13-42 Fracture surface topography extending between two adjacent fastener holes, case history 13-8.

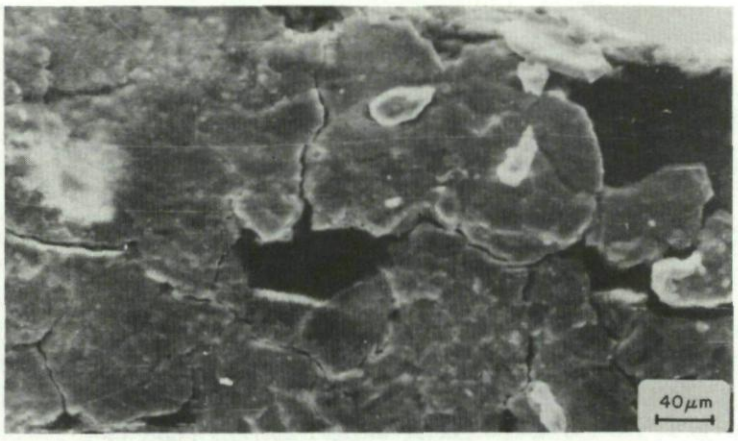

Fig. 13-43 Scanning electron micrograph of a fracture surface from case history 13-8, showing secondary intergranular cracking.

Case history 13-9. Failure of a 2014 aluminium alloy nose wheel steering damper.

During a visual inspection of a fighter aircraft, a crack was found in the body of the nose wheel steering damper. The component is shown in Figure 13-44(a), where the location of the crack on the outside body is indicated by the arrow. The protective coating and metal in the region of the crack had been scraped away prior to delivery to the laboratory for examination, and a number of impact marks were noticed in this region. A section perpendicular to the crack front was prepared for metallographic examination, and this showed that the crack had propagated over two-thirds of the way through the thickness of the part, which was identified as being 2014 aluminium alloy. The crack was intergranular in nature over most of its length, as indicated in Figure 13-44(c), and it had propagated at about 45° to the external surface following the grain flow in the component. Figure 13-44(d) shows the crack path at higher magnification and reveals both intergranular facets, indicated by solid arrows, and transgranular facets, indicated by open arrows. The remainder of the crack was opened up for examination and the fracture surface exhibited a flat brittle appearance (Fig. 13-44(e)), although the finer features of the fracture surface were obliterated by heavy corrosion.

It was concluded that stress corrosion was the most probable cause of failure, and as noted in Section 13-5, 2014 aluminium is one of the most susceptible 2000 series alloys to SCC in the T4 or T6 conditions. It was impossible to determine how, or where the crack had initiated since the initiation site had been obliterated. However the tool marks visible near the crack indicate that the protective surface anodizing had been removed in these areas, exposing end grains to the corrosive environment. The service operating stresses in this part were not unduly high, and it is likely that residual stresses contributed to the SCC process. Also the surface indentations would have created a stress concentration effect and it is possible that the SCC cracks initiated at these locations.

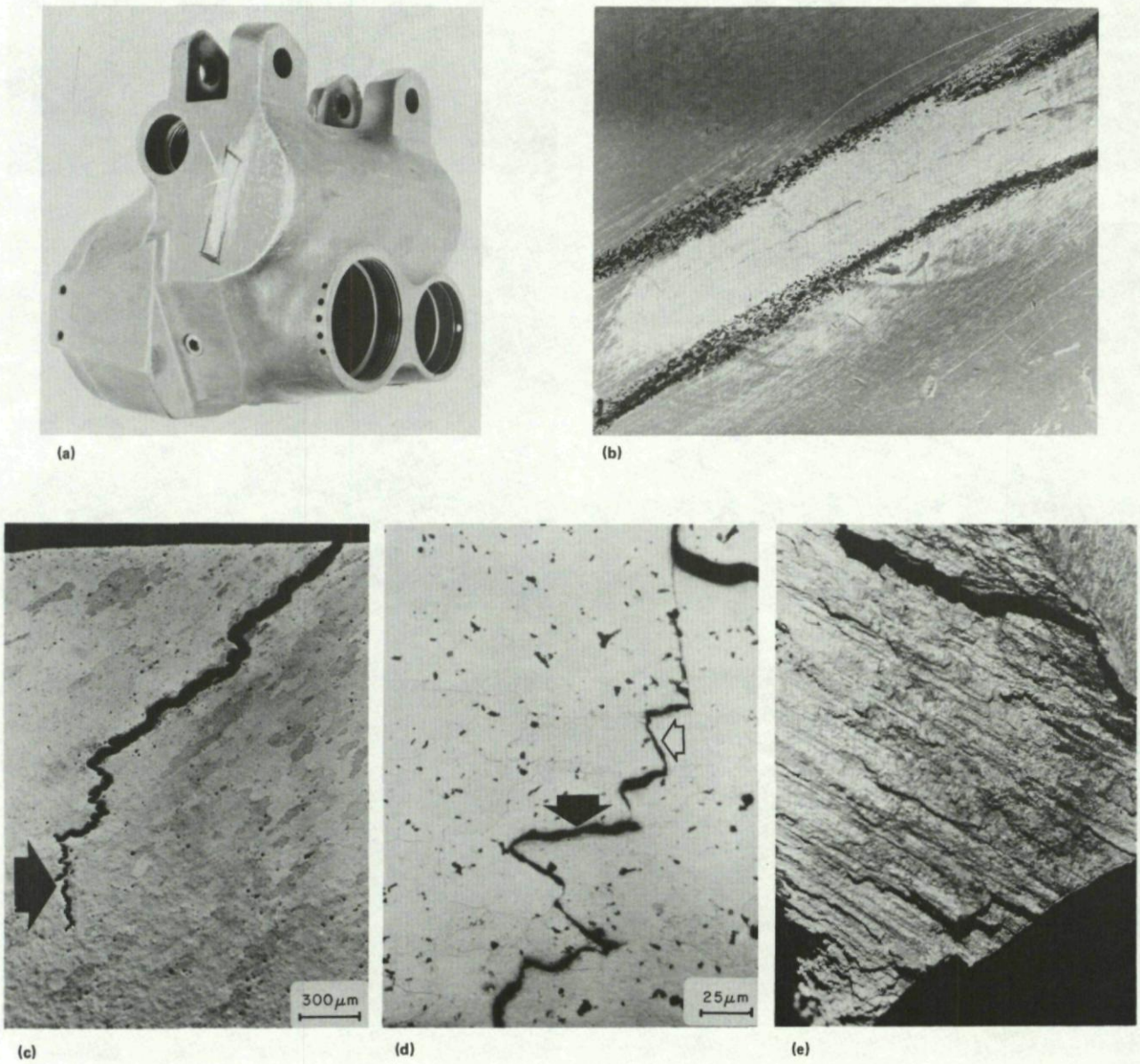

Fig. 13-44 Cracking in a 2014 aluminium nose wheel steering damper, case history 13-9.

(a) Arrow indicates the location of cracking.
(b) Close-up of the surface crack.
(c) Microstructure near the surface of the part showing the grain structure and crack path. Arrow indicates location of Figure 13-44(d).
(d) Crack path showing intergranular facets (solid arrows) and transgranular facets (open arrows).
(e) Fracture surface topography.

Case history 13-10. Corrosion induced failure of an aluminium-copper alloy main landing gear part.

A landing gear forging of an aircraft, Figures 13-45(a) and 13-45(b) failed during ground operations. The crack initiated on an interior surface at the junction of an axial bore and a radial bore, Figures 13-45(c) and 13-45(d). The fracture surface to the right of the radial bore, see Figure 13-45(c), contained a dark corroded area, which had propagated to a considerable length as indicated by the open arrows. This was surrounded by a light, non-corroded, overload region which formed a narrow band between the dark corroded region and the outer surface of the part. This indicates that the growing crack had not broken through to the outside until the final overload failure had occurred, and therefore the pre-crack had remained hidden until this final failure. The presence of the narrow band of overload fracture suggests that growth of the pre-crack had been suppressed by compressive residual stresses in the surface layers, which presumably did not exist, or had been removed by machining on the interior surfaces. Figures 13-45(c) and 13-45(d) show that severe corrosion and pitting occurred on the interior surface of the radial bore, and deep corrosion pits were present in the crack initiation regions.

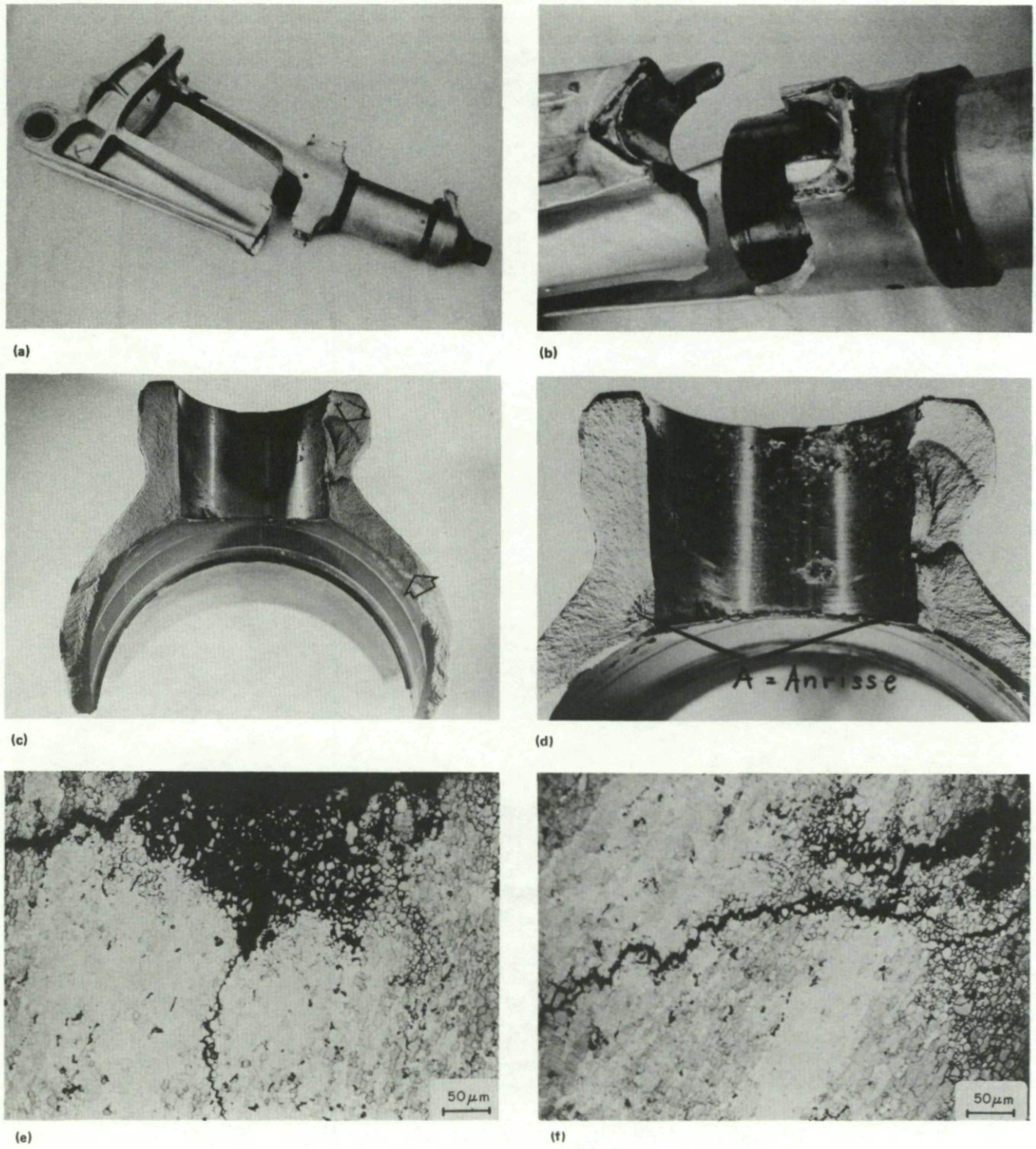

Fig. 13-45 Failure of an Al-Cu main landing gear part, case history 13-10.

(a) Fracture component.
(b) Close-up of the fracture area.
(c) Arrows indicate the extent of corrosion induced cracking.
(d) Crack initiation sites at the junction of the axial and radial bores.
(e) Sub-surface intergranular cracking adjacent to the radial bore.
(f) Sub-surface intergranular cracking adjacent to the axial bore.

The component was made from an AlCuSiMn alloy, conforming to the German specification WLB 3.1254. This alloy contains about 4.3% Cu, and is similar to 2017 aluminium. Metallographic examination showed that the material had a very fine recrystallized grain structure, with a grain size of about 10-20 μm. Cross sections prepared through the component adjacent to the radial and axial bores showed severe intergranular corrosion immediately adjacent to the machined internal surfaces as shown in Figures 13-45(e) and 13-45(f) respectively. In both figures long cracks can be seen growing out of the regions of intergranular cracking to penetrate deeply into the wall thickness. These cracks resemble stress corrosion cracks, propagating intergranularly and exhibiting signs of crack branching.

It was concluded that the failure occurred by stress corrosion cracking and this produced the dark pre-crack shown in Figures 13-45(c) and 13-45(d). Although the strength of the alloy was not given in this failure report, it is known that alloys of this type are sensitive to intergranular corrosion and stress corrosion cracking, particularly when heat treatment leads to the formation of solute-depleted regions adjacent to grain boundaries which are anodic with respect to the grain boundaries and grain interiors. Little specific data appears to be available on 2017 aluminium, but Reference 13-45 indicates that stress corrosion service failures can be expected in 2017-T4 or 2017-T451 when sustained tensile stress acts in the short transverse direction relative to the grain structure. In this particular component there was very little directionality in grain structure, but as indicated in Section 13-5 equiaxed structures of the type observed might represent a worst-case condition with respect to SCC.

Case history 13-11. Stress corrosion cracking of an AZ-91C-T6 brake housing.

Magnesium alloys are not usually associated with SCC, however it can occur in alloys containing more than 2.5% aluminium, and where the sustained stress is more than about 90% of the yield strength. Alloys AZ81 and AZ91 fall in the susceptible category since they contain about 7.6% Al and 8.6% Al respectively, and although their ultimate tensile strengths are in the 275 MPa range their yield strengths are only about 83 and 195 MPa respectively.

The brake housing castings of a popular light aircraft were frequently being found cracked and leaking at the brake line union, leading to brake failure. A typical cracked casting is shown in Figure 13-46(a).

On breaking open the crack in the laboratory it was found that the crack had grown only as far as the line union had been threaded into the casting (Fig. 13-46(b)). The required driving stress was the hoop stress caused by a tight fitting union. The crack stopped growing when it reached a zone where the local hoop stress fell below the threshold required for stress corrosion cracking. It was thought that as the crack leaked fluid, the operator had tightened the union further, thus raising the local hoop stress and causing the crack to propagate further.

The problem was solved by increasing the section thickness in the casting around the brake line union so that the hoop stress caused by insertion of the union was lowered below the SCC threshold stress, and hence SCC could not occur.

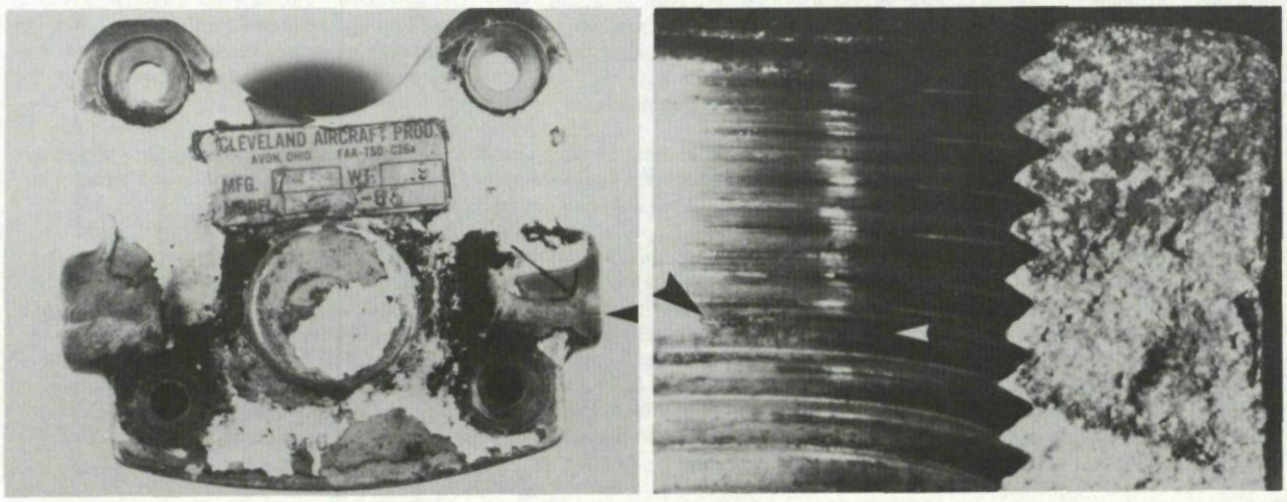

(a) (b)

Fig. 13-46 Stress corrosion cracking of a magnesium alloy brake housing, case history 13-11.

(a) General view of the as-received brake cylinder housing, indicating location of crack (arrow).
(b) Fracture surface and internal thread. Bright area of fracture is overload region. Note dark area of fracture stops at same depth as union (see Loctite remains and chip arrowed in thread root).

Case history 13-12. Transgranular stress corrosion cracking of an AZ-91C magnesium alloy nose-wheel.

A magnesium alloy nose-wheel of a fighter aircraft failed and caused a tire blow-out. The wheel was produced as a casting using the MgAlZn alloy, AZ-91C, and this failed through the formation of a major crack in the fillet between the flange and the rim. This crack had caused the flange to be partly torn from the wheel body, as shown in Figure 13-47(a). Visual inspection revealed corrosion pits and small cracks in the fillet between the flange and the rim at the surface of contact with the tire-bead. The fractographic investigation failed to reveal any indications of fatigue or intergranular failure. The fracture surfaces were dirty and severely damaged, and the only recognizable features were lamellar components of the microstructure protruding from the fracture surface at various angles, as indicated in Figure 13-47(b).

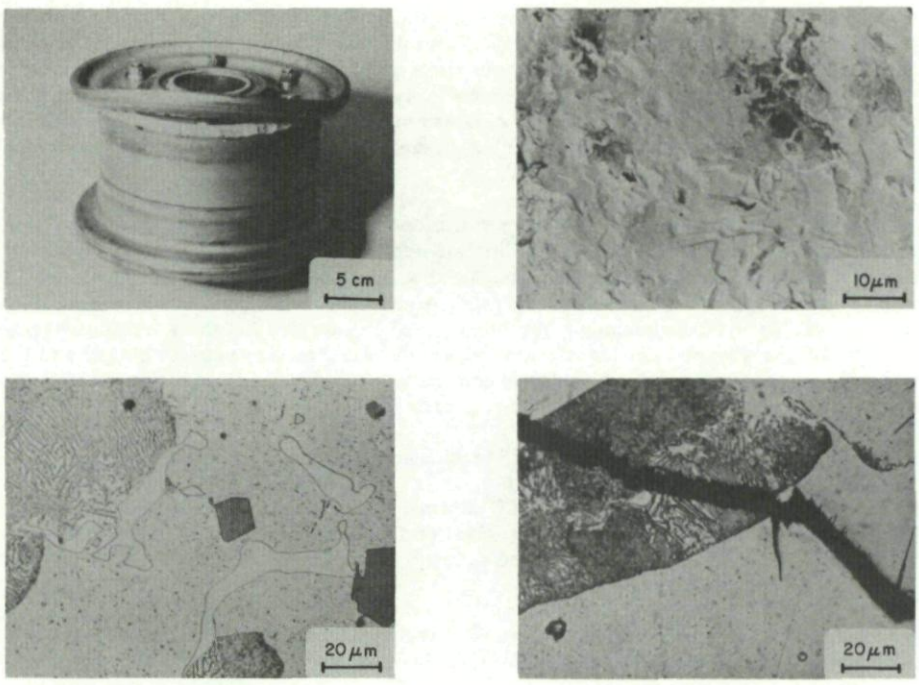

Fig. 13-47 Stress corrosion cracking of a magnesium alloy nose wheel, case history 13-12.

(a) Fractured wheel.
(b) Fracture surface topography.
(c) Microstructural constituents.
(d) Section through a crack showing transgranular propagation.

A microstructural examination of the alloy revealed a magnesium alloy matrix containing various precipitated phases. These included: (a) pools of eutectic containing lamellar particles of the compound Mg_3Al_2, (b) coarse white particles containing zinc which may have been $Mg_3Al_2Zn_3$ or $MgZn_2$, and (c) grey angular particles of a manganese bearing compound MgMnAl or Al_4Mn. These constituents can be seen in Figure 13-47(c). Figure 13-47(d) shows a crack cutting through a patch of lamellar eutectic and propagating transgranularly through the magnesium solid solution matrix. Some secondary cracking can be seen propagating out of the main crack, and this appears to be following specific crystallographic planes.

The fact the corrosion pits were clearly visible in the region of crack initiation suggested that corrosion may have played an important role both in the initiation and crack propagation processes, and since propagation was largely transgranular and sensitive to grain orientation it was felt that stress corrosion cracking was a possible cause of fracture.

Magnesium alloys are known to exhibit both intergranular and transgranular stress corrosion cracking, and intergranular cracking is often associated with heavy grain boundary precipitation. Transgranular cracking is the more usual form of SCC in magnesium alloys, and this is believed to be influenced by the precipitation of iron and aluminium compounds on the basal planes of the hexagonal grain structure. It is also known that the corrosion resistance of magnesium alloys is extremely sensitive to the presence of impurities such as iron, nickel and copper, and that their effect becomes marked above a critical concentration known as the tolerance limit (Ref. 13-52). For iron the tolerance limit is about 0.017%, while for copper and nickel the tolerance limits are about 0.1% and 0.0005% respectively. A chemical analysis of this particular magnesium alloy indicated iron and copper contents each of 0.02%. The iron content was therefore above the tolerance limit and this might be expected to cause the alloy to be susceptible to general corrosion and to transgranular stress corrosion cracking.

No information was given in this report on the corrosion protection system employed, however as noted in Chapter 6, it is most important to isolate magnesium alloys from the environment by providing a fully protective envelope. It is also important to use primers with a very high chromate content and appropriate leaching characteristics to maintain a high concentration of inhibitor at any exposed metal surface.

Case history 13-13. Stress corrosion induced failure of an alloy steel undercarriage hinge pivot.

A large commercial turboprop aircraft suffered collapse of its left main undercarriage shortly after touchdown while landing. The aircraft settled onto the left wingtip, slewed off the runway and was extensively damaged by the subsequent fire. It was found that the right hand trunnion shaft, which acts as the hinge pivot for the gear assembly, had fractured as indicated in Figures 13-48(a) and 13-48(b).

Fractographic analysis of the shaft fracture surface (Fig. 13-48(c)), showed that about 90% of the cross-section had cracked progressively. Crack initiation had occurred in the region of the white arrow, marked 'a,b,c' in Figure 13-48(c), and stable slow crack propagation had occurred across the fracture surface to the location marked 'f', except for a band of overload rupture at 'g'. This overload band extended across the diameter of the shaft and consisted of mixed cleavage and ductile dimpling. It was ascribed to a previous heavy landing. The bulk of the fracture surface, including areas marked 'a, b, c, d, h and f' in Figure 13-48(c), exhibited well defined intergranular facets as indicated in Figure 13-48(d). The final overload rupture occurred as the crack reached the location marked 'e' in Figure 13-48(c).

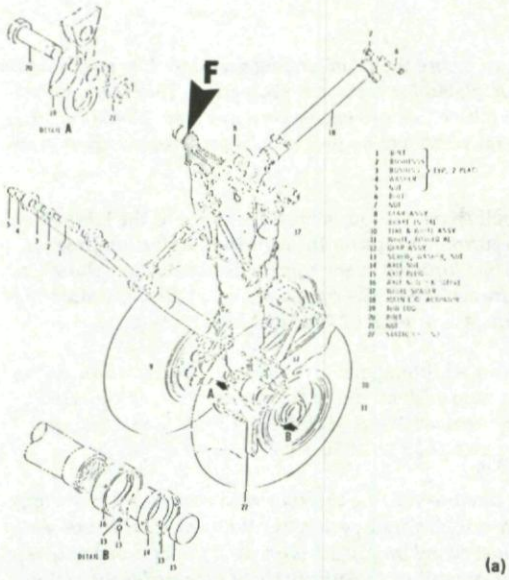

(a)

(b)

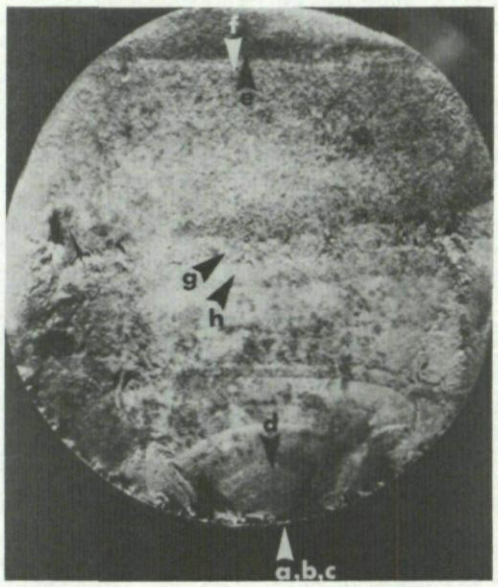

(c)

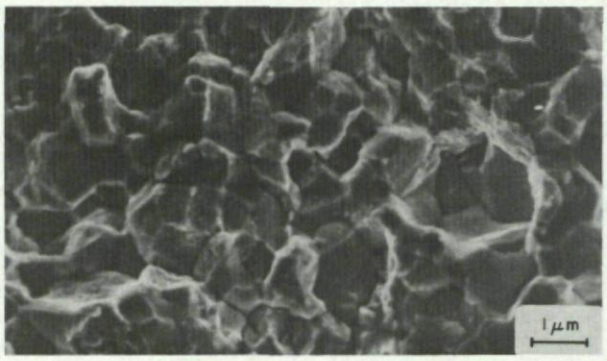

(d)

(e)

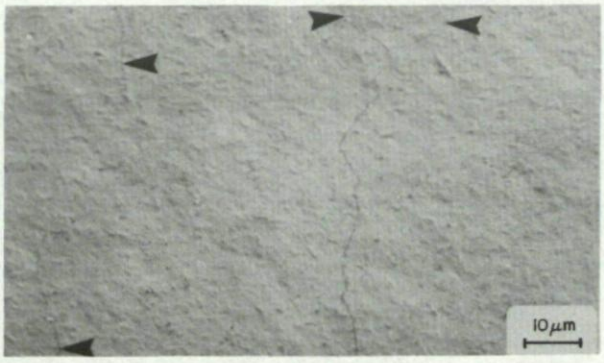

(f)

Fig. 13-48 Environmentally enhanced fracture of a steel landing *gear trunnion, case history 13-13.*

(a) MLG assembly showing trunnion failure location F.
(b) Fractured right hand trunnion arm shaft, and unfailed left hand trunnion.
(c) Fracture surface showing origin at a, b, c.
(d) Intergranular fracture as observed at sites a, b, c, d, h and f.
(e) Axial section near fracture shows cracking under chromium plating.
(f) Surface of shaft after stripping of plating, showing circumferential grinding cracks (arrowed).

The presence of intergranular fracture and the clear evidence of stable slow crack propagation led to the view that an environmentally enhanced fracture process was involved. Stress corrosion was suspected, although it was found that the threshold stress level for stress corrosion cracking in this particular steel was 620 MPa while the design maximum surface tensile stress was 276 MPa. Further investigation showed that crack initiation was due to the presence of surface grinding cracks, which were produced on the shaft during rework to repair prior corrosion damage. These pre-cracks were hidden by the subsequent hard chromium plating used to rebuild the shaft to size, but they were revealed by post-fracture sectioning, as indicated in Figure 13-48(e), and later confirmed by stripping the plating and viewing the original steel surface as indicated in Figure 13-48(f).

The conditions for stress corrosion cracking were not met unless the grinding cracks were present under the chromium plating, since although the steel was known to be susceptible to SCC, and the natural crack network in the chromium plating would allow a corrosive medium to reach the steel, normal stresses were far below the threshold level for SCC. However the stress concentration effect of the pre-existing grinding cracks provided the necessary stress levels at the crack tips to cause crack propagation to occur. The authorized rework procedure required post-grinding inspection for such cracks, this was not performed in this particular case. This failure would have been avoided had the authorized overhaul procedure been strictly followed.

Case history 13-14. Stress corrosion cracking of a 4335 steel bolt.

Steel bolts fabricated from 4335V modified low alloy steel were used to secure the main landing gear door hinge on a fighter aircraft. The bolts were heat treated to a hardness of R_c 46-48 and were cadmium plated for corrosion protection. They were made with an interconnecting hole in the top and on the side for hinge lubrication, and these features can be seen in Figure 13-49(a) and Figure 13-49(b), which show a failed bolt. The bolts had been in service for several years, and no previous failures had occurred prior to the failure of the one shown in Figure 13-49.

Optical examination showed that corrosion pits were present on the bolt shank and on the inside surface of the lubrication hole, as indicated in Figure 13-49(a) and Figure 13-49(c). The fracture had occurred on a plane through the lubrication hole, as indicated in these figures. Further fractographic analysis showed that the failure had initiated at the upper edge of the hole shown in Figure 13-49(c), and had progressed in a counter-clockwise direction. The fracture surface on the opposite side of the lubrication hole exhibited a rougher, more fibrous fracture appearance, and appeared to have formed as a result of final overload rupture.

Scanning electron fractographic examination of the failed bolt revealed an intergranular fracture in the initiation region (region 1 in Figure 13-49(c)), and both secondary cracking and corrosion pitting were evident on the fracture surface, as indicated in Figure 13-49(d). Chemical analysis of the steel showed that it satisfied the requirements AMS 6428B, for 4335V mod. steel, and hardness was in the specified range indicating an ultimate tensile strength in the range 1517 to 1655 MPa.

The presence of corrosion pits in the crack initiation area, and on the fracture surface, together with intergranular cracking suggested an environmentally enhanced fracture process, and a stress corrosion cracking/hydrogen embrittlement mechanism was considered. Hydrogen embrittlement might have occurred as a result of the original cadmium plating process, if the bolt had not been adequately baked after plating. However it was felt that failure would then have occurred in a relatively short time under the action of sustained tensile stresses in service. However, as noted previously, the bolt had performed satisfactorily for several years. It was concluded therefore that stress corrosion cracking was the most probable cause of cracking, where sustained service stresses and the corrosive nature of the operating environment contributed to failure by a process possibly involving hydrogen evolution, embrittlement of the steel and cracking.

Since this bolt was one of several that had been in service for a long period of time, it was considered likely that the remaining bolts may also be affected by corrosion. All of the hinge bolts were removed and replaced with new bolts protected with a low embrittlement cadmium plating. However, since service induced corrosion was the major source of damage, as opposed to plating induced embrittlement, a program of regular inspections was implemented.

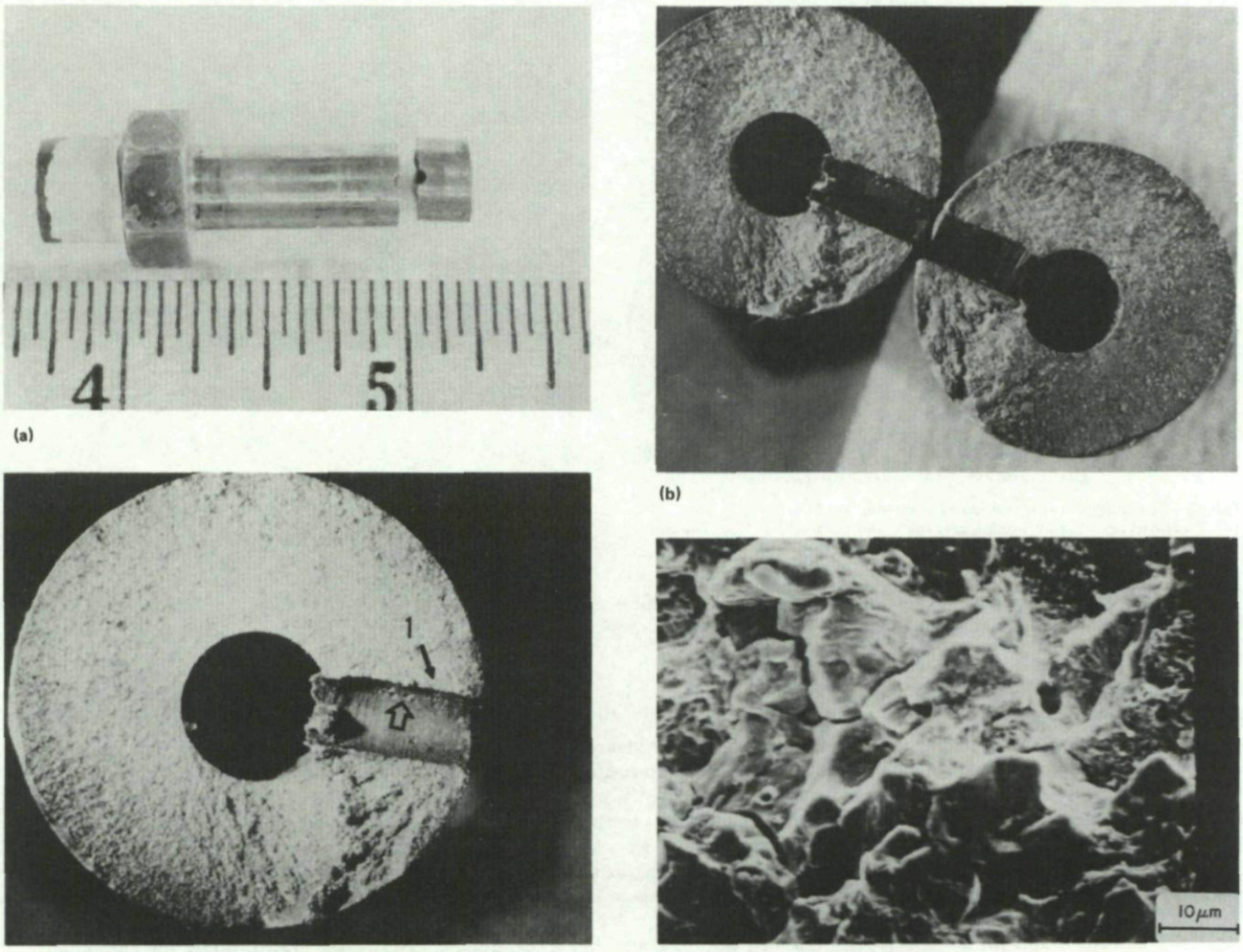

(a) (b) (c) (d)

Fig. 13-49 Corrosion induced fracture of a 4335V steel bolt, case history 13-14.

(a) Cracked MLG hinge bolt.
(b) Mating fracture surfaces showing flat fracture.
(c) Corrosion pits in the lubricating hole.
(d) Intergranular fracture observed in the initiation region (area 1 in Fig. 13-49(c)).

Case history 13-15. Failure of an 18-Ni maraging steel pressure vessel.

A pressurized cylinder containing helium at 55 MPa ruptured and fragmented while in storage. The cylinder was made from 18-Ni maraging steel with a hardness of R_c-43, and a minimum yield strength of 1420 MPa. It was part of the auxiliary power unit of a missile, and was designed to leak and not fragment when subjected to over-pressure.

Visual examination of the cylinder inner wall showed numerous cracks running along the length of the cylinder, and there was no evidence of deformation associated with the crack sites, as indicated in Figure 13-50(a). Further examination of the open fracture faces showed that crack initiation had occurred on the inner surface of the cylinder, and indicated that before final overload fracture occurred the crack fronts were establishing a stable, slow crack growth configuration. The cracks had propagated through about 80% of the wall thickness before final overload rupture occurred, as indicated in Figure 13-50(b). In this figure, the symbols 'A', 'B' and 'C' indicate the overload fracture region, the region of slow crack growth, and the initiation region respectively.

Fractographic examination showed that the fracture mode in the initiation region and the region of slow crack growth was intergranular, and heavy corrosion products partly obscured the grain facets in the initiation region. Figure 13-50(c) shows the fracture topography in region B, while Figure 13-50(d) shows the transition zone between the region of slow crack growth (B) and the overload region A. This latter region showed ductile dimples, characteristic of overload rupture. Metallographic cross-sections through the wall of the cylinder showed extensive intergranular cracking with multiple crack paths, as indicated in Figure 13-50(e).

The presence of corrosion products and intergranular fracture in the region of slow crack growth suggested that an environmentally induced fracture mode was operating. The inner surface of the cylinder was found to be covered by a thin film of oil which was analysed and found to be an established hydraulic fluid. Because of the small amount of oil available for analysis it was not possible to determine whether any contaminants were present that might cause corrosion. However, as noted in Section 13-6, it is known that many light oils and hydraulic fluids contain small amounts of water which are sufficient to cause stress corrosion cracking in some susceptible alloys. No other source of corrosion was identified, and in the absence of alternative explanations the failure was attributed to stress corrosion cracking.

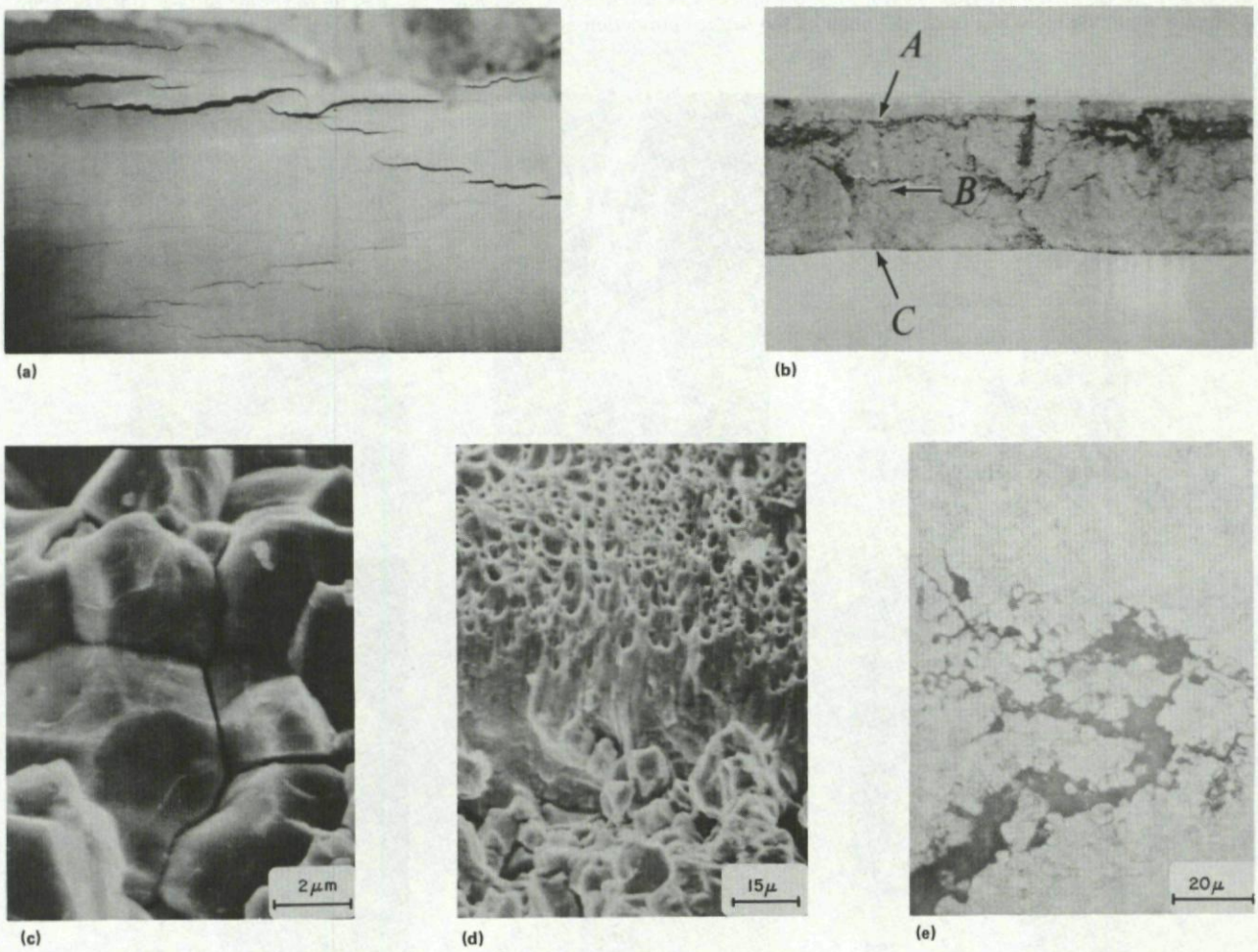

Fig. 13-50 Failure of a 18-Ni maraging steel pressure vessel, case history 13-15.

(a) View of the cylinder inner surface showing longitudinal cracks.
(b) Macrograph of a fracture surface showing inner wall (C), region of stable crack growth (B), and overload region (A).
(c) Intergranular fracture in region B.
(d) Transition from intergranular to transgranular dimpled fracture, region B→A.
(e) Metallographic section across wall showing extensive intergranular attack.

Case history 13-16. Failure of some 4340 main landing gear retraction cylinders.

Over a short period of time four retraction cylinders from the main landing gear of a fleet of fighter aircraft suffered failures. Two cylinders failed at the peripheries of the down-lock lugs, and two others failed at the boundary between the cylinder and the rod end. Figure 13-51(a) shows the appearance of these extreme ends of the cylinder.

The first cylinder failed at the peripheries of the down-lock lugs, and a portion of the fracture surface is shown in Figure 13-51(b). It was noted that the failure had been initiated by a shallow crack growing inward from the undercut at the transition from lug to cylinder wall. Initiation is seen as a bright ledge indicated by an arrow in Figure 13-51(b). Study of replicas of the fracture surface with the electron microscope revealed many dimpled areas associated with ductile rupture, but also intergranular failure, which indicated that the failure had been initiated by either stress corrosion or hydrogen embrittlement.

The second cylinder, which came from the same aircraft as the first cylinder, contained cracks in the periphery of the down-lock lugs (Fig. 13-51(c)). Some metallographic specimens featuring the undercuts at the edges of the down-lock lugs were prepared. In one of them an intergranular crack was found running at an angle to the surface of the main crack. Figure 13-51(d) shows a detail of this crack and reveals its intergranular nature. The cylinder failed, however, at the boundary between cylinder and rod end. At this location the cylinders were weakened by a circumferential groove in the inner surface. Figure 13-51(e) shows a part of the fracture surface where a flat plateau exists and which appeared to contain the initiation site on the inside surface of the cylinder.

The third cylinder had failed in the undercut at the periphery of the down-lock lugs. Again a ledge was found at the edge of one of the lugs, similar to that shown in Figure 13-51(b).

The fourth cylinder failed in the boundary between the cylinder and the rod end, and again the fracture surface contained a circumferential ledge which indicated that the fracture had initiated at the inner surface in the groove described previously. The location of the ledge is indicated by the arrows in Figure 13-51(f). Electron fractography showed that the fracture surface in this region was predominantly intergranular.

The topography of the fracture surfaces and the nature of the cracks found in metallographic specimens provided clear evidence that cracking was due to a stress corrosion or hydrogen embrittlement mechanism. Two of the four cylinders failed as a result of cracks initiated on the external surface, while the other two failed due to cracks which initiated on the inside surface. Unfortunately no information was given in this investigation of the surface protection systems used on the external and internal surfaces of the

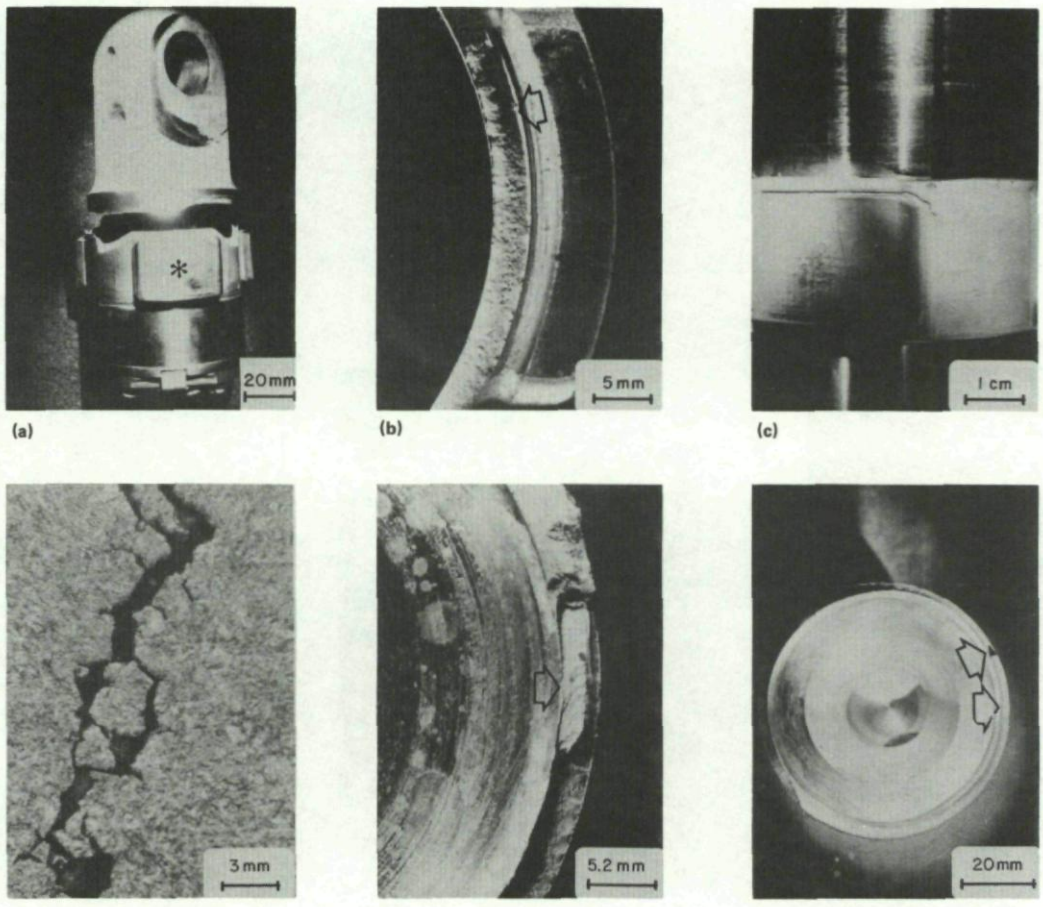

Fig. 13-51 Corrosion induced failure of four 4340 landing gear retraction cylinders, case history 13-16.

(a) Extreme ends of cylinder, asterisk (*) indicates down lock lugs.
(b) Fracture surface of first cylinder, indicating initiation zone, (arrow).
(c) Cracking at the periphery of the down-lock lug in cylinder No. 2.
(d) Intergranular cracking in cylinder No. 2.
(e) Crack initiation region on the inside surface of cylinder No. 2.
(f) Crack initiation region on the inside surface of cylinder No. 4.

cylinder, or on the type of hydraulic fluid contained inside the cylinder. However it is reasonable to assume that damage to external coatings would lead to exposure of bare metal to water or salt spray, which would cause stress corrosion cracking in 4340 steel. It is also possible that the inner surface was left bare on the assumption that corrosive attack would not occur in the presence of hydraulic fluids. Very little information is available in the literature on stress corrosion cracking of steels in organic liquids, but Reference 13-42 provides examples of SCC of 4340 in methanol, acetone, butyl alcohol and carbon tetrafluoride. In some cases traces of water and hydrochloric acid in the organic liquids were suspected to be the damaging species. Reference 13-11 has pointed out that hydraulic fluids usually contain sufficient water to cause SCC in high strength aluminium alloys, and therefore the question arises whether they can produce similar effects in high strength steels.

The problem was solved by redesign of the cylinders, which provided increased wall thickness to lower stresses, and a more generous radius in the undercut at the rod end side to reduce the stress concentration effect.

Case history 13-17. Corrosion induced failure of a helicopter nose gear door bolt.

The securing bolts from a military helicopter nose landing gear door began to fail, several failures being reported over a fairly short period of time. One such bolt which was examined was found to be cadmium plated and to have a countersunk head with a common screwdriver slot. The straight slotted head was not common military issue, which suggested that the bolt had been installed by a contractor as part of a modification.

Figure 13-52(a) shows the fracture face of the bolt with the nut still attached. The fracture originated at a thread root, in the region indicated by the solid arrow, and propagated across the cross-section in a time dependent manner. A pattern of crack arrest lines was visible over about 60% of the fracture surface, and these lines terminated at a region of relatively flat overload fracture, as indicated by the open arrows in Figure 13-52(a). The topography of the slow crack growth region was quite rough and more granular in appearance than would be expected from pure mechanical fatigue, and this led to the view that a corrosion induced failure mechanism might be operative.

Several cracks, other than the one leading to complete failure, were observed in the bolt. Figure 13-52(b) shows a crack just below the bolt head, which was almost at the point of separation, and Figure 13-52(c) shows a cross-section through the bolt and another long crack which had initiated at the root of the thread.

Examination of the surface of the bolt in the shank area showed that the cadmium plating was in poor condition, and patches of bare steel were observed in several areas. There was evidence of extensive intergranular cracking in these exposed areas, as indicated in Figure 13-52(d), and examination of the primary fracture surface with a scanning electron microscope revealed corroded intergranular fracture facets and areas of what appeared to be transgranular fracture containing poorly defined fatigue striations.

The bolt was analysed spectrographically and was found to be 1040 plain carbon steel, which was not an approved material for this application. The attached nut was found to be stainless steel. It was concluded that the failure was due to intergranular stress corrosion cracking, and that crack propagation may have been assisted for short periods of time by corrosion fatigue. The problem was due primarily to the use of a bolt which did not meet aerospace requirements, and all similar bolts were removed and replaced with approved fasteners.

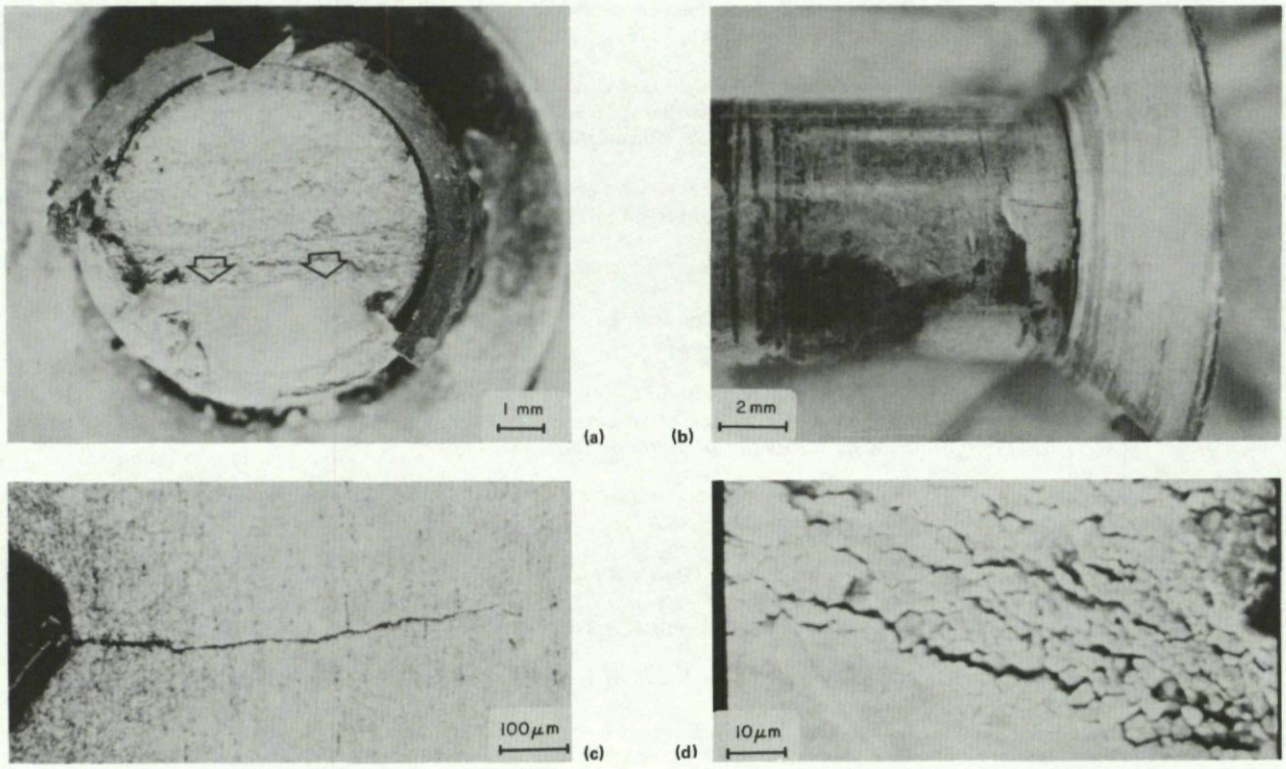

Fig. 13-52 Corrosion induced failure of a 1040 plain carbon steel bolt, case history 13-17.

(a) Fracture surface of the bolt showing initiation site (solid arrow) and extent of stable crack growth (open arrows).
(b) Head and shank of the bolt showing secondary cracking.
(c) Cross-section showing a secondary crack growing out of thread root.
(d) Scanning electron micrograph of shank surface showing network of intergranular cracking.

13.8 References

13-1 Speidel, M.O. *Stress Corrosion Cracking of Aluminium Alloys.* Metallurgical Transactions, 6A, April 1975, pp. 631-651.

13-2 Logan, H.L. J. Res. National Bureau of Standards, 48, 1952, p. 99.

13-3 Champion, F.A. *Int. Symposium on Stress in Metals and Alloys.* Inst. of Metals, London, 1948, p. 468.

13-4 Kruger, J. *Failure by Stress Corrosion Cracking — Current Approaches Toward Failure Prediction.* IN Stress Corrosion Cracking, ed. J. Yahalom and A. Aladjem, 1980, Freund Publishing House, Tel Aviv, pp. 5-37.

13-5 Uhlig, H.H. *An Evaluation of Stress Corrosion Cracking Mechanisms.* Proc. Conf. Fundamental Aspects of Stress Corrosion Cracking, National Association of Corrosion Engineers, Houston, 1969, pp. 86-91.

13-6 Uhlig, H.H. *Stress Sorption Cracking and the Critical Potential.* Proc. Int. Conf. on Stress Corrosion Cracking and Hydrogen Embrittlement of Iron Base Alloys, Unieux-Firminy, France, 1973, National Association of Corrosion Engineers, Houston, 1977.

13-7 Parkin, R.N. *Stress Corrosion Cracking of Low-Strength Ferritic Steels.* IN The Theory of Stress Corrosion Cracking in Alloys, ed. J.C. Scully, NATO, Brussels, 1971, pp. 167-185.

13-8 Staehle, R.W. *Stress Corrosion Cracking of the Fe-Cr-Ni Alloy System.* IN The Theory of Stress Corrosion Cracking in Alloys, ed. J.C. Scully, NATO, Brussels, 1971, pp. 223-286.

13-9 Thompson, A.W. *Effect of Metallurgical Variables on Environmental Fracture of Engineering Materials.* IN Environment—Sensitive Fracture of Engineering Materials, ed. Z.A. Foroulis, Metallurgical Society of AIME, 1979, pp. 379-410.

13-10 Rhodes, P.R. *Mechanism of Chloride Stress Corrosion Cracking of Austenitic Stainless Steels.* Corrosion, 25, 1969, pp. 462-472.

13-11 Speidel, M.O., Hyatt, M.V. *Stress Corrosion Cracking of High Strength Aluminium Alloys.* IN Advances in Corrosion Science and Technology, Vol 2, ed. M.G. Fontana and R.W. Staehle, Plenum Press, New York, 1972, pp. 115-335.

13-12 Brown, R.H., Sprowls, D.O., Shumaker, M.B. *The Resistance of Wrought High Strength Aluminium Alloys to Stress Corrosion Cracking.* IN Stress Corrosion Cracking of Metals — A State of the Art, ASTM STP-518, American Society for Testing and Materials, Philadelphia, 1972, p. 87.

13-13 Speidel, M.O. *Current Understanding of Stress Corrosion Crack Growth in Aluminium Alloys.* IN Theory of Stress Corrosion Cracking in Alloys, NATO, Brussels, 1971, pp. 289-353.

13-14 Thompson, A.W., Bernstein, I.M. *Environmental Fracture of Aluminium Alloys and Stainless Steels as a Function of Composition and Microstructure.* IN Stress Corrosion Cracking, ed. J. Yahalom and A. Aladjem, Freund Publishing House, Tel Aviv, 1980, pp. 193-230.

13-15 Sprowls, D.O., Brown, R.H. *Stress Corrosion Mechanisms for Aluminium Alloys.* IN Fundamental Aspects of Stress Corrosion Cracking, NACE-1, ed. R.W. Staehle and A.J. Forty, National Association of Corrosion Engineers, 1967.

13-16 Urishino, K., Sugimoto, K. *Stress Corrosion Cracking of Aged Al-Cu-Mg Alloys in NaCl Solution.* Corr. Sci., 19, 1972, pp. 225-236.

13-17 Hunsicker, H.Y. *Development of Al-Zn-Mg-Cu Alloys for Aircraft.* Rosenhain Centenary Conference: Contributions of Physical Metallurgy to Engineering Practice, 22-24 September 1975, pub. Royal Society, London, 1976, pp. 359-376.

13-18 Polmear, I.J. *The Influence of Small Additions of Silver on the Structure and Properties of Aged Aluminium Alloys.* J. Metals, 20, No. 6, 1968, pp. 44-51.

13-19 Staley, J.T. *Stress Corrosion Cracking in Aluminium Alloys.* Met. Eng. Quart, 13, No. 4, 1973, pp. 52-61.

13-20 Staley, J.T., Brown, R.H., Schmidt, R. *Heat Treating Characteristics of High Strength Al-Zn-Mg-Cu Alloys With and Without Silver Additions.* Met. Trans, 3, 1972, pp. 191-199.

13-21 Scamans, G.M.
Tuck, C.D.S.
The Role of Hydrogen in Environmentally Sensitive Mechanical Behaviour of Al Zn Mg Alloys.
IN Mechanisms of Environment Sensitive Cracking of Metals, The Metals Society, London, 1977, pp. 482-491.

13-22 Christodoulou, L.
Flower, H.M.
Hydrogen Embrittlement and Trapping in Al-6% Zn-3% Mg.
Acta Met., 28, 1980, pp. 481-487.

13-23 Rajan, K.
Wallace, W.
Beddoes, J.C.
Microstructural Study of a High Strength Stress Corrosion Resistant 7075 Aluminum Alloy.
J. Mat. Sci., 17, 1982, pp. 2817-2824.

13-24 Cina, B.
Ranish, B.
New Technique for Reducing Susceptibility to Stress Corrosion of High Strength Aluminum Alloys.
IN Aluminum Industrial Products, pub. Pittsburgh Chapter, American Society for Metals, 1974.

13-25 Wallace, W.
Beddoes, J.C.
de Malherbe, M.C.
A New Approach to Stress Corrosion Cracking in 7075 Aluminum.
Canad. Aero. and Space Journ., 27, 1981, p.p. 222-232.

13-26 Cong, D.N.
Rajan, K.
Wallace, W.
A TEM Study of Microstructural Changes During Retrogression and Reaging in 7075 Aluminum.
Met. Trans., 14A, 1983, pp. 1843-1850.

13-27 Park, J.K.
Ardell, A.J.
Effect of Retrogression and Reaging Treatments on the Microstructure of Al-7075-T651.
Met. Trans., 15A, 1984, pp. 1531-1543.

13-28 Phelps, E.H.
Liginow, A.W.
Stress Corrosion of Steels for Aircraft and Missiles.
Corrosion, 16, 1960, p. 325t.

13-29 Kerns, G.E.
Wang, M.T.
Staehle, R.W.
Stress Corrosion Cracking and Hydrogen Embrittlement in High Strength Steels.
IN Stress Corrosion Cracking and Hydrogen Embrittlement of Iron Base Alloys, NACE-5, National Association of Corrosion Engineers, Houston, 1977, pp. 700-735.

13-30 Brown, B.F.
Stress Corrosion Cracking of High Strength Steels.
IN The Theory of Stress Corrosion Cracking in Alloys, ed. J.C. Scully, NATO Scientific Affairs Division, Brussels, 1971, pp. 186-203.

13-31 Benjamin, W.D.
Steigerwald, E.A.
Effect of Composition on the Environmentally Induced Delayed Failure of Pre-cracked High Strength Steel.
Met. Trans., 2, 1971, pp. 606-608.

13-32 Sandoz, G.
A Unified Theory for Some Effects of Hydrogen Source, Alloying Elements, and Potential on Crack Growth in Martensitic AISI 4340 Steel.
Met. Trans., 3, 1972, pp. 1169-1176.

13-33 Sandoz, G.
The Effect of Alloying Elements on the Susceptibility to Stress Corrosion Cracking of Martensitic Steels in Salt Water.
Met. Trans., 2, 1971, pp. 1055-1063.

13-34 Hughes, P.C.
Lamborn, I.R.
Liebert, B.B.
Delayed Fracture of a Low Alloy Steel in Corrosive Environments.
J.I.S.I., 203, 1965, p. 156.

13-35 Wang, M.T.
Staehle, R.W.
Effect of Heat Treatment and Stress Intensity Parameters on Crack Velocity and Fractography of AISI 4340 Steel.
IN Hydrogen in Metals, Proc. International Conference, May-June 1972, p. 342.

13-36 Lillys, P.
Nehrenberg, A.E.
Effect of Stress Corrosion Cracking and Hydrogen Embrittlement of Martensitic Stainless Steels.
Trans. ASM, 48, 1956, pp. 327-346.

13-37 Banerjee, B.R.
Fracture Micromechanics in High Strength Steels, Structure and Properties of Ultrahigh Strength Steels.
ASTM-STP-370, American Society for Testing and Materials, Philadelphia, 1965, p. 94.

13-38 Dautovich, D.P.
Floreen, S.
Stress Corrosion Cracking and Hydrogen Embrittlement of Maraging Steels.
IN Stress Corrosion Cracking and Hydrogen Embrittlement of Iron Base Alloys, NACE-5, National Association of Corrosion Engineers, Houston, 1977, pp. 798-815.

13-39 Latanision, R.M.
Staehle, R.W.
Stress Corrosion Cracking of Iron-Nickel-Chromium Alloys.
IN Fundamental Aspects of Stress Corrosion Cracking, National Association of Corrosion Engineers, Houston, 1969, pp. 214-296.

13-40 Okada, H.
Hosoi, Y.
Abe, S.
Scanning Electron Microscopic Observation of Fracture Surface of Austenitic Stainless Steels in Stress Corrosion Cracking.
Corrosion, 27, 1971, pp. 424-428.

13-41 Sedriks, A.J. *Stress Corrosion Cracking of Stainless Steels and Nickel Alloys.* J. Inst. Metals, 101, 1973, pp. 225-232.

13-42 Carter, C.S., Hyatt, M.V. *Review of Stress Corrosion Cracking in Low Alloy Steels with Yield Strengths Below 150 Ksi.* IN Stress Corrosion Cracking and Hydrogen Embrittlement of Iron Base Alloys, NACE-5, National Association of Corrosion Engineers, Houston, 1977, pp. 524-600.

13-43 Carter, C.S. *Fracture Toughness and Stress Corrosion Characteristics of a High Strength Maraging Steel.* Met. Trans., 2, 1971, pp. 1621-1626.

13-44 Gerberich, W.W., Van Stone, R.H., Gunderson, A.W. *Fracture Properties of Carbon and Alloy Steels.* IN Application of Fracture Mechanics for Selection of Metallic Structural Materials, ed. J.E. Campbell et al., American Society for Metals, 1982, pp. 41-103.

13-45 Fontana, M.G., Greene, N.D. *Corrosion Engineering.* McGraw Hill Book Company, New York, 1967.

13-46 Feeney, J.A., Blackburn, M.J. *The Status of Stress Corrosion Cracking of Titanium Alloys in Aqueous Solutions.* IN The Theory of Stress Corrosion Cracking in Alloys, NATO Scientific Affairs Division, Brussels, 1971.

13-47 Johnson, H.H., Willner, A.M. *Moisture and Stable Crack Growth in a High Strength Steel.* App. Mats. Res., 4, 1965, p. 33.

13-48 Green, J.A.S., Haney, E.G. *Relationships Between Electrochemical Measurements and Stress Corrosion Cracking of Maraging Steel.* Corrosion, 23, 1967, pp. 5-10.

13-49 Helfrich, W.F. *Influence of Stress and Temperature on Short Transverse Stress Corrosion Cracking of an Al-4.2 Zn-2.5 Mg Alloy.* IN Stress Corrosion Testing Methods, ASTM STP 425, American Society for Testing and Materials, Baltimore, Md., 1967.

13-50 Williams, D.P., Nelson, H.G. *Embrittlement of 4130 Steel by Low Pressure Gaseous Hydrogen.* Metallurgical Transactions, 1, 1970, p. 60.

13-51 Sawicki, V.R. Ph.D Dissertation, Cornell University, Ithaca, New York, 1971. (Reported in Ref. 13-29.)

13-52 Uhlig, H.H. *Corrosion and Corrosion Control.* 2nd Edition, John Wiley and Sons, Inc., New York, 1971.

CHAPTER 14

CORROSION FATIGUE

14.1 Introduction

Fatigue involves the initiation and growth of cracks in solids which are subjected to repeated cyclic stresses. The mechanical loads involved are generally quite small, and the stresses resulting from these loads are usually less than the yield strength of the material. Fatigue cracks usually initiate at free surfaces and at stress concentration sites such as abrupt changes in section, key-ways, filet radii, fastener holes, or internal discontinuities such as inclusions or cavities. The total fatigue life of a component may be considered in terms of the number of cycles of stress required to cause crack initiation, and the number of cycles required to cause the crack to grow to a size where the remaining load bearing cross-sectional area can no longer sustain the applied loads. Sudden catastrophic rupture of the remaining ligament then occurs.

A wide range of variables can affect the fatigue behaviour of a given material. These include the amplitude of the stress cycles, the mean stress, the frequency and wave-shape of the applied stress cycles and the environment to which the material is exposed. Some of the terms used to describe fatigue are explained in Figure 14-1. To determine the effects of the external variables a wide range of standard tests are available. The relationship between stress amplitude and number of stress cycles to failure is usually determined from tests on carefully machined specimens, either with or without notches machined in their gauge lengths. These tests give rise to the well known S-N curves of the type shown in Figure 14-2(a). For materials such as aluminium or magnesium lives increase as the applied stress amplitudes decrease, but for some materials such as steel a point will be reached at low stresses where fatigue life becomes independent of stress. This is known as the fatigue limit, and it is generally assumed that if a metal is stressed below its fatigue limit it will endure an infinite number of cycles without fracture. If the specimen used in a fatigue test is notched prior to testing, so that a stress concentration exists, then the fatigue strength will be reduced by an amount depending on the radius or sharpness of the notch and on the stress concentration that it creates.

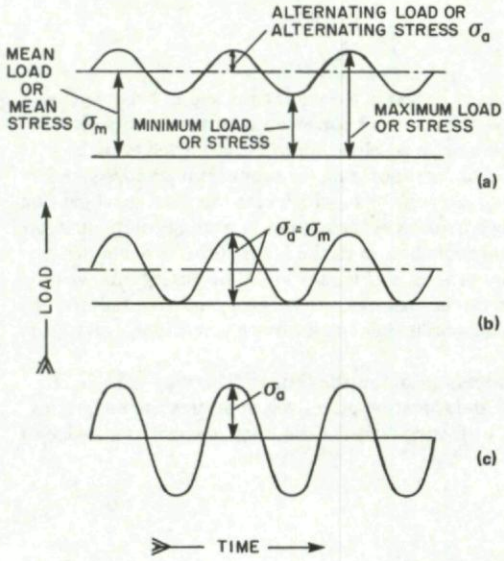

MEAN LOAD = THE AVERAGE BETWEEN THE MAXIMUM AND MINIMUM LOADS OF THE FATIGUE LOADING CYCLE.

ALTERNATING LOAD = THE AMPLITUDE OF THE CYCLICAL LOAD, OR HALF THE DIFFERENCE OF MAXIMUM AND MINIMUM LOADS.

A REPEATED LOAD IS DEFINED AS THE REPEATED APPLICATION AND REMOVAL OF A TENSILE (OR COMPRESSIVE) LOAD.

A REVERSED LOAD IS ONE IN WHICH THE MAXIMUM TENSILE AND COMPRESSIVE LOADS ARE OF EQUAL AMPLITUDE.

$2\sigma_a$ = RANGE OF ALTERNATING STRESS

$\sigma_m + \sigma_a$ = THE MAXIMUM STRESS

$\sigma_m - \sigma_a$ = THE MINIMUM STRESS

$$\frac{\sigma_m - \sigma_a}{\sigma_m + \sigma_a} = \frac{\text{MINIMUM STRESS}}{\text{MAXIMUM STRESS}} = R = \text{STRESS RATIO}$$

Fig. 14-1 Types of constant amplitude fatigue load cycles (Ref. 14-1)

(a) Fluctuating tension load cycle.
(b) Repeated load cycle (stresses $\sigma_a \pm \sigma_a$, or $-\sigma_a \pm \sigma_a$)
(c) Reversed load cycle (stresses $0 \pm \sigma_a$)

The determination of fatigue crack growth rates is usually performed on specimens having notches machined on their edges, or at their centres in the case of sheet specimens. Fatigue cracks can then be initiated under controlled conditions from the notches and allowed to propagate so that their lengths can be monitored as a function of elapsed time or the number of stress cycles applied. Fatigue crack growth rates may be determined under conditions of constant amplitude loading, and also under conditions of variable amplitude or spectrum loading to simulate the conditions existing in service during ground, flight and air-ground operations.

Fatigue crack growth rate (da/dn) is dependent on the range of stress intensity (ΔK) applied to the crack tip during cycling. Figure 14-2(b) shows schematically the relationship between the stress intensity range (ΔK) and fatigue crack growth rates for typical engineering materials. Three regimes of crack growth can usually be identified, as indicated in Figure 14-2(b). Crack growth occurs very slowly at low values of ΔK, and a threshold value of ΔK (ΔK_{th}) can usually be identified below which the crack growth either ceases or is so slow as to be insignificant. As crack tip stress intensity range ΔK is gradually increased, crack growth rates also increase and a point will be reached where log (da/dn) increases linearly with log (ΔK) over a fairly wide range. This point marks the transition between the threshold regime (Region 1) and the intermediate regime (Region 2) of crack growth. Region 2 is often referred to as the linear regime or Paris regime of crack growth, and growth rates can be described by the equation:

$$da/dn = C(\Delta K)^m$$

where C and m are constants.

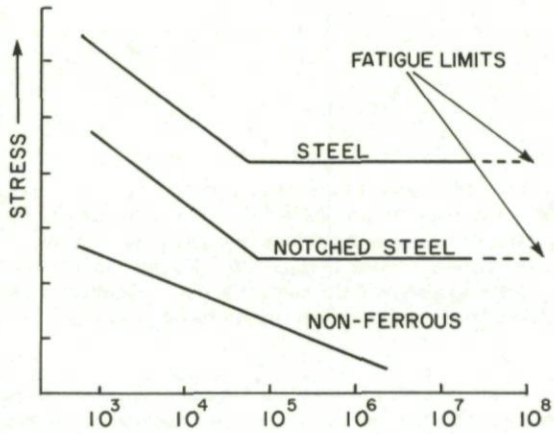

Fig. 14-2(a) Schematic illustration of the fatigue behaviour of ferrous and non-ferrous alloys

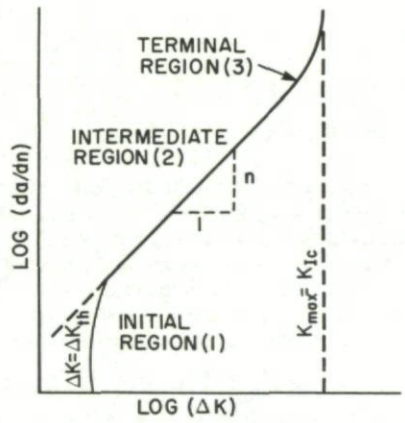

Fig. 14-2(b) The three stages of fatigue crack growth

At even higher values of ΔK crack growth rates increase at an accelerating rate and unstable crack growth occurs as the peak stress intensity in the cycle (K_{max}) approaches the fracture toughness (K_c) of the material. This period of accelerating growth rate at high values of ΔK is known as stage 3, or the terminal stage of crack growth.

14.2 Effects of Corrosive Environments

When fatigue occurs in the presence of a corrosive environment failure usually occurs in a shorter time and in fewer cycles than would be the case in a dry or benign environment. This synergistic effect between fatigue and corrosion is known as corrosion fatigue, and it may involve either a decrease in the number of cycles to crack initiation or an acceleration of fatigue crack growth rates, or both. An important feature of corrosion fatigue is that mechanical damage and corrosion damage occur simultaneously and synergistically. In many cases the two modes of degradation will occur successively or alternately, in which case the damage would not be attributed to corrosion fatigue. This might be the case, for example, when pitting corrosion occurred first in a metal component, and then fatigue crack propagation occurred from the base of a corrosion pit. The fatigue contribution to the failure process could occur even in the absence of a corrosive environment. The correct description of the failure process in this case would be pitting followed by fatigue, rather than corrosion fatigue. However, while hypothetical failure processes can be classified quite easily, and even failures produced under laboratory conditions, it is not always easy to correctly classify failures occurring under service conditions.

Although not very common, cases have been reported where corrosion processes can impede fatigue. This may arise due to the formation of dense oxide scales which help to carry the externally applied loads and therefore effectively reinforce the underlying metal. Similarly, if thick oxide scales or other corrosion products form at the tip of a growing fatigue crack they may act as a wedge to

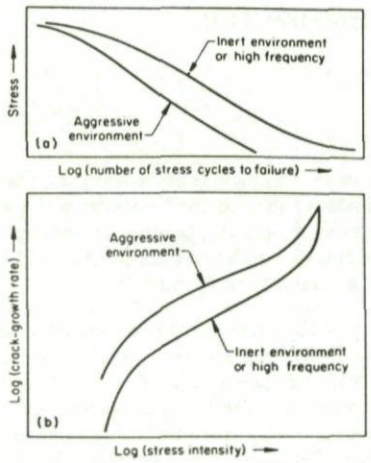

Fig. 14-3(a) Typical fatigue behaviour in aggressive environment compared with fatigue behaviour in inert environment or at high frequency shown (top) as an S-N curve and (bottom) as variation of crack growth with stress intensity. (Ref. 14-2)

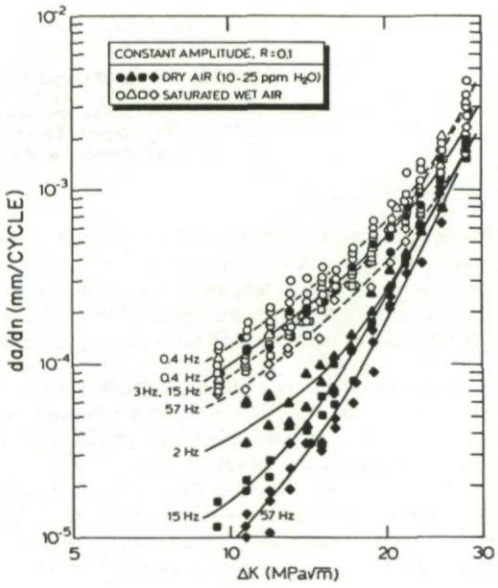

Fig. 14-3(b) The effects of frequency on fatigue crack growth in 1 mm thick Alclad sheet of 2024-T3 aluminium. (Ref. 14-3)

prevent the crack faces from closing completely during the load decreasing part of the fatigue cycle. In this way they may lower the effective range of stress intensity applied at the crack tip and lower the growth rate. Corrosion therefore does not always reduce fatigue life, and cyclic stressing does not always increase rates of corrosion.

In the more general case the effect of a corrosive environment is to reduce fatigue life, either by decreasing the time to crack initiation and, or, by increasing the rate of fatigue crack growth. These effects can be seen quite easily in laboratory tests where they give rise to results of the type indicated in Figure 14-3(a). The decrease in fatigue life or acceleration of crack growth rate depends on cyclic frequency, stress amplitude, mean stress and wave shape. In general terms, conditions which provide the aggressive environment with easy access to the bare metal, for example at the crack tip, and which provide time to allow corrosive reactions to occur will lead to the most noticeable reduction in fatigue life.

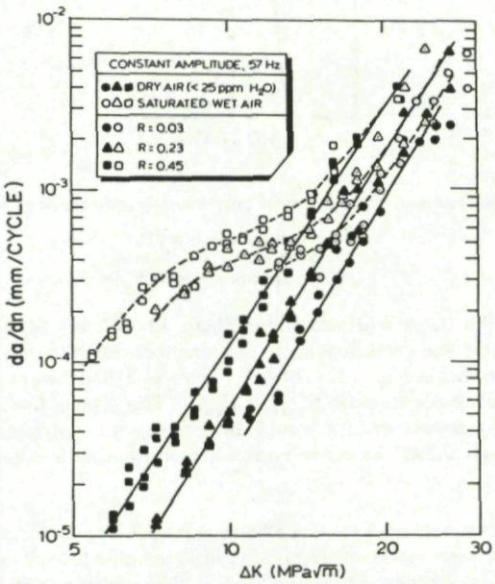

Fig. 14-4 The effect of stress ratio (R) on fatigue crack growth rates of 1 mm thick clad sheet of 7075-T6 aluminium in dry air and saturated wet air. (Ref. 14-3)

Since corrosion is a time-dependent process, low frequency cyclic straining promotes corrosion fatigue by allowing time for corrosion degradation to occur and to contribute to mechanical degradation during the fatigue process. Frequency dependent fatigue strength or fatigue crack growth rates are therefore often taken as a clear indication of corrosion fatigue. The effects of frequency in corrosion fatigue will be most pronounced at low stress amplitudes or low crack tip stress intensities where mechanical damage accumulates slowly. Some examples of the effects of frequency on fatigue crack growth in Alclad 2024-T3 sheet in dry air and saturated wet air are given in Figure 14-3(b).

High stress amplitudes and high crack tip stress intensities lead to short fatigue lives and rapid crack growth rates. The opportunity for corrosion to contribute to the degradation process is therefore diminished and the S-N curves, or curves of log (da/dn) versus log (ΔK) for aggressive and non-aggressive environments tend to merge. These effects can be seen in Figure 14-3(a) and Figure 14-3(b).

The mean stress applied to a specimen during cycling determines the portion of time that the crack is open during each stress cycle. For a zero mean stress (fully reversed loading, Fig. 14-1) the crack would normally be closed during the compressive half-cycle, and open only during the tensile half-cycle. If a static tensile component is introduced to raise the mean stress of the cycle above zero the crack will be open for a greater part of the cycle, and therefore for a given frequency a longer time will exist during each cycle when corrosion may occur at the crack tip. When the mean stress is equal to or greater than the stress amplitude (Fig. 14-1(a) and (b)), the crack should be open throughout the cycle. Under these conditions corrosion should be able to occur throughout the cycle and corrosion fatigue should be pronounced. The greater is the stress ratio the greater is the crack opening and the easier it should be for the corrosive environment to reach the crack tip and cause corrosion fatigue. This effect is shown in Figure 14-4, where high R values lead to higher crack growth rates in 7075-T6 clad sheet.

14.3 Stress Corrosion Fatigue

When fatigue loading is applied to materials which are susceptible to stress corrosion cracking there is a possibility that this will also contribute to the overall fracture process. The result may be a more rapid rate of crack growth compared to those expected for either pure mechanical fatigue or true corrosion fatigue. This phenomenon may lead to the appearance of a sudden step-like increase in growth rate at a certain value of ΔK in plots of log (da/dn) versus ΔK, as indicated in Figure 14-5.

The step-like increase in growth rate might be expected to appear when the peak stress intensity reached in the fatigue cycle first equals the threshold stress intensity for stress corrosion cracking. Only then should a stress corrosion contribution to crack growth be possible. However there are indications that the threshold stress intensity for stress corrosion cracking may be lower under cyclic loading conditions than for static loading conditions, and therefore the use of SCC data from static tests may be misleading. Having recognized the possible contribution of stress corrosion cracking to fatigue crack growth, it is possible to describe three basic types of

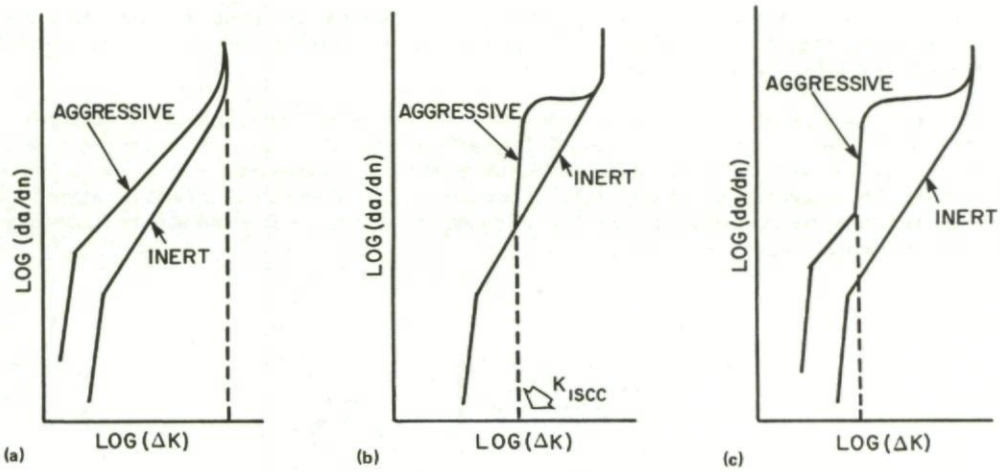

Fig. 14-5 Schematic illustrations of basic types of corrosion fatigue crack growth behaviour (Ref. 14-4)

(a) True corrosion fatigue (TCF).
(b) Stress corrosion fatigue (SCF).
(c) SCF superimposed on TCF.

corrosion fatigue crack growth. These are illustrated schematically in Figure 14-5. Figure 14-5(a) shows true corrosion fatigue where a synergistic reaction occurs between corrosion and cyclic loading to cause an increase in fatigue crack growth rates. This increase is most pronounced at low values of ΔK and diminishes at high values of ΔK. Figure 14-5(b) shows pure stress corrosion fatigue, where a stress corrosion contribution to fatigue crack growth occurs when $K_{max} \geqslant K_{ISCC}$. This type of behaviour is unlikely to occur in practice since the corrosive environment required for stress corrosion would also induce a true corrosion fatigue contribution. The more likely situation is shown in Figure 14-5(c), which shows the stress corrosion contribution superimposed on a true corrosion fatigue contribution.

The variables of frequency, mean stress and wave-shape become particularly important when the test material is susceptible to stress corrosion cracking. The higher the mean stress, or stress ratio, in a corrosion fatigue test, the sooner will the condition that $K_{max} = K_{ISCC}$ be reached. This will lead to the appearance of the 'step' in the corrosion fatigue crack growth curve at lower values of ΔK, as indicated in Figure 14-6(a).

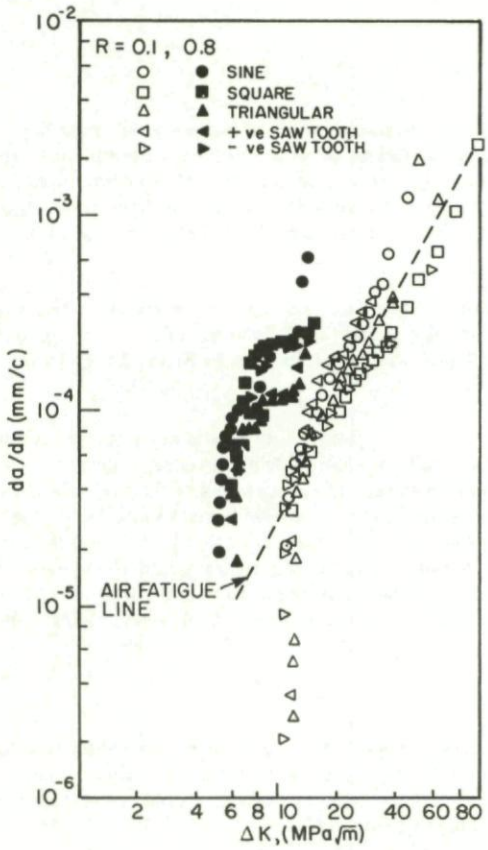

Fig. 14-6(a) The effect of cyclic waveform on true corrosion fatigue (R = 0.1) and stress corrosion fatigue (R = 0.8) for 835M30 steel in 3.5% NaCl solution. (Ref. 14-4)

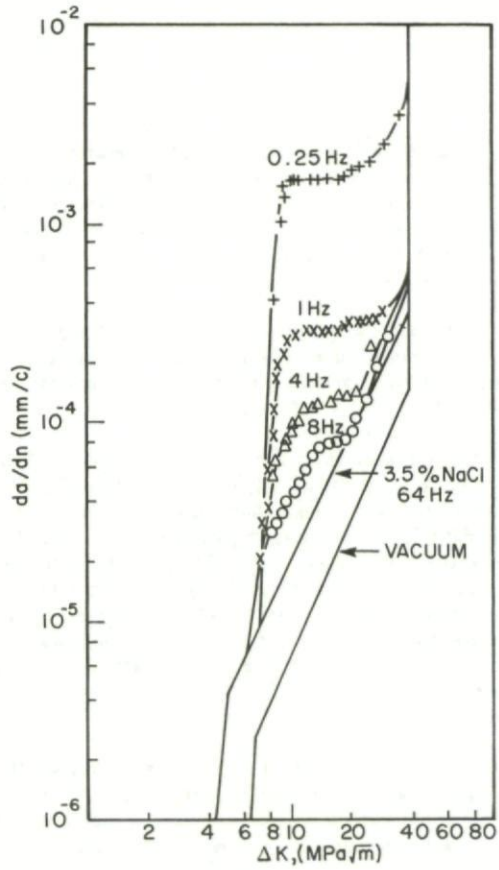

Fig. 14-6(b) The effect of frequency on stress corrosion fatigue for 835M30 steel in 3.5% NaCl solution. (Ref. 14-4)

Lower frequencies lead to greater environmental contributions to crack growth, because of the longer time per cycle during which corrosion processes may occur. This is true for both corrosion fatigue and stress corrosion fatigue, and the effects of frequency for this latter process can be seen in Figure 14-6(b) for 835M30 steel in 3.5% NaCl solution.

Wave-shape is important with respect to stress corrosion fatigue since stress corrosion cracking can only occur above some critical value of stress intensity. Thus the longer the time in each cycle spent above this critical value the greater will be the contribution to crack growth from SCC. Wave-shapes which maximize the time at peak stress therefore tend to promote SCC. This can be seen in Figure 14-7, where a pronounced step increase in crack growth rate, due to stress corrosion cracking, can be seen in an Al-Zn-Mg alloy tested in a corrosive environment with a square waveform at 0.1 Hz. The step diminishes as the frequency is increased to 10 Hz, and disappears entirely when the waveform is changed to a triangular or sawtooth form. Figure 14-7 indicates that the stress corrosion contribution, even at 0.1 Hz, disappears when ΔK falls below the stress corrosion threshold. It also indicates that the true corrosion fatigue contribution to crack growth is very small below K_{ISCC}, when a square waveform is used. However the true corrosion fatigue contribution remains quite large in this regime when a triangular or sawtooth waveform is used. This suggests that true corrosion fatigue crack growth, like pure (mechanical) fatigue, only occurs during the load increasing part of the cycle. From this, it may be inferred that cyclic loading under a triangular, trapezoidal, positive-slope-sawtooth or sinusoidal stress wave is more likely to effect a reduction in fatigue life in detrimental environments than is cyclic loading under a negative-slope-sawtooth or square wave.

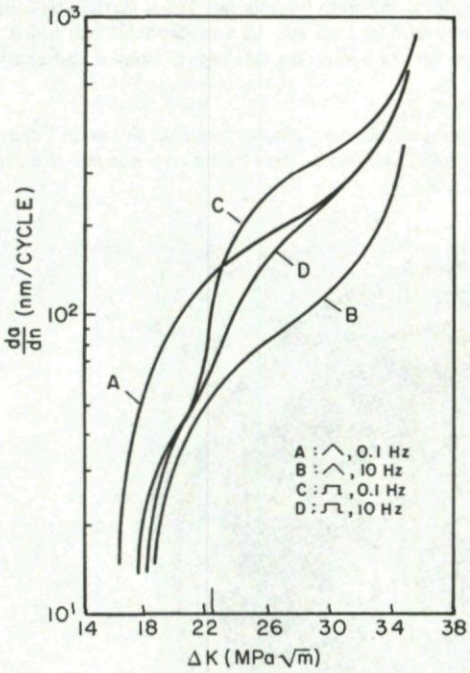

Fig. 14-7 Crack growth rates da/dn versus stress intensity range ΔK for a Al-Cu-Mg alloy showing the effect of waveform and frequency at R = 0.04. (Ref. 14-5)

14.4 Case Histories

Case history 14-1. Corrosion fatigue of a magnesium alloy (AZ-91C) main landing gear wheel.

A large rim section was found broken from the rim of a STOL transport aircraft main wheel after landing (Fig. 14-8(a)). The cause of fracture was found to be corrosion fatigue cracking which had grown completely through the rim section. Cracking initiated from the tyre bead seat radius, and the corrosion products were typical of a marine environment.

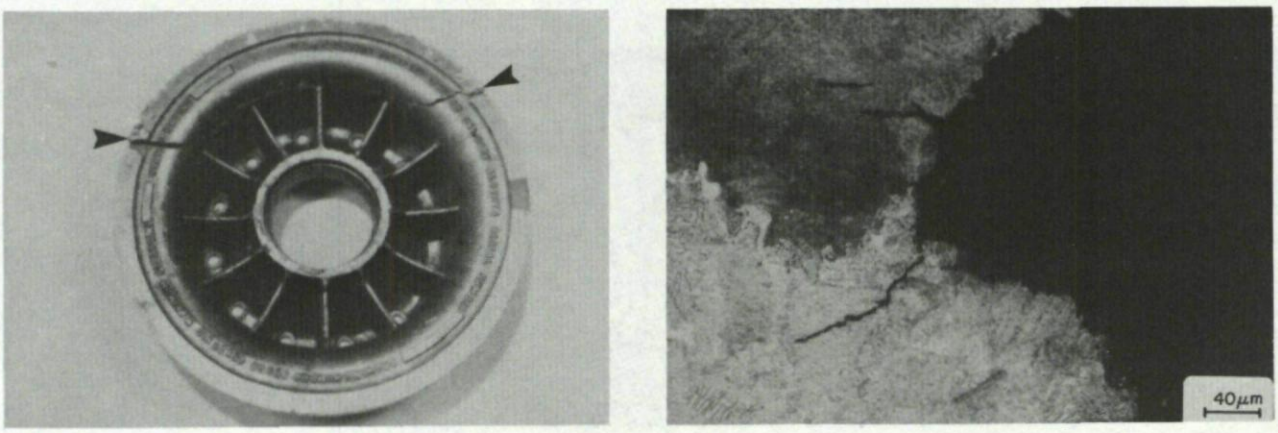

(a) (b)

Fig. 14-8 Corrosion fatigue of a magnesium alloy (AZ-91C) main landing gear wheel

(a) General view of the failed wheel and the crack indicated by arrows.
(b) Section through a typical pit showing multiple corrosion fatigue cracks. Nital etch. (Mag. × 250)

These experimental low pressure tyre wheels allowed salt moisture to penetrate the tyre bead seat area between tyre and rim, aided by frequent tyre changes. The wheel was a magnesium alloy casting (AZ-91C) and fatigue crack initiation occurred at the base of deep corrosion pits. Figure 14-8(b) shows a typical pit with multiple crack origins.

Such failures are not likely to occur until the cracking is substantial and then only when side loaded during taxiing, since tyre pressure loads are small. Dye penetrant or eddy current inspection to detect cracking during tyre changes would prevent in-service failures. In this case the frequent experimental tyre changes increased the availability of the corrosive media to the growing undetected cracks.

Case history 14-2. Corrosion fatigue failure of a magnesium alloy (QE-22A) main landing gear wheel.

Long cracks were found during visual inspection of a fighter aircraft main landing gear wheel. The cracks were approximately 125 mm long and were found to run between the rim of the wheel and a bolt hole, as shown in Figure 14-9(a). The crack initiation site is indicated by the arrow in Figure 14-9(b).

Metallurgical analysis showed that the wheel was made from a magnesium alloy casting, QE-22A with a nominal composition Mg-2.5% Ag-2.0% Di-0.4% Zr. The microstructure (Fig. 14-9(c)), showed heavily cored but equiaxed grains with precipitates of an intermetallic compound believed to be a magnesium-rare earth phase (Mg_9R) along grain boundaries. The material was found to have a tensile strength of 215 MPa and hardness of BHN-70, determined with a 500 kg load and 10 mm diameter ball indenter. These properties and microstructure are typical of the T6 heat treatment consisting of a solution treatment, quench and artificial age (Ref. 14-6).

Heavy surface corrosion was observed over most of the wheel and polished sections, such as that shown in Figure 14-9(c), showed several through cracks and partial cracks initiating from corrosion pits. The cracks were found to propagate in a predominantly intergranular mode, as indicated in Figure 14-9(c).

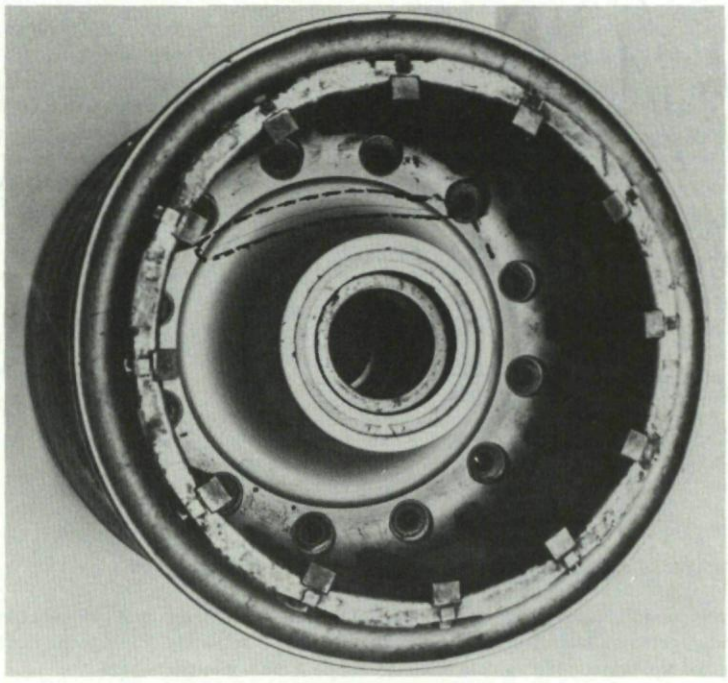

(a)

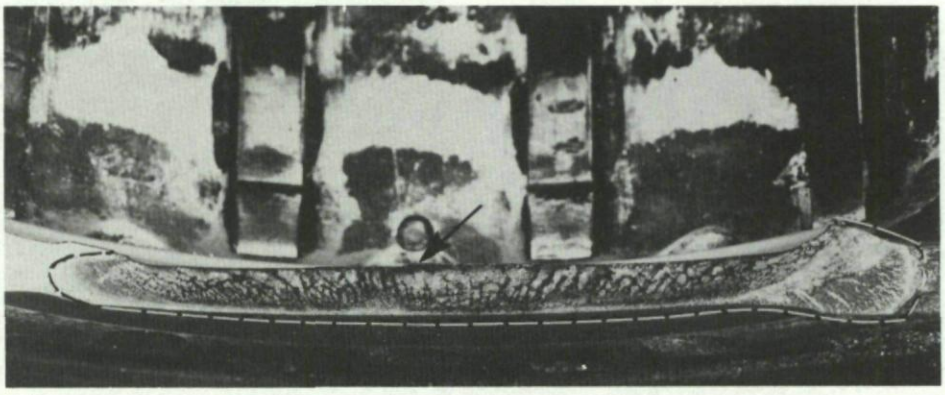

(b)

Fig. 14-9 Corrosion fatigue of a magnesium alloy (QE-22A) main landing gear wheel

(a) General view of the wheel showing the crack.
(b) Fracture surface showing the crack initiation site indicated by arrows.

(c)

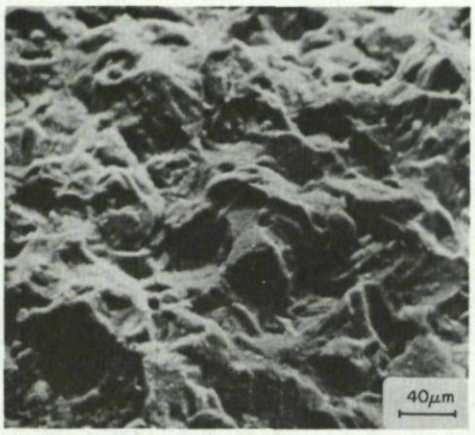

(d)

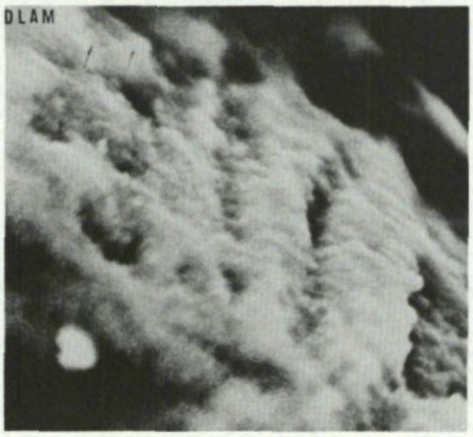

(e)

Fig. 14-9 Corrosion fatigue of a magnesium alloy (QE-22A) main landing gear wheel

(c) Secondary cracking initiating from corrosion pits.
(d) Area showing intergranular fracture on the heavily corroded fracture face. (Mag. × 220)
(e) Heavy corrosion products largely obscuring fatigue striations running normal to the direction of crack propagation indicated by the arrow.

Scanning electron microscopy showed that the fracture surface was covered by thick corrosion products, but the intergranular nature of the fracture was still clearly evident in many areas (Fig. 14-9(d)). The fine features of the fracture surface were largely obscured by the corrosion products, but isolated areas could be found which showed what appeared to be fatigue striations (Fig. 14-9(e)).

QE-22A, like other magnesium alloys, is subject to general and pitting corrosion in industrial, marine and moist environments. However, with suitable surface treatments and painting, it performs satisfactorily in all types of natural environments with the exception of continuous immersion in water (Ref. 14-7). The alloy has low susceptibility to stress corrosion cracking (Ref. 14-8). The wheel in question had been operated in the Mediterranean region, and exposure to a warm moist salt atmosphere was no doubt a factor in the failure. The critical crack had initiated on the exterior surface of the wheel, which fortunately was visible, and this probably occurred in an area where the corrosion protection system was damaged. Regular inspection and repair of the paint system should have prevented this failure. Because of the clear evidence of corrosion and the indications of fatigue striations on a heavily corroded fracture surface the failure was attributed to corrosion fatigue.

Case history 14-3. Corrosion fatigue failure of a magnesium alloy (AZ-91C) nose wheel.

Multiple cracks were found propagating out of bolt housings during a visual and liquid penetrant inspection of the nose wheels of a fleet of fighter aircraft. Many wheels were found to be affected, and typical cracks are indicated by the arrows shown in Figure 14-10(a).

Metallurgical analysis showed that the wheels were made of a magnesium alloy casting, AZ-91C, with a nominal composition Mg-9% Al-0.7% Zn. The microstructure (Fig. 14-10(b)) consisted of equiaxed grains with fine precipitates of an intermetallic compound along grain boundaries. Brinell hardness determined with a 500 kg load and a 10 mm diameter ball indenter was found to be BHN-51 to 59, which is typical of materials in the T4 heat treatment condition.

Several cracks were opened in the laboratory, and these showed a dark zone, covered by corrosion products, which extended up to the bright overload zone produced during opening (Fig. 14-10(c)). The inner surfaces of the bolt holes were also examined. These were found to contain deep corrosion pits of the type shown in Figure 14-10(d). Examination of the fracture surfaces using a scanning electron microscope showed that intergranular cracking had occurred in the initiation regions (Fig. 14-10(e)), while transgranular fracture had occurred at longer crack lengths (Fig. 14-10(f)). Both the intergranular and transgranular zones were badly corroded, but fatigue striations were clearly visible in the transgranular areas (Fig. 14-10(f)).

Pitting attack in the bolt holes may have been influenced by galvanic effects, or by crevice conditions existing between the wheel and the steel bolts. However, the presence of heavy corrosion across the fracture faces and the clear evidence of striations suggests that corrosion fatigue was responsible for at least the later stages of crack propagation. This aircraft had operated in the Mediterranean region which is also a significant factor. This, and the two preceding case histories, suggest that magnesium alloy castings are not good choices for aircraft wheels.

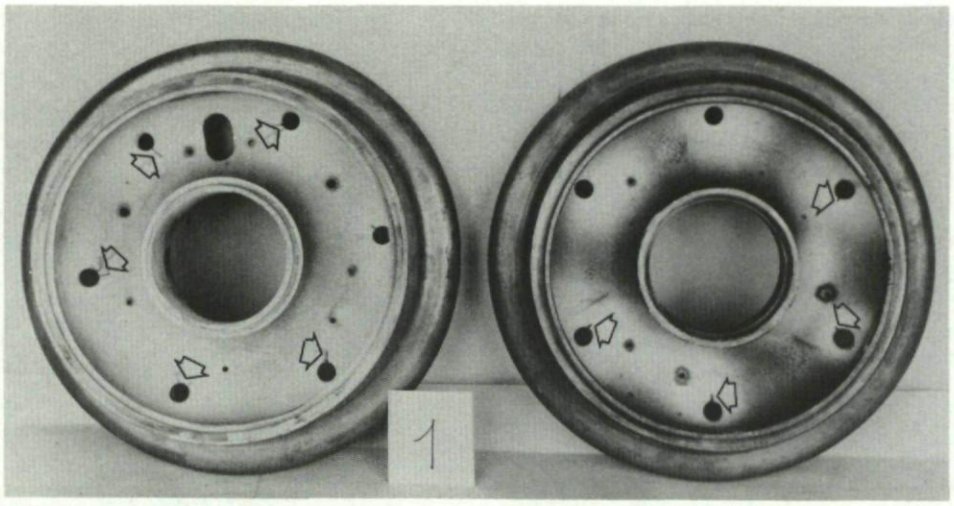

(a)

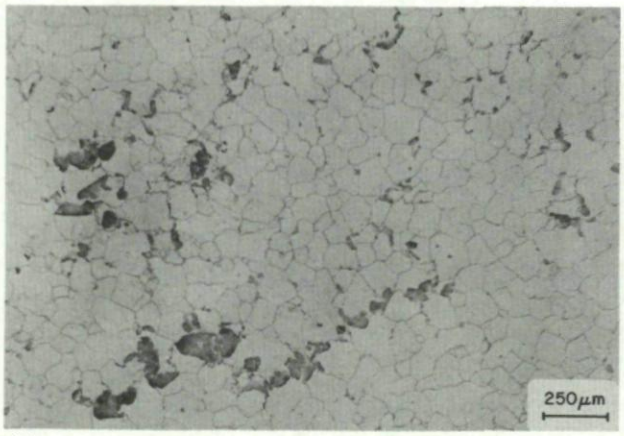

(b)

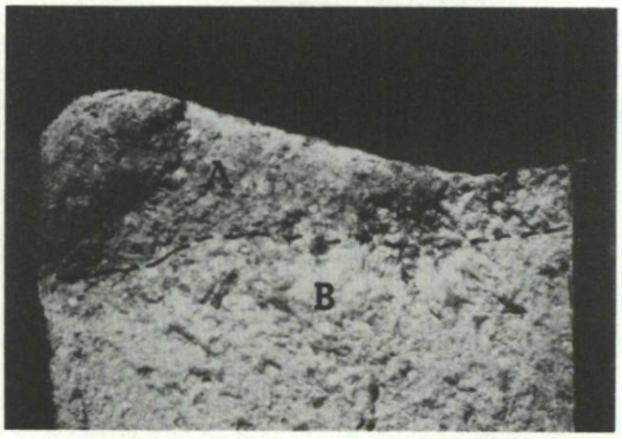

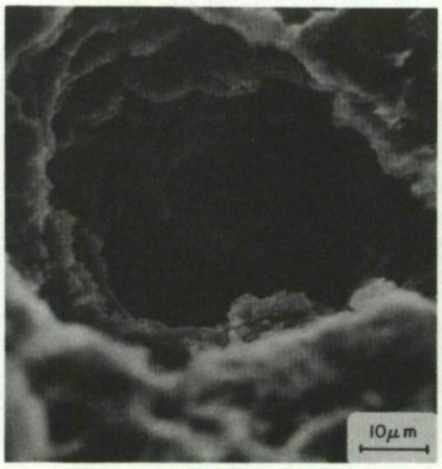

(d)

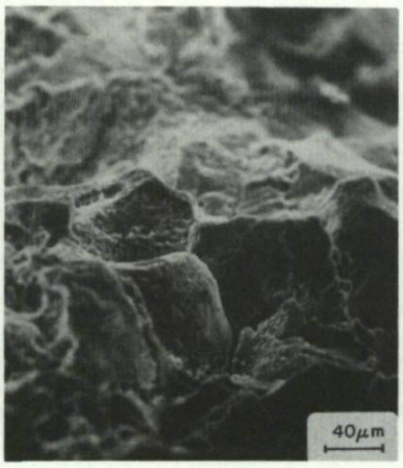

(e)

(f)

Fig. 14-10 Corrosion fatigue of a magnesium alloy (AZ-91C) nose wheel

(a) General view of two wheels showing cracks (arrows) growing out of bolt holes.
(b) Microstructure of the AZ-91C magnesium alloy. (Mag. × 45)
(c) Fracture surface showing the corroded (dark) pre-cracked area 'A', and the bright final fracture zone 'B'.
(d) Inner surface of a bolt hole showing a deep corrosion pit. (Mag. × 1200)
(e) Intergranular cracking in the initiation zone. (Mag. × 260)
(f) Fatigue striations in a transgranular portion of the fracture surface. (Mag. × 650)

Case history 14-4. Corrosion fatigue of a rocker arm journal bearing.

Severe vibration and noise led to the tear-down and inspection of an aircraft engine. A rocker arm journal bearing was found to be fractured and was submitted for laboratory examination. The journal bearing and fractures are shown in Figures 14-11(a) and 14-11(b).

Examination of the bearing surface revealed the presence of numerous deep pits and score marks (Fig. 14-11(c)). The fracture surfaces were found to be covered by corrosion products and brittle fatigue straitions were found in zone 'F', 3-4 mm from the bearing surface, as shown in Figure 14-11(d). However the most noticeable feature of these fractures was the presence of large pockets of what appear to be interdendritic shrinkage cavities running along the bearing surface (Figs. 14-11(e) and 14-11(f)). The fatigue cracks initiate at these cavities and propagate radially outwards, away from the bearing surface, as indicated in Figure 14-11(e).

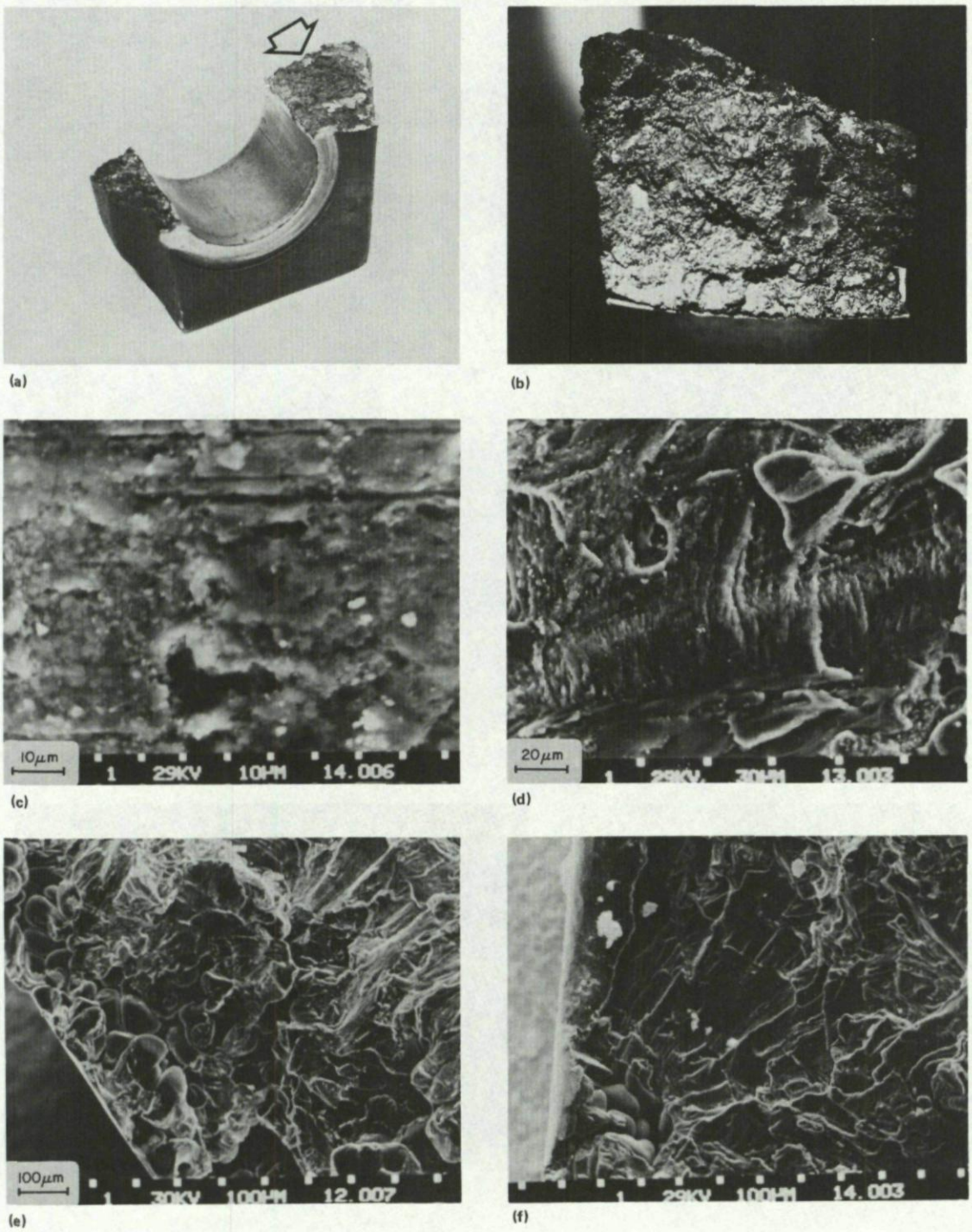

Fig. 14-11 Corrosion fatigue of a cast aluminium rocker arm journal bearing

(a) Portion of the fractured journal bearing.
(b) Portion of the fracture surface ('A' in Fig. 14-11(a)).
(c) SEM picture of the bearing surface showing pitting. (Mag. × 1070)
(d) Fatigue striations observed in zone 'F', 3-4 mm from the bearing surface. (Mag. × 540)
(e) and (f) Interdendritic shrinkage cavities observed on the fracture at the bearing surface. (Mag. × 100)

Metallurgical examination confirmed that the journal bearing was made from an aluminium alloy casting, and the microstructures confirmed the presence of a coarse grained dendritic structure with intermetallic compounds and large shrinkage cavities in the interdendritic regions. Chemical analysis showed that the casting was an aluminium-copper-nickel-magnesium-silicon alloy, AA-242 (formerly 142), Al-4% Cu, 2% Ni, 1.5% Mg, 1% Fe, 0.7% Si, 0.35% Zn, 0.25% Cr. The material was found to have a Brinell hardness number HB = 58, determined using a 500 kg load and 10 mm diameter ball.

The primary cause of this failure was the use of a poor quality casting in a fatigue critical application. This was the result of poor foundry practice and poor quality control procedures which failed to detect gross porosity in the casting. However, the evidence indicates that once in service the failure progressed by fatigue and that corrosion contributed to the fracture process, and thus corrosion fatigue was a factor.

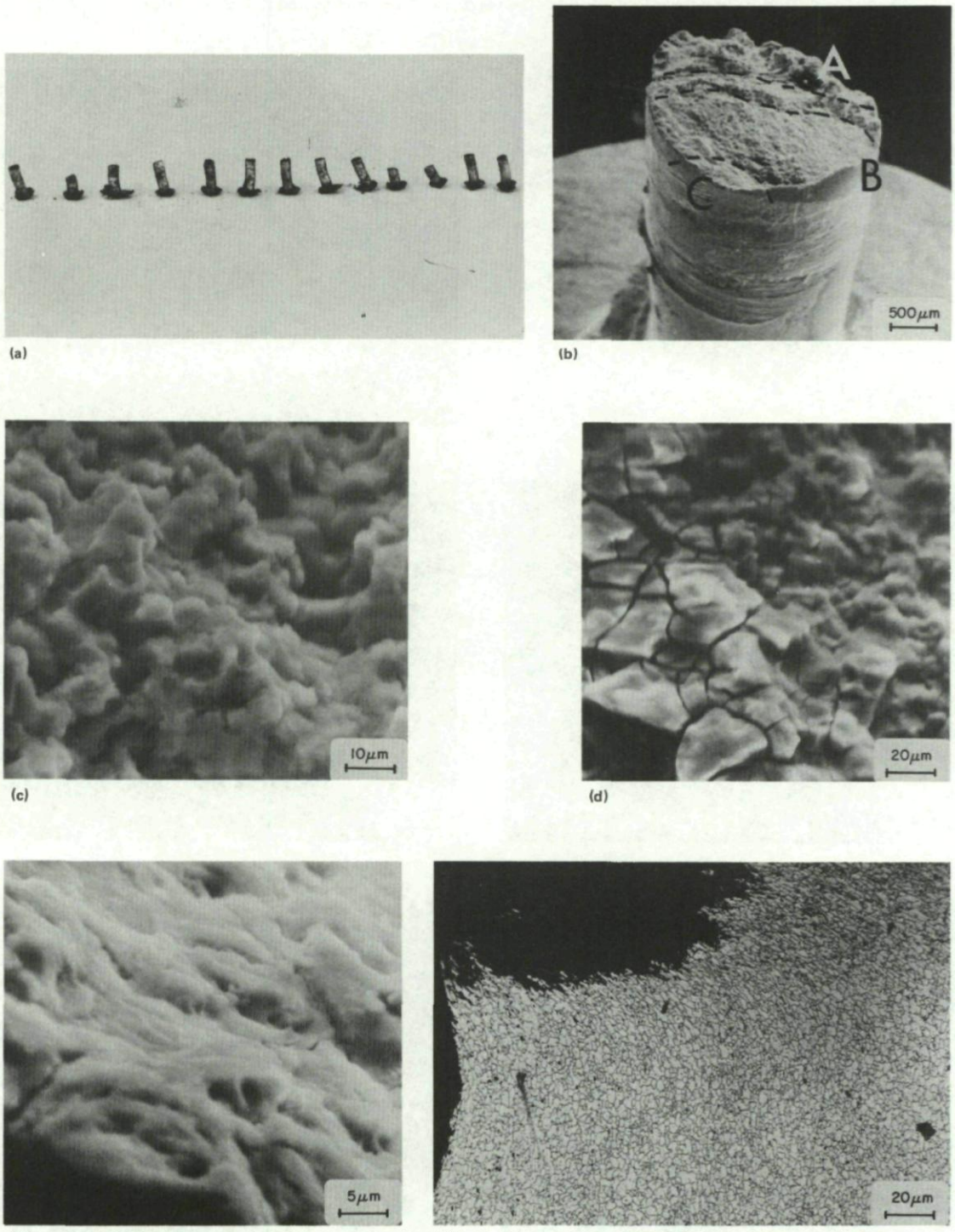

Fig. 14-12 Corrosion fatigue of 5052 aluminium alloy rivets

(a) Rivets removed from the structure for examination.
(b) Fracture surface of a rivet showing three zones of fracture. (Mag. × 20)
(c) Intergranular fracture observed in zone 'A'. (Mag. × 1000)
(d) Mud-crack pattern observed in fracture zone 'A'. (Mag. × 500)
(e) Fracture surface appearance in fracture zone 'B'. (Mag. × 2000)
(f) Grain structure in the rivets. The deformation is due to tearing in an overload region. (Mag. × 500)

Case history 14-5. Corrosion fatigue of 5052 aluminium alloy rivets.

Visual inspection of a set of rivets, used to hold a filter housing in a helicopter, showed that several were fractured. The rivets were removed and inspected. Many of the rivets (Fig. 14-12(a)), were badly deformed and they were all badly corroded. Closer examination in a scanning electron microscope showed that the sides of the rivets were badly scored and pitted, while the fracture surfaces typically showed three or four distinct zones of fracture as indicated in Figure 14-12(b).

Zone A in Figure 14-12(b) was found to contain predominantly intergranular fracture (Fig. 14-12(c)), but large areas were covered by corrosion deposits having a mud-crack appearance as shown in Figure 14-12(d). Zone B in Figure 14-12(b) was found to be fairly smooth and was also covered by heavy corrosion products. However some areas were found which had a striated appearance, as shown in Figure 14-12(e), suggesting the presence of underlying fatigue striations. The fact that the rivets failed in an essentially brittle manner, with little evidence of necking or other signs of ductility in the fracture process suggests that fatigue was involved. The absence of clearly defined fatigue striations is not uncommon in corrosion fatigue and this often complicates the interpretation of service induced fracture surfaces. Zone C in Figure 14-12(b), and the intermediate zone between zones B and A, were rougher in texture suggesting that these may have formed by tearing during the final stages of fracture of the rivets. These zones were also covered by thick layers of corrosion debris.

Microstructural analysis of these rivets showed they were made from wrought aluminium alloy 5052 (Al-2.5% Mg-0.25% Cr), with a very small equiaxed grain structure (Fig. 14-12(f)). The material had a Vickers hardness, Hv = 112 ± 8. This alloy is generally resistant to corrosion in normal marine and industrial atmospheres, and to salt water in the tempers normally used for rivets. The presence of corroded fracture surfaces and the macroscopic and microscopic aspects of the fracture surfaces indicate that corrosion fatigue was the primary cause of failure.

Case history 14-6. Corrosion fatigue of a 6061 aluminium alloy pitot support tube.

A pitot support tube (Fig. 14-13(a)), on a military aircraft was found to be cracked during a routine visual inspection. The crack encircled the tube more than 300° and had existed for a considerable period of time. The tube did not separate from the pitot boom because it contained air hoses and electrical wiring which hold it in place to some degree. The appearance of the magnified crack (Fig. 14-13(a)), suggested that extensive corrosion of an old fracture had occurred. The intergranular nature of the corrosive attack is shown in the metallographic cross-section of Figure 14-13(b). The crack was carefully broken open so that the most recent portion which was not so severely corroded could be studied by scanning electron microscopy. The fracture surface was found to contain fatigue striations amid the corrosion debris and secondary cracking (Fig. 14-13(c)).

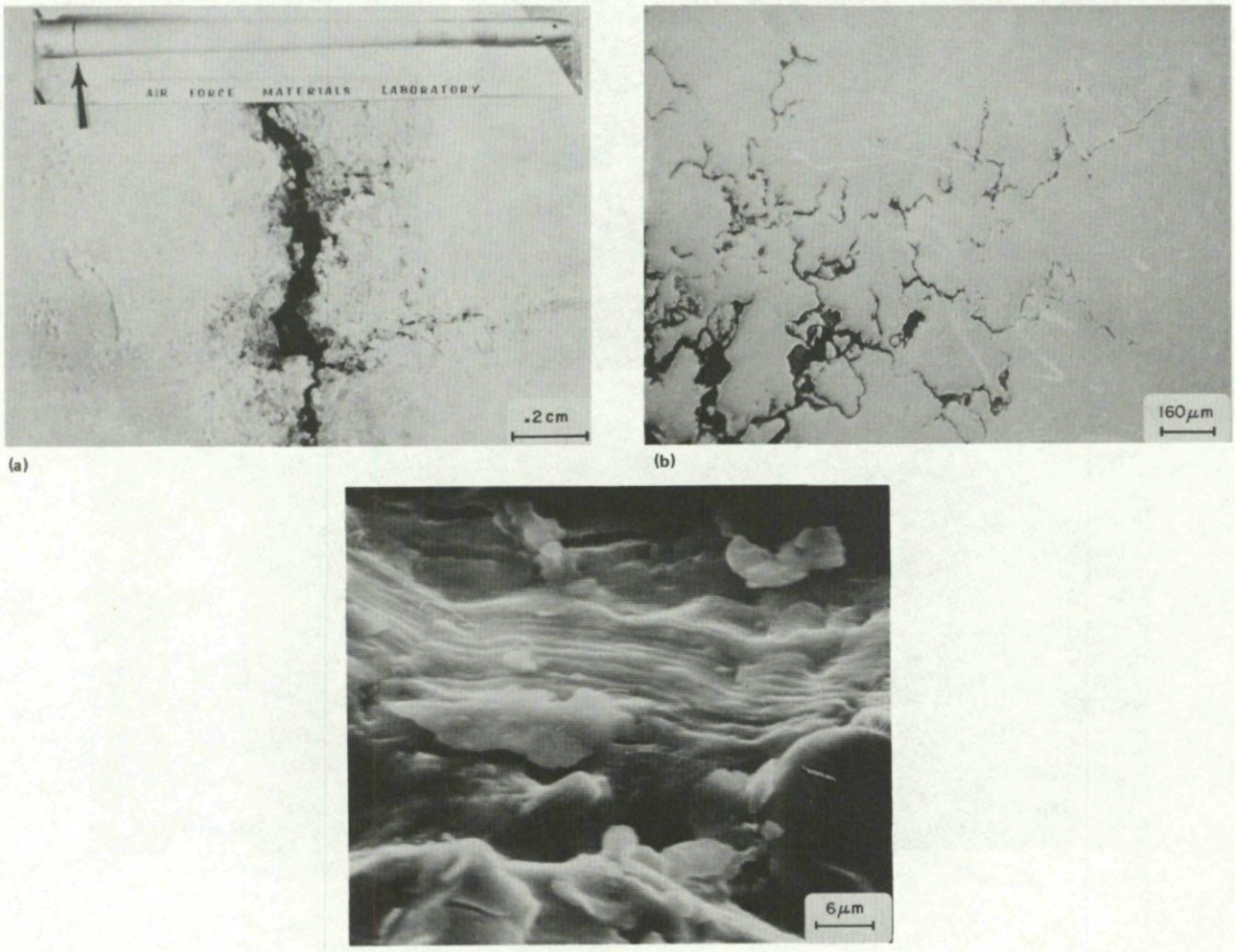

Fig. 14-13 Corrosion fatigue in a 6061 aluminium pitot support tube

(a) Corroded crack encircling the tube (arrow inset). (Mag. × 7)
(b) Cross-section showing intergranular corrosion attack. (Mag. × 62.5)
(c) Scanning electron fractograph showing fatigue striations. (Mag. × 1700)

The stress contribution of the corrosion fatigue failure was believed to be due to aerodynamically induced vibration of the tube, since it was otherwise a very lightly loaded structure. The corrosion could not be identified other than being due to general environmental corrosion of the unprotected aluminium fracture surface. A possibility exists that a rigid foam type material located in the pitot boom at the connection to the pitot support tube may have contributed to the corrosive environment, however this was not confirmed. Some galvanic corrosion was observed around the securing bolts of the pitot support tube but this could not be related to the failure.

The tube material was identified as 6061 aluminium alloy. This alloy is among the best of the heat treatable aluminium alloys with respect to corrosion resistance, and these properties are not significantly affected by variations in heat treatment. A thin invisible oxide film forms in air which is normally expected to protect the metal from further oxidation and to provide corrosion resistance to all but alkalis, which are among the few substances which attack the oxide film (Ref. 14-9). However the material is known to be susceptible to galvanic corrosion, and fatigue crack propagation rates are increased by the presence of moisture. There is insufficient data to establish the magnitude of this effect, but it is less pronounced in this alloy than in the 2000 and 7000 series alloys (Refs. 14-10, 14-11).

The failure of the pitot support tube was therefore attributed to corrosion fatigue, although the corrosive medium could not be specifically identified and aerodynamic loading was the only significant source of stress. No material or design deficiency could be identified, other than the vibrational loading situation.

Case history 14-7. Corrosion fatigue of a 321 stainless steel hose assembly.

A visual inspection was carried out on a turbojet engine from a fighter aircraft after a flame-out. A hose assembly, shown in Figure 14-14(a), was found to be completely fractured, the fracture occurring towards one end of the tube close to a weld. Prior to failure the engine had been in service in the Mediterranean region where it would be exposed to warm and humid salt atmospheres.

The fracture appeared to have initiated in the region indicated by the arrow in Figure 14-14(b), and examination of the fracture surface in this region revealed the presence of fatigue striations (Fig. 14-14(c)), partially covered by corrosion products. Examination of the outer surface of the tubing adjacent to the fracture surface revealed the presence of surface pits, longitudinal scratches, and superficial intergranular cracking (Fig. 14-14(d)).

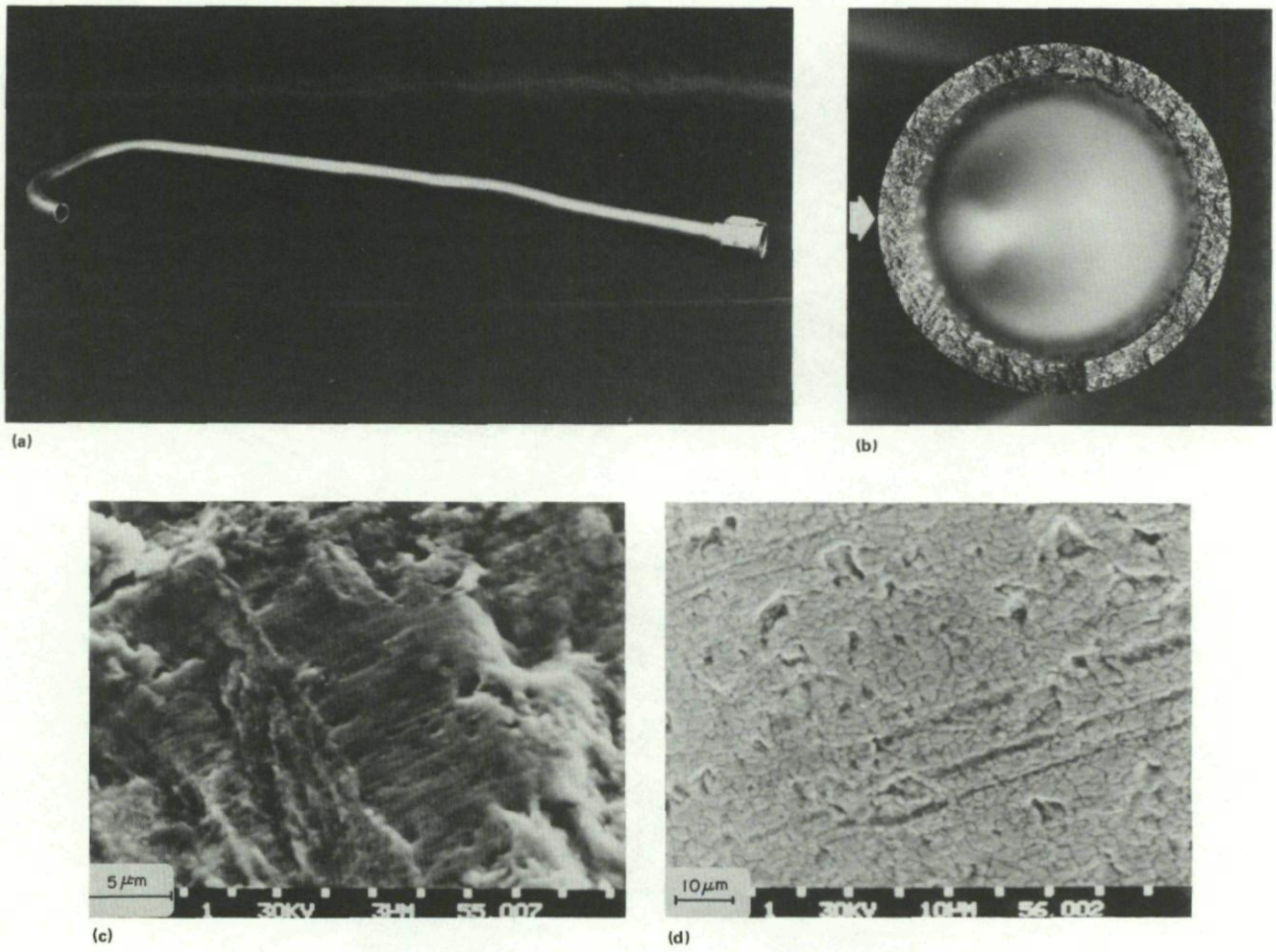

Fig. 14-14 Corrosion fatigue of a 321 stainless steel hose assembly

(a) General view of the tube showing fractured end (left).
(b) Fracture surface and the crack initiation site indicated by arrow.
(c) Fatigue striations on the corroded and pitted fracture surface close to the initiation zone. (Mag. × 3300)
(d) Surface of the tube close to the fracture face showing corrosion pits and intergranular crevices. (Mag. × 1050)

Microstructural analysis of the tubing showed that it was made from an austenitic, type 321, stainless steel (Fe - 18% Cr - 10% Ni + Ti), with a fine grained (15-30 μm) wrought microstructure showing appreciable deformation twinning.

Type 321 stainless steel is a highly corrosion resistant material which contains small amounts of titanium to stabilize the carbides. Titanium carbides form randomly throughout the grains and this prevents the formation of chromium carbides at grain boundaries in the sensitizing range of 425-870°C. Because of this it has good resistance to intergranular corrosion. It is also resistant to general corrosion and stress corrosion when in contact with dense hydrocarbon fuels (Ref. 14-12). However while it is resistant to stress-corrosion cracking in sea water, it is known to be susceptible to both stress corrosion and pitting corrosion in marine atmospheric environments such as sea shores and aboard ships (Ref. 14-13).

The presence of pitting (Fig. 14-14(d)) and fatigue (Fig. 14-14(c)) in a stabilized, corrosion resistant stainless steel suggests that fatigue, or corrosion fatigue was the primary mode of failure. There is little information on the corrosion fatigue behaviour of stainless steels, but the fact that stress corrosion cracking may occur in salt laden atmospheres under static loading conditions suggests that an environmental contribution to fatigue crack growth might also occur under certain conditions of cyclic loading. Zinc and aluminium rich coatings are effective in preventing or retarding stress corrosion and pitting in salt laden atmosphers (Ref. 14-13).

Case history 14-8. Corrosion fatigue failure of 4340 steel helicopter rotor components.

A military helicopter lost a rotor blade in flight and crashed. Several parts from the rotor blade attachment assembly and the blade were recovered from the crash site and were submitted for laboratory examination. These parts included the horizontal hinge pin and the associated nut and locking washer, which are shown in Figures 14-15(a)-(c).

Visual examination revealed that the hinge pin was broken, and the fracture face showed a flat beach mark indicating the presence of a pre-existing crack. The fracture surface and beach mark are shown in Figures 14-15(d) and 14-15(e) respectively. Also noteworthy was a dent on one side of the threaded area of the hinge pin (Fig. 14-15(f)). The threaded area was examined carefully to determine whether the nut was on the pin at the time of the crash. The nut was not recovered.

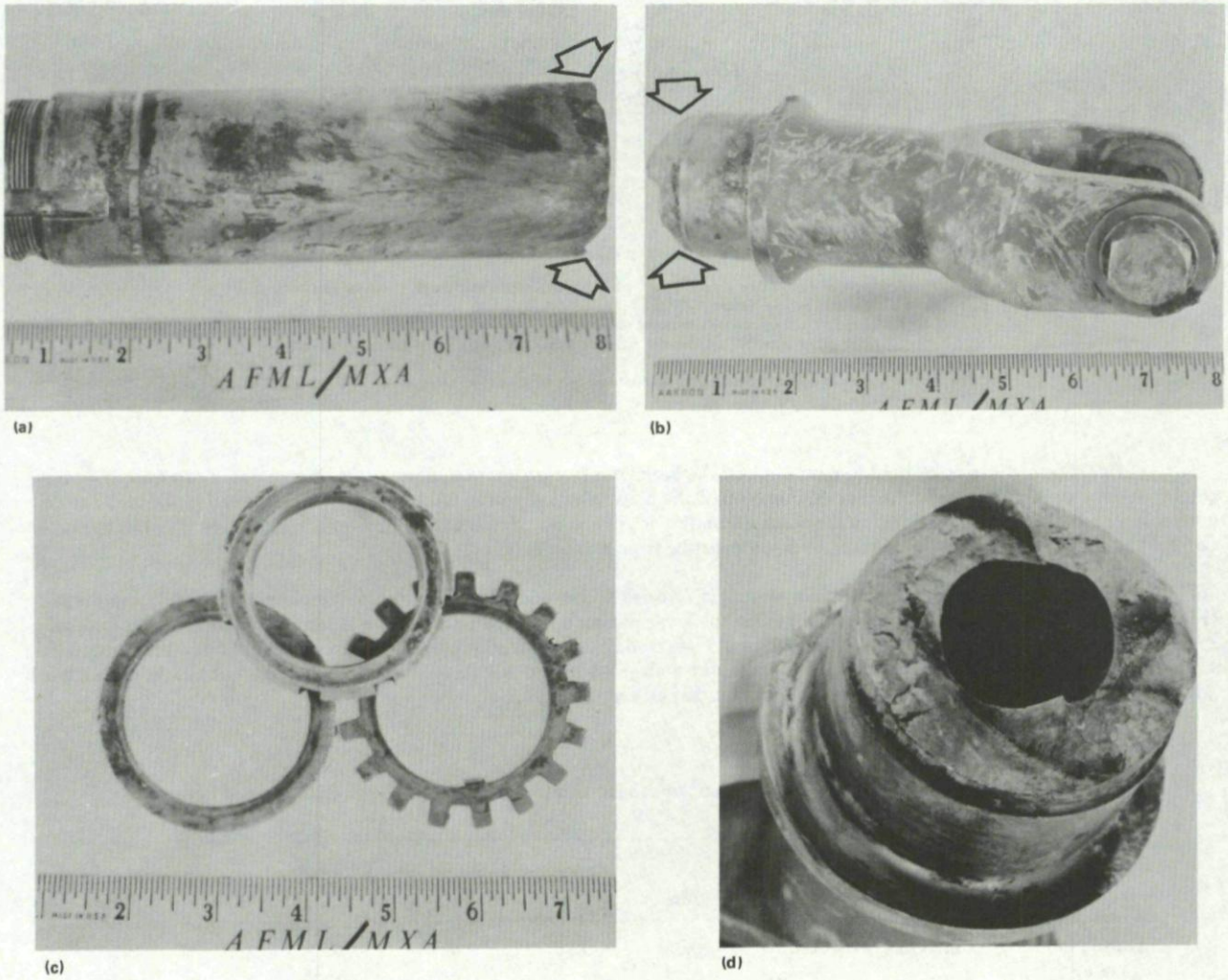

Fig. 14-15 Corrosion fatigue of a 4340 steel rotor attachment assembly

(a) Threaded end of the horizontal hinge pin with arrows indicating fracture location.
(b) Mating part of the hinge pin with arrows indicating fracture location.
(c) Nut and locking washer from the failed pin.
(d) Fracture face of the pin before cleaning.

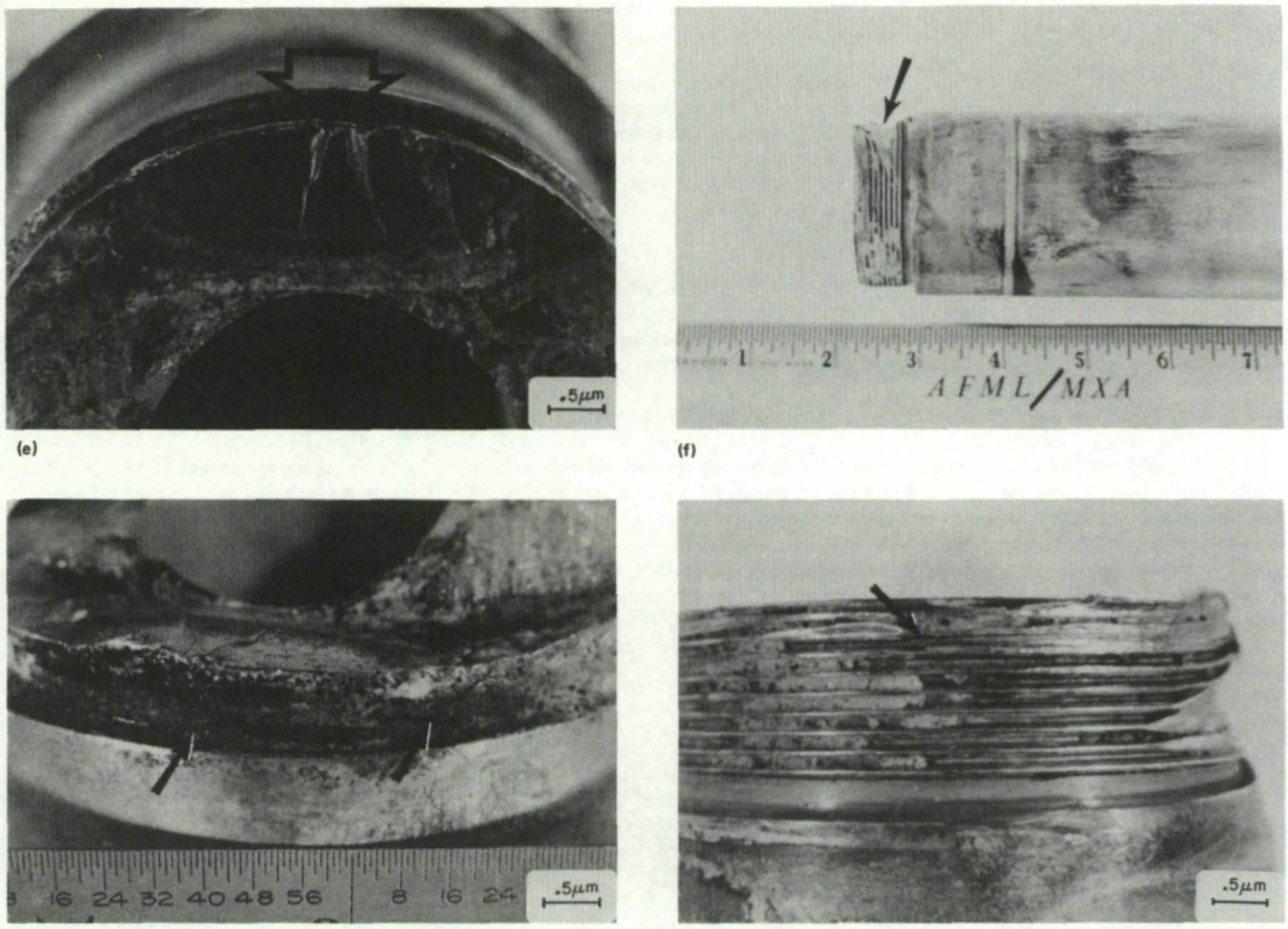

Fig. 14-15 Corrosion fatigue of a 4340 steel rotor attachment assembly

(e) Fracture face after cleaning, showing beach marks and crack plateaus in the initiation region. (Mag. × 2)
(f) Threaded end of the pin showing damaged threads.
(g) Outer circumference of the pin at the fracture showing secondary cracks and pits indicated by arrows. (Mag. × 2)
(h) Close-up of threads showing embedded thread at arrow. (Mag. × 2)

Optical examination of the hinge pin showed the beach mark or pre-crack had progressed across about one quarter of the total cylinder cross-sectional area. Further examination of the hinge pin close to the fracture initiation site revealed the presence of corrosion pits and secondary cracking on the outer circumference of the pin adjacent to the primary fracture face. The cracks ran parallel to the primary fracture and seemed to be propagating from small pits (Fig. 14-15(g)).

Examination of the threaded portion of the pin revealed an embedded thread which did not appear to come from the pin (Fig. 14-15(h)). Chemical analyses were performed on the hinge pin, an associated attachment nut, and the embedded thread. The results, shown in Table 14-1, indicated that the hinge pin was made from 4340 alloy steel, while the locking nut and the thread were made from the same 4130 low alloy steel. This suggests the embedded thread was from a nut, and that the nut had been in contact with the pin just before the sequence of events occurred that caused the crash.

Table 14-1 Chemical analysis of hinge pin, embedded thread, and attachment nut from crashed helicopter

Part		Chemical Composition, Weight %						
		Cr	Mn	Mo	Si	C	Ni	Fe
Hinge pin	(analysis)	0.80	0.65	0.23	0.35	0.40	1.90	Balance
4340 Steel AMS 6415H	Min	0.70	0.65	0.20	0.20	0.38	1.65	Balance
	Max	0.90	0.85	0.30	0.35	0.43	2.0	Balance
Embedded thread	(analysis)	1.0	0.50	0.17	0.31	0.33	—	Balance
Attachment nut	(analysis)	0.99	0.49	0.17	0.32	0.33	—	Balance
4130 Steel AMS 6370H	Min	0.80	0.40	0.15	0.20	0.28	—	Balance
	Max	1.10	0.60	0.25	0.35	0.33	—	Balance

The failure of the horizontal hinge pin was attributed to corrosion fatigue. The failure initiated in areas of localized corrosion pits, and propagated by fatigue to the depth indicated in Figure 14-15(e). The 4340 steel was found to have a hardness of R_c 41, which was within the specified range of R_c 39-43 for this part, and the part was found to be cadmium plated. As noted in Chapter 9, 4340 steel has poor corrosion resistance and corrosion protection is required in most normal operating environments. The presence of pitting in the hinge pin suggests that the cadmium plating had deteriorated to expose the underlying steel.

It was noted that the rotor assemblies were more than 11 years old, and a complete inspection and overhaul was recommended for all components, regardless of the flying hours for individual helicopters. All the rotors were disassembled and the hinge pins were inspected to ascertain the presence of cracks, corrosion pits and general corrosion. Those pins that were determined to be satisfactory for further use were stripped of cadmium, shot-peened, and re-coated with cadmium to a minimum thickness of 12.5 μm.

14.5 *References*

14-1	Heywood, R.B.	*Designing Against Fatigue.* Chapman and Hall Ltd., London, 1962.
14-2		*Corrosion Fatigue Failures.* Metals Handbook Volume 10, Failure Analysis and Prevention, American Society for Metals, Metals Park, Ohio, 1975, pp. 240-249.
14-3	Hartman, A. Jacobs, F.A. Nederveen, A. de Rijk, P.	NLR TR M2182, National Aerospace Laboratory, The Netherlands, May 1967.
14-4	Austen, I.M. Walker, E.F.	Proc. Conference on The Influence of Environment On Fatigue, Inst. Mech. Eng., and Soc. Env. Eng., London, May 1977, pp. 1-10.
14-5	Bowen, A.W.	*Corrosion Fatigue of Aircraft Materials.* AGARD Report No. 659, Neuilly Sur Seine, France, October 1977.
14-6	Kaltus, J.R.	Aerospace Structural Metals Handbook, Vol. 3, U.S. Department of Defence, Belfour Stulen Inc., Code 3406, Revised 1977.
14-7		*The Corrosion of Magnesium Alloys.* ASM Metals Handbook, 8th Edition, Vol. 1, American Society for Metals, Metals Park, Ohio, 1961, pp. 1086-1094.
14-8	Whitehead, D.J.	Trans. American Foundry Society, 69, 1961, pp. 442-456.
14-9	Brown, W.F. Jr	IN Aerospace Structural Metals Handbook, Vol. 3, Code 3206, U.S. Department of Defence, Belfour Stulen Inc., 1972.
14-10	Williams, D.N.	*Environmental Corrosion-Fatigue Behaviour of Aluminium Alloys.* DMIC Memo 249, Battelle Columbus Laboratories, Ohio, June 1970.
14-11	Speidel, M.O.	Paper 2.2, Proc. Eighth ICAF Symposium, ed. J. Branger and F. Berger, Lausanne, June 1975.
14-12	Kaltus, J.R.	See Reference 14-6, Code 1308.
14-13	Morrison, J.D.	*Corrosion Study of Bare and Coated Stainless Steel.* NASA TN D-6519, July 1972.

CHAPTER 15

MICROBIOLOGICAL CORROSION

by

Dr. P.V. Kandachar
Technological Centre
Fokker B.V.
P.O. Box 7600, 1117 ZJ Schiphol
The Netherlands

SUMMARY

Under suitable conditions, micro-organisms can flourish in the fuel tank environment and contaminate the aircraft integral fuel tanks. Unless preventive steps are taken in time, this contamination can lead to corrosion of the fuel tanks, and in extreme situations disastrous consequences can follow. In this review, several aspects of micro-organisms, their growth, their corrosive behaviour and the preventive measures that have been found to be effective in controlling the problem in aircraft integral fuel tanks have been discussed.

15.1 Introduction

Microbiological corrosion may be defined as the corrosion of metals caused by the presence and/or growth of microbiological organisms. In the beginning of 1960's, several reports and publications appeared in the technical and scientific literature describing this type of corrosion in aircraft, which was till then virtually unknown (Refs. 15-1 to 15-17). It is suggested that the interaction of two advances in aircraft design which were introduced in this period is responsible for this phenomenon which appeared after nearly fifty years of aviation development: firstly, the entry into worldwide service of kerosene-powered turbo-prop and turbo-jet engines, instead of the till then exclusively used petrol-driven piston engines. Secondly, increased adoption of the integrally machined or "wet wing" type of fuel tank in place of the rubberized fabric containers ("bag tanks") used earlier. Kerosene fuels, and water, which is either present dissolved in the fuel itself precipitating out at lower temperatures during flight or which can condense in the aircraft tanks when warm and humid air enters a cold tank, provide the nutrition for the growth of micro-organisms. This growth can cause corrosion of the metal structure of the wing tanks, even when the best corrosion protective system known is applied. Microbiological contamination can also cause plugging of fuel filters, malfunctioning of fuel probes, engine flame out or other operational difficulties. However, the scope of this review is limited to corrosion of aluminium alloy wing tanks caused due to conditions existing underneath the microbiological contamination. Extensive research investigations have been carried out in this field so that the problem is reasonably well understood, at least to an extent that control measures could be devised. This, however, does not mean that this problem is always controlled or that it can now be ignored.

Reports on microbiological corrosion of aircraft fuel tanks are often incomplete and clouded by secrecy for obvious reasons. Microbiological corrosion cannot be attributed to one single factor, but to a complex interaction between aircraft design, materials, construction, manufacture, operation, maintenance and fuel quality. Since there are at least three parties involved — the aircraft manufacturer, the aircraft operator and the fuel supplier — it is almost impossible to pinpoint which party is to be held responsible. In addition, several disciplines — aeronautical engineering, metallurgy, chemistry, microbiology, fuel technology, etc. — interact with each other in the contamination and corrosion process, making the approach towards the solution exceedingly complex. Nevertheless this problem should be seen as a common enemy and concerted efforts together and trust in each other could only produce the desired solution.

The growth, and consequences of growth of micro-organisms in the actual aircraft depend on a large number of factors: temperature, humidity, amount of water, amount of fuel, type of fuel, their conditions of storage and transportation, distribution of water in the fuel, aircraft movements affecting the distribution, aircraft idle periods, turn-around periods, the operational environment, presence of other bacteria which could affect the behaviour of corrosion causing fungus and/or bacteria, materials used in the tank construction, corrosion protection system, etc. This large number of variables makes laboratory simulation of the conditions almost impossible, while experiments in the actual aircraft is either inefficient or inconvenient or both. In addition, even if simulation is somehow achieved, the problem of relating the accelerated corrosion results from the laboratory to actual practice remains, since one has to bear in mind that the aircraft and its protective system are designed to last for decades. Nevertheless, laboratory investigations have their own value since they give some insight into the processes going on in the actual aircraft. One should, however, be extremely cautious in relating the results of the laboratory research investigations to the actual aircraft findings and vice-versa. It is therefore useful to keep in mind that the results of the many laboratory investigations cited in this review may not truly represent what is going on in the actual aircraft, although they might enlighten a particular aspect of the whole situation.

15.2 Micro-Organisms

Micro-organisms are so small that they can be seen only with the aid of special equipment like a light or electron microscope. Micro-organisms found in the aircraft wing tanks is a general term applied to microbes, bacteria, fungus, moulds, etc. Microbes are minute living beings, either plants or animals. Bacteria are small, unicellular organisms which reproduce by fission, the cell merely dividing itself in half to give two daughter cells. Under the right conditions this process may take place every fifteen minutes so that large colonies, which are readily visible, are rapidly produced (Ref. 15-19).

The cells exist in any one of the three basic shapes: rods, curved or spiral rods and spheres. The spheres average about 0.5 to 1.0 μm (micrometers; microns) in diameter; the rods from 0.2 to 1.5 μm in diameter and up to 10 or more μm in length. Spiral forms vary greatly in size. Some bacterial cells, primarily certain rod forms, are capable of forming endospores (spores with a cell). The spores, when transplanted to a suitable medium, germinate to form single cells again. Spores generally exhibit a high tolerance to heating and other inimical agencies.

Fig. 15-1 Cladosporium resinae. Scanning Electron Micrograph (Mag. × 2160)

The fungi are a heterogeneous group of plantlike organisms without flowers and without chlorophyll feeding on non-living organic material or growing as parasites on other living organisms. The fungal forms which are generally found alone or in association with corroding metals are primarily filamentous or yeastlike (non-filamentous oval cells). In contrast to some bacteria, the fungi usually require some oxygen to grow. They may obtain their energy from a substrate (a carbohydrate, for example) by a fermentative (anaerobic) or an oxidative (aerobic) mechanism. Various organic acids such as citric acid, oxalic acid, gluconic acid, dodecanoic acid, etc., which may be corrosive to metals, are products of an oxidative metabolism. The main growth of fungi consists of thread-like hyphae which form a heavily-branched, tangled growth called a mycelium. The hyphae are 2-5 μm in diameter but grow to great lengths and the mycelium can be easily visible to the naked eye. Under certain conditions specialized hyphae, called conidiophores, develop, terminating in bodies called conidia. Conidia are readily detached as spores which are equivalent to the seeds of flowering plants. Typical spores are about 5-6 μm long and 2-3 μm in diameter, and are produced in vast numbers, spreading the species about by wind, wave, insect and every other method of transport. A new plant can start growing from a piece of hyphae which has broken away from the maingrowth, just as a rose can be grown from a cutting.

Microbial growths occur often as dark, almost felt-like, slimes or sludges at any interface between water and fuel. Parbery (Ref. 15-26) has listed about 60 different fungi, 10 different yeasts and 20 different types of bacteria which are found in aviation fuel tanks (Table 15-1). Not all of them are capable of growing well in aviation kerosene. Further, of those capable of growing well, not all of them are capable of inducing severe corrosion of alloys used in the aircraft wings. The most commonly found micro-organisms in aviation fuels are the fungus CLADOSPORIUM RESINAE and the bacterium PSEUDONOMAS AERUGINOSA. Each is capable of causing severe corrosion under experimental conditions, while the fungus is the more commonly associated with the corrosion problem on a world basis. *Cladosporium resinae* was also one of the most prevalent species found in 78 aviation fuel samples examined in a programme carried out by British Aircraft Corporation under the sponsorship of U.K. Ministry of Defence (Procurement Executive) (Ref. 15-34). *Cladosporium resinae* was found in 78 percent of all jet aircraft fuel tank samples examined in Australia in 1961 and 1962, and 80 percent of samples from integral fuel tanks of 59 jet aircraft in California, examined in 1966 (Ref. 15-20). The aviation department of Shell International Petroleum Company. London, has carried out an extensive study of samples taken out worldwide in 1961 (Ref. 15-22). They have sampled and identified 380 samples originating from Europe, Near East, Africa, India and Pakistan, Far East, Australia, Pacific, North America and South America. 86 samples showed the presence of *Cladosporium resinae*, out of which 43 samples originated in Near East (Hong Kong, Manila, Singapore and Tokyo). Only two samples showed the presence of *Pseudonomas aeruginosa* in the Shell survey.

It is however possible that *Cladosporium resinae* is more capable of surviving in aviation fuel than *Pseudonomas aeruginosa*. According to Sheridan (Ref. 15-20), microbiological contamination (and corrosion), although found worldwide, appears to affect worst the tropical countries (Refs. 15-18 to 15-22).

Table 15-1 A list of micro-organisms found in aviation fuel tanks. Ability to grow in the fuel is indicated where tests were made

Name	Growth in kerosene	Information source
Fungi		
Alternaria tenuis	+	Hedrick et al. (1963)
sp. (tenuis group)	+++	Darby et al. (1968)
Aspergillus clavatus	–	Darby et al. (1968)
fischeri	++	Darby et al. (1968)
flavipes	++	Darby et al. (1968)
flavus		Anon. (1961 d); Inoue (1968)
fumigatus	++	Darby et al. (1968)
niger	–	Darby et al. (1968)
niger°	++	Hedrick et al. (1963)
niger	+	Inoue and Takao (1966); Inoue (1965)
niger		Anon. (1961 d)
ustus	–	Darby et al. (1968)
sp.	–	Darby et al. (1968)
Aureobasidium pullulans	–	Darby et al. (1968)
pullulans (as Pullularia pullulans)		Anon. (1961 d)
Botrytis cinerea		Anon. (1961 d)
Cephalosporium sp.		Anon. (1961 d)
sp.	+	Darby et al. (1968)
sp.		Kuo (1967)
Chaetomium globosum	+	Kuo (1967)
globosum		Inoue (1968)
sp.	+	Inoue (1968)
Cladosporium cladosporioides	++	Inoue (1968)
cladosporioides		Anon. (1961 d)
herbarum	–	Darby et al. (1968)
resinae	+++	Darby et al. (1968)
f. avellaneum°°	+++	Elphick (1961); many others
resinae f. resinae	+++	Hendey (1964)
sphaerosperma		Inoue (1966)
sphaerosperma	++	Darby et al. (1968)
Curvularia lunata	+	Darby et al. (1968)
geniculata	–	Darby et al. (1968)
Epicoccum nigrum	+	Darby et al. (1968)
Fusarium moniliforme	+	Davis (1967)
oxysporum		Anon. (1961 d)
roseum		Hedrick et al. (1963)
sp.	+++	Darby et al. (1968)
Geotrichum candidum	–	Darby et al. (1968)
Helminthosporium sp.	+	Darby et al. (1968)
Humicola grisea	++	Darby et al. (1968)
Isaria sp.	+	Darby et al. (1968)
Monocillium sp.	+	Darby et al. (1968)
Paecilomyces varioti	+++	Darby et al. (1968)
varioti		Leathern and Kinsel (1963)
varioti		Anon. (1961 d)
Penicillium citrinum		Anon. (1961 d)
citrinum		Inoue (1968)
cyclopium		Anon. (1961 d)
frequentans		Anon. (1961 d)
expansum		Anon. (1961 d)
luteum		Churchill (1963)
ochryochloron	+	Hedrick et al. (1963)
spinulosum		Anon. (1961 d)
spp.		Darby et al. (1968)
sp.		Anon. (1961 d)
Phoma sp.		Anon. (1961 d)
Rhinocladiella sp.		Anon. (1961 d)
Sordaria fimicola		Anon. (1961 d)
Spicaria violacea	–	Hedrick et al. (1963)
sp.		Hedrick et al. (1963)
Stemphylium sp.		Hazzard (1963)
Syncephalastrum sp.		Hazzard (1963)
Trichoderma sp.		Hazzard (1963)
sp.	–	Darby et al. (1968)
Ulociadium sp.	++	Darby et al. (1968)
Miscellaneous fungi		Darby et al. (1968)

Table 15-1 A list of micro-organisms found in aviation fuel tanks. Ability to grow in the fuel is indicated where tests were made (Cont'd)

Name	Growth in kerosene	Information source
Yeasts		
Candida albicans	+	Tanaka and Fukui (1968)
intermedia	++	Tanaka and Fukui (1968)
humicola	++	Kuo (1967)
lipolytica	++	Anon. (1961 d); Kuo (1967)
sp.		Anon. (1961 d); Kuo (1967)
tropicalis	+	Anon. (1961 d); Kuo (1967)
Hansenula mrakii		Anon. (1961 d); Kuo (1967)
Rhodotorula rubra	+	Hedrick et al. (1963)
Torulopsis famata		Anon. (1961 d)
Miscellaneous		Anon. (1961 d)
		Darby et al. (1963)
Bacteria		
Aerobacter aerogenes	+	Hedrick et al. (1963)
Alcaligenes faecalis	+	Inoue and Takao (1966)
Achromobacter cycloclastes		Hedrick et al. (1963)
Bacillus cereus	++	Hedrick et al. (1963)
cereus	+	Kuo (1967)
subtilis	++	Hedrick et al. (1963)
subtilis	+	Inoue and Takao (1966)
Clostridium sporogenes		Hedrick et al. (1963)
Comamonas sp.°	+++	Inoue and Takao (1966)
		Inoue (1968)
Desulfovibrio desulfuricans	+	Hedrick et al. (1963)
desulfuricans°	+	Iverson (1967)
Escherichia coli	+	Inoue and Takao (1966)
Flavobacterium arborescens	+	Hedrick et al. (1963)
Micrococcus caseolyticus°°		Inoue (1968)
radiodurans	+	Hedrick et al. (1963)
Pseudomonas aeroginosa°°	+++	Widely reported
cohaerens	+	Kuo (1967)
Marinoglutenosa	+	Kuo (1967)
fluorescens	++	Hedrick et al. (1963)
Sphaerotilis notans	++	Hedrick et al. (1963)
Vibrio faecalis°	+	Inoue (1968)
Miscellaneous		Hedrick et al. (1963)

– = unable to grow in kerosene; + = able to grow; ++ = able to grow very well;
° = capable of inducing corrosion; °° = capable of inducing severe corrosion.

Taken from Parbery (Ref. 15-26).

15.3 Sources of Micro-Organisms

The literature contains several references to the same fungus type and it is therefore relevant to briefly describe the history of *Cladosporium resinae*. Lindau was the first scientist who originally isolated the fungus in Germany from the resin Pinus excelsior and named it *Harmodendrum resinae Lindau* (Ref. 15-24). The status of the genus *Harmodendrum* was questioned by de Vries (Ref. 15-20) and *Cladosporium resinae* is the currently accepted name as a correct one. *Cladosporium resinae*, however, is the imperfect state (also called asexual state) of *Amorphotheca resinae*. Four forms of *Cladosporium resinae* (also denoted as *C. resinae*) are reported to exist: *f. avellaneum*, *f. resinae*, *f. albidium* and *f. sterile*, although only *C. resinae*, *f. avellaneum* is the more common in nature (Fig. 15-2). Parbery (Ref. 15-26) suggests therefore this as the possible reason for its being the more common in aviation kerosene. From its natural habitat, namely the soil where it is a natural component of the soil microflora, *Cladosporium resinae*, because of its profuse sporulation and ease with which its spores become airborne, causes widespread contamination (Ref. 15-24). As well as growing readily in kerosene, it grows on creosote used to impregnate telegraph poles and fence posts, on resinous woods, such as pine, and on asphalt used for street pavement. Some of the more obvious routes the fungi find their way into aviation fuel systems include: (1) Air, water vapour and dust drawn into storage tanks and aircraft fuel systems through vents; (2) Floating roof tanks which permit leakage of contaminated rainwater past roof seals; (3) Fuel added from tankers and barges which have been ballasted with contaminated sea water; (4) Cross-contamination from parts of a system already contaminated. Spores of *C. resinae* are also found in outdoor air. Sheridan et. al. (Ref. 15-21) have shown that in their examinations over Wellington, in New Zealand in 1970-71, that *C. resinae* forms a significant component of the airspore. According to Sheridan, *C. resinae* is also found on chicken and gull feathers and these and other birds may be important disseminating media. Rainfall is another factor. According to Parbery (Ref. 15-26), there appears to be some positive correlation between rainfall and occurrence of *C. resinae* in soils in Australia. Sheridan (Ref. 15-21), however, could not find this correlation in New Zealand.

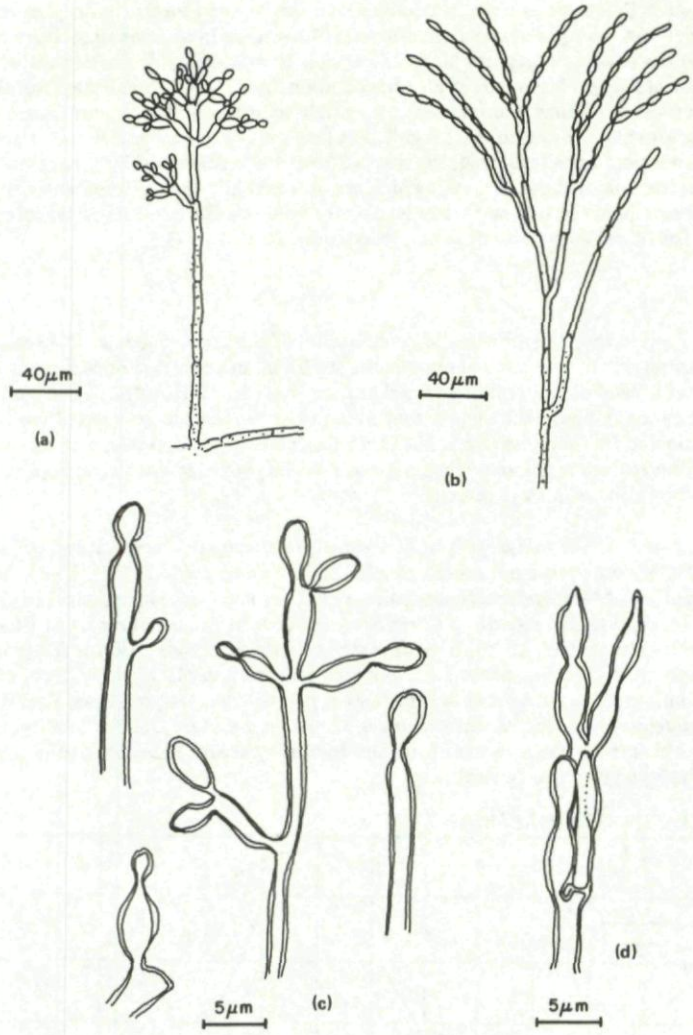

Fig. 15-2 Cladosporium resinae and its forms (Ref. 15-24)

(a) Habit study of C. resinae f. avellaneum. (c. × 300)
(b) Habit study (fertile portion of conidiophore) of C. resinae f. resinae. (c. × 300)
(c) Conidium development in forma avellaneum. (Mag. × 2200)
(d) Conidium development in forma resinae. (Mag. × 2200)

15.4 Nutritional Aspects

Micro-organisms, being the first type of life on our planet, are often regarded as "primitive"; yet, they are in a sense the most successful form of life, having survived something like 2000 million years with their amazing adaptability and having colonized almost every type of environment (Ref.15-66). Fundamentally, all micro-organisms (and all other living organisms) are the same in an important respect: their life processes are directed towards growth of the organisms and, eventually, some form of reproduction to perpetuate the species. In order to accomplish this they all require the presence of at least traces of water and sources of the other elements besides hydrogen and oxygen that are essential to life: carbon, nitrogen, phosphorous, sulphur, potassium, magnesium, calcium, iron and several "trace elements". Being microscopic in size, micro-organisms are in intimate contact with their environment, which almost always include moisture. In fact, they cannot be grown in completely water-free situations (Ref. 15-57). Due to their microscopic size and hence their extremely high surface to volume ratios, they are capable of absorbing their own weight of dissolved nutrients within a very short time in favourable environments and build more of their living material. In addition, kerosene fuel used in aircraft is more viscous and retains more water and solids than gasoline (Ref. 15-58). Once these substances are absorbed into the cell, work must be done on them into the large, complex, functional molecules (proteins, carbohydrates, nucleic acids, etc.) which constitute the living organism.

Thus an external source of energy is also required, to enable these transformations to be carried out. This energy may be derived from the oxidation of one or more of enormous range of organic substances which usually provide at the same time a source of carbon for the synthetic reactions (Ref. 15-66).

Micro-organisms obtain their nutritional requirements in an aircraft integral fuel tank from the aviation fuel and its additives, water, rubber, paints and extraneous matter. Bushnell and Haas (Ref. 15-27) have shown that petrol, kerosene, light and heavy mineral oils and paraffin wax could be used as sources of carbon. Though they examined "waterbottoms" from various petroleum storage tanks, they recorded only bacteria (*Pseudomonas* and *Coryne bacterium*). However, Hendey (Ref. 15-42) has demonstrated that kerosene vapour can provide sufficient nutriment to support the growth of *C. resinae*, provided the relative humidity is high enough. Kerosene

does not kill *C. resinae* or other moulds immersed in it; in fact conidia of *C. resinae* can survive in dry kerosene (i.e., containing no water vapour) up to 2½ years, while "wet" kerosene favours the survival of bacteria. In the overall mixture of petroleum products, microbiological growth is usually at the expense of a particularly susceptible hydrocarbons or fractions (Ref. 15-12). Parbery has shown that *C. resinae*, during its growth on jet fuel preferentially utilize the component C9 to C13 n-alkanes (Ref. 15-26). On the other hand, gasoline which contains mostly short-chain alkanes is usually not susceptible to attack by the fungus (Ref. 15-28) and this perhaps accounts for the failure of microbiological corrosion to reach significant levels in piston-engined aircraft (Ref. 15-8). Between 20 and 50 percent of the carbon assimilated is used as cell material, the rest is digested and converted by the metabolic system into oxidized compounds, such as carbon dioxide, organic acids, esters, etc., which are excreted into the environment. One of the results of this process is a reduction in surface tension between fuel and water leading into a more diffused fuel/water interface, so that the zone in which water and fuel are available for fungal growth is considerably extended (Ref. 15-17).

15.5 Growth and Survival

Although the fuel is the food source, the growth and proliferation of the micro-organisms take place in the presence of a water phase, and the highest concentrations of microbial contaminants are found in water bottoms. Fungal spores can be retained in a viable state in dry fuel, while water is needed for germination and growth (Ref. 15-4). However, when fuel is sampled, fuel is also found to contain micro-organisms, although not to the same extent as in water. Several surveys carried out to demonstrate the extent of the problem of microbially contaminated fuel supplies (Refs. 15-22, 15-32) have shown that micro-organisms were present in a high proportion of fuel samples taken from storage tanks, tankers, pipelines, refueling vehicles and aircraft tanks. The fungus *C. resinae* and bacteria of the genus *Pseudonomas* were almost always present.

The main physical factors that affect the growth of *C. resinae* in culture are: temperature, pH and relative humidity. Temperatures between 5°C and 40°C are noted, the optimum being 25-35°C on agar medium (Fig. 15-3). As regards pH is concerned, its influence is not so well known as that of temperature. Some isolents of *C. resinae* can reduce the pH in certain media to less than 2 and still survive. Parbery (Ref. 15-33) reports that growth of *C. resinae* will occur in a range of media of which the initial pH's varied between 3 and 9.6. Laboratory investigations (Ref. 15-33) have shown that large containers used for the growth of *C. resinae* provided a greater surface area for oxygen uptake by the fungus into corresponding reduction in pH. Shaking the containers inhibited growth unless the area exposed to air was limited when the growth was increased. It is thought that increased fungal growth due to increase in both the amount of fuel over the aqueous phase and its surface area is due to increased oxygen availability. Growth of micro-organisms is synonymous with their producing chemical change in their food and food they accept in aqueous solutions. Hence they are, as noted earlier, primarily associated with the aqueous phase (water).

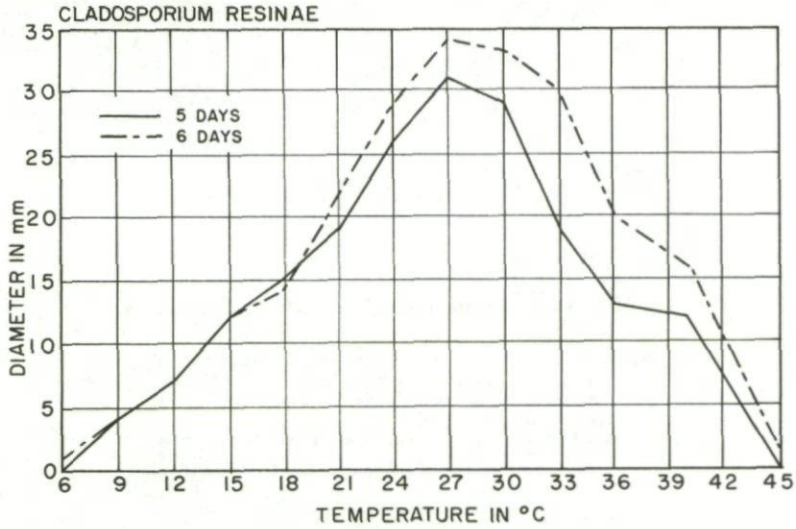

Fig. 15-3 Temperature range of Cladosporium resinae on 2% saltextract agar after 5 and 6 days

The microbiological organisms in fuel water bottom are generally oxidative and readily obtain their oxygen from that dissolved in the hydrocarbon phase provided there is adequate fuel turnover (Ref. 15-32).

Hill et. al. (Ref. 15-31) quote an air saturation level of oxygen in kerosene of 322 ppm and have shown that kerosene in equilibrium with air would, in conditions of modest turbulence, pass oxygen to an aqueous bottom at a rate and to a level which would satisfy the needs of aerobic (oxygen-requiring) organisms. Where the system remains stagnant for long periods, however, the aqueous phase is finally depleted of oxygen by the aerobic organisms there and growth of anaerobic (oxygen-disliking) organisms can occur.

Little is known of the precise effects of relative humidity, although, according to Parbery (Ref. 15-33), higher relative humidity encourages growth while at lower relative humidities growth is slow. *Cladosporium resinae* seems to survive longer in dry fuel while *Pseudomonas* survives longer in kerosene containing water (Ref. 15-31, Figs. 15-4 and 15-5).

Most of the work on microbial contamination of fuel systems has been concentrated on *Cladosporium resinae*, and the bacteria have been largely ignored. Survival of micro-organisms in jet fuel varies, from species to species, from a few hours to several months (Ref. 15-31). Organisms which do not grow on fuel, but are isolated from hydrocarbon fuel systems do not survive in fuel for as long as fuel-degrading organisms. Cooney and Kule (Ref. 15-32) found that out of 33 bacteria isolated from a hydrocarbon system, only three strains of *Pseudonomas aeruginosa* were capable of good growth and long term survival (greater than one month) in a water-fuel system. Other organisms isolated could survive for 1-11 days. The failure of the majority of these fuel isolates to survive suggests that they are chance contaminants introduced through inadequate field sampling techniques or through recent fuel contamination (Ref. 15-30).

William et. al. (Ref. 15-30) have isolated several bacterial species from samples of AVTUR (aviation turbine) fuel and found them to grow rapidly using the jet fuel on the sole source of carbon and energy. One organism, identified as *Pseudonomas putida* survived in the fuel phase for periods of up to one month. They also found that this organism grew on and oxidated a wide range of alkanes, with optimum growth occurring on octane.

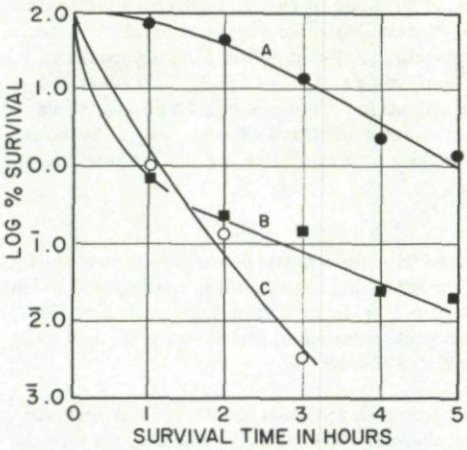

Fig. 15-4 Survival of Pseudomonas sp. strain E in aviation kerosene at 25°C. Curve A (full circles) 100 percent relative humidity kerosene. Curve B (full squares) 94 percent relative humidity kerosene. Curve C (open circles) dry kerosene. (Ref. 15-31)

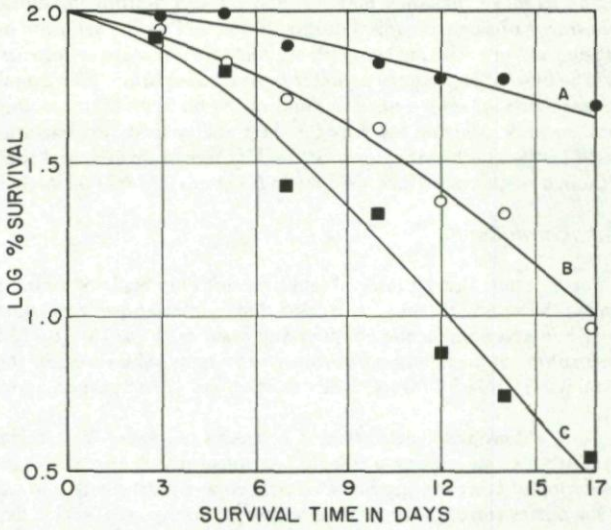

Fig. 15-5 Survival of Cladosporium resinae in aviation kerosene at 25°C. Curve A (full circles) dry kerosene. Curve B (open circles) 50 percent relative humidity kerosene. Curve C (full squares) 100 percent relative humidity kerosene. (Ref. 15-31)

Table 15-2 Evaluation of microbiological test kits (Ref. 15-37)

Parameter	Kit	Manufacturer	Type	Shelf life	Detection time	Remarks	End point sensitivity (organisms/ml)
Total microbial count	Grotan	Lehn & Fink, Montvale, N.J.	Dipslide	12-24 wk (cold); 3-6 wk (room temp)	48 h	Easy to handle; results easy to read; good agreement with lab standards	150
	Biostix	Biosan Labs., Ferndale, Mich.	Dip-pad	1-2 yr	48 h	Easy to use but pouch opening somewhat small; easy to read; good agreement with lab standards	150
	Millipore Total Count	Millipore Corp., Bedford, Mass.	Dipslide	1 yr	2-3 days	Easy to handle; hard to read; less sensitive than lab standards but may be too old	>1,000
	Microb Monitor	Boron Oil Co., Cleveland, Ohio	Vial	?	3 days	Requires syringe; negative test; medium may not be suitable for marine bacteria	$> 12 \times 10^{-7}$
	Keimindikator GK-T	Biotest, Frankfurt, West Germany	Dipslide	2 mo	2 days	Easy to handle; results easy to read; agrees with lab standards	150
	Keimindikator GK-A	Biotest, Frankfurt, West Germany	Dipslide	2 mo	2-3 days	Easy to handle; results harder to read; agrees with lab standards	150
	Easicult TTC	Orion Diagnostica, Helsinki, Finland	Dipslide	6 mo	2 days	Easy to handle; results easy to read; good agreement with lab standards	150
Fungi and Yeast	Mycostix	Biosan Labs., Ferndale, Mich.	Dip-pad	1-2 yr	3 days	Easy to handle, but pouch opening rather small; easy to read; agrees with lab standards	50
	Keimindikator HS	Biotest, Frankfurt, West Germany	Dipslide	2 mo	3 days	Easy to handle; easy to read; agrees with lab standards	50
	Millipore yeast-mold	Millipore Corp., Bedford, Mass.	Dipslide	1 yr	3 days	Easy to handle; fairly easy to read; agrees with lab standards	50
	Easicult M	Orion Diagnostica, Helsinki, Finland	Dipslide	6 mo	2 days	Easy to handle; results easy to read; good agreement with lab standards	50
	Microb Monitor	Boron Oil Co., Cleveland, Ohio	Vial	?	3 days	Requires syringe; easy to read; agrees with lab standards	50
Sulfate-reducing bacteria	S-R Deeps	Biosan Labs., Ferndale, Mich.	Tube	1-2 yr	3-7 days	Capillary difficult to handle	Less sensitive than lab standard
	API broth	Difco Labs., Detroit, Mich.	Vial	1-2 yr, not formally specified	1-3 weeks	Requires syringe	Less sensitive than lab standard
	Easicult-S	Orion Diagnostica, Helsinki, Finland	Tube	6 mo	5 days +	Capillary difficult to handle; no positive test in lab sample but positive in field sample	

15.6 Field Detection of Contamination

The problem of sampling and identification of micro-organisms is not a simple one (Refs. 15-37 to 15-39). In sampling, the minute size of bacteria and spores makes it difficult to collect all the significant organisms present, while the living nature of the organisms mean that they may be changing and multiplying during transit. Identification is complicated by the variation in the appearance of single organism during its life, and by the variation between individuals of the same species. Nevertheless a reasonably fast method of detecting contamination at an early stage is necessary, because of the impossibility of keeping storage facilities sterile and the inevitable presence of water from condensation, poor maintenance or its deliberate addition as ballast in shipboard tanks. Consequently, there is a need to monitor the build up of microbiological contamination. Bailey and May (Ref. 15-37) have tested commercially available test kits for their ability to detect bacterial and fungal contamination in hydrocarbon fuel systems (see Table 15-2). The handling ease of the kits was evaluated, and their sensitivity was compared with that of conventional methods. Although these evaluations were made for shipboard fuel tanks there is no reason why these data cannot be applied to aircraft tanks.

15.7 Corrosion

Since aircraft integral tanks are not only made of metals but are also provided with sealants and coatings to protect the metal against the corrosion, metal corrosion due to micro-organisms takes place following either the degradation of the coatings and sealants or at imperfections in the coatings and sealants (Figs. 15-6 to 15-9). The literature, however, lacks information concerning the mechanisms of degradation of protective systems, while most of the investigations have concentrated on the corrosion mechanism of metal itself (Refs. 15-40 to 15-68). A summary of the proposed mechanisms is given in this chapter.

Microbiological corrosion processes fall under the category of electrolytical corrosion processes in which electrochemical reactions play an important role. Micro-organisms are thought to cause corrosion by enhancing these reactions primarily through the formation of corrosive products, oxygen concentration cells and cathodic depolarization (Ref. 15-51). Menzies (Ref. 15-56) notes that at the outset corrosion brought about by microbiological action usually occurs by a number of mechanisms which are, in themselves, reasonably well understood as corrosion phenomena per se. Some of the major mechanisms of interest here in relation to microbiological action are, according to him:

1. the production of corrosive metabolic products;
2. the production of differential aeration and concentration cells;
3. depolarization of cathodic processes;
4. disruption of natural and other protective films; and
5. the breakdown of corrosion inhibitors.

When the above named general mechanisms are applied to corrosion induced by micro-organisms on aluminium alloys employed in the wing structure, two principal mechanisms emerge, viz., (1) production and secretion into environment of a wide variety of water soluble organic acids as waste products of the metabolism of the micro-organisms, (2) a hypothesis based on oxygen concentration gradient. Since little or no oxygen can reach the lower layers of an actively growing microbiological colony, an oxygen concentration gradient is established which is supposed to cause an adequate potential difference leading to electrochemical corrosion (Ref. 15-51). The galvanic cells so produced may have voltage differences of up to 60 milli-volts, sufficient to cause rapid pitting of the alloys (Ref. 15-71). Such a condition may also lead to undesirable effects as suggested by Iverson (Ref. 15-45). He suggests that under conditions of severe oxygen depletion, *Pseudomonas aeruginosa*, the fungus *Cladosporium* and other aerobic or facultative organisms live in close association with the anaerobic sulphate reducer *Desulfovibro* to form, along with the corrosion products, a visible tubercular mass on the tank bottom. Once such deposits consisting of corrosion products and masses of micro-organisms are formed, a pit usually develops under a tubercle and corrosion is likely to proceed almost independent of the metabolic activity of the micro-organisms.

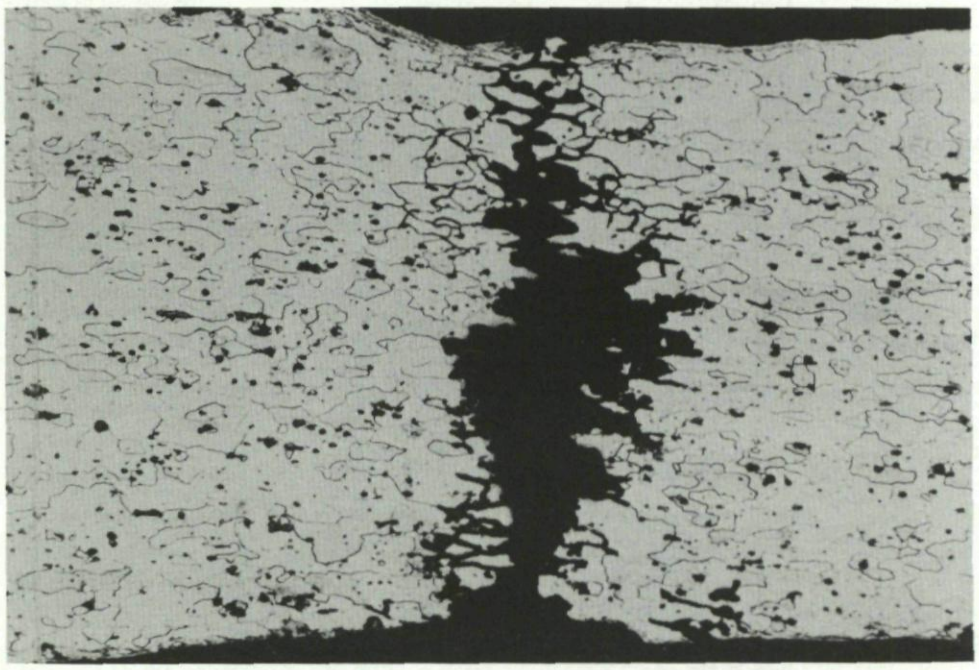

Fig. 15-6 Typical perforation corrosion caused by micro-organisms. Alloy: 2024 (Al-Cu-Mg)

Hedrick (Ref. 15-52) has proposed another mechanism wherein the corrosion of aluminium alloys by micro-organisms, particularly bacteria, is considered to be a result of the removal of metallic atoms (major and minor) from the basic structure of the alloy by extracellular enzyme activity. Engel (Ref. 15-53) supports this hypothesis. It is unlikely that a single mechanism is operating under all circumstances. As noted by Iverson (Ref. 15-51), biologically stimulated corrosion in natural environments is in all probability due to a number of mechanisms, operating either simultaneously or in succession.

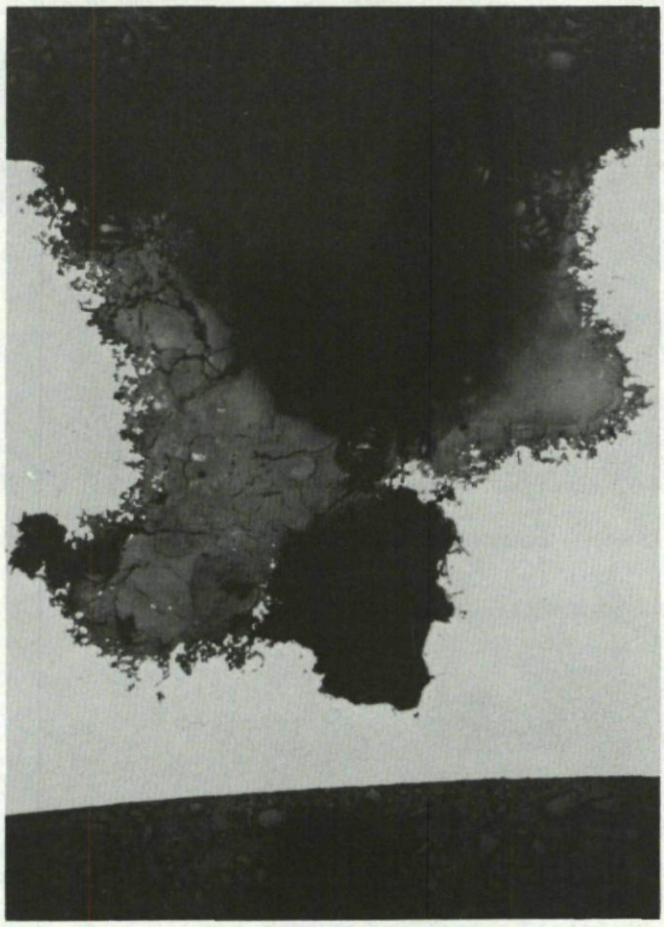

Fig. 15-7 Typical microbiological corrosion. Alloy 5052 (Al-Mg)

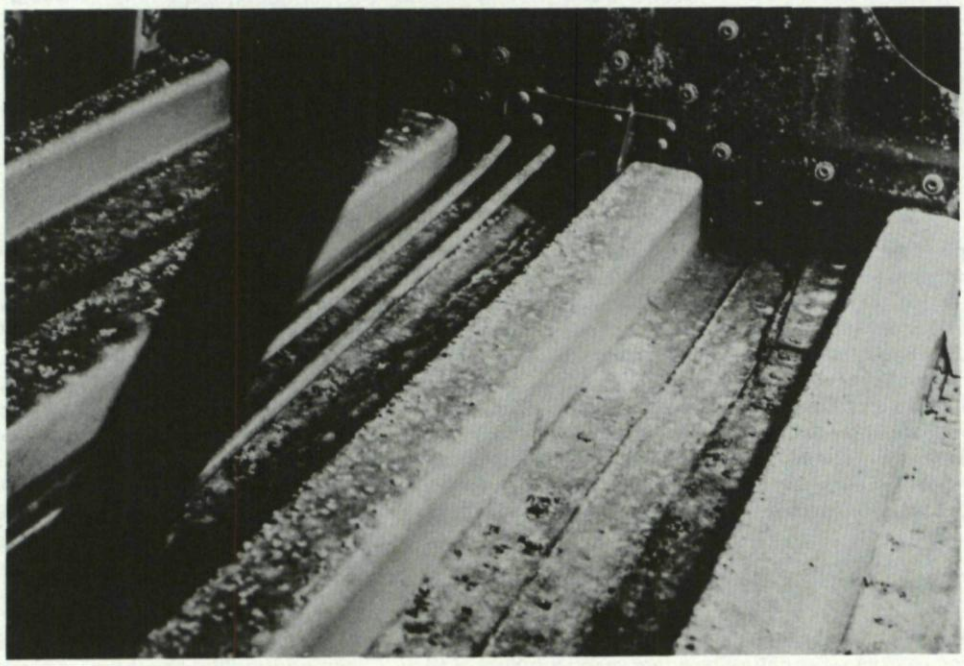

Fig. 15-8(a) Typical view of integral fuel tanks with microbiological corrosion

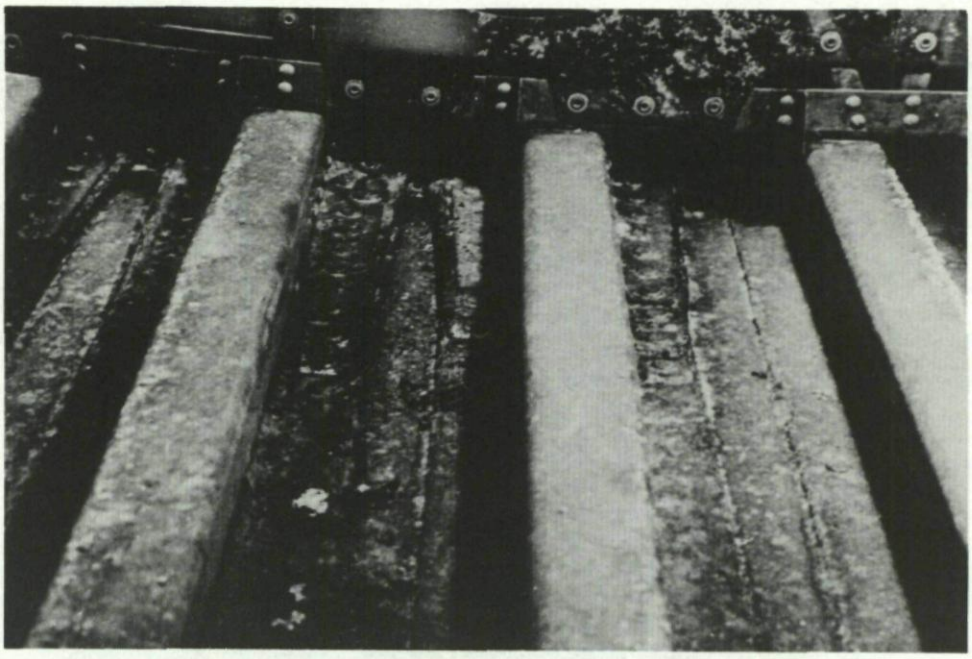

Fig. 15-8(b) Typical view of integral fuel tanks with microbiological corrosion

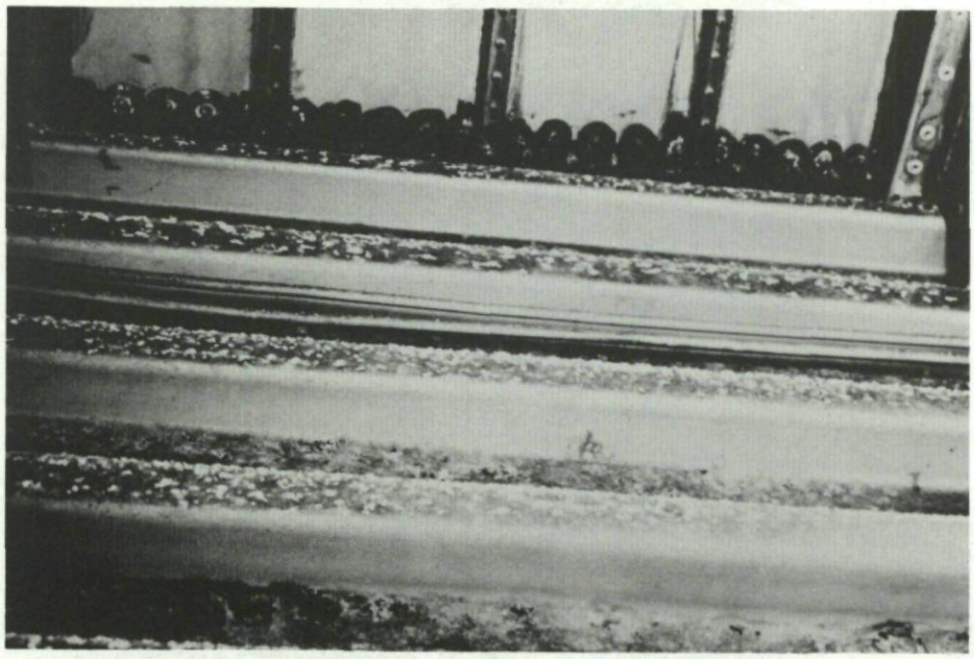

Fig. 15-9 Typical view of integral fuel tanks with microbiological corrosion

Attempts to get an insight into the mechanism of microbiological corrosion have also revealed results of interest to aircraft manufacturers and operators. For example: (1) 2024 alloy corrodes more rapidly than 7075 when exposed to *Cladosporium* (Ref. 15-12, Fig. 15-10); (2) polarization curves of aluminium alloy 2024-T351 in the aqueous phase in equilibrium with jet fuel could provide a means for determining the effectiveness of maintenance operations performed or stored fuel (Ref. 15-63); (3) the Air Force Materials Laboratory at Wright-Patterson Air Force Base, Ohio, USA, has attempted to determine the effects of microbiological corrosion on the fatigue life of aluminium fuel cell skins. They have investigated the materials 7075-T651, 7079-T651, 7178-T651 and 2024-T351 aluminium alloys. They found that chemical and microbiological corrosion produced in the laboratory could closely duplicate the appearance of the corrosion found in integral fuel cell skins from Air Force service aircraft. They could test a limited number of microbiologically corroded specimens for their fatigue lives and found that microbially corroded pits with depths equivalent to the chemically corroded pits could be expected to have a slightly more detrimental effect on the fatigue life of the alloy. In fact, a chemically corroded pit of 0.25 mm depth would reduce the fatigue life of the alloys by 50 to 70% according to this investigation (Ref. 15-43, Fig. 15-11).

15.8 Preventive Measures

Once it is recognized that micro-organisms are found on spores practically everywhere on earth and can flourish in the presence of aviation fuel and water optimally at temperatures typical of tropical countries, it is obvious, as has long been recognized, to take preventive measures concentrated on removing water, the main culprit. Although the solution appears simple, it is not always practical, since it is almost impossible to remove all water at all times (Refs. 15-69 to 15-84).

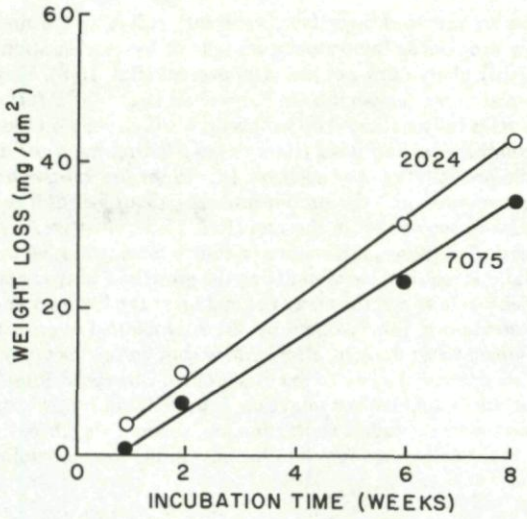

Fig. 15-10 Corrosion of aircraft alloys by Cladosporium (Ref. 15-12)

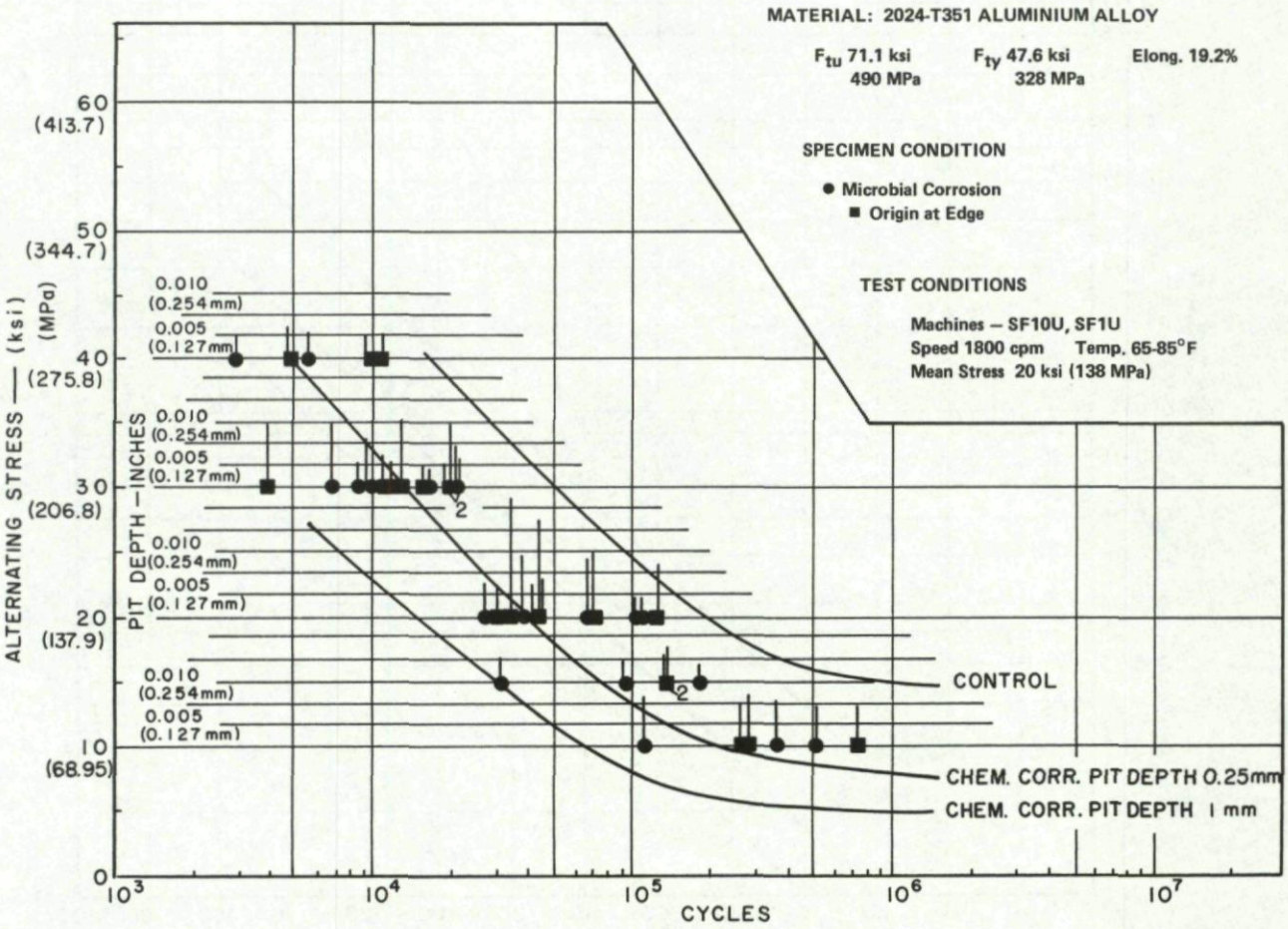

Fig. 15-11 Fatigue curve, microbial corrosion, 2024-T351 alloy, mean stress 20 ksi (138 MPa) (Ref. 15-43)

15.8.1 Water

Aircraft manufacturers after several years of experience in designing and constructing wing tanks have largely improved the wing tanks to such an extent that most water can be drained away, at least if drained regularly. For instance, blind areas of the tank and areas which may allow water accumulation are eliminated by design or redesign. Cross-feed drains are placed through the stiffening members in the bottom of the tank allowing free drainage of water to the low point drains. Drainage of the tanks is also aided by the use of ramp seals which are made in place by tailoring fuel tank sealing compound into desired contours to direct the flow of fluids along the tank bottom and to the low point drains. Water removal systems, such as scavengers, drain spirals combined with fuel ejectors have also been used (Ref. 15-80).

Although good drainage facilities are provided these days, water may still enter the aircraft fuel tanks either by precipitation of the dissolved water in the fuel forming droplets as the temperature falls or by condensation of warm moist air within the tank coming into contact with cold structure, particularly during or just after descent (Ref. 15-6). Very approximately, kerosene contains a parts per million (ppm) water content equal to the temperature in Fahrenheit i.e., at 70°F fuel can contain about 70 ppm dissolved water (Fig. 15-12). Whether the aviation fuel is fully saturated up to this limit will depend on the relative humidity of the atmosphere in contact with it, provided equilibrium conditions are achieved (Henry's law). Therefore, if fuel is cooled in flight from say 70°F to say 30°F, up to 40 ppm of free water could precipitate out of solution. Due to the low relative humidity of the atmosphere at high altitudes, much of this precipitated water evaporates into the air, but probably about half of it remains in the fuel tank, some of which collects at the bottom, whilst some remains in suspension in the fuel (Ref. 15-6). However, according to Elphick the amount of dissolved water is so small, that for all practical purposes, this water as a source in contributing towards the growth of micro-organisms may be neglected. He suggests that free water is required for stimulating the growth of micro-organisms. Condensed water in the form of droplets may not obey the expected drainage laws and thus may not end up at the lowest points in the wing tanks where the drainage points are often located. Further water retention is also favoured by the microbiological growth since the fungus mat is capable of retaining water. One could consider postponing water draining after landing (but before take-off) to a later stage as possible to give sufficient time for condensed water to settle down and move to the drainpoints. One could consider also refuelling as soon as possible to reduce the airspace above the fuel and thus minimize condensation, especially on longer stops and particularly under humid conditions. Since higher humidity increases the likelihood of contamination, particularly where it is associated with high fluctuating temperatures, aircraft based permanently in the tropics are found to be most prone to microbiological contamination and eventually corrosion (Ref. 15-6).

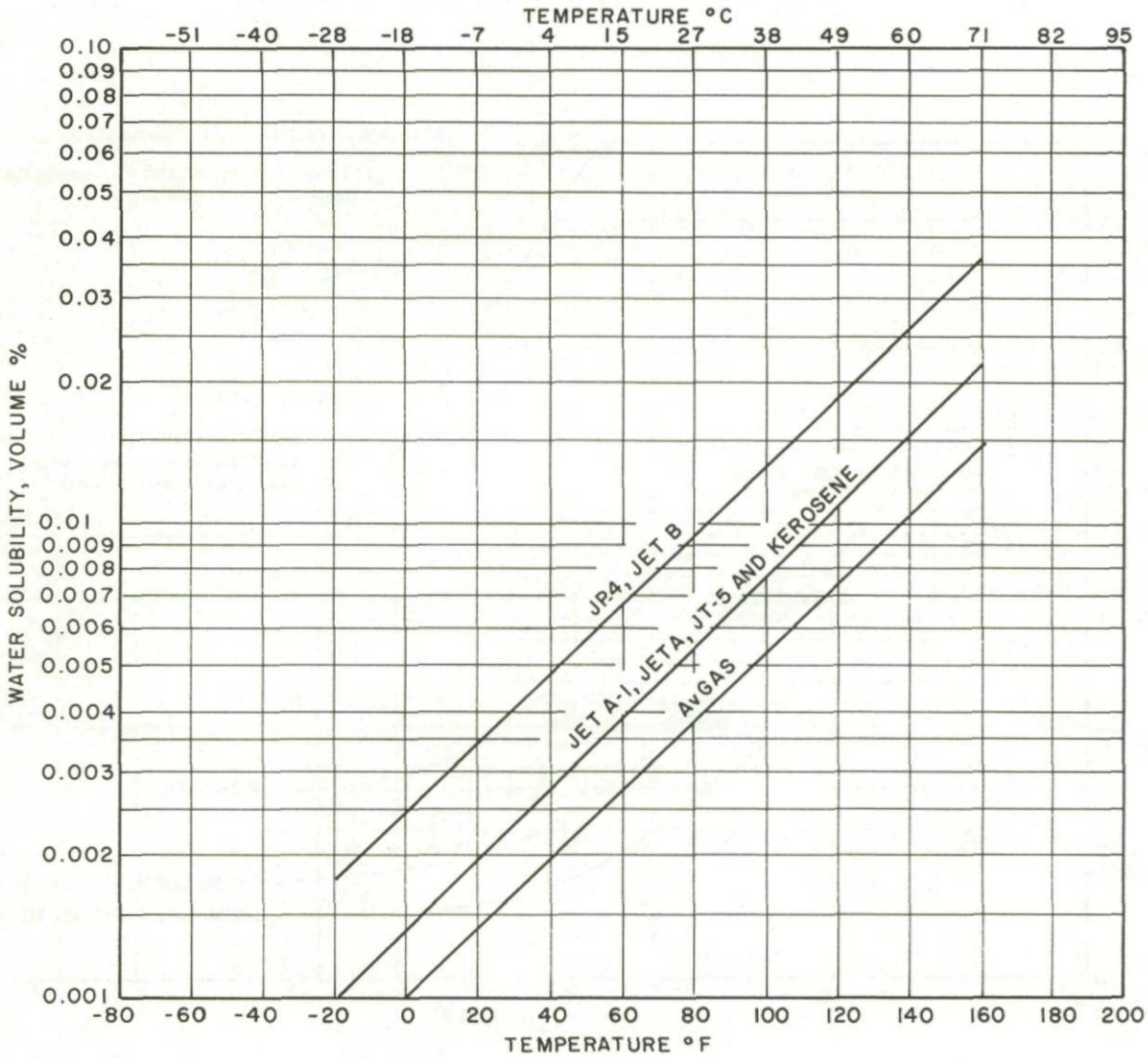

Fig. 15-12 Solubility of water in aviation fuels

15.8.2 Tank protective coatings

Inspite of all the measures, water still enters the fuel tank and therefore aircraft manufacturers have also sought to protect the wing tank bottoms by application of fuel tank coatings, such as Buna-N rubber films, through etch primers, epoxy polyurethane coatings, polysulphide sealants, etc. All these coatings are more or less permeable to moisture or to acid products (Ref. 15-43) especially at weak spots in the coating, giving rise to the possibility of localized attack.

Miller et. al. (Ref. 15-71) have tested 3-mil (75 microns) films of Buna-N, fluorocarbon EC-1981, silicone rubber and polyurethane PR-1560 for their water vapour transmission characteristics. Buna-N had the lowest moisture transmission rate of all the films tested while the polyurethane and silicone rubber were relatively permeable to moisture. Further they also tested Buna-N and polyurethane films to determine whether or not they could be penetrated by micro-organisms. These tests demonstrated that both films are permeable to the passage of fuel-bottom micro-organisms with the polyurethane film being the more resistant of the two. The rate of oxygen uptake by *Cladosporium resinae* and *Pseudomonas aeruginosa* is also higher in a polymer of acrylnitrile and butadien (EC 776) compared to polyurethanes (PR 1560, DeSoto 1080) according to Hedrick (Ref. 15-52). Buna-N coatings are thin and this is perhaps the reason for its generally outspoken poor performance, although several aircraft with Buna-N coating are still flying without any problems of microbiological corrosion. Further, Buna-N rubber coatings can be utilized and penetrated by *Cladosporium resinae* (Ref. 15-57). Thicker coatings are obviously of some help because of increased protection, although this would have to be chosen at the expense of some weight. The better protection is mainly due to the higher resistance to penetration by micro-organisms due to the greater thickness. Their use is worth considering in critical areas where contamination is likely or where access for cleaning or repair is difficult (Ref. 15-7).

Unlike most synthetic resins, polyurethanes have frequently been found to be subject to direct attack by micro-organisms, especially by fungi. According to Seal and Pathirana (Ref. 15-84) there is considerable presumptive evidence that the polyester type of polyurethanes is commonly attacked by fungi whereas polyethers may be completely or almost completely resistant.

15.8.3 Fuel cleanliness

Although aviation fuel produced at a refinery is in itself sterile and free from biological contamination, it may get contaminated during transportation by ship, rail, road or pipeline to the airfield. During this process fuel may become contaminated by other petroleum products, dirt, water, surfactants and by microbiological material. All the major fuel suppliers usually take steps to minimize these contaminations by one or more of the several ways: handling aviation fuel in segregated systems, filtration, provision of filter/water separators at various stages in the system, particularly in airfields, etc. As far as microbiological contamination is concerned, very little can be done to prevent the presence of spores except by addition of biocides which of course makes the fuel costlier. Further, since microbiological spores are found everywhere even outside the fuel system and since, due to their size, they cannot be removed adequately by filtration (and only a few need to get through), they will always grow if fuel and water and optimum temperature conditions are available.

15.9 Biocides

In the previous sections, it has been shown that microbiological contamination of turbine fuels in aircraft fuel tanks and fuel distribution systems has been a quality control problem since the late 1950's. Since micro-organisms require water to grow, good housekeeping and water removal practices are important at all points in the distribution system. This would include refinery, pipeline, bulk terminal, airfield system and the aircraft itself. The practice of allowing sufficient settling time in all storage tanks, maintaining filter/separator equipment in serviceable condition and sumping or draining free water regularly from all storage tanks, filter sumps, refueller tanks and aircraft tanks will help insure fuel free of water and particulate matter. However, often this is not enough. Microbiological fuel tank contamination problems vary considerably from one operator to another. In addition to the aforementioned good housekeeping practices, which are often beyond the operator's control, there are many other variables. Some of these are: type of aircraft in their fleet; how well the aircraft tanks drain and if they have a water scavenging system; their geographic routes and flight schedules; fuel tank inspection practices and frequency; use of fuel biocides; etc. Since there are many factors beyond the operator's control, a number of airlines either have or are using chemical methods on a periodic basis to control their microbiological fuel tank contamination (Refs. 15-85 to 15-96). Physical methods of inhibiting microbial growth are not very practical, although gamma-ray sterilization of integral tanks has been considered (Ref. 15-91). The use of chemicals which kill micro-organisms (biocides — the collective name for fungicides and bactericides) or merely prevent their reproduction (biostat) is the more usual approach. In practice the same chemical may act in either way according to dilution and the distinction between the words tends to become vague (Ref. 15-91).

Rogers and Kaplan (Ref. 15-89) have listed the requirements for an ideal biocide. The characteristics for an ideal fuel biocide do not differ greatly from those for any other fungicide or bactericide but are dictated to some degree by its specific use. The biocide must:

(1) be toxic to both fungal and bacterial organisms at low concentrations, preferably at 5-10 ppm,

(2) be non-toxic to mammals at use concentrations,

(3) be fuel- and/or water soluble,

(4) be stable over a range of operational temperatures (18°C-55°C),

(5) be harmless to materials with which the biocide may come in contact (non-corrosive to metals and compatible with other fuel additives and fuel tank coatings),

(6) not form soaps or emulsions with fuel,

(7) have a low ash content,

(8) be easily handled and capable of being readily mixed with fuel or water bottom,

(9) be stable in storage,

(10) be easily detected by a simple quantitative analytical procedure to monitor concentration,

(11) be reasonable in price, and

(12) have no deleterious effect on engine performance and engine.

No generally accepted biocide has met all of the above criteria. Roger and Kaplan (Ref. 15-89) have also made a comprehensive screening of 97 possible water and fuel soluble materials. Active laboratory investigations continue to take place, while only three

biocides have so far received any significant practical application in aircraft fuel systems, namely various chromates, ethylene glycol monomethyl ether (EGME) and a proprietory mixture of two organic compounds:

2,2′-oxybis(4,4,6-trimethyl-1,3,2-dioxaborinane) and

2,2′-(1-methyltrimethylenedioxy)bis-(4-methyl-1,3,2-dioxaborinane).

A water soluble, fuel-insoluble material such as sodium or potassium or strontium chromate or dichromate has obvious attractions, not least among which are the anti-corrosive properties of these compounds. However, free water persists not only at the lowest level of a fuel tank, but also at numerous sites along its floor, e.g. where condensed water drips from protrusions in the upper wing structure. The application and replenishment of chromate materials at such diverse sites presents considerable practical difficulties, bearing in mind the high rates of leaching which may prevail (Ref. 15-90). For example, strontium chromate is known to be a good inhibitor of metal corrosion and is extensively incorporated into paints applied to the internal surfaces of aircraft integral wing fuel tanks or their rubber sealants. It is an oxidizing agent and has microbiocidal activity under correct conditions. Strontium itself is reputed to have activity against some fungi as are chromium and chromates (Ref. 15-92). This has prompted some manufacturers to place strontium chromate in the form of tablets at strategic locations in the fuel tank where water is expected to collect, since strontium chromate is soluble in water but not in aviation kerosene. No cases of microbiological contamination have been reported from aircraft installed with strontium chromate. On the other hand, Rubidge (Ref. 15-92) found that strontium chromate tablets in which a binder was used to hold the chromate in tablet form is not a powerful biocide since the binder itself was a microbial nutrient. However, he found that strontium chromate in pure state does inhibit *Cladosporium resinae*, provided the biocide can be made to reach water, since strontium chromate does not dissolve in fuel. EGME and organoboron compounds on the other hand, are applied as solutions in the fuel. By virtue of their high partition coefficients with respect to water, comparitively low concentrations in the fuel phase can build up higher, biostatic or biotoxic, concentrations in a water phase in contact with the fuel (Ref. 15-90). Hill (Ref. 15-91) has examined the influence of aviation kerosene/water ratios on biocide and has conducted experiments with EGME and the proprietory organoborate mixture (Biobor JF). He found that for acceptable treatment levels, sterilization required several days to achieve. Elphick and Hunter (Ref. 15-90) have also examined the effectiveness of EGME and organoboron compounds as intermittent biocidal treatments against *Cladosporium resinae*. In this connection, Elphick and Hunter make the following relevant remarks to show how critical the action of biocides in the actual aircraft is:

> "The combined effects of fuel impregnation of the inoculum and the rate of partition of biocide into the water phase may exert a considerable effect on the efficiency of a biocide. Nevertheless, intermittent application of biocide to aircraft fuel systems may be clearly successful in controlling fungal contamination under suitable conditions. However, when one considers the possible implications of other factors which may intervene in practical applications of biocides to aircraft, the situation becomes more complex. Agitation of the fuel and water phase during flight will increase the rate of partition, while reduced fuel temperatures during flight will increase the partition coefficient, particularly of EGME. On the other hand, dilution of biocide-treated fuel with untreated fuel at subsequent refuelling points, and leaching of biocide from the fuel and dilution of biocide in the water phase by precipitated or condensed water, will serve to diminish biocidal efficiency.
>
> Of perhaps even greater importance are the environmental factors which will dictate whether, and to what extent, microbial growth will occur in a particular aircraft. It is well established that an aircraft operating predominantly in temperate regions is unlikely to develop significant fungal growth in its fuel tank. The same aircraft, if operated in tropical or subtropical regions, may develop extensive growth within a few months of entering service in these regions. Temperature by itself would at first glance seem unlikely to exert such a dramatic effect; *Cladosporium resinae* and other micro-organisms isolated from aircraft fuel systems are capable of rapid growth at ambient temperatures prevailing in temperate areas. An indication of a possible explanation lies in the persistence of ice in aircraft wing tanks. After a transatlantic flight, ice may persist inside the integral tanks of a large airliner for more than 24 hours after landing at London on a normal "temperate" day. The temperature of any associated free water in the tank during this period will probably remain too low for appreciable microbial growth to occur. Indeed, it may prove that water in the fuel tanks of aircraft regularly operating even short-haul services in temperate regions attain temperatures conducive to microbial growth for surprisingly limited periods. In the tropics, fuel tank temperatures during flight may be somewhat lower, and moreover the wing will heat up and ice in the fuel tanks will melt much more rapidly after landing. Hence factors which will affect the temperature of free water in the fuel tanks, such as duration and altitude of flight, amount of fuel remaining in the tank on landing, duration of time spent on the ground, and ambient sun and shade temperatures on the ground, may all combine to influence the extent of growth.
>
> Another major consideration is the extent to which an aircraft is exposed to microbial contamination. Although it must be assumed that all aircraft will receive contaminated fuel from time to time, inoculum potential may be an important factor. Cases where "cleaning up" ground installations has apparently resulted in a reduction of microbial problems in aircraft using these facilities has at least provided positive *prima facie* evidence. The interaction of all these factors, and undoubtedly others, suggest that there may well be a very narrow borderline between a set of conditions under which an aircraft will remain virtually free of microbiological growth, and those under which significant growth will occur. When conditions near to this borderline prevail, intermittent use of even a relatively inefficient biocide such as EGME may be sufficient to swing the balance in favour of trouble-free service. On the other hand, under really severe operating conditions an even more efficient material such as organoboron may fail to keep the problem in check unless it is used very frequently. At present the nature and extent of the imponderables is such that an accurate forecast of a minimum effective treatment schedule is impossible."

Therefore, as Rogers and Kaplan (Ref. 15-89) point out, the crucial test of the effectiveness of a fuel/water biocide is a full-scale field exposure evaluation with close observation and careful analysis under conditions which arise in practice. The field exposure test conditions of expected use should be the primary criterion for evaluating the effectiveness of biocide treatments and should be the standard against which the laboratory biocide test method is calibrated.

As noted earlier in Section 1, the laboratory evaluation of a microbial problem is carried out under conditions that attempt to simulate field conditions. These conditions necessarily differ from the wide spectrum of field conditions in order to meet workable and practical laboratory limitations. It is therefore not possible to accurately predict the performance of a biocide in the field on the basis of its laboratory performance. However, without laboratory test data it is impossible to assess the comparative merits of different compounds and laboratory methods and to relate the laboratory test results back to actual field performance (Ref. 15-89).

15.10 Concluding Remarks

Considerable experience has been collected on the subject of microbiological corrosion since the occurrence of the first serious problem in aviation so as to devise preventive measures to control the problem. Although the application of corrosion protection systems and the use of biocides have been found to be successful, the best control appears to be the elimination of stagnant water from the fuel supply system and aircraft fuel system.

15.11 Acknowledgements

The author gratefully acknowledges, Ir. R.J. Schliekelmann, Manager, Fokker Technological Centre for providing permission to publish this review, his several colleagues for many helpful discussions and comments, Dr. H.P. van Leeuwen of National Aerospace Laboratory, The Netherlands for stimulating him to write this chapter, Dr. W. Wallace of National Aeronautical Council, Canada and Mrs. T. Kijlstra of KLM-Royal Dutch Airlines for providing helpful literature. Many thanks are due to Mrs. J. van Zanten for her help and patience in realizing this manuscript.

15.12 References

Inspite of the relatively large number of publications listed below, the author does not pretend this to be a complete coverage, especially in view of the many unpublished internal reports of manufacturers, suppliers and aircraft operators. The literature available to the author and compiled to produce this review can be broadly classified as those containing general information covering practically all aspects of microbiological corrosion (on which Section 1 is based) and those containing specialized information (on which the remaining sections are based), although in many cases they overlap, due to the complex nature of the subject. The reader is advised to bear this in mind when referring to the particular publication.

Section 1: Introduction

15-1	Donahue, T.B.	*Microbiological Fuel Contamination and Corrosion.* Lockheed Field Service Digest, 7 (5), 3-13 (1961).
15-2	Digman, W.J.	*Effects of Fuel Contamination on Corrosion of Aircraft Fuel Systems.* National Aerospace Engineering and Manufacturing Meeting, Los Angeles, Calif., Oct. 8-12, 1962, Paper 575A.
15-3	Anon	*Microbial Contamination and Corrosion in Integral Fuel Tanks.* Convair Traveller, Jan./Feb. 1963, 3-11.
15-4	Lansdown, A.R.	*Microbiological Attack in Aircraft Fuel Systems.* Journal of the Royal Aeronautical Society, 69, 763-767 (1965).
15-5	Boggs, W.A.	*Contamination + Microbes = Corrosion + Malfunctions: An Equation Which Yields Trouble for Aircraft Integral Fuel Tanks.* S.A.E. Paper 680231, Society of Automotive Engineers, Business Aircraft Meeting, Wichita, Kansas, April 3-5, 1968.
15-6		Symposium on the Microbiological Contamination of Integral Fuel Tanks, organized by British Aircraft Corporation, Weybridge, June 10, 1970.
15-7	Scott, J.A.	*Microbiological Contamination of Aircraft Fuel Tanks — Airframe Considerations.* SAE Paper 710438, Society of Automotive Engineers, National Air Transportation Meeting, Atlanta, Ga, May 10-13, 1971.
15-8	Elphick, J.J.	*Microbial Corrosion in Aircraft Fuel Systems.* IN Microbial Aspects of Metallurgy, J.D.A. Miller (Ed.), Medical and Tech. Pub. Co. Ltd., Aylesbury, U.K., 1971, Chapter Six, 157-172.
15-9	Scott, J.A. Hill, E.C.	*Microbiological Aspects of Subsonic and Supersonic Aircraft.* Paper presented at a symposium on microbiology, held at Mount Royal Hotel, London, 27-28 January 1971.
15-10	Iverson, W.P.	*Biological Corrosion.* IN Advances in Corrosion Science and Technology, Vol. 2, M.G. Fontana and R.W. Staehle (Editors), Plenum Press, New York-London, 1972, 1-42.
15-11	Allan, K.	*Treatment of Corrosion on Airframes.* Anti-corrosion, 9-14 (October 1973).
15-12	McKenzie, P. Akbar, S.A. Miller, J.D.A.	*Fungal Corrosion of Aircraft Fuel Tank Alloys.* I.P. Symposium 29 April 1976, Issued at Institute of Petroleum, Technical Paper 37/50.
15-13	Arnold, J.B.	*Microbes and Materials.* Engineering, August 1978, 772-774.
15-14	Boeing Commercial Airplane Company	*Wing Tank Microbial Growth and Corrosion.* Boeing/Airline Regional Conference, Singapore/Nairobi/Miami, 1980.

15-15 Anon — *The Microbiology of Aircraft.* Materials Quality Assurance Directorate, U.K. Ministry of Defence, 1980 (?).

15-16 Lingus, Aer — *Microbiological Fuel Tank Corrosion.* Presented at the 15th Meeting of the European Airlines Committee for Materials Technology, Dublin, September 1980.

15-17 Anon — *Microbiological Contaminations of Aviation Fuels.* Air B.P. International, 1981.

Section 2: Micro-organisms

15-18 Hedrick, H.G., Carroll, M.T., Owen, H.P., Pritchard, D.J. — *Viability of Selected Micro-Organisms in Hydrocarbon Fuels.* Appl. Microbiol., 11, 472-475 (1963).

15-19 Miller, J.D.A. — *Introductory Microbiology.* IN Microbial Aspects of Metallurgy, J.D.A. Miller (Editor), Medical and Technical Publishing Co. Ltd., Aylesbury, U.K., 1971.

15-20 Sheridan, J.E. — *Studies on the Kerosene Fungus Amorphotheca Resinae in New Zealand.* Int. Biodetn. Bull., 8 (2), 65-74 (1972).

15-21 Sheridan, J.E., Soteros, J.J. — *A Survey of Fungi in Jet Aircraft Fuel Systems in New Zealand.* Int. Biodetn. Bull., 10 (4), 105-107 (1974).

15-22 Anon — *An Analysis of Certain Microbiological Matter in Aircraft Fuels.* Shell International Petroleum Co. Ltd., London (1961).

Section 3: Sources of micro-organisms

15-23 Hazzard, G.F. — *Fungal Growth in Aviation Fuel Systems (Part 1).* Report 252, Australian Defence Scientific Service (1961).

15-24 Parbery, D.G. — *Amorphoteca Resinae Gen. Nov. Sp. Nov.: The Perfect State of Cladosporium Resinae.* Aust. J. Bot., 17, 331-57 (1969).

15-25 Parbery, D.G. — *The Soil as a Natural Source of Cladosporium Resinae.* IN Biodeterioration of Materials, A.H. Walter and J.J. Elphick, Elsevier Publishing Co. Ltd., Amsterdam, 371-380 (1969).

15-26 Parbery, D.G. — *Biological Problems in Jet Aviation Fuel and the Biology of Amorphotheca Resinae.* Material und Organismen, 6, 161-208 (1971).

Section 4: Nutritional aspects

15-27 Bushnell, L.D., Haas, H.F. — *The Utilization of Certain Hydrocarbons by Micro-Organisms.* J. of Bacteriology, 41, 653-673 (1941).

15-28 Teh, J.S., Lee, K.H. — *Utilization of n-alkanes by Cladosporium Resinae.* App. Microbiology, 25 (3), 454-457 (1973).

15-29 Siporin, C., Cooney, J.J. — *Extracellular Lipids of Cladosporium (Amorphotheca) Resinae Grown on Glucose and n-alkanes.* Applied Microbiology, 29 (5), 604-609 (1975).

15-30 Williams, G.R., Cumins, E., Gardner, A.C., Palmier, M., Rubidge, T. — *The Growth of Pseudomonas Putida in AVTUR Aviation Turbine Fuel.* J. App. Bact., 50, 551-557 (1981).

Section 5: Growth and survival

15-31 Hill, E.C., Evans, D.A., Davies, I. — *The Growth and Survival of Micro-Organisms in Aviation Kerosine.* Jour. Inst. Petroleum, 53 (524), 280-284 (1967).

15-32 Cooney, J.J., Kula, T.J. — *Growth and Survival of Organisms Isolated from Hydrocarbon Fuel System.* Int. Biodetn. Bull., 6 (3), 109-114 (1970).

15-33 Parbery, D.G. — *Physical Factors Influencing Growth of Amorphotheca Resinae in Culture.* Int. Biodetn. Bull., 7 (1), 5-9 (1971).

15-34 Scott, J.A., Forsyth, T.J. — *Thermophilic Micro-Organisms in Aircraft Fuel.* Int. Biodetn. Bull., 12 (1), 1-4 (1976).

15-35 Klug, M.J.
Markoretz, A.J.
Utilization of Aliphatic Hydrocarbons by Micro-Organisms in Adv. Microbiol. Physiol.
Vol. 5, A.H. Rose and J.F. Wilkinson (Editors), Academic Press, London, 1-43 (1971).

15-36 Thomas, A.R.
Hill, E.C.
Aspergillus Fumigatus and Supersonic Aviation, 1. Growth of Aspergillus Fumigatus.
Int. Biodetn. Bull., 12 (3), 87-94 (1976).

Section 6: Field detection of contamination

15-37 Bailey, C.A.
May, M.E.
Evaluation of Microbiological Test Kits for Hydrocarbon Fuel Systems.
App. & Env. Microbiol., 37 (5), 871-877 (1979).

15-38 Peacock, A.T.
Engle, W.B.
Detection and Prevention of Aviation Turbine Fuel Contaminants.
Douglas Service, 32-42, September-October 1980.

15-39 Cabral, D.
Corrosion by Micro-Organisms of Jet Aircraft Integral Fuel Tanks, Part 1: Analysis of Fungal Contamination.
Int. Biodetn. Bull., 16 (1), 23-27 (1980).

Section 7: Corrosion

15-40 Ward, C.B.
Corrosion Resulting from Microbial Fuel Tank Contamination.
Materials Protection, June, 10-16 (1963).

15-41 Churchill, A.V.
Microbial Fuel Tank Corrosion: Mechanisms and Contributing Factors.
Materials Protection, June, 19-23 (1963).

15-42 Hendey, N.I.
Some Observations on Cladosporium Resinae as a Fuel Contaminant and its Possible Role in the Corrosion of Aluminium Alloy Fuel Tanks.
Trans. Brit. Mycol. Soc., 47 (4), 467-475 (1964).

15-43 Halkias, J.E. et. al.
Microbiological Corrosive Effects on Structural Materials Used in Aircraft Fuel Tanks.
Technical Report AFML-TR-65-95, March 1965, Air Force Materials Laboratory, Wright-Patterson Air Force Base, Ohio, U.S.A.

15-44 Inoue, M.
Takao, H.
Studies on Corrosions Caused by Micro-Organisms in Aircraft Fuel Tank of Aluminium Alloy.
The Ninth Japanese Congress on Testing Materials, March 1966, 88-90.

15-45 Iverson, W.P.
A Possible Role for Sulphate Reducers in the Corrosion of Aluminium Alloys.
Electrochem. Tech., 5 (3-4), 77-79 (1967).

15-46 Blanchard, G.C.
Goucher, C.R.
Aluminium Corrosion Processes in Microbial Cultures.
Electrochem. Tech., 5 (3-4), 79-83 (1967).

15-47 Hedrick, H.G.
Crum, M.G.
Reynolds, R.J.
Culver, S.C.
Mechanism of Microbiological Corrosion of Aluminium Alloys.
Electrochemical Tech., 5, 75-77 (1967).

15-48 Hedrick, H.G.
Reynolds, R.J.
Crum, M.G.
Factors Influencing the Mechanism of Corrosion of Aluminium Alloys by Aerobic Bacteria.
Dev. Ind. Microbiol., 8, 267-274 (1967).

15-49 Parbery, D.G.
The Role of Cladosporium Resinae in the Corrosion of Aluminium Alloys.
Int. Biodet. Bull., 4 (2), 79-81 (1968).

15-50 Landerkin, G.B.
le Cheminant, A.N.
Microbial Induction of Corrosion in Aircraft Aluminium Alloy Sheet.
Canadian Aero. and Space J., April 1968, 131-135.

15-51 Iverson, W.P.
Mechanisms of Microbial Corrosion.
IN Biodeterioration of Materials, A.H. Walters and J.J. Elphick (Editors), Elsevier Publishing Co. Ltd., Amsterdam (1969), 28-43.

15-52 Hedrick, H.G.
Microbiological Corrosion of Aluminium Alloys.
Proceedings 25th Conference NACE, Houston, Texas, March 10-14, 1969, 609-619.

15-53 Engel, W.B.
Role of Metallic Ion Concentrating Micro-Organisms in the Corrosion of Metals.
Proceedings 25th Conference NACE, Houston, Texas, March 10-14, 1969, 588-596.

15-54 Calderson, O.H.
Staffeldt, E.E.
Coleman, C.B.
Metal-Organic Acid Corrosion and Some Mechanisms Associated With These Corrosion Processes.
IN Biodeterioration of Materials, A.H. Walters and J.J. Elphick (Editors), Elsevier Publishing Co. Ltd., Amsterdam (1969), 356-363.

15-55 Hedrick, H.G.
Microbiological Corrosion of Aluminium.
Material Protection, 27-31, January 1970.

15-56 Menzies, I.A. *Introductory Corrosion.* IN Microbial Aspects of Metallurgy, Editor: J.D.A. Miller, Medical and Techn. Publ. Co. Ltd., Aylesbury, U.K., 34-60 (1971).

15-57 Miller, J.D.A. *Corrosion: The Influence of Micro-Organisms.* Microbiology Group Symposium, 28 April 1976, Institute of Petroleum, London Publication IP 77-001, 3-11.

15-58 Thomas, A.R., Hill, E.C. *Aspergillus Fumigatus and Supersonic Aviation, 2. Corrosion.* Int. Biodetn. Bull., 12 (4), 116-119 (1976).

15-59 Smith, I.E. *Microbial Spoilage of Engineering Materials, Part 2: The Extent of Biodeterioration in Industry.* Tribology International, October 1976, 225-230.

15-60 de Mele, M.F.L., Salvarezza, R.C., Videla, H.A. *Microbial Contaminants Influencing the Electrochemical Behaviour of Aluminium and its Alloys in Fuel/Water System.* Int. Biodetn. Bull., 15 (2), 39-44 (1979).

15-61 Salvarezza, R.C., de Mele, A.F.L., Videla, H.A. *The Use of Pitting Potential to Study the Microbial Corrosion of 2024 Aluminium Alloy.* Int. Biodetn. Bull., 15 (4), 125-132 (1979).

15-62 de Schiapparelli, E.R., de Meybaum, B.R. *The Role of Dodecanoic Acid in the Microbiological Corrosion of Jet Aircraft Integral Fuel Tanks.* Int. Biodetn. Bull., 16 (3), 61-66 (1980).

15-63 de Meybaum, B.R., de Schiapparelli, E.R. *A Corrosion Test for Determining the Quality of Maintenance in Jet Fuel Storage.* Materials Performance, August, 41-44 (1980).

15-64 Williams, G.R., Lugg, M. *The Significance of Bacteria in Aviation Turbine Fuel Containing Anti-Icing Additive.* Int. Biodetn. Bull., 16 (4), 103-106 (1980).

15-65 de Meybaum, B.R., de Schiapparelli, E.R. *Corrosion by Micro-Organisms of Jet Aircraft Integral Fuel Tanks, Part 2: Corrosion.* Int. Biodetn. Bull., 16 (2), 31-36 (1980).

15-66 Miller, J.D.A. *Principles of Microbial Corrosion.* Br. Corros. J., 15 (2), 92-94 (1980).

15-67 Salvarezza, R.C., de Mele, M.F.L., Videla, H.A. *Redox Potential and the Microbiological Corrosion of Aluminium and its Alloys in Fuel/Water Systems.* Brit. Corros. J., 16 (3), 162-168 (1981).

15-68 Salvarezza, R.C., de Mele, M.F.L., Videla, H.A. *Mechanisms of the Microbial Corrosion of Aluminium Alloys.* Corrosion, 39 (1), 26-32 (1983).

Section 8: Preventive measures

15-69 ZoBell, C.E., Beckwith, J.D. *The Deterioration of Rubber Products by Micro-Organisms.* J. Am. Water Works Ass., 36, 439-453 (1944).

15-70 Kereluk, K., Baxter, R.M. *Microbial Activity in Integral Fuel Tanks, II. The Effect of Buna-N on the Growth of Pseudomonas Aeruginosa and Hormodendron.* Dev. Ind. Microbiol., 4, 235-244 (1963).

15-71 Miller, R.N., Herron, W.C., Krigens, A.G., Cameron, J.L., Terry, B.M. *Micro-Organisms Cause Corrosion in Aircraft Fuel Tanks.* Material Protection, September, 60-67 (1964).

15-72 Hedrick, H.G., Gilmartin, J.N. *A Detection Study of Microbiological Penetration of Aircraft Fuel Tank Coatings.* Dev. Ind. Microbiol., 6, 124-132 (1964).

15-73 Reynolds, R.J., Crum, M.G., Hedrick, H.G. *Studies on the Microbiological Degradation of Aircraft Fuel Tank Coatings.* Dev. Ind. Microbiol., 8, 260-266 (1967).

15-74 Kaplan, A.M., Darby, R.T., Greenberger, M., Rogers, M.R. *Microbial Deterioration of Polyurethane Systems.* Dev. Ind. Microbiol., 9, 201-217 (1968).

15-75 Darby, R.T., Kaplan, A.M. *Fungal Susceptibility of Polyurethanes.* App. Microbiol., 16, 900-905 (1968).

15-76 Ross, R.T. Sladen, J.B. Wienert, L.A.
Biodeterioration of Paint and Paint Films.
IN Biodeterioration of Materials, A.H. Walters and J.J. Elphick (Editors), Elsevier Publishing Co. Ltd., Amsterdam, 317-325 (1969).

15-77 Hueck, H.J.
The Biodeterioration of Material — An Appraisal.
IN Biodeterioration of Materials, A.H. Walters and J.J. Elphick (Editors), Elsevier Publishing Co. Ltd., Amsterdam, 6-12 (1969).

15-78 Wälchli, O.
Biodeterioration Test Methodology.
IN Biodeterioration of Materials, A.H. Walters and J.J. Elphick (Editors), Elsevier Publishing Co. Ltd., Amsterdam, 242-251 (1969).

15-79 Hedrick, H.G.
Microbiological Degradation of Aircraft Materials.
Proceedings Society of Aerospace Material and Process Engineers, 15, 817-827 (1969).

15-80 Boggs, W.A.
Changes in Aircraft Design, Fabrication and Finish Techniques and Maintenance Requirements Dictated by Microbe Infested Jet Fuel Sources.
Proceedings 25th Conference NACE, Houston, Texas, March 10-14, 1969, 624-637.

15-81 Rubidge, T.
A New Selective Medium for the Screening of Aircraft Fuels for Biodeteriogenic Fungi.
Int. Biodetn. Bull., 10 (2), 53-55 (1974).

15-82 Rubidge, T.
Techniques for Selective Isolation of Fungi from Aircraft Fuel.
IN Biodeterioration Investigation Techniques, A.H. Walters (Ed.), Applied Science Publishers, London (1977), 221-226).

15-83 Dallemagne, G.
Resistance des protections de fonds de reservoirs aux micro-organismes.
Aerospatiale, septembre 1980.

15-84 Seal, K.J. Pathirana, R.A.
The Microbiological Susceptibility of Polyurethanes — A Review.
Int. Biodetn. Bull., 18 (3), 81-85 (1982).

Section 9: Biocides

15-85 London, S.A. Finefrock, V.H. Killian, L.N.
Microbial Activity in Airforce Jet Fuel Systems.
Dev. Ind. Microbiol., 6, 61-79 (1964).

15-86 Hitzmann, D.O.
The Control of Bacterial and Fungal Growth in Jet Fuels by Use of a Fuel Additive.
Dev. Ind. Microbiol. 6, 105-116 (1965).

15-87 De Gray, R.J. Fitzgibbons, W.O.
Mechanism of Microbiocidal Action of Organo-Borates in Fuel-Water Systems.
Dev. Ind. Microbiol., 7, 384-391, (1966).

15-88 Allgood, M.A.
Microbes in Aircraft Wing Tanks — Fuel Additives to Inhibit Microbial Growth.
Materials Protection, 26-28, 8 (1967).

15-89 Rogers, M.R. Kaplan, A.M.
Screening of Prospective Biocides for Hydrocarbon Fuels.
Dev. Ind. Microbiol., 2, 448-476 (1968).

15-90 Elphick, J.J. Hunter, S.K.P.
Evaluating Biocidal Fuel Additives for Intermittant Use in Aircraft Fuel Systems.
IN Biodeterioration of Materials, A.H. Walters and J.J. Elphick (Editors), Elsevier Publishing Co. Ltd., Amsterdam (1969), 364-370.

15-91 Hill, E.C.
The Control of Micro-Organisms in Aircraft Fuel Systems.
Il. Inst. of Petroleum, 56 (549), 138-146 (1970).

15-92 Rubidge, T.
Inadequacy of a Strontium Chromate Formulation for Control of Fungal Growth in a Kerosene/ Water System.
Int. Biodetn. Bull., 11 (4), 133-135 (1975).

15-93 Thomas, A.R. Hill, E.C.
Aspergillus Fumigatus and Supersonic Aviation, 4 Biocidal Control.
Int. Biodetn. Bull., 13 (2), 31-37 (1977).

15-94 Neihof, R.A. Baily, C.A.
Biocidal Properties of Anti-Icing Additives for Aircraft Fuels.
App. & Env. Microbiol., 35 (4), 698-703 (1978).

15-95
Aircraft Fuel Tank Corrosion Group, Survey on the Use and Experience of Aircraft Fuel Biocides.
Coordinating Research Council Inc., New York, January 1979, C.R.C. Report No. 504.

15-96 Gardner, A.C. Williams, G.R.
The Growth of Pseudomonas Putida in Fuel Samples Containing 2-Methoxyethanol (2-ME).
Int. Biodetn. Bull., 18 (3), 93-94 (1982).

ACKNOWLEDGEMENTS

The authors would like to thank members of the Corrosion Subcommittee of the AGARD Structures and Materials Panel for their help and encouragement during the preparation of this handbook. Special thanks are due to Mr. Thomas Kearns, former Chairman of the subcommittee who suggested this project, and to Mr. Richard Schmidt who later assumed responsibilities for this chairmanship. Many organizations have provided information which has been used in the handbook and their co-operation is gratefully acknowledged. These organizations include:

- Aviation Safety Bureau, Department of Transport Canada.
- Quality Engineering Test Establishment, Department of National Defence, Canada.
- Industrieanlagen-Betriebsgesellschaft (IABG), Germany.
- National Aerospace Laboratory (NLR), Holland.
- Aeritalia, Societa Aerospaziale, Italy.
- Aeronautica Militare, Italy.
- Hellenic Air Force, Research and Technology Division, Keta, Athens, Greece.
- Department of Defence, Norway.
- Ministry of Defence, United Kingdom.
- United States Air Force, Air Force Materials Laboratory, Wright Aeronautical Laboratories, Dayton, Ohio.
- Naval Air Development Center, Warminster, Pennsylvania.
- Naval Air Systems Command, United States Department of the Navy.

The authors would also like to thank the graduate students of the Structural Integrity, Fatigue and Fracture Mechanics Research Laboratory of the Department of Mechanical Engineering, University of Toronto, who assisted in the preparation of the case histories. We would like to mention the following names: Dr. D. Cameron, Mr. A. MacDonald, Mr. D. Mann, Ms. E. Mann, Mr. S. Missana, Dr. I. Sherman, Mr. F. Smith and Mr. D. Wu.

REPORT DOCUMENTATION PAGE

1. Recipient's Reference	2. Originator's Reference	3. Further Reference	4. Security Classification of Document
	AGARD-AG-278 Volume 1	ISBN 92-835-1505-6	UNCLASSIFIED

5. Originator
Advisory Group for Aerospace Research and Development
North Atlantic Treaty Organization
7 rue Ancelle, 92200 Neuilly sur Seine, France

6. Title
AGARD AG 278 VOLUME 1
AIRCRAFT CORROSION: CAUSES AND CASE HISTORIES

7. Presented at

8. Author(s)/Editor(s)	9. Date
W.Wallace, D.W.Hoeppner and P.V.Kandachar	July 1985

10. Author's/Editor's Address	11. Pages
Various	208

12. Distribution Statement
This document is distributed in accordance with AGARD policies and regulations, which are outlined on the Outside Back Covers of all AGARD publications.

13. Keywords/Descriptors

Corrosion
Corrosion prevention
Aircraft
Corrosion tests
Corrosion inhibitors

14. Abstract

A need exists to keep aircraft operators and maintenance personnel aware of the science and technology of corrosion as it applies to aircraft structures. This handbook provides information on the aircraft operating environment, corrosion theory, common airframe materials and their response to corrosion, the detection of corrosion, and methods employed to control corrosion in aircraft structures and materials.

The handbook also gives case histories of the deterioration or failure of components in typical aircraft and details the means of detection and the remedial action taken. An additional chapter is devoted to microbiological corrosion.

The handbook is intended to assist in the early diagnosis of developing corrosion problems and in the selection of appropriate corrective measures.

This AGARDograph was prepared on behalf of the Corrosion Subcommittee of the Structures and Materials Panel of AGARD.

AGARD

NATO OTAN

7 RUE ANCELLE · 92200 NEUILLY-SUR-SEINE

FRANCE

Telephone 745.08.10 · Telex 610176

DISTRIBUTION OF UNCLASSIFIED AGARD PUBLICATIONS

AGARD does NOT hold stocks of AGARD publications at the above address for general distribution. Initial distribution of AGARD publications is made to AGARD Member Nations through the following National Distribution Centres.Further copies are sometimes available from these Centres, but if not may be purchased in Mircrofiche or Photocopy form from the Purchase Agencies listed below.

NATIONAL DISTRIBUTION CENTRES

BELGIUM
Coordonnateur AGARD — VSL
Etat-Major de la Force Aérienne
Quartier Reine Elisabeth
Rue d'Evere, 1140 Bruxelles

CANADA
Defence Scientific Information Services
Dept of National Defence
Ottawa, Ontario K1A 0K2

DENMARK
Danish Defence Research Board
Ved Idraetsparken 4
2100 Copenhagen Ø

FRANCE
O.N.E.R.A. (Direction)
29 Avenue de la Division Leclerc
92320 Châtillon

GERMANY
Fachinformationszentrum Energie,
Physik, Mathematik GmbH
Kernforschungszentrum
D-7514 Eggenstein-Leopoldshafen

GREECE
Hellenic Air Force General Staff
Research and Development Directorate
Holargos, Athens

ICELAND
Director of Aviation
c/o Flugrad
Reyjavik

ITALY
Aeronautica Militare
Ufficio del Delegato Nazionale all'AGARD
3 Piazzale Adenauer
00144 Roma/EUR

LUXEMBOURG
See Belgium

NETHERLANDS
Netherlands Delegation to AGARD
National Aerospace Laboratory, NLR
P.O. Box 126
2600 AC Delft

NORWAY
Norwegian Defence Research Establishment
Attn: Biblioteket
P.O. Box 25
N-2007 Kjeller

PORTUGAL
Portuguese National Coordinator to AGARD
Gabinete de Estudos e Programas
CLAFA
Base de Alfragide
Alfragide
2700 Amadora

TURKEY
Department of Research and Development (ARGE)
Ministry of National Defence, Ankara

UNITED KINGDOM
Defence Research Information Centre
Station Square House
St Mary Cray
Orpington, Kent BR5 3RE

UNITED STATES
National Aeronautics and Space Administration (NASA)
Langley Research Center
M/S 180
Hampton, Virginia 23665

THE UNITED STATES NATIONAL DISTRIBUTION CENTRE (NASA) DOES NOT HOLD STOCKS OF AGARD PUBLICATIONS, AND APPLICATIONS FOR COPIES SHOULD BE MADE DIRECT TO THE NATIONAL TECHNICAL INFORMATION SERVICE (NTIS) AT THE ADDRESS BELOW.

PURCHASE AGENCIES

Microfiche or Photocopy
National Technical
Information Service (NTIS)
5285 Port Royal Road
Springfield
Virginia 22161, USA

Microfiche
ESA/Information Retrieval Service
European Space Agency
10, rue Mário Nikis
75015 Paris, France

Microfiche or Photocopy
British Library Lending
Division
Boston Spa, Wetherby
West Yorkshire LS23 7BQ
England

Requests for microfiche or photocopies of AGARD documents should include the AGARD serial number, title, author or editor, and publication date. Requests to NTIS should include the NASA accession report number. Full bibliographical references and abstracts of AGARD publications are given in the following journals:

Scientific and Technical Aerospace Reports (STAR)
published by NASA Scientific and Technical
Information Branch
NASA Headquarters (NIT-40)
Washington D.C. 20546, USA

Government Reports Announcements (GRA)
published by the National Technical
Information Services, Springfield
Virginia 22161, USA

Printed by Specialised Printing Services Limited
40 Chigwell Lane, Loughton, Essex IG10 3TZ

ISBN 92-835-1505-6